UNIVERSITAT DE BARCELONA

Mitochondria as a therapeutic target for neurodevelopmental disorders

Uliana Musokhranova Matveeva

ADVERTIMENT. La consulta d'aquesta tesi queda condicionada a l'acceptació de les següents condicions d'ús: La difusió d'aquesta tesi per mitjà del servei TDX (**www.tdx.cat**) i a través del Dipòsit Digital de la UB (**diposit.ub.edu**) ha estat autoritzada pels titulars dels drets de propietat intel·lectual únicament per a usos privats emmarcats en activitats d'investigació i docència. No s'autoritza la seva reproducció amb finalitats de lucre ni la seva difusió i posada a disposició des d'un lloc aliè al servei TDX ni al Dipòsit Digital de la UB. No s'autoritza la presentació del seu contingut en una finestra o marc aliè a TDX o al Dipòsit Digital de la UB (framing). Aquesta reserva de drets afecta tant al resum de presentació de la tesi com als seus continguts. En la utilització o cita de parts de la tesi és obligat indicar el nom de la persona autora.

ADVERTENCIA. La consulta de esta tesis queda condicionada a la aceptación de las siguientes condiciones de uso: La difusión de esta tesis por medio del servicio TDR (**www.tdx.cat**) y a través del Repositorio Digital de la UB (**diposit.ub.edu**) ha sido autorizada por los titulares de los derechos de propiedad intelectual únicamente para usos privados enmarcados en actividades de investigación y docencia. No se autoriza su reproducción con finalidades de lucro ni su difusión y puesta a disposición desde un sitio ajeno al servicio TDR o al Repositorio Digital de la UB. No se autoriza la presentación de su contenido en una ventana o marco ajeno a TDR o al Repositorio Digital de la UB (framing). Esta reserva de derechos afecta tanto al resumen de presentación de la tesis como a sus contenidos. En la utilización o cita de partes de la tesis es obligado indicar el nombre de la persona autora.

WARNING. On having consulted this thesis you're accepting the following use conditions: Spreading this thesis by the TDX (**www.tdx.cat**) service and by the UB Digital Repository (**diposit.ub.edu**) has been authorized by the titular of the intellectual property rights only for private uses placed in investigation and teaching activities. Reproduction with lucrative aims is not authorized nor its spreading and availability from a site foreign to the TDX service or to the UB Digital Repository. Introducing its content in a window or frame foreign to the TDX service or to the UB Digital Repository is not authorized (framing). Those rights affect to the presentation summary of the thesis as well as to its contents. In the using or citation of parts of the thesis it's obliged to indicate the name of the author.

Universitat de Barcelona

PhD Thesis

MITOCHONDRIA AS A THERAPEUTIC TARGET FOR NEURODEVELOPMENTAL DISORDERS

EL MITOCONDRI COM A DIANA TERAPÈUTICA EN TRASTORNS DEL NEURODESENVOLUPAMENT

Thesis submited by **Uliana Musokhranova**

To obtain the degree of Philosophy Doctor (PhD)

PhD program: Doctorat en Biomedicina, Universitat de Barcelona

Research has been conducted at the “Synaptic metabolism and personalized therapies” laboratory of Institut de Recerca Sant Joan de Déu - Hospital Sant Joan de Déu, Barcelona.

Directors | Dr. Alfonso Luis de Oyarzábal Sanz, Dr. Mònica Mir Llorente

Tutor | Dr. Raúl Estévez Povedano

PhD Candidate | Uliana Musokhranova Matveeva

Barcelona, January 2025

The work included in this Thesis has been performed at Institut de Recerca Sant Joan de Déu. Part of the experimental work was conducted in the facilities of Bellvitge Biomedical Research Institute (IDIBELL) and Institute for Bioengineering of Catalonia (IBEC) in academic collaborations.

This work has been supported by the predoctoral grant PFP00201-PERIS, from Departament de Salut of Generalitat de Catalunya, awarded to Uliana Musokhranova. Additionally, the experimental work has been carried out with the support of the following grants: PI18/00011, PI21/00073, both from Instituto de Salud Carlos III, awarded to Dr. Àngels García-Cazorla, RTC-2017-5867, CPP2021-008554 both from Ministerio de Ciencia e Innovación, awarded to Dr. Alfonso de Oyarzábal, and PID2022-1422273OB-I00 by Ministerio de Cienca e Innovación, awarded to Dr. Mònica Mir. Finally, generous recurrent donations from the Rett patients associations “Mi Princesa Rett” and “Rettando al Síndrome de Rett” have made possible this work.

INDEX

Abstract 1

Introduction 9

1. Rett syndrome, a paradigmatic neurodevelopmental disease 11
   1.1. Clinical and genetic aspects
   1.2. Molecular pathophysiology
      Neuronal maturation delay
      Excitatory and inhibitory (E/I) neurotransmitter systems imbalance
      Glial cell dysfunction
   1.3. Other events contributing to Rett pathophysiology: mitochondrial dysfunction, metabolism, and systemic inflammation
   1.4. Current therapeutic landscape
      Symptomatic treatments
      Gene therapy: beyond classic gene replacement
      Pharmacological approaches for brain development
      Future therapeutic options

2. Mitochondrial function and related disorders in the light of neurodevelopment and synaptic communication 18
   2.1. Mitochondria are multifunctional and diverse organelles
   2.2. Energy metabolism in neurotransmission
   2.3. Mitochondria in neurodevelopment
   2.4. Mitochondrial diseases and current therapeutic options
      Current treatments for mitochondrial disorders

3. Organs on a chip (OoC): a new technology towards personalized medicine 25
   3.1. Organ on a chip (OoC) current perspectives
   3.2. Synapse on a chip (SoC): a sub-specialization of the system

Hypothesis and objectives 29

Materials & Methods 33

1. Materials 35
   1.1. Reagents and kits
   1.2. Antibodies
   1.3. Primers
   1.4. Informatic resources

2. Samples 39
   2.1. Patients and control fibroblasts
   2.2. Mouse colony
   2.3. Human neural progenitor cells (hNPCs)

3. Cell culturing 41
   3.1. Fibroblasts cell culture and treatments
   3.2. Cortical neuron differentiation
   3.3. Dopaminergic neuron differentiation

4. Microfluidic device fabrication 42
4.1. Design and SU-8 master fabrication
4.2. Fabrication of the PDMS chip replicas
4.3. Inclusion and differentiation of neurons in the device

5. Molecular biology 44
5.1. Immunofluorescence on conventional culture and confocal microscopy
TOMM20 quantification
8-OHdG intensity quantification
5.2. Immunofluorescence on chip and confocal microscopy
Quantifications
5.3. Time-lapse confocal microscopy in live cells
5.4. Transmission electron microscopy (TEM)
5.5. Immunohistochemistry
5.6. RT-qPCR
5.7. Western blotting
5.8. Oxygen consumption rate
5.9. ATP content measurement
5.10. Analysis of intracellular $O_2^{\cdot-}$ by flow cytometry
5.11. TBARS assay
5.12. Cytokines multiplex
5.13. High-performance liquid chromatography (HPLC)

6. Behavioral tests 49
6.1. General Health Score (GHS)
6.2. Novel Object Recognition Test (NORT)
6.3. Elevated Plus Maze (EPM) test

7. Statistical analysis 49
7.1. GraphPad Prism
7.2. R Software

Results 51

1 | MITOCHONDRIAL DYSFUNCTION IN RETT SYNDROME AND ITS MODULATION AS A THERAPEUTIC STRATEGY 53

1. Mitochondrial homeostasis studies on Rett patients' primary fibroblasts 55
1.1. Mitochondrial network morphology and ultrastructure in Rett fibroblasts
1.2. Mitochondrial bioenergetic profile in Rett patients' fibroblasts

2. Leriglitazone treatment on Rett patients' primary fibroblasts 62
2.1. Leriglitazone effect on the PPARγ pathway: assessment of gene and protein expression
2.2. Evaluation of leriglitazone on mitochondrial homeostasis modulation in treated Rett patients' fibroblasts
2.3. Validation of leriglitazone effect on the PPARγ pathway with the inhibitor GW9662
2.4. Summary of mitochondrial performance and its modulation in patients' fibroblasts

3. Studies on animal models: female Rett mice for assessment of brain bioenergetic function, neuroinflammation and behavior 69
3.1. Bioenergetic characterization: ATP characterization and oxidative stress
3.2. Neuroinflammatory component
3.3. Phenotypic outcome and behavior analysis
3.4. Additional results: neuronal markers expression
3.5. Summary of mitochondrial homeostasis alterations in Rett mice and their modulation with leriglitazone

2 | PERSONALIZED TREATMENTS FOR MITOCHONDRIAL DISORDERS WITH ALTERATIONS IN NEUROTRANSMISSION 79

1. Functional studies for mutations characterization 82
   - 1.1. Mitochondrial dynamics
   - 1.2. Mitochondrial structure
   - 1.3. Mitochondrial genes translation
   - 1.4. Mitochondrial OXPHOS complexes subunits expression and assembly
   - 1.5. Intermediate metabolism

2. Personalized therapeutic approach 103
   - 2.1. Pharmacological treatment: leriglitazone
   - 2.2. Nutraceutical treatment: spermidine
   - 2.3. Metabolic treatment: ketogenic diet
   - 2.4. Non-responsive (non-treated) patients
   - 2.5. Summary of mitochondrial dysfunctions and responses to personalized treatments

3 | SYNAPSE ON A CHIP (SoC): AN ADVANCED TOOL FOR STUDYING THE IMPLICATION OF MITOCHONDRIA IN SYNAPTIC COMMUNICATION IN NEURODEVELOPMENTAL DISORDERS 117

1. Microfluidic device “synapse on a chip” (SoC): design and characterization 120
   - 1.1. Synapse on a chip device design and fabrication
   - 1.2. Synapse on a chip device characterization

2. Cortical neurons growth and characterization in the microfluidic device 121
   - 2.1. Human neural progenitor cell (hNPC)-derived cortical neurons growth and differentiation in the microfluidic device
   - 2.2. Characterization of cortical neurons in the microfluidic device
   - 2.3. Neurotransmitters’ measurement in the synaptic chamber

3. Dopaminergic neurons growth and characterization in the microfluidic device 127
   - 3.1. Human ventral midbrain neural progenitor cell (vmNPC)-derived dopaminergic neurons growth and differentiation in the microfluidic device
   - 3.2. Mitochondrial characterization of dopaminergic neurons in the microfluidic device
   - 3.3. Dopamine measurement and mitochondrial disturbance in the synaptic chamber

Discussion 131

1. Mitochondrial homeostasis is altered in Rett syndrome and represents a new therapeutic target 133
   Mitochondrial homeostasis alterations are detected in the two studied Rett syndrome models
   Mitochondrial modulation through leriglitazone is a potential treatment for Rett syndrome

2. Personalized treatment approach for mitochondrial disorders 140
   Characterization of mitochondrial homeostasis in selected disorders
   Therapeutic approaches for neurodevelopmental disorders with mitochondrial involvement

3. Advanced *in vitro* platforms for synaptic function analysis 147

4. Integrative view of mitochondria as a therapeutic target 149

Conclusions 151

Bibliography 155

Paper publications 175

LIST OF FIGURES

Figure 1. Rett syndrome main clinical features, developmental stages and molecular pathways affected.

Figure 2. Schematic representation of the energetic metabolism of glucose.

Figure 3. Schematic representation of energy metabolism in the developing brain.

Figure 4. Synapse on a chip (SoC) microfluidic devices.

Figure 5. Schematic representation of dopaminergic neuron differentiation from vmNPCs.

Figure 6. Microfluidic device design in AutoCAD and master photolithography fabrication.

Figure 7. Pipeline of mitochondrial network analysis with TOMM20 IF staining.

Figure 8. Pipeline of mitochondrial dynamics and morphology analysis with Mitometer add-in for MATLAB.

Figure 9. Parameters analyzed for mitochondrial ultrastructure quantification.

Figure 10. Schematic representation of the methods used for mitochondrial homeostasis characterization of Rett patients' fibroblasts.

Figure 11. Analysis of the mitochondrial network shape in Rett fibroblasts.

Figure 12. Mitochondrial dynamics evaluation in Rett fibroblasts: expression of dynamics proteins and live-cell visualization.

Figure 13. Description of mitochondrial ultrastructure in Rett fibroblasts.

Figure 14. Mitochondrial energy production in Rett fibroblasts: oxygen consumption profile and ATP concentrations.

Figure 15. Reactive oxygen species (ROS) production and metabolism in Rett fibroblasts: evaluation of superoxide anion, antioxidant enzymes and oxidative damage.

Figure 16. PPARɣ mechanism of action in cells and treatment with the agonist LGZ.

Figure 17. Regulation of the PPARɣ pathway: detection of genes and proteins' expression under its control.

Figure 18. Mitochondrial network structure in Rett patients' fibroblasts after treatment with LGZ.

Figure 19. Assessment of mitochondrial dynamics in LGZ-treated Rett fibroblasts: protein expression and live-cell mitochondrial movement.

Figure 20. Evaluation of the bioenergetic profile in Rett fibroblasts after LGZ treatment: mitochondrial ATP synthesis and ROS metabolism.

Figure 21. Appraisal of the effects of blocking the PPARɣ pathway with GW9662 antagonist: ATP measurement and ROS generation.

Figure 22. Evaluation of Rett mice on brain bioenergetic function, neuroinflammation and phenotype.

Figure 23. Bioenergetic characterization of pre-symptomatic (3 m.o.) and symptomatic (7 m.o.) Rett mice: ATP concentration and lipid peroxidation.

Figure 24. Assessment of ATP concentration fluctuations over time.

Figure 25. Analysis of LGZ effect on the bioenergetic component in the brain areas: ATP concentration and oxidative stress evaluation on lipid peroxidation, oxidative damage and antioxidant metabolism.

Figure 26. Cytokine profile of the three brain areas (cortex, hippocampus and cerebellum) at pre-symptomatic and symptomatic stages of the disease.

Figure 27. Assessment of LGZ effect on the neuroinflammatory component in symptomatic Rett mice, differentiating between the three studied brain areas.

Figure 28. Phenotypical characterization of Rett female mice: general health status and behavioral assessment.

Figure 29. Neuronal markers (cFos, NeuN and DCX) expression in pre-symptomatic and symptomatic brain areas, in basal and LGZ-treated Rett mice.

Figure 30. Summary of the main parameters for studying mitochondrial homeostasis in pediatric patients with primary mitochondrial disorders.

Figure 31. Schematic representation of the selected neuropediatric patients, according to the functional groups.

Figure 32. Description of the mutations and dynamics proteins' expression in the five DNM1L patients' fibroblasts.

Figure 33. Mitochondrial dynamics markers detection in the five DNM1L patients' fibroblasts.

Figure 34. Evaluation of mitochondrial network structure in the five DNM1L patients' fibroblasts.

Figure 35. Evaluation of mitochondrial bioenergetics in the five DNM1L patients' fibroblasts.

Figure 36. AFG2A patients' description of mutations and mitochondrial homeostasis characterization in fibroblasts from the patients.

Figure 37. Validation of the mutation in CHCHD6 patient's fibroblasts and its effect on mitochondrial homeostasis maintenance.

Figure 38. Evaluation of the mutation in WARS2 patient's fibroblasts and its effect on mitochondrial homeostasis maintenance.

Figure 39. Evaluation of the mutation in GFM1 patient's fibroblasts and its effect on mitochondrial homeostasis maintenance.

Figure 40. Evaluation of the mutation in NDUFS1 patient's fibroblasts and its effect on mitochondrial homeostasis maintenance.

Figure 41. Evaluation of the mutations in NDUFAF6 patient's fibroblasts and their effect on mitochondrial homeostasis maintenance.

Figure 42. Evaluation of the mutations in SCO2 patient's fibroblasts and their effect on mitochondrial homeostasis maintenance.

Figure 43. Evaluation of the mutations in two SURF1 patients' fibroblasts (SURF1_P1 and SURF1_P2), and their effect on mitochondrial homeostasis maintenance.

Figure 44. Evaluation of the mutations in SLC25A22 patient fibroblasts and their effect on mitochondrial homeostasis maintenance.

Figure 45. Evaluation of the mutation in COASY patient fibroblasts and its effect on mitochondrial homeostasis maintenance.

Figure 46. Evaluation of the mutation in PDHX patient fibroblasts and its effect on mitochondrial homeostasis maintenance.

Figure 47. Bioenergetic profile in NDUFS1 patient's fibroblasts after LGZ treatment.

Figure 48. Mitochondrial function performance in DNM1L patients' fibroblasts after LGZ treatment.

Figure 49. SPM mechanism of action and mitochondrial pediatric patients studied.

Figure 50. Evaluation of spermidine (SPM) effect on the bioenergetic function in mitochondrial patients' fibroblasts.

Figure 51. Evaluation of SPM clinical effect on mitochondrial pediatric patients through Vineland test.

Figure 52. Evaluation of the mutation in SMS patient fibroblasts and its effect on mitochondrial homeostasis maintenance.

Figure 53. Evaluation of the KD-mimicking media effect on mitochondrial dynamics and bioenergetics in the three AFG2A patients' fibroblasts.

Figure 54. Assessment of mitochondrial function in GFM1, COASY and SLC25A22 patients' fibroblasts after different personalized treatments.

Figure 55. Workflow followed for synapse on a chip (SoC) device fabrication and validation.

Figure 56. PDMS microfluidic device synapse on a chip (SoC) fabrication.

Figure 57. PDMS microfluidic device synapse on a chip (SoC) characterization.

Figure 58. Optimization of cell seeding conditions in the SoC microfluidic device for cortical neuron differentiation from hNPCs.

Figure 59. Cortical neuron differentiation in the SoC microfluidic device seeding 150,000 progenitors and maintaining proliferation factors EGF and FGF2 for 48 hours.

Figure 60. Characterization of CTRL2#8 hNPC-derived cortical neurons in the SoC microfluidic device.

Figure 61. Synaptic activity evaluation of cortical neurons in SoC microfluidic device.

Figure 62. Neurotransmitters' measurement through HPLC in synaptic chamber of SoC microfluidic devices.

Figure 63. Optimization of cell seeding conditions in the SoC microfluidic device for DA neuron differentiation from vmNPCs.

Figure 64. Characterization of DA neurons derived from the SP11 TH-reporter TdT line in the SoC microfluidic device.

Figure 65. Mitochondrial dynamics characterization in the DA neuron-microfluidic device.

Figure 66. Neurotransmitters' measurement through HPLC in synaptic chamber of SoC microfluidic devices.

Figure 67. Schematic representation of the alterations in Rett mice cerebellum.

LIST OF TABLES

Table 1. Reagents and other materials.

Table 2. List of kits.

Table 3.List of primary antibodies used for Western blot, immunocytochemistry (ICC) and immunohistochemistry (IHC).

Table 4. List of secondary antibodies.

Table 5. List of fluorescent conjugates and probes.

Table 6. List of primers.

Table 7. List of informatic resources.

Table 8. Rett patients' fibroblasts samples.

Table 9. Mitochondrial patients' fibroblasts samples.

Table 10. Combinations of primary and secondary antibodies for on-chip immunofluorescence.

Table 11. Summary of *in vitro* results for the Rett patients studied per technique.

Table 12. Summary of results obtained for Rett mice brains.

Table 13. Genes coding for mitochondrial proteins studied, number of patients per affected gene, protein function and main clinical symptomatology of these patients.

Table 14. Summary of the main findings for each patient studied.

ABBREVIATIONS

2-DG: 2-deoxy-D-glucose

8-OHdG: 8-hydroxy-2'-deoxyguanosine

AFG2A: ATPase family gene 2 protein homolog A

ATP: Adenosine Triphosphate

BBB: Blood-Brain Barrier

BDNF: Brain-Derived Neurotrophic Factor

CAMKII: Calcium/Calmodulin-Dependent Protein Kinase II

COASY: Coenzyme A Synthase.

CRMs: Caloric Restriction Mimetics

CSF: Cerebrospinal Fluid

DA: Dopamine

DAPI: 4',6-Diamidino-2-Phenylindole

DCX: Doublecortin

DNM1L: Dynamin-related protein 1

Drp1: Dynamin-related protein 1

ER: Endoplasmic Reticulum

ETC: Electron Transport Chain

EPM: Elevated Plus Maze

FAO: Fatty Acid Oxidation

FCCP: Carbonyl cyanide-p-trifluoromethoxyphenylhydrazone

FGF2: Fibroblast Growth Factor 2

GABA: Gamma-Aminobutyric Acid

GDNF: Glial cell line-Derived Neurotrophic Factor

GFM1: Mitochondrial elongation factor G1

GPx: Glutathione Peroxidase

HK2: Hexokinase 2

hNPCs:Human Neural Progenitor Cells

HPLC: High-Performance Liquid Chromatography

HVA: Homovanillic Acid

IF: Immunofluorescence

IMM: Inner Mitochondrial Membrane

KD: Ketogenic Diet

KCl: Potassium Chloride

LGZ: Leriglitazone

MAP2: Microtubule-Associated Protein 2

MeCP2: Methyl-CpG-Binding Protein 2

Mfn2: Mitofusin 2

MICOS: Mitoc. Contact site and Cristae Organizing System

MnSOD: Manganese Superoxide Dismutase

NDUFS1: NADH:Ubiquinone Oxidoreductase Core Subunit S1

NDUFAF6: Complex I assembly factor

NeuN: Neuronal Nuclei Protein

NORT: Novel Object Recognition Test

NT: Neurotransmitters

OCR: Oxygen Consumption Rate

OPA1: Optic Atrophy 1

OSR: Oligomycin-Sensitive Respiration

OXPHOS: Oxidative Phosphorylation

pCAMKII: Phosphorylated CAMKII

PDHX: Pyruvate Dehydrogenase Complex Component X

PDMS: Poly-Dimethyl-Siloxane

PE: Phycoerythrin

PGC1α: Peroxisome Proliferator-Activated Receptor Gamma Coactivator 1-alpha

PPAR-ɣ: Peroxisome Proliferator-Activated Receptor Gamma

RFP: Red Fluorescent Protein

ROS: Reactive Oxygen Species

RTT: Rett syndrome

SCO2: Cytochrome c oxidase assembly protein 2

SLC25A22: Mitochondrial glutamate carrier 1

SMS: Spermine Synthase

SoC: Synapse on a Chip

SPATA5: Spermatogenesis Associated Protein 5.

SREBP2: Sterol Regulatory Element-Binding Protein 2

SURF1: Surfeit locus 1 protein

TCA: Tricarboxylic Acid cycle

TH: Tyrosine Hydroxylase

TOMM20: Translocase of the Outer Mitochondrial Memb. 20

TUJ-1: Neuronal Class III β-Tubulin

VDAC1: Voltage-Dependent Anion Channel 1

vmNPCs: Ventral Midbrain Neural Progenitor Cells.

WARS2: Mitochondrial tryptophanyl-tRNA synthetase

* Only most relevant abbreviations have been included. Expansion for all the abbreviations used has been included at their first instance.

ABSTRACT

MITOCHONDRIA AS A THERAPEUTIC TARGET FOR NEURODEVELOPMENTAL DISORDERS

The brain's unique functions and its capacity to grow, adapt, and establish complex networks during infancy and childhood relies heavily on the multiple mitochondrial functions. These organelles not only fuel the energy required for neuronal proliferation, differentiation, and synaptogenesis but also regulate key signaling pathways, calcium dynamics, reactive oxygen species, and the synthesis of key metabolites. The importance of brain energy metabolism in neurodevelopment is made evident both through the diseases that arise from primary defects of brain energy homeostasis and the defects in mitochondrial homeostasis that underly in the pathophysiology of several neurodevelopmental diseases, such as Rett syndrome.

Building upon this understanding, in this Thesis we hypothesize that mitochondria being cross-sectional to neurodevelopmental diseases, constitute a potential common therapeutic target for their treatment. To demonstrate so, we divided this work in three sections.

First, we studied the mitochondrial homeostasis alterations in a paradigmatic neurodevelopmental disease, Rett syndrome, using two pre-clinical models. We evaluted the mitochondrial alterations in fibroblasts from Rett patients in terms of mitochondrial network structure and dynamics, along with bioenergetic function and oxidative stress metabolism. Once the alterations were described, we tested the metabolic modulator drug leriglitazone, a PPAR-ɣ agonist, achieving an improvement on the bioenergetic function in fibroblasts. After that, we moved on to a female Rett mouse model in which we studied the bioenergetic function and neuroinflammation at two developmental stages (pre- and post-symptomatic mice) and differentiating between brain areas (cortex, hippocampus and cerebellum). We observed that these alterations are different between brain regions of symptomatic mice, and that a bioenergetic dysfunction in pre-symptomatic cerebellum stands out. Continued treatment with leriglitazone from weaning to symptom development prevents some of the described bioenergetic and inflammatory alterations. Moreover, these biochemical changes translate into improvements in the phenotypic and behavioral features of the female mice. This work has confirmed that mitochondria is an interesting therapeutic target in neurodevelopmental pathologies in which it is not the main cause of the disease, and has led to the approval of a clinical trial with leriglitazone on Rett patients.

Second, we analyzed the mitochondrial homeostasis in a selection of 20 pediatric patients with complex neurological phenotypes due to primary defects in mitochondrial function. These patients recapitulated different aspects of mitochondrial homeostasis, including dynamics, cristae structure, mitochondrial gene translation, electron transport chain complexes structure and assembly, and intermediary metabolism. The characterization of the mitochondrial alterations in patients fibroblasts led to the description of novel pathogenic variants and phenotypes, providing support for their diagnosis. Based on the pathophysiology of these diseases, we have implemented an algorithm for the design of personalized therapies in mitochondrial diseases that could be implemented in a molecular biology laboratory with a real clinical-time repsonse. Moreover, we evaluated three theapeutic approaches (pharmacologic, nutraceutical and metabolic) in the patients' cells based on the bioenergetic characterization. The positive *in vitro* results obtained led to a series of n-of-1 clinical trials in these patients, who recovered in variable degrees cognitive and motor functions.

Finally, in response to the need for advanced models for the study of synaptic function, we developed a "synapse on a chip" model, a microfluidic device to study mitochondrial function in synaptic communication. The preliminary results obtained on neurons derived from human neural progenitor cells endorse the development of the microfluidic platform for its application on personalized medicine studies.

In conclusion, in this Thesis we have defined mitochondrial alterations in several neurodevelopmental diseases and we have defined different avenues for its modulation as therapeutic strategies. The work has had a direct impact on patients, with novel diagnoses, several clinical trials and personalized treatments implementation.

Keywords: Mitochondria; Energy metabolism; Neurodevelopmental disorders; Personalized Therapies; Organ on a chip.

EL MITOCONDRI COM A DIANA TERAPÈUTICA EN TRASTORNS DEL DESENVOLUPAMENT

La gran especialització funcional del cervell i la seva capacitat per créixer, adaptar-se i establir xarxes complexes durant la infància i la infantesa depenen, en gran part, de les múltiples funcions mitocondrials. Aquests orgànuls no només proporcionen l'energia necessària per a la proliferació, diferenciació neuronal i sinaptogènesi, sinó que també regulen rutes de senyalització, les concentracions dinàmiques de calci, les espècies reactives d'oxigen i la síntesi de metabòlits essencials. La importància del metabolisme energètic cerebral en el neurodesenvolupament es fa evident en observar tant les malalties que sorgeixen per defectes primaris en l'homeòstasi energètica cerebral com la descripció de defectes en l'homeòstasi mitocondrial subjacents a la fisiopatologia de diverses malalties del neurodesenvolupament, com per exemple la síndrome de Rett.

Partint d'aquesta base, en aquesta Tesi plantegem la hipòtesi que els mitocondris, com a element transversal en les malalties del neurodesenvolupament, constitueixen una possible diana terapèutica comuna pel seu tractament. Per demostrar-ho, hem dividit aquest treball en tres seccions:

En primer lloc, estudiem les alteracions en l'homeòstasi mitocondrial en una malaltia paradigmàtica del neurodesenvolupament, la síndrome de Rett, utilitzant dos models pre-clínics. Avaluem les alteracions mitocondrials en fibroblasts dels pacients en termes d'estructura i dinàmica de la xarxa mitocondrial, juntament amb la funció bioenergètica i el metabolisme de l'estrès oxidatiu. Una vegada descrites les alteracions, provem el fàrmac leriglitazona, un agonista de PPAR-γ i per tant modulador del metabolisme, aconseguint una millora en la funció bioenergètica en els fibroblasts. Posteriorment, analitzem un model murí de femella Rett, estudiant la funció bioenergètica i la neuroinflamació en dues etapes del desenvolupament (ratolins pre- i post-simptomàtics) i diferenciant entre àrees cerebrals (escorça, hipocamp i cerebel). Observem que aquestes alteracions són diferents entre les regions cerebrals en ratolins simptomàtics, destacant una disfunció bioenergètica en el cerebel pre-simptomàtic. El tractament continu amb leriglitazona, des del deslletament fins a l'aparició dels símptomes, redueix algunes de les alteracions bioenergètiques i inflamatòries descrites. A més, aquests canvis bioquímics es tradueixen en millores fenotípiques i conductuals en els ratolins femella. Aquest treball ha confirmat que els mitocondris són una diana terapèutica prometedora en patologies del neurodesenvolupament on el seu defecte no és la causa principal de la malaltia, la qual cosa ha portat a l'aprovació d'un assaig clínic amb leriglitazona en pacients amb Rett.

En segon lloc, analitzem l'homeòstasi mitocondrial en una selecció de 20 pacients pediàtrics amb fenotips neurològics complexos a causa de defectes primaris en la funció mitocondrial. Aquests pacients comparteixen diverses alteracions de l'homeòstasi mitocondrial, incloent la dinàmica, l'estructura de les crestes, la traducció de gens mitocondrials, l'estructura i l'acoblament dels complexos de la cadena de transport d'electrons i el metabolisme intermediari. La caracterització de les alteracions mitocondrials en fibroblasts de pacients va permetre descriure variants i fenotips patogènics nous, donant suport al seu diagnòstic. Basant-nos en la fisiopatologia d'aquestes malalties, implementem un algoritme per a l'estudi de teràpies personalitzades en malalties mitocondrials que pot ser aplicat en un laboratori de biologia molecular oferint una resposta en temps clínic real. A més, avaluem tres enfocaments terapèutics (farmacològic, nutracèutic i metabòlic) en les cèl·lules dels pacients basant-nos en la seva caracterització bioenergètica. Els resultats positius *in vitro* van portar a una sèrie d'assajos clínics *n-of-1* en aquests pacients, recuperant les funcions cognitives i motores en diferents graus.

Finalment, en resposta a la necessitat de models avançats amb la finalitat d'estudiar la funció sinàptica, desenvolupem un model de "sinapsi en xip", un dispositiu microfluídic per a l'estudi de la funció mitocondrial en la comunicació sinàptica. Els resultats preliminars obtinguts en neurones derivades de cèl·lules progenitores neuronals humanes recolzen el desenvolupament d'aquesta plataforma microfluídica per a la seva aplicació en estudis de medicina personalitzada.

En conclusió, en aquesta Tesi hem definit les alteracions mitocondrials en diverses malalties del neurodesenvolupament i hem identificat diferents vies modulables com a estratègies terapèutiques. Aquest treball ha tingut un impacte directe en els pacients, oferint diagnòstics nous, diversos assajos clínics i la implementació de tractaments personalitzats.

Paraules clau: Mitocondri; Metabolisme energètic; Malalties del neurodesenvolupament; Teràpies personalitzades; *Organ on a chip.*

LA MITOCONDRIA COMO DIANA TERAPÉUTICA PARA EL TRATAMIENTO DE PATOLOGÍAS DEL NEURODESARROLLO.

La gran especialización funcional del cerebro y su capacidad para crecer, adaptarse y establecer redes complejas durante la infancia y la niñez dependen en gran medida de las múltiples funciones mitocondriales. Estas organelas no solo proporcionan la energía necesaria para la proliferación, diferenciación neuronal y sinaptogénesis, sino que también regulan rutas de señalización, las concentraciones dinámicas de calcio, las especies reactivas de oxígeno y la síntesis de metabolitos esenciales. La importancia del metabolismo energético cerebral en el neurodesarrollo se hace evidente al observar tanto las enfermedades que surgen de defectos primarios en la homeostasis energética cerebral como la descripción de defectos en la homeostasis mitocondrial subyacentes en la fisiopatología de varias enfermedades del neurodesarrollo, como por ejemplo el síndrome de Rett.

Partiendo de esta base, en esta Tesis planteamos la hipótesis de que las mitocondrias, al ser un elemento transversal en las enfermedades del neurodesarrollo, constituyen una posible diana terapéutica común para su tratamiento. Para demostrarlo, hemos dividido este trabajo en tres secciones:

En primer lugar, estudiamos las alteraciones en la homeostasis mitocondrial en una enfermedad paradigmática del neurodesarrollo, el síndrome de Rett, utilizando dos modelos preclínicos. Evaluamos las alteraciones mitocondriales en fibroblastos de pacientes con Rett en términos de la estructura y dinámica de la red mitocondrial, junto con la función bioenergética y el metabolismo del estrés oxidativo. Una vez descritas las alteraciones, probamos el fármaco leriglitazona, un agonista de PPAR-ɣ y por tanto modulador del metabolismo, logrando una mejora en la función bioenergética en los fibroblastos. Posteriormente, analizamos un modelo murino hembra de Rett, estudiando la función bioenergética y la neuroinflamación en dos etapas del desarrollo (ratones pre- y post-sintomáticos) y diferenciando entre áreas cerebrales (corteza, hipocampo y cerebelo). Observamos que estas alteraciones son diferentes entre las regiones cerebrales en ratones sintomáticos, destacando una disfunción bioenergética en el cerebelo presintomático. El tratamiento continuo con leriglitazona desde el destete hasta el desarrollo de los síntomas previene algunas de las alteraciones bioenergéticas e inflamatorias descritas. Además, estos cambios bioquímicos se traducen en mejoras fenotípicas y conductuales en los ratones hembra. Este trabajo ha confirmado que las mitocondrias son una diana terapéutica interesante en patologías del neurodesarrollo donde no son la causa principal de la enfermedad, lo que ha llevado a la aprobación de un ensayo clínico con leriglitazona en pacientes con Rett.

En segundo lugar, analizamos la homeostasis mitocondrial en una selección de 20 pacientes pediátricos con fenotipos neurológicos complejos debido a defectos primarios en la función mitocondrial. Estos pacientes recogen defectos en diferentes aspectos de la homeostasis mitocondrial, incluidos dinámica, estructura de crestas, traducción de genes mitocondriales, estructura y ensamblaje de los complejos de la cadena de transporte de electrones y metabolismo intermediario. La caracterización de las alteraciones mitocondriales en fibroblastos de pacientes ha permitido describir variantes y fenotipos patogénicos novedosos, apoyando su diagnóstico. Basándonos en la fisiopatología de estas enfermedades, implementamos un algoritmo para el diseño de terapias personalizadas en enfermedades mitocondriales que puede ser aplicado en un laboratorio de biología molecular ofreciendo una respuesta en tiempo clínico real. Además, evaluamos tres enfoques terapéuticos (farmacológico, nutracéutico y metabólico) en las células de los pacientes basándonos en la caracterización bioenergética. Los resultados positivos *in vitro* llevaron a una serie de ensayos clínicos *n-of-1* en estos pacientes, recuperando en grados variables funciones cognitivas y motoras.

Finalmente, en respuesta a la necesidad de modelos avanzados para el estudio de la función sináptica, desarrollamos un modelo de "sinapsis en chip", un dispositivo microfluídico para estudiar la función mitocondrial en la comunicación sináptica. Los resultados preliminares obtenidos en neuronas derivadas de células progenitoras neuronales humanas respaldan el desarrollo de esta plataforma microfluídica para su aplicación en estudios de medicina personalizada.

En conclusión, en esta Tesis hemos definido las alteraciones mitocondriales en varias enfermedades del neurodesarrollo y hemos identificado diferentes vías para su modulación como estrategias terapéuticas. Este trabajo ha tenido un impacto directo en los pacientes, ofreciendo diagnósticos novedosos, varios ensayos clínicos y la implementación de tratamientos personalizados.

Palabras clave: Mitocondria; Metabolismo energético; Enfermedades del neurodesarrollo; Terapias personalizadas, *Organ on a chip.*

INTRODUCTION

The brain's remarkable capacity to grow, adapt, and establish complex networks during infancy and childhood relies heavily on the multiple mitochondrial functions. These organelles not only fuel the energy required for neuronal proliferation, differentiation, and synaptogenesis but also regulate key signaling pathways, calcium dynamics, reactive oxygen species, and the synthesis of key metabolites. These processes are essential for neurotransmitter release and synaptic plasticity, and shaping the development of neuronal circuits, highlighting the intricate connection between mitochondrial homeostasis and synaptic metabolism.

Whereas energy function in the aging brain and their related diseases has been explored in more detail, there is only limited knowledge about the molecular mechanisms and brain networks of energy metabolism at infancy and childhood. Despite its great interest, we only have scarce understanding on substrate utilization during neonatal and following periods, with most knowledge coming from studies in animal models such as rodents. From an energy metabolism point of view, the main players to be taken into account in neurodevelopment are glucose, lactate and ketone bodies. On one side, glucose is metabolized through the glycolytic pathway to pyruvate, and further metabolized either to lactate or to Acetyl-CoA, entering the TCA (tricarboxylic acid) cycle in the mitochondria. On the other side, lactate may be metabolized back to pyruvate, further processed in mitochondria, and ketone bodies are transported into the mitochondria for metabolism into Acetyl-CoA.

The importance of brain energy metabolism in neurodevelopment is made evident through the diseases that arise from primary defects of brain energy homeostasis. These are genetic diseases of brain metabolism (inborn errors of metabolism, IEM) with symptoms due to, at least in part, a deficiency in energy production or utilization within the nervous system. Most of them are pediatric-onset diseases, and therefore, they represent excellent models to study how energy is used in the neurodevelopmental brain. According to the simplified classification of IEM, these disorders include defects of membrane carriers of energetic molecules, cytoplasmic energy defects, and mitochondrial defects. They encompass numerous diseases with diverse clinical manifestations which may appear as movement disorders, stroke-like episodes, and neuro-muscular signs amongst others.

Besides primary cause of disease, defects on brain metabolism and in mitochondrial homeostasis underly in the pathophysiology of several neurodevelopmental diseases, ranging from autism spectrum and epileptic encephalopathies to genetic diseases such as Fragile-X syndrome or Rett syndrome. In the latest, several alterations including defective bioenergetic function or abnormal mitochondrial dynamics have been described in different diseases models, as will be further reviewed. Setting the focus on mitochondria as a target for Rett syndrome has resulted in various pre-clinical and clinical studies, aiming to improve mitochondrial dysfunction to rescue the neurological phenotype, representing an innovative therapeutic strategy for these diseases.

In fact, and considering the above, mitochondrial homeostasis can constitute not only a common pathway through different diseases, but also a common therapeutic target. It is most likely that precise information on energy metabolism in the pathophysiology of neurodevelopmental diseases will provide new horizons in mitochondria-targeted treatments regardless of the etiology of the neurological disease.

1 Rett syndrome, a paradigmatic neurodevelopmental disease

Rett syndrome (RTT, OMIM #312750) is a severe neurodevelopmental disorder that affects 1 in 10,000 people, mostly women (Petriti et al., 2023). First described in 1966 by the Austrian pediatrician Andreas Rett, it was recognized internationally in 1983 when Hagberg et al. described a large cohort of patients. The disease is commonly caused by *de novo* mutations in the *MECP2* gene (Amir et al., 1999), located on the X-chromosome. Its product, methyl CpG-binding protein 2 (MeCP2), is a master regulator of transcription mostly expressed in the brain (Chahrour and Zoghbi, 2007). Despite it is considered a rare disease, is the second cause of intellectual disability in females, only after Down syndrome (Hagberg, 1995). Rett syndrome is a very complex disorder, clinically and molecularly, and besides detecting *MECP2* mutations, its diagnosis is mostly based on clinical symptomatology (Neul et al., 2010). Nowadays, there is still no specific treatment for this devastating neurological disorder.

1.1 Clinical and genetic aspects

Rett is typically characterized by a regression in neurodevelopment between 6 and 18 months of age, after normal early development. Patients experience a loss of acquired abilities, such as communication skills, and a plethora of symptoms including features of severe autism, loss of purposeful use of hands, stereotypies, organ dysfunctions, apnea/hyperpnea, and seizures (Leonard et al., 2017).

The disorder progresses through four developmental stages (Ehrhart et al., 2016; Banerjee et al., 2019).

Stage I – Early onset stage (6-18 months): initial normal development with subtle signs such as reduced eye contact, delayed motor skills, and decreased interest in toys. Growth retardation and deceleration of head growth (acquired microcephaly). Muscle hypotonia and postural weakness may appear.
Stage II – Developmental regression (1-4 years): rapid loss of acquired skills, including purposeful hand use and spoken language. Development of repetitive hand movements (wringing, clapping, flapping, mouthing), gait abnormalities, and social withdrawal. Breathing irregularities, sleep disturbances, and autistic features. Gross motor abnormalities, ataxia, apraxia, and sound hypersensitivity.
Stage III – Plateau or Pseudostationary period (2-10 years): slowing of rapid regression with partial recovery in communication and social interaction. Improved gross motor skills, although gait ataxia and hand apraxia persist. Development of seizures, behavioral abnormalities (bruxism, inappropriate laughing/crying, anxiety), and osteopenia. Scoliosis and rigidity become apparent.
Stage IV – Late motor deterioration (10 years and older): continued decline in motor abilities, leading to reduced mobility and wheelchair dependence. Worsening scoliosis, rigidity, dystonia, and Parkinsonian features. Additional autonomic dysfunctions (vasomotor disturbances, dysphagia, constipation, cardiac dysfunction). Despite physical decline, cognitive and communication skills often remain stable or improve slightly. Some patients survive beyond 40 years in a severely impaired physical condition.

Between the 90-95% of cases, Rett is caused by **loss-of-function (LOF) mutations in *MECP2*** (OMIM *300005) (Percy et al., 2007). Less common cases are caused by mutations in genes encoding Cyclin-Dependent Kinase-Like 5 (*CDKL5*), the early onset seizures variant, and Forkhead box G1 (*FOXG1*) that causes the congenital form (Weaving et al., 2004; Ariani et al., 2008; Fehr 2013). *MECP2* mutations can be missense (the DNA change results in a different amino acid encoded in that position), nonsense (the sequence change gives rise to a stop codon), frameshift (insertion or deletion of nucleotide bases in numbers that are not multiples of three) and large deletions. No correlation has been established between genotype and phenotype, with the exception of missense and late-truncating mutations, that are associated with a milder phenotype, opposite to nonsense mutations or large deletions (Cuddapah et al., 2014).

MECP2 is located on the long arm of the X-chromosome (Xq28) between the Interleukin-1 receptor associated kinase (*IRAK1*) gene and the red opsin (*RCP*) gene. Alternative splicing of *MECP2* gene generates two isoforms (e1 and e2), which are identical except for the N-terminus (Kriaucionis and Bird, 2004). Given its chromosomal localization, *MECP2*, like most X-linked genes, is subject to X-chromosome inactivation (XCI). This process, in which mammalian female cells silence one of the X chromosomes to compensate for gene dosage, occurs randomly during embryonic development. Because of this, Rett is more often observed in females, and XCI patterns may contribute to phenotypic differences among patients with identical mutations. However, the extent of this influence remains unclear (Xiol et al., 2019). Hemizygous males with a severe mutation are generally not compatible with life, but there are several non-lethal mutations which can lead to severe congenital encephalopathy, Rett-like syndrome, and mild to severe intellectual disability in males (Bienvenu and Chelly, 2006). In addition, overexpression of *MECP2* has neurological consequences, causing the *MECP2* duplication syndrome (Van Esch et al., 2005).

The *MECP2* gene codes for a 52 kDa protein in which we can differentiate five main domains: the N-terminal domain (NTD), the methyl binding domain (MBD) for binding the methylated DNA, the interdomain region (ID), the transcription repressor domain (TRD) that interacts with co-repressors (Lyst et al., 2013), and the C-terminal domain (CTD). From a functional point of view, MeCP2 is defined as an epigenetic regulator of gene expression.

As aforementioned, MeCP2 is a transcriptional regulator, therefore, its main molecular function is to recognize and bind methylated DNA, both methyl CG dinucleotides as well as non-canonical methyl CAC sites that are enriched in neurons via its MBD domain (Lagger et al., 2017). MeCP2 interacts with NCOR (nuclear receptor co-repressor) and SMRT (also known as NCOR2) through the NCOR-SMRT interaction domain (NID), mapped to the TRD (Lyst et al., 2013). MeCP2 influences various biological mechanisms, such as transcriptional regulation, chromatin remodeling, alternative splicing, and micro-RNA processing (Maunakea et al., 2013; Ragione et al., 2016; Urdinguio et al., 2010; Young et al., 2005), that depending on context, can repress or stimulate gene expression (Chahrour et al., 2008; Yasui et al., 2007). Through these processes, MeCP2 acts as a multifunctional protein that regulates gene expression at both transcriptional and post-transcriptional levels, exerting control over numerous genes across the entire genome (Guy et al., 2011).

MeCP2 is ubiquitously expressed throughout the body, showing the highest expression levels in brain (where the e1 isoform is predominant) together with lungs and spleen (Liyanage and Rastegar, 2014). Within the central nervous system, its highest expression levels are found in the cortex and cerebellum, and it is predominantly expressed in neurons, although the expression is different between neuronal subpopulations (Sugino et al., 2014). It is also present at lower levels in glia (astrocytes, oligodendrocytes and microglia) (Sharma et al., 2018). Interestingly, the expression of MeCP2 is dynamic through development; it is already expressed at the earliest stages of embryonic development, when it is responsible for prenatal neurogenesis, reaching its peak in mature neurons (Feldman et al., 2016). In postmitotic neurons, the increase in expression coincides with dendritic growth, branching and spine morphogenesis for synapse formation, and it has a role in synaptic transmission and plasticity (Luikenhuis et al., 2004). This delayed expression pattern of MeCP2 could be contributing to the apparent normal early development observed in individuals with Rett. In addition, high expression levels are maintained throughout adulthood. In fact, late-deletion of Mecp2 recapitulates key phenotypes of the disease (Du et al., 2016; McGraw et al., 2011), suggesting that MeCP2 is also important for the maintenance of neuronal circuits in adult brain.

1.2 Molecular pathophysiology

Within the complex heterogeneity in Rett, the disorder stands in three main pathophysiological pillars: (1) **neuronal maturation delay** and (2) **imbalance between excitatory and inhibitory neurotransmitter systems**, together with (3) **glial dysfunction** (Fig. 1). These mechanisms collectively disrupt neuronal circuit formation, synaptic function, and brain homeostasis, contributing to the diverse clinical symptoms characteristic of Rett, as studied in animal models and patients.

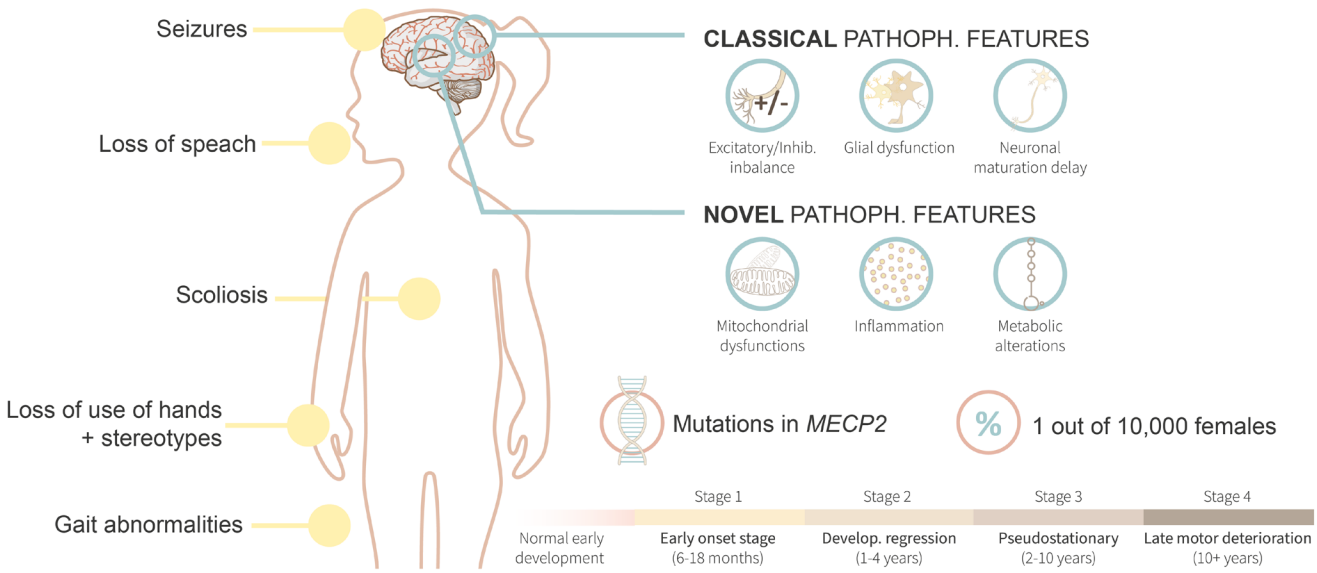

Figure 1. Rett syndrome main clinical features, developmental stages and molecular pathways affected.

Neuronal maturation delay

The molecular pathology of Rett reveals significant structural and functional abnormalities in neurons, as shown in human postmortem analyses and animal models of Mecp2 LOF (Li and Pozzo-Miller, 2012). Previous studies have demonstrated that selective removal of MeCP2 from neurons is sufficient to induce a Rett-like phenotype in mice (Chen et al., 2001; Guy et al., 2001) and region and cell-specific deletions in *Mecp2*-KO mouse brains have been correlated to different aspects of the phenotype (Liyanage and Rastegar, 2014).

Human postmortem studies consistently show an overall reduction in brain volume in Rett patients, with specific deficits such as decreased volume in the dorsal parietal cortex, a hallmark of Rett on MRI, and anterior frontal lobe reductions correlating with clinical severity (Carter et al., 2008). Structural alterations are also evident at cellular levels, and include impaired dendritic arborization, reduced synaptic spine maturation, and cytoskeletal deficiencies, all of which compromise neuronal connectivity and structural integrity (Bedogni et al., 2014; Sala and Pizzorusso, 2013). These deficits are linked to *MECP2* regulation of genes essential for dendritic growth and branching and its modulation of the BDNF (Brain Derived Neurotrophic Factor) pathway, a key player in neuronal development (Li and Pozzo-Miller, 2014).

From a neurophysiological perspective, Rett neurons exhibit reduced long-term potentiation (LTP) and long-term depression (LTD), essential mechanisms for learning and memory (Monteggia and Kavalali, 2009). MeCP2 expression responds to neuronal activity, adapting gene expression to the functional demands of maturing neurons. Loss of this dynamic regulation hinders activity-dependent maturation processes. The result is a significant delay or arrest in neuronal development, leaving the affected neurons structurally and functionally immature. Therefore, MeCP2's role appears to be more critical in maintaining neuronal integrity than in initial development, suggesting that Rett may be treatable with gene restoration therapies (Gold et al., 2024).

Excitatory and inhibitory (E/I) neurotransmitter systems imbalance

In close relationship with the neuronal maturation delay, the balance between excitatory and inhibitory (E/I) neurotransmitter systems is also critically disrupted in Rett syndrome (Ip et al., 2018). Rather than deficits in excitation or inhibition alone, Rett is marked by an altered spatiotemporal interplay between these two processes (Banerjee et al., 2019) and a hindered maturation of the GABAergic neurotransmission. This imbalance involves key neurotransmitter systems, including GABAergic, glutamatergic, and dopaminergic pathways, and contributes to the characteristic neurological and motor symptoms observed in Rett, as reviewed in (Li, 2022).

Ionotropic GABA receptors allow for the exchange of chloride (Cl^-); given the low Cl^- concentrations in mature neurons, GABAergic receptors activation results in the import of Cl^- and subsequent membrane hyperpolarization. This prevents the propagation of an action potential and therefore GABA is usually referred to as the main inhibitory neurotransmitter in the CNS. Interestingly, in early phases of development GABA acts as an activator, and only after fine tuning of specific transporters it changes to its inhibitory function. This developmental shift does not rely on GABA itself but on the expression of neuronal chloride co-transporters NKCC1 and KCC2. During early phases of brain development, the predominant activity of NKCC1 transporter (that imports Cl^- in the cell) leads to high intracellular chloride concentration, and GABA activation results in chloride extrusion, thus acting as a depolarizer. It is only as the brain matures that the increase in the expression of the KCC2 cotransporter (that transports Cl^- out of the cell) lowers intracellular chloride levels, switching GABA's action from excitatory to inhibitory—a crucial change for the formation of functional neural circuits. This NKCC1/KCC2 expression equilibrium is diminished in Rett patients (Duarte et al., 2013), leading to the abolishment of the GABA developmental shift (Lozovaya et al., 2019).

The co-transporters expression are not the only alteration regarding GABAergic neurotransmission in Rett pathophysiology, as reviewed in (Benke and Möhler, 2018). One of the key features is also diminished expression of GABA receptors subunits, which interestingly are also altered during development and detectable in presymptomatic mice consistently (Oyarzabal et al., 2020), highlighting the importance of time frame when addressing potential treatments for the disease. GABAergic dysfunction has been associated to several Rett features, such as ataxia, repetitive behaviors, and deficits in motor coordination (Chao et al., 2010). Its crucial role in Rett pathophysiology was made evident in 2016, when it was shown that restoration of MeCP2 activity in just GABAergic neurons of Mecp2 KO mice was sufficient for partial rescue of Rett-like symptoms (Ure et al., 2016). Not only highlighted the importance of GABAergic neurotransmission in Rett, but also opened a new horizon for its treatment and symptoms reversibility.

E/I imbalance has been reported not only in Rett but also in related neurodevelopmental and neurodegenerative disorders, such as Autism Spectrum Disorders (ASD) and Parkinson's disease, which share overlapping molecular pathways and phenotypic traits (Michele et al., 2013; Rubenstein et al., 2003). A key gene implicated in this imbalance in Rett is *GRID1*, which is downregulated in the absence of functional MeCP2. *GRID1* dysregulation links mutations to impaired neurotransmitter dynamics and, consequently, the Rett phenotype (Livide et al., 2015).

Finally, alterations in other neurotransmitters and neurotransmitter-related metabolites have been described in Rett syndrome samples. One example is tryptophan metabolism, precursor of serotonin, which is altered in Rett syndrome, together with other neurodevelopmental disorders in which glutamatergic signaling is compromised, as we demonstrated in (Illescas et al., 2023). Finally, glutamate have been described as consistently elevated in Rett patients. This overexcitation leads to increased glutamate uptake and conversion to glutamine, triggering compensatory downregulation of glutamate receptors (Viola et al., 2007). Excess glutamate can amplify excitotoxicity, further contributing to neuronal dysfunction.

Glial cell dysfunction

While neuronal dysfunction is central to the Rett pathophysiology, other studies have highlighted the contribution of glial cells to disease progression. Initially, MeCP2 deficiency in neurons was considered the primary cause of Rett, as MeCP2 is predominantly expressed in the brain (Chahrour and Zoghbi, 2007). However, increasing evidence has shown that non-neuronal cells, including glia, play a significant role in Rett pathogenesis (Kahanovitch et al., 2019; Lioy et al., 2011).

Microglia, for instance, show altered activity, including increased glutamate release, which may exacerbate neuronal dysfunction in Rett (Maezawa and Jin, 2010). Microglia have been implicated in inflammation and synaptic pruning in Rett, although their exact role remains unclear (O'Driscoll et al., 2013). Jin et al. (Jin et al., 2015) have found that MeCP2 acts as a microglia-specific transcriptional repressor of SNAT1, a major glutamine transporter. MeCP2 downregulation (or SNAT1 overexpression) impairs glutamine homeostasis resulting in mitochondrial dysfunction and overproduction of glutamate. Nonetheless, early attempts to restore wild-type microglia as a therapeutic strategy by bone marrow transplants (Derecki, 2012) were not reproducible and selective re-expression of *Mecp2* in microglia did not rescue Rett-like phenotypes in mice (Wang et al., 2015).

Astrocyte-specific deletion of MeCP2 results in non-cell-autonomous effects (Maezawa et al., 2009), affecting neuronal and synaptic function, which can be partially ameliorated by re-expression of MeCP2 (Lioy, 2011). Alterations in Rett astrocytes include impaired calcium signaling (Turovsky et al., 2015), aberrant metabolic support for synaptic function failing to provide sufficient metabolites (Saywell et al., 2006; De Filippis et al., 2012) and altered ion homeostasis affecting maintenance of the E/I balance in neuronal cells (Kahanovitch et al., 2018). De Filippis and collaborators (De Filippis et al., 2012) were able to reverse signs of atrophy in astrocytes and restore metabolic deficiencies in mice treated with the bacterial cytotoxic necrotizing factor 1 (CNF1), which activates RhoGTPases, shapes the actin cytoskeleton and enhances neurotransmission and synaptic plasticity in mouse brains.

The selective ablation of MeCP2 in oligodendrocytes induces behavioral impairments, further implicating glial cells in Rett's pathophysiology (Nguyen et al., 2013). Restoration of Mecp2 in oligodendrocyte progenitor cells (OPCs) of *Mecp2* mice from both sexes increased lifespan and improved the locomotor deficits and hindlimb clasping. These findings support the hypothesis that glial cells, beyond just neurons, play a crucial role in Rett syndrome pathology.

1.3 Other events contributing to Rett pathophysiology: mitochondrial dysfunction, metabolism, and systemic inflammation

In recent years more elements than the aforementioned have been described to contribute to Rett syndrome pathophysiology. **Mitochondrial dysfunction**, **oxidative stress**, **inflammation**, and **metabolic alterations** have demonstrated to be pivotal to the pathophysiology of Rett, significantly contributing to the multisystemic manifestations of the disease. Remarkably, their modulation may constitute an attractive therapeutic approach, as it is more easily approachable than neuronal modulation, and complementary to it.

Mitochondrial dysfunction plays a critical role in the pathophysiology of Rett, affecting both neuronal and non-neuronal cells. As a matter of fact, in the earliest studies, before *MECP2* mutations were identified as causative of Rett syndrome, the disorder was proposed to be a mitochondrial disease based on observed abnormalities in mitochondrial structure and metabolism in patients (Cardaioli et al., 1999; Cornford et al.,1994; Dotti et al., 1993; Eeg-Olofsson et al., 1988, 1990; Wakai et al., 1990). Recently, mitochondrial disease was suspected in a boy before Rett syndrome diagnosis (Balicza et al., 2024). Subsequent studies have highlighted significant alterations in mitochondrial bioenergetic function and oxidative stress in both human and animal models, as reviewed previously in (Filosa et al., 2015; Müller, 2019; Shulyakova et al., 2017). The relationship between MeCP2 and mitochondrial homeostasis is hypothesized to be through the dysregulation of ANT1 (adenine nucleotide translocase), a mitochondrial protein repressed by MeCP2 (Forlani et al., 2010).

Studies in mouse model brains reveal decreased ATP levels in both male (Saywell et al., 2006) and female mice (De Filippis et al., 2015a). The decrease in ATP could be caused by decreased activity in oxidative phosphorylation (OXPHOS) complexes II, III and IV, impairing ATP synthesis and leading to energy depletion in mice and MeCP2-KO SH-SY5Y cells (Gibson et al., 2010; Gold et al., 2014; Valenti et al., 2017). Other studies have reported upregulated expression of nuclear-encoded components of OXPHOS complexes together with increased respiration rates, although with lower efficiency, in Mecp2-null mice brains (Kriaucionis et al., 2006; Grosser et al., 2012) and upregulation and downregulation of proteins related to mitochondrial biogenesis (Gold et al., 2014; Pecorelli et al., 2013).

Rett fibroblasts and mice models display a dysregulated redox state, with elevated oxidative damage in lipids and proteins and decreased levels of critical antioxidants like glutathione (GSH). These oxidative changes exacerbate cellular damage (Cervellati et al., 2015; De Filippis et al., 2015b; Signorini et al., 2014). Oxidative stress occurs early in disease progression, as shown in *Mecp2*-deficient mice, and can be ameliorated by reactivating *Mecp2* in brain (De Felice et al., 2014). Particularly, glial cells contribute to the increased oxidative stress in Rett phenotype, such as microglia from *Mecp2*-KO mice (Jin et al., 2015) and astrocytes from *Mecp2*-mutant mice (Tomasello et al., 2024).

Several omics studies (transcriptomic, proteomic and metabolomic) highlight altered mitochondrial and lipid metabolism in human cell lines and mouse models (Zlatic et al., 2023), including phospholipid profiles in Mecp2-mutant mice (Viola et al., 2007). Since phospholipids are essential for membrane synthesis, these changes could contribute to the reduced neuronal network connectivity observed in Rett. Dysregulated cholesterol metabolism has been observed, potentially impairing membrane dynamics and synaptic functionality, key to maintaining neural plasticity (Buchovecky et al., 2013; Justice et al., 2014; Kyle 2018). Altered creatine metabolism has been implicated in Rett, potentially contributing to energy deficits and respiratory dysfunctions observed in some Rett patients (Halbach et al., 2012). Various metabolic and central signaling pathways have been described to be altered, such as the mTOR-AKT axis that regulates metabolic adaptations and protein synthesis for synaptic organization (Ricciardi et al., 2011).

Another component of Rett's pathophysiology is the **inflammatory component**, as reviewed in (Pecorelli et al., 2020). Inflammation plays an intersecting role with mitochondrial dysfunction. ROS production and mitochondrial DNA (mtDNA) activate inflammatory signaling pathways (Riley and Tait, 2020), creating a vicious cycle of oxidative damage and cellular stress. Non-neuronal cells, particularly astrocytes and microglia, contribute significantly to this pro-inflammatory environment by releasing molecules such as glutamate and cytokines (Jin et al., 2015). In addition, lipid metabolism has been directly related to inflammation (Schulman et al., 2017). Systemic inflammatory profiles have been described in patients' tissues, such as plasma (Leoncini et al., 2015), serum (Pecorelli et al., 2019), peripheral blood mononuclear cells (O'Driscoll et al., 2015), and saliva (Byiers et al., 2020), together with plasma of female Rett mice (Cortelazzo et al., 2017).

Mitochondrial dysfunction together with redox alterations and the inflammatory component have been previously targeted to treat Rett syndrome, shaping mitochondrial homeostasis as an approachable and **modulable therapeutic target**. Treatment approaches range from nutrient supplementations to drug repurposing and gene therapy. Nonetheless, many of the observed effects were mild and not clinically translatable, hence other therapies could potentially be assayed.

Antioxidants and redox modulators: vitamin E analogue Trolox showed oxidative stress reduction and behavioral improvements in a mouse model of Rett (Baroncelli et al., 2022; Bebensee et al., 2017; Janc and Muller 2014; Janc et al., 2016); a cocktail of vitamin E, N-acetyl cysteine (NAC) and α-lipoic acid in male and female mice improved head growth and hippocampal synaptic plasticity but failed to improve behavior, breathing issues, or overall survival (Hayek, 2015) and long-term treatment could aggravate metabolic disturbances (Baroncelli et al., 2022); flavonoids such as quercetin upregulated the mitochondrial respiratory complex-II, complex-III, and complex-IV activities in dose-dependent manner in Mecp2-deficient astrocytes (Dave et al., 2019); coenzyme Q10 (ubiquinone), which enhances mitochondrial electron transport, reduced oxidative stress-induced damage in Rett erythrocytes (Di Pierro et al., 2020); ω-3 polyunsaturated fatty acid (ω-3 PUFA) supplementation showed anti-oxidative protection in *in vitro* models and reduction in the clinical severity of symptoms (Ciccoli et al., 2012; De Felice et al., 2012; Dave and Pillai, 2022). However, antioxidant therapies are considered controversial, and effects in patients are weak.

Mitochondrial bioenergetic function: the anti-diabetic drug metformin was able to increase bioenergetics but did not exert a phenotypical amelioration on fully-symptomatic female mice (Zuliani et al., 2020); pharmacological stimulation of serotonin receptor 7 (5-HT7R) with LP-211 rescued mitochondrial electron transport chain impairments and translated into phenotype recovery in Rett mice (De Filippis 2015a; Valenti 2017); CNF1-toxin activation of Rho GTPases, enzymes that participate in mitochondrial motility and transport, rescued mitochondrial morphology in fibroblasts and OXPHOS activity and cognitive defects in female mouse model (Cittadini et al., 2023; De Filippis et al., 2012; De Filippis et al., 2015b; Urbinati et al., 2021); pharmacological inhibition of the CB1 cannabinoid receptor with rimonabant rescued bioenergetic and behavioral phenotypes in a female mouse model (Cosentino et al., 2024).

Metabolism-based treatments: creatine supplementation increased global DNA methylation, but scores reflecting clinical improvement were lower for creatine than for placebo (Lopes et al., 2024); cholesterol biosynthesis regulation through statins failed to improve motor symptoms in Mecp2-null mice (Villani et al., 2016) whereas AAV-based CYP46A1 overexpression, enzyme involved in the cholesterol pathway, has shown behavioral ameliorations in male and female *Mecp2*-KO mice (Audouard et al., 2024); dietary therapy with triglycerides such as triheptanoin increased levels of TCA cycle intermediates and normalized glucose and fatty acid biochemical pathways consistent with the improved metabolic phenotype in *Mecp2*-KO mice (Park et al., 2014). Triheptanoin has been used in two clinical trials, but no results are available (Percy et al., 2024).

Inflammatory component: vitamin D supplementation rescued aberrant NF-κB pathway activation and ameliorated neocortical dendritic morphology and soma size phenotypes in *Mecp2* hemizygous null males and female Het mice, and modestly improved phenotype progression and lifespan of *Mecp2*-null males (Ribeiro et al., 2020); treatment with monoclonal antibody against semaphorin 4D (anti-SEMA4D) ameliorated Rett

syndrome-specific symptoms and improved behavioral functions in both pre-symptomatic and symptomatic cohorts of hemizygous male mice (Mao et al., 2021); N-Acetylcysteine (precursor to glutathione) conjugated to dendrimer (D-NAC) resulted in improved behavioral phenotype, sleep and glial inflammatory profile in Mecp2-heterozygous female mice (Khoury et al., 2024).

1.4 Current therapeutic landscape

Besides the previous therapeutic approaches targeting mitochondrial dysfunction and related components, the current therapeutic landscape for Rett syndrome includes a combination of symptomatic treatments, supportive care, and experimental therapies aimed at addressing the underlying genetic, molecular, and cellular dysfunctions caused by *MECP2* mutations.

Despite being a rare neurodevelopmental disorder, many pharmacological treatments are being developed for Rett, with more than 60 clinical trials finished or in progress (Panayotis et al., 2023). Nonetheless, these approaches have not been sufficient to treat the disease and Rett syndrome still lacks a specific therapeutic option. Since the demonstration that reversal of many of the features that characterize Rett is possible (Guy et al., 2007), diverse approaches targeting specific features such as epileptic activity or breathing abnormalities have been made. However, many of these trials failed to improve clinical aspects of the disease, or the effects were very subtle. Clinical trials are mostly focused on genetic therapy, although their efficacy and reach are still dubious.

Symptomatic treatments

These therapies manage the day-to-day symptoms of Rett syndrome and improve the quality of life but do not address the underlying cause of the disease. Some of them are currently being used whereas others are in clinical trial as recently reviewed in (Percy et al., 2024). For seizure management pharmacological interventions with valproate and levetiracetam are recommended (Amin et al., 2024), cannabidiol is currently in phase 3 clinical trial (Desnous et al., 2024), and metabolic approaches such as ketogenic diet are also prescribed (Liebhaber et al., 2003). For motor dysfunctions and scoliosis physiotherapeutic interventions are common (Kapel et al., 2022; Romano et al., 2022), along with the use of drugs for muscle rigidity management as baclofen or botulinum toxin. Treatments for gastrointestinal alterations are used such as proton pump inhibitors for gastroesophagic reflux or polyethylene glycol for constipation. Treatments targeting anxiety or sleep disturbances, including serotonin uptake inhibitors or melatonin respectively (Buchanan et al., 2022); and for breathing abnormalities, buspirone or the noradrenaline reuptake inhibitor desipramine can be used (Mancini et al., 2018).

Gene therapy: beyond classic gene replacement

Studies show that MeCP2 absence during development does not cause irreversible damage in mice. Reactivating MeCP2 in neurons of Mecp2-null male and heterozygous female mice corrects neuronal morphology, increasing soma size and dendritic complexity (Guy et al., 2007), and improves survival and rescues Rett features, including motor coordination, anxiety, breathing irregularities, and epileptiform activity, restoring phenotypes to near wild-type levels (Guy et al., 2007; Robinson et al., 2012; Ure et al., 2016). These findings confirm that Rett is not solely a neurodevelopmental disorder. Instead, MeCP2 primarily supports neuronal maturation and maintenance, fine-tuning gene expression critical for dendritic growth and synaptogenesis (Nguyen et al., 2012). In this manner, MeCP2 deficiency arrests neuronal development in an immature state, not causing neurodegeneration, and its reactivation can reverse these effects (Robinson et al., 2012).

Considering MeCP2 dysfunction reversibility, several gene therapy approaches are being developed and demonstrate promise (Bassuk, 2022). However, the level of MeCP2 in a cell is critical and tightly modulated, and restoring MeCP2 function without producing overexpression, which can cause *MECP2* duplication syndrome, is a considerable challenge (Leonard et al., 2017). To prevent this, several methodologies have been applied to limit the gene expression (Percy et al., 2024).

There are currently two ongoing clinical trials on **gene replacement therapy**. The first (REVEAL) evaluates Taysha 102 (NCT05606614 in adults and NCT061522237 in children). This is a recombinant, non-replicating, self-complementary AAV9 (scAAV9) vector carrying a miniMECP2 gene and 3' UTR features to limit overexpression of the virally delivered miniMECP2 (Percy et al., 2024). It has showed safety and tolerability in Rett adults and children. The second ongoing trial is NGN-401 (NCT05898620), which evaluates Neurogene, an AAV9 vector encompassing MECP2 gene in its full length and with a transgene regulation technology, a synthetic miRNA that eliminates excess transcript.

Additional interventions that are currently in preclinical development include **genome editing**, which has corrected specific mutations *in vitro* (Croci et al., 2020), **RNA editing** that has demonstrated phenotypic amelioration in male

mice's brainstem (Sinnamon et al., 2022) and **X-chromosome reactivation** (Grimm et al., 2022). The latter is being examined by Alcyone Therapeutics (XGR-101) and consists of an AAV9-delivered pharmacological inhibitors for X-reactivation that has shown to reactivate silent Mecp2 in cortical neurons in living mice (Przanowski et al., 2018).

Pharmacological approaches for brain development

Several compounds targeting neurotransmitter systems, neuronal growth factors and related signaling pathways have been developed. Fingolimod, a sphingosine-1 phosphate receptor modulator, showed preclinical improvements in a mouse model but failed to demonstrate an increase either in BDNF levels (blood and CSF) or in gray matter volume during the clinical trial (Naegelin et al., 2021). Blarcamesine, a sigma 1 receptor agonist improved homeostasis in the CNS with increased synaptic development, increased GABA and BDNF levels, and led to a reduction in seizures and markers of neurodegeneration in a mouse model (Kaufmann et al., 2019). These results led to a clinical trial with Anavex 2-73 that failed to achieve significant differences between the placebo and study groups (Percy et al., 2024). Similar results were achieved with N-methyl-d-aspartate receptor (NMDAR) antagonists ketamine and dextromethorphan, serotonin and dopamine receptor agonist sarizotan, and the immunomodulator glatiramer acetate, compounds that were successful in preclinical models but failed or had conflicting outcomes in clinical trials (Percy et al., 2024). We highlight the recently approved clinical trial with leriglitazone (currently under the recruiting phase) that will be carried out in Hospital Sant Joan de Déu based on the positive results presented in this Thesis, as will be further developed.

Efforts in the field have led to the very recent approval of the drug **trofinetide** (Neul et al., 2023) by the Food and Drug Administration (FDA) for the treatment of Rett syndrome in the United States (U.S. Food and Drug Administration 2023). Trofinetide is an IGF-1 (Insulin Growth Factor 1) synthetic analog that has been studied for more than fifteen years in the context of Rett (Tropea et al., 2009). It showed partial increases in spine density, synaptic amplitude, and cortical plasticity, along with increased survival, reduced breathing and cardiac issues, and improved motor performance in male mice. Whereas it is the first treatment approved, clinical trials have shown many severe secondary effects and an over 50% abandonment rate, along with very limited amelioration in symptomatology (Camillo et al., 2024).

Future therapeutic options

The complexity of MeCP2 deficiency in Rett syndrome calls for treatments targeting multiple neural systems rather than a single signaling pathway or neurotransmitter system. To date, emulating MeCP2 function using a pharmacological approach as a treatment for Rett has not been the most successful strategy (Vidal et al., 2019). Gene therapy has emerged as a key focus, with current trials exploring the safety of gene replacement while addressing the challenge of *MECP2* dosage balance. Innovative approaches like X-chromosome reactivation, gene editing, and mRNA editing offer potential for disease modification. Nonetheless, all resources should not be directed to the same approach, since gene therapy is still under development and safety issues can arise (Lykken et al., 2018). In addition, considering the relatively late diagnosis of Rett, a combination of drug and gene treatments is a possibility for preventing progression and even reversing clinical manifestations (Gold et al., 2024).

Therefore, the urgency to find innovative and effective strategies persists, by overcoming the current limitations of gene therapy with advanced methods as nanoparticles delivery (Palmieri et al., 2023) and exploring new treatments that target cellular components key for various neural systems. Regarding the latter, mitochondrial modulation is being shaped as an attractive therapeutic target that can be actioned in different cell types (including neurons and glia) and influence several cellular processes that are disrupted in MeCP2 deficiency. This can be applied not only to Rett syndrome, but also to other neurodevelopmental disorders with compromised mitochondrial homeostasis.

2 Mitochondrial function and related disorders in the light of neurodevelopment and synaptic communication

Mitochondria, beyond their classical role as bioenergetic hubs of the cell, are central to a multitude of processes critical for proper neurodevelopment and synaptic communication (Rangaraju et al., 2019a). As thoroughly reviewed by Monzel and collaborators (Monzel et al., 2023), these organelles participate in calcium homeostasis, redox signaling, and apoptosis, all of which influence brain development and function. In the context of neurodevelopment, mitochondria contribute not only to energy production but also to the regulation of cell differentiation, migration, and synapse formation (Khacho and Slack, 2018; Mattson et al., 2008). Furthermore, the substantial energy demands of neurotransmission confer a unique reliance on mitochondrial performance, underscoring their pivotal role in sustaining synaptic communication.

2.1 Mitochondria are multifunctional and diverse organelles

Mitochondria are multifaceted and multifunctional organelles. They are very heterogeneous and specialized, presenting different phenotypes between tissues and cell types. They can also present different morphologies inside the compartments of a same cell (Picard and Shirihai, 2022), and they are capable of reversibly adapting and responding to the energetic cellular demands, as well as to environmental factors and stressors (Monzel et al., 2023).

Mitochondria have a central role in **energy metabolism**, converting nutrients such as glucose (metabolized via glycolysis into pyruvate), fatty acids (through beta-oxidation) and amino acids (processed via the urea cycle), into energy in the form of adenosine triphosphate (ATP). This process, known as oxidative respiration, involves the decarboxylation of pyruvate by pyruvate dehydrogenase (PDH), the incorporation of acetyl-CoA into the tricarboxylic acid (TCA) cycle and the oxidation of reducing equivalents (NADH and $FADH_2$) in the respiratory chain (Fig. 2).

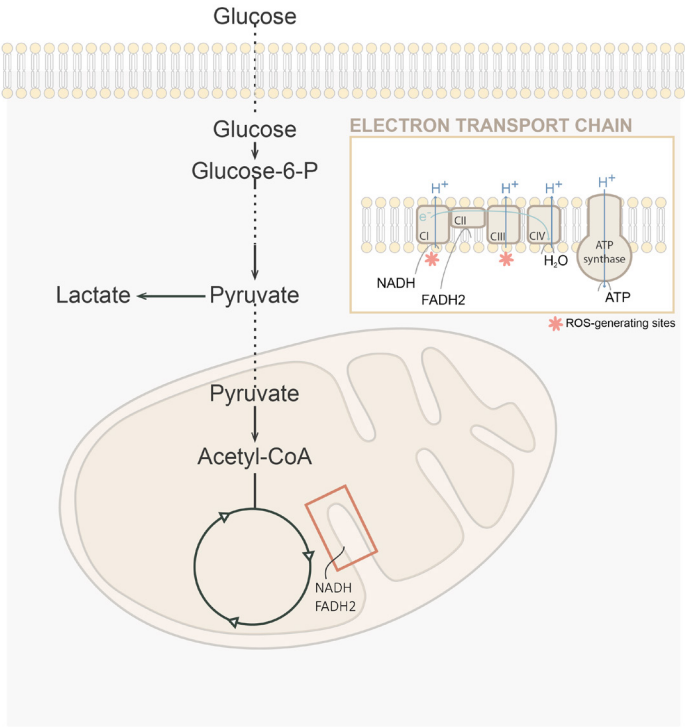

Figure 2. Schematic representation of the energetic metabolism of glucose, involving glycolysis, TCA cycle, and oxidative phosphorylation.

Mitochondria harbor the oxidative phosphorylation (OXPHOS) system, a set of five multi-subunit complexes (complexes I-V), and two mobile electron carriers, coenzyme Q (CoQ) and cytochrome c. Four of the complexes (complexes I-IV), known as the electron transport chain (ETC), pass free electrons derived from the oxidation of NADH (via complex I) and $FADH_2$ (via complex II) from the TCA cycle (and other non-canonical sources) into molecular oxygen, the final electron acceptor. The electron transfer is coupled to the active proton pumping across the inner membrane, creating an electrochemical gradient. The resulting transmembrane potential is used by complex V (ATP synthase) to drive the synthesis of ATP from ADP and inorganic phosphate. Beyond ATP synthesis, this gradient supports several mitochondrial functions, including ion uptake (calcium, sodium, manganous), protein import, synthesis of iron-sulfur (Fe/S) clusters, antioxidant regeneration by nicotinamide nucleotide transhydrogenase, and antiviral and apoptotic signaling (Monzel et al., 2023). Furthermore, the electrochemical gradient is also necessary for maintaining the mitochondrial permeability transition pore, and regulating cristae shape and dynamics processes.

Besides energy production, mitochondria participate in the synthesis (anaplerosis) and elimination (cataplerosis) of intermediary metabolites of the TCA cycle. These metabolites can later be used in the cytoplasm for the synthesis of lipids and other molecules and macromolecules necessary for cell growth, division and maintenance, or for cell signaling both intra- and inter-cellularly. Other important mitochondrial functions include mtDNA maintenance and expression, heat production (thermogenesis), synthesis and degradation of neurotransmitters, synthesis of hormones, and **reactive oxygen species (ROS) production**. ROS, mainly superoxide anion ($O_2^{\cdot-}$) and hydrogen peroxide (H_2O_2) are produced at complexes I and III from the free electrons that react with molecular oxygen. They are generally considered as by-products of respiration and excessive production is associated with malfunction and disease. However, they are major signaling molecules and are involved in cellular adaptation and stress resistance (Sies and Jones, 2020; Palma et al., 2023).

Mitochondria play a critical role in maintaining **mitochondrial DNA (mtDNA)**, which encodes essential components of the OXPHOS system. Proper mtDNA maintenance is crucial for the accurate expression of mitochondrial-encoded subunits of OXPHOS complexes. The nuclear-encoded aminoacyl-tRNA synthetases (ARS2) are key for this process, as they ensure proper mitochondrial protein synthesis by charging mitochondrial tRNAs with their corresponding amino acids. Dysfunction in ARS2 leads to impaired mitochondrial translation, which can compromise the assembly and function of the OXPHOS complexes (Sissler et al., 2017).

Mitochondria specialize between tissues, cell types, and subcellular compartments. The specialization of mitochondria comes with changes in their morphology, which can be grossly classified into two categories: tubular and branched versus rounded and fragmented. In the CNS, mitochondria from different neuronal populations have distinct protein composition, lipid metabolism, Ca^{2+} buffering properties, and interactions with other organelles (Fecher et al., 2019). As reviewed in (Pekkurnaz and Wang, 2022), in neurons, axonal and synaptic mitochondria have adapted as smaller and shorter organelles since they must travel long distances, compared to much longer and branched dendritic mitochondria that are less mobile and contribute to local Ca^{2+} buffering, ATP production and other possible roles (Rangaraju et al., 2019a). In the neuron cell body (soma) is where most of the mitochondrial biogenesis takes place, which seem to represent the source population of mitochondria feeding both axonal and dendritic mitochondrial pools. In consequence, populations in the neuron soma exhibit intermediate size and morphological complexity (Faitg et al., 2021).

The changes in morphology, quantity and position of mitochondria inside a cell come from the tightly regulated **mitochondrial dynamics processes** (Chen et al., 2023), which maintain a healthy mitochondrial network. These encompass fission and fusion processes, in which the first is observed usually under nutrient excess conditions and contributes to mitochondrial division for biogenesis, transport and quality control by elimination of impaired or dysfunctional mitochondria, and promoting apoptosis (Suen et al., 2008). Fusion is associated with high-energy cellular demands and helps mitigate the effects of stress by mixing the contents of partially damaged mitochondria (Rossignol et al., 2004; Youle and van der Bliek, 2012). Fusion is a process coordinated between GTPase proteins of the outer mitochondrial membrane (OMM) and the inner mitochondrial membrane (IMM). The OMM fusion is mediated by the Mitofusins 1 and 2 (Mfn1 and Mfn2), which seem to have similar functions (Chen et al., 2003), while the IMM fusion is mediated by the Optic Atrophy 1 (OPA1) protein, which is localized close to mitochondrial cristae (Olichon et al., 2002). Conversely, the main protein that participates in the fission process is the GTPase dynamin-like protein (Dnm1L or Drp1), which is located in the cytosol and is recruited to the OMM where it oligomerizes. There, is activated and stabilized by cardiolipin (lipid on the IMM) before constricting mitochondria with aid of the endoplasmic reticulum (ER) and actin cytoskeleton (Francy et al., 2017; Korobova et al. 2013; Li et al., 2015; Otera et al., 2013). Adaptor proteins are also needed as receptors for Drp1 during mitochondrial fission, including mitochondrial fission 1 (Fis1) protein, mitochondrial fission factor (Mff), and mitochondrial dynamics proteins MiD-49 and MiD-51 (Otera et al., 2013). Interestingly, the site of mitochondrial fission determines its outcome: midzone fission typically supports biogenesis, while peripheral fission, preceded by lysosomal contact, directs damaged mitochondria towards mitophagy, the process of elimination of damaged mitochondria (Kleele et al., 2021). Both processes are Drp1-dependent but involve distinct modulators, with the ER and Mff promoting midzone fission for biogenesis, and Fis1 regulating peripheral fission for quality control.

Depending on the stimuli, mitochondria reoganize their **internal structure** by modifying the shape of the cristae (Cogliati et al., 2016). These invaginations of the IMM into the mitochondrial matrix are the site of the OXPHOS system, with the ATP synthase forming dimers at the edge of cristae and the other complexes along both sides assembling into supercomplexes (Davies et al., 2011). This seems a necessary organization for the creation of the proton gradient. The maintenance of the cristae shape is regulated by the protein family that conform the mitochondrial contact site and cristae-organizing system (MICOS) complex. This complex is formed by at least seven subunits (Pfanner et al., 2014) and multiple interactors. MICOS subunits interact with complexes III and IV, cardiolipin, and with proteins of the IMM and OMM, including OPA1, for the maintenance of cristae shape. The fusion-related protein OPA1, controls cristae remodeling during apoptosis (Frezza et al., 2006; Landes et al., 2010) and regulates supercomplexes stability (Cogliati et al., 2013), directly connecting mitochondrial cristae architecture with the bioenergetic output.

Therefore, mitochondria are multifunctional and highly dynamic organelles that respond to internal and external stimuli by reorganizing their morphology and internal structure. In this manner, they are able to function according to cell-type specific needs, by generating energy, signaling for several biological processes, maintaining ion homeostasis (e.g. Ca^{2+} buffering), and performing a quality control to eliminate damaged mitochondria (mitophagy).

2.2 Energy metabolism in neurotransmission

As mentioned previously, neurotransmission consumes most of the energy demand of the brain, with mitochondria providing 93% of this energy and only 7% coming from glycolysis (Harris et al., 2012), although glycolysis in neurons could contribute to synapsis in a larger extent under energetic stress (Jang et al., 2016). Energy storage in the brain, in the form of glycogen uniquely, is located in astrocytes (Gruetter et al., 2003). Pellerin and Magistretti (Pellerin and Magistretti, 1994) proposed an **astrocyte-neuron lactate shuttle**, in which astrocytes, mainly glycolytic, increase their metabolic activity after neuronal stimulation. Astrocytes generate lactate that is exported to neurons, where it is converted to pyruvate for ATP generation in mitochondria. However, to what extent astrocytes "feed" neurons for synaptic activity is still a controversial debate (Bak and Walls, 2018). Recent studies have demonstrated that astrocytes support neurotransmission through the metabolization of ketone bodies (KB) from fatty acid oxidation during starvation, and neurons, which cannot oxidize fatty acids, uptake these KB as fuel (Ioannou et al., 2019; Silva et al., 2022).

Mitochondrial heterogeneity is crucial in polarized cells, such as neurons, where they must travel long distances to arrive to synaptic sites. Mitochondria undergo bidirectional **transport** through kinesin and dynein motors on microtubules or actin filaments (Kuznetsov et al., 2009). In axons, kinesins move mitochondria from the soma towards the synaptic terminals, and dyneins move them back to the soma. In dendrites, both motors can operate in either direction, since microtubule polarity is mixed (Sheng and Cai, 2012). The far ends of synaptic terminals, such as dendritic spines and presynaptic boutons, are devoid of microtubules but enriched with actin filaments (Morris and Hollenbeck, 1995). During intense and repeated synaptic firing, mitochondria can be further guided into synapses by actin-mediated movement. Other important players are involved in mitochondrial transport, such as the fission protein Drp1, which controls transport of mitochondria and dendritic arborization in Purkinje cells (Fukumitsu et al., 2016). The distribution of mitochondria along axons and dendrites is essential for a correct synaptic communication, outstanding the importance of fission dynamics in this process (Rawson et al., 2014; Oettinghaus et al., 2016).

Once mitochondria reach their final destinations in distal neurites, they are unloaded from microtubules by increased concentrations of intracellular Ca^{2+} and they are immobilized where needed most for supporting synaptic activity (Pekkurnaz and Wang, 2022). At the **synaptic boutons**, mitochondria are used directly for energy production for synaptic transmission and other functions including Ca^{2+} buffering and neurotransmitters release (Ly and Verstreken, 2006). Approximately 50% of axonal mitochondria are located at the synapses (Smith et al., 2016). Although not all synapses contain mitochondria (half of the synapses lack the organelle), the presence of mitochondria at the presynaptic terminals increases synaptic longevity and increases the number of synaptic vesicles (Lees 2020; Smith et al., 2016).

Despite the large energy demands of neurons required for neurotransmission, these cells do not store energy but rather synthesize it rapidly and locally in the form of ATP through OXPHOS (Rangaraju et al., 2014). These high energy demands, together with the absence of protection from mtDNA methylations and elevated exposure to ROS, makes synaptic mitochondria very vulnerable (Hill et al., 2018). Several quality control mechanisms have been suggested, including local protein translation (Kuzniewska et al., 2020) and transport of damaged mitochondria back to soma through microtubules (Goldsmith et al., 2022).

At the **postsynaptic site**, dendritic spines usually do not contain mitochondria in the resting state, but they can be confined within short distances serving as energy reserves (Rangajaru et al., 2019b) and they are recruited transiently during synaptic transmission and plasticity, processes with high energy consumption (Li et al., 2004; Harris et al., 2012). Therefore, stability and dynamics of the mitochondrial network are critical for postsynaptic activity. At both the pre- and post-synaptic sites, neuronal activity drives the positioning, morphology, and function of mitochondria to align with local bioenergetic requirements (Pekkurnaz and Wang, 2022).

Finally, mitochondria in synapses are also involved in **synthesis of neurotransmitters and vesicle trafficking**. At the resting state, maintenance of the synaptic-vesicle pool filled with neurotransmitters consumes a major part of basal presynaptic energy (Pulido and Ryan, 2021). Mitochondria are involved in the synthesis of cofactor BH4 (tetrahydrobiopterin), used to synthesize catecholamines (dopamine, norepinephrine and epinephrine), serotonin, melatonin, and nitric oxide (Monzel et al., 2023). They can also degrade catecholamines, participate in GABA metabolism and generate ATP necessary for vesicle recycling (Pathak et al., 2015).

2.3 Mitochondria in neurodevelopment

As reviewed by us in (Oyarzabal et al., 2021), the brain consumes more ATP during development and less in adolescence and adulthood. This peak in energy consumption coincides with the growth of neurites from the neuronal cell body to form synaptic connections with other neurons. Then, energy demand decreases as pruning starts and GABAergic synapses shift from excitatory during development to inhibitory (Harris et al., 2012). In parallel, mitochondrial biogenesis peaks during synaptogenesis (Cheng et al., 2012) and axonal growth in developing neurons (Agostini et al., 2016).

Mitochondrial dynamics have an important role in neurogenesis and stem cell fate decision, as suggested by (Khacho and Slack, 2018). Neurogenesis begins at the prenatal stage and continues even in adult brains (mostly in the hippocampal dentate gyrus) (Son and Han, 2018). As neural stem cells (NSCs) begin to differentiate, mitochondria first adopt a fragmented morphology in neural progenitor cells (NPCs) (Khacho et al., 2016), to later increase mitochondrial biogenesis and elongation, together with increased number of cristae in differentiated neurons. Mfn2 expression levels increase as NPCs differentiate (Fang et al., 2016) and OPA1 seems to influence mitochondrial bioenergetics during embryonic development in zebrafish (Rahn et al., 2012). Drp1 is necessary for cerebellar development and developmental apoptosis during neural tube formation in mice (Wakabayashi et al., 2009).

The change in mitochondrial dynamics during neurogenesis is paired to a **metabolic shift** from glycolysis to reliance on OXPHOS for energy production (Beckervordersandforth et al., 2017; Mandal et al., 2011; Shyh-Chang et al., 2013; Takubo et al., 2013), and an increase in mitochondrial mass and mtDNA copy number in postmitotic neurons (Wang et al., 2010; 2011). During this process, NSCs are highly vulnerable to oxidative stress, and accumulation of mtDNA damage results in failure to properly differentiate into neurons. In the study developed by Khacho and collaborators (Khacho et al., 2017), they demonstrated that the alteration of mitochondrial bioenergetic function in embryonic forebrain development disrupts NSC self-renewal capacity, proliferation and differentiation, causing defective cortical and hippocampal structures. In addition, adult NPCs have decreased mitochondrial mass and altered metabolism, which could contribute to their decreased capacity of self-renewal and differentiation (Stoll et al., 2011).

After neurogenesis, neurons mature and grow their neurites. One these neurites will grow rapidly and acquire the molecular, structural and functional characteristics of an axon, a process called **axogenesis**, whereas the other neurites will develop into dendrites. Interestingly, mitochondria accumulate at the base of the neurite that will become an axon (Mattson and Partin, 1999), possibly promoting microtubule polymerization by reducing Ca^{2+} concentration, to later be transported through the microtubules together with other essential cargos (Hollenbeck and Saxton, 2012).

From an **energy metabolism** point of view (Fig. 3), the main metabolites taken into account during brain development are glucose, lactate and KBs (acetoacetate, acetone and β-hydroxybutyrate). In the neonatal brain, the ratio of lactate and KBs over glucose is higher than in adults, and lactate utilization can even be higher in fetal brain (Lust et al., 2003). This preference for lactate and KBs is reflected in the expression of specific transporters in the blood-brain barrier (BBB), and the expression of glycolytic enzymes (Brekke et al., 2015; Rafiki et al., 2003). During development, KBs serve as source of acetyl-CoA for the synthesis of lipids, fatty acids and cholesterol. For synaptic function, it seems that neonatal brain prefers lactate over glucose when both substrates are present at equal concentrations (Kasischke et al., 2011).

Along early infancy to childhood, brain lactate metabolism decreases and glucose uptake and metabolism increase. Particularly interesting during this period is the non-oxidative metabolism of glucose, that is, aerobic glycolysis, when in presence of oxygen glucose is not fully oxidized to CO_2. It has been proposed that aerobic glycolysis represents a way to sustain synaptogenesis as brain mass increases, together with other uses of glucose during development, such as neurotransmitter homeostasis (Lund et al., 2009) and myelination (Rinholm et al., 2011).

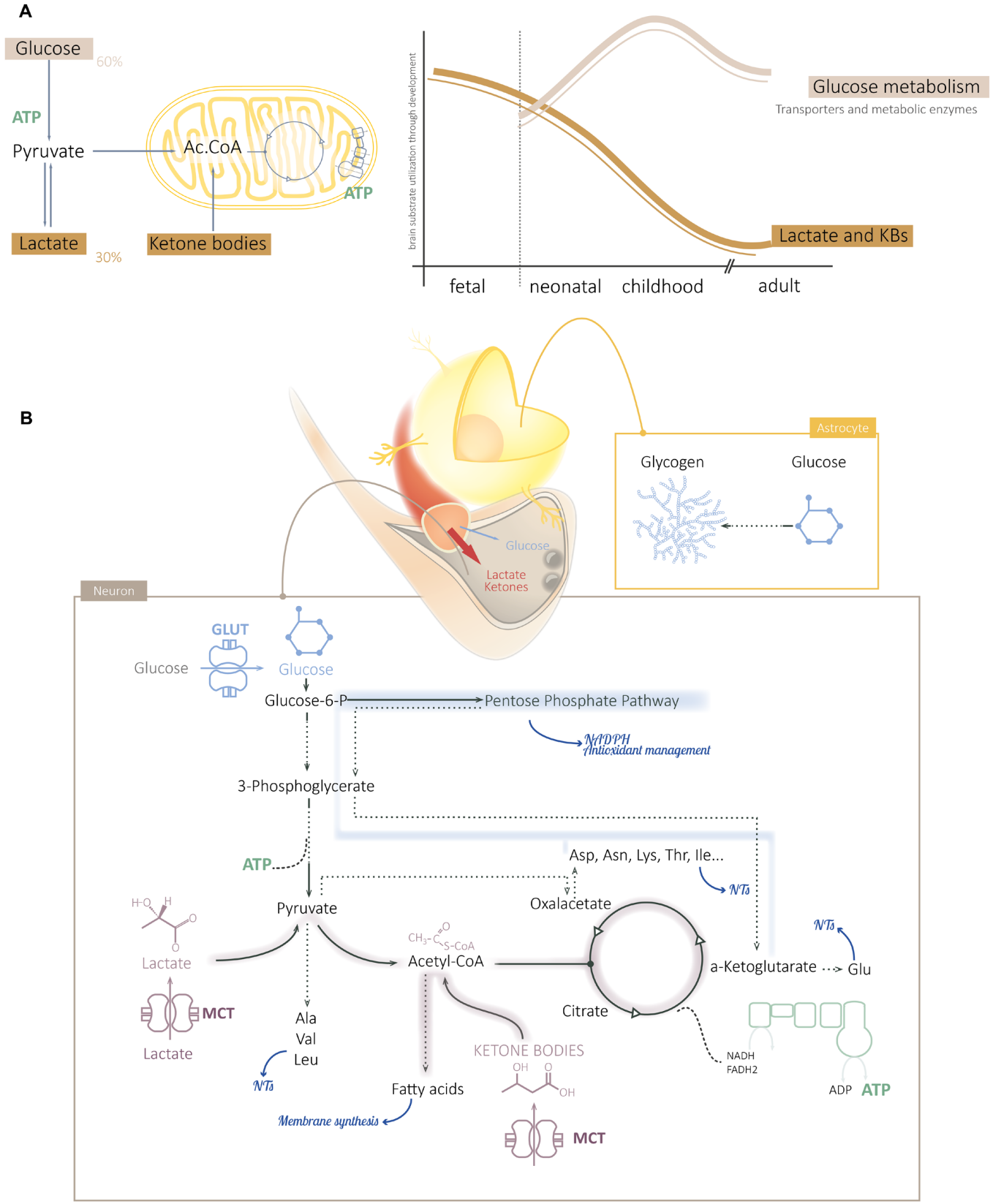

Figure 3. Schematic representation of energy metabolism in the developing brain. (A) Key molecules and their dynamics: glucose, lactate and ketone bodies (KB). Basic pathways for energy production and substrate utilization dynamics in the brain through development. (B) Perinatal to early infancy metabolism in the neuron. In the neonatal brain, lactate and ketone bodies uptake versus glucose ratio is higher than in the adult brain. Upon importation of glucose into the neuron, it will be preferentially metabolized through the pentose phosphate pathway, generating both NADPH and precursors for the synthesis of nucleotides, as well as key element in the antioxidant defense of the cell. Glucose might also be further metabolized for the generation of oxalacetate, α–Ketoglutarate and pyruvate, all precursors of amino acids which also have specific roles as neurotransmitters (NTs), as is the synthesis of glutamate. Lactate and KBs are taken up by the cell at much higher rates than found in adults. They undergo metabolism for the production of Acetyl CoA, which can either enter the TCA cycle, producing NADH used by the mitochondrial electron transport chain for ATP synthesis, or for sterol synthesis, such as cholesterol, a key element for neurodevelopment signaling and essential component of membranes. KBs are preferentially used over lactate for fatty acid synthesis.

2.4 Mitochondrial diseases and current therapeutic options

Mitochondrial functions are diverse, and alterations in mitochondrial homeostasis are associated with a wide range of diseases, from inborn errors of metabolism (IEM) to age-dependent neurodegeneration. **Primary mitochondrial disorders**, or "mitochondriopathies", represent the most common group of IEMs (Gorman et al., 2016). They are due to either *de novo* or inherited mutations genes affecting any of the mitochondrial functions. They can have any pattern of inheritance, including autosomal and X-linked for nuclear DNA (nDNA) and maternal inheritance for mitochondrial DNA (mtDNA), in which heteroplasmy, that is, the presence of both mutated and non-mutated copies, usually occurs (Payne et al., 2013). Clinically, they represent a heterogeneous group of diseases, but usually show a chronic, slowly progressive course varying onset between birth and late adulthood. Overall, mitochondrial disorders have an incidence in the general population of 11.5 per 100,000 (Chinnery, 2000), half of which develop a neurological syndrome (van der Ven et al., 2021).

Mitochondrial disorders are typically multisystemic, with symptoms frequently involving tissues that have high energy demands, such as the brain, skeletal muscle, heart, liver, and kidneys. The severity and pattern of involvement vary depending on the specific mutation and its distribution, although in many mitochondrial disorders, neurological symptoms are especially common due to CNS's reliance on mitochondria for ATP generation and Ca^{2+} regulation. Clinical symptomatology includes muscle weakness and pain, seizures, loss of motor control, decreased visual and auditory functions, metabolic acidosis, acute developmental regression, and immune system dysfunction (Thornton et al., 2014). This results in severe disabilities, diminished quality of life, and reduced life expectancy for many patients.

Economically, mitochondrial disorders place a heavy burden on healthcare systems and families, due to frequent medical consultations, diagnostic tests, long-term treatments, and the need for specialized care. Costs are comparable to patients with ALS and multiple sclerosis (AJMC 2021). From a social perspective, families and caregivers face emotional stress and social isolation while managing the unpredictable course of these diseases. Moreover, the lack of curative treatments can lead to frustration and feelings of helplessness among affected individuals and their communities (Zhao et al., 2024a). Efforts to enhance awareness, promote early diagnosis, and improve therapeutic options are crucial to mitigating the impact of mitochondrial disorders on society.

Current treatments for mitochondrial disorders

Treatments of mitochondrial diseases currently focus on symptomatic management (anti-seizure and lactic acidosis medications, cardiac support and physical therapy) rather than ameliorating the biochemical defect caused by a particular mutation (McFarland et al., 2010; Russell et al., 2020). Consequently, there is an urgent need to define therapeutic agents (drugs or other compounds, such as nutraceuticals), which correct aspects of mitochondrial dysfunction. Due to the high functional heterogeneity of mitochondrial alterations and the high-throughput sequencing and advanced omics approaches enabling better characterization of individual mutations and their functional consequences (Rahman and Rahman, 2018), personalized therapies are one promising avenue to solve this gap in their treatment.

The existing therapeutic options include (Hirano et al., 2018):

Dietary and nutritional supplements: multiple vitamins and cofactors, including CoQ_{10}, riboflavin, thiamine, idebenone, alpha-lipoic acid, vitamins C and E, and L-carnitine, which functions as a mitochondrial substrate. However, these therapies are not standardized and the results on their efficacy are usually inconclusive.
Ketogenic diet: this high-fat, low-carbohydrate dietary regimen shifts metabolism towards fatty acid oxidation of ketone bodies as the primary energy source, is considered for treatment of refractory (drug-resistant) epilepsy in mitochondrial patients and is contraindicated in mtDNA deletion-related myopathy (Zweers et al., 2021).
Exercise: aerobic endurance training has proven to be beneficial in trials with mtDNA patients by stimulating mitochondrial biogenesis.

Several therapeutic approaches are being assayed for mitochondrial disorders. The main approaches are pharmacological interventions, which include:

Bezafibrate: activates peroxisome proliferator-activated receptors (PPARs) to stimulate mitochondrial biogenesis, has been assayed *in vitro* for complex IV-deficient cells where it has restored neuronal morphogenesis (Casarin et al., 2012; Inak et al., 2021). There is an on-going clinical trial in which its efficacy is being evaluated in mtDNA patients (NCT02398201) (Hirano et al., 2018).
Metformin: this metabolic modulator has shown *in vitro* amelioration of mtDNA disease model by rescuing mitophagy defects (Chen et al., 2021).
MTP-131 (**elamipretide**): targets IMM by stabilizing cardiolipin, has corrected ATP deficiency and ROS generation *in vitro*, and is currently in clinical trial for several mitochondrial diseases (Hirano et al., 2018).

AICAR (**5-aminoimidazole-4-carboxamide ribonucleotide**): an AMP (adenosine monophosphate) analog, is an agonist of AMPK (AMP-activated protein kinase), which phosphorylates the peroxisome proliferator-activated receptor-gamma coactivator (PGC)-1α, increasing its activity as mitochondrial biogenesis stimulator. It has been assayed in several complex IV-deficiencies, showing improvement in motor functions in a mouse model (Viscomi et al., 2011).

Resveratrol: polyphenolic compound with antioxidant properties, enhances mitochondrial function by activating sirtuins (SIRT1) and AMPK pathways, which are associated with improved mitochondrial biogenesis.

Rapamycin: targets mitophagy by mTOR inhibition. It has shown amelioration of the clinical phenotype in mice, but the mechanism of action is unknown (Johnson et al., 2013; Siegmund et al., 2017).

Other approaches that are being developed are **gene editing** as gene replacement therapies, which have been assayed for complex IV deficiency *in vitro* (Miliotou et al., 2023) and heteroplasmy shift to reduce the amount of mtDNA mutations below pathogenic threshold (Bacman et al., 2018). Also, replacement of mutant mtDNA in oocytes or single-cell embryos by **mitochondrial replacement therapy** is being assayed, which is a novel method to prevent maternal transmission of mtDNA mutations (Rai et al., 2018).

3 Organs on a Chip (OoC): a new technology towards personalized medicine

The complexity of neurodevelopmental disorders highlights the urgent need for more precise and advanced technologies to explore their underlying mechanisms. These disorders arise from intricate interactions between genetic, molecular, and environmental factors that disrupt neuronal development and connectivity. Traditional models, including animal studies and conventional cell cultures from primary cultures or cell lines often fail to fully reproduce the cellular diversity, spatial organization, and dynamic processes that characterize the human brain. Furthermore, animal models lack the ability to reflect patient-specific variability and despite they exhibit phenotypes similar of a particular human disease, the underlying molecular and cellular mechanisms can sometimes be different (Horejs, 2021). To overcome these limitations, innovative platforms are required to replicate the microenvironments of neuronal systems that allow straightforward characterization, for a deeper understanding of cellular behavior, network formation, and synaptic dysfunction. By enabling a more precise resolution of neuronal and metabolic interactions, these advancements have the potential to unveil the complex biology of neurodevelopmental disorders and guide the development of targeted therapeutic strategies.

3.1 Organ on a chip (OoC) current perspectives

Organs on a chip (OoC) are microfluidic platforms designed to mimic physiological and pathological characteristics of human tissues and organs *in vitro*. These systems are characterized by their small size, customizable architecture, and capability for precise fluid flow control, in combination with three-dimensional (3D) cell co-culture, enabling advanced studies of human biology (Ramadan and Zourob, 2020). OoC are usually fabricated using precise techniques including photolithography and soft lithography to assure high accurate microstructures (Joseph et al., 2022). Microfluidic devices integrate micro-channels and compartments that recreate key aspects of organ functionality and are usually fabricated with transparent biologically inert and gas-permeable materials, such as PDMS (polydimethylsiloxane). This makes them compatible with cell culture and characterization techniques s like optical or high-resolution video microscopy allowing easier monitoring of the culture over time (Moutaux et al., 2018).

OoCs address several limitations of traditional *in vitro* and *in vivo* models, such as the lack of tissue architecture, limited cell-cell interactions, and biological variability in animal models, thus offering a scalable, cost-effective, and ethically favorable alternative (Zhang et al., 2018). These miniaturized platforms use small amount of resources (Rodrigues et al., 2020) and can provide significant insights into drug permeability, therapeutic efficacy, and disease mechanisms in controlled environments. In this manner, this reduces the reliance on animal models and helps bridge the gap between preclinical and clinical outcomes (Low et al., 2021; Ma et al., 2021; Palasantzas et al., 2023).

OoCs can incorporate biomaterials and 3D cell culture tissue, such as organoids and spheroids, to better mimic *in vivo* environments (Zhao et al., 2024b). Moreover, they allow the control of mechanical cues, including physiological flow, such as blood and interstitial flow, and tissue deformation as breathing, peristalsis and heartbeat (Esch et al., 2015).

The versatility of OoC platforms facilitates research into complex tissue interactions, including multi-organ systems for evaluating drug effects in a systemic approach. Their compatibility with high-throughput applications makes OoCs particularly suitable for the development and validation of pharmaceutical interventions (Ingber, 2022). By replicating human organ physiology more accurately, these devices represent a transformative tool for the study of disease mechanisms and offers the possibility of using cells derived from patients, opening this technology to personalized medicine studies.

3.2 Synapse on a chip (SoC): a sub-specialization of the system

Brain on a chip (BoC) models have been developed to overcome the limitations of two- and three-dimensional cultures, as well as of brain organoids (Amirifar et al., 2022). Two-dimensional (2D) models establish non-specific, multidirectional and uncontrolled connections between neuronal populations (Hong and Nam, 2022), and therefore, do not replicate the complex architecture and functionality of human neuronal networks. Organoids typically lack a stable vasculature and can have compromised survival due to limited nutrient diffusion. Other limitations to overcome include heterogeneity, reproducibility and scalability (Coronel et al., 2024).

BoC models have been developed to address the limitations found in these models. They have been used with human cells and dynamic systems to create microphysiological models exhibiting specific functions and unique brain tissue regions (Amirifar et al., 2022). BoC models can compartmentalize neuronal bodies and neurites to study neuritogenesis, axonal guidance and transport, and synaptic communication between neurons; the latter named synapse on a chip (SoC) models. SoC devices can have compartments with different neuronal populations mimicking specific brain circuits such as cortico-hippocampal (Lenoir et al., 2021) or cortico-striatal (Lassus et al., 2018) pathways. These devices have been used to model specific neurodegenerative disorders such as Huntington's (Virgoleux et al. 2018), Alzheimer's (Deleglise et al., 2014) and Parkinson's disease (Freundt et al., 2012), to better understand the mechanism of these pathologies and accelerate the development of effective and personalized therapies. Devices to study the synaptic alterations of neurodevelopmental disorders have also been developed, as the microfluidic device for characterizing the electrophysiological activity of iPSC-derived neurons of patients with Kleefstra syndrome, a neurodevelopmental disorder caused by mutations in the Euchromatin Histone Methyltransferase1 (*EHMT1*) gene (Frega et al., 2018). Finally, BoC models can also recreate neuron-glia interactions (Wevers et al., 2016), such as the supporting roles of oligodendrocytes in myelinization, the astrocyte-neuron junctions and microglia in immune function, and mimic complex structures as the blood-brain-barrier (BBB on a chip) by co-culturing endothelial and neuronal cells (Palma-Florez et al., 2023).

BoC microfluidic devices – particularly SoC – are characterized by microchannels that are able to separate axons or dendrites from the neuronal cell bodies (Fig. 4). These channels usually have very small heights and, depending on the length, only axons can access (Taylor et al., 2010). Virlogeux et al. (Virlogeux et al., 2018) used a three-compartment device connected by microchannels to study the cortico-striatal network in a Huntington's disease model. They used the chambers and microchannels to create three compartments: a presynaptic chamber with cortical neurons, a post-synaptic with striatal neurons, and a synaptic region where both populations established connections through the microchannels. The chambers were connected with microchannels of different length, so axons from the cortical neurons would access, while from the striatal chamber, with shorter microchannels, mainly dendrites would cross. Kamudzandu and collaborators (Kamudzandu et al., 2019) developed a microfluidic device to mimic the complex brain circuitry *in vitro* with five chambers connected by microchannels where different basal ganglia (BG) neuronal subtypes were cultured. Iannielli et al. (Iannielli et al., 2019) recreated the human nigro-striatal circuit between medium spiny and dopaminergic neurons in a Parkinson's disease model with OPA1 mutations. In this device, they studied the dopaminergic synapses and the influence of mitochondrial homeostasis on the synaptic communication.

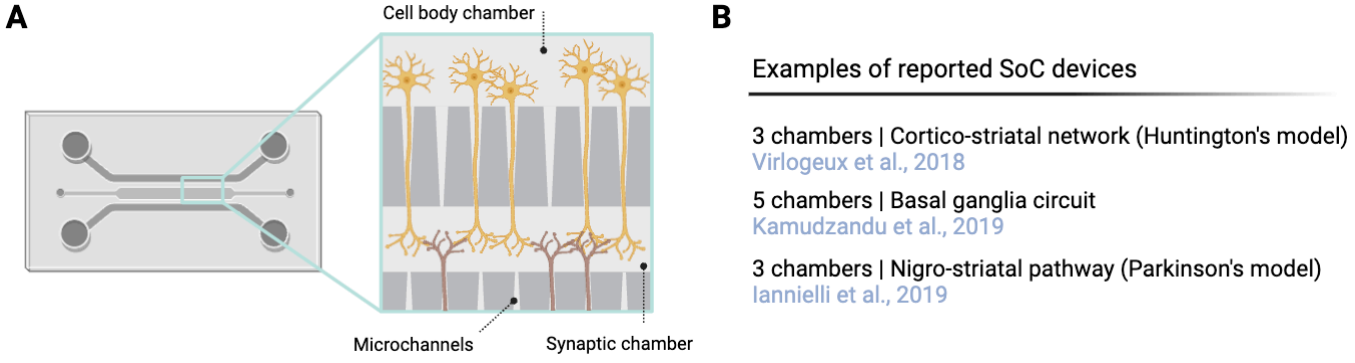

Figure 4. Synapse on a chip (SoC) microfluidic devices (A) schematic view and (B) examples of different systems defined.

These microfluidic devices have an enormous potential in the development of personalized therapies for neurological disorders, particularly for rare neurodevelopmental disorders for which an animal model has not been generated. Fibroblasts from the patients can be obtained and reprogrammed into iPSCs, which can later be differentiated in a particular neuronal type, generating a personalized model for the study of the pathophysiology of these patients. The SoC devices allow the *in vitro* study of specific mechanisms that can be involved in the disease at a synaptic level and allow the evaluation of the direct influence of a certain compound on the synaptic communication.

HYPOTHESIS & OBJECTIVES

This work builds on the **hypothesis** that mitochondrial dysfunctions being cross-sectional to neurodevelopmental diseases constitute a potential common therapeutic target for their treatment.

The **main objective** of this Thesis is the study of the mitochondria as a target for the treatment of neurodevelopmental disorders.

The **specific objectives** for its achievement are the following:

1. Characterization of mitochondrial homeostasis in the neurodevelopmental disorder Rett syndrome and its validation as a therapeutic target.

2. Functional characterization of mitochondrial disorders with congenital errors of neurotransmission, and evaluation of potential therapeutic approaches in clinical-time response.

3. Development of a “synapse on a chip”, an advanced *in vitro* system for the study of mitochondrial homeostasis in the context of synaptic communication.

MATERIALS & METHODS

1 Materials

1.1 Reagents and kits

Table 1. Reagents and other materials

Name	Reference	Commercial Provider
2-Chloro-5-nitro-N-phenylbenzamide (GW9662)	M6191	Sigma-Aldrich
2'-Deoxy-D-Glucose (2-DG)	D8375	Sigma-Aldrich
4-12% Tris-Glycine gels	4561096	Bio-Rad
30% Acrylamide/Bis Solution, 29:1	1610157	Bio-Rad
β-hydroxybutyrate (HBA)	H6501	Sigma-Aldrich
β-mercaptoethanol	M3148	Sigma-Aldrich
Acetoacetate (AA)	A8509	Sigma-Aldrich
Amersham HyperFilm™ ECL Sheets 18 x 24 cm	28-9068-37	BioLab
Amersham™ Protran® Western blotting membranes	GE10600001	Sigma-Aldrich
Antimycin A	A8674	Sigma-Aldrich
B27™ supplement (without vitamin A)	17054-04	Gibco
(Quick Start™) Bradford 1X Dye Reagent	5000205	Bio-Rad
Bovine Serum Albumin (BSA)	A2153	Sigma-Aldrich
Brain-Derived Neurotrophic Factor (BDNF)	450-02	Miltenyi
Carbonyl cyanide 4-(trifluoromethoxy)phenylhydrazone (FCCP)	C2920	Sigma-Aldrich
cOmplete™ Mini EDTA-free Protease Inhibitor Cocktail	11836170001	Sigma-Aldrich
Dimethyl sulfoxide (DMSO)	D2650	Sigma-Aldrich
Doxycycline (DOX)	D9891	Sigma-Aldrich
Dulbecco's Modified Eagle Medium Nutrient Mixture F-12 (Ham) (DMEM/F12)	11320-033	Gibco
Dulbecco's Modified Essential Medium high glucose (4.5 g/L)	702549	Corning
Dulbecco's Modified Essential Medium low glucose (1 g/L)	D5546	Sigma-Aldrich
Epidermal Growth Factor (EGF)	AF-100-15	Peprotech
Fetal Bovine Serum (FBS) heat inactivated	A5256801	Gibco
Fibroblast growth factor 2 (FGF2)	100-18B	Peprotech
Fibroblast growth factor 8 (FGF8)	100-25	Peprotech
Fluoromount™ Aqueous Mounting Medium	F4680	Sigma-Aldrich
Galactose (GAL)	G0750	Sigma-Aldrich
Glial cell-Derived Neurotrophic Factor (GDNF)	450-10	Miltenyi
GlutaMAX™ supplement	35050061	Gibco
Hanks' Balanced Salt Solution (HBSS)	55037C	Sigma-Aldrich
HiMark™ Pre-Stained High Molecular Weight Protein Standard	LC5699	Invitrogen
Horse Serum (HS) heat inactivated	26050070	Gibco
Laminin (LAM)	L2020	Sigma-Aldrich
L-Glutamine 200 mM (100X)	25030-024	Gibco
N2™ supplement	17502-048	Gibco
Neurobasal™ medium	21103049	Gibco
NuPAGE™ 3-8% Tris-Acetate gels	EA0378BOX	Invitrogen
NuPAGE™ Transfer Buffer	NP0006	Invitrogen
NuPAGE™ Tris-Acetate SDS Running Buffer	LA0041	Invitrogen
NZYTaq II 2x Green Master Mix	MB35802	NZYtech
Oligomycin	O4876	Sigma-Aldrich
Paraformaldehyde (PFA)	1.00496.8350	Sigma-Aldrich

Name	Reference	Commercial Provider
PageRuler™ Prestained Protein Ladder	26616	Thermo Fisher
Penicillin / Streptomycin	15140-122	Gibco
Phenol red	P3532	Sigma-Aldrich
Phosphate Buffered Saline (PBS)	P3813	Sigma-Aldrich
PhosSTOP™ Inhibitor Tablets	4906837001	Sigma-Aldrich
Pierce™ ECL Western blotting substrate	32109	Thermo Fisher
Poly-L-Ornithine (PO)	P4957	Sigma-Aldrich
ProLong™ Diamond Antifade Mountant with DAPI	P36966	Thermo Fisher
Polydimethylsiloxane (Sylgard 184) (PDMS)	DCE-1673921	Dow Corning
PowerUp™ SYBR™ Green Master Mix	A25741	Applied Biosystems
Radioimmunoprecipitation assay (RIPA) buffer	R0278	Sigma-Aldrich
Skim Milk Powder	70166	Sigma-Aldrich
Sodium Bicarbonate	S5761	Sigma-Aldrich
Sodium Pyruvate	P2256	Sigma-Aldrich
Sonic Hedgehog (SHH)	100-45	Peprotech
Spermidine (SPM)	S0266	Sigma-Aldrich
SuperScript™ III First-Strand Synthesis SuperMix	11752050	Invitrogen
Triton X-100	X-100	Sigma-Aldrich
Trypsin-EDTA (0.05%)	25300062	Thermo Fisher
TWEEN® 20 BioXtra	P7949	Sigma-Aldrich
Whatman™ cellulose papers for chromatography	731-2503	VWR

Table 2. List of kits

Kit	Reference	Commercial Provider
ATP Bioluminescence Assay Kit CLS II	11 699 695 001	Roche (Sigma-Aldrich)
LEGENDplex™ Mouse Inflammation Panel (13-plex) with V-bottom Plate	740446	BioLegend
Lipid Peroxidation (MDA) Assay Kit (Colorimetric)	ab118970	Abcam
RNeasy Fibrous Tissue Mini Kit	74004	Qiagen

1.2 Antibodies

Table 3. List of primary antibodies used for Western blot, immunocytochemistry (ICC) and immunohistochemistry (IHC)

Primary Antibody	Reference	Commercial Provider	Species	Dilution	Use
Anti-8-OHdG	sc-66036	Santa Cruz Biotechnology	Mouse	1:250	ICC; IHC
Anti-Bassoon	ab82958	Abcam	Mouse	1:100	ICC
Anti-Beta III Tubulin (TUJ-1)	AB9354	Sigma-Aldrich	Chicken	1:250	ICC
	801202	Biolegend	Mouse	1:500	ICC
Anti-CAMKII	PA5-19128	Thermo Fisher	Goat	1:50	ICC
Anti-Calbindin	14479-1-AP	Proteintech	Rabbit	1:100	IHC
Anti-c-Fos	ab184666	Abcam	Mouse	1:1000	Western blot
Anti-CHCHD6	66597-1-Ig	Proteintech	Mouse	1:1000	Western blot
Anti-COASY	sc-100474	Santa Cruz Biotechnology	Mouse	1:200	Western blot
Anti-Doublecortin	ab207175	Abcam	Rabbit	1:10000	Western blot
Anti-Drp1	ab184247	Abcam	Rabbit	1:500, 1:1000	Western blot
Anti-EIF5A	11309-1-AP	Proteintech	Rabbit	1:20000	Western blot
Anti-Fis1	sc-376469	Santa Cruz Biotechnology	Mouse	1:500	Western blot
Anti-GAPDH	60004-1-Ig	Proteintech	Mouse	1:20000	Western blot
Anti-GC-1	ab137614	Abcam	Rabbit	1:1000	Western blot
Anti-GFM1	PA5-109763	Thermo Fisher	Rabbit	1:1000	Western blot
Anti-GPx	ab108427	Abcam	Rabbit	1:1000	Western blot
Anti-HSP60	ADI-SPA-829-F	Enzo	Mouse	1:10000	Western blot
				1:1000	ICC

Primary Antibody	Reference	Commercial Provider	Species	Dilution	Use
Anti-Hypusine	ABS1064-I	Sigma-Aldrich	Rabbit	1:10000	Western blot
Anti-MAP2	M9942	Sigma-Aldrich	Mouse	1:500	ICC
Anti-MCU	ab219827	Abcam	Mouse	1:500	Western blot
Anti-Mfn2	ab124773	Abcam	Rabbit	1:500	Western blot
Anti-MnSOD	ADI-SOD-111-F	Enzo	Rabbit	1:80000	Western blot
Anti-NeuN	ab177487	Abcam	Rabbit	1:5000	Western blot
Anti-NDUFS1	12444-1-AP	Proteintech	Rabbit	1:2000	Western blot
Anti-OPA1	BD-612607	BD Biosciences	Mouse	1:2000	Western blot
Anti-OxPhos Human WB Cocktail	45-8199	Thermo Fisher	Mouse	1:500	Western blot
Anti-PDHX	10951-1-AP	Proteintech	Rabbit	1:1000	Western blot
Anti-phospho-CAMKII	MA1-047	Thermo Fisher	Mouse	1:100	ICC
Anti-RFP	ab34771	Abcam	Rabbit	1:400	ICC
Anti-SCO2	PA5-117084	Thermo Fisher	Rabbit	1:500	Western blot
Anti-SMS	15979-1-AP	Proteintech	Rabbit	1:1000	Western blot
Anti-SURF1	15379-1-AP	Proteintech	Rabbit	1:500	Western blot
Anti-TH	P60101-0	Pel-Freez	Sheep	1:500	ICC
Anti-TOMM20	ab186735	Abcam	Rabbit	1:250	ICC
				1:10000	Western blot
Anti-α-Tubulin	ab7291	Abcam	Mouse	1:250	ICC
				1:50000	Western blot
Anti-VDAC1	ab14734	Abcam	Mouse	1:5000	Western blot
Anti-Vinculin	sc-59803	Santa Cruz Biotechnology	Mouse	1:20000	Western blot
Anti-WARS2	AV52366	Sigma-Aldrich	Rabbit	1:500	Western blot

Table 4. List of secondary antibodies

Secondary Antibodies	Reference	Commercial Provider	Species	Dilution	Use
Anti-Chicken IgY (H+L) Alexa Fluor® 647	ab150171	Abcam	Goat	1:500	ICC
Anti-Goat IgG (H+L) Alexa Fluor® 546	A-11056	Thermo Fisher	Donkey	1:500	ICC
Anti-Mouse IgG (H+L) Alexa Fluor® 488	A-11001	Thermo Fisher	Goat	1:500	ICC
Anti-Mouse IgG (H+L) Alexa Fluor® 546	A-11030	Thermo Fisher	Goat	1:500	ICC
				1:400	IHC
Anti-Mouse IgG (H+L) Alexa Fluor® 555	A-21427	Thermo Fisher	Rabbit	1:500	ICC
Anti-Mouse IgG (H+L) Alexa Fluor® 647	715-605-150	Jackson Immunoresearch	Donkey	1:200	ICC
Anti-Mouse IgG (H+L) HRP	A-16017	Thermo Fisher	Donkey	1:5000	Western blot
Anti-Rabbit IgG (H+L) Alexa Fluor® 488	A-11034	Thermo Fisher	Goat	1:500	ICC
				1:400	IHC
Anti-Rabbit IgG (H+L) HRP	31458	Thermo Fisher	Donkey	1:5000	Western blot
Anti-Sheep IgG (H+L) Alexa Fluor® 488	713-545-147	Jackson Immunoresearch	Donkey	1:200	ICC
Cyanine 3 Anti-Rabbit IgG (H+L)	711-165-152	Jackson Immunoresearch	Goat	1:200	ICC

Table 5. List of fluroescent conjugates and probes

Probes	Reference	Commercial Provider	Dilution	Use
DAPI (4',6-diamidino-2-phenylindole)	62248	Invitrogen	1:5000	ICC
Hoechst 33342	H3570	Invitrogen	1:2000	ICC
			1:10,000	IHC
MitoSOX™ Red	M36008	Invitrogen	5 µM	Flow cytometry
Mitotracker™ Green	M7514	Invitrogen	300 nM	Live-cell imaging
Phalloidin CruzFluor™ 647 Conjugate	sc-363797	Santa Cruz Biotechnologies	1:1,000	ICC

1.3 Primers

Table 6. List of primers

Gene	Forward (5' – 3')	Reverse (3' – 5')
CO1	ACCCTAGACCAAACCTACGC	TGTATGCATCGGGGTAGTCC
CO2	TCATGAGCTGTGTCCCCACATT	ACGATGGGCATGAAACTGTG
CO3	CCTAATGACCTCCGGCCTAG	GTGTTACATCGCGCCATCAT
HK2	ATGTGGTTGCTGTGGTGAAC	CTTCCACCAGTTCCACGTTG
MnSOD	TTTTGGGGTATCTGGGCTCC	CCTGGTACTTCTCCTCGGTG
mtND1	ATATGACGCACTCTCCCCTG	TGAGTTGGTCGTAGCGGAAT
PGC-1α	AGCGCCGTGTGATTTATGTC	TGCGTCCACAAAAGTACAGC
SREBP2	GCCCTGGAAGTGACAGAGAG	CCACCACCCAGCTTAACAAT

1.2 Informatic resources

Table 7. List of informatic resources

Program	Use	URL/App
AlphaFold	Protein structure prediction	https://alphafold.com/
AutoCAD	Design and drawing of masks	https://www.autodesk.com/
Biorender	Scientific illustration	https://www.biorender.com/
Concensus	Bibliographic search	https://consensus.app/search/
Ensembl	DNA sequence query	https://www.ensembl.org/index.html
Fiji (ImageJ)	Microscopy image and densitometry analysis	App
Franklin	Mutation pathogenicity classification	https://franklin.genoox.com/clinical-db/home
GeneCards	Disease associations to gene	https://www.genecards.org/
Genome Browser (In-Silico PCR)	Oligonucleotide design verification	https://genome.ucsc.edu/cgi-bin/hgPcr
GraphPad Prism 10.0	Statistical analysis and data visualization	App
Human Genome Mutation Database (HGMD)	Variants query	https://www.hgmd.cf.ac.uk/ac/index.php
MutPred2	Prediction of protein structure alteration	http://mutpred.mutdb.org/#qform
Online Mendelian Inheritance in Man (OMIM)	Gene-phenotype relationships	https://omim.org/
Primer 3	Oligonucleotide design	https://primer3.ut.ee/
Protein Data Bank (PDB)	Protein structure query	https://www.rcsb.org/
PubMed	Bibliographic search	https://pubmed.ncbi.nlm.nih.gov/
PyMol	3D protein structure visualization	App
RStudio Software	Data analysis and visualization	App
STRING	Protein-protein interaction networks	https://string-db.org/
Uniport	Protein query	https://www.uniprot.org/

2 Samples

2.1 Patients and control fibroblasts

Fibroblast samples were collected with legal tutors informed consent, and ethical approval for its collection, use and storage was granted by the Institutional Ethics Committee of the Hospital Sant Joan de Déu. For *in vitro* studies in patients, skin biopsies were obtained from the internal part of the upper arm and primary fibroblast cell lines were established using standard procedure. Controls were unrelated surgery surpluses from eight healthy donors, both males and females of pediatric age.

For the experiments in fibroblasts from Rett patients, a total of eight cell lines were used, from female patients with different *MECP2* mutations and clinical severities, as detailed in Table 8. Clinical severity of the diagnosed Rett patients was measured using the clinical severity score designed by Dr Pineda (Monrós et al., 2001).

Table 8. Rett patients' fibroblasts samples. Patient ID, sex, age of the patient when the skin biopsy was performed, mutation, domain affected and clinical severity.
F = Female; * = nonsense mutation; TRD = transcription repression domain; NLS = nuclear localization sequence; MBD = methyl-DNA binding.

ID	Sex	Age	Mutation (systematic name)	Domain	Phenotype
RTT_P1	F	3	c.502C>T (p.Arg168*)	Inter-domain region	Severe
RTT_P2	F	3-10	c.916C>T (p.Arg306Cys)	TRD	Mild
RTT_P3	F	11	c.502C>T (p.Arg168*)	Inter-domain region	Severe
RTT_P4	F	15	c.808C>T (p.Arg270*)	NLS	Severe
RTT_P5	F	2	c.423C>G (p.Tyr141*)	MBD	Severe
RTT_P6	F	2	c.423C>G (p.Tyr141*)	MBD	Severe
RTT_P7	F	13	c.880C>T (p.Arg294*)	TRD	Mild
RTT_P8	F	3	c.763C>T (p.Arg255*)	TRD	Severe

For the experiments in fibroblasts from pediatric patients with mutations in proteins affecting mitochondrial functions, a total of 20 patients were studied, detailed in Table 9. Mutations were identified at the Genetic Diagnosis Service of Hospital Sant Joan de Déu or at other hospitals where the patient was first diagnosed before transferring to HSJD.

Table 9. Mitochondrial patients' fibroblasts samples. Patient ID, sex, gene, mutation if available and protein affected.
Not confirmed genetic diagnosis. F = Female; M = Male; del = deletion; dup = duplication, fs = frameshift, * = nonsense mutation.

ID	Sex	Gene	Mutation (systematic name)	Protein
DNM1L_P1	-	*DNM1L*	Not available	Dynamin-1-like protein or Dynamin-related protein 1 (Drp1)
DNM1L_P2	-		Not available	
DNM1L_P3	-		Not available	
DNM1L_P4	M		c.2167A>G (p.Arg723Gly)	
DNM1L_P5	F		c.1084G>A (p.Gly362Ser)	
AFG2A_P1	M	*AFG2A (SPATA5)*	c.251G>A (p.Arg84Gln)	ATPase family gene 2 protein homolog A (AFG2A) or Spermatogenesis associated 5 (SPATA5).
AFG2A_P2	M		c.327_328del (p.Lys110fs), c.1631T>G (p.Leu544Arg)	
AFG2A_P3	M		c.251G>A (p.Arg84Gln), c.1064T>C (p.Ile355Thr)	
CHCHD6	F	*CHCHD6*	c.142C>T (p.Pro48Ser), c.572G>A (p.Arg191His)	MICOS complex subunit Mic25
WARS2	F	*WARS2*	c.515+5 G>A	Tryptophan-tRNA ligase, mitochondrial (WARS2)
GFM1	M	*GFM1*	c.2011C>T (p.Arg671Cys)	Elongation factor G, mitochondrial (GFM1)
NDUFS1	F	*NDUFS1*	c.2144G>A (p.Ser715Asn)	NADH-ubiquinone oxidoreductase 75 kDa subunit, mitochondrial (NDUFS1)
NDUFAF6	M	*NDUFAF6*	c.523G>C (p.Ala178Pro), c.420+784C>T	NADH dehydrogenase (ubiquinone) complex I, assembly factor 6 (NDUFAF6)
SCO2	M	*SCO2*	c.244_246delAAG (p.Lys82del), c.703G>A (p.Gly235Ser)	Protein SCO2 homolog, mitochondrial (SCO2)

ID	Sex	Gene	Mutation (systematic name)	Protein
SURF1_P1	M	*SURF1*	c.817C>T (p.Gln273*), c.503T>G (p.Val177Gly)	Surfeit locus protein 1 (SURF1)
SURF1_P2	F		c.809_826dup AGCATCTGCAGTACATCG (p.Glu270_Ile275dup), c.815_825dup TGCAGTACATC (p.Val276Cysfs*5)	
SLC25A22	M	*SLC25A22*	Not available	Mitochondrial glutamate carrier 1 (GC-1)
COASY	M	*COASY*	c.140dupT (p.Ala48fs)	Bifunctional coenzyme A synthase (COASY)
PDHX	M	*PDHX*	c.906delT (p.Tyr302fs)	Pyruvate Dehydrogenase Complex Component X (or E3 Binding Protein) (PDHX)
SMS	F	*SMS*[#]	c.733G>T (p.Pro258Leu)	Spermine synthase (SMS)

2.2 Mouse colony

The mouse colony was maintained in the Animal Facilities of the University of Barcelona. All animal procedures were carried out according to European Union guidelines (Directive 2010/63/EU) and were approved by the University of Barcelona Committee on Animal Use and Care.

Both *Mecp2*$^{+/-}$ female mice Brid's model (Guy et al., 2001) (B6.129P2(C)-*Mecp2*$^{tm1.1Bird}$/J) and control littermates (C57BL/6J) were used (Jackson Laboratories). Only female mice have been used to increase the translational value of the work as they have been reported to better recapitulate the disease phenotype. Mice were housed in standard cages with *ad libitum* access to food and water and in controlled environmental conditions of light (12 h dark/light cycle starting at 7:30 am), temperature (22°C) and humidity (60%). Mice were genotyped following the provider recommendations: ear samples were digested in lysis buffer (25 mM NaOH, 2mM EDTA, pH 12) at 95°C for 1h, followed by neutralization neutralized with 40 mM Tris-HCl, pH 5. For PCR, lysed DNA sample was added to a pre-mix of water and primers and added to the PCR MIX (containing buffer with $MgCl_2$ nucleotides, Taq polymerase, and loading buffer). Samples were spun down and subjected to PCR cycling (2' 94°C - 10x(20'' 94°C-15'' 65°C - 1' 68°C)-28x(15'' 94°C, 15'' 50°C, 1' 72°C)- 5' 72°C- 4°C). Post-PCR, samples were loaded onto an agarose gel with GelRed and subjected to electrophoresis at 110 V for 40 minutes. The gel was visualized under UV light.

The primers were mutant (R: CCACCTAGCCTGCCTGTACT), wild-type (R: CTGTATCCTTGGGTCAAGCTG) and common (F: AAATTGGGTTACACCGCTGA).

When stated, leriglitazone was delivered orally with the food at a 75 mg/kg/day dose. Mice were fed pellets with or without leriglitazone from weaning until 7 months, when they are considered symptomatic mice. Leriglitazone plasmatic levels were confirmed by LC–MS/MS post animal sacrifice to confirm the proper intake.

At endpoint, mice brains were dissected into three areas (cortex, hippocampus and cerebellum) and discerning between left and right hemispheres. Dissected samples were stored at –80°C until corresponding analysis.

2.3 Human neural progenitor cells (hNPCs)

We used two human neural progenitor cell (hNPC) lines from healthy controls, previously obtained at Institut d'Investigació Biomèdica de Bellvitge (IDIBELL) from human induced pluripotent stem cells (hiPSC) and approved by the Spanish competent authorities (Commission of Guarantees concerning the Donation and the Use of Human Tissues and Cells of the Carlos III National Institute of Health). One healthy control was used for differentiation to cortical neurons (Ctrl2-Ep6F-8 line, namely CTRL2#8), whereas for differentiation to dopaminergic neurons (DAn), we used ventral midbrain progenitor cells (vmNPCs) from another control (SP11 line). These DA progenitors were obtained from the TH-TdTomato hiPSC reporter cell line generated by CRISPR/Cas9, following the same procedure as specified in (Calatayud et al., 2019).

3 Cell culturing

3.1 Fibroblasts cell culture and treatments

We used primary cultures of skin fibroblasts from patients and age-matching controls. Dermal fibroblasts were grown following standard culture conditions in Dulbecco's Minimal Essential Medium (DMEM) high glucose (4.5 g/L) supplemented with 1% glutamine, 10% fetal bovine serum (FBS) and 1% penicillin–streptomycin. Unless stated otherwise, experiments were accomplished when fibroblasts were at 80% confluence and between the 7th and 14th passages.

For galactose experiments, DMEM (8.3 g/L, pH 6.8 – 7.2) with no glucose was prepared. Sodium bicarbonate (3.7 g/L), sodium pyruvate (110 mg/L), phenol red (15 mg/L), L-glutamine (2 mM) and galactose (5.6 mM) were added to the DMEM solution and sterilized by filtration. DMEM galactose 1 g/L was supplemented with 10% FBS and 1% penicillin-streptomycin and cells were incubated for 48 hours prior to experimentation.

Leriglitazone (LGZ) (MW = 408.9 g/mol) was kindly supplied by Minoryx Therapeutics S.L. 3.4 mg were resuspended in 831 µL DMSO to obtain a 10 mM stock solution (100% DMSO). Then a 0.1 mM stock solution was prepared in DMEM (10% DMSO) and stored at -20ºC for less than one month. For the working solutions, an intermediate 1 µM working solution with 1% DMSO was prepared from the 0.1 mM stock solution. For LGZ treatment, cells were incubated for 48 hours with 100 nM or 500 nM LGZ in the same medium, complemented with 1% DMSO.

GW9662 (MW = 276.68 g/mol) was used as a PPARγ antagonist. 5 mg of GW9662 were resuspended in 1.8 mL of DMSO to obtain a 10 mM stock solution, stored at -20ºC. From this, a 1 mM intermediate stock solution was prepared in DMEM and 10% DMSO. Cells were treated with a 1 µM working solution in DMEM and 1% DMSO for 72 hours.

Spermidine (SPM) (MW = 145.25 g/mol) was resuspended in milli-Q H_2O for 6.4 M stock solution and stored at 4ºC. Two intermediate stock solutions were prepared: first at 1 M in milli-Q H_2O and from this at 1 mM in milli-Q H_2O, both stored at -20ºC. For treatment, cells were incubated for 24 hours with 1 µM spermidine in DMEM.

Media mimicking ketogenic diet (KD) was achieved by using complete DMEM low glucose (1 g/L) with a final concentration of 5 mM of acetoacetate (MW = 108.02 g/mol) and β-hydroxybutyrate (MW = 126.09 g/mol), obtained from 0.25 M and 0.5 M stock solutions, respectively. Prior to experiments, cells were treated for five consecutive days with this medium, changing for fresh medium every 48 hours.

Doxycycline (DOX) (MW = 512.94 g/mol) was resuspended in milli-Q H_2O for a 40 mM stock solution and stored at -20ºC. For treatment, cells were incubated with 40 µM DOX in DMEM for 48 hours prior to experimentation.

3.2 Cortical neuron differentiation

For the growth and differentiation of cortical neurons, the correspondent hNPCs were thawed and maintained in 12-well plates coated with 0.01% poly-L-ornithine and 1 mg/mL laminin (POLAM). For the coating, first poly-L-ornithine (PO) was incubated overnight at 37ºC and then laminin overnight at 37ºC. The cells were maintained with proneural (PN) medium, which consisted of DMEM/F12 medium and Neurobasal medium at 1:1 ratio, together with 1% B27 without vitamin A, 0.5% N2, 0.1% β-mercaptoethanol, 1% glutaMAX, and 1% penicillin/streptomycin. This medium was supplemented with 10 ng/mL EGF and 10 ng/mL FGF2 growth factors for proliferation of undifferentiated hNPCs. Once expanded, they were seeded in the POLAM-coated microfluidic devices, where the differentiation to cortical neuron started after removing the growth factors.

3.3 Dopaminergic neuron differentiation

For the growth and differentiation of dopaminergic neurons (DAn), the correspondent vmNPCs were thawed on 6-well POLAM-coated plates and the protocol specified in (Calatayud et al. 2019) was followed (Fig. 5). In brief, first the neural progenitors were expanded on PN medium supplemented with 10 ng/mL EGF and 10 ng/mL FGF2. Then the medium was changed to DAn induction medium, which consisted of N2B27 medium (DMEM/F12 and Neurobasal media (1:1), 1% B27 without vitamin A, 0.5% N2, 1% glutaMAX and 1% penicillin/streptomycin) supplemented with 200 ng/mL SHH and 100 ng/mL FGF8. The cells were maintained in this medium for 6 days. Ultimately, the fate-inducted progenitor cells were maintained in N2B27 for 10 days, when the neuronal differentiation process started. Then the DA-inducted neurons were detached and seeded in the POLAM-coated microfluidic devices, where the final differentiation phase began, maintaining the cells with N2B27 medium supplemented with 20 ng/mL BDNF and 20 ng/mL GDNF.

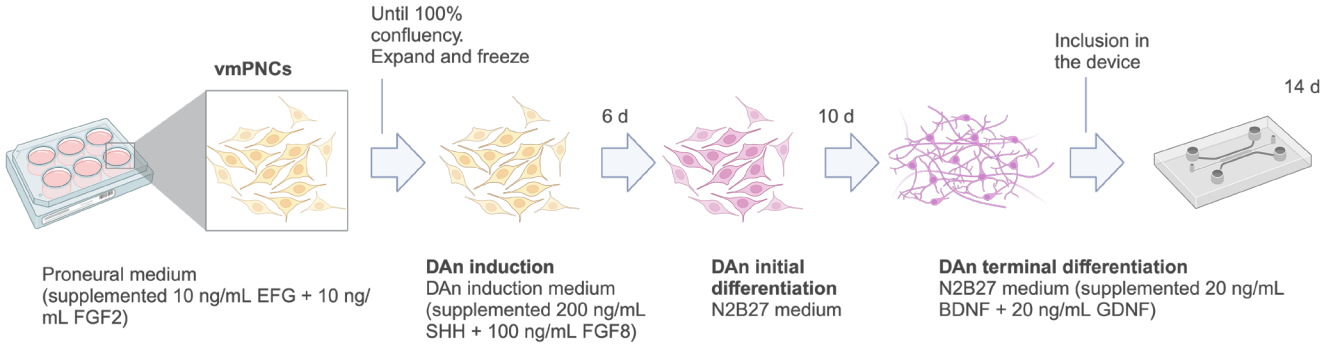

Figure 5. Schematic representation of dopaminergic neuron differentiation from vmNPCs. Created with BioRender.

4 Microfluidic device fabrication

4.1 Design and SU-8 master fabrication

The design of the microfluidic device (synapse on a chip, SoC) and the masks required for its manufacture is done using AutoCAD. The design consists of three chambers, each of them connected by microchannels. All chambers have one inlet and outlet of two 8 mm diameter reservoirs (Fig. 6A). The lateral chambers (namely pre- and post-synaptic) have a length of 10 mm, width of 1 mm and height of 200 µm, and therefore, a volume of 2 mm^3 (or µL), while the central chamber (namely synaptic chamber) is thinner with 500 µm width (Fig. 6B). The lateral chambers are connected to the central chamber through 189 parallel microchannels of 500 µm length, 5 µm height and asymmetric shape for axon guidance: starting from 5 µm on the lateral chambers, to end at 2 µm on the central chamber.

We use two masks to fabricate the master on silicon wafers by photolithography and the molds with SU-8 photoresist (Microchemicals, Ulm, Germany), which contains the 3D negative image of the microfluidic system (Fig. 6C). For this chip, which contains channels and chambers at different heights (5 µm and 200 µm respectively), is required two masks and two microaligned photolithography processes with SU-8 to obtain the 3D chip. The master was manufactured by the MicroFabSpace service at the Institute for Bioengineering of Catalonia (IBEC). The fabrication process began with preparing a 4-inch silicon wafer. The wafer was first desiccated at 200°C for 15 minutes and then plasma-cleaned (Harrick Plasma, PCD-002-CE) for 1 minute at high potency to activate the surface. A base layer (~10 µm thick) was created by spin-coating SU-8 2010 photoresist onto the wafer. This involved an initial spin at 500 rpm (10 seconds, 100 rpm/s acceleration), followed by a second spin at 4000 rpm (120 seconds, 300 rpm/s acceleration). The layer was exposed to 120 mJ/cm^2 of UV light and post-baked at 95°C for 4 minutes. For the fabrication of the negative 3D structure of the 5 µm height microchannels, SU-8 2005 photoresist was spin-coated with the same initial spin but with a final spin at 8000 rpm (55 seconds, 300 rpm/s acceleration) to obtain a final SU-8 thickness of 5 µm. After soft baking (2 minutes at 95°C), UV exposure (125 mJ/cm^2) was performed using a chrome mask containing the microchannel patterns, followed by a post-bake at 95°C for 2 minutes. Two thicker layers of SU-8 2100 (for the chambers and features at 200 µm height) were added sequentially. Each layer was spin-coated (500 rpm for 10 seconds, then 3500 rpm for 30 seconds) and soft-baked, first at 65°C (5–10 minutes) and then at 95°C (20–40 minutes). The patterns were then exposed to UV light (270 mJ/cm^2) using the second chrome mask with the chambers pattern, followed by post-baking (65°C for 5 minutes, then 95°C for 10 minutes). The development stage involved immersing the wafer in SU-8 developer for 10 minutes to remove unexposed photoresist, followed by a wash with isopropanol. A hard bake was performed (95°C for 30 minutes, then 65°C for 10 minutes) to stabilize the structures. To facilitate PDMS demolding during device fabrication, the masters were coated with trichloroperfluorosilane in a vacuum chamber for 1 hour.

The structure of the micrometric channels in the silicon master were characterized to ensure their correct structure. To do this, the surface topography was measured with an optical profilometer (Wyko NT1100), and their structure was checked in Bright Field with a Nikon Eclipse L150 microscope.

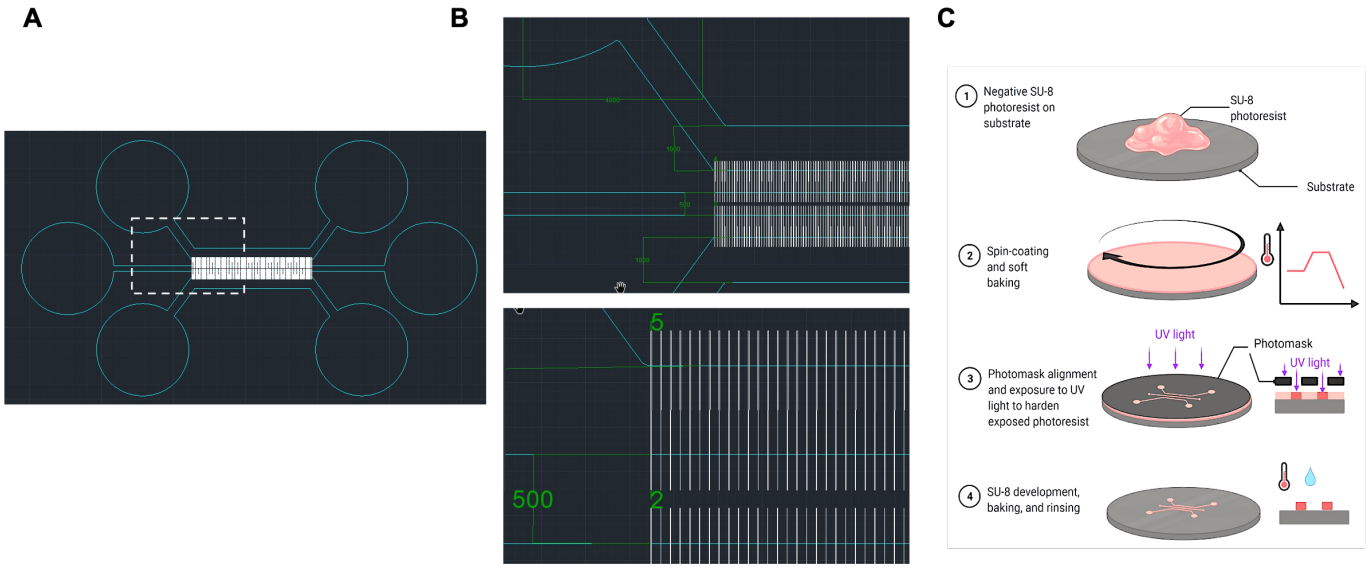

Figure 6. Microfluidic device design in AutoCAD and master photolithography fabrication. (A) General view of the synapse-on-a-chip (SoC) design in AutoCAD, with three chambers connected to two reservoirs each, and microchannels between the lateral (pre- and post-synaptic) and central (synaptic) chambers. (B) Zoomed sections from the dotted white square: upper image shows the length of the chambers (1000 µm for lateral chambers, 500 µm for central chamber) and 4000 µm radius for the reservoirs; lower image is a closer section to show the width of microchannels: 5 µm at the lateral chambers, 2 µm at the central chamber (units in the image in µm, green color). (C) Schematic representation of the mold fabrication in a silicon wafer through photolithography (adapted from (Scott and Ali, 2021)).

4.2 Fabrication of the PDMS chip replicas

A mixture of silicone elastomer, polydimethylsiloxane (PDMS), and its curing agent (The SYLGARD™ 184 Silicone Elastomer Kit, Ellsworth (WI, USA)) (10:1 ratio) was poured on the master attached to a Petri dish. After degassing and allowing the elastomer to solidify (12 hours at room temperature or 2 hours at 65°C), the PDMS replicas (chips) were removed from the master, which allowed us to obtain four devices at a time. The chips were cut out and the holes for the reservoirs were drilled with 8 mm biopsy punches (Harris Uni-Core). To make the chips usable for neuron culture, the chambers and microchannels of the device need to be sealed with another material. In this case, PDMS was bonded to thin cover glass slides (#1.5; Menzel-Gläser). Both PDMS replicas and cover glass slides were washed and sonicated for 5 minutes in three steps: (1) water and soap, (2) acetone and (3) isopropanol, finally washed with ethanol 70% and dried out. In the clean room, they were placed in a vacuum plasma generator to activate the surfaces for 30 seconds at 30W and constant oxygen pressure (0.8 torr). The active surface of the chips (where the chambers and microchannels are located) was irreversibly bonded together with the slides, left for 5 minutes at 95°C and then at 85°C overnight to finish solidifying the bond. Their structure was checked in Phase Contrast with a Nikon Eclipse L150 microscope and the number of functional microchannels was evaluated by manual counting.

4.3 Inclusion and differentiation of neurons in the device

Two days before seeding, the chip was activated in the plasma generator (5 minutes at 11W) in the clean room to decrease internal hydrophobicity in the microchannels (to facilitate water flow within them) and milli-Q H_2O was added to protect activation. In the cell culture room, the chip chambers and microchannels were washed with 70% ethanol and sterilized after exposure to UV light for 15-20 minutes in the laminar-flow hood. They were washed 3 times with milli-Q H_2O and 1 time with PBS and POLAM coating was performed (first 0.01% poly-L-ornithine coating overnight at 37°C and then 1 mg/mL laminin coating overnight at 37°C). On the day of seeding, cells were counted and seeded with a volume of 10 µL per chamber to avoid the formation of bubbles.

For cortical neurons inclusion, 100,000, 150,000 or 200,000 cells were seeded per chamber (pre- and post-synaptic). The cells were maintained in PN medium after seeding for two days, before removing the 10 ng/mL EGF and 10 ng/mL FGF2 growth factors to start cortical neuron differentiation. Experiments were performed between weeks 3 and 5 of differentiation in the microfluidic device. For dopaminergic neurons (DAn) inclusion, 150,000, 200,000 or 250,000 cells were seeded per chamber (pre- and post-synaptic). Two approaches were performed: adding DAn terminal differentiation medium (N2B27 + 20 ng/mL BDNF and 20 ng/mL GDNF) at the time of seeding or maintaining the cells with N2B27 medium for two days before changing to DAn terminal differentiation medium. Experiments were performed after 14 days of differentiation in the microfluidic device. The correspondent medium in the reservoirs was half changed every 2-3 days, and the chips were kept in a humid chamber to avoid evaporation of the medium. For TH-TdTomato live imaging, DA neurons were observed in the microfluidic device through a Zeiss Observer Z1 inverted epi-fluorescence microscope (Zeiss, Germany).

5 Molecular biology

5.1 Immunofluorescence on conventional culture and confocal microscopy

Cells were seeded onto coverslips placed in 24 multi-well plates at 80% confluence and fixed with paraformaldehyde (PFA) 4% for 20 minutes. Cells were permeabilized with 0.1% Triton X-100 for 15 minutes and incubated with a blocking solution (10% FBS in PBS) for 1 hour at room temperature. Primary antibodies were used against TOMM20 and α-tubulin for mitochondrial network imaging, and 8-OHdG for DNA oxidative damage imaging. They were incubated for 1 hour at room temperature in a PBS 1% FBS solution. Secondary antibodies anti-Rabbit (Alexa Fluor 488) and anti-Mouse (Alexa Fluor 546) were incubated for 1 hour at room temperature in the same solution and mounted on slides with antifade mounting medium with DAPI. Fluorescence was visualized either using Leica TCS SP8 confocal microscope (Leica Microsystems) or Zeiss LSM 880 confocal microscope (Zeiss, Germany), both with 63x, 1.4 N.A. immersion oil objective. Quantifications were performed using Fiji (ImageJ) software.

TOMM20 quantification

For TOMM20 quantification, analysis was automatized using ImageJ Macro language and the Mitochondria Analyzer plug-in (Chaudhry et al., 2020). In brief, first a mask was created from the tubulin and DAPI channels for ROI selection (each cell was considered a ROI). Then, the channel containing TOMM20 staining was Z projected using sum slices and pre-processed for enhancing the signal-to-noise ratio. Finally, Mitochondria Analyzer plug-in was used for thresholding and quantification of mitochondrial network morphology and branching parameters per cell (Fig. 7). The most representative parameters for each patient's mitochondrial network were selected: total area (sum of area occupied by signal in the image), independent networks ratio (inverse of total area corrected by number of structures), mean aspect ratio (a shape measure given by d_{max}/d_{min}, ranges from 0 (round) to 1 (elongated), expressed as mean AR of objects in image), mean form factor (MFF, defined as a shape measure given by $P^2/(4\pi A)$, where 1 indicates round object and increases with elongation and expressed as mean FF of objects in image), branches per mitochondria (number of branches per individual structure), mean branch length (total branch length corrected by number of branches), mean branch diameter (width of branches across all structures, measured on the long axis), and interconnectivity (correlation between branch end points and branch junctions).

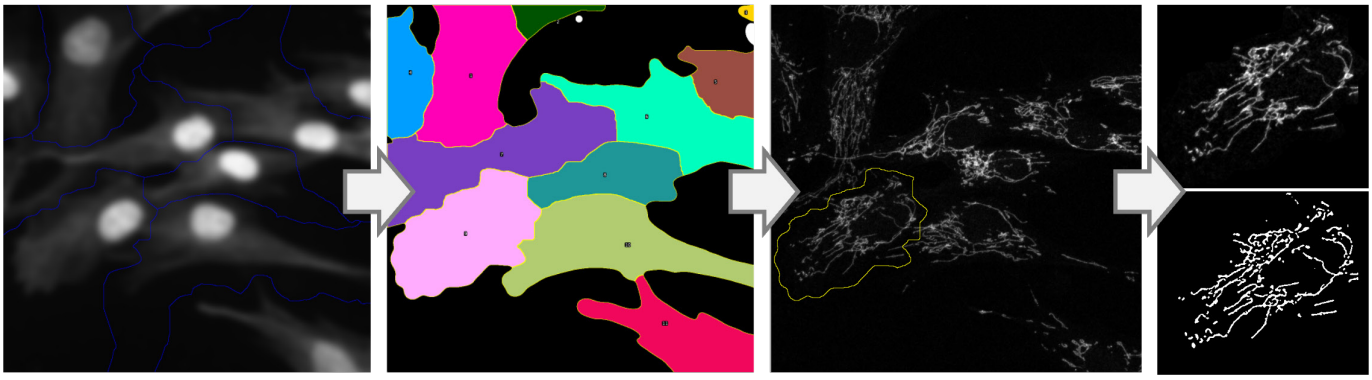

Figure 7. Pipeline of mitochondrial network analysis with TOMM20 IF staining. First a mask was created from adding tubulin and DAPI channels for individualizing each cell as a ROI (and subsequent manual review for any incorrect ROI selection). Then the ROIs were applied on the TOMM20 z-projected images, thresholded with Mitochondria Analyzer plug-in and parametrized.

8-OHdG intensity quantification

For 8-OHdG quantification, gray values in nuclei were measured using histogram tool in ImageJ software. For this, 8-OHdG channel was Z projected using sum slices and pre-processed for enhancing signal-to-noise ratio. Then, the signal throughout nuclei was selected with segmented line and measures were recorded with histogram tool. Ultimately, mean gray values per nuclei were obtained for comparative analysis between the groups.

5.2 Immunofluorescence on chip and confocal microscopy

For on-chip immunofluorescence, chips were fixed with 4% PFA for 20 minutes, permeabilized with 0.1% Triton X-100 for 15 minutes and blocked with 10% FBS for 1 hour at room temperature. Combinations of primary antibodies were incubated overnight at 4°C against, specified in Table 10: (1) TUJ-1 and MAP2, (2) Bassoon and TUJ-1, (3) pCAMKII, CAMKII and TUJ-1, and (4) RFP, TH and TUJ-1. Correspondent secondary antibodies were incubated for 2 hours at room temperature and 10-15 minutes with DAPI or Hoechst for nuclei staining. The chips were left for a maximum of one week in PBS-0.2% sodium azide until visualization on a Zeiss LSM 880 confocal microscope (Zeiss, Germany), using objectives 10x/0.45 M27 (dry), 25x/0.8 Imm Korr DIC M27 (oil), and 63x/1.4 DIC M27 (oil). Quantifications were performed using Fiji (ImageJ) software.

Table 10. Combinations of primary and secondary antibodies for on-chip immunofluorescence. A total of five different combinations were used for chip IF visualization: in cortical neurons, a series of (1) neuronal, (2) mitochondrial, (3) synaptic and (4) calcium-related markers were assayed, whereas in the case of dopaminergic neurons, (5) specific markers for these neurons were assayed.

Combination	Primary antibody	Species	Secondary antibody	Species
1	TUJ-1	Chicken	Anti-Chicken (Alexa Fluor 647)	Goat
	MAP2	Mouse	Anti-Mouse (Alexa Fluor 488)	Goat
2	Bassoon	Mouse	Anti-Mouse (Alexa Fluor 555)	Rabbit
	TUJ-1	Chicken	Anti-Chicken (Alexa Fluor 647)	Goat
3	pCAMKII	Mouse	Anti-Mouse (Alexa Fluor 555)	Rabbit
	CAMKII	Goat	Anti-Goat (Alexa Fluor 546)	Donkey
	TUJ-1	Chicken	Anti-Chicken (Alexa Fluor 647)	Goat
4	RFP	Rabbit	Anti-Rabbit (Cyanine-3)	Goat
	TH	Sheep	Anti-Sheep (Alexa Fluor 488)	Donkey
	TUJ-1	Mouse	Anti-Mouse (Alexa Fluor 647)	Donkey

Quantifications

For synaptic activity analysis, Bassoon marker was visualized using 63x 1.4 N.A. immersion oil objective and measured in terms of count and occupied area. In synaptic chamber, individual axons were first selected on TUJ-1 channel and used as a mask. A total of five ROIs per image were selected, each of them representing a section of an axon. Next, in Bassoon channel and after sum slices Z projection and image pre-processing, analyze particles tool was used on each ROI with size from 0.09 – 2 μm^2 (Manrique et al., 2021).

For calcium activity-related markers, ratio pCAMKII/CAMKII was visualized using 63x 1.4 N.A. immersion oil objective and measured in terms of average intensity. In post-synaptic chamber, in nuclei channel, area encompassing neuronal somas (nuclei and area around them) was used as a mask, considering each area as a ROI. Then, in the pCAMKII and CAMKII channels, average intensity was calculated per each ROI and their ratio was compared between the groups.

5.3 Time-lapse confocal imaging in live cells

Cells were incubated with 300 nM MitoTracker™ Green for 30 minutes at 37°C and 5% CO_2, whereas neurons in the pre-synaptic chamber of the microfluidic device were incubated with 600 nM at the same conditions, together with 50 µM FCCP for the correspondent assays. For KCl treatment, the neurons in the pre-synaptic chamber were incubated with 50 mM KCl for 10 minutes at 37°C and 5% CO_2 following MitoTracker™ staining. Immunofluorescence was visualized using Leica TCS SP8 microscope (Leica Microsystems) with a 63x/1.4 N.A. oil-immersion objective, 2.75 electronic zoom, and at a frame size of 512 x 512 pixels. A 495 nm white laser was used, and videos were recorded for 2 minutes with 0.73 seconds between each frame, maintaining cell culture conditions. Mitochondrial dynamics and morphology analysis in 2D was performed with the MATLAB add-in Mitometer (Lefebvre et al., 2021), detailed in Figure 8. First, individual cells were selected and pre-processed as maximum projections for enhancing signal-to-noise ratio in ImageJ. Then, images were uploaded to Mitometer, where a threshold was performed and tracking analysis gave the dynamics parameters: (1) directionality, defined as the total distance traveled by a mitochondrion divided by the maximum displacement of the track, (2) median speed in µm/s, (3) the ratio of the median to the maximum speed, suggesting the propensity for mitochondria to have bursts of motion, and (4) fusion and fission number of events per track (which gives the track number for which the mitochondrion fused or fissioned). Analysis with Mitometer also gave the morphology parameters: (1) mitochondrial area in μm^2, (2) mitochondrial perimeter in µm and (3) aspect ratio, as the ratio between the major and minor axes of the mitochondrion in µm.

(see next page)

Figure 8. Pipeline of mitochondrial dynamics and morphology analysis with Mitometer add-in for MATLAB. Selection of individual cells in ImageJ, and posterior upload to Mitometer with specification of pixel size and time between frames. Mitometer performed a threshold with background removal, and object labelling for tracking.

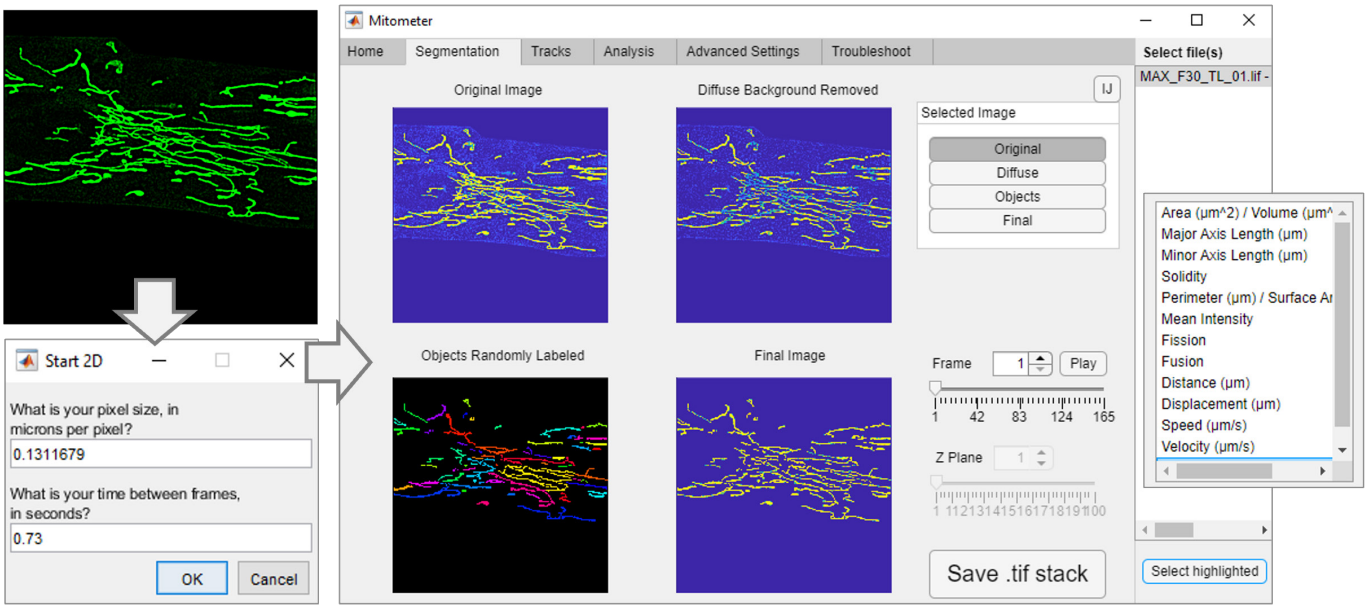

5.4 Transmission electron microscopy (TEM)

Mitochondrial ultrastructure was analyzed by electron microscopy. Fibroblasts were fixed in the culture plate at room temperature for 1 hour with a mixture of 4% paraformaldehyde and 2% glutaraldehyde in phosphate buffer (pH 7.4) and post-fixed with 1% osmium tetroxide plus 1% potassium ferricyanide in distilled water for 1 hour at 4°C. Fibroblasts were dehydrated in ethanol and embedded in epoxy resin EML-812 (TAAB Laboratories), still attached to the culture plate. Small pieces of the thin layer of resin containing the cells were separated from the culture plate and glued to blocks of resin to cut ultrathin sections (70 nm) oriented parallel to the cell base. Sections were collected on 100-meshgrids, stained with uranyl acetate and lead citrate, and examined at 80 kV in a Jeol JEM-1010 (Tokyo, Japan) electron microscope. Images were recorded with 4 k CMOS F416 camera from TVIPS (Gauting, Germany). Electron transmission images were taken at the Electron Microscopy Service at Centro de Biología Molecular Severo Ochoa in Madrid.

Images were analyzed using Fiji software quantifying the following ultrastructure parameters: (1) mitochondrial aspect ratio (Fig. 9A) measured as major:minor axis ratio using segmented line tool; (2) electrodensity (Fig. 9B), as the mean gray value inside the mitochondrial matrix, measured as average from three ROIs (rectangle tool) in the mitochondrial matrix, without selecting cristae, compared to average from three ROIs outside the mitochondria (selecting cytosol); and the cristae parameters (Fig. 9C) (3) length axis of the crista relative to the IMM (segmented line), (4) width axis of the crista (segmented line) and (5) cristae angle, measured as the angle of each crista relative to the IMM, using the angle tool.

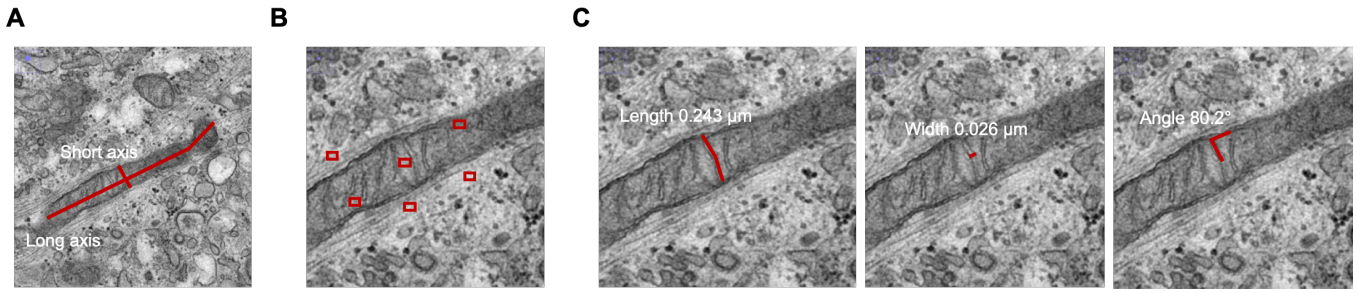

Figure 9. Parameters analyzed for mitochondrial ultrastructure quantification. (A) Mitochondrial aspect ratio as the major:minor axis per mitochondrion; (B) electrodensity, as the mean gray value inside the mitochondrial matrix compared to the cytosol, and (C) cristae length, width and angle relative to IMM. Measurements highlighted in red.

5.5 Immunohistochemistry

Mice were anaesthetized with Ketamine/Xylazine at a concentration of 100 mg/kg and 10 mg/kg respectively and perfused intracardially with 4% paraformaldehyde (PFA). Brains were extracted and post-fixed in a solution of 4% PFA overnight, cryoprotected in 30% sucrose and kept frozen at −80°C. Sagittal sections of 40-µm thick were obtained using a cryostat, collected in a cryoprotective solution (30% glycerol, 30% ethylene glycol in 0.1M phosphate buffer) and kept at −20°C until processing. For immunohistochemistry analysis, the slices were washed three times with washing solution (0.01% Triton X-100 in PBS), permeabilized with 0.25% Triton X-100 in PBS for 15 minutes and incubated with blocking solution (0.25% Triton X-100, 10% Horse Serum, 2% BSA) for 2 hours at room

temperature. Subsequently, slices were incubated with mouse anti-8-OHdG, rabbit anti-calbindin, rabbit anti-GFAP or rabbit anti-Iba in blocking solution at 4°C overnight. The slices were then washed with washing solution before the incubation with Alexa Fluor 488-conjugated goat anti-rabbit IgG or Alexa Fluor 546-conjugated goat anti-mouse IgG antibody, and Hoechst in blocking solution for 2 hours at room temperature. Finally, slices were washed three times with PBS and then mounted with Fluoromount Aqueous Mounting Medium in glass slides coated with 0.2% gelatin. Fluorescence images at 10x/0.45 N.A. were captured using a Zeiss LSM 880 confocal microscope (Zeiss, Germany).

Quantifications were done using Fiji (ImageJ) software. For oxidative damage analysis, 8-OHdG fluorescence intensity in cells of hippocampal and cerebellar slices was quantified. In hippocampus, ROI was selected for dentate gyrus and 8-OHdG-positive cells were counted and their intensity was measured. In cerebellum, Purkinje cells were identified as calbindin-positive and the 8-OHdG intensity was quantified per cell. For neuroinflammatory analysis in cortex, Iba1 marker for microglia and GFAP for reactive astrocytes were used. Three slices were visualized per mice, each slice was divided in cortex frontal, medial and dorsal, and two ROIs were quantified per area. Comparison was done after averaging the two ROIs and the three areas per slice.

5.6 RT-qPCR

RNA for RT-qPCR was extracted using RNeasy Fibrous Tissue Mini Kit, following the manufacturer's instructions. The total RNA was eluted in 40 µL of RNAse-free water and stored at -80°C. The RNA concentration was measured using the NanoDrop 2000 Spectrophotometer (Thermo Fisher). qPCRs were carried out following a two-step protocol. First, cDNA was synthesized from a total of 500 ng of RNA per reaction, following the recommendations provided with SuperScript III First-Strand Synthesis SuperMix for RT-qPCR. After the RT-PCR reaction, the cDNA from control and Rett fibroblasts was pooled. Second, qPCR was performed in a QuantStudio 6 Flex Real Time PCR System (Thermo Fisher) with PowerUp SYBR Green Master Mix. The data were analyzed using a comparative method, correlating the initial template concentration with the cycle threshold (Ct) to obtain the relative quantity (RQ) of the RNA. The RQ is defined as $2^{-\Delta\Delta Ct}$, where ΔΔCt is the ΔCt of the patient cell line minus the ΔCt of the control cell line, and ΔCt is the Ct of the target gene minus Ct of the endogenous gene (*RPLP0*). Primers used for determination of mitochondrial mass were: *mtND1*, *CO1*, *CO2*, *CO3* and *HK2*. Primers used for detection of PPARγ pathway were: *PGC1a*, *MnSOD*, *SREBP2*.

5.7 Western blotting

Proteins were extracted from cultured fibroblasts or mouse brain tissue through a 30-minute cold incubation with RIPA and protease and phosphatase inhibitors. Following extraction, proteins were quantified by Bradford method and prepared at a homogenous concentration in Laemmli Buffer in reductive denaturing conditions. Protein solutions were loaded on 10 or 12% gels, or 4-20% pre-cast gels and subjected to SDS-PAGE at 120-160V and transferred to a nitrocellulose membrane at 100V for 1 hour at 4°C. Membranes were blocked with TBS-Tween (0.05%):milk 5% for 1 hour at room temperature. Primary antibodies (Drp1, Fis1, OPA1, Mfn2, MnSOD and GPx) were incubated overnight at 4°C in blocking buffer, at concentrations detailed in Table 3. For the OXPHOS complexes detection, proteins were denatured in a non-reductive buffer and incubated after SDS-PAGE and Western blot with OXPHOS Human WB Antibody Cocktail. For the oligomeric Drp1 detection, the NuPAGE™ system (Invitrogen) for high molecular weight proteins was followed using 3-8% Tris-Acetate gels and the correspondent buffers. Vinculin, tubulin or GAPDH were used as a loading controls.

The secondary antibodies HRP-conjugated goat anti-Rabbit and goat anti-Mouse IgG were incubated 1-2 hours at room temperature and were detected using the Pierce™ ECL Western Blotting substrate. Quantification of protein expression was performed using Fiji software by calculating protein densitometry relative to controls and normalized to vinculin or GAPDH for fibroblasts, or tubulin for mice brain samples.

5.8 Oxygen consumption rate

Oxygen consumption rate (OCR) was measured using the XF24 Extracellular Flux Analyzer (Seahorse Bioscience, Izasa Scientific). 80,000 fibroblasts per well were seeded in XF 24-well cell culture microplates (Seahorse Bioscience) in 250 µL of DMEM 10% FBS and incubated in normal conditions for 24 h in DMEM containing 1 g/L glucose. Two hours previous to the assay, the growth medium was replaced with 700 µL of fresh medium, allowing the media temperature and pH to reach equilibrium before the first measurement. After an OCR baseline measurement, 50 µL of oligomycin, carbonylcyanide-4-(trifluoromethoxy) phenylhydrazone (FCCP), rotenone and antimycin solutions were sequentially added to each well to reach working concentrations of 6 µM, 50 µM, 1 µM and 1 µM respectively. Results were normalized to 30,000 cells after the experiment.

A series of parameters were calculated from the OCR: (1) basal respiration, detected at the beginning of the experiment before the addition of oligomycin; (2) oligomycin-sensitive respiration (OSR) considered ATP-linked

respiration, calculated as the difference between basal and oligomycin-induced OCR; and (3) maximal respiration or Rmax, calculated as the difference between FCCP-induced OCR and the OCR after inhibition with antimycin A.

5.9 ATP content measurement

ATP concentration was evaluated both in fibroblasts and mice brains. In the former, cells at 80% confluency were harvested and resuspended in boiling ATP extraction buffer (100 mM Tris–HCl, 4 mM EDTA pH 7.7). Finally, ATP concentration was assayed by bioluminescence using a luciferin-luciferase system according to manufacturer's instructions. ATP concentration was corrected per mg of protein. To discriminate between glycolytic and non-glycolytic ATP, cells were grown either in complete DMEM 10% FBS or supplemented with the hexokinase inhibitor 2′-deoxy-D-glucose at a concentration of 100 mM for 1.5 hours prior to extraction.

For analysis of ATP concentration in the different brain areas, brains were dissected, and samples were kept in cryopreservation buffer (50 mM K-Mes pH 7.1, 3 mM K_2HPO_4, 9.5 mM $MgCl_2$, 3 mM ATP, 20% glycerol, 10 mg/mL BSA) at −80°C until experiment. Samples were weighted, homogenized in pre-cooled 10% $HClO_4$, neutralized with KOH 2.5 M and the supernatant diluted in 100 mM Tris–4 mM EDTA, as described in (Khan, 2003). Total ATP concentration was detected by luciferin–luciferase bioluminescence assay and corrected by mg of tissue.

5.10 Analysis of intracellular $O_2^{\cdot-}$ by flow cytometry

Superoxide anion ($O_2^{\cdot-}$) concentration was measured using MitoSOX™ Red probe. Fibroblasts were grown in 24-well plates until 80% confluency and on the day of the experiment, alive cells were incubated with the dye at a concentration of 5 µM for 10 minutes at 37°C according to manufacturer's instructions. Cells were subsequently resuspended in HBSS and analyzed by flow cytometry in a NovoCyte Flow Cytometer (ACEA Biosciences). For fluorescence quantification, alive fibroblasts were identified according to forward *vs*. side scatter (FSC *vs*. SSC) density plot, based on their size and granularity. For this selection or gating, the mean fluorescence intensity at 610 nm was measured for the cells.

5.11 TBARS assay

Lipid peroxidation is the oxidative degradation of lipids, in which free radicals take electrons from the lipids (generally in cell membranes), resulting in cell damage. In brain samples it was detected using a colorimetric assay in which the by-product malonaldehyde (MDA) present in the samples reacted with thiobarbituric acid (TBA) to form the MDA-TBA adduct. During the assay, butylated hydroxytoluene (BHT) was added to the samples to protect the intact lipids from artificial peroxidation. In brief, samples were homogenized in 303 µL lysis solution (300 µL MDA lysis buffer + 3 µL BHT) for hippocampus and cerebellum, and 606 µL for cortex, and centrifuged at 13,000g for 10 minutes. Then 200 µL of supernatant were collected and added 600 µL of TBA reagent. Samples were incubated at 95ºC for 30 minutes and cooled to room temperature previous to absorbance measurement at 532 nm. Measurements were corrected by mg of protein.

5.12 Cytokines multiplex

A panel of thirteen cytokines (IL-1α, IL-1β, IL-6, IL-10, IL-12p70, IL-23, IL-27, IFN-β, IL-17A, MCP-1, TNF-α, IFN-γ, GM-CSF) developed by Biolegend was detected by flow cytometry using an immunoassay based on bead-fluorescence detection on a V-bottom plate according to the manufacturer's guidelines. For sample preparation, samples were weighted and homogenized with lysis buffer (1x PBS, 1% NP-40 and 1x protease inhibitor) as specified in (Amsen et al., 2009). Next, they were incubated with rotation for 1 hour at 4ºC, sonicated and centrifuged at 14,000 rpm (19,500g) for 15 minutes at 4ºC. Supernatant was collected and centrifuged at 14,000 rpm (19,500g) for 15 minutes at 4ºC. For the multiplex assay, 25 µL of sample were added to 25 µL of assay buffer and 25 µL mixed beads and incubated for 2 hours shaking at room temperature. Beads were spun down, washed and 25 µL of detection antibodies were added and incubated for 1 hour shaking at room temperature. Then 25 µL of streptavidin-PE (SA-PE) were added and incubated for 30 minutes shaking at room temperature. Finally, beads were spun down, samples were added 150 µL of wash buffer and were read on a flow cytometer. Measurements were corrected by mg of protein.

5.13 High-performance liquid chromatography (HPLC)

Supernatant was collected from the synaptic chamber reservoirs from cortical and dopaminergic neurons and kept directly at -80ºC until the time of analysis. Glutamate/GABA from cortical neurons chips and dopamine from DAn chips were measured by high-performance liquid chromatography (HPLC) at the Biochemistry Service at Hospital Sant Joan de Déu. Glutamate and GABA metabolites were measured following the protocol in (Casado et al., 2018). Dopamine and dopamie-1,1,2,2-d4 hydrochloride were analyzed on a Waters ACQUITY UPLC H-class instrument with a ACQUITY UPLC HSS T3 1.8 µm 2.1 x 100 mm column using water and acetonitrile with 0.1% formic acid as the mobile phases (run time = 4 minutes). The detection was performed with a Waters Xevo TQ-S

cronos triple-quadrupole mass spectrometer using positive electrospray ionization in the multiple reaction monitoring mode.

6 Behavioral tests

6.1 General Health Score (GHS)

The health scale was carried out every two weeks, from 3 months to the day of sacrifice. Mice were placed onto a laboratory bench for observation and received a score foreach category (0 = absent or normal appearance; 1 = present or moderate phenotype; 2 = severe phenotype). The resulted phenotype was calculated by the sum of the scores of each mouse and then averaging all animals within each group. The categories taken into account were gait, mobility, breathing, hind limb clasping, tremors, general condition, kyphosis (i.e., increased curvature of the frontal part of the spine), fur and seizures.

6.2 Novel object recognition test (NORT)

The NOR test is widely used to evaluate object recognition memory in mice. To test recognition, on the first day of the test (familiarization phase) mice were placed in a box (35 x 35 x 35 cm) with two identical objects (such as chess figures) and let freely explore the objects (meaning physically interact with them) for a total of 20 seconds of physical contact, or a maximum of 10 minutes in the cage even if the exploration time did not sum 20 seconds. 24 hours later, on the second day of the test (test phase), mice were placed again in the box with the initial object explored during the familiarization phase and a novel object, for 10 minutes. The time spent exploring each object was calculated manually (exploration of an object was defined as the mouse placing its nose within 2 cm of the zone where the object located). Maximum exploration time was recorded at 20 seconds.

6.3 Elevated Plus Maze (EPM) test

The EPM test is one of the most widely used tests for measuring anxiety-like behavior. The EPM apparatus consists of a cross-shaped maze elevated 60 cm above the floor with two open arms (35 x 5 cm) and two closed arms (35 x 5 x 15 cm). Mice were placed in the center of the maze (facing an open arm) and the amount of time spent in either the closed and open arms and the number of entries in each arm were recorded for 5 minutes.

7 Statistical analysis

7.1 GraphPad Prism

GraphPad Prism 10.0 software was used for statistical analysis. First, outliers are identified by ROUT test and discarded, and then data normality was determined. If two groups were compared, unpaired T test with Welch's correction for parametric data or Mann-Whitney test for parametric data were performed. If more than two groups were compared, (Brown-Forsythe and Welch) ANOVA for parametric data or Kruskal–Wallis for non-parametric data were performed, with posterior multiple comparisons analysis correction when appropriate. Equal standard deviations were not assumed. Two-way ANOVA was used for comparing groups and two or more variables, with post-hoc Tukey multiple comparisons correction.

Results were represented as mean for parametric data, or median for non-parametric data, together with individual values; as mean ± SD or median ± interquartile range; box plot with individual values; floating bars from min. to max. values with line at mean if data were parametric or median if non-parametric; or column with median and interquartile range. Differences were considered as statistically significant at $p < 0.05$, and coded through the figures as follows: $*p < 0.05$, $**p < 0.01$, $***p < 0.001$, and $****p < 0.0001$.

7.2 R Software

For more specific analyses and representations, RStudio software was used. Fluorescence measurements were represented as density plots, and box plots were represented with mean values per patient and lines connecting each patient response between groups.

Hotelling's T^2 test, a multivariate statistical method, was used to compare the combined means of two groups

(control and DNM1L patients) across two related variables, branch junctions and branch end points. This test accounts for the correlation between variables, providing a more robust analysis of group differences than univariate tests.

A supervised model was trained to classify subjects as DNM1L patients, other mitochondrial disease patients, or healthy controls using mitochondrial network morphology parameters. First, because of the high intercorrelation of the variables, redundancy analysis (*Hmisc*) was used to eliminate those variables that could be predicted with a high *R2* using the values of the remaining variables. The variables selected were Mean Aspect Ratio, Mean Branch Length, Branch End Points, Mitochondrial Count, and Mean Branch Diameter. Three different algorithms were fit using them as predictors to perform multiclass classification: Random Forest (RF, *randomForest*), Support Vector Machine (SVM, *kernlab*), and Multinomial logistic regression (NN, *nnet* package). Their performance was compared on training data and SVM was selected due to higher performance according to Accuracy and Kappa. Finally, the model was tested on unseen data. All predictors were log2-transformed to reduce skewness and standardized to ensure comparability before inclusion in the models.

RESULTS

1| MITOCHONDRIAL DYSFUNCTION IN RETT SYNDROME AND ITS MODULATION AS A THERAPEUTIC STRATEGY

2| PERSONALIZED TREATMENTS FOR MITOCHONDRIAL DISORDERS WITH ALTERATIONS IN NEUROTRANSMISSION

3| SYNAPSE ON A CHIP (SoC): AN ADVANCED TOOL FOR STUDYING THE IMPLICATION OF MITOCHONDRIA IN SYNAPTIC COMMUNICATION IN NEURODEVELOPMENTAL DISORDERS

1 MITOCHONDRIAL DYSFUNCTION IN RETT SYNDROME AND ITS MODULATION AS A THERAPEUTIC STRATEGY

1 Mitochondrial homeostasis studies on Rett patients' primary fibroblasts

1.1. Mitochondrial network morphology and ultrastructure in Rett fibroblasts
- Mitochondrial network morphology and dynamics
- Mitochondrial ultrastructure

1.2. Mitochondrial bioenergetic profile in Rett patients' fibroblasts
- Mitochondrial respiration and ATP synthesis
- Mitochondrial reactive oxygen species (ROS) generation and metabolism

2 Leriglitazone treatment on Rett patients' primary fibroblasts

2.1. Leriglitazone effect on the PPARγ pathway: assessment of gene and protein expression

2.2. Evaluation of leriglitazone on mitochondrial homeostasis modulation in treated Rett patients' fibroblasts
- Mitochondrial network morphology and dynamics
- Bioenergetic profile: mitochondrial ATP synthesis and ROS generation and metabolism

2.3. Validation of leriglitazone effect on the PPARγ pathway with the inhibitor GW9662

2.4. Summary of mitochondrial performance and its modulation in patients' fibroblasts

3 Studies on animal models: female Rett mice for assessment of brain bioenergetic function, neuroinflammation and behavior

3.1. Bioenergetic characterization: ATP concentration and oxidative stress
- Basal: pre-symptomatic and symptomatic mice
- Effect of leriglitazone treatment on bioenergetics

3.2. Neuroinflammatory component
- Basal: pre-symptomatic and symptomatic mice
- Effect of leriglitazone treatment in the inflammatory profile

3.3. Phenotypic outcome and behavior analysis

3.4. Additional results: neuronal markers expression

3.5. Summary of mitochondrial homeostasis alterations in Rett mice and their modulation with leriglitazone

In this first chapter, we study the mitochondrial homeostasis in Rett syndrome, a neurological disorder that affects 1:10,000 people, mostly girls, and it is caused by *de novo* mutations in the X-linked gene *MECP2* (Amir et al., 1999). While altered neurotransmission and brain development are the center of its pathophysiology, mitochondrial dysfunction also plays a key role in the natural history of the disease, as reviewed in (Shulyakova et al., 2017). This shapes mitochondria as an attractive target for the treatment of the disorder. With this in mind, we studied the effect of leriglitazone (LGZ), a PPARγ agonist, as a potential modulator of mitochondrial function to change the phenotype of the disease.

In this context, we characterized the mitochondrial dysfunction in two models of Rett syndrome: primary fibroblasts of up to eight different patients, and B6.129P2(C)-*Mecp2*$^{tm1.1Bird}$/J female mice, a validated mouse model for Rett syndrome. In summary, we described the mitochondrial homeostasis in primary fibroblasts from the patients, based on the mitochondrial network structure and dynamics and the bioenergetic function, in terms of ATP production and reactive oxygen species (ROS) generation and metabolism. Based on these parameters, we then studied the response to LGZ treatment in the fibroblasts of the patients. In parallel, we studied in female mice the brain bioenergetic function (regarding ATP synthesis and lipid peroxidation) and the neuroinflammatory component, topped with a phenotypical characterization. Working with mice allowed to study two aspects of the disease: the temporary evolution (pre-symptomatic and symptomatic mice) and the possible spatial brain alterations in three main areas (cortex, hippocampus and cerebellum). To assay the effect of LGZ on the mice, we explored a long treatment approach from weaning until sacrifice in the symptomatic stage.

Most of the results presented in this part are included in the paper "Musokhranova U, Grau C, Vergara C, Rodríguez-Pascau L, Xiol C, Castells AA, Alcántara S, Rodríguez-Pombo P, Pizcueta P, Martinell M, García-Cazorla A, Oyarzábal A. Mitochondrial modulation with leriglitazone as a potential treatment for Rett syndrome. J Transl Med. 2023 Oct 26;21(1):756. doi: 10.1186/s12967-023-04622-5".

1 Mitochondrial homeostasis studies on Rett patients' primary fibroblasts

We studied both mitochondrial shape (network dynamics and ultrastructure) and bioenergetic homeostasis (energy metabolism and oxidative stress) in fibroblasts from eight Rett patients (RTT_P1-P8 as can be consulted in Table 8) compared to a total of eight different healthy controls (Fig. 10). These patients presented different *MECP2* mutations and different severity presentations of the disease. Due to technical capability, the number of both controls and patients' fibroblasts used varied between experiments.

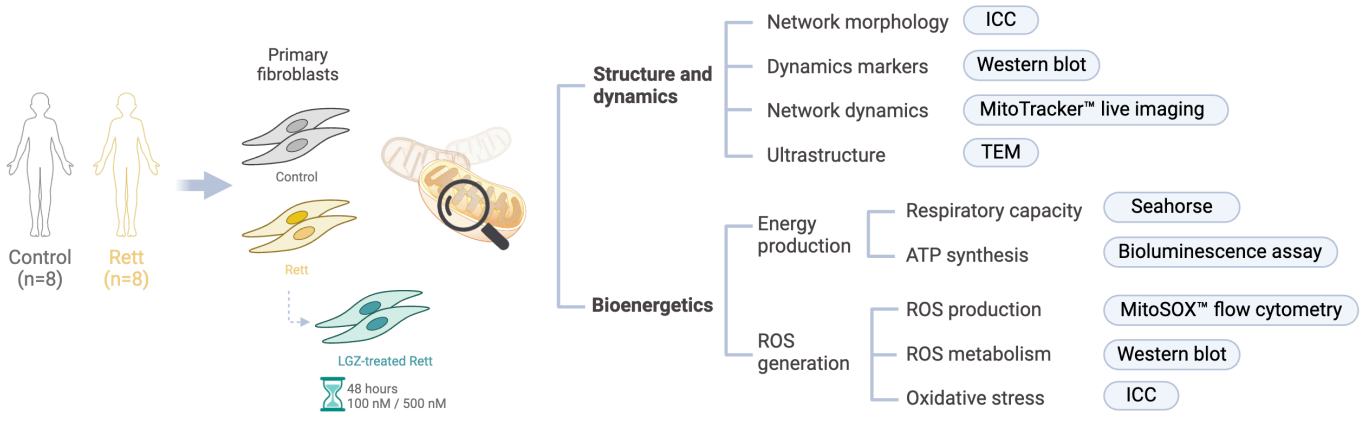

Figure 10. Schematic representation of the methods used for mitochondrial homeostasis characterization of Rett patients' fibroblasts. Created with BioRender. ICC = immunocytochemistry; TEM = Transmission Electron Microscopy, LGZ = leriglitazone.

1.1 Mitochondrial network morphology and ultrastructure in Rett fibroblasts

Mitochondrial network morphology and dynamics

First, we analyzed mitochondrial network by immunofluorescence with the mitochondrial membrane marker TOMM20 (Translocase of Outer Mitochondrial Membrane 20) (Fig. 11A) and parametrized its structure with Mitochondria Analyzer plug-in for ImageJ (Fig. 11B) in four Rett patients' fibroblasts (RTT_P1-P4) compared to three different controls. We observed alterations in mitochondrial grid number and morphology compared to control fibroblasts, as Rett mitochondrial networks had 1.5 times more independent networks, 20% reduction in mean form factor, and 10% reduced number of branches per network, together with 25% decreased branch length and a minor 16nm decrease in branch diameter. In other words, Rett mitochondria were less interconnected and less ramified than controls.

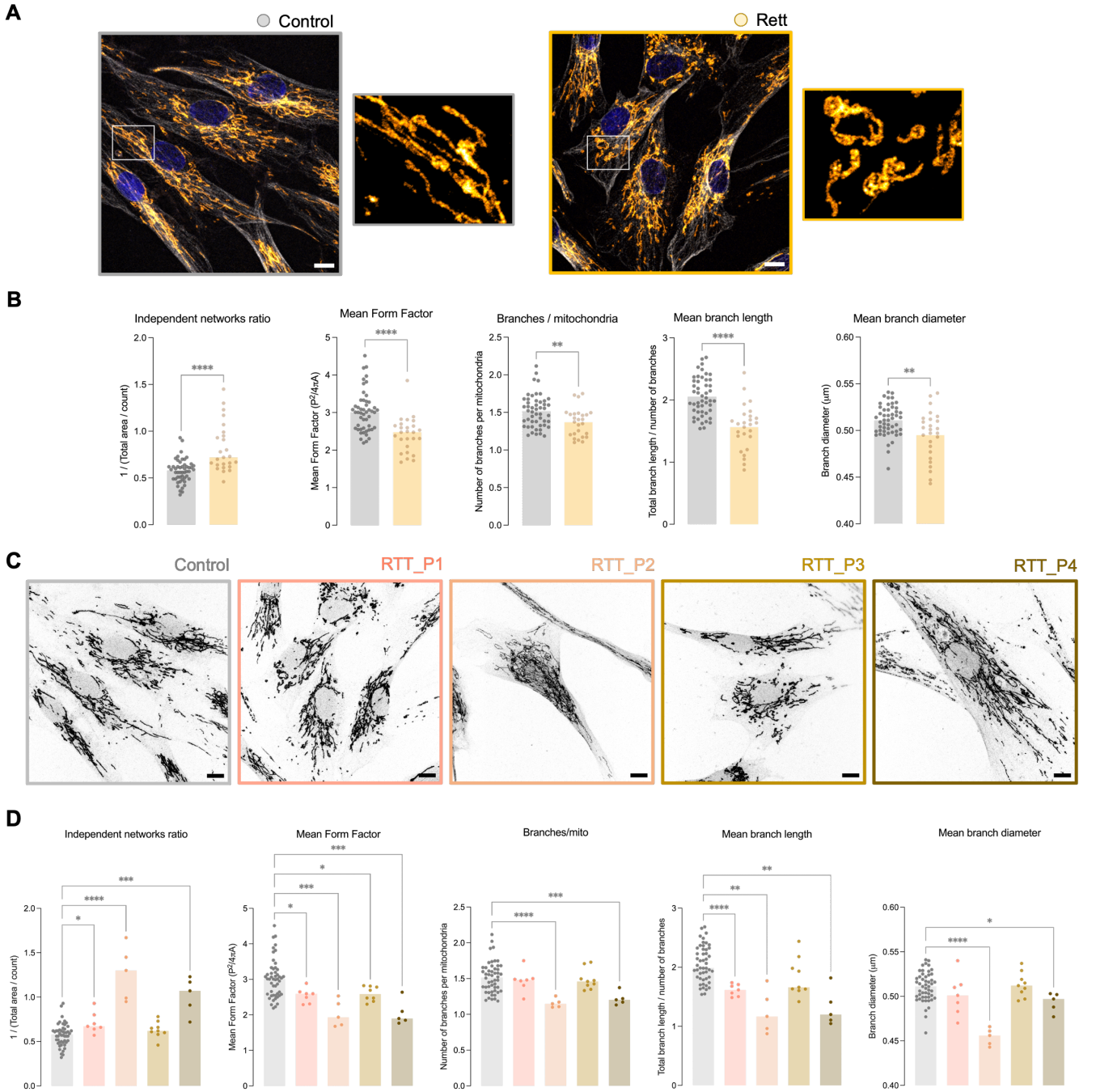

Figure 11. Analysis of the mitochondrial network shape in Rett fibroblasts.
(see next page)

(from previous page)
(A) Representative image of mitochondrial network IF (TOMM20 in yellow, nuclei in blue, and tubulin in grey; scale bar 10 µm; 6x zoomed section included in the white box). (B) Parametrization with Mitochondria Analyzer plug-in for ImageJ of the number of independent networks corrected by area, mean form factor (a shape measure given by: $P^2/(4\pi A)$ where 1 indicates round object and increases with elongation, expressed as mean FF of objects in image), number of branches per mitochondrial network, and mean branch length and diameter (n=50 mitochondria from three controls, n=26 mitochondria from RTT_P1-P4). (C) Representative image of mitochondrial network IF for Rett patients P1-P4 (TOMM20 in black; scale bar 10 µm). (D) Table with the five parameters in columns and their values for controls and patients RTT_P1-P4, giving the average value, the fold change over average of controls, and *p* value from the correspondent statistical test. (E) Spider plot showing the parametrization of the number of independent networks (1/Mean area), mean form factor, number of branches per mitochondrial network, and mean branch length and diameter, expressed as folds over control (n=50 mitochondria from three controls; n=7 mitochondria for P1, n=5 for P2, n=9 for P3, n=5 for P4). *(cont. next page)*
Data represented as (B) mean for parametric data or median for non-parametric data, + individual values, and (E) folds per patient over control. Comparative analysis control *vs*. Rett done with Welch's test for parametric, and Mann-Whitney for non-parametric data. *P* value represents **<0.01, ****<0.0001.

While these results summarize the general picture, they, however, were not homogeneous within the patients. Some individualities were found along the different cell lines (Fig. 11C, D). For example, we can observe that fibroblasts from patients 1 (RTT_P1) and 3 (RTT_P3), who have the same mutation (see Table 8), have a similar mitochondrial network structure and follow a similar pattern (Fig. 11D). Compared to control cells, RTT_P1 and P3 have modestly higher ratios of independent mitochondrial networks – by 22% and 10%, respectively – with statistical significance for P1. They also show reduced mean branch length by 22% and 12%, respectively, only significant for P1. In contrast, patients 2 (RTT_P2) and 4 (RTT_P4) display more pronounced network alterations, with a 2.2-fold and 1.8-fold increase in the ratio of independent networks and even shorter branches per network – 40% shorter for P2 and 37% for P4 compared to controls.

The other parameters analyzed follow a similar pattern. Compared to control fibroblasts, the mean form factor is reduced by 30% for P2 and P4, while P1 and P3 show only a 15% and 10% decrease, respectively. In addition, significant decreases are seen only in P2 and P4 for branch number per network (20% decrease) and mean branch diameter (56nm and 18nm decrease respectively). All these findings suggest that mitochondrial network structure is more altered in Rett patients 2 and 4, while the other two patients with the same mutation present a milder phenotype.

As mitochondrial network maintenance is closely regulated through mitochondrial dynamics (Fig. 12A), we studied the expression of Drp1 (Dynamin-related protein 1) and Fis1 (Fission, mitochondrial 1) as fission-regulating proteins, and OPA1 (Optic Atrophy 1) and Mfn2 (Mitofusin 2) as fusion mediating proteins through Western blot (Fig. 12B). We registered a significant decrease in the expression of both proteins involved in mitochondrial fission, with a 20% decrease in Drp1 and 30% in Fis1 (Fig. 12C), compared to controls. On the contrary, we did not detect changes in the proteins responsible for the fusion processes Mfn2 or OPA1 (Fig. 12D), but a minor decrease of 10% in OPA1 80:100 ratio (p=0.0481), compared to controls. This ratio is the comparison between the short (80 kDa, S-OPA1) and long (100 kDa, L-OPA1) isoforms of OPA1, being the short isoform related to a more fragmented morphology (Dotto et al., 2018). All these results together suggest a reduction in the fission:fusion rate.

This was supported by time-lapse image acquisition of mitochondria in live cells, stained with the probe MitoTracker™. The dynamics processes were visualized by confocal microscopy, recording during 2 min with 0.7 s between each frame (Fig. 12E), as described in Materials and Methods. Subsequent analysis of the mitochondrial movement with the MATLAB add-in Mitometer (Fig. 12F) showed a 10% increase in directionality, defined as the total distance traveled divided by the maximum displacement of the mitochondria, together with a 5% decrease in median speed and 5% increase in median:max speed ratio, that is, the bursting of mitochondria. More importantly, on top of these subtle alterations, the analysis confirmed a 23% decrease in the fission rate of Rett mitochondria compared to controls. This means that Rett mitochondria have less fission events and move more slowly overall but in a more directed and bursting-like behavior than controls. All these results are compatible within each other and support that Rett fibroblasts bear elongated and non-fragmented mitochondria.

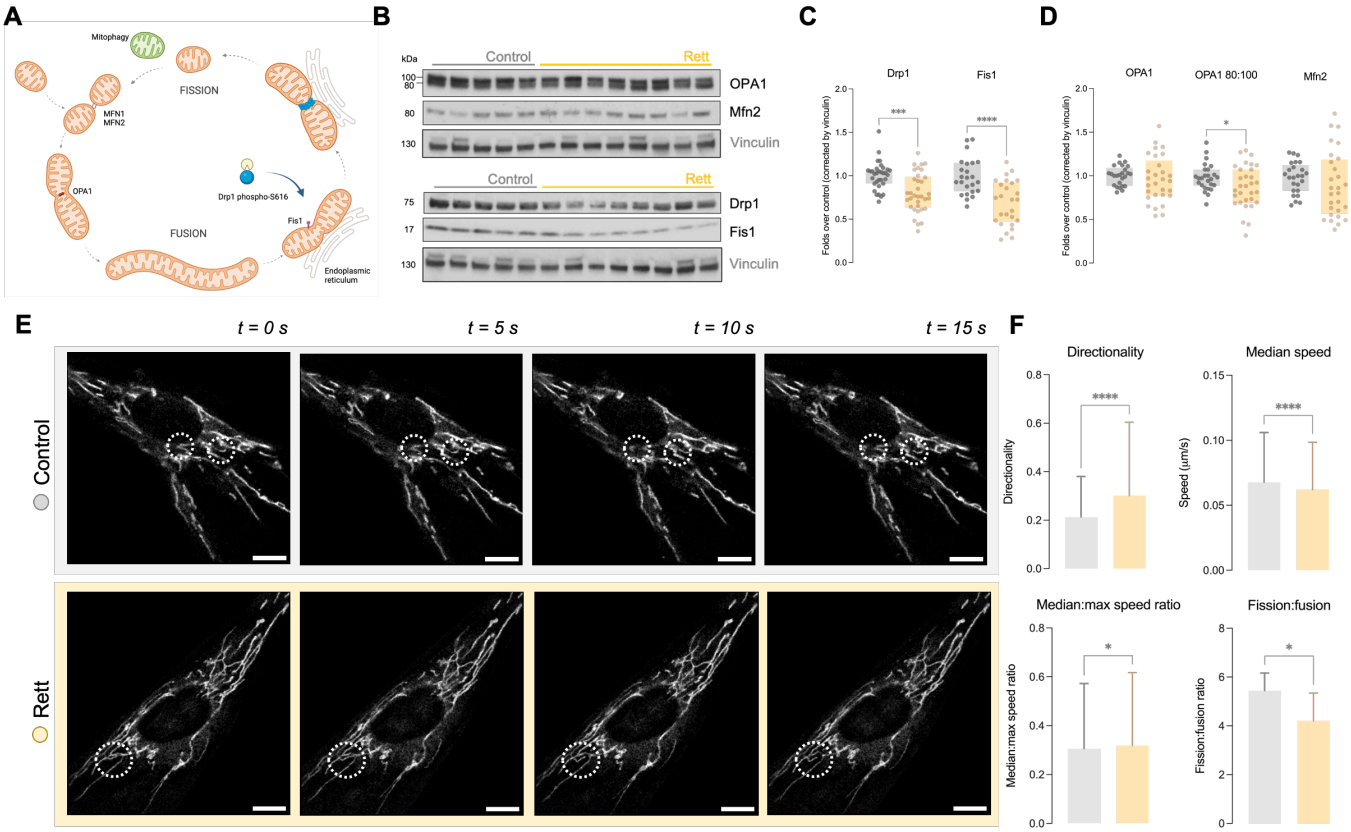

Figure 12. Mitochondrial dynamics evaluation in Rett fibroblasts: expression of dynamics proteins and live-cell visualization. (A) Schematic illustration of the mitochondrial dynamics processes, with OPA1 and Mfn2 involved in mitochondrial fusion, and Drp1 and Fis1 involved in fission (adapted from (Chen et al., 2023) using BioRender). (B) Representative images and densitometry quantification with ImageJ of mitochondrial dynamics associated proteins, (C) Drp1 and Fis1, (D) OPA1, ratio 80:100 kDa OPA1 (S-OPA1 vs L-OPA1) and Mfn2, by Western blot and corrected by vinculin; each lane represents a different cell line: controls 1-5 and patients Rett_P1-8 (n=8-10 experiments). (E) Representative frames of control and Rett mitochondrial network stained with MitoTracker™ Green, highlighting fission and fusion events at different time points (0s, 5s, 10s and 15s) (mitochondria in grey, scale bar 10 µm). (F) Quantification with Mitometer of the directionality, median speed, median:max speed ratio (bursting of mitochondria), and fission and fusion events ratio (calculated as explained in Materials and Methods) from time-lapse imaging of mitochondrial network (n=4285 mitochondria tracks for control, n=4637 tracks for Rett_P1 and P6; for fission:fusion ratio n=6 mitochondria for control, n=8 mitochondria for patients).
Data expressed as (C, D) folds over controls from the same experiment and represented as box plot + individual values; in (F) represented as mean + SD for parametric data or median + interquartile range for non-parametric data. Comparative analysis control *vs*. Rett done with Welch's test for parametric, and Mann-Whitney for non-parametric data. *P* value represents *<0.05, ***<0.001, ****<0.0001.

Mitochondrial ultrastructure

In addition to network dynamics, mitochondria reorganize their internal structure by modifying cristae shape (Cogliati et al., 2016). To analyze mitochondrial internal structure (or ultrastructure) differences between two Rett patients' fibroblasts (RTT_P2 and RTT_P3) and two controls we used transmission electron microscopy (TEM) imaging (Fig. 13A). As detailed in Materials and Methods, we focused on the parametrization of: (1) aspect ratio (major:minor axis ratio), (2) number of cristae per mitochondria, (3) cristae length, (4) width, (5) angularity, and (6) matrix electrodensity (Fig. 13B).

In Rett mitochondria we found a hyperfused phenotype, as the major:minor axis ratio was 1.5 times higher than controls and homogeneous between the two studied patients. On top of that, Rett fibroblasts' mitochondria showed structural abnormalities regarding cristae: patients had 15% less cristae than controls, which were also 11% shorter, 21% wider and their angularity – defined as the crista angle relative from the IMM – differed from controls in a 11% decrease, meaning that Rett cristae were less perpendicular to the IMM than cristae in controls. Moreover, the mitochondrial matrix in Rett fibroblasts was 10% more electrodense than in controls. Together, these results suggest that mitochondria in Rett patients show a 'condensed' phenotype, similar to a pro-apoptotic state with wider and 'disorganized' cristae and protein-dense matrix.

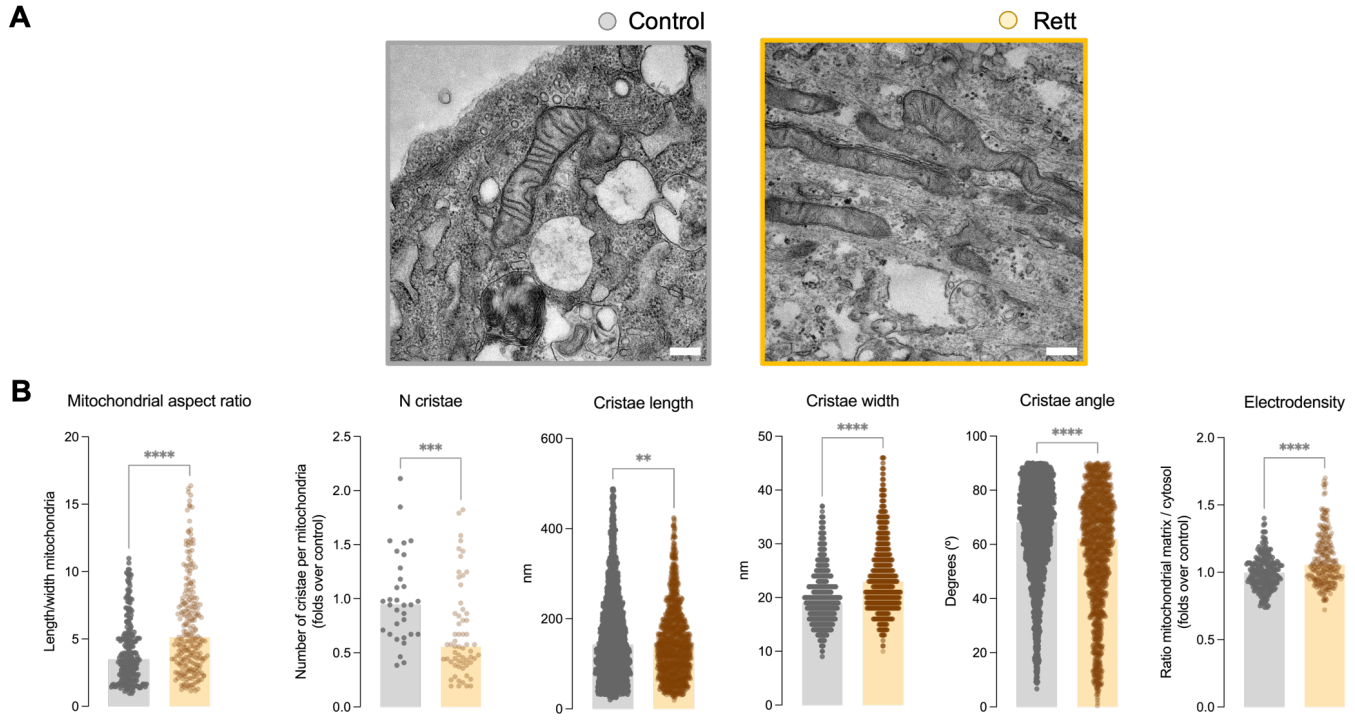

Figure 13. Description of mitochondrial ultrastructure in Rett fibroblasts. (A) TEM representative images of control and Rett mitochondria (scale bar 300 nm). (B) Parametrization of mitochondrial aspect ratio by measuring major:minor axis ratio (n=236 controls' mitochondria, n=246 patient's mitochondria), the number of cristae per mitochondria (n=32 images from controls, n=65 patient images), cristae length, width and angularity (n=2406 control cristae, n=1646 patient cristae), and electrodensity (n = 226 control matrices, n = 243 patient matrices).
Data represented as box plot with individual values. Analysis on non-parametric data done with Mann-Whitney test. *P* value represents **<0.01, ***<0.001, ****<0.0001.

1.2 Mitochondrial bioenergetic profile in Rett patients' fibroblasts

Mitochondrial respiration and ATP synthesis

After describing the mitochondrial network shape and dynamics and the ultrastructure deficiencies in Rett fibroblasts, we next analyzed the mitochondrial bioenergetic performance, focusing on respiratory capacity, measured by Seahorse, and ATP production detected by a bioluminescence assay.

We measured real-time oxygen consumption rate (OCR) of Rett and control fibroblasts in basal conditions and after addition of different drugs into the cell media. This allowed the calculation of several bioenergetic parameters relevant for the cells: (1) basal respiration (OCR), detected at the beginning of the experiment; (2) oligomycin-sensitive respiration (OSR or ATP-linked respiration, since oligomycin blocks ATP synthase), calculated as the difference between basal and oligomycin-induced OCR; and (3) maximal respiration or Rmax, calculated as the difference between FCCP-induced OCR and the OCR after inhibition with antimycin A and rotenone. FCCP (carbonyl cyanide-4-(trifluoromethoxy) phenylhydrazone) uncouples the oxygen consumption from ATP synthesis, causing the electron transport chain to work at its maximal capacity, whereas antimycin and rotenone block complex III and I of the oxidative phosphorylation (OXPHOS) system, respectively.

The analysis revealed an overall reduction in the OCR in the MeCP2-deficient cells (Fig. 14A). Rett fibroblasts showed a significant lowered both basal respirations and maximal respiration, with 40% and 55% decreases over controls, respectively (Fig. 14B). Moreover, patients also showed a significant 43% reduction in the oligomycin-sensitive respiration (OSR), this is, the fraction of oxygen consumed for ATP production. These results were consistent with an impairment in mitochondrial bioenergetic function in Rett fibroblasts.

Since ATP-linked respiration was decreased in Rett fibroblasts, we went on to study ATP concentration in control and patient cells by luciferin-luciferase bioluminescence assay. To discriminate between total and non-glycolytic (and hence mitochondrial) ATP, we measured ATP concentration in the presence of 2-deoxy-D-glucose (2-DG), a non-metabolizable glucose analog that inhibits glycolysis via hexokinase, and therefore forces mitochondria to use other substrates (from fatty acid β-oxidation and amino acid metabolism). Analysis revealed reduction of 47% in total and 53% in mitochondrial ATP (Fig. 14C) compared to controls, meaning that Rett fibroblasts' mitochondria produce half ATP than controls without any compensatory mechanism.

Opposite to the observed regarding mitochondrial network morphology, these results were consistent along all the studied patients (Fig. 14D). Detection of total ATP synthesis showed that Rett patients 1, 2 and 3 had significant decreases of 37%, 69% and 54% over the controls, respectively. Mitochondrial ATP was also decreased in the same trend (59%, 71% and 39% over the controls, respectively), being Rett patient 2 the most severely affected in terms of bioenergetic production.

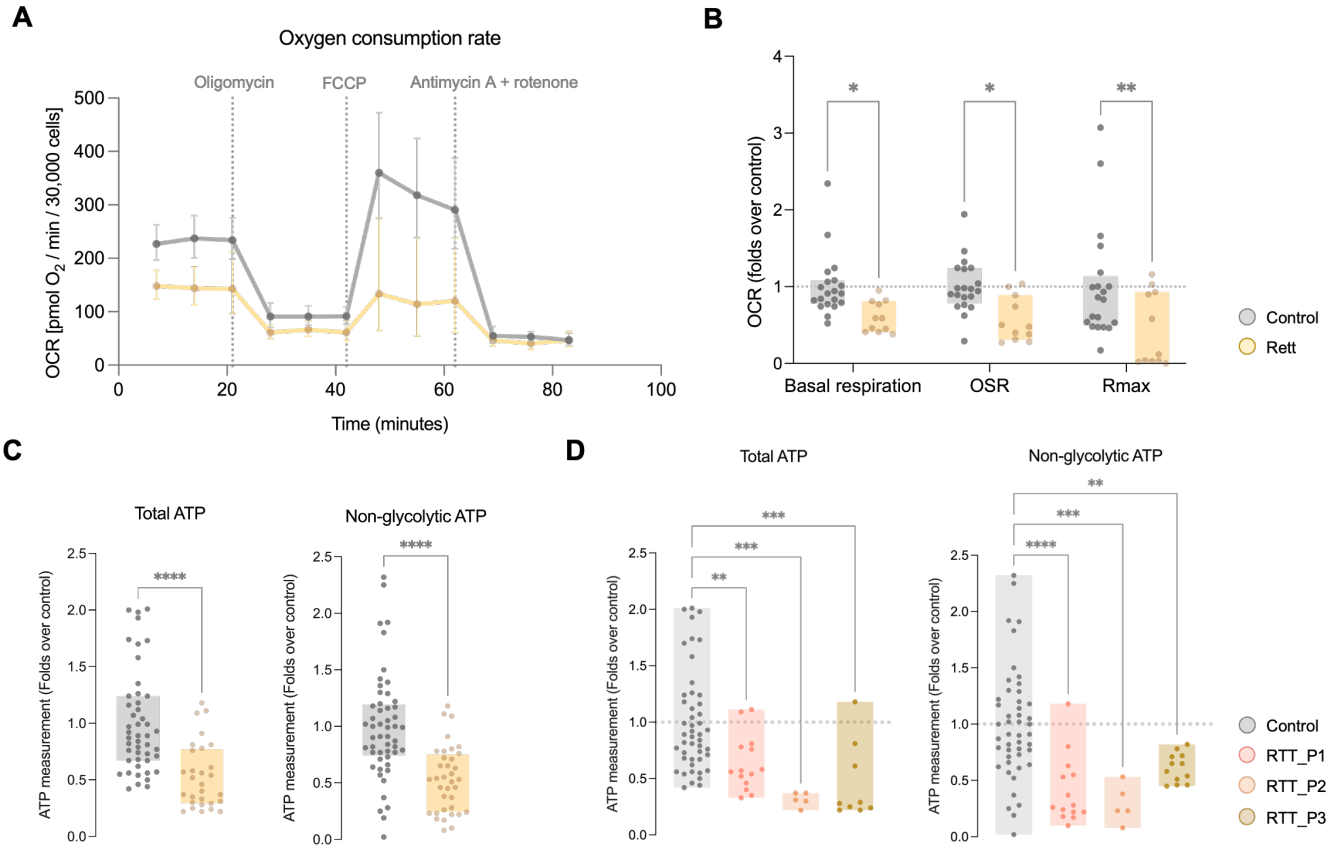

Figure 14. Mitochondrial energy production in Rett fibroblasts: oxygen consumption profile and ATP concentrations. (A) Mitochondrial respiratory efficiency in control and patient's fibroblasts was measured by Seahorse in the presence of oligomycin, FCCP, antimycin A and rotenone. (B) Calculation of three respiratory parameters: basal respiration as the average OCR until 20 minutes of experiment, oligomycin-sensitive respiration (OSR) as the difference of oxygen consumption before and after adding oligomycin (considered as ATP-linked respiration), and maximal respiration (Rmax) as the difference between oxygen consumption after adding FCCP and before antimycin A (n=3 experiments from RTT_P1 and P2 and two controls). (C) Total and non-glycolytic ATP production – assumed as mitochondrial ATP – measured by luciferin-luciferase luminescence upon incubation with 100 mM 2-deoxy-D-glucose (n=3 experiments, 4-6 technical replicates from three Rett patients and a total of four controls). (D) Total and mitochondrial ATP production in RTT_P1 (n=3 experiments with 4-6 replicates), P2 (n=1 experiment with 5 replicates) and P3 (n=2 experiments with 5-6 replicates). Data represented as (A) mean ± SD over time and (B-D) box plot with individual values expressed as folds over control. Two-way ANOVA analysis with post-hoc multiple comparisons uncorrected Fisher's LSD, comparing only control vs. patient groups. Comparative analysis for two groups done with Welch's test for parametric and Mann-Whitney for non-parametric data; Kruskal-Wallis test for non-parametric data when comparing the different groups over control. *P* value represents *<0.05, **<0.01, ***<0.001, ****<0.0001.

Mitochondrial reactive oxygen species (ROS) generation and metabolism

Mitochondrial respiration defects often result in excessive ROS generation, that can cause oxidative damage in the cells. Therefore, we detected through flow cytometry the superoxide anion ($O_2^{\cdot-}$), measuring its fluorescence with the probe MitoSOX™ Red. Superoxide anion is a reactive oxygen species (ROS) molecule produced as a byproduct during ATP synthesis in the OXPHOS system. We recorded that Rett fibroblasts were exposed to 1.9-fold higher concentrations of $O_2^{\cdot-}$ compared to controls (Fig. 15A, B). Similar to ATP production, these results were consistent through all the studied patients (Fig. 15B): 1.90 folds in RTT_P1, 2.11 in P2, 1.81 folds in P3 and 1.77 folds in P4, being patient 2 the one that bears the highest increase over the controls.

Superoxide anion is metabolized through superoxide dismutase, that can be cytoplasmatic (SOD1), mitochondrial (SOD2 or MnSOD) and extracellular (SOD3). As detailed in Figure 15C, in mitochondria MnSOD catalyzes the partition of $O_2^{\cdot-}$ into normal molecular oxygen (O_2) and hydrogen peroxide (H_2O_2). Then glutathione peroxidase (GPx) reduces H_2O_2 to O_2 and water by using monomeric glutathione (GSH) as an electron donor. Despite a general 1.9-fold increase in $O_2^{\cdot-}$ production in the Rett patients' fibroblasts, antioxidant MnSOD and GPx enzymes expression was not homogeneous between the different Rett patients (Fig. 15D,E). Patient RTT_P2 showed a 2.5-fold increased expression in MnSOD (yet not statistically significative, Welch's t test p=0.054), while patient RTT_P4

revealed a significant 52% decrease in GPx expression (Welch's t test p=0.0007), compared to controls. Therefore, densitometry quantification did not reveal any significant differences in the expression of the antioxidant enzymes in Rett patients compared to controls (Fig. 15E).

To detect if this increase in $O_2^{\cdot-}$ generation in Rett mitochondria is causing oxidative damage to the cells, we detected immunofluorescence of 8-OHdG (8-hydroxy-2'-deoxyguanosine) (Fig. 15F), a widely accepted marker of DNA oxidative damage. Quantification of the 8-OHdG fluorescence intensity revealed a 15% increase in Rett cells compared to controls (Fig. 15G, H). These results suggest that Rett patients, besides having a decreased respiratory rate and energy production, have exacerbated oxidative stress because of increased ROS production.

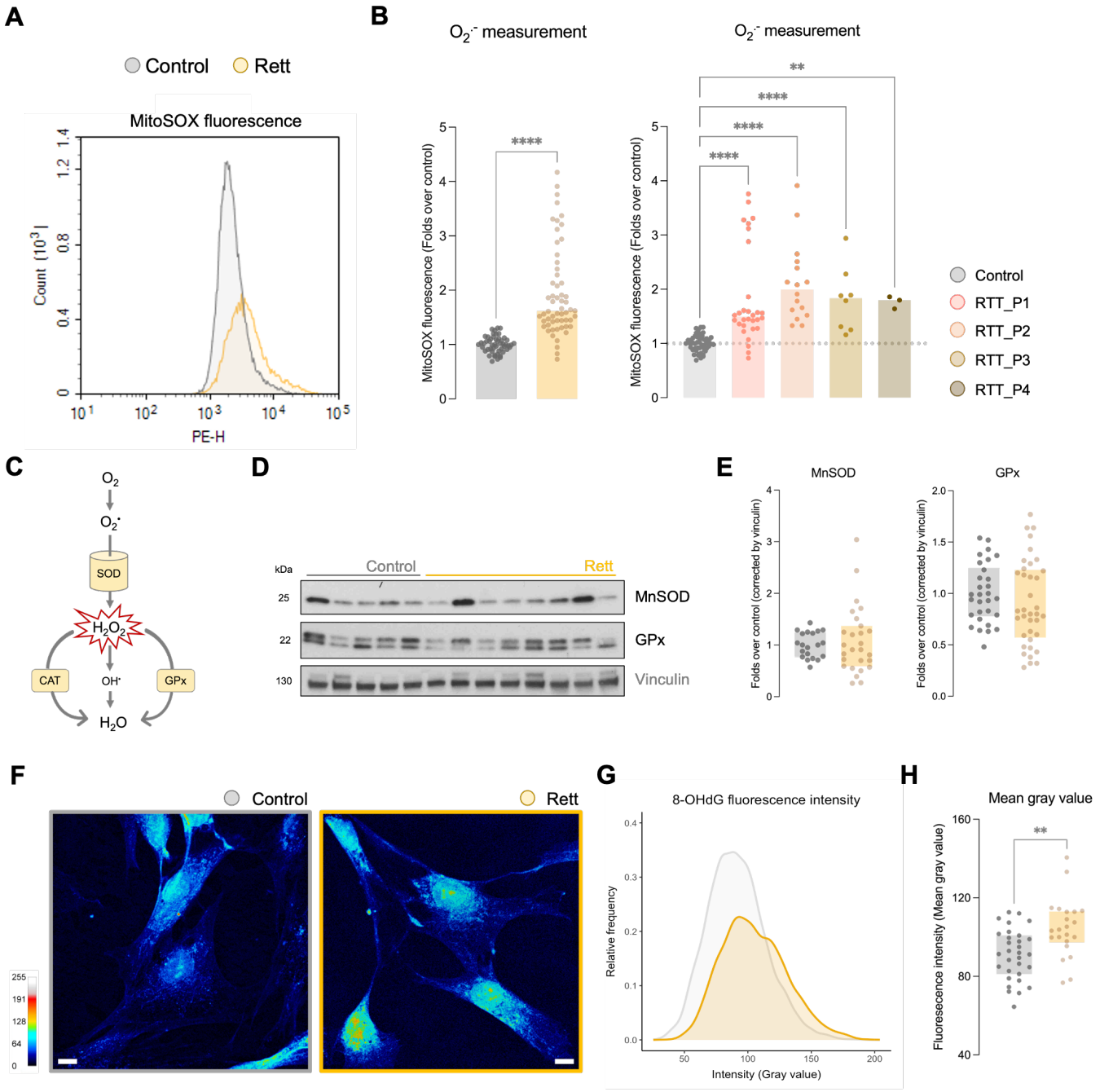

Figure 15. Reactive oxygen species (ROS) production and metabolism in Rett fibroblasts: evaluation of superoxide anion, antioxidant enzymes and oxidative damage. (A) Flow-cytometer visualization and quantification of $O_2^{\cdot-}$ production, detected with MitoSOX™ probe fluorescence, in Rett patients' fibroblasts and expressed as folds over controls from the same experiment (n=10 experiments, 3-6 technical replicates with three controls and patients RTT_P1-4). (B) $O_2^{\cdot-}$ detection in RTT_P1 (n=8, 3-6 replicates), P2 (n=5, 2-5 replicates), P3 (n=2, 2-6 replicates) and P4 (n=1, 3 replicates) compared over average of controls. (C) Schematic representation of the antioxidant enzymes pathways to reduce $O_2^{\cdot-}$ into H_2O through a series of steps that involve the enzymes superoxide dismutase (SOD) and glutathione peroxidase (GPx), amongst others (adapted from (Pandey et al., 2010)). (D) Representative image of the expression of MnSOD and GPx detected by Western blot, and (E) densitometry quantification, corrected by vinculin and expressed as folds over controls; each lane represents a different cell line, in order: five controls and patients RTT_P1-P3, P5-P8 and P4 (n=9-11 experiments). (F) IF detection of DNA oxidative damage with 8-OHdG marker and visualized with the intensity-revealing LUT "royal" (calibration bar on the left side of the images; scale bar 10 µm). Quantification of 8-OHdG fluorescence intensity in each cell's nucleus (detailed in Materials and Methods) and represented as (G) relative frequency of intensity values and (H) as mean gray value in two controls (n=31 cells) and two Rett patients' fibroblasts (n=23 cells, patients RTT_P1 and P6).

(cont. next page)

(from previous page)
Data represented as (A) histogram distribution of alive cells (gated) with MitoSOX™ Red fluorescence, (B) median + individual values, (E, H) box plot with individual values, and (G) density plot of gray values of controls and patients. Comparative analysis for two groups done with Welch's test for parametric and Mann-Whitney for non-parametric data; Kruskal-Wallis test for non-parametric data when comparing the different patients over control. *P* value represents **<0.01, ****<0.0001.

2 Leriglitazone treatment on Rett patients' primary fibroblasts

Given the mitochondrial alterations in the studied model, we next investigated if these dysfunctions could be corrected with leriglitazone (LGZ). Leriglitazone is a selective peroxisome proliferator-activated receptor gamma (PPARγ) agonist that can efficiently cross the blood–brain barrier (BBB) (Rodríguez-Pascau et al., 2021a). Activation of the PPARγ/PGC1α pathway stimulates mitochondrial biogenesis, reduces oxidative stress and improves mitochondrial function (Fig. 16A). LGZ has demonstrated preclinical efficacy in the correction of the phenotype in *in vitro* and *in vivo* models of other neurodevelopmental diseases such as X-linked adrenoleukodystrophy (X-ALD) (Rodríguez-Pascau et al., 2021a) and Friedreich's ataxia (FA) (Rodríguez-Pascau et al., 2021b) and clinical benefit for X-ALD and FA patients in clinical trials (Pandolfo et al., 2022; Köhler et al., 2023; Golse et al., 2024).

We investigated the *in vitro* effect of LGZ in Rett fibroblasts incubating the cells at two different concentrations, 100 and 500 nM, for 48 hours (Fig. 16B), as detailed in Materials and Methods. First, we evaluated the effect of LGZ on the PPARγ pathway through detection of genes and proteins expression under its regulation. Then, we studied the functional effect of LGZ on mitochondrial homeostasis regarding mitochondrial dynamics and bioenergetics, and ultimately validated the response on Rett fibroblasts as a direct consequence of the PPARγ pathway activation with a molecular inhibitor.

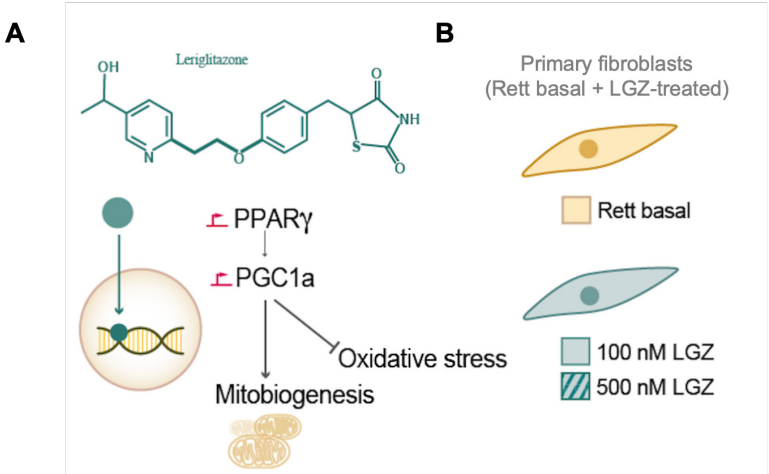

Figure 16. PPARγ mechanism of action in cells and treatment with the agonist LGZ. (A) Schematic representation of LGZ and its activity as a PPARγ agonist in a cell: LGZ binds to PPARγ, activating the expression of the genes under its regulation through interaction with PGC1α. (B) LGZ effect evaluation on Rett fibroblasts at two concentrations, 100 nM and 500 nM for 48 hours.

2.1 Leriglitazone effect on the PPARγ pathway: assessment of gene and protein expression

PPARγ belongs to a family of ligand-regulated nuclear receptors (PPARs) together with isoforms α and β. These three isoforms share a highly conserved DNA binding domain that recognizes specific DNA sequences known as Peroxisome Proliferator Response Elements (PPREs). We investigated the effect of LGZ on the expression of three genes under the PPARγ pathway: (1) *PGC-1α* gene, a PPARγ coactivator (Puigserver et al., 1999) (2) *MnSOD* gene, with three PPRE motifs where one of them is a binding site for PPARγ (Venkatachalam et al., 2009) and (3) *SREBP2* gene, which codes for the processed sterol regulatory element-binding protein 2 and is negatively regulated by PPARγ (Rogue et al., 2010; Han et al., 2019). These genes represent different key pathways under its modulation: mitochondrial biogenesis and function, antioxidant metabolism, and lipid homeostasis, respectively.

Upon LGZ incubation for 48 hours in Rett patients' fibroblasts, by qPCR analysis we detected a 1.9-fold increase in the *PGC1α* transcript with the 500 nM concentration over basal condition, and 1.5 and 2.2-fold increases in *MnSOD* transcripts at 100 nM and 500 nM concentrations, respectively (Fig. 17A). However, we did not detect significative differences for the *SREBP2* transcript. These results verify that leriglitazone can effectively modulate PPARγ-signaling pathway in the patients' fibroblasts in terms of mitochondrial biogenesis and antioxidant metabolism.

To further investigate the effect of LGZ on mitochondrial biogenesis we quantified by qPCR the expression of the mitochondria-encoded genes *mt-ND1* (Mitochondrially encoded NADH:ubiquinone oxidoreductase core

subunit 1), *CO1* (Cytochrome c oxidase subunit I), *CO2* (Cytochrome c oxidase subunit II), and *CO3* (Cytochrome c oxidase subunit III). The first gene codes for a subunit of complex I of the respiratory chain, while the other three code for subunits of complex IV. The expression of these transcripts was corrected over the nuclear-encoded gene *HK2* (hexokinase 2), which function is the phosphorylation of glucose into glucose-6-P, the first step of glycolysis. We compared the expression of the transcripts in Rett patients' fibroblasts over the average of controls in basal condition and after treatment, and compared the treated over the non-treated patients' cells (Fig 17B). Quantification of the transcripts' expression in Rett showed a general increase in the four genes (*mtND1*: 1.8 folds, *CO1*: 1.5 folds, *CO2*: 1.5 folds, *CO3*: 2.2 folds) compared to controls. Additionally, the LGZ-treated Rett cells showed a significant increase in both concentrations compared to controls for *mtND1* (100 nM: 2.7 folds, 500 nM: 2.1 folds), *CO1* (100 nM: 1.9 folds, 500 nM: 1.5 folds), *CO3* (100 nM: 2.5 folds, 500 nM: 2.2 folds), and only significant for 100 nM in *CO2* (1.9 folds). Regarding the effect on the patients' fibroblasts, these increases were significant for 100 nM in *mtND1* (1.5 folds over basal) and 100 nM in *CO3* (1.2 folds over basal). These results point towards an increased expression of respiratory complexes in Rett patients that is augmented with LGZ treatment.

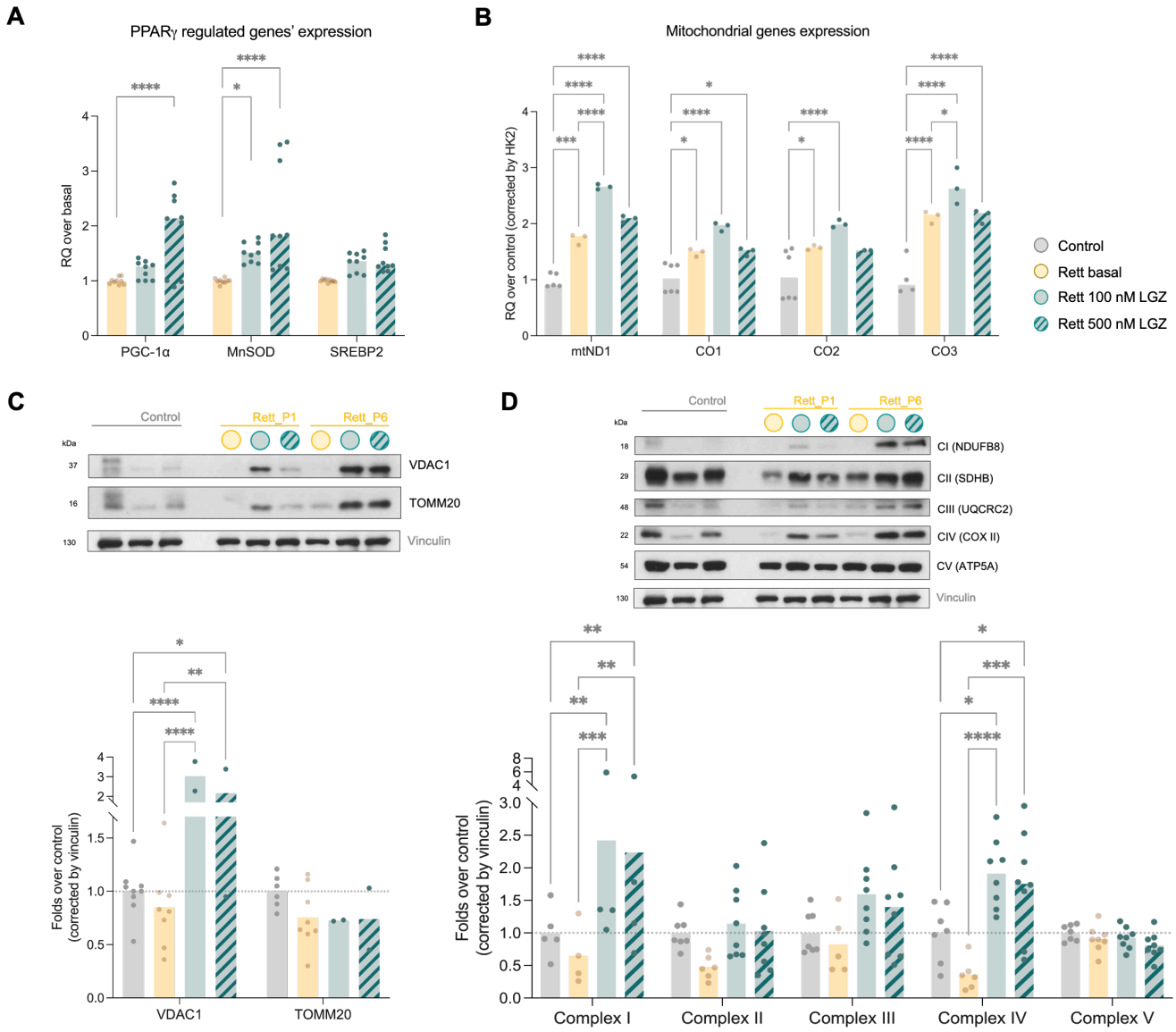

Figure 17. Regulation of the PPARγ pathway: detection of genes and proteins' expression under its control. (A) Detection of the expression of PPARγ regulated transcripts *PGC1α*, *MnSOD*, and *SREBP2*, measured by qPCR, expressed as relative quantification (RQ) over basal (triplicates from three controls and Rett patients P1-4). (B) Estimation of mitochondrial biogenesis by quantification of mitochondria-encoded genes *mtND1*, *CO1*, *CO2* and *CO3*, corrected over nuclear-encoded gene *HK2*, and measured by qPCR, expressed as RQ over basal (triplicates of controls and Rett). (C) Representative image of three controls and two Rett patients and densitometry quantification of the mitochondrial outer membrane proteins VDAC1 and TOMM20, detected by Western blot and corrected by vinculin (n=3-4 experiments, a total of four different controls and three patients (Rett_P1, P3 and P6). (D) Representative image of three controls and two Rett patients and densitometry quantification of the electron-transport chain complexes from the OXPHOS system, detected by Western blot and corrected by vinculin (n=3 experiments from four controls and Rett patients P1 and P6).
Data represented as median for non-parametric data (A-B) or mean for parametric (C-D) together with individual values. The test used was two-way ANOVA analysis, with Tukey post-hoc correction for multiple comparisons when comparing all the different groups. *P* value represents *<0.05, **<0.01, ***<0.001, ****<0.0001.

To determine if these changes in mitochondrial mass are translatable at protein level, we detected by Western blot and quantified the expression of the mitochondrial proteins VDAC1 (Voltage Dependent Anion Channel 1), the most abundant protein of the mitochondrial outer membrane, and TOMM20 (previously detected by immunofluorescence) in the patients at basal conditions and after LGZ treatment (Fig. 17C). We did not detect significant changes in both proteins' expression in Rett patients compared to controls, but confirmed a 3-fold and 2.2-fold increased expression in VDAC1 expression for the 100 nM and 500 nM treated conditions both compared to control and basal condition in the patients.

In line with the previous results, we analyzed the expression of the proteins from the OXPHOS system, main site responsible for ATP production in mitochondria, detected by Western blot (Fig. 17D). This system consists of five complexes (I, II, III, IV and V or ATP synthase) and two electron carriers embedded in the inner mitochondrial membrane. Quantification of the different complexes' expression showed a general decrease in complexes I-IV in Rett patients' cells compared to controls, and a general trend to increase upon LGZ treatment in the same complexes. In particular, these differences were statistically significant for the expression increases in complex I (100 nM: 2.4 folds, 500 nM: 2.2 folds) and IV (100 nM: 1.9 folds, 500 nM: 1.8 folds) compared both to controls and to the basal condition in the patients (complex I 2.7 folds in 100 nM and 2.6 folds in 500 nM; complex IV 3.8 folds in 100 nM and 3.2 folds in 500 nM).

Taken together, these results suggest that, besides detecting an increase in mitochondrial mass and complexes subunits at transcript level in basal condition, this is not translated to protein expression. In contrast, LGZ effect on mitochondrial biogenesis is detected both at transcript and protein level in Rett patients' fibroblasts.

2.2 Evaluation of leriglitazone on mitochondrial homeostasis modulation in treated Rett patients' fibroblasts

Mitochondrial network morphology and dynamics

As previously mentioned, Rett fibroblasts are characterized by an increase in independent networks, together with reduced number of branches per structure. These branches, in addition, are shorter and have a thinner diameter than controls. Therefore, we went to analyze if these alterations could be corrected by treating patients' cells with 100 nM and 500 nM LGZ for 48 hours. TOMM20 immunofluorescence showed no statistical differences for the measured parameters at the treated conditions over basal in patients (Fig. 18 A, B).

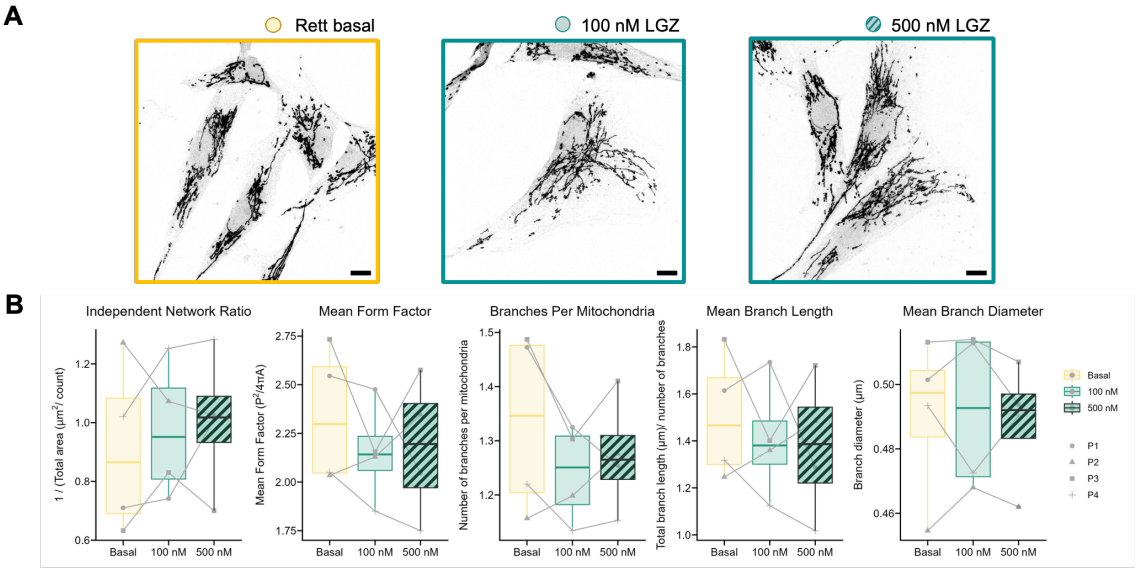

Figure 18. Mitochondrial network structure in Rett patients' fibroblasts after treatment with LGZ. (A) Representative images of TOMM20 IF in a patient (RTT_P3) for basal, 100 nM and 500 nM LGZ conditions (TOMM20 in black; scale bar 10 μm). (B) Parametrization of the network with Mitochondria Analyzer, showing the previously altered parameters in basal, differentiating amongst the responses per patient, connected with grey lines between the three conditions (n= 26 mitochondria for basal, n=19 for 100 nM, n=23 for 500 nM, from four Rett patients P1-P4, indicated each with a different symbol).
Data represented as box plot and average values per patient in each condition, connected by a line. One-way ANOVA or Kruskal-Wallis for parametric and non-parametric data respectively, with multiple comparisons between groups.

However, some individualities were observed between the patients. Similar to basal condition, where RTT_P1 and P3 grouped together with a milder mitochondrial phenotype while RTT_P2 and P4 showed more severe alterations, LGZ-treated fibroblasts also grouped in two responses. Two-way ANOVA analysis with multiple comparisons over basal condition, detected statistical differences for patients RTT_P1 and P3 regarding individual networks ratio (42% increase for P1 500 nM, p=0.0051), mean form factor (20% decrease for P1 500 nM, p=0.02, and 21% decrease for P3 100 nM, p=0.0068), branches per mitochondria (10% decrease for P1 100 nM, p=0.048, 15% decrease for P1 500 nM, p=0.004, and 12% decrease for P3 100 nM, p=0.013), and mean branch length (24% decrease for P3 100 nM, p=0.013) over basal condition. Regarding patients P2 and P4, we only detected differences for P2 at the independent networks ratio (19% decrease for P2 500 nM, p=0.038). Therefore, these results suggest that there is an exacerbation of the mitochondrial network alterations in the patients with milder network phenotype and a slight correction for one of the patients with severe network alterations.

Regarding mitochondrial dynamics balance, in Rett cells there is a decrease in fission proteins expression Drp1 and Fis1, together with a decrease in the short isoform of OPA1 (S-OPA1) over the long isoform (L-OPA1), but no significative changes in the total OPA1 nor Mfn2, related to fusion processes. We investigated the expression of these proteins by Western blot in the Rett patients after LGZ treatment (Fig. 19A). Similarly to the mitochondrial network results, we did not detect significant differences in the dynamics markers expression in the LGZ-treated cells over basal condition, both for fission (Fig. 19B) and fusion proteins (Fig. 19C).

Moreover, Rett patients' mitochondria have a decreased fission:fusion ratio, with slowly but directed and bursting-like movement. We observed the dynamics of the mitochondrial network by time-lapse imaging using MitoTracker™ Green probe (Fig. 19D) and quantified these parameters with Mitometer (Fig. 19E). We detected a 12% increase in median speed in treated cells and a non-significative 37% increase the fission:fusion ratio over basal condition. Therefore, at the assayed treatment concentrations and incubation time, LGZ can correct the speed of the mitochondrial movement but without significant differences in directionality, bursting and fission:fusion dynamics deficiencies.

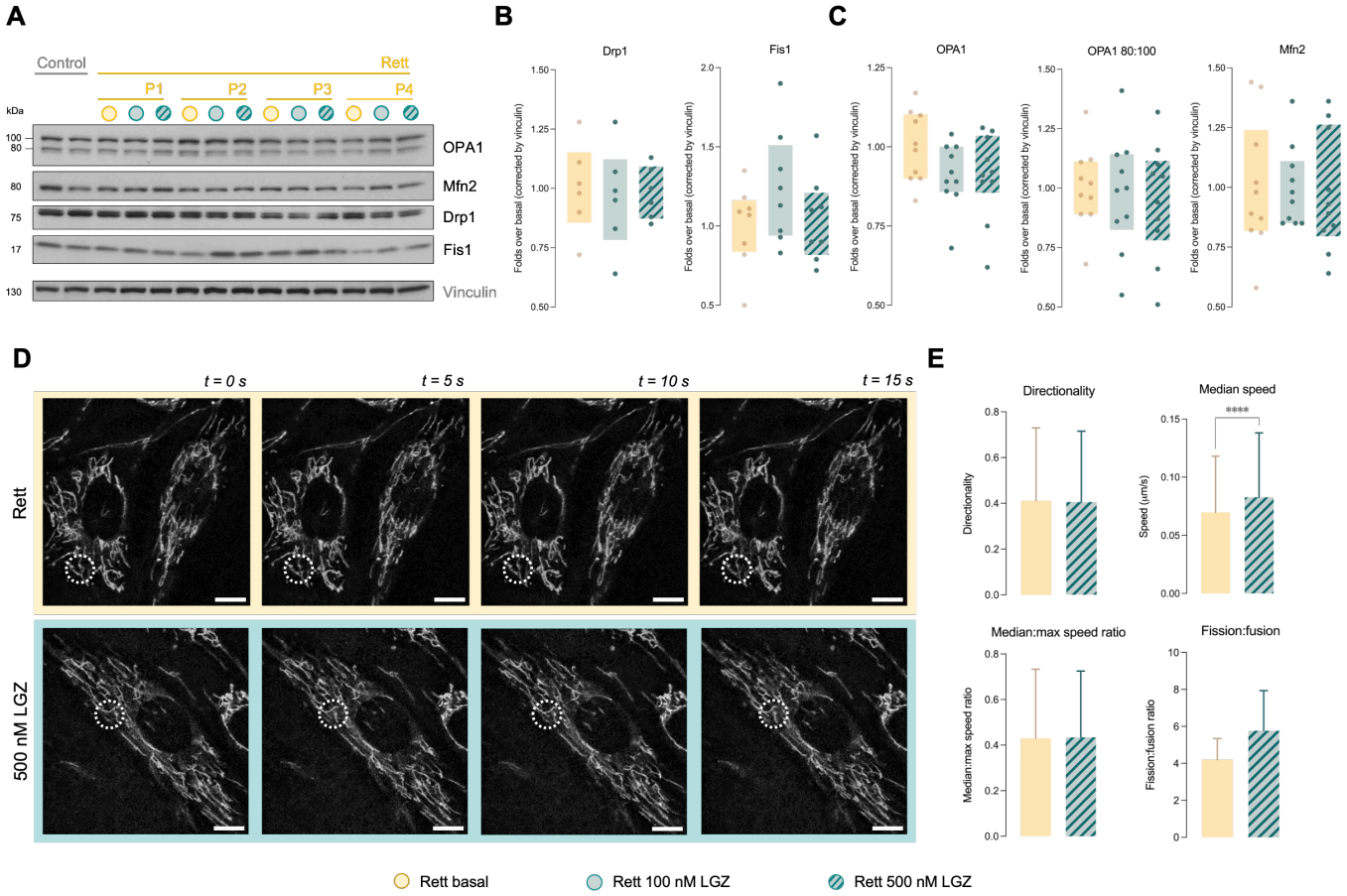

Figure 19. Assessment of mitochondrial dynamics in LGZ-treated Rett fibroblasts: protein expression and live-cell mitochondrial movement. (A) Representative images of two controls and four Rett patients (RT_P1-P4) treated with 100 nM and 500 nM LGZ. Densitometry quantification of (B) fission –Drp1 and Fis1– and (C) fusion –OPA1, 80:100 OPA1, and Mfn2– mitochondrial dynamics markers expression detected by Western blot and corrected by vinculin, expressed as folds over basal (n=2-4 experiments, with a total of four controls, and patients RTT_P1-P4). (D) Representative frames of basal and 500 nM LGZ-treated Rett fibroblasts (RTT_P6) at different time points (0s, 5s, 10s and 15s) from the time-lapse imaging with MitoTracker™ Green probe (mitochondria in grey; dashed white circle highlights dynamic events; scale bar 10 µm). (E) Quantification with Mitometer of the directionality, median speed, median:max speed ratio (bursting of mitochondria), and fission and fusion events ratio (n=4637 tracks for basal RTT_P1 and P6, n=2765 tracks for LGZ-treated; for fission:fusion ratio n=8 basal mitochondria, n=7 LGZ-treated mitochondria). *(cont. next page)*

(from previous page)
Data expressed as (B, C) folds over basal from the same experiment and represented as box plot + individual values; in (E) represented as mean + SD for parametric data or median + interquartile range for non-parametric data. Comparative analysis Rett basal vs. treatment done with Welch's test for parametric, and Mann-Whitney for non-parametric data if two groups; Brown-Forsythe and Welch ANOVA tests for comparing 100 nM and 500 nM groups over basal. *P* value represents ****<0.0001.

Bioenergetic profile: mitochondrial ATP synthesis and ROS generation and metabolism

The bioenergetic deficiencies in Rett fibroblasts are characterized by a decrease in respiration rate and ATP synthesis –total and particularly mitochondrial– paired with an increase in ROS generation, in terms of $O_2^{\cdot-}$ accumulation, ultimately causing DNA oxidative damage. These deficiencies were homogeneous between the studied patients (RTT_P1-P4). Given that LGZ modulates mitochondrial biogenesis and function, we went to analyze if the treatment could correct the bioenergetic alterations described in Rett patients.

Using luciferin-luciferase bioluminescence analysis we detected that 100 nM LGZ treatment for 48 hours was able to correct the deficient mitochondrial ATP production in Rett fibroblasts (Fig. 20A), increasing ATP synthesis in a 56% compared to basal condition. In addition, MitoSOX™ fluorescence measured through flow cytometry (Fig. 20B) showed a 25% decrease in $O_2^{\cdot-}$ production for the 500 nM LGZ concentration over basal condition (Fig. 20C). Concerning ROS metabolism, LGZ treatment on Rett fibroblasts did not produce a significant change in antioxidant enzymes expression (Fig. 20D).

Regarding oxidative stress, we measured immunofluorescence intensity of the marker 8-OHdG in Rett fibroblasts in basal and treated conditions (Fig. 20E). Quantification of the fluorescence intensity revealed 25% and 26% decreases in DNA oxidative damage for both 100 nM and 500 nM LGZ, respectively, over basal condition in the patients (Fig. 20 F, G). Taken together, these results suggest an enhancement on mitochondrial energy production with a decrease in ROS generation and, therefore, an amelioration in the overall oxidative damage for Rett cells.

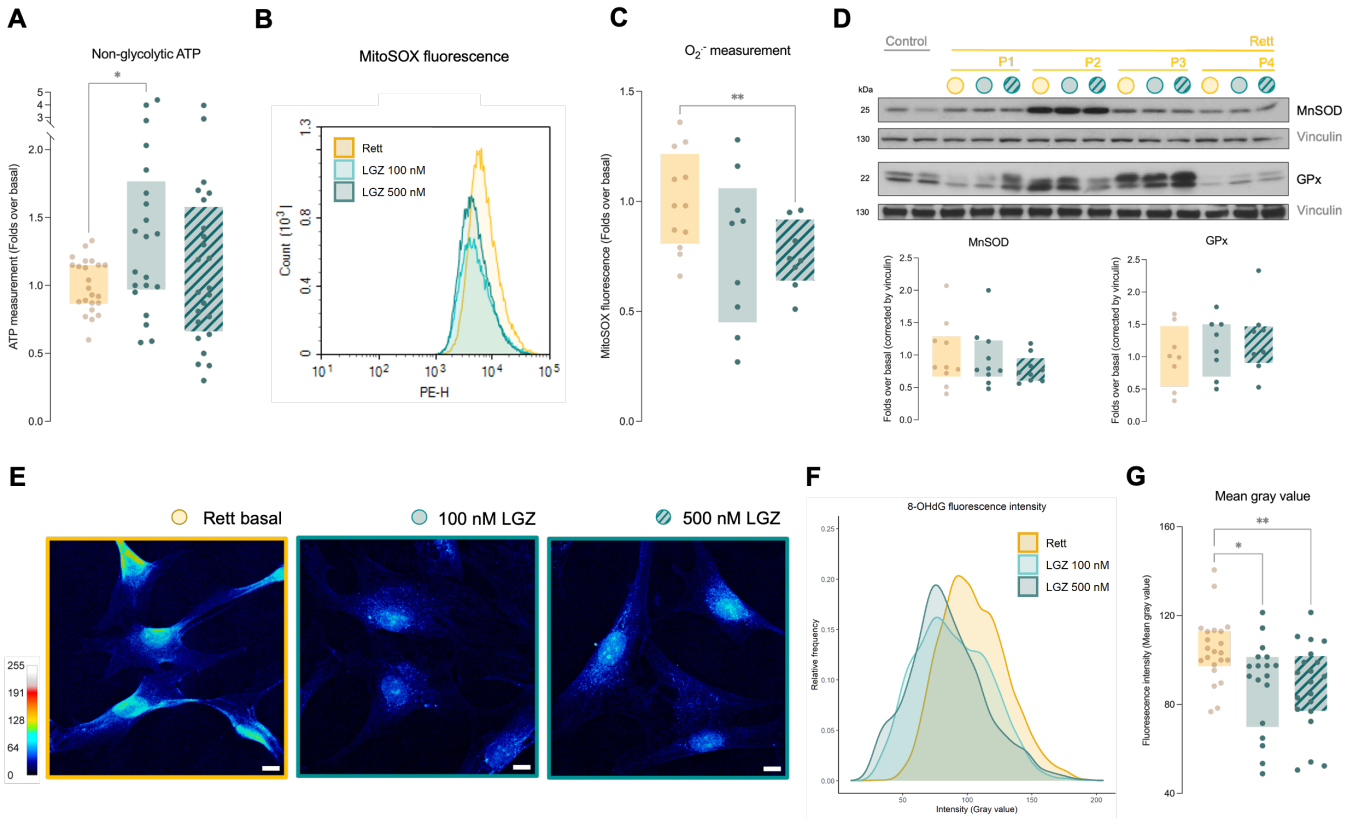

Figure 20. Evaluation of the bioenergetic profile in Rett fibroblasts after LGZ treatment: mitochondrial ATP synthesis and ROS metabolism. (A) Mitochondrial ATP production in Rett cells detected by luciferine-luciferase bioluminescence assay and expressed as folds over basal (n=3 experiments, triplicates from Rett patients RTT_P1-P3). (B) MitoSOX™ fluorescence visualization and (C) quantification of basal and treated Rett fibroblasts, detected by flow cytometry and expressed as folds over basal from the same experiment (n=2 experiments, triplicates from patients RTT_P2 and P3). (D) Representative image of antioxidant enzymes MnSOD and GPx expression detected by Western blot from two controls and patients RTT_P1-P4 and their densitometry quantification, corrected by vinculin and expressed as folds over basal (n=3-4 experiments, with a total of four controls and four patients). (E) Representative images of 8-OHdG IF in basal and treated conditions (LUT "royal" with calibration bar on the left side of the images, scale bar 10 µm). Fluorescence intensity quantification as (F) relative frequency of intensity values and (G) mean gray value (patients RTT_P1 and P6; n=23 basal cells, n=18 LGZ 100 nM cells, n=20 LGZ 500 nM cells).
Data represented as (A, C, D, G) box plot with individual values, (B) histogram of PE fluorescence of alive cells and (F) density plot of intensity values' relative frequency of basal, 100 nM LGZ and 500 nM LGZ Rett fibroblasts. Brown-Forsythe and Welch ANOVA test for parametric data and Kruskal-Wallis for non-parametric data, with multiple comparisons between 100 nM and 500 nM groups over basal. *P* value represents *<0.05, **<0.01.

2.3 Validation of leriglitazone effect on the PPARγ pathway with the inhibitor GW9662

LGZ treatment in Rett fibroblasts was able to correct the bioenergetic alterations in terms of mitochondrial ATP deficiency and increase in $O_2^{\cdot-}$ production. To confirm that these changes were a direct consequence of PPARγ pathway activation, we treated the cells with the PPARγ-signaling inhibitor GW9662 (Fig. 21A) at a concentration 1 µM for 72 hours. This molecule inhibits PPARγ by covalently modifying a specific cysteine residue in its ligand-binding domain, leading to irreversible inhibition of its activity, with minimal effects on other PPARs (Leesnitzer et al., 2002).

Mitochondrial ATP production, detected by bioluminescence, was evenly decreased when Rett fibroblasts were treated with either GW9662 or a combination of LGZ + GW9662 (50% and 54% decreases, respectively), which means that LGZ cannot recover ATP production in presence of the antagonist (Fig. 21B). Analogously, $O_2^{\cdot-}$ production, measured by flow cytometry, was not reduced after treatment with the antagonist nor LGZ + GW9662 (Fig. 21C). Therefore, pathway inhibition blocked the effect of LGZ regarding the observed measures and confirmed the beneficial effect of PPARγ pathway activation in the recovery of the bioenergetic deficits in Rett syndrome fibroblasts.

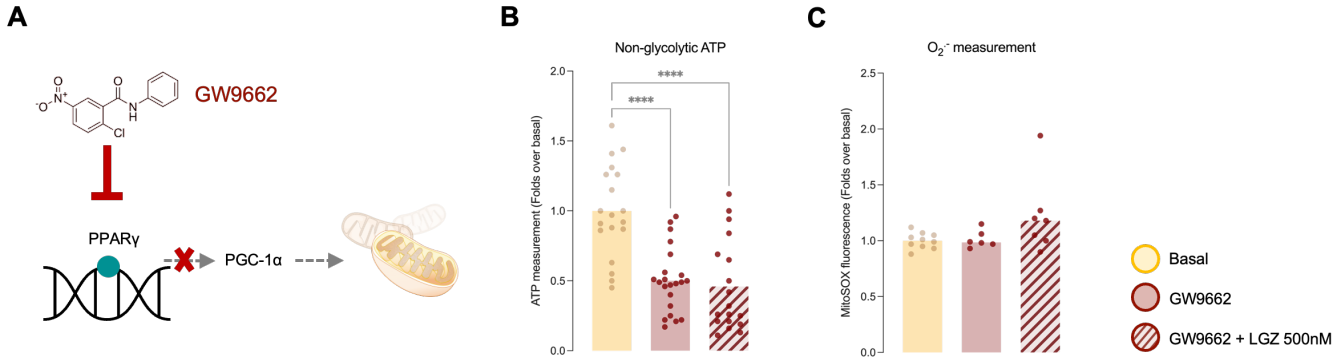

Figure 21. Appraisal of the effects of blocking the PPARγ pathway with GW9662 antagonist: ATP measurement and ROS generation. (A) Schematic representation of the inhibtion with GW9662. (B) Mitochondrial ATP production in Rett fibroblasts, detected by luciferin-luciferase bioluminiscence, after treatment with the PPARγ antagonist GW9662 at 1 µM for 72 hours, and a combination of GW9662 1 µM + LGZ 500 nM, expressed as folds over basal (n=2 experiments, 6 replicates from patients RTT_P1, P3 and P6). (C) Detection of $O_2^{\cdot-}$ generation by flow cytometry with MitoSOX™ Red probe, and quantification of GW9662 and GW9662 1 µM + LGZ 500 nM treated cells, expressed as folds over basal (n=2 experiments, 1-2 replicates from patients RTT_P1, P3 and P6).
Data represented as (B) mean for parametric or (C) median for non-parametric data, with individual values. Brown-Forsythe and Welch ANOVA test for parametric data and Kruskal-Wallis for non-parametric data, with multiple comparisons between GW9662 and GW9662+LGZ groups over basal. *P* value represents ****<0.0001.

2.4 Summary of mitochondrial performance and its modulation in patients' fibroblasts

For the *in vitro* analysis, we studied the mitochondrial homeostasis in fibroblasts from a total of eight different patients (as can be reviewed in Table 8 in Materials and Methods), and the potential effect of LGZ in the correction of the altered parameters. In Table 11, we summarize the mitochondrial alterations regarding mitochondrial structure and network and mitochondrial bioenergetics for the eight Rett patients (RTT_P1-P8), indicating which patient was used per technique and their response to LGZ treatment for 48 hours.

To recapitulate, the studied patients showed differences in mitochondrial network structure, discerning between two phenotypes: one milder (patients RTT_P1 and P3) and another more severe (patients RTT_P2 and P4). However, the alterations in ultrastructure and decreased fission dynamics were similar between the studied patients. In the same line, we detected a homogeneous profile in bioenergetic alterations, with decreases in mitochondrial respiration and ATP synthesis and increased oxidative stress, outstanding the deficiencies in patient P2.

Regarding mitochondrial homeostasis modulation with the PPARγ agonist LGZ, the treatment was able to recover the bioenergetic deficiencies in all the studied patients, in terms of mitochondrial ATP synthesis and oxidative stress. However, the treatment did not recover the dynamics alterations at the assayed time and concentrations, detecting only an increase in mitochondrial motility speed.

Table 11. Summary of *in vitro* results for the Rett patients studied per technique.

			RTT_P1	RTT_P2	RTT_P3	RTT_P4	RTT_P5	RTT_P6	RTT_P7, P8
Mitochondrial network structure and dynamics	Network	TOMM20 IF	↑ Indep. networks ratio ↑ ↓ MFF ↓ ↓ Mean branch length ↓ Branches per mito	↑ Indep. networks ratio ↓ ↓ MFF ↓ Branches per mito ↓ Mean branch length ↓ Mean branch diameter	↓ MFF ↓ ↓ Branches per mito ↓ Mean branch length	↑ Indep. networks ratio ↓ MFF ↓ Branches per mito ↓ Mean branch length ↓ Mean branch diameter			
	Ultrastructure	TEM		↑ Aspect ratio ↓ Cristae per mito ↓ Cristae legth ↑ Cristae width ↓ Angularity (≠ 90º) ↑ Electrodensity	↑ Aspect ratio ↓ Cristae legth ↑ Cristae width ↓ Angularity (≠ 90º)				
	Dynamics markers	WB	↓ Drp1, Fis1 ↓ OPA1 80:100	↓ Drp1, Fis1 ↓ OPA1 80:100	↓ Drp1, Fis1 ↓ OPA1 80:100	↓ Drp1, Fis1 ↓ OPA1 80:100	↓ Drp1, Fis1 ↓ OPA1 80:100	↓ Drp1, Fis1 ↓ OPA1 80:100	↓ Drp1, Fis1 ↓ OPA1 80:100
	Network dynamics	MitoTracker™ time-lapse imaging	↑ Directionality ↓ Median speed ↑ ↑ Bursting ↓ Fission:fusion rate					↑ Directionality ↓ Median speed ↑ ↑ Bursting ↓ Fission:fusion rate	
Mitochondrial bioenergetics	Respiration rate	Seahorse	↓ Basal respiration ↓ Rmax ↓ OSR	↓ Basal respiration ↓ Rmax ↓ OSR					
	ATP production	Bioluminescence assay	↓ Total ATP ↓ Mitochondrial ATP ↑	↓ Total ATP ↓ Mitochondrial ATP *(more severe)* ↑	↓ Total ATP ↓ Mitochondrial ATP ↑				
	ROS	MitoSOX™, WB	↑ Superoxide anion ↓	↑ Superoxide anion *(more severe)* ↓ ↑ MnSOD expression	↑ Superoxide anion ↓	↑ Superoxide anion ↓ ↓ GPx expression			
	Oxidative stress	8-OHdG IF	↑ Intensity ↓					↑ Intensity ↓	

3 Studies on animal models: female Rett mice for assessment of brain bioenergetic function, neuroinflammation and behavior

Encouraged by the alterations found in fibroblasts, and the bioenergetic correction with LGZ, we moved towards the analysis of mitochondrial homeostasis in the brain of a Rett animal model. We aimed to elucidate three aspects: (1) whether the dysfunction would be homogeneous through the different brain areas, (2) if such dysfunction was steady through neurodevelopment, and (3) whether it could be treated with leriglitazone. For that, we studied female mice from the Rett "Bird's model" (B6.129P2(C)-*Mecp2*$^{tm1.1Bird}$/J strain), as they are a validated model of the disease and recapitulate many elements of its phenotype (Ribeiro and MacDonald, 2020) and compared the results with C57BL/6J *wild-type* (*wt*) littermates.

First, to analyze mitochondrial performance and evaluate if alterations could be area-dependent, we analyzed three different brain areas separately: cortex, hippocampus, and cerebellum, as detailed in Figure 22. Interestingly, as patients do, female mice also go through an early normal or non-phenotypic phase, and only after a few months they develop the full Rett phenotype. Therefore, to bring neurodevelopment into the equation, we study differences at two developmental stages: pre-symptomatic (3 months old) and fully symptomatic (7 months old) in female mice. Finally, to evaluate LGZ effect in Rett mice, the drug was orally administered mixed with the diet at a 75 mg/kg/day dose from weaning and until analysis at the correspondent time point (7 m.o.). Its intake was controlled at sacrifice through quantification of leriglitazone concentration in plasma by LC–MS/MS.

We have defined the mitochondrial homeostasis in Rett mice based on three main readouts: (1) brain bioenergetic characterization, regarding ATP concentration and oxidative stress, which is assessed through lipid peroxidation; (2) neuroinflammatory component regarding cytokine production; and (3) phenotypic and behavioral evaluation.

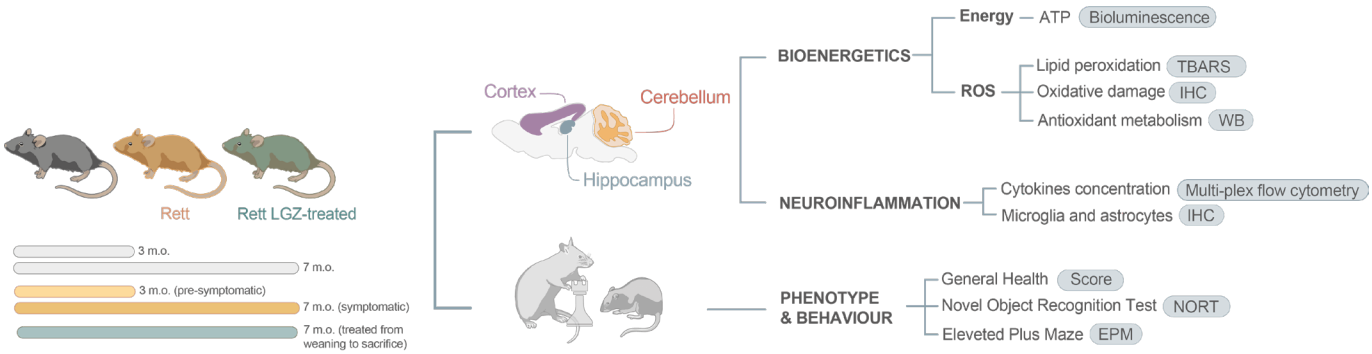

Figure 22. Evaluation of Rett mice on brain bioenergetic function, neuroinflammation and phenotype. Schematic representation of the different brain areas and their color code: cortex in purple, hippocampus in blue, and cerebellum in orange; and the studied groups *wild-type* and Rett mice at two time points (3 m.o. and 7 m.o.) and LGZ treatment (continued treatment from weaning until sacrifice at 7 months). TBARS = Thiobarbituric acid-reactive substance; IHC = immunohistochemistry; WB = Western blot.

3.1 Bioenergetic characterization: ATP concentration and oxidative stress

Basal: pre-symptomatic and symptomatic mice

In the previous analyses in Rett fibroblasts we detected a decrease in total and mitochondrial ATP, together with an increase in $O_2^{\cdot-}$ generation and consequent oxidative stress damage. Based on that, we analyzed in Rett mice brains the ATP concentration by luciferin-luciferase bioluminescence, and oxidative stress by TBARS assay detecting the by-product of lipid peroxidation malondialdehyde (MDA). As mentioned, we differentiated between brain areas (cortex, hippocampus and cerebellum) and between two disease stages: the pre-symptomatic phase was defined at 3 m.o. and the symptomatic phase at 7 m.o.

We detected alterations in ATP concentration already in pre-symptomatic mice (Fig. 23A), which were brain area-specific: ATP concentration in Rett cerebellums was 17% decreased over *wt*, which was within control values in cortex and hippocampus samples. Lipid peroxidation, which is the oxidative degradation of lipids, displayed differences as well. We observed a significant 35% decrease in pre-symptomatic Rett cortex samples compared to *wt*, along with non-significant changes in hippocampus and cerebellum.

As expected, the variations in these two parameters were more evident when we moved into symptomatic 7 months-old mice brains (Fig. 23B). The observed reduction in ATP concentration in cerebellum of pre-symptomatic mice was continued in the symptomatic ones at a 32% compared to same-aged *wt*. At this stage, a reduction of 36% in hippocampus ATP concentration was also evident in symptomatic Rett mice. Opposite to that, a 15% increase

in ATP concentration was detected in Rett cortex compared to *wt*. Concerning lipid peroxidation in symptomatic mice, we detected decreases in lipid peroxidation of 50% in hippocampus and 30% in cerebellum, contrary to a significant 40% increase observed in Rett cortex. These results suggest that alterations are dynamic both between brain areas and through neurodevelopment.

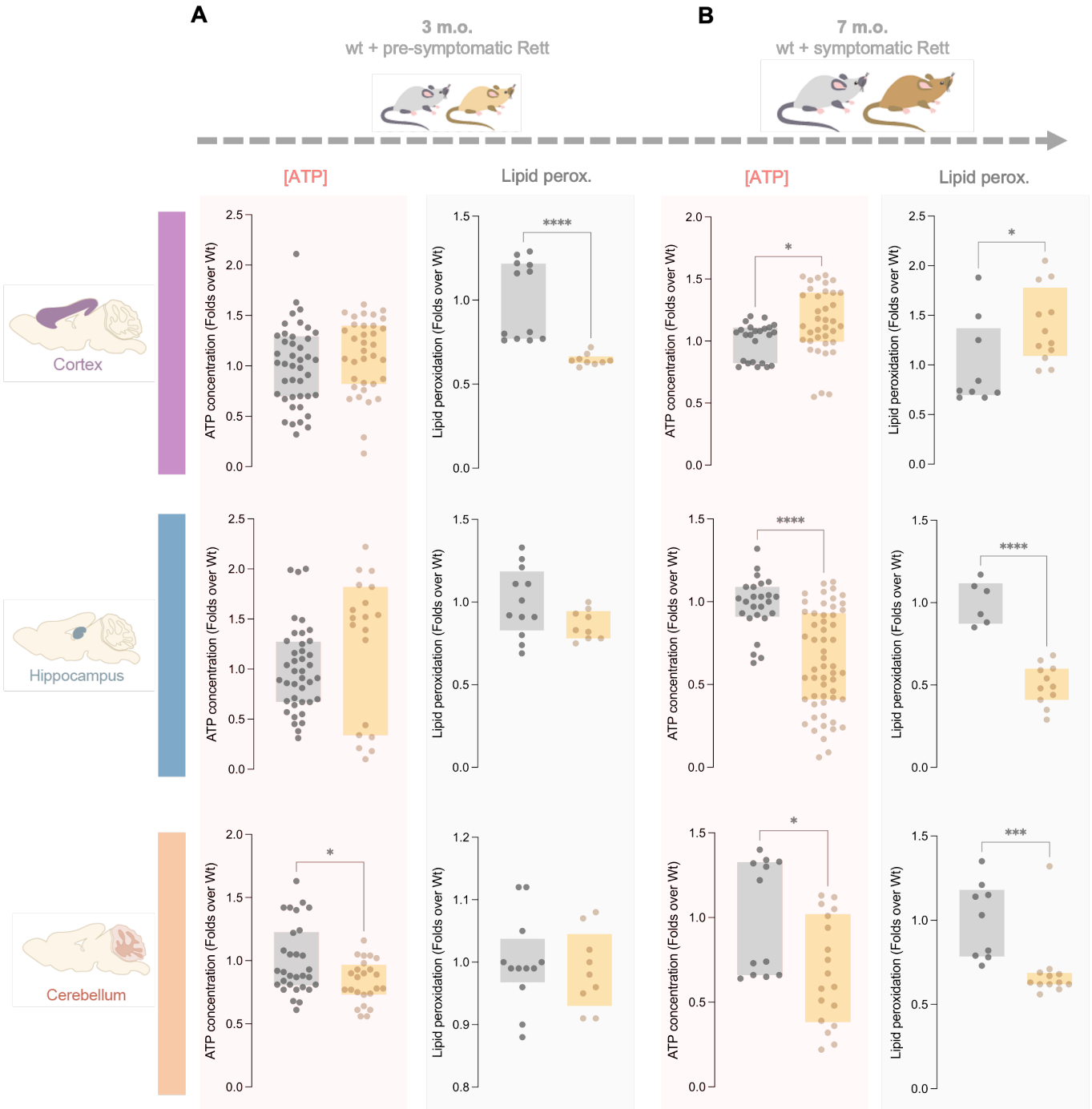

Figure 23. Bioenergetic characterization of pre-symptomatic (3 m.o.) and symptomatic (7 m.o.) Rett mice: ATP concentration and lipid peroxidation. Analyses of ATP concentration (detected by luciferin-luciferase bioluminescence assay) and lipid peroxidation (detected by TBARS assay) were performed in three brain areas – cortex, hippocampus and cerebellum – at two time points: (A) at 3 months old, when Rett mice are considered pre-symptomatic and (B) at 7 months old, when they are fully symptomatic (n=4 experiments for ATP, n=1 experiment for lipid peroxidation, from minimum three mice per group, with technical triplicates).
Data are expressed as folds over wild-type and represented as box plots with individual values. Comparative analysis done with Welch's test for parametric data and Mann-Whitney for non-parametric data. *P* value represents *<0.05, ***<0.001, ****<0.0001.

To understand whether brain ATP concentration was variable through development, we compared the observed changes between both timepoints, setting the measurement of *wt* at 3 months as the baseline, and maintaining the distinction between brain areas. In *wt* mice, ATP concentration was significantly increased at 7 months in 1.3 folds for cortex (Fig. 24A) and 1.9 folds for hippocampus (Fig. 24B). Rett mice did not show statistically significant variations in any of both areas. Whereas in cerebellum (Fig. 24C), ATP was decreased in older mice both for *wt* (80%) and Rett (84%). In summary, these results hallmark the time-sensitiveness and area-dependence of bioenergetic features in the pathophysiology of Rett syndrome.

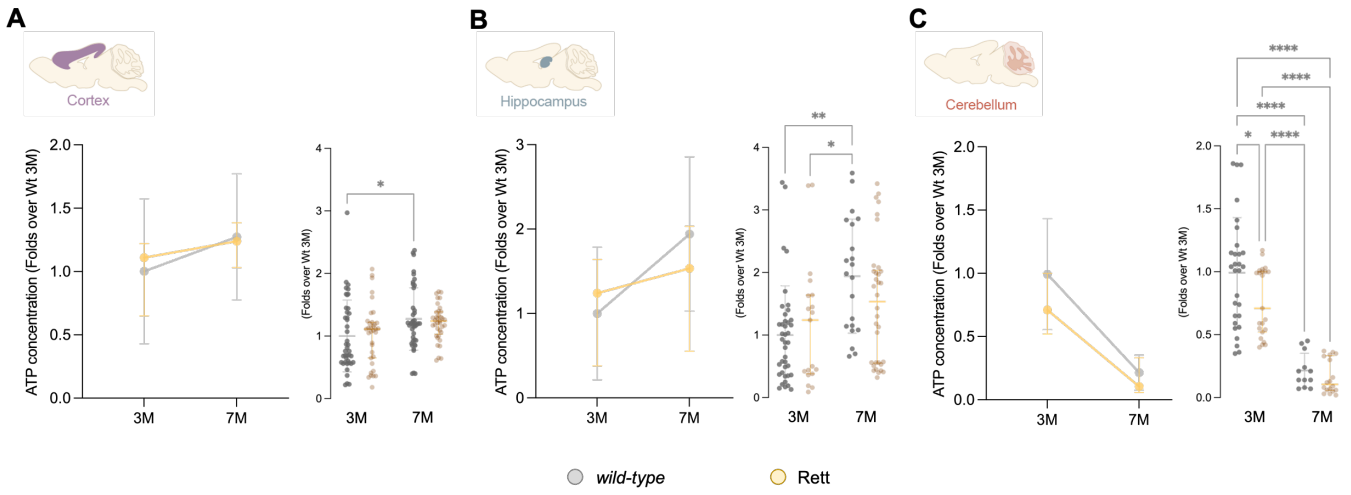

Figure 24. Assessment of ATP concentration fluctuations over time. ATP concentrations have been compared between both time points in the three different areas: (A) cortex, (B) hippocampus and (C) cerebellum, expressed as folds over *wt* 3 m.o. (n=4 experiments, minimum three mice per group, with technical triplicates. Data represented as mean ± SD and a line connecting the 3 m.o. and 7 m.o. groups (left graph) or individual values (right graph). Two-way ANOVA test, with post-hoc Tukey multiple comparisons correction. *P* value represents *<0.05, **<0.01, ****<0.0001. 3M = 3 months old; 7M = 7 months old.

Effect of leriglitazone treatment on bioenergetics

Encouraged by the positive results of LGZ treatment observed in fibroblasts (correction of bioenergetic deficiencies by increasing mitochondrial ATP production and ameliorating the oxidative stress), we studied the potential LGZ effect in the animal model regarding the bioenergetic parameters ATP and lipid peroxidation. Animals were treated from weaning until sacrifice at 7 months old at a dose of 75/mg/kg/day, orally provided through diet. At the moment of sacrifice, plasma was obtained and LGZ concentration was measured by LC-MS/MS, detecting a value of 2.49 ± 0.44 µg/mL.

We analyzed the effect on the different studied brain areas. While leriglitazone did not correct the ATP and lipid peroxidation increases found in 7 m.o. cortex (Fig. 25A), differences upon treatment were observed in hippocampus and cerebellum, in which both ATP concentration and lipid peroxidation were decreased. LGZ treatment increased ATP concentration in 1.45 folds and lipid peroxidation in 1.26 folds in hippocampus (Fig. 25B), together with increases of 2.38 folds for [ATP] and 1.37 folds for lipid peroxidation in cerebellum (Fig. 25C) compared to non-treated Rett mice.

To delve into the oxidative stress, we measured oxidative damage through the quantification of 8-OHdG fluorescence in 7 m.o. mice in hippocampus and cerebellum (Fig. 25D, E). Fluorescence intensity analysis showed a significant 16% decrease in the dentate gyrus of hippocampus from symptomatic mice, that was recovered with LGZ, with an increase of 11% over non-treated mice (Fig. 25F). Interestingly, Rett mice cerebellum showed an increase of 10% in 8-OHdG intensity levels compared to *wt*, that were within control values in LGZ-treated mice with a recovery of 19% over basal group (Fig. 25G). In this context, hippocampus maintained the decrease in oxidative stress detected previously as lipid peroxidation alteration and was corrected in the treated group, whereas cerebellum showed an opposite profile with an increase in oxidative stress and correction with LGZ.

To deepen the analysis of the effect of LGZ in the management of oxidative stress, we analyzed the expression of the ROS-metabolizing enzymes MnSOD and GPx in 7 m.o. LGZ-treated Rett mice by Western blot (Fig. 25H). Quantitative two-way ANOVA analysis (Fig. 25I) showed a significant 1.2-fold increase in GPx expression in cortex of symptomatic mice (p=0.034), which was not corrected in the treated group. In hippocampus, we did not detect any significant changes in the enzymes' expression for the studied groups. On the contrary, as happened in the ATP concentration and lipid peroxidation corrections, the most significant LGZ effect was a 30% and 38% decrease in both MnSOD and GPx expression, respectively, in cerebellum. Therefore, these results outstand cerebellum not only as one of the most affected areas regarding bioenergetic functions but also as one of the most LGZ-respondent areas in Rett animal models.

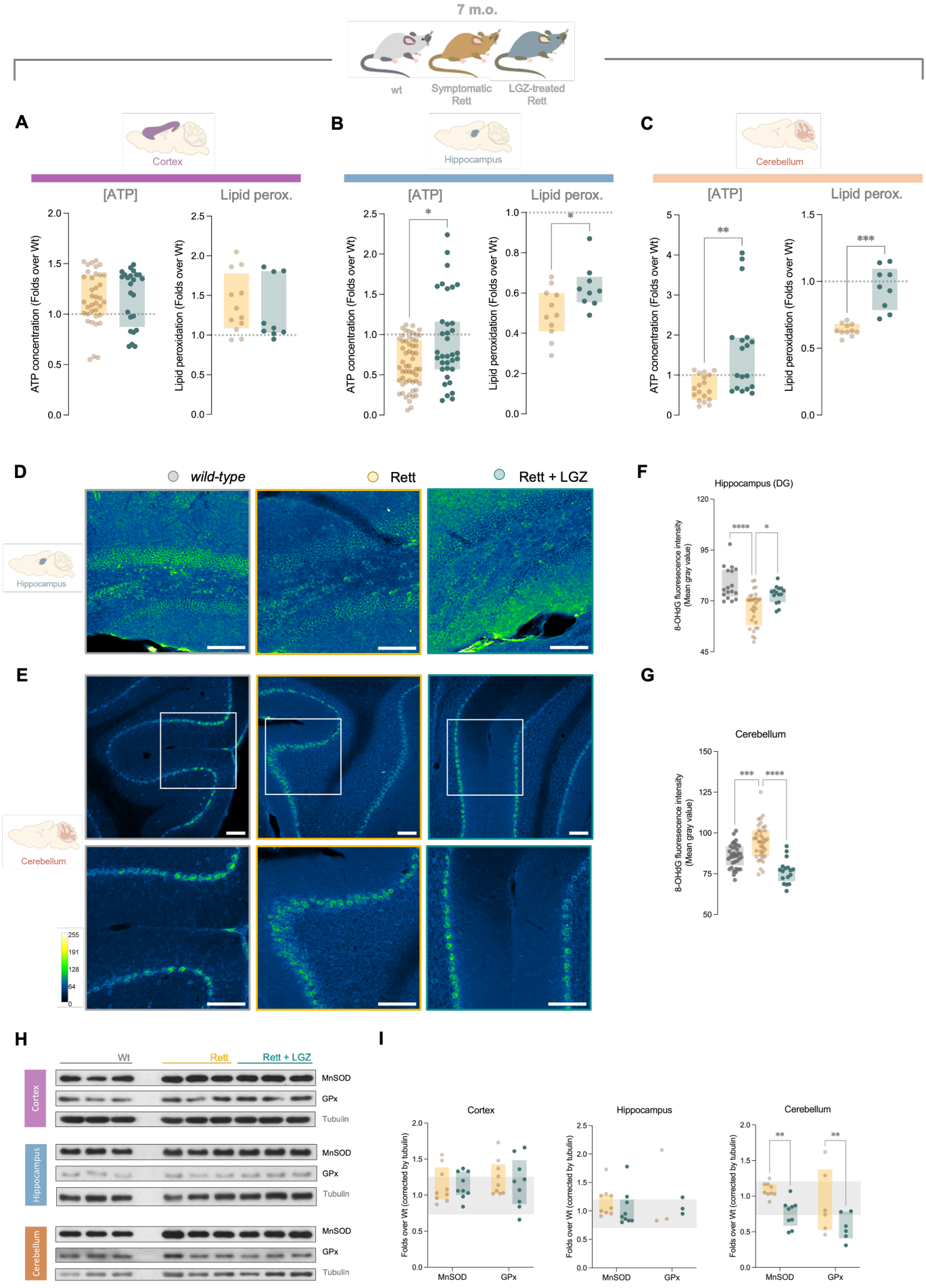

Figure 25. Analysis of LGZ effect on the bioenergetic component in the brain areas: ATP concentration and oxidative stress evaluation on lipid peroxidation, oxidative damage and antioxidant metabolism.
(cont. previous page)

(from previous page)
Figure 25. Analysis of LGZ effect on the bioenergetic component in the brain areas: ATP concentration and oxidative stress evaluation on lipid peroxidation, oxidative damage and antioxidant metabolism. Both ATP concentration (detected by bioluminescence) and lipid peroxidation (detected by TBARS) were assayed in untreated and LGZ-treated Rett mice in (A) cortex, (B) hippocampus and (C) cerebellum, expressed as folds over *wt* from the same experiment (n=4 experiments for ATP, n=1 experiment for lipid peroxidation, from minimum three mice per group, with technical triplicates). Detection of the oxidative damage marker 8-OHdG in (D) hippocampus and (E) cerebellum by immunofluorescence (8-OHdG marker is shown with the intensity-revealing LUT "Green Fire Blue"; scale bar represents 100 µm). Quantification of the fluorescence intensity in (F) hippocampal dentate gyrus and (G) Purkinje cells in cerebellum, expressed as mean gray value (in hippocampus: n=17 *wt* cells, n=29 Rett cells, n=15 Rett+LGZ cells; in cerebellum: n=37 *wt* cells, n=37 Rett cells, n=17 Rett+LGZ cells). (H) Representative images of antioxidant markers MnSOD and GPx expression in cortex, hippocampus, and cerebellum detected by Western blot, and (I) their respective densitometry quantification, corrected by tubulin and expressed as folds over *wt*; each lane represents a different mouse (n= 1-3 experiments with three mice per group).
Data represented as box plot with individual values; in (A-C) dashed line shows value 1 on y-axis, and in (I) grey shade delimits highest and lowest value for *wt*, as a reference of fold-change over wt. Comparative analysis for two groups done with Welch's test for parametric, and Mann-Whitney for non-parametric data; when more than two groups, Brown-Forsythe and Welch ANOVA test for parametric data and Kruskal-Wallis for non-parametric data, with multiple comparisons between *wt vs*. Rett and Rett *vs*. Rett+LGZ; if two variables, two-way ANOVA analysis with multiple comparisons between the groups. *P* value represents *<0.05, **<0.01, ***<0.001, ****<0.0001.

3.2 Neuroinflammatory component

Previous reports have suggested increased inflammatory signaling in Rett syndrome, detected in peripheral tissues of both Rett animal models and patient samples, and a neuroinflammatory component that may contribute to the pathophysiology of the disease. To broaden the knowledge on this neuroinflammatory component, we performed a cytokine detection panel in the three brain areas and at the two disease stages –pre-symptomatic and symptomatic– compared to age-matched controls. Since PPARγ pathway activation has an anti-inflammatory effect via NF-κB modulation, we investigated the possible regulation of LGZ on neuroinflammation in the treated mice.

Basal: pre-symptomatic and symptomatic mice

To characterize the role of inflammation through neurodevelopment we used a panel of thirteen cytokines: the broadly considered pro-inflammatory cytokines IL-1α, IL-1β, IL-6, IL-12p70, IL-23, IL-17A, MCP-1, TNF-α, IFN-γ and GM-CSF, and the anti-inflammatory (or regulatory) cytokines IL-10, IL-27 and IFN-β. The cytokine expression in each brain area was detected by flow cytometry using an immunoassay based on bead-fluorescence detection.

Analysis of the pre-symptomatic mice (Fig. 26A) revealed no differences in the inflammatory profile in cortex, which only had a significant 32% decrease in IL-1α expression compared to *wt* group. Similarly, hippocampus did not show any significant changes in cytokine expression, whereas cerebellum displayed a pro-inflammatory profile, as all the measured cytokines were significantly increased in average 1.6 folds over the wild types.

When we moved to the symptomatic mice (Fig. 26B), we observed that the inflammatory profile was modified. While in the pre-symptomatic cortex we did not detect significant changes, symptomatic mice showed average 1.4-fold significant increases in several cytokines (IFN-β, IFN-γ, IL-10, IL-27, IL-17A, MCP-1 and TNF-α) compared to 7 m.o. *wt* mice. In addition, hippocampus showed significant 47% and 30% decreases in expression of cytokines IL-1α and TNF-α respectively, and a 2.4-fold increase in IFN-β expression. Symptomatic cerebellum, which in the prodromal stage showed an increased expression in all the detected cytokines, only had a decreased expression of the pro-inflammatory cytokine IL-1α compared to *wt* mice. Therefore, the inflammatory profile varies between brain areas and through neurodevelopment, underlining the pro-inflammatory environment in cerebellum from pre-symptomatic mice, in which we also detected bioenergetic deficiencies, and the cortex of symptomatic mice.

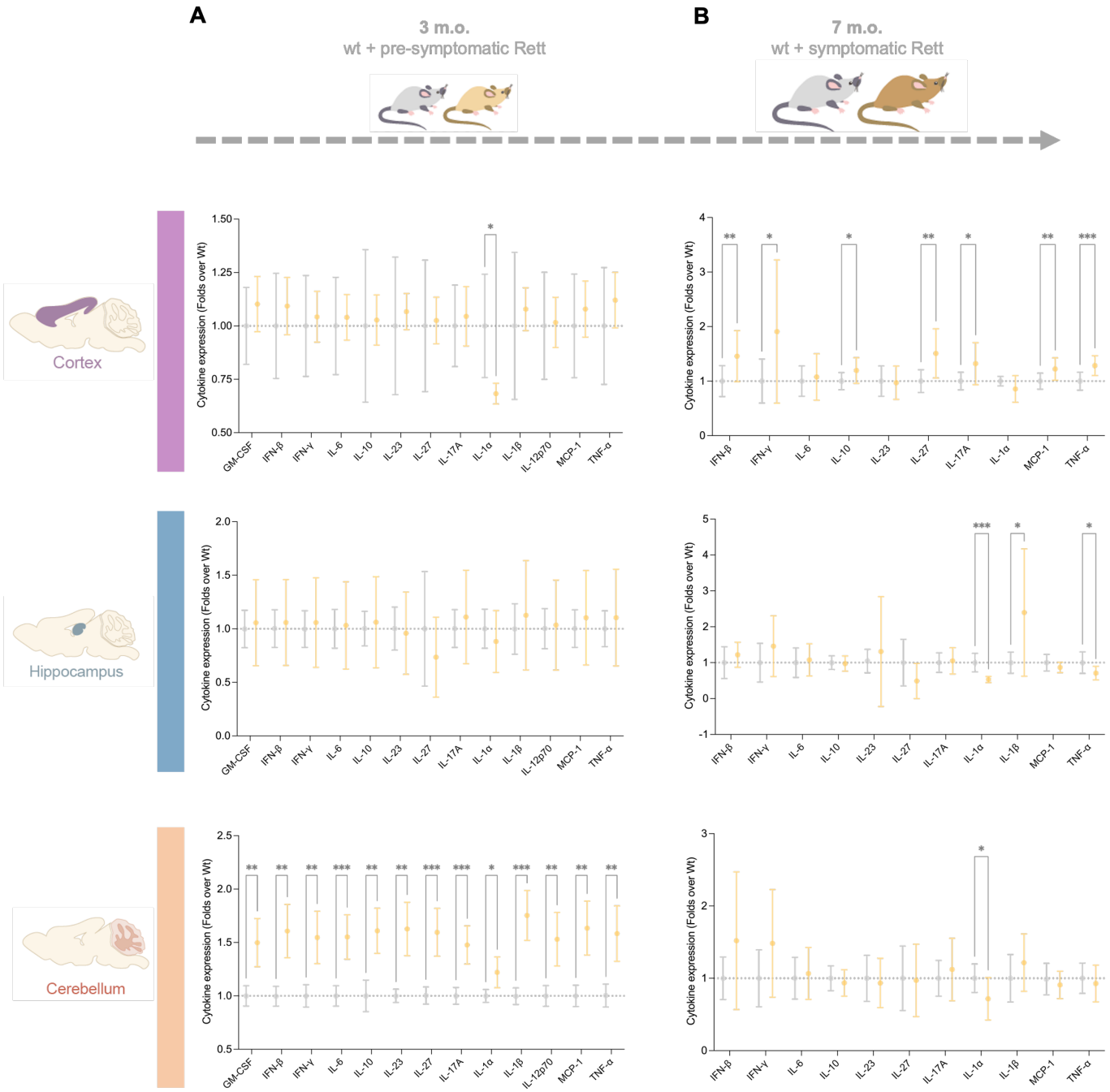

Figure 26. Cytokine profile of the three brain areas (cortex, hippocampus and cerebellum) at pre-symptomatic and symptomatic stages of the disease. Measurement of 13 cytokines expression (IL-1α, IL-1β, IL-6, IL-10, IL-12p70, IL-23, IL-27, IFN-β, IL-17A, MCP-1, TNF-α, IFN-γ and GM-CSF) by flow cytometry using an immunoassay based on bead-fluorescence detection. Grouped representation of the cytokine panel for (A) pre-symptomatic mice at 3 m.o. and (B) post-symptomatic mice at 7 m.o., with data expressed as folds over *wt* (n=1 experiment, three mice per group and technical duplicates).
Data represented as mean ± SD, and line at y=1 as reference for *wt* mean. Group comparison analysis was performed with unpaired T test with Welch's correction. *P* value represents *<0.05, **<0.01, ***<0.001.

Effect of leriglitazone treatment in the inflammatory profile

After describing the developmental differences in inflammation through the different brain areas, we wanted to assay if the continued LGZ treatment was able to prevent the pro-inflammatory status in cortex. In this context, LGZ-treated group showed average 0.57-fold decreased expression in the detected cytokines (IFN-β, IFN-γ, IL-6, IL-10, IL-23, IL-27, IL-17A, IL-1α and MCP-1) compared to non-treated 7 m.o. Rett mice (Fig. 27A). In hippocampus, we detected significant increases of 1.6 folds for IL-17A and 1.7 folds for IL-1β (Fig. 27B), without corrections in the other altered cytokines (IL-1α and TNF-α). In symptomatic cerebellum, we did not detect any significant changes in LGZ-treated mice compared to non-treated group (Fig. 27C). These results suggest that there is a correction in the neuroinflammatory component in cortex of symptomatic Rett mice.

To complement the analysis on the inflammatory status in symptomatic cortex, we evaluated the presence of microglia and mature astrocytes by immunohistochemistry with the markers Iba1 (Fig. 27D) and GFAP (Fig. 27F),

respectively. Quantitative analysis showed an increase of 21% Iba1-positive cells in Rett mice cortex compared to 7 m.o. *wt* mice (Fig. 27E), which was decreased 13% in the treated group respect to basal condition. In the same line, GFAP-positive cells were increased in 35% over *wt*, and its number was decreased with the treatment in 45% compared to the basal group. These results ratify the neuroinflammatory component in cortex of symptomatic Rett mice, which can be significantly corrected with LGZ treatment.

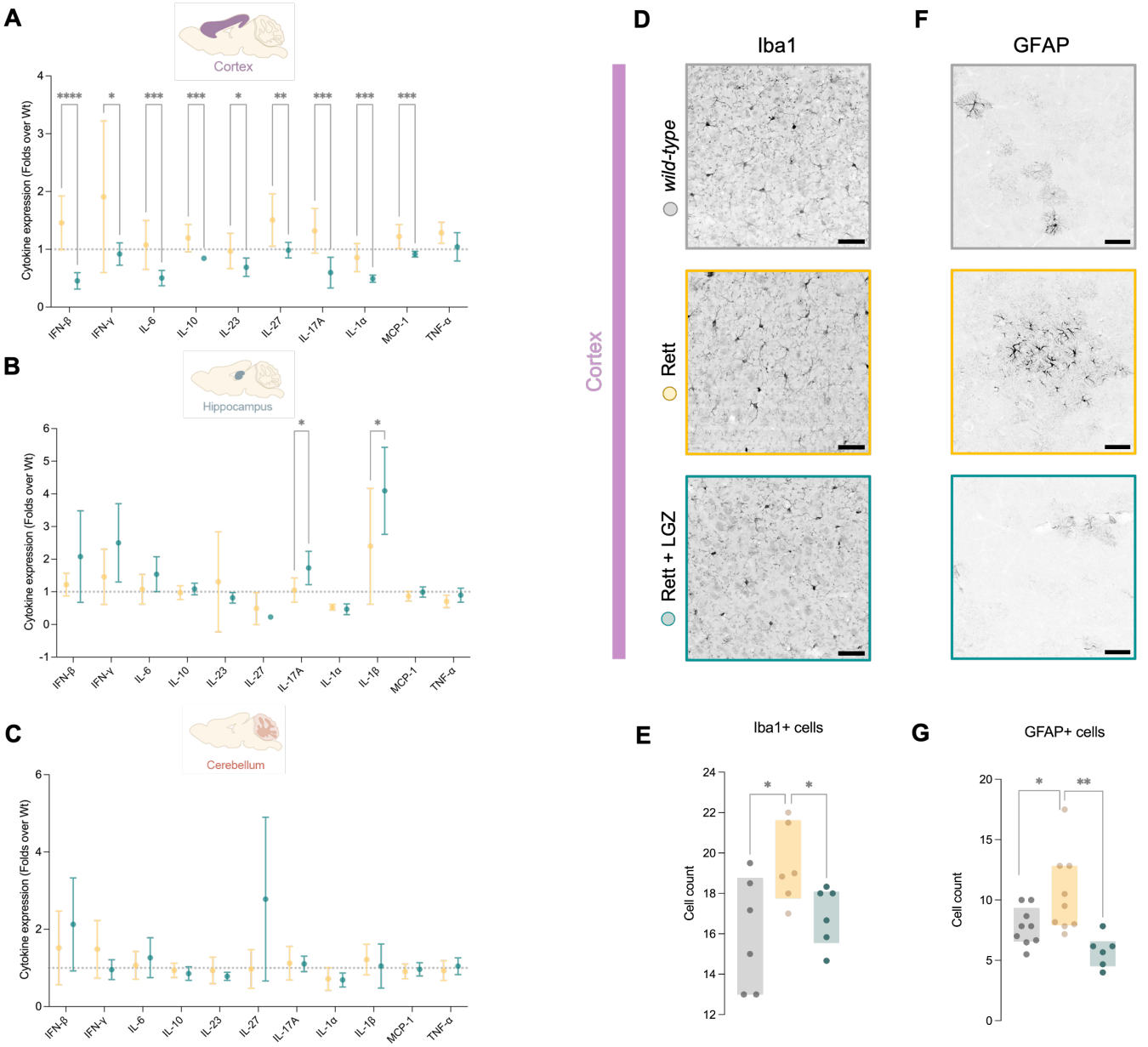

Figure 27. Assessment of LGZ effect on the neuroinflammatory component in symptomatic Rett mice, differentiating between the three studied brain areas. Cytokine panel detection by flow cytometry based on bead immunofluorescence in LGZ-treated and non-treated symptomatic Rett mice in (A) cortex, (B) hippocampus and (C) cerebellum, expressed as folds over *wt* (n=1 experiment, three mice per group with technical duplicates). Representative IF images of markers (D) Iba1 for microglia and (F) GFAP for mature astrocytes in cortex of 7 m.o. mice (cells shown in grey; scale bar 50 µm). Quantification of number of (E) Iba1-positive cells and (G) GFAP-positive cells (n=2 mice per group, 3 slices each).
Data represented as (A-C) mean ± SD, with line at y=1 as reference for *wt* mean; and (E, G) box plot and individual values. Group comparison analysis was performed with unpaired T test with Welch's correction for LGZ-treated mice over non-treated; and Brown-Forsythe and Welch ANOVA test for parametric data for *wt vs*. Rett and Rett *vs*. Rett-LGZ comparisons. *P* value represents *<0.05, **<0.01, ***<0.001.

3.3 Phenotypic outcome and behavior analysis

Rett "Bird's model" (B6.129P2(C)-*Mecp2*$^{tm1.1Bird}$/J strain) recapitulate many elements of the disease. As in humans, Rett phenotype displays sex differences in mice. Female mice recapitulate the neurodevelopmental regression, showing an apparently normal early development and being fully symptomatic around 6-7 months old. While they are more phenotypically variable because of the cellular mosaicism due to X-inactivation, the symptomatic phenotype often includes low exploratory activity, breathing abnormalities, hindlimb clasping and weight gain.

Therefore, the translational value of female mice as a pre-clinical model is considered higher, along with fulfilling sex perspective research.

To assess the ultimate effect of LGZ as a potential drug for the treatment of Rett syndrome, we studied its effect on Rett mice phenotype correction through the General Health Score, a scale that evaluates the most relevant features in Rett mice such as mobility, breathing abnormalities, tremor or physical deterioration. In addition, to understand whether the effect of LGZ at a biochemical level has an impact on cognitive behavior, we assayed two behavioral tests: novel object recognition test (NORT) to evaluate the discrimination between objects as a measure of cognitive and explorative behavior, and elevated plus maze (EPM) test to consider possible anxiolytic effects for LGZ on Rett mice.

When Rett female mice start developing the symptomatology, they are primarily characterized by increased weight and gait and motor abnormalities because of hindlimb clasping (Fig. 28A). We detected an average 8g weight increase in Rett symptomatic mice compared to *wt* (Fig. 28B). One of the possible secondary effects of LGZ is an increase in weight, but treated Rett mice showed no differences compared to non-treated ones. Interestingly, general health evaluation from 3 m.o. already indicated increased scores for Rett mice compared to *wt* (Fig. 28C). LGZ effectively ameliorated the overall health status in the treated mice, since they developed a milder form of the disease, quantified with lower score values. This difference was evident from the beginning of the assessment (12 weeks) and especially significant in fully symptomatic mice at 7 m.o. scoring 2.3 points compared to the 4.1 in non-treated mice (Fig. 28D).

Regarding behavioral tests, we did not detect significant changes in discrimination between new and old objects for NORT in both pre-symptomatic and symptomatic Rett mice compared to age-paired *wt* (Fig. 28E). However, in symptomatic mice we detected a significant 14% decrease in total exploration time, that is, time exploring the objects without distinction between new and old objects. 7 m.o. LGZ-treated mice increased in 20% the exploring time compared to non-treated symptomatic mice, suggesting an enhanced explorative behavior (Fig. 28F). EPM test did not show any significant differences for both evolutionary stages in Rett mice (Fig. 28G) and no significant differences in LGZ-treated group (Fig. 28H), showing no changes for anxiety-like behavior in Rett mice. In this regard, continued LGZ treatment from weaning can effectively ameliorate the phenotypic outcome in Rett mice, together with improvements in explorative behavior and without apparent secondary effects.

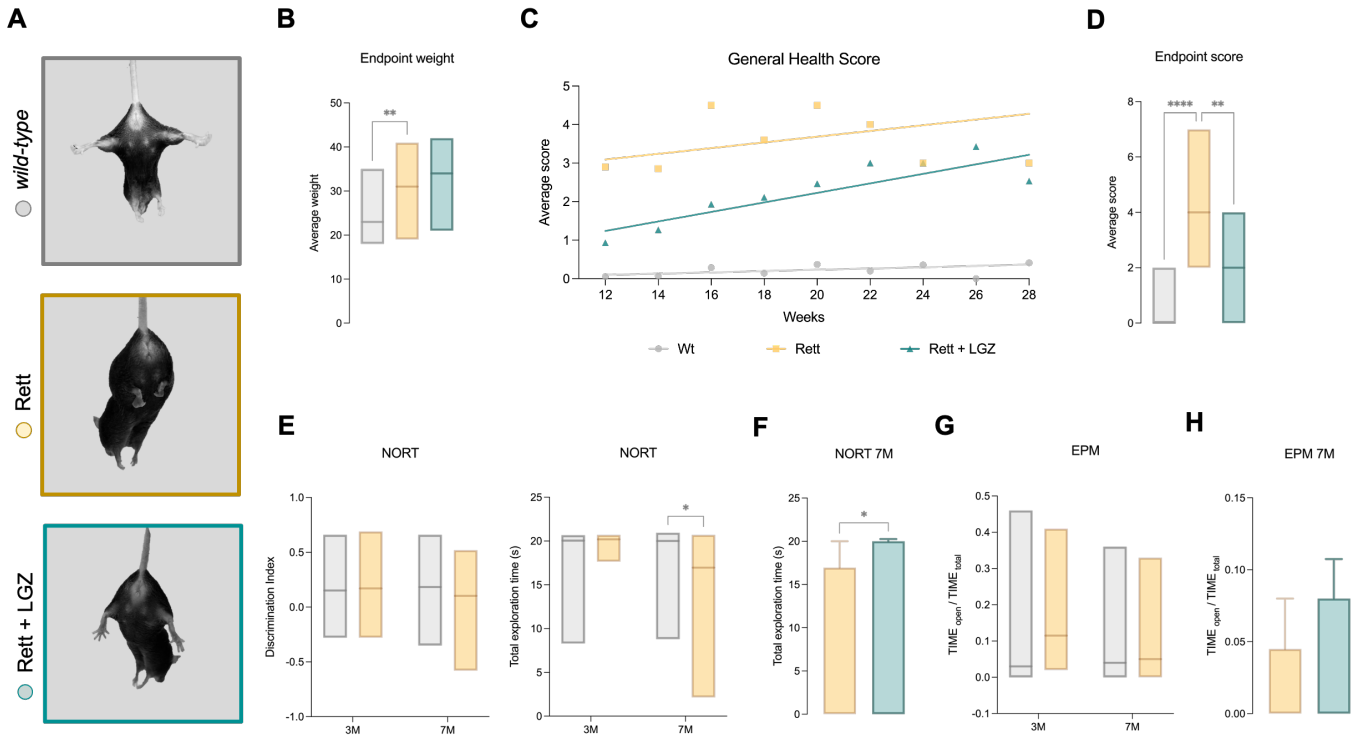

Figure 28. Phenotypical characterization of Rett female mice: general health status and behavioral assessment. (A) Representative pictures from wild-type, Rett and LGZ-treated Rett mice at 7 m.o. (B) Weight measurement for the three groups at endpoint (7M) (n=21 wt, n=10 Rett, n=15 Rett+LGZ). General Health Score (GHS) evaluated the following parameters: gait, mobility, breathing, hind limb clasping, tremors, general condition, kyphosis, fur and seizures. GHS measured (C) from 3 m.o. (12 weeks) until sacrifice at 7 m.o. (28 weeks), with evaluations every two weeks, and (D) GHS score at endpoint (7 m.o.) (n=21 wt, n=10 Rett, n=15 Rett+LGZ). (E) Novel object recognition test (NORT) measurements as discrimination index (time spent exploring the new object minus time with the old object, divided by total time) and total exploration time in seconds for both objects, at pre-symptomatic (3M) and symptomatic stages (7M), compared to age-paired controls (n=10-25 mice per group). (G) Elevated plus maze (EPM) measurements expressed as time spent on open arms over total time, at 3 m.o. and 7 m.o. (n=10-25 mice per group). (F, H) NORT total exploration time and EPM measurements for non-treated and treated symptomatic Rett mice (n=8-24 mice per group). *(cont. next page)*

(from previous page)
Data represented as (A, D, E, F) floating bars from min. to max. values with line at mean if data were parametric, or line at median if data were non-parametric; (C) simple linear regression with symbols showing average for each time point, or (G) column with median and interquartile range. Kruskal-Wallis for multiple comparisons between *wt vs.* Rett and Rett *vs.* Rett+LGZ groups; two-way ANOVA analysis with multiple comparisons between *wt* and Rett at the two time points (3M and 7M); Mann-Whitney for non-parametric data when comparing two groups (Rett *vs.* Rett+LGZ). *P* value represents *<0.05, **<0.01, ****<0.0001.

3.4 Additional results: neuronal markers expression

One of the hallmarks of Rett syndrome is the imbalance in glutamatergic/GABAergic neurotransmission, together with alteration in neuronal maturation. These alterations are responsible for many of the neurological symptoms, including stereotypies, motor coordination deficiencies, breathing abnormalities, seizures, and learning dysfunctions (Li, 2022). In particular, seizures occur in 80% of Rett patients and are associated with age and clinical severity (Jian et al., 2007). We analyzed by Western blot the expression of the neuronal markers (1) cFos, a proto-oncogene considered as a marker for neuronal activity, (2) NeuN (neuronal nuclei protein), a marker for neuron differentiation and therefore it identifies mature neurons, and (3) DCX (doublecortin), a microtubule-associated protein required for initial steps of neuronal dispersion, used as a marker of immature neurons.

In pre-symptomatic mice (Fig. 29A), cFos expression is significantly increased 1.2 folds in cortex and 1.7 folds in hippocampus, compared to 3 m.o. *wt* mice. Prodromic cortex also shows decreases of 27% in NeuN expression and 70% in DCX compared to *wt*. We did not detect significant changes in hippocampus for NeuN and DCX, nor in cerebellum for cFos and NeuN, while we could not measure DCX. Therefore, in presymptomatic mice we report less neurons, both mature and immature, but with increased activity in cortex and hippocampus.

In symptomatic mice (Fig. 29B), the increase in cFos in cortex and hippocampus is maintained: 1.4 folds in cortex and 1.6 folds in hippocampus. In addition, we detect a non-significant increase of 1.2 folds in cerebellum. However, the LGZ treated group does not show differences in expression of this marker for the three brain areas. Regarding the mature neuron marker NeuN, we detect an increased expression of 1.5 folds in cortex and 1.7 folds in cerebellum, with no significant differences for hippocampus. This increase is corrected in the LGZ-treated group with a decrease of 37% for cortex and 30% for cerebellum. We did not detect significant changes in expression for the immature neuron marker DCX, both for basal and LGZ conditions in symptomatic brains. Overall, these results suggest that cFos increased expression is maintained through development in the different brain areas, while NeuN and DCX change through time. Prolonged LGZ treatment from weaning can correct the abnormal expression of mature neurons in symptomatic cortex and cerebellum.

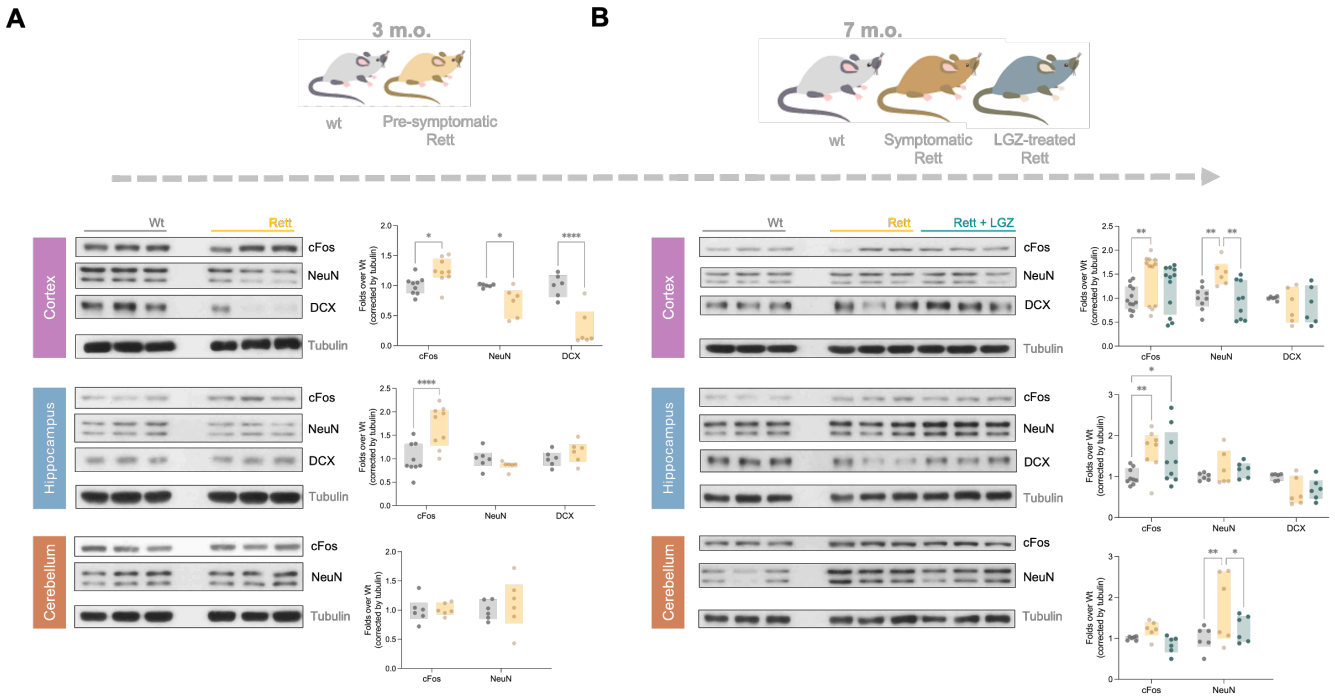

Figure 29. Neuronal markers (cFos, NeuN and DCX) expression in pre-symptomatic and symptomatic brain areas, in basal and LGZ-treated Rett mice. Representative images of the neuronal markers expression detected by Western blot in (A) pre-symptomatic Rett mice in basal conditions and (B) symptomatic Rett mice in basal and treated conditions, together with their densitometry quantifications corrected by tubulin. Each lane represents a different mouse (n=2-3 experiments, with three mice per group).
Data represented as box plot and individual values. Two-way ANOVA with multiple comparisons between *wt vs.* Rett, and Rett *vs.* Rett+LGZ for each area. *P* value represents *<0.05, **<0.01, ****<0.0001.

3.5 Summary of mitochondrial homeostasis alterations in Rett mice and their modulation with leriglitazone

In Table 12, we recapitulate the findings in the female mouse model of Rett syndrome and the corrections in the LGZ-treated groups, at the two developmental stages (pre-symptomatic and symptomatic) and discerning between the three brain areas studied: cortex, hippocampus and cerebellum. The parameters studied were (1) bioenergetics, focusing on ATP production and oxidative stress through lipid peroxidation and other oxidative damage markers, as well as ROS metabolism; (2) neuroinflammatory component, through cytokines detection and glial cells markers; (3) phenotypic and behavioral assessment along the development of the disease; and (4) additional results, which were the detection of neuronal markers in the brain areas.

Table 12. Summary of results obtained for Rett mice brains.
Arrows indicate variations over wild-type. Squared in turquoise, leriglitazone correcton over basal conditions.

		Cortex		Hippocampus		Cerebellum	
		Pre (3 m.o.)	**Post (7 m.o.)**	**Pre (3 m.o.)**	**Post (7 m.o.)**	**Pre (3 m.o.)**	**Post (7 m.o.)**
Bioenergetics	ATP concentration (Bioluminescence assay)	No changes	↑	No changes	↓ ↑	↓	↓ ↑
	Lipid peroxidation (TBARS)	↓	↑	No changes	↓ ↑	No changes	↓ ↑
	Oxidative stress (IHC, WB)				↓ 8-OhdG int. ↑		↑ 8-OhdG int. ↓ ↓ MnSOD, GPx expression
Neuroinflammation	Cytokines (Multiplex assay)	↓ IL-1α	↑ IFN-β, IFN-γ, IL-10, IL-27, IL-17A, MCP-1 ↓ ↑ TNF-α ↓ IL-6	No changes	↓ IL-1α, TNF-α ↑ IL-1β ↑ ↑ IL-17A	↑ GM-CSF, IFN-β, IFN-γ, IL-6, IL-10, IL-23, IL-27, IL-17A, IL-1α, IL-1β, IL-12p70, MCP-1, TNF-α	↓ IL-1α
	Glia markers (IHC)		↑ Iba and GFAP+ cell count ↓				
Phenotype and behavior	General Health Score (GHS) (Scale evaluation)	↑ weight ↑ GHS score since 12 weeks until endpoint ↓					
	Behavior (NORT, EPM)	No changes in pre-symptomatic mice ↓ total exploration time in symptomatic mice ↑					
Additional results	Neuronal markers (WB)	↑ cFos ↓ NeuN, DCX	↑ cFos ↑ NeuN ↓	↑ cFos	↑ cFos	No changes	↑ NeuN ↓

2 PERSONALIZED TREATMENTS FOR MITOCHONDRIAL DISORDERS WITH ALTERATIONS IN NEUROTRANSMISSION

1 Functional studies for mutations characterization

1.1. Mitochondrial dynamics
- Mitochondrial fission: *DNM1L*
- Mitochondrial dynamics: *SPATA5*

1.2. Mitochondrial structure
- Mitochondrial cristae structure: *CHCHD6*

1.3. Mitochondrial genes translation
- Mitochondrial amino-acyl-tRNA synthetases: *WARS2*
- Mitochondrial gene translation elongation factor: *GFM1*

1.4. Mitochondrial OXPHOS complexes subunits expression and assembly
- Complex I subunits: *NDUFS1*
- Complex I assembly factors: *NDUFAF6*
- Complex IV assembly factors: *SCO2*
- Complex IV assembly factors: *SURF1*

1.5. Intermediate metabolism
- Glutamate transport: *SLC25A22*
- Coenzyme A synthesis: *COASY*
- Pyruvate Dehydrogenase complex: *PDHX*

2 Personalized therapeutic approach

2.1. Pharmacological treatment: leriglitazone

2.2. Nutraceutical treatment: spermidine
- Effect of spermidine on the bioenergetic profile in mitochondrial patients
- Effect of spermidine treatment on the clinical phenotype of mitochondrial patients
- Spermidine accumulation consequences on mitochondrial bioenergetic function

2.3. Metabolic treatment: ketogenic diet

2.4. Non-responsive (non-treated) patients

2.5. Summary of mitochondrial dysfunctions and responses to personalized treatments

Besides conditions as the previously presented, which pathophysiology includes several mitochondrial deficiencies, primary alterations in mitochondrial homeostasis often lead to a spectrum of different pathologies themselves. Mitochondrial diseases are clinically heterogeneous, although with an outstanding neurological affectation, they can occur at any age and manifest with a wide range of clinical symptoms. Particularly, childhood-onset mitochondrial disorders commonly include hypotonia, generalized weakness, failure to thrive, dysautonomia, fatigue, exercise intolerance, vomiting, seizures and encephalopathy (Gorman et al., 2016). Despite their impact and prevalence (1:5.000), mitochondrial diseases are still a major therapeutic challenge.

To overcome this need and study new potential treatments for mitochondrial pathologies, we have studied the mitochondrial dysfunction in primary fibroblasts of a selection of 20 pediatric patients with a neurological phenotype and due to defects in mitochondrial functions (as described previously in Table 9 in Materials and Methods section). Remarkably, the patients were referred because of decreases in homovanillic acid (HVA) or 5-hydroxyindoleacetic acid (5-HIAA) in CSF, rather than alterations in lactate.

The selected patients recapitulate different aspects of mitochondrial function, including mitochondrial dynamics (*DNM1L, AFG2A*), mitochondrial cristae structure (*CHCHD6*), mitochondrial gene translation (*WARS2, GFM1*), electron transport chain complexes subunits (*NDUFS1*), complexes assembly (*NDUFAF6*, *SCO2*, *SURF1*), and intermediate metabolism related to mitochondria (*SLC25A22*, *COASY*, *PDHX*, *SMS*).

We focused on two main aspects of mitochondrial homeostasis (Fig. 30): (1) mitochondrial network structure and dynamics through immunofluorescence; and (2) bioenergetics, through ATP bioluminescence detection and ROS generation and metabolism (by MitoSOX™ fluorescence measured with flow cytometry and antioxidant enzymes expression by Western blot). These parameters were used to characterize the pathophysiology and to evaluate potential therapeutic approaches.

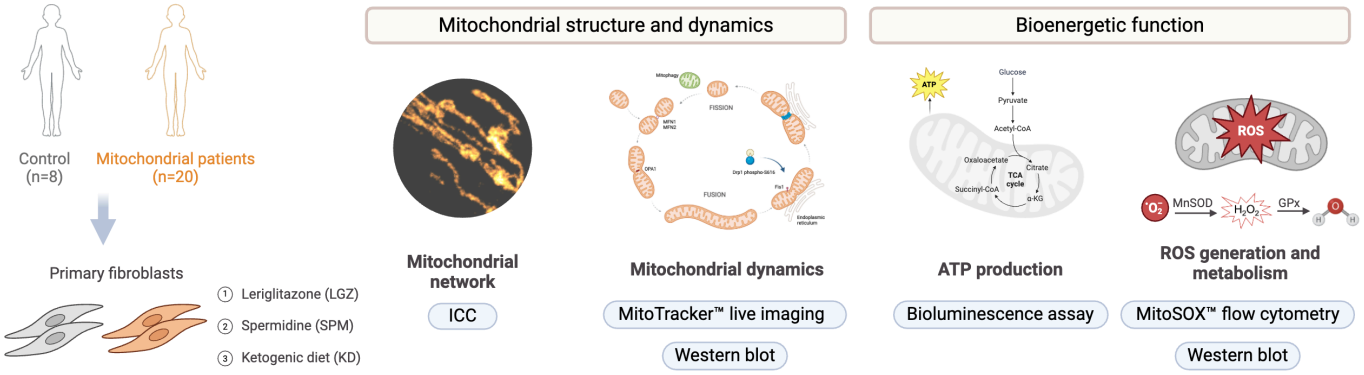

Figure 30. Summary of the main parameters for studying mitochondrial homeostasis in pediatric patients with primary mitochondrial disorders. Created with BioRender.

This chapter is organized in two sections. First, molecular characterization of the different mutations and evaluation of their effect on mitochondrial homeostasis, and second, evaluation of therapeutic alternatives. The latter is divided in three main approaches investigated: (1) pharmacological, (2) nutraceutical, and (3) a metabolic treatment. Finally, we describe the research performed in the group of patients that did not show a positive response to any treatment assayed.

1 Functional studies for mutations characterization

We selected a total of 12 genes involved in different aspects of mitochondrial homeostasis, described in Table 13 and represented in Figure 31. They have been classified in five main categories according to mitochondrial functions: (1) dynamics, (2) structure, (3) gene translation, (4) oxidative phosphorylation, and (5) intermediate metabolism.

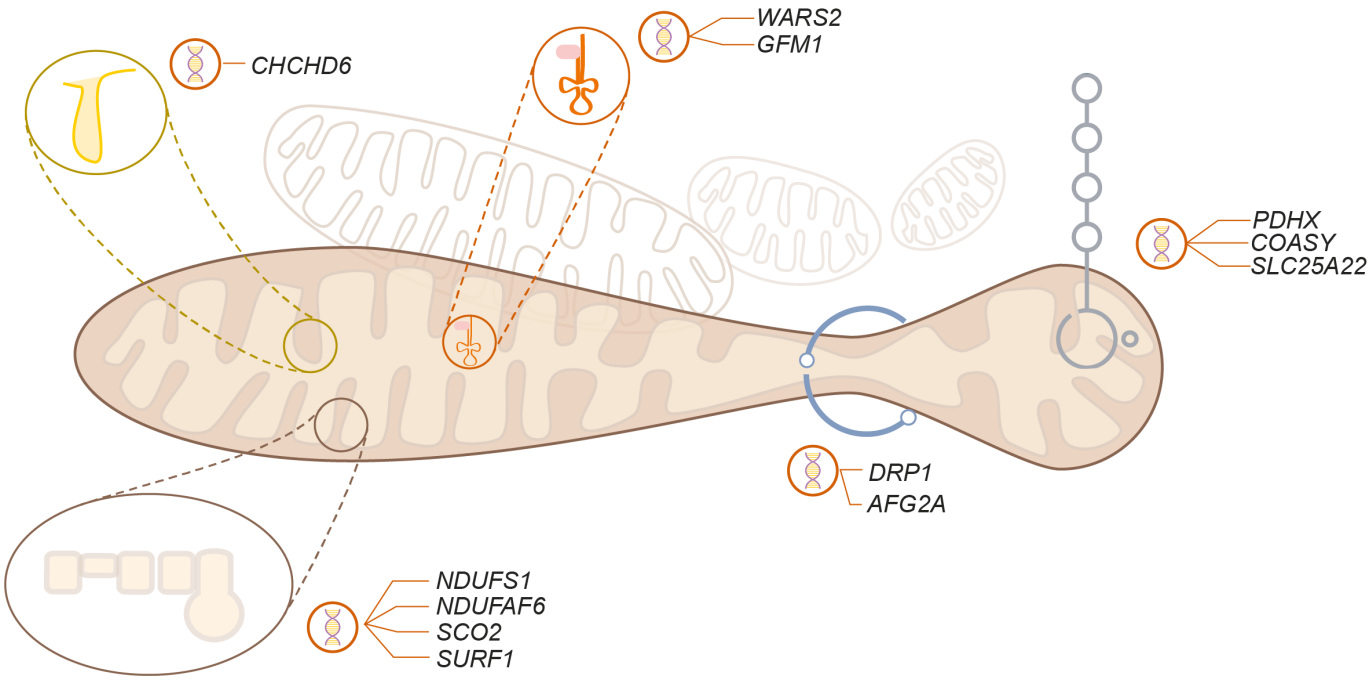

Figure 31. Schematic representation of the selected neuropediatric patients, according to the functional groups.

We have followed the same working and presentation scheme in all these cases: we first describe the main clinical aspects of the patients; following, we focus on the mutations' evaluation, performing an *in-silico* prediction of possible molecular mechanisms of pathology with MutPred2 (Pejaver et al., 2020), and validate the mutation on the protein expression *in vitro*. Finally, after mutation validation and diagnosis confirmation, we evaluate its potential consequences on mitochondrial homeostasis for each neuropediatric patient.

Table 13. Genes coding for mitochondria proteins studied, number of patients per affected gene, protein function and main clinical symptomatology of these patients.

Functional group	Gene	N patients	OMIM*	Protein	Protein function	Presented symptomatology in studied patients
Dynamics	*DNM1L*	5	603850	Dynamin-related protein 1 (Drp1)	Fission of mitochondria and peroxisomes.	Parkinsonism motor pattern, first with a hypokinetic-rigid syndrome that progressively evolved into a dystonic-parkinsonism pattern.
	AFG2A	3	613940	ATPase family gene 2 protein homolog A (AFG2A)	Morphological and functional mitochondrial transformations during spermatogenesis	Microcephaly, neurodevelopmental delay, intellectual disability and impairments in auditory, visual, gastrointestinal and motor functions. Epileptic symptoms from 14-27 months of age, as infantile spasms that were uncontrolled besides several anti-epileptic treatments
Structure	*CHCHD6*	1	615634	Mic25	Mitochondria contact site and cristae organizing system (MICOS) complex	Hypokinetic-rigid syndrome with evolution to hypotonic-hyperkinetic, and dystonic movements on lower limbs.
Translation	*WARS2*	1	604733	Tryptophanyl-tRNA synthetase 2 (WARS2)	Aminoacylation of tRNA(trp) with tryptophan.	Pediatric parkinsonism and associated intellectual disability along with other neurological symptoms over time. Diagnosed with hypokinetic-rigid syndrome.
	GFM1	1	606639	Mitochondrial elongation factor G1 (GFM1)	Catalyzes the GTP-dependent ribosomal translocation step during translation elongation.	Global developmental delay, mild cognitive delay, poor language, congenital left eye nystagmus and global hypotonia. Slow positive progression over time.
OXPHOS	*NDUFS1*	1	157655	NADH-ubiquinone oxidoreductase Fe-S protein 1 (NDUFS1)	Subunit of the complex I of the OXHPOS system.	Several motor and cognitive regression symptoms appeared during a mild viral infectious process. Severe truncal hypotonia with increase tone on the lower limbs with hyperreflexia. Necrotizing leukoencephalopathy indicating mitochondrial encephalopathy. Autistic-spectrum features, respiratory apneas and dysphagia worsening that resulted in inability to oral feeding.
	NDUFAF6	1	612392	NADH dehydrogenase (ubiquinone) complex I assembly factor 6 (NDUFAF6)	Early-stage assembly factor of the complex I of the OXPHOS system.	Mitochondrial encephalopathy (Leigh syndrome) and did not present epilepsy nor cardiopathies.
	SCO2	1	604272	SCO cytochrome c oxidase assembly protein 2	Synthesis and maturation of cytochrome c oxidase subunit II (COX II).	Pure neuroaxonal neuropathy, gait impairment with marked imbalance and tremor.
	SURF1	2	185620	Surfeit locus 1 protein (SURF1)	Component of the MITRAC complex (Mitochondrial Translation Regulation Assembly intermediate of COX complex).	Debut at 6 months of age. Ataxia and gastrointestinal problems. Hypotonia, neurodevelopmental delay, and digestive problems.
Intermediate metabolism	*SLC25A22*	1	609302	Glutamate carrier 1 (GC-1)	Transporter for glutamate from the cytosol into the mitochondrial matrix.	Psychomotor retardation and cerebral palsy. Epilepsy from the first months of life.
	COASY	1	609855	Coenzyme A synthase (COASY)	Bifunctional enzyme that catalyzes the two last steps in CoA synthesis.	Neurodevelopmental delay, refractory epileptic spasms and severe neurodevelopmental encephalopathy.
	PDHX	1	608769	Pyruvate dehydrogenase complex, component X (PDHX)	Catalyzes the oxidative decarboxylation of pyruvate to form acetyl CoA	Global developmental delay.

1.1 Mitochondrial dynamics

Mitochondrial fission: *DNM1L*

DNM1L (OMIM *603850) encodes for the dynamin 1-like or dynamin-related protein 1 (Drp1), a protein that belongs to the dynamin family of large GTPases that mediate membrane remodeling during a variety of cellular processes. Drp1 is crucial for regulating the morphology of the mitochondrial network according to the cellular energetic needs, with an important role in fission of mitochondria and peroxisomes (Fig. 32A). Patients with mutations in this gene are characterized by developmental delay, epilepsy, motor disturbances (such as muscle weakness, ataxia, and dystonia), and sensory neuropathy.

We performed *in vitro* studies on fibroblasts form a total of five patients with different mutations in the *DNM1L* gene that caused molecular alterations on the protein structure (Fig. 32B). For patients DNM1L_P1, P2 and P3 the specific mutation name and clinical symptomatology was not available.

DNM1L_P4 presented a parkinsonism motor pattern, first with a hypokinetic-rigid syndrome that progressively evolved into a dystonic-parkinsonism pattern. Cerebrospinal fluid (CSF) study showed decreased levels of homovanillic acid (HVA), suggesting a defective dopaminergic neurotransmission. Treatment with L-Dopa + Carbidopa resulted in improvement in motor function, however, neurological clinical signs continued. This patient carried the *DNM1L* c.2167A>G (p.Arg723Gly) mutation in heterozygosis with a *de novo* inheritance. Mutations in this gene have not been previously associated with the patient's symptomatology, but causative of encephalopathy in an autosomal dominant negative manner (Waterham et al., 2007). The mutation was predicted as pathogenic, and potentially causing an altered coiled coil (probability 0.92, $p = 7.7 \times 10^{-4}$) that could disrupt oligomerization, analyzed with MutPred2.

DNM1L_P5 carried a mutation in c.1084G>A (p.Gly362Ser), previously reported to be associated with microcephaly and pain insensitivity (Sheffer et al., 2016). The mutation was predicted as pathogenic and could be inducing an altered ordered interface (probability 0.28, $p = 3.4 \times 10^{-3}$). Meaning that, in this patient, the mutation in Drp1 could be affecting the protein's ability to bind the mitochondrial membrane or its oligomerization, ultimately affecting its function on mitochondrial fission.

We analyzed the protein expression of Drp1 by Western blot in the five DNM1L patients' fibroblasts (Fig. 32C). We detected that the monomeric form of Drp1 was significantly decreased for patients DNM1L_P1 (0.38 folds), P2 (0.39 folds) and P3 (0.44 folds), whereas P4 did not show significant changes in expression and P5 showed a 2.37-fold increase (not significative) compared to control fibroblasts. Since we did not detect a decrease for Drp1 expression in its monomeric form for patients DNM1L_P4 and P5, we performed a high-molecular weight Western blot to detect the oligomeric form of Drp1 (Fig. 32D). For mitochondrial fission process, Drp1 is recruited from cytosol to the mitochondrial outer membrane, where it assembles into oligomers to form a contractile ring. Densitometry quantification of the ratio oligomeric:monomeric forms of Drp1 expressed as folds over controls, showed a 3.16-fold increase in the ratio for DNM1L_P4 whereas a non-statistically significant 9.62-fold increase for DNM1L_P5 compared to controls.

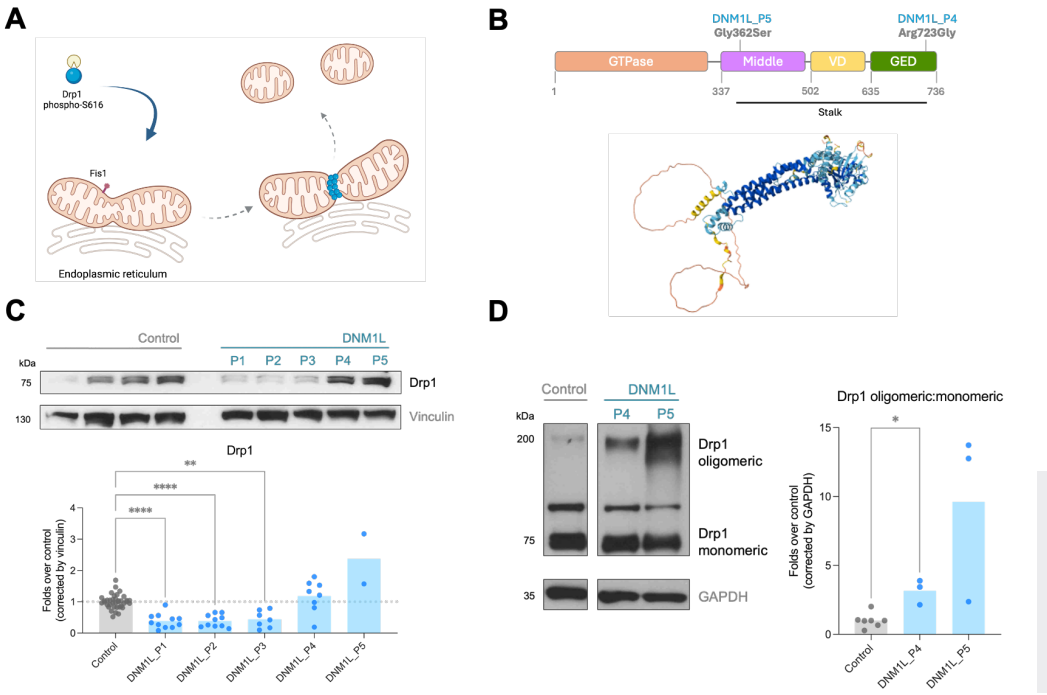

Figure 32. Description of the mutations and dynamics proteins' expression in the five DNM1L patients' fibroblasts.
(see next page)

(from previous page)

Figure 32. Description of the mutations and dynamics proteins' expression in the five DNM1L patients' fibroblasts. (A) Schematic representation of Drp1 function in the mitochondrial fission process: Drp1 assembles into constriction rings around mitochondria and hydrolyzes GTP to divide the organelle into two segments; created with BioRender. (B) 3D Drp1 protein structure and location of the mutations, observed through PyMOL, and linear protein representation highlighting the main domains: GTPase domain (facilitates GTP binding and hydrolysis), middle domain (contributes to dimerization and oligomerization), Variable Domain (VD, regulates membrane interactions) and GTPase Effector Domain (GED, links the GTPase and middle domains, aiding in oligomerization and coupling GTP hydrolysis to mechanical activity). (C) Representative image of the Drp1 protein expression in four controls (each lane represents a different cell line) and the five DNM1L patients, detected by Western blot, and densitometry quantification, compared to controls and corrected by vinculin (n=12 experiments). (D) Representative image of the detection of monomeric (75 kDa) and oligomeric (200 kDa) Drp1 protein expression in control and patients by Western blot, with GAPDH used as loading control and densitometry quantification of the oligomeric:monomeric ratio per patient compared to controls (n=3 experiments).
Data represented as mean and individual values. (Brown-Forsythe) ANOVA analysis for comparing DNM1L_P1-P5 over control group. *P* value represents *<0.05, **<0.01, ****<0.0001.

After Drp1 expression detection in the patients, we analyzed the mitochondrial dynamics markers expression by Western blot (Fig. 33A), both fusion (OPA1 and Mfn2) and fission (Fis1) proteins. We observed that, as happened with Drp1, the expression for both groups of proteins differed between the DNM1L patients (Fig. 33B). Regarding the fusion proteins, we detected significative increases in OPA1 for DNM1L_P3 (1.29 folds), P4 (1.4 folds) and P5 (1.57 folds), while the ratio of the OPA1 short isoform over the long isoform (OPA1 80:100, in which the short isoform of 80 kDa is associated to a more fragmented morphology) was increased in 1.28 folds in DNM1L_P1. Mfn2 showed no significant differences for the patients' fibroblasts compared to controls. Regarding the fission Fis1 protein, expression was reduced in 41% only in P2. In consequence, we observe that the five *DNM1L*-mutated patient cells are characterized by different expressions of the dynamics proteins.

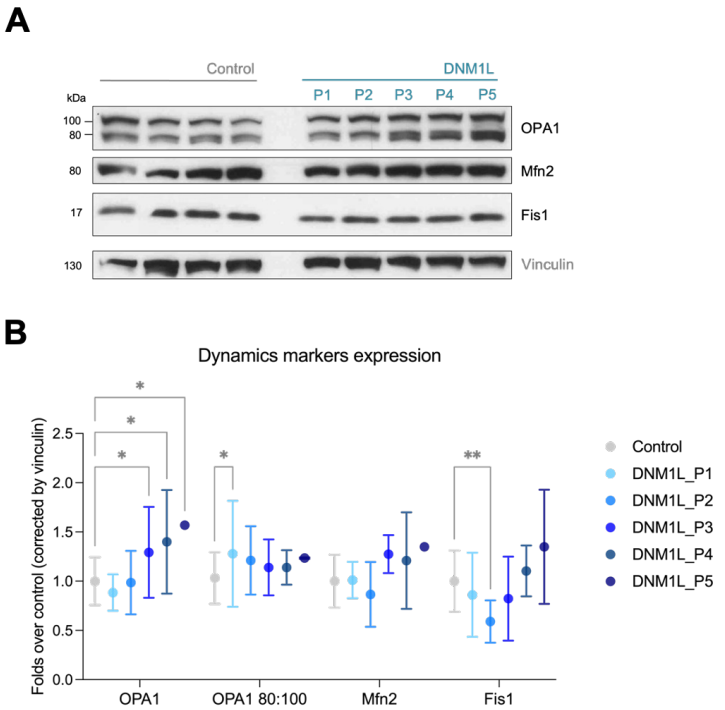

Figure 33. Mitochondrial dynamics markers detection in the five DNM1L patients' fibroblasts. (A) Representative image of the dynamics proteins in four controls (each lane represents a different cell line) and the five DNM1L patients, detected by Western blot. (B) Densitometry quantification of the fusion proteins expression OPA1, ratio OPA1 80:100 kDa, and Mfn2, and the fission protein Fis1 in the DNM1L patients compared to controls, corrected by vinculin (n=7-9 experiments).

Data represented as mean value ± SD. Two-way ANOVA analysis with multiple comparisons of each patient over control, per protein. *P* value represents *<0.05, **<0.01.

To understand how these mutations could be influencing mitochondrial homeostasis, we first analyzed mitochondrial network structure by immunofluorescence with TOMM20 (Fig. 34A). The parametrization of the mitochondrial network (Fig. 34B) showed that the DNM1L fibroblasts have a distinctive morphology characterized by 1.8-fold more area occupied by mitochondria, with a 26% increased mean form factor, 11% increased mean branch length and decreased branch diameter in 27 nm compared to controls. These results suggest that DNM1L patients' fibroblasts have an accumulation of elongated mitochondrial networks with longer and thinner branches per network, in addition to an increased interconnectivity of these ramifications, calculated by the relationship between branch end points and branch junctions compared to controls (Hotelling's T^2 test, $p = 4.64 \times 10^{-8}$). In summary, DNM1L cells show a unique mitochondrial network with polygonal shapes.

Based on this characteristic mitochondrial network, and considering that the heterogenous clinical presentation and the difficulty of some variants interpretation can harness the correct diagnosis of these patients, we created a machine learning classification model that could discern DNM1L mitochondrial network structure from other mitochondrial diseases and from healthy controls (Fig. 34C). To do this, we first selected those parameters obtained with Mitochondria Analyzer plug in that were considered more informative, defined as those parameters

not inferred from the measurement of another parameter and therefore that were not highly predictable from the other variables. The selected parameters were mitochondrial count, mean aspect ratio, mean branch length, branch end points and mean branch diameter. Then we trained and compared three models to perform multiclass classification: Random Forest (RF), Support Vector Machine (SVM) and Multinomial logistic regression (NN). Based on their performance during cross-validation on training data, we compared the Accuracy and Kappa median values for each model, where Accuracy measures what proportion of values are on the real class and Kappa gives a value between -1 and 1, with a value more than zero meaning that the classification did better than random. The model with highest median values was SVM (Accuracy = 0.83, Kappa = 0.74). Finally, the model was validated on testing data, with the metrics showing that SVM was highly accurate in predicting samples as members of the DNML1 group while being less efficient in the separation of other mitochondrial (OTHERMIT) samples from CONTROL samples. The difference between Accuracy and No Information Rate (NIR), used to evaluate whether the overall accuracy rate is greater than the rate of the largest class (OTHERMIT), is statistically significant ($p = 4.27 \times 10^{6}$). In addition, the Mcnemar's Test P-Value, which evaluates if one the classes is being less accurately classified compared to the others, was non-significative. These results suggest that DNM1L fibroblasts' networks are homogeneous and differ from other mitochondrial disorders and healthy controls, who show a more heterogeneous profile. In this context, this analysis could aid the diagnosis for those suspected *DNM1L* patients with variants of uncertain pathogenicity.

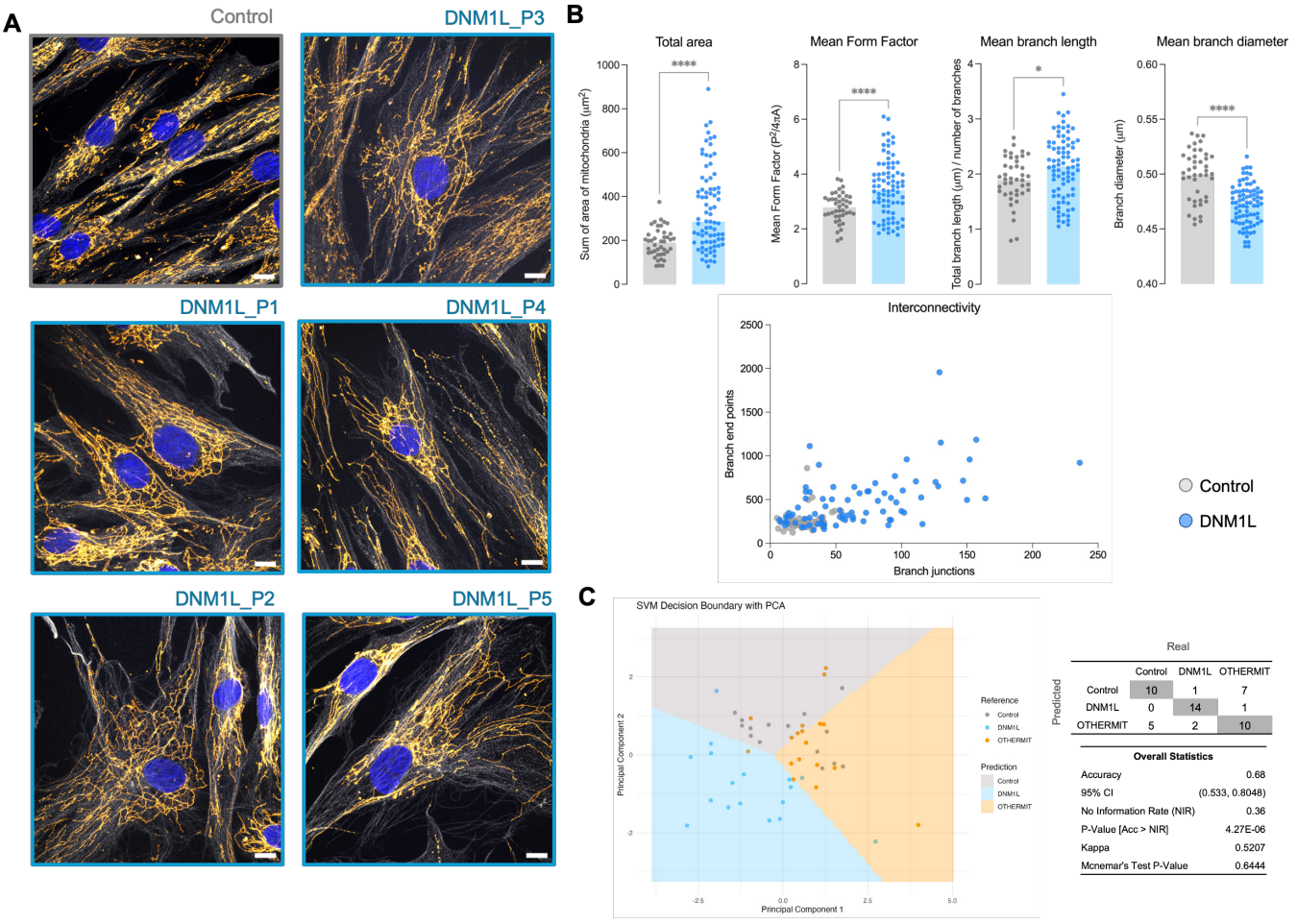

Figure 34. Evaluation of mitochondrial network structure in the five DNM1L patients' fibroblasts. (A) Representative image per patient of the mitochondrial network IF (TOMM20 in yellow, tubulin in grey, nuclei in blue; scale bar 10 µm). (B) Parametrization of the total area of signal occupied by mitochondria, mean form factor, mean branch length and diameter, and interconnectivity, expressed as the relationship between the number of branch end points and branch junctions; quantified with Mitochondria Analyzer (n=42 control, n=81 patients' mitochondria). (C) Prediction of the DNM1L mitochondrial signature compared to other mitochondrial patients (OTHERMIT) and controls with the Support Vector Machine (SVM) model. The figure shows a projection of the validation data on its two first principal components. The space is colored according to the selected model's prediction on the validation set, and points are colored according to each sample's real class (n=50 samples).
Data represented as (B) mean for parametric data or median for non-parametric data with individual values; or (C) projection of the validation data on its two first principal components, the space is colored according to the selected model's prediction on the validation set, and points are colored according to each sample's real class. Comparative analysis control vs. DNM1L done with Welch's test for parametric, and Mann-Whitney for non-parametric data. *P* value represents *<0.05, ****<0.0001.

On the other hand, the bioenergetic profile was not consistent between patients. We analyzed both total and mitochondrial ATP production in the five patients' fibroblasts compared to controls (Fig. 35A). Total ATP was increased in four of the patients (1.8 folds for DNM1L_P1, 1.4 folds for P2, 1.7 folds for P3, and 1.3 folds for P5), without significant changes in DNM1L_P4. Regarding mitochondrial ATP, patients DNM1L_P1 and P2 fibroblasts showed an increase in 1.4 folds concentration, 1.5 folds for P3, a significant 30% decrease for patient DNM1L_P4, and no changes for DNM1L_P5 fibroblasts. For the last patient, since we did not detect significant changes for mitochondrial ATP production, we forced the reliance on oxidative phosphorylation incubating the cells with galactose for 48 hours (Fig. 35B). Fibroblasts are highly glycolytic cells and therefore the mitochondrial dysfunction could be masked. However, no significant differences were detected for total ATP in the DNM1L_P5 when cells were grown in galactose media compared to controls.

$O_2^{\cdot-}$ detection (Fig. 35C) recorded similar increases in MitoSOX fluorescence for patients DNM1L_P1, P2 and P3 (1.7, 2 and 2.6 folds respectively), and a 5.6-fold increase for DNM1L_P4, compared to controls. On the contrary, DNM1L_P5 fibroblasts showed a significant 30% decrease compared to controls. In addition, antioxidant enzymes expression detected by Western blot (Fig. 35D) showed a significant 61% decreased MnSOD expression for patient DNM1L_P3 and a 28% decrease in GPx expression for patient DNM1L_P1 and 30% decrease for patient DNM1L_P2 compared to controls, without significant differences for the other patients.

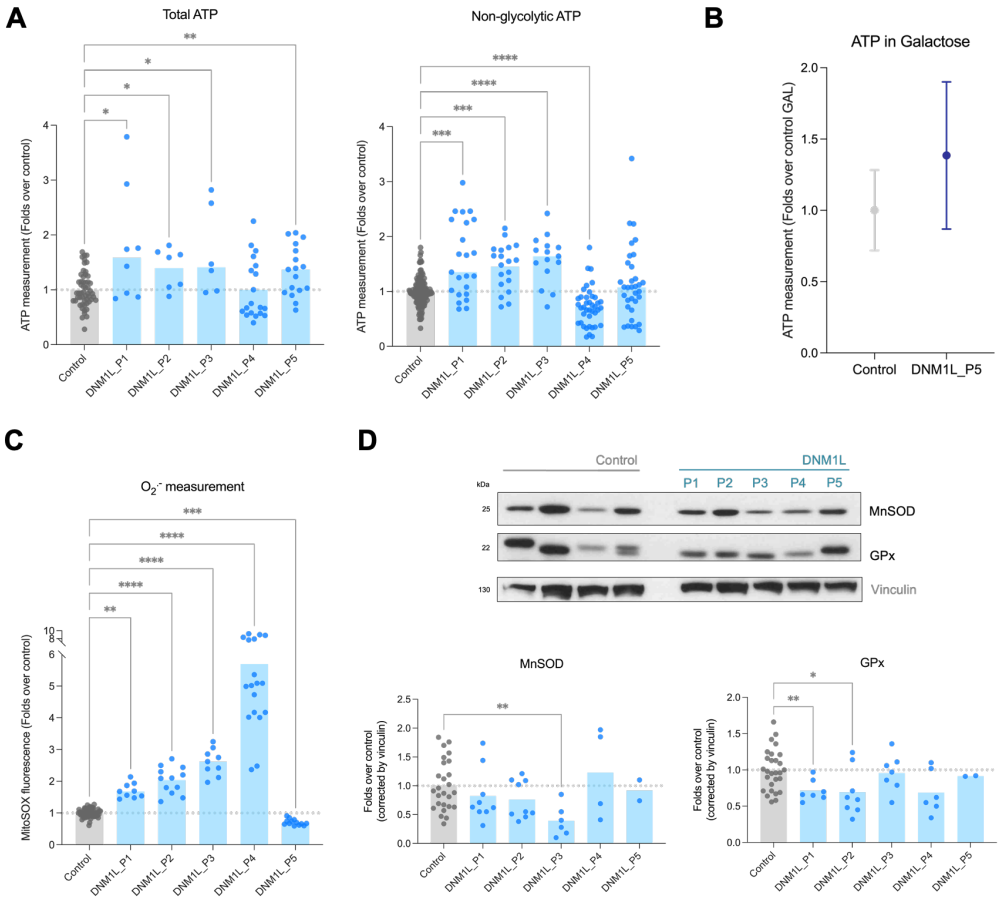

Figure 35. Evaluation of mitochondrial bioenergetics in the five DNM1L patients' fibroblasts. (A) Total and mitochondrial ATP concentration in DNM1L patients compared to controls, measured by luciferin-luciferase bioluminescence after incubation with 2-DG (n=13 experiments with minimum duplicates), and (B) in DNM1L_P5 after incubation with galactose 48 hours. (C) $O_2^{\cdot-}$ production in DNM1L fibroblasts compared to controls, measured by flow cytometry with MitoSOX™ probe (n=13 experiments with triplicates). (D) Representative image of antioxidant enzymes MnSOD and GPx expression in patients compared to four controls (each lane represents a different cell line) detected by Western blot and densitometry quantification with ImageJ and corrected by vinculin (n=8-10 experiments).

Data represented as (A, C, D) mean for parametric data or median for non-parametric data with individual values; (B) mean as symbol ± SD. Comparative analysis performed with Welch's t test for two group comparison; (Brown-Forsythe and Welch) ANOVA for parametric data and Kruskal-Wallis for non-parametric, and multiple comparisons between controls and the five patients. *P* value represents *<0.05, **<0.01, ***<0.001, ****<0.0001.

In brief, fibroblasts of patients DNM1L_P1, P2 and P3 displayed a more homogeneous behavior, showing *increased* ATP production and ROS, along with *decreased* expressions of antioxidant enzymes. On the other hand, DNM1L_P4 was characterized by *decreased* mitochondrial ATP and *increased* ROS, while DNM1L_P5 showed *no changes* for mitochondrial ATP when grown in DMEM nor galactose medium, together with *decreased* ROS production. In conclusion, *DNM1L* patients' fibroblasts present a distinctive hyperfused mitochondrial network but different bioenergetic profiles.

Mitochondrial dynamics: *AFG2A*

AFG2A (*SPATA5*) (OMIM *613940) encodes for the ATPase family gene 2 protein homolog A or Spermatogenesis associated protein 5 (SPATA5), an ATP-dependent chaperone involved in morphological and functional mitochondrial transformations during spermatogenesis. Mutations in this gene cause AFG2A-related encephalopathy and to the present day, only 43 patients have been reported. Despite partial insights reporting mitochondrial dynamics and bioenergetic alterations together with impaired axonal growth in rat cortical neurons (Puusepp et al., 2018) and defective bioenergetics in patients' mononuclear cells and platelets (Raggio et al., 2023), the molecular causes of the disease remain unclear.

We performed *in vitro* studies of three diagnosed *AFG2A* patients to understand the mitochondrial involvement in the physiopathology. The three patients (AFG2A_P1, AFG2A_P2 and AFG2A_P3) were male and aged 7 (P1 and P3) and 11 (P2) at the moment of the diagnosis. The three patients had microcephaly, neurodevelopmental delay, intellectual disability and impairments in auditory, visual, gastrointestinal and motor functions. They presented abnormal electroencephalograms (EEGs) and started with epileptic symptoms from 27 (P1) and 14 months of age (P2 and P3), as infantile spasms. The seizures were uncontrolled besides several anti-epileptic treatments, meaning they presented refractory epilepsy. In addition, patients AFG2A_P2 and P3 had mild elevation of lactate without other alterations in mitochondrial biomarkers.

The patients harbored different mutations in *AFG2A* gene (Fig. 36A), which caused several molecular changes in the protein structure (Fig. 36B). AFG2A_P1 carried the c.251G>A (p.Arg84Gln) mutation, predicted as likely pathogenic and causing loss of allosteric site at R84 (probability 0.28, $p = 7.5 \times 10^{-3}$). AFG2A_P2 carried two mutations, namely c.327_328del (p.Lys110fs) and c.1631T>G (p.Leu544Arg), which were predicted as variants of uncertain significance (VUS). However, no protein prediction was achieved for these frameshift and missense mutations, respectively. AFG2A_P3 carried two mutations, namely c.251G>A (p.Arg84Gln) and c.1064T>C (p.Ile355Thr), predicted as likely pathogenic and causing possible losses of allosteric site at R84 (probability 0.28, $p = 7.5 \times 10^{-3}$) and Y352 (probability 0.28, $p = 7.4 \times 10^{-3}$), respectively. Only mutation Arg84Gln was previously reported by Tanaka and collaborators (Tanaka et al., 2015).

To study mitochondrial homeostasis in the fibroblasts of these patients, we first visualized mitochondrial morphology and dynamics with the probe MitoTracker™ Green using *live cell* time-lapse confocal microscopy (Fig. 36C). Network dynamics parametrization with Mitometer revealed a decrease of 14% in directionality (the total distance traveled divided by the maximum displacement of the mitochondria), a decrease of 8% for median:max speed ratio (i.e. rapid movements of mitochondria) and a 53% decrease in fusion:fission ratio compared to healthy controls, while no significant differences were detected for median speed (Fig. 36D). Morphology quantification showed alterations in all the measured parameters (Fig. 36E). AFG2A patients' fibroblasts had 53% decreased mitochondrial area, 34% decreased aspect ratio and 53% decreased perimeter, whereas showed a 19% increase in solidity (calculated as the ratio of the volume of individual mitochondria to their convex hull, which gives information on how branched the mitochondria are) compared to controls. In consequence, these patients' cells have an aberrant mitochondrial network with less, round-shaped and slightly more branched mitochondria. More importantly, these mitochondria have a decreased motility characterized by undirected and slower bursting-like movement, together with fewer fusion events ultimately causing a fragmented morphology.

While dynamic movements were homogeneous in the studied patients' cells, the bioenergetic profile showed differences between them. Bioluminescence ATP measurement revealed a significant 55% decrease for AFG2A_P1 and 24% decrease for P2, while no significant differences were detected for P3 compared to control fibroblasts (Fig. 36F). Mitochondrial ATP detection after incubation with 2-DG showed no statistically significant differences for the AFG2A patients compared to controls. On the contrary, $O_2^{\cdot-}$ was altered for the three patients in a similar manner, with increases of 1.68 folds for AFG2A_P1, 1.53 folds for P2, and 2.42 folds for P3 compared to controls (Fig. 36G). Interestingly, besides having the same increase in ROS production, antioxidant enzymes expression differed between the three patients (Fig. 36H). MnSOD expression showed a 4.39-fold increase for P3, without significant differences for the other two patients, while GPx was 40% decreased for P1 and 1.95-fold increased for P2, without differences for P3 fibroblasts. These results suggest that there is a mitochondrial homeostasis impairment with different bioenergetic implications between the studied patients.

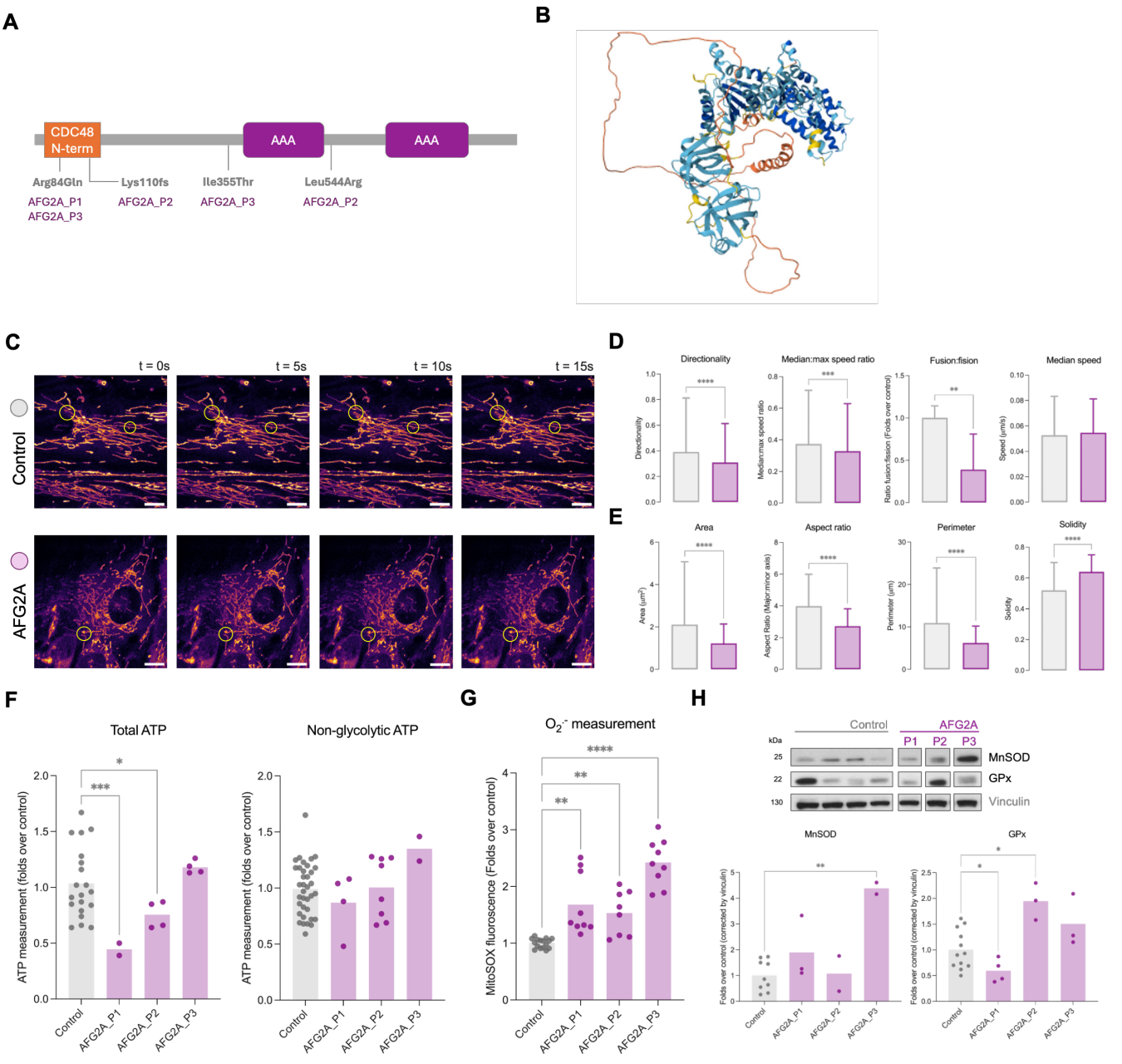

Figure 36. AFG2A patients' description of mutations and mitochondrial homeostasis characterization in fibroblasts from the patients. (A) Schematic representation of the mutations in the AFG2A for AFG2A_P1 (c.251G>A (p.Arg84Gln)), AFG2A_P2 (c.327_328del (p.Lys110fs) and c.1631T>G (p.Leu544Arg)), and AFG2A_P3 (c.251G>A (p.Arg84Gln) and c.1064T>C (p.Ile355Thr)); CDC48 = evolutionarily conserved substrate recognition domain that binds to polypeptides, prevents protein aggregation, and is involved in protein folding (Tanaka et al., 2015), AAA = ATPase associated with diverse activities domain. (B) 3D protein structure representation and location of the mutations, observed through PyMOL (C-E) Mitochondrial dynamics and shape characterization of control and patients' fibroblasts using MATLAB add-in Mitometer. (C) Frames obtained from time-lapse images at different time points (0s, 5s, 10s, 15s) showing in yellow the fusion-fission dynamics in the mitochondrial network, detected with MitoTracker™ Green (ImageJ LUT inferno, scale bar 10 µm). (D) Quantification of the dynamics parameters: median speed (µm/s), median:max speed ratio (capacity of burst movement), directionality (defined as the total distance traveled divided by the maximum displacement of the track), and fusion:fission ratio. (E) Quantification of mitochondrial shape parameters: area occupied by signal, perimeter and aspect ratio (calculated as the ratio between the major and minor axes of mitochondria) (n=1579-1863 tracks for controls, n=1616-1895 tracks for patients' mitochondria; n=4 control, n=7 patients' cells). (F) Total and mitochondrial ATP production in fibroblasts from the three AFG2A patients, detected by bioluminescence assay and expressed as folds over control (n=3 experiments with minimum duplicates). (G) $O_2^{\cdot-}$ production expressed as folds over controls, measured by flow cytometry with MitoSOX™ probe (n=3 experiments with triplicates). (H) Antioxidant enzymes MnSOD and GPx expression detected by Western blot, and densitometry analysis corrected to vinculin and expressed as folds over average of four controls (each lane represents a different cell line; n=2 experiments).
Data represented as mean for parametric data or median for non-parametric data, (D, E) with interquartile range or standard deviation respectively, and (F-H) individual values. Comparative analysis control *vs.* AFG2A done with Welch's test for parametric, and Mann-Whitney for non-parametric data, and (Brown-Forsythe and Welch) ANOVA for parametric data and Kruskal-Wallis for non-parametric, and multiple comparisons between controls and the three patients. *P* value represents *<0.05, **<0.01, ***<0.001, ****<0.0001. P1 = AFG2A patient 1, P2 = AFG2A patient 2, P3 = AFG2A patient 3.

1.2 Mitochondrial structure

Mitochondrial cristae structure: *CHCHD6*

The present patient presented hypokinetic-rigid syndrome with evolution to hypotonic-hyperkinetic, dystonic movements on lower limbs and HVA decreased levels in CSF. All these symptoms suggested a pediatric parkinsonism with dopaminergic affectation.

Whole exome sequencing revealed two heterozygous mutations in the nuclear gene *CHCHD6* (Coiled-Coil-Helix-Coiled-Coil-Helix Domain Containing 6) (OMIM *615634), that codes for the protein Mic25. This mitochondrial protein forms part of the Mitochondria contact site and Cristae Organizing System (MICOS) complex (Fig. 37A), involved in the maintenance of mitochondrial cristae architecture and not previously associated to disease. The mutations, namely c.142C>T (p.Pro48Ser) and c.572G>A (p.Arg191His) (Fig. 37B) were detected as variants of uncertain significance (VUS) and no *in silico* prediction was achieved with MutPred2. However, the presence of both variants resulted in a decrease in Mic25 protein detection by Western blot (Fig. 37C), supporting the pathological character of the mutations. In addition, we analyzed mitochondrial inner membrane structure by transmission electron microscopy (TEM) in collaboration with the Mitochondrial Biogenesis and Pathology group led by Dr. Julio Montoya from Universidad de Zaragoza. As can be observed in Figure 37D, patient mitochondria had altered cristae both in structure and number, supporting the diagnosis.

After description and confirmation of the mitochondrial-related diagnosis, we evaluated the impact of the *CHCHD6* mutations in the mitochondrial homeostasis. First, we observed the mitochondrial network by TOMM20 IF (Fig. 37E). The network parametrization with Mitochondria Analyzer (Fig. 37F), showed cells with a 5.87-fold increase in total area and 35% more independent networks, together with a decrease of 22 nm in mean branch diameter compared to controls. However, we did not detect significant changes for number of branches per network and mean branch length. In summary, CHCHD6 patient's fibroblasts have more mitochondrial networks with thinner branches, but not more or longer branches per network. Ultimately, the bioenergetic profile in the Mic25-deficient cells showed a 40% decrease in mitochondrial ATP detected by bioluminescence without significative changes for total ATP (Fig. 37G), and a 3.2-fold increase in $O_2^{\cdot-}$ accumulation (Fig. 37H), compared to control fibroblasts. However, we did not detect significant differences for expression of antioxidant enzymes MnSOD and GPx in the patient cells (Fig. 37I). In brief, mutations in *CHCHD6* are responsible for mitochondrial structure and bioenergetic deficiencies, causing mitochondrial disease with pediatric parkinsonism.

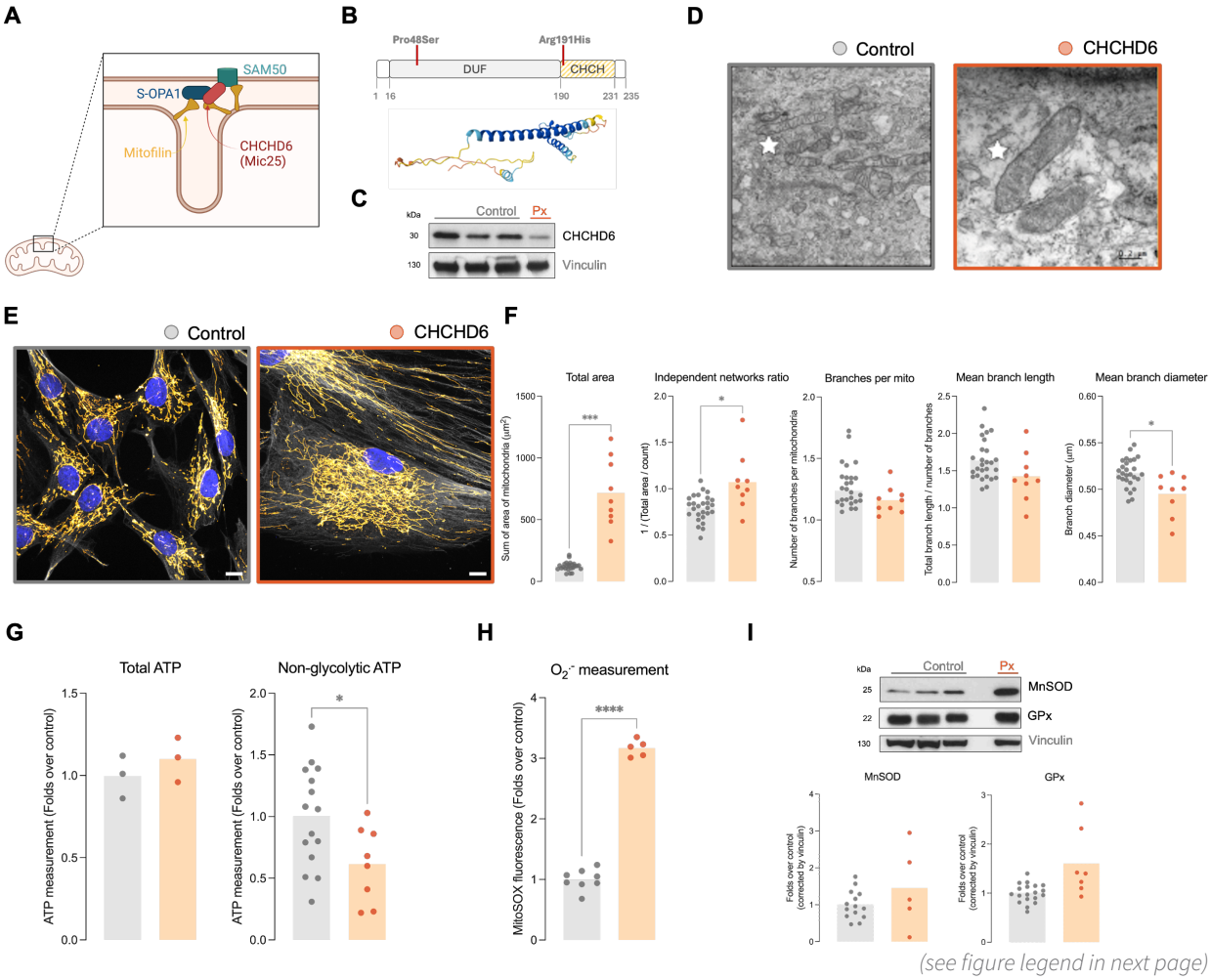

(see figure legend in next page)

(from previous page)
Figure 37. Validation of the mutation in CHCHD6 patient's fibroblasts and its effect on mitochondrial homeostasis maintenance. (A) Schematic representation the Mic25 (CHCHD6) protein function in the mitochondria IMM and cristae structure, as hypothesized in (Ding et al., 2015); created with BioRender. (B) Schematic representation of the heterozygous mutations c.142C>T (p.Pro48Ser) and c.572G>A (p.Arg191His) in CHCHD6 and 3D Mic25 protein structure and location of the mutations, observed through PyMOL; DUF = domain of unknown function. (C) Detection of Mic25 protein expression in three controls (each lane represents a different cell line) and patient by Western blot, with vinculin used as loading control. (D) Representative images of mitochondrial ultrastructure visualized by TEM (scale bar 0.2 µm). (E-I) Studies on mitochondrial homeostasis regarding network structure and bioenergetics. (E) Representative image of the mitochondrial network IF (TOMM20 in yellow, tubulin in grey, nuclei in blue; scale bar 10 µm). (F) Parametrization with Mitochondria Analyzer of the total area, mean form factor (a shape measure given by $P^2/(4\pi A)$), number of branches per mitochondrial network, and mean branch length and diameter (n = 27 control, n = 9 CHCHD6 mitochondria). (G) Total and mitochondrial (non-glycolytic) ATP concentration expressed in folds over controls, measured by luciferin-luciferase bioluminescence after incubation with 2-DG (n=3 experiments with minimum technical duplicates). (H) $O_2^{\cdot-}$ production expressed as folds over controls, measured by flow cytometry with MitoSOX™ probe (n=2 experiments with minimum technical duplicates). (I) Antioxidant enzymes MnSOD and GPx expression detected by Western blot, and densitometry analysis, corrected to vinculin and expressed as folds over average of controls (n=4-6 experiments).
Data represented as mean for parametric data or median for non-parametric data, with individual values. Comparative analysis control *vs*. CHCHD6 done with Welch's test for parametric, and Mann-Whitney for non-parametric data. *P* value represents *<0.05, ****<0.0001. Px = patient.

1.3 Mitochondrial genes translation

Mitochondrial amino-acyl-tRNA synthetases: *WARS2*

This patient presented with pediatric parkinsonism and associated intellectual disability along with other neurological symptoms over time. She was eventually diagnosed with hypokinetic-rigid syndrome and showed a global improvement after treatment with L-Dopa + Carbidopa. Biochemical analyses revealed constant reduced levels of HVA in CSF. The patient carried a homozygous mutation in the nuclear gene *WARS2* (OMIM *604733), a mitochondrial aminoacyl-tRNA synthetase that catalyzes the aminoacylation of tRNA(trp) with tryptophan (Fig. 38A), associated with parkinsonism of childhood onset. The mutation *WARS2* c.515+5 G>A was inherited from both parents, and produced exon 4 skipping, detected by cDNA sequencing (Fig. 38B). The mutation, predicted as VUS and not previously reported, resulted in the absence of protein detected in patient fibroblasts (Fig. 38C).

After confirmation of diagnosis, we visualized the mitochondrial network structure in the patient with TOMM20 IF (Fig. 38D). Parametrization analysis through Mitochondria Analyzer (Fig. 38E) showed no significant differences for mitochondrial network shape and branching in WARS2-patient cells compared to controls. Besides no alterations in the network, the bioenergetic profile in the neuropediatric patient showed significative decreases of 32% in total ATP and 57% in mitochondrial ATP concentration (Fig. 38F), together with a 1.6-fold significant increase in $O_2^{\cdot-}$ generation (Fig. 38G) compared to control fibroblasts. Regarding ROS metabolism, WARS2 fibroblasts expressed 67% less MnSOD compared to controls, while no differences were detected for GPx expression (Fig. 38H). These results suggest that while mitochondrial structure is not altered, there can be deficiencies in the bioenergetic function affecting mitochondrial homeostasis in WARS2 patients' fibroblasts.

(see next page)
Figure 38. Evaluation of the mutation in WARS2 patient's fibroblasts and its effect on mitochondrial homeostasis maintenance. (A) Schematic representation of the WARS2 function in mitochondrial gene translation, ultimately responsible for the synthesis of OXPHOS complexes subunits; created with BioRender. (B) Schematic representation of homozygous mutation c.515+5 G>A in *WARS2* gene, showing the exon 4 skipping, detected by cDNA sequencing. (C) Detection of WARS2 protein expression in fibroblasts of three controls (each lane represents a different cell line) and patient by Western blot, with vinculin used as loading control. (D-H) Mitochondrial network structure and bioenergetics studies on WARS2 fibroblasts. (D) Representative image of the mitochondrial network IF (TOMM20 in yellow, tubulin in grey, nuclei in blue; scale bar 10 µm). (E) Parametrization of the independent networks ratio corrected by area, mean form factor, mean branch length and mean branch diameter (n = 48 control, n = 23 patient mitochondria). (F) Total and mitochondrial (non-glycolytic) ATP concentration in patient compared to controls, measured by luciferin-luciferase bioluminescence after incubation with 2-DG (n=4 experiments with minimum duplicates). (G) $O_2^{\cdot-}$ production compared to controls, measured by flow cytometry with MitoSOX™ probe (n=6 experiments with minimum triplicates). (H) Antioxidant enzymes MnSOD and GPx expression detected by Western blot, and densitometry analysis, corrected to vinculin and expressed as folds over average of controls from the same experiment (n=4-6 experiments).
Data represented as mean for parametric data or median for non-parametric data, with individual values. Comparative analysis control *vs*. WARS2 done with Welch's test for parametric, and Mann-Whitney for non-parametric data. *P* value represents **<0.01, ****<0.0001. Px = patient.

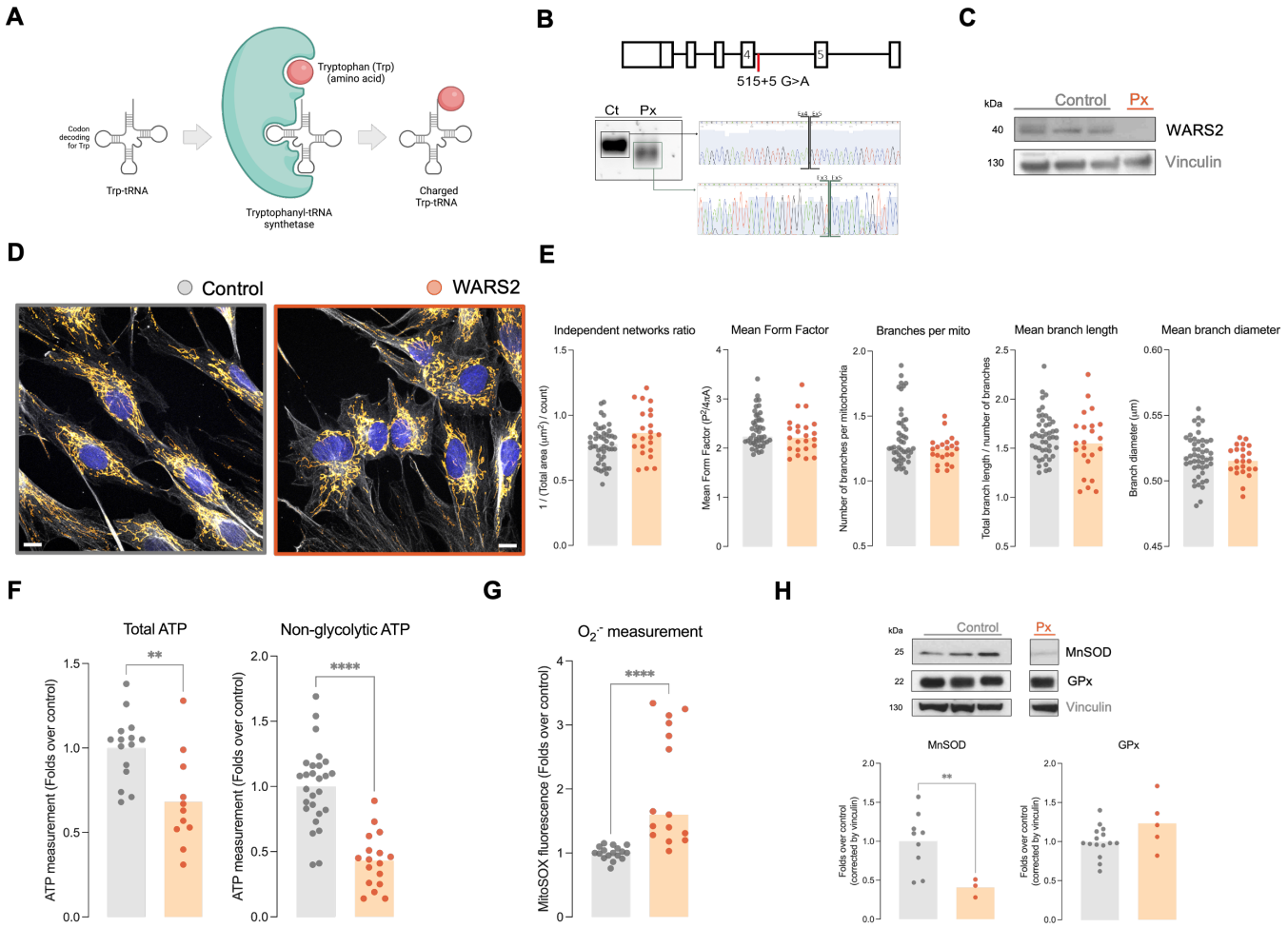

Mitochondrial gene translation elongation factor: *GFM1*

This patient presented global developmental delay, mild cognitive delay, poor language, congenital left eye nystagmus and global hypotonia. He carried a homozygous mutation in *GFM1* gene (OMIM *606639), detected by WES. This nuclear gene codes for the mitochondrial elongation factor G1, a mitochondrial GTPase that catalyzes the GTP-dependent ribosomal translocation step during translation elongation (Fig. 39A) and has been associated with oxidative phosphorylation deficiencies. The mutation c.2011C>T (p.Arg671Cys) (Fig. 39B), previously reported by Galmiche et al. (Galmiche et al., 2012), was predicted as pathogenic and to cause altered metal binding (probability 0.56, $p = 3.4 \times 10^{-3}$) or a loss of the catalytic site at R671 (probability 0.27, $p = 3.6 \times 10^{-3}$) between other mechanisms, detected with the *in silico* predictor MutPred2. *In vitro* studies of protein expression showed a decrease in GFM1 expression in patient fibroblasts (Fig. 39C).

As previously, we started the study of mitochondrial homeostasis by visualizing the mitochondrial network structure in the patient's fibroblasts (Fig. 39D). Network parametrization revealed a 16% significant increase in mean branch length in patient's mitochondria compared to controls, whereas the other parameters, when corrected to the total count did not show statistical differences. Regarding the bioenergetic profile, we did not detect significant alterations for total and mitochondrial ATP production in the patient's fibroblasts (Fig. 39F). Since fibroblasts are highly glycolytic cells, the mitochondrial energy dysfunction could be masked. Therefore, to increase the reliance on oxidative phosphorylation and improve the detection of mitochondrial dysfunction, we incubated the cells in medium with galactose for 48 hours (Fig. 39G). Interestingly, we detected a significant 1.77-fold increase in total ATP in the GFM1-patient cells grown in galactose compared to controls in the same conditions. In addition, $O_2^{\cdot -}$ generation was 1.56-fold increased in the patient compared to control (Fig. 39H) and MnSOD showed 55% decreased expression in the patient, with no significant differences for GPx expression compared to controls (Fig. 39I). Therefore, GFM1 cells show a subtle mitochondrial dysfunction with enlarged network branches and impaired ROS metabolism, and a bioenergetic alteration that becomes apparent under mitochondria-reliance conditions.

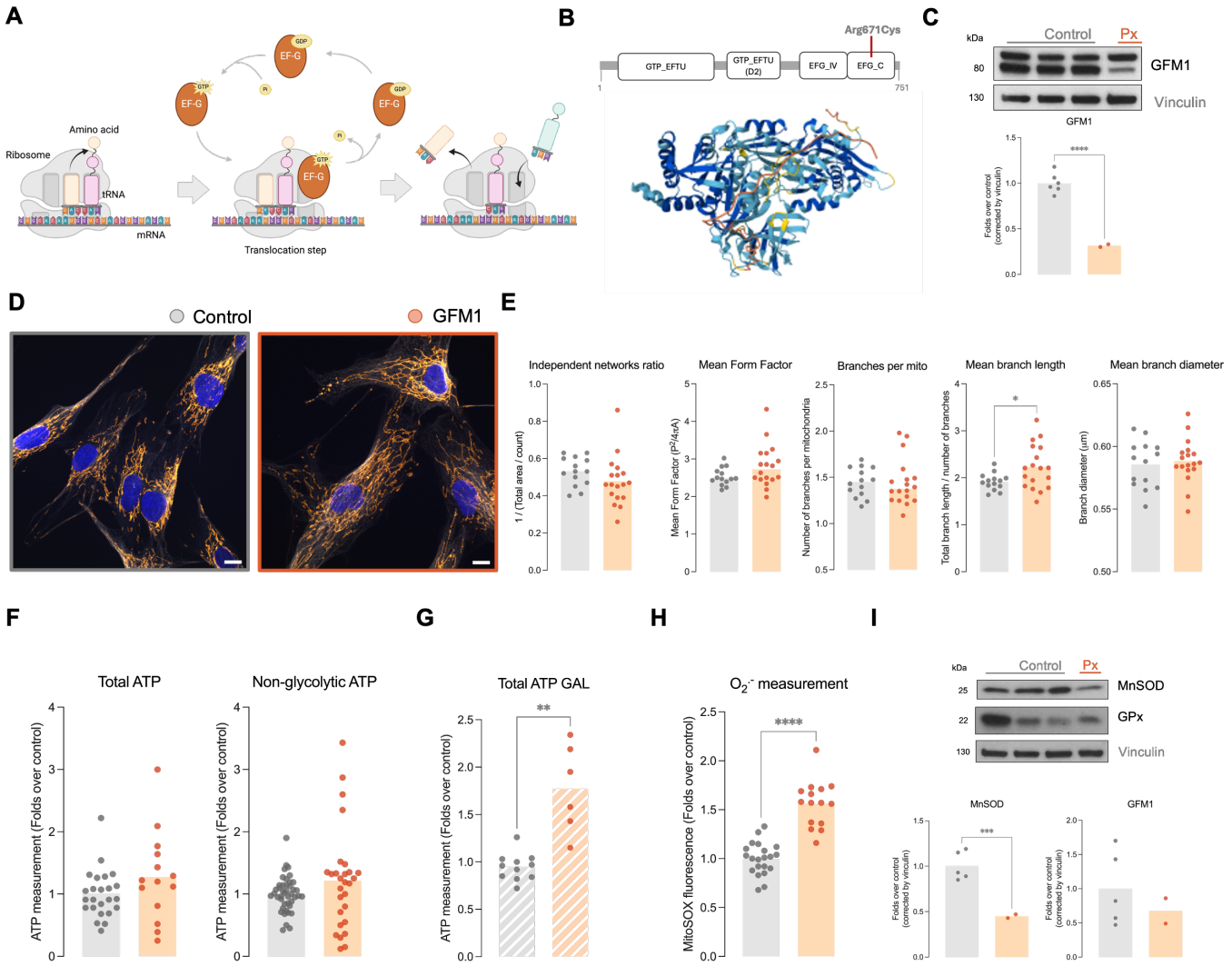

Figure 39. Evaluation of the mutation in GFM1 patient's fibroblasts and its effect on mitochondrial homeostasis maintenance. (A) Schematic representation of the ribosomal translocation step during translation: the elongation factor G (EF-G) binds and hydrolyzes GTP to GDP to drive a conformational change that facilitates the movement of tRNAs and mRNA within the ribosome by one codon; created with BioRender. (B) Schematic representation of the GFM1 sequence and location of the mutation; GTP_EFTU = Elongation factor Tu GTP binding domain, GTP_EFTU_D2 = Elongation factor Tu domain 2, binds the charged tRNA, EFG_IV = Elongation Factor G Domain IV, interacts with the ribosome, EFG_C = Elongation Factor G C-terminal domain, where the mutation is located, helps in the interaction with the ribosome. (C) GFM1 protein expression detection by Western blot in three controls (each lane represents a different cell line) and the patient, with vinculin as loading control (n=2 experiments). (D-I) Mitochondrial network structure and bioenergetics studies on GFM1 fibroblasts. (D) Representative image of the mitochondrial network IF (TOMM20 in yellow, tubulin in grey, nuclei in blue; scale bar 10 µm). (E) Parametrization of the independent networks ratio corrected by area, mean form factor, mean branch length and mean branch diameter (n=13 control, n=18 patient mitochondria). (F) Total and mitochondrial (non-glycolytic) ATP concentration in patient compared to controls both in DMEM high glucose and (G) total ATP after incubation with galactose for 48h, measured by luciferin-luciferase bioluminescence after incubation with 2-DG (n=3-5 experiments with minimum duplicates for total ATP, minimum four technical replicates for mitochondrial ATP). (H) $O_2^{\cdot-}$ production compared to controls, measured by flow cytometry with MitoSOX™ probe (n=4 experiments with triplicates). (I) Representative image of Western blot detection of antioxidant enzymes MnSOD and GPx expression, in three controls (each lane represents a different cell line) and patient, densitometry quantification corrected over vinculin (n=2 experiments).

Data represented as mean for parametric data or median for non-parametric data, with individual values. Comparative analysis control *vs*. GFM1 done with Welch's test for parametric, and Mann-Whitney for non-parametric data. *P* value represents *<0.05, **<0.01, ****<0.0001. Px = patient.

1.4 Mitochondrial OXPHOS complexes subunits expression and assembly

Complex I subunits: *NDUFS1*

This patient had a mitochondrial encephalopathy with pediatric parkinsonism features. Whole exome sequencing and directed analysis through HPOs (Human Phenotype Ontology) revealed a homozygous mutation in *NDUFS1* (OMIM *157655). This nuclear gene encodes a 75 kDa subunit of NADH-ubiquinone oxidoreductase (or complex I) of the oxidative phosphorylation (OXPHOS) system (Fig. 40A). Deficiencies in complex I are the most common between OXPHOS congenital disorders (Kirby et al., 1999). The mutation c.2144G>A (p.Ser715Asn) (Fig. 40B), not previously reported, was located in the isoform 2 and predicted as VUS, potentially causing a gain of allosteric site at R716 (probability 0.34, p = 5 x 10^{-4}) or, with a lower probability but pathogenic, a loss of catalytic site at R716 (probability 0.13, p = 0.03). Ultimately, the mutation resulted in 37% residual protein expression in the patient fibroblasts (Fig. 40C), detected by Western blot.

After diagnosis confirmation, we performed an immunofluorescence with TOMM20 (Fig. 40D) and network parametrization using Mitochondria Analyzer (Fig. 40E). *NDUFS1* mutation in patient's fibroblasts resulted in 10% increased independent networks ratio, 6% increased mean aspect ratio, and 8% decreased mean branch length, with no statistically significant differences for the other parameters compared to controls. These subtle changes represent more individual and round-shaped mitochondrial structures with shorter branches per network in the patient. When we analyzed the bioenergetic profile in this patient, we observed that while total ATP was increased in 1.7-folds, mitochondrial ATP was 32% decreased in the patient compared to controls (Fig. 40F). Regarding ROS generation, we detected a significative increase of 1.48 folds in $O_2^{\cdot-}$ accumulation in the patient fibroblasts compared to controls (Fig. 40G). However, we did not record changes in the expression of antioxidant enzymes MnSOD and GPx in the patient (Fig. 40H), detected by Western blot. These results suggest that in the NDUFS1-deficient cells there is a mitochondrial homeostasis alteration in terms of network structure and deficient bioenergetic function.

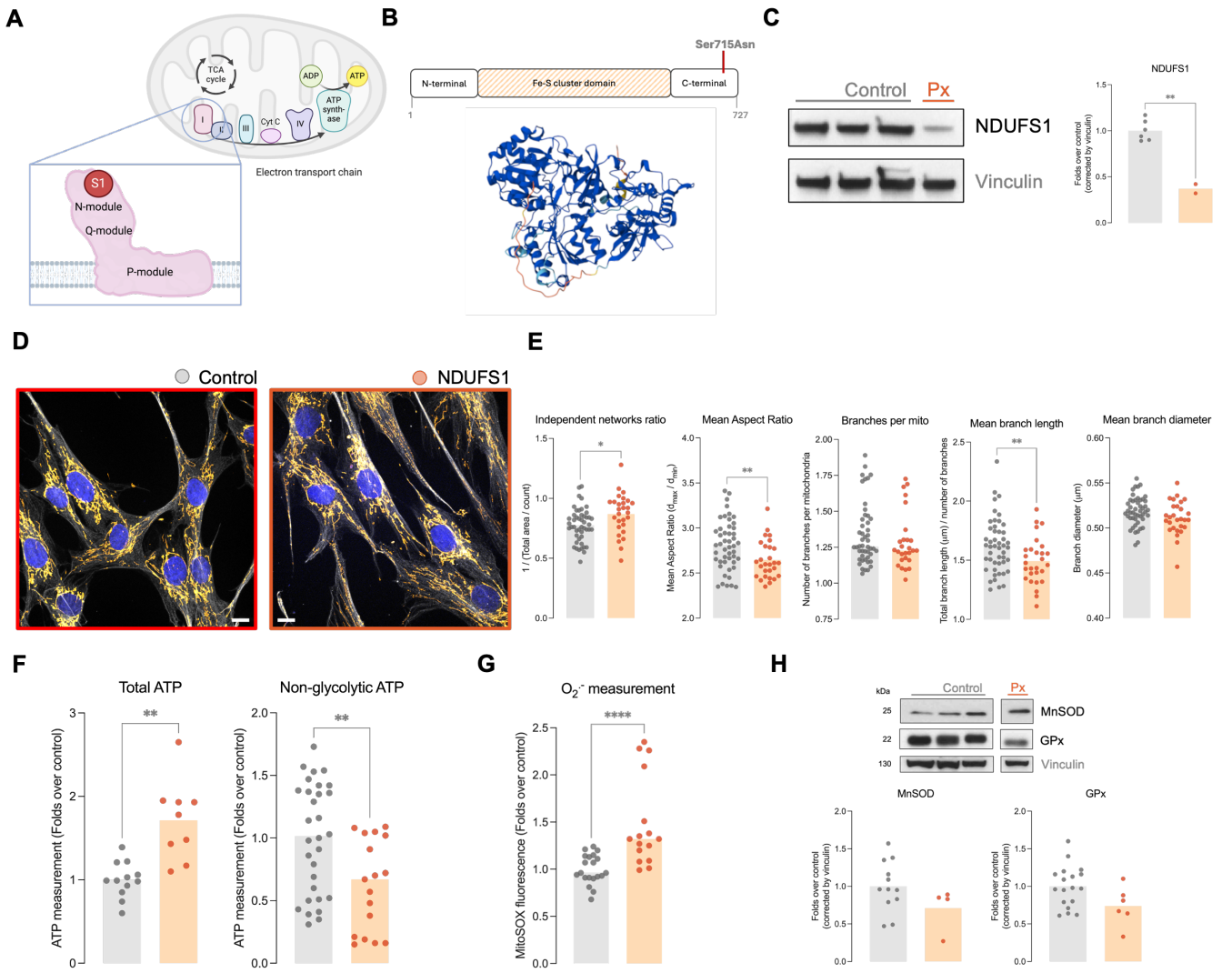

Figure 40. Evaluation of the mutation in NDUFS1 patient's fibroblasts and its effect on mitochondrial homeostasis maintenance.
(cont. next page)

(from previous page)

Figure 40. Evaluation of the mutation in NDUFS1 patient's fibroblasts and its effect on mitochondrial homeostasis maintenance. (A) Schematic representation of the OXPHOS complex I and its subunits; subunit S1 is located in the N module (dehydrogenase module), which accepts electrons from NADH; created with BioRender. (B) Schematic linear representation of the mutation Ser715Asn in NDUFS1, and 3D protein structure, observed through PyMOL; the mutation is located in the C-terminal domain, which interacts with iron-sulfur clusters necessary for electron transfer. (C) Detection of NDUFS1 protein expression in three controls (each lane represents a different cell line) and patient by Western blot, with vinculin used as loading control. (D-H) Mitochondrial network structure and bioenergetics studies on NDUFS1 fibroblasts. (D) Representative image of the mitochondrial network IF (TOMM20 in yellow, tubulin in grey, nuclei in blue; scale bar 10 µm). (E) Parametrization of the number of independent networks corrected by area, mean aspect ratio, number of branches per mitochondrial network, and mean branch length and diameter (n=48 control, n=28 patient mitochondria). (F) Total and mitochondrial (non-glycolytic) ATP concentration in the patient compared to controls, measured by luciferin-luciferase bioluminescence after incubation with 2-DG (n=4 experiments with minimum triplicates). (G) $O_2^{\cdot-}$ production in NDUFS1 fibroblasts compared to controls, measured by flow cytometry with MitoSOX™ probe (n=5 experiments with triplicates). (H) Representative image of antioxidant enzymes MnSOD and GPx expression in patient compared to three controls (each lane represents a different cell line) detected by Western blot and densitometry quantification corrected by vinculin (n=3-5 experiments).
Data represented as mean for parametric data or median for non-parametric data, with individual values. Comparative analysis control *vs*. NDUFS1 done with Welch's test for parametric, and Mann-Whitney for non-parametric data. *P* value represents *<0.05, **<0.01, ****<0.0001. Px = patient.

Complex I assembly factors: *NDUFAF6*

This patient was diagnosed with mitochondrial encephalopathy (Leigh syndrome) and did not present epilepsy nor cardiopathies. He carried two heterozygous mutations, namely c.523G>C (p.Ala178Pro) and c.420+784C>T, in the nuclear gene *NDUFAF6* (OMIM *612392), detected by WES (Fig. 41A). This gene codes for the assembly factor 6 of the OXPHOS complex I, essential for its maturation (McKenzie et al., 2011). The detected mutations were already reported as pathogenic (Catania et al., 2018) and related to complex I deficiencies. *In silico* prediction showed that the amino acid change A178P could cause an altered coiled coil (probability 0.95, $p = 3.8 \times 10^{-4}$) or a pathogenic loss of helix (probability 0.30, $p = 6.7 \times 10^{-3}$). Protein expression of the complex I (by Western blot detection of the subunit NDUFB8) showed a decrease of 91% in the patient compared to controls (Fig. 41B), therefore validating the mutation effect.

Mitochondrial network structure studies by TOMM20 IF (Fig. 41C) showed 14% increase in total area occupied by mitochondria in the cell, 7% decrease in mean aspect ratio and 9% decrease in mean branch length compared to controls, without differences for number of branches per structure nor mean branch diameter (Fig. 41D). Therefore, in the NDUFAF6 patient fibroblasts there are more mitochondria, with round-shaped structures and shorter branches per network, similar to the NDUFS1 patient. Regarding the bioenergetic profile, despite total ATP synthesis was unaffected, mitochondrial ATP was decreased in 73% compared to controls (Fig. 41E). Similarly, $O_2^{\cdot-}$ production was altered, showing an increase in 1.7 folds over controls (Fig. 41F) but no changes were detected for the antioxidant enzymes MnSOD and GPx in the patient (Fig. 41G). All together, these results suggest that *NDUAF6* mutations are affecting mitochondrial network with more mitochondria but with decreased aspect ratio and branches, and deficient bioenergetic function.

(see next page)

Figure 41. Evaluation of the mutations in NDUFAF6 patient's fibroblasts and their effect on mitochondrial homeostasis maintenance. (A) Schematic representation of the mutations c.523G>C (p.Ala178Pro) and c.420+784C>T in the *NDUFAF6* gene, detected by whole exome sequencing. (B) Detection of complex I subunit NDUFB8 protein expression in two controls (each lane represents a different cell line) and patient by Western blot, and densitometry quantification with vinculin used as loading control (n=5 experiments). (C-G) Mitochondrial network structure and bioenergetics studies on NDUFAF6 fibroblasts. (C) Representative image of the mitochondrial network IF (TOMM20 in yellow, tubulin in grey, nuclei in blue; scale bar 10 µm). (D) Parametrization of the total area occupied by signal, mean aspect ratio, number of branches per mitochondrial network, and mean branch length and diameter (n=61 control, n=34 patient mitochondria). (E) Total and mitochondrial (non-glycolytic) ATP concentration in the patient compared to controls, measured by luciferin-luciferase bioluminescence after incubation with 2-DG (n=3 experiments with duplicates for total ATP and minimum quadruplicates for mitochondrial ATP). (F) $O_2^{\cdot-}$ production in NDUFAF6 fibroblasts compared to controls, measured by flow cytometry with MitoSOX™ probe (n=3 experiments with minimum duplicates). (G) Representative image of antioxidant enzymes MnSOD and GPx expression in patient compared to three controls (each lane represents a different cell line) detected by Western blot and densitometry quantification corrected by vinculin (n=4 experiments).
Data represented as mean for parametric data or median for non-parametric data, with individual values. Comparative analysis control *vs*. NDUFAF6 done with Welch's test for parametric, and Mann-Whitney for non-parametric data. *P* value represents *<0.05, **<0.01, ***<0.001, ****<0.0001. Px = patient.

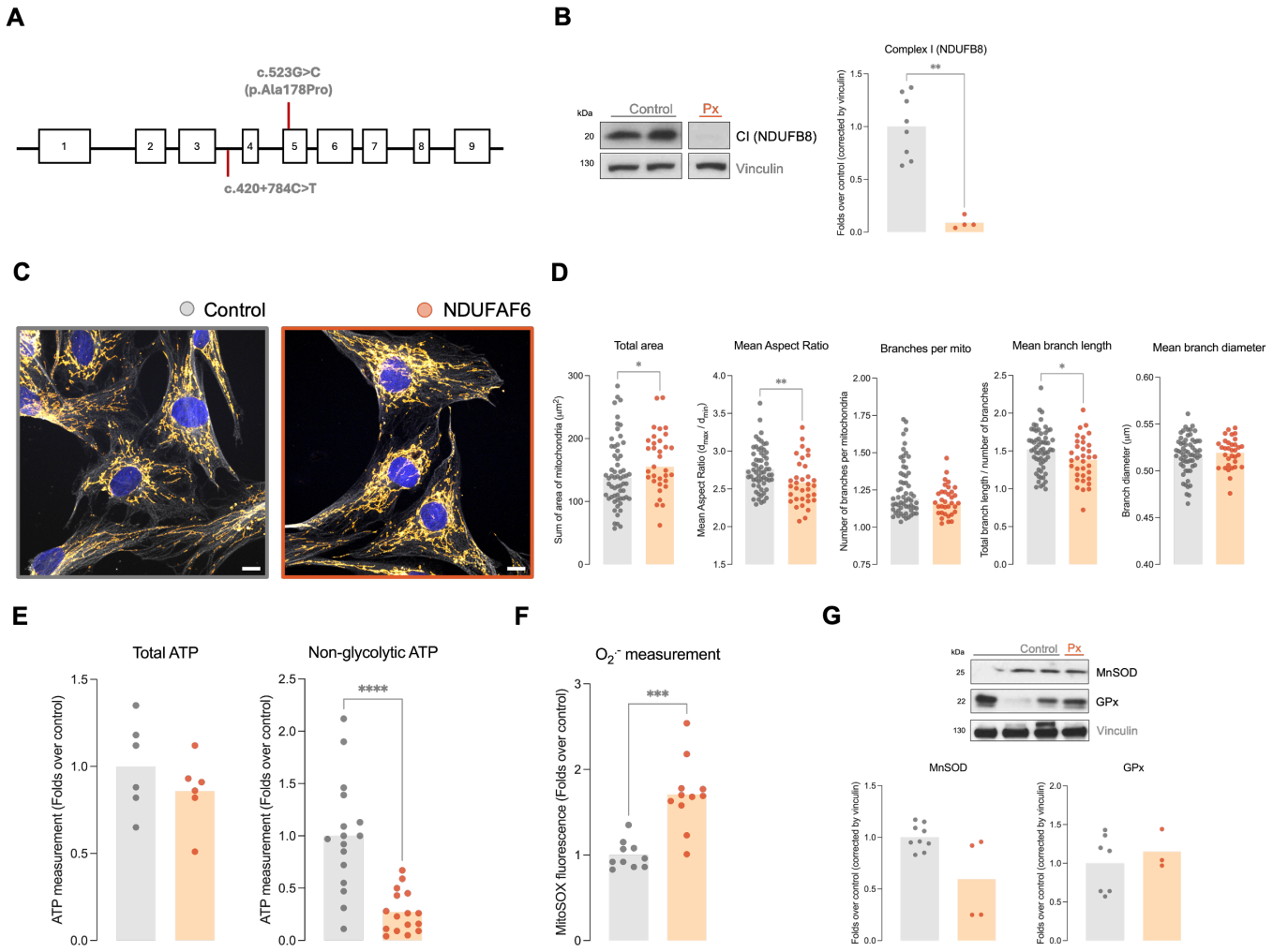

Complex IV assembly factors: *SCO2*

The patient was diagnosed with pure neuroaxonal neuropathy, gait impairment with marked imbalance and tremor. He carried two mutations in nuclear *SCO2* gene (OMIM *604272). This gene codes for the cytochrome c oxidase (COX, or complex IV) assembly protein 2, a copper metallochaperone essential for the synthesis and maturation of COX subunit II (COX II) (Fig. 42A) and has been related to mitochondrial complex IV deficiencies. The two mutations c.244_246delAAG (p.Lys82del) and c.703G>A (p.Gly235Ser) (Fig. 42B) were detected by WES and were predicted to be likely pathogenic. The first mutation was previously reported in patients with high myopia (Zheng et al., 2021). The missense mutation Gly253Ser was *in silico* predicted to cause altered metal binding (probability 0.34, p = 8.3 x 10^{-4}) or a pathogenic loss of strand (probability 0.26, p = 0.04), between other non-pathogenic possibilities. Detection of SCO2 protein expression by Western blot showed a non-significative 38% decrease in patient fibroblasts compared to healthy controls (Fig. 42C), whereas detection of COX II showed a significative 44% decreased expression compared to control cells (Fig. 42D). Therefore, the detected *SCO2* mutations may not be affecting protein expression but influencing complex IV synthesis, particularly COX II subunit.

After confirmation of the mutations effect on complex IV stability, we observed mitochondrial network structure in the patient cells (Fig. 42E). Parametrization showed a significant 48% increase in total area occupied by mitochondria, a 16% decrease in mean form factor, 10% decrease in branches per structure, and 16% decrease in mean branch length without significant changes for mean branch diameter, compared to controls (Fig. 42F). In short, *SCO2*-mutated cells have more mitochondria with less and shorter branches. Regarding ATP synthesis in the patient, total ATP was not affected while mitochondrial ATP was decreased in a 39% compared to controls (Fig. 42G). In the same context, $O_2^{\cdot-}$ production was increased 2.83 folds in the patient compared to controls (Fig. 42H), paired with a 61% decrease in MnSOD expression (Fig. 42I). These results suggest that *SCO2* mutations cause a defective mitochondrial network together with an inefficient bioenergetic function.

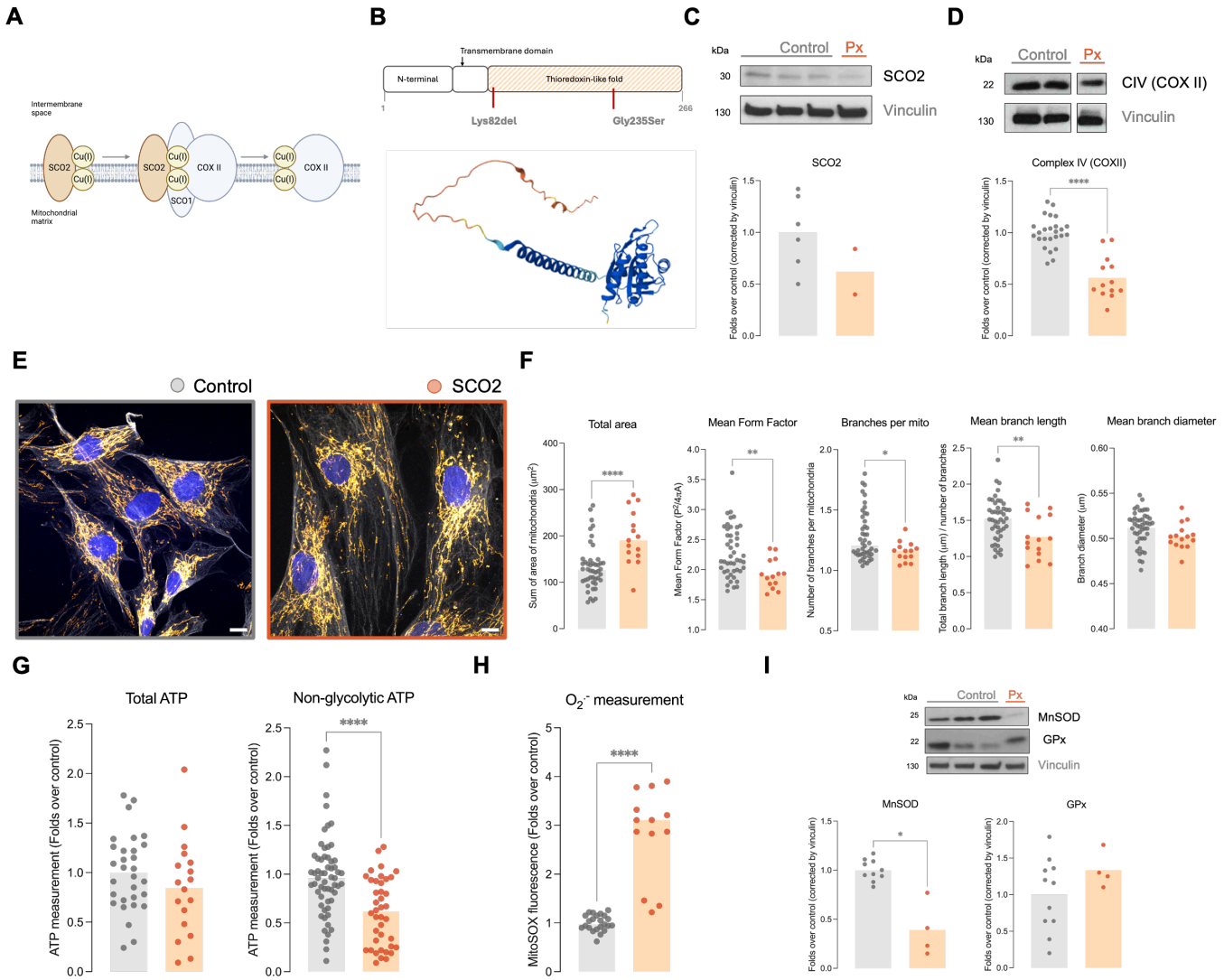

Figure 42. Evaluation of the mutations in SCO2 patient's fibroblasts and their effect on mitochondrial homeostasis maintenance. (A) Schematic representation of the assembly factor SOC2 function: it delivers two coppers to COXII necessary for the catalytic site of complex IV; created with BioRender. (B) Schematic representation of the mutations Lys82del and Gly235Ser in SCO2, and 3D protein structure and location of the mutations, observed through PyMOL. Detection of (C) SCO2 and (D) COX II subunit from complex IV protein expressions in three and two controls respectively (each lane represents a different cell line) and patient by Western blot, and densitometry quantification with vinculin used as loading control (n=2 experiments for SCO2, n=11 experiments for COX II). (E-I) Mitochondrial network structure and bioenergetics studies on SCO2 fibroblasts. (E) Representative image of the mitochondrial network IF (TOMM20 in yellow, tubulin in grey, nuclei in blue; scale bar 10 µm). (F) Parametrization of the total area occupied by signal, mean form factor, number of branches per mitochondrial network, and mean branch length and diameter (n=46 control, n=15 patient mitochondria). (G) Total and mitochondrial (non-glycolytic) ATP concentration in the patient compared to controls, measured by luciferin-luciferase bioluminescence after incubation with 2-DG (n=7 experiments with duplicates for total ATP and minimum quadruplicates for mitochondrial ATP). (H) $O_2^{\cdot-}$ production in SCO2 fibroblasts compared to controls, measured by flow cytometry with MitoSOX™ probe (n=4 experiments with minimum duplicates). (I) Representative image of antioxidant enzymes MnSOD and GPx expression in patient compared to three controls (each lane represents a different cell line) detected by Western blot and densitometry quantification corrected by vinculin (n=4 experiments). Data represented as mean for parametric data or median for non-parametric data, with individual values. Comparative analysis control *vs*. SCO2 done with Welch's test for parametric, and Mann-Whitney for non-parametric data. *P* value represents *<0.05, **<0.01, ****<0.0001. Px = patient.

Complex IV assembly factors: *SURF1*

The first patient presented ataxia and gastrointestinal problems, debuting at 6 months of age. The second patient, who also debuted at 6 months, presented hypotonia, neurodevelopmental delay, and digestive problems. These two patients were diagnosed by WES with mutations in *SURF1* gene (OMIM *185620) and will be identified as SURF1_P1 and SURF1_P2. This gene encodes for the surfeit locus 1 protein (SURF1), component of the MITRAC complex (Mitochondrial Translation Regulation Assembly intermediate of COX complex) that regulates complex IV assembly (Fig. 43A). Mutations in this gene have been broadly related to Leigh syndrome.

SURF1_P1 carried two heterozygous mutations in c.817C>T (p.Gln273*) and c.503T>G (p.Val177Gly), previously reported (Dixon-Salazar et al., 2012; Yuksel et al., 2006), both predicted as pathogenic. The missense mutation can potentially be causing altered stability (probability 0.33, p = 4.4 x 10^{-3}). SURF1_P2 carried two heterozygous

mutations in c.809_826dup AGCATCTGCAGTACATCG (p.Glu270_Ile275dup) and c.815_825dup TGCAGTACATC (p.Val276Cysfs*5) predicted as pathogenic and likely pathogenic respectively (Fig. 43B). For both SURF1 patients' fibroblasts, Western blot analysis revealed residual SURF1 protein expression of 0.19 folds for P1 and 0.30 folds for P2 (Fig. 43C) and COXII subunit from complex IV (Fig. 43D) with 86% decrease for P1 and 92% decrease for P2 compared to control cells.

98| Mitochondrial network detection by TOMM20 IF (Fig. 43E) revealed similar alterations for both patients' cells. Parametrization detected a significant increase in total area of 1.42 folds and a subtle but significant 10 nm decrease in mean branch diameter, for both SURF1 patients compared to controls (Fig. 43F), without significant alterations in mean form factor, branches per structure and mean branch length. Therefore, SURF1 fibroblasts have more mitochondria with slightly thinner branches. Regarding the bioenergetic profile, SURF1-deficient cells showed different alterations: total ATP was significantly decreased in 31% for SURF1_P2 without changes for P1, whereas mitochondrial ATP was analogously decreased for both patients (67% for P1 and 64% for P2) compared to controls (Fig. 43G). In addition, ROS production showed differences between the patients. $O_2^{\cdot-}$ generation was 1.56-fold increased for SURF_P1 while SURF1_P2 fibroblasts showed a significant decrease in 24% compared to healthy controls (Fig. 43H). Antioxidant enzymes expression showed no statistically significant differences for both patients over the controls (Fig 43I). In this context, SURF1 patients show a distinctive mitochondrial homeostasis alteration, with similar network morphology but different bioenergetic shifts.

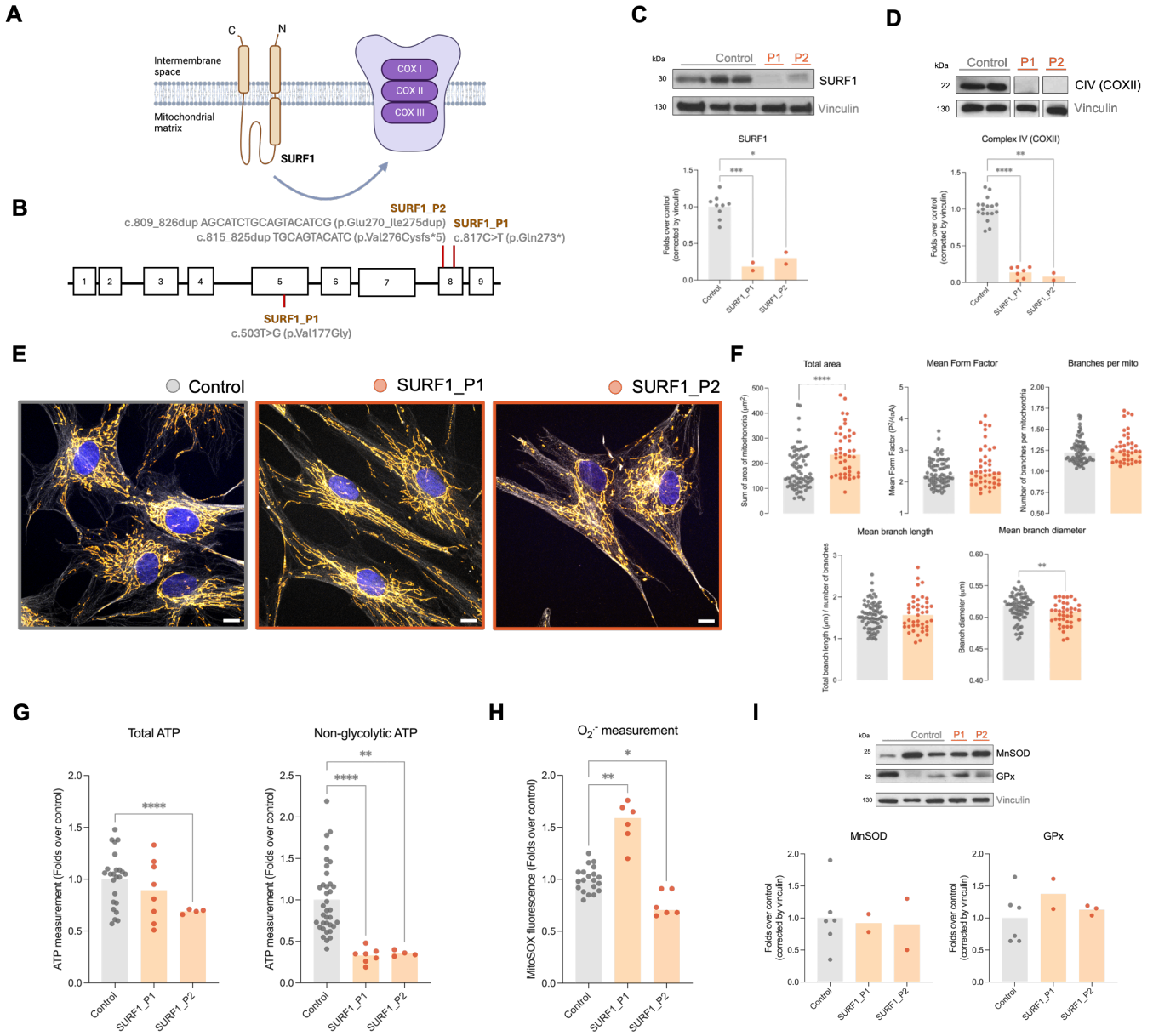

Figure 43. Evaluation of the mutations in two SURF1 patients' fibroblasts (SURF1_P1 and SURF1_P2), and their effect on mitochondrial homeostasis maintenance. (A) Schematic representation of SURF1 in the assembly of the subunits COX I, II and III that form the catalytic core of complex IV; created using BioRender. (B) Schematic representation of the mutations c.817C>T (p.Gln273*) and c.503T>G (p.Val177Gly) for P1, and c.809_826dup AGCATCTGCAGTACATCG (p.Glu270_Ile275dup) and c.815_825dup TGCAGTACATC (p.Val276Cysfs*5) for P2, in the *SURF1* gene, detected by whole exome sequencing. Detection of (C) SURF1 and (D) COX II subunit from complex IV protein expressions in three and two controls respectively (each lane represents a different cell line) and *(cont. next page)*

(from previous page) SURF1 patients by Western blot, and densitometry quantification with vinculin used as loading control (n=2-7 experiments). (E-I) Mitochondrial network structure and bioenergetics studies on SURF1_P1 and P2 fibroblasts. (E) Representative image of the mitochondrial network IF (TOMM20 in yellow, tubulin in grey, nuclei in blue; scale bar 10 µm). (F) Parametrization of the total area occupied by signal, mean form factor, number of branches per mitochondrial network, and mean branch length and diameter (n=78 control, n=43 patients' mitochondria). (G) Total and mitochondrial (non-glycolytic) ATP concentration in the two patients compared to controls, measured by luciferin-luciferase bioluminescence after incubation with 2-DG (n=3 experiments with minimum quadruplicates). (H) $O_2^{\cdot-}$ production in both *SURF1* patients' fibroblasts compared to controls, measured by flow cytometry with MitoSOX™ probe (n=3 experiments with minimum triplicates). (I) Representative image of antioxidant enzymes MnSOD and GPx expression in both patients compared to three controls (each lane represents a different cell line), densitometry quantification corrected over vinculin (n=3 experiments).
Data represented as mean for parametric data or median for non-parametric data, with individual values. Comparative analysis control *vs*. *SURF1* done with Welch's test for parametric, and Mann-Whitney for non-parametric data; for multiple comparison of the two patients over the control (Brown-Forsythe and Welch) ANOVA if parametric or Kruskal-Wallis if non-parametric. *P* value represents *<0.05, **<0.01, ****<0.0001. P1 = SURF1 patient 1, P2 = SURF1 patient 2.

1.5 Intermediate metabolism

Glutamate transport: *SLC25A22*

This patient was diagnosed with psychomotor retardation and presented a very severe neurological phenotype with cerebral palsy and neonatal seizures. He had a mutation in the *SLC25A22* gene, called Solute Carrier Family 25 (Mitochondrial carrier, glutamate), member 22 (OMIM *609302). This gene codes for the mitochondrial glutamate carrier 1 (GC-1), one of the transporters for glutamate from the cytosol into the mitochondrial matrix (Fig. 44A). Mutations in this gene have been associated with developmental and epileptic encephalopathies (Spoto et al., 2021), and downregulation of this gene has been associated with Alzheimer's disease onset (Tian et al., 2024), suggesting a role in neurodegeneration as well. However, the exact mutation for this patient was not available for *in silico* studies. Protein detection by Western blot showed residual 14% GC-1 expression in the patient fibroblasts compared to controls (Fig. 44B).

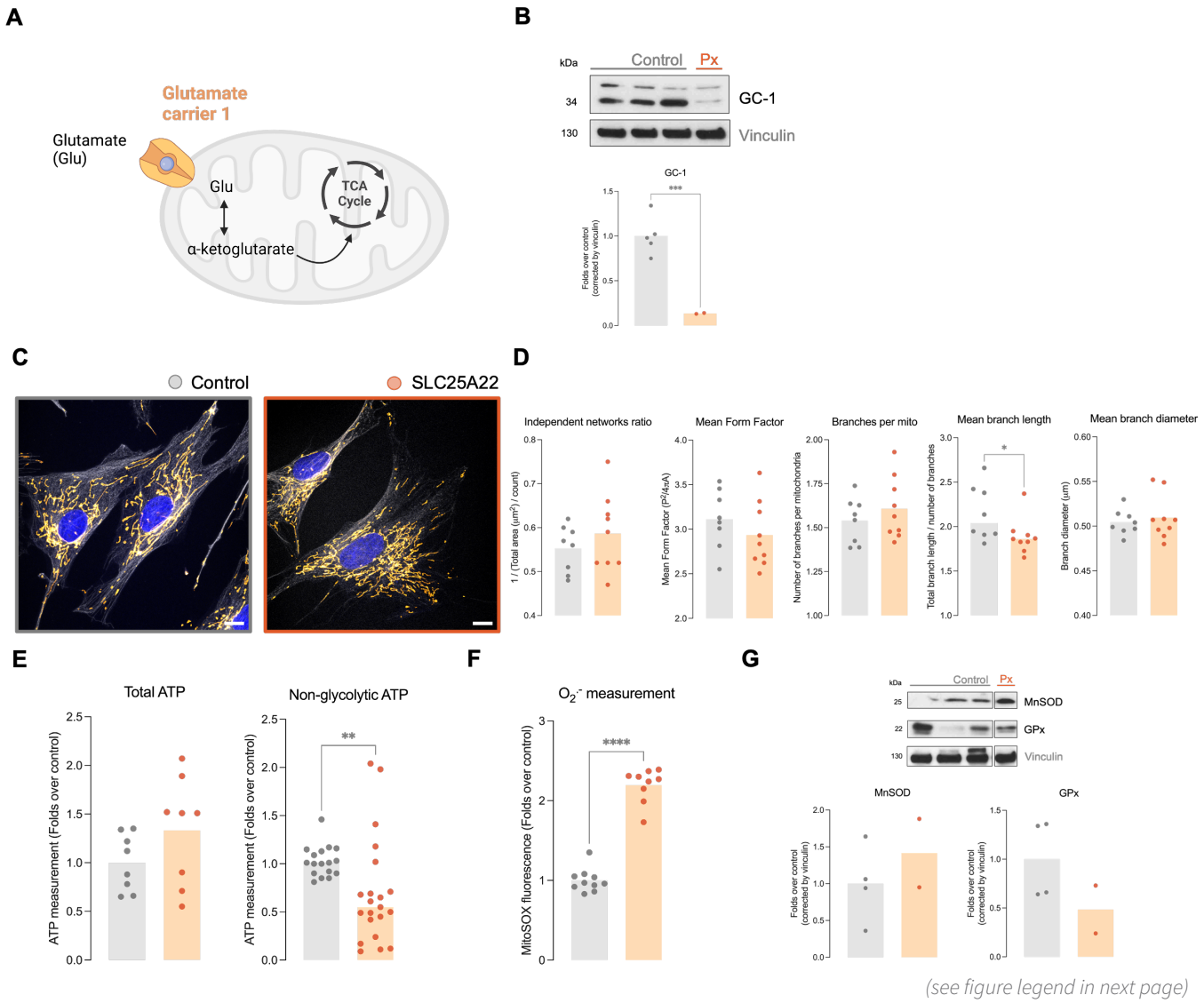

(see figure legend in next page)

(from previous page)
Figure 44. Evaluation of the mutations in SLC25A22 patient fibroblasts and their effect on mitochondrial homeostasis maintenance. (A) Schematic representation of the glutamate carrier 1 (GC-1) in the transport of glutamate from the cytosol into the mitochondrial matrix and its posterior use in metabolism; created with BioRender. (B) Detection of GC-1 protein expression in three controls (each lane represents a different cell line) by Western blot, with vinculin used as loading control (n=2 experiments). (C-G) Mitochondrial network structure and bioenergetics studies on SLC25A22 fibroblasts. (C) Representative image of the mitochondrial network IF (TOMM20 in yellow, tubulin in grey, nuclei in blue; scale bar 10 µm). (D) Parametrization of the independent networks ratio, mean form factor, number of branches per mitochondrial network, and mean branch length and diameter (n=8 control, n=9 patient mitochondria). (E) Total and mitochondrial (non-glycolytic) ATP concentration in the patient compared to controls, measured by luciferin-luciferase bioluminescence after incubation with 2-DG (n=4 experiments with duplicates for total ATP, 6 technical replicates for mitochondrial ATP). (F) $O_2^{\cdot-}$ production in patient compared to controls, measured by flow cytometry with MitoSOX™ probe (n=3 experiments with minimum duplicates). (G) Representative image of antioxidant enzymes MnSOD and GPx expression in patient compared to three controls (each lane represents a different cell line), densitometry quantification corrected over vinculin (n=2 experiments).
Data represented as mean for parametric data or median for non-parametric data, with individual values. Comparative analysis control *vs*. *SLC25A22* done with Welch's test for parametric, and Mann-Whitney for non-parametric data. *P* value represents *<0.05, **<0.01, ****<0.0001. Px = patient.

After diagnosis confirmation, we analyzed mitochondrial homeostasis in the patient cells. TOMM20 IF (Fig. 44C) showed a mitochondrial network with 11% decrease in mean length of branches, without significative alterations for the other parameters compared to controls (Fig. 44D). Measurement of total ATP revealed no significant differences for the patient, whereas mitochondrial ATP showed a 30% decrease in SLC25A22 patient compared to controls (Fig. 44E). Ultimately, ROS production was increased in 2.2 folds compared to controls (Fig. 44F), without significative changes in antioxidant enzymes MnSOD and GPx expression (Fig. 44G). Therefore, mutations in the mitochondrial glutamate carrier 1 cause minor mitochondrial morphology alterations with a decrease in branch length together with important bioenergetic deficiencies.

Coenzyme A synthesis: *COASY*

This patient was diagnosed with neurodevelopmental delay, refractory epileptic spasms and severe neurodevelopmental encephalopathy. He carried a mutation in the *COASY* gene (OMIM *609855) that codes for the coenzyme A (CoA) synthase, a bifunctional enzyme that catalyzes the two last steps in CoA synthesis (Fig. 45A). CoA is a pivotal metabolic cofactor essential for catabolism, anabolism and metabolic signaling. Mutations in this gene have been related to COASY protein-associated neurodegeneration (COPAN) and other rare disorders that continue to be identified. Detected by WES, the homozygous mutation c.140dupT (p.Ala48fs) was identified for the isoform 2 (Fig. 45B), not previously reported, and was predicted as likely pathogenic. Western blot detection of COASY expression in patient cells showed a residual 13% expression (Fig. 45C), therefore confirming the pathogenicity of the mutation.

Mitochondrial network structure analysis by TOMM20 IF (Fig. 45D) showed significant alterations for all the measured morphology and branching parameters (Fig. 45E). The patient mitochondria presented an increase of 2.11 folds in the independent networks ratio, a 34% decrease in mean form factor, a 21% decrease in number of branches per structure, a decrease of 43% for mean branch length, and a significant decrease of 40 nm in branches diameter compared to controls. Therefore, the patient has more mitochondrial networks with less, thinner and shorter branches. Regarding the bioenergetic profile, we did not detect alterations for both total and mitochondrial ATP (Fig. 45F), but a 3.17-fold increase in $O_2^{\cdot-}$ generation in the patient cells compared to controls (Fig. 45G) together with a 3.43-fold increase in MnSOD expression (Fig. 45H). These results suggest that the *COASY* mutation severely affects mitochondrial network structure and ROS generation and metabolism whereas ATP synthesis is unaffected in patient's fibroblasts.

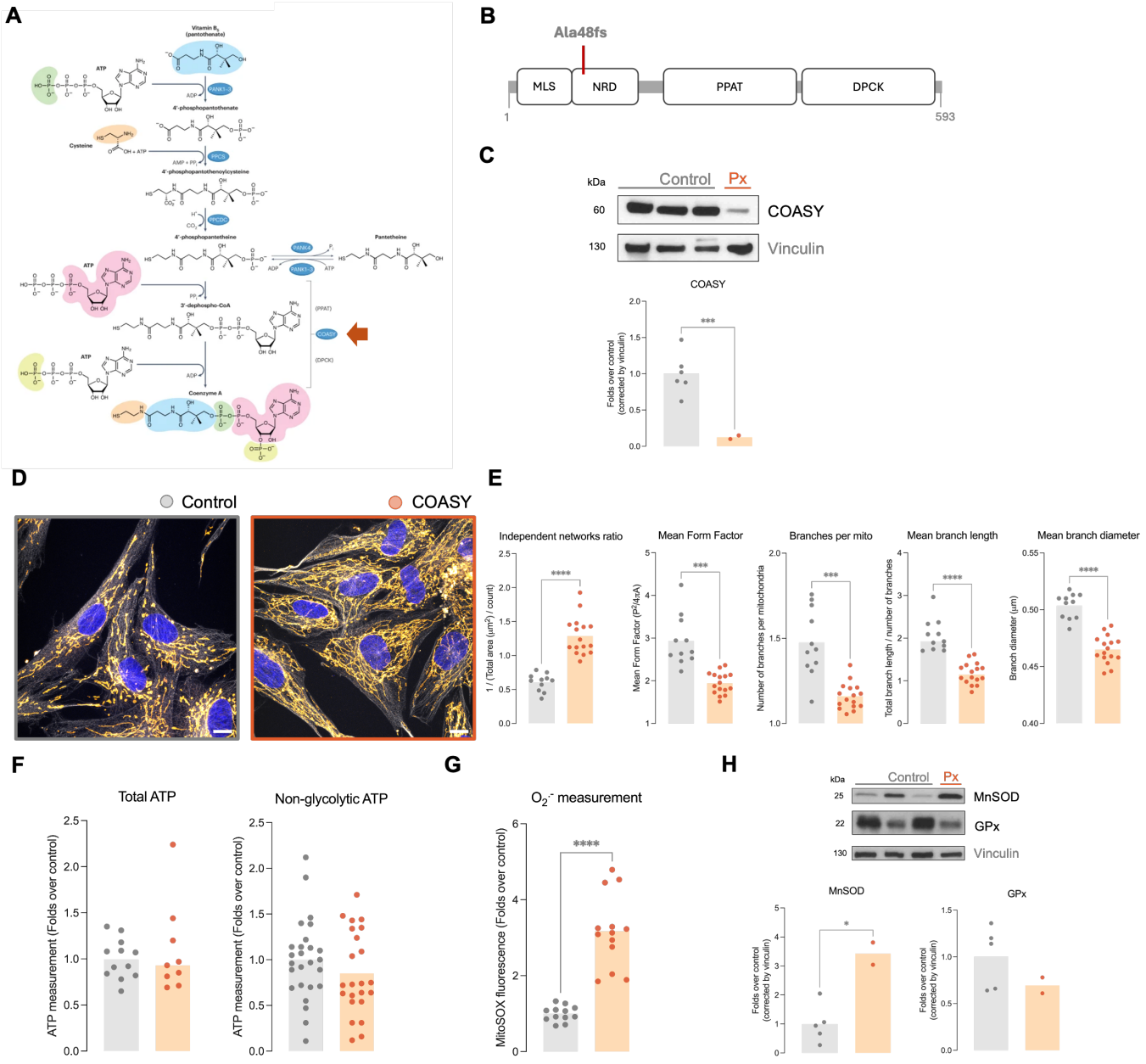

Figure 45. Evaluation of the mutation in COASY patient fibroblasts and its effect on mitochondrial homeostasis maintenance. (A) Schematic representation of the coenzyme A (CoA) biosynthesis, in which COASY catalyzes the last two steps; adapted from (Barritt et al., 2024). (B) Schematic representation of the mutation Ala48fs in COASY, located on the Nucleotide Recognition Domain (NRD); MLS = Mitochondria Localizing Sequence, PPAT = Phosphopantetheine Adenylyltransferase, DPCK = Dephospho-CoA Kinase. (C) Detection of COASY protein expression in three controls (each lane represents a different cell line) by Western blot, with vinculin used as loading control (n=2 experiments). (D-H) Mitochondrial network structure and bioenergetics studies on COASY fibroblasts. (D) Representative image of the mitochondrial network IF (TOMM20 in yellow, tubulin in grey, nuclei in blue; scale bar 10 µm). (E) Parametrization of the independent networks ratio, mean form factor, number of branches per mitochondrial network, and mean branch length and diameter (n=11 control, n=16 patient mitochondria). (F) Total and mitochondrial (non-glycolytic) ATP concentration in the patient compared to controls, measured by luciferin-luciferase bioluminescence after incubation with 2-DG (n=5 experiments with duplicates for total ATP, quadruplicates for mitochondrial ATP). (G) $O_2^{\cdot-}$ production in patient compared to controls, measured by flow cytometry with MitoSOX™ probe (n=4 experiments with minimum duplicates). (H) Representative image of antioxidant enzymes MnSOD and GPx expression in patient compared to three controls (each lane represents a different cell line), densitometry quantification corrected over vinculin (n=2 experiments).

Data represented as mean for parametric data or median for non-parametric data, with individual values. Comparative analysis control *vs*. COASY done with Welch's test for parametric, and Mann-Whitney for non-parametric data. *P* value represents ***<0.001, ****<0.0001. Px = patient.

Pyruvate Dehydrogenase complex: *PDHX*

The patient, diagnosed with global developmental delay, carried a mutation in the *PDHX* gene (OMIM *608769). This gene encodes for pyruvate dehydrogenase E3-binding protein (also called X), subunit part of the pyruvate dehydrogenase complex (PDC), which catalyzes the oxidative decarboxylation of pyruvate to form acetyl CoA and plays a crucial role in energy metabolism (Fig. 46A). Mutations in this gene have been related to lactic acidemias.

Detected by WES, the patient carried an homozygous mutation inherited from consanguineous parents, namely c.906delT (p.Tyr302fs) (Fig. 46B), not previously reported. Western blot analysis revealed absence of the PDHX protein expression in patient fibroblasts compared to controls (Fig. 46C), confirming the diagnosis.

To study the implications of this mutation on mitochondrial homeostasis, we first observed the network structure by TOMM20 IF (Fig. 46D). Its parametrization revealed a 1.34-fold increase in total area occupied by mitochondria in the cell and 10% increase in mean branch length without differences in mean form factor, number of branches and diameter compared to controls (Fig. 46E). In consequence, PDHX patient fibroblasts have more mitochondrial mass with longer ramifications. Bioenergetic profile analysis revealed no changes in total ATP but a 36% significant decrease in mitochondrial ATP synthesis in the patient cells compared to control (Fig. 46F). Regarding ROS production, MitoSOX™ fluorescence showed a significant increase of 1.83 folds compared to controls (Fig. 46G) that was paired to a 61% decrease in MnSOD expression (Fig. 46H). Therefore, mutations in enzymes that catalyze steps previous to mitochondrial reactions (e.g. Krebs cycle), can affect its homeostasis.

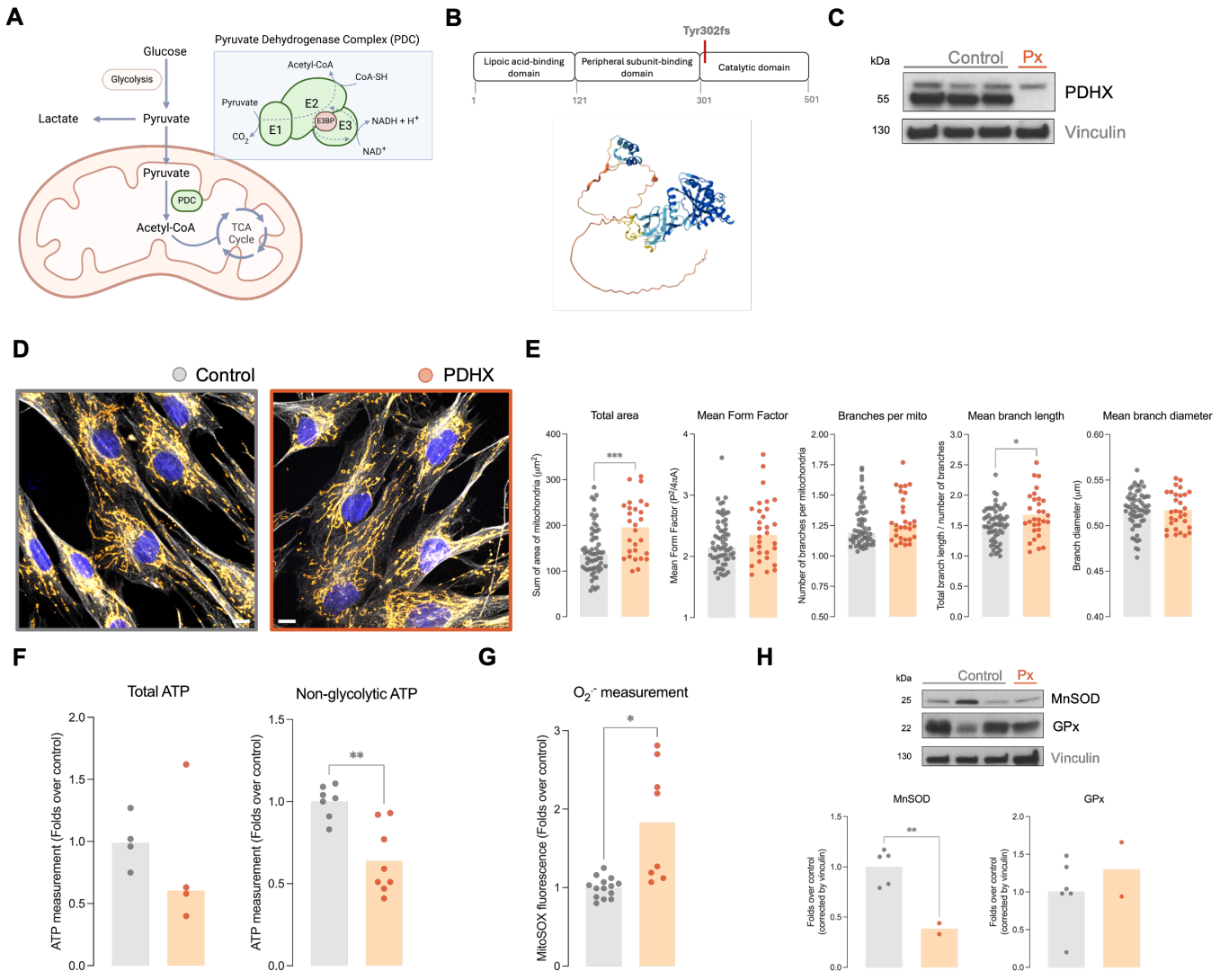

Figure 46. Evaluation of the mutation in PDHX patient fibroblasts and its effect on mitochondrial homeostasis maintenance. (A) Schematic representation of PDC function: in mitochondria, it catalyzes the oxidative decarboxylation of pyruvate into acetyl-CoA, which later enters the Krebs cycle. It has three subunits: E1 = pyruvate dehydrogenase, E2 = dihydrolipoamide acetyltransferase, E3 = dihydrolipoamide dehydrogenase, and the E3BP (X) = E3 binding protein; created with BioRender. (B) Schematic representation of the mutation Tyr302fs in the PDHX and 3D protein structure, observed through PyMOL. (C) Detection of PDHX protein expression in three controls (each lane represents a different cell line) by Western blot, with vinculin used as loading control (D-H) Mitochondrial network structure and bioenergetics studies on PDHX fibroblasts. (D) Representative image of the mitochondrial network IF (TOMM20 in yellow, tubulin in grey, nuclei in blue; scale bar 10 µm). (E) Parametrization of the total area, mean form factor, number of branches per mitochondrial network, and mean branch length and diameter (n=61 control, n=30 patient mitochondria). (F) Total and mitochondrial (non-glycolytic) ATP concentration in the patient compared to controls, measured by luciferin-luciferase *(cont. next page)*

(from previous page)
bioluminescence after incubation with 2-DG (n=2 experiments with duplicates for total ATP and quadruplicates for mitochondrial ATP). (G) $O_2^{\cdot-}$ production in patient compared to controls, measured by flow cytometry with MitoSOX™ probe (n=2 experiments with quadruplicates). (H) Representative image of antioxidant enzymes MnSOD and GPx expression in patient compared to three controls (each lane represents a different cell line), densitometry quantification corrected over vinculin (n=2 experiments).
Data represented as mean for parametric data or median for non-parametric data, with individual values. Comparative analysis control *vs*. PDHX done with Welch's test for parametric, and Mann-Whitney for non-parametric data. *P* value represents ***<0.001, ****<0.0001. Px = patient.

2 Personalized therapeutic approach

2.1 Pharmacologic treatment: leriglitazone

We studied the potential application of the already presented PPARγ agonist leriglitazone (LGZ) in the recovery of mitochondrial alterations in mitochondrial diseases.

We first investigated its effect in fibroblasts from the *NDUFS1*-mutated patient. As previously explained, these cells had decreased mitochondrial ATP paired with an augmented ROS generation. To assess the effect of LGZ, we treated the patient fibroblasts with 100 nM and 500 nM LGZ for 48 hours. Mitochondrial ATP in the patient showed significant increases with the two concentrations assayed (5.16 folds for 100 nM and 4.87 folds for 500 nM), compared to the basal ATP concentration in the patient (Fig. 47A). Importantly, the oxidative species generation was decreased in the patient with both concentrations (27% and 24% respectively) compared to basal condition (Fig. 47B). This suggests that LGZ treatment can efficiently correct the main mitochondrial dysfunction in the complex I-deficient NDUFS1 patient.

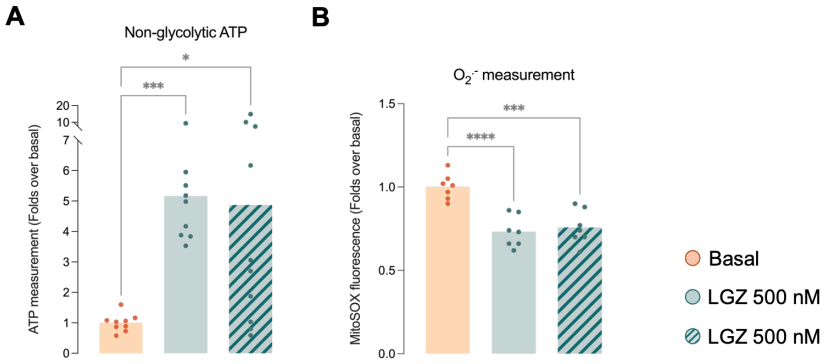

Figure 47. Bioenergetic profile in NDUFS1 patient's fibroblasts after LGZ treatment. (A) Mitochondrial (non-glycolytic) ATP concentration in the treated *NDUFS1*-mutated patient's cells compared to basal condition, measured by luciferin-luciferase bioluminescence after incubation with 2-DG (n=3 experiments with minimum triplicates). (B) $O_2^{\cdot-}$ production in the treated fibroblasts compared to basal, measured by flow cytometry with MitoSOX probe (n=3 experiments with minimum duplicates).
Data represented as mean for parametric data or median for non-parametric data, with individual values. Comparative analysis basal *vs*. 100 nM and 500 nM done with (Brown-Forsythe and Welch) ANOVA if parametric or Kruskal-Wallis if non-parametric. *P* value represents *<0.05, ***<0.001, ****<0.0001.

Enlightened by the positive results, we wondered whether this could be extrapolated to other conditions such as defects in mitochondrial dynamics. For that, we investigated the effect of LGZ treatment on fibroblasts of the five DNM1L patients. Since these patients are characterized by a distinctive network structure, we explored if LGZ would be able to exert an effect on this parameter (Fig. 48A). For DNM1L patients P1 and P4, parametrization of the mitochondrial network detected with TOMM20 IF, showed no significant differences for the representative parameters after 500 nM LGZ treatment for 48 hours, detecting only a significant but subtle increase in 14 nm for the branch diameter (Fig. 48B). Regarding the bioenergetic profile, bioluminescence detection of mitochondrial ATP concentration did not reveal any significant differences (Fig. 48C) compared to the basal condition. Regarding $O_2^{\cdot-}$ generation measured through flow cytometry, we detected significant decreases in 24% for DNM1L_P1 and 23% for P2, but it was further increased in patients DNM1L_P3 (1.6 folds) and P4 (1.4 folds), the latter who had the highest increment in basal conditions (Fig. 48D). In this manner, LGZ does not correct the bioenergetic deficiencies in DNM1L patients at the assayed treatment conditions.

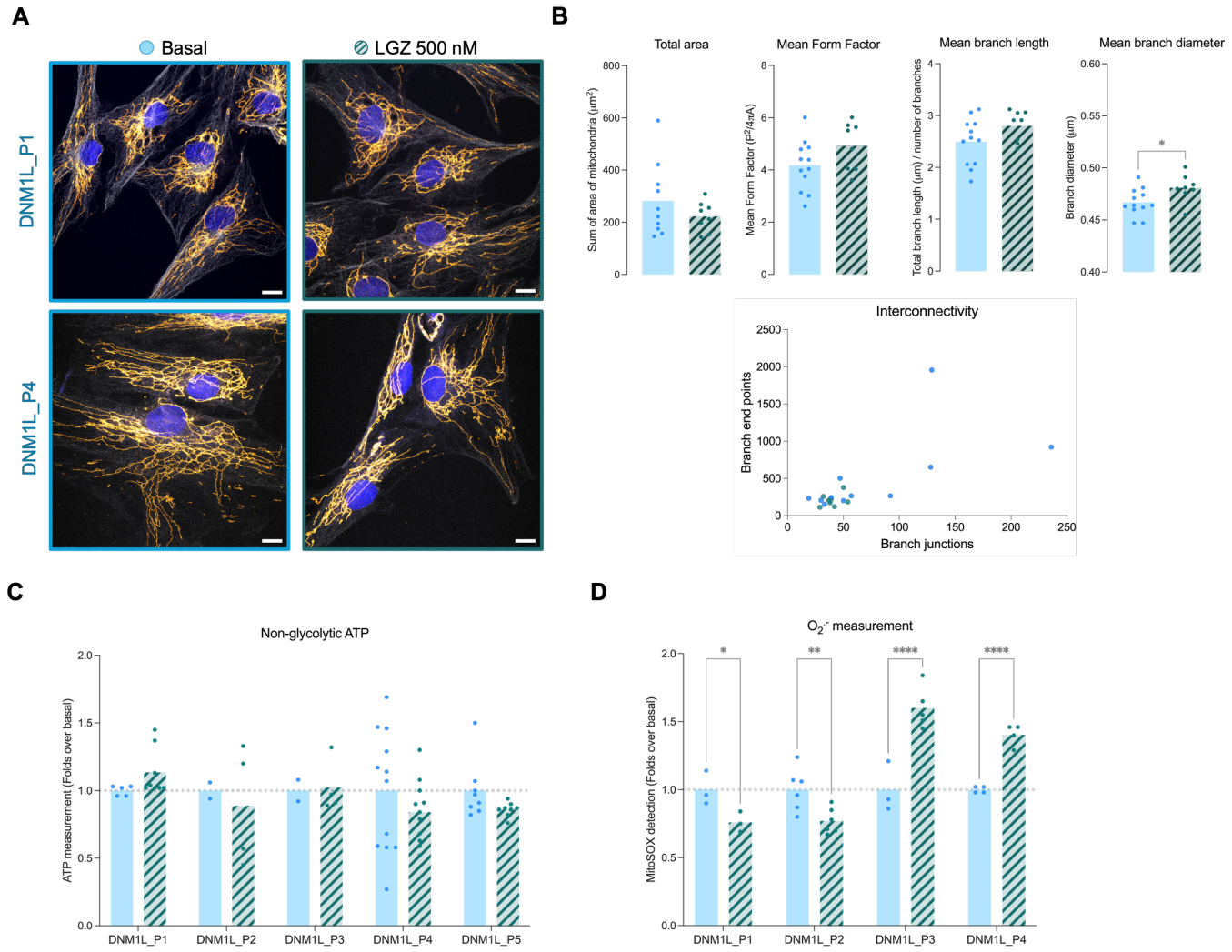

Figure 48. Mitochondrial function performance in DNM1L patients' fibroblasts after LGZ treatment. (A) Representative image for DNM1L_P1 and P4 of the mitochondrial network IF, in basal and LGZ-treated conditions (TOMM20 in yellow, tubulin in grey, nuclei in blue; scale bar 10 µm). (B) Parametrization of the total area of signal occupied by mitochondria, mean form factor, mean branch length and diameter, and interconnectivity, expressed as the relationship between the number of branch end points and branch junctions; quantified with Mitochondria Analyzer (n=12 basal, n=8 LGZ-treated patients' mitochondria). (C) Mitochondrial (non-glycolytic) ATP concentration in the treated *DNM1L*-mutated patients' cells compared to basal condition, measured by luciferin-luciferase bioluminescence after incubation with 2-DG (n=2-3 experiments with minimum duplicates). (D) $O_2^{\cdot-}$ production in treated fibroblasts compared to basal, measured by flow cytometry with MitoSOX probe (n=2 experiments with minimum duplicates).
Data represented as mean for parametric data or median for non-parametric data, with individual values. Comparative analysis basal *vs.* 500 nM done with Welch's t test if parametric or Mann-Whitney if non-parametric; two-way ANOVA with multiple comparisons for the five DNM1L patients between basal and treated 500 nM LGZ groups. *P* value represents *<0.05, **<0.01, ****<0.0001.

2.2 Nutraceutical treatment: spermidine

Nutraceuticals are compounds or food supplements that, at certain concentrations, can have a pharmacological effect. These compounds have shown to be modulators of several cellular functions (Alba et al., 2023) and brain development (Ip et al., 2017). This is the case of the polyamine spermidine, a natural compound found in cells that regulates autophagy and mitochondrial biogenesis in healthy population (McCarty, 2022; Wang et al., 2020). In this part of the work, we tested the potential use of spermidine for the recovery of molecular alterations in mitochondrial diseases (Fig. 49A).

From the previous described mitochondrial patients, we selected eight patients that can be grouped in the five functional categories (Fig. 49B): (1) mitochondrial cristae structure (CHCHD6), (2) gene translation (WARS2), (3) dynamics (DNM1L_P4), (4) intermediate metabolism (PDHX), and (5) OXPHOS-related functions (NDUFS1, NDUFAF6, SCO2, SURF1_P1). Building on the characterized mitochondrial dysfunction, we studied the *in vitro* response to the nutraceutical spermidine (SPM) at 1 µM for 24 hours, in order to establish it as a safe-to-use personalized treatment for neuropediatric disorders.

SPM serves as the aminobutyl group donor for the synthesis of hypusine (N^{ε}-[4-amino-2-hydroxybutyl]-lysine) at a specific lysine residue of the eukaryotic translation initiation factor 5A (eIF5A), essential for its activity (Liang et al.,

2021) (Fig. 49C). Since hypusinated eIF5A is an important effector of SPM, we studied the ratio of hypusine/eIF5A in the patients before and after SPM treatment, detected by Western blot (Fig. 49D). The SPM-treated fibroblasts of patients WARS2, PDHX and NDUFS1 showed increased trends in hypusination compared to basal, and NDUFAF6 patient had a significative 1.85-fold increase compared to basal. DNM1L_P4 showed a decreased trend in eIF5A hypusination when treated with SPM 1 µM and no changes were observed for SCO2 and SURF1_P1 (Fig. 49E).

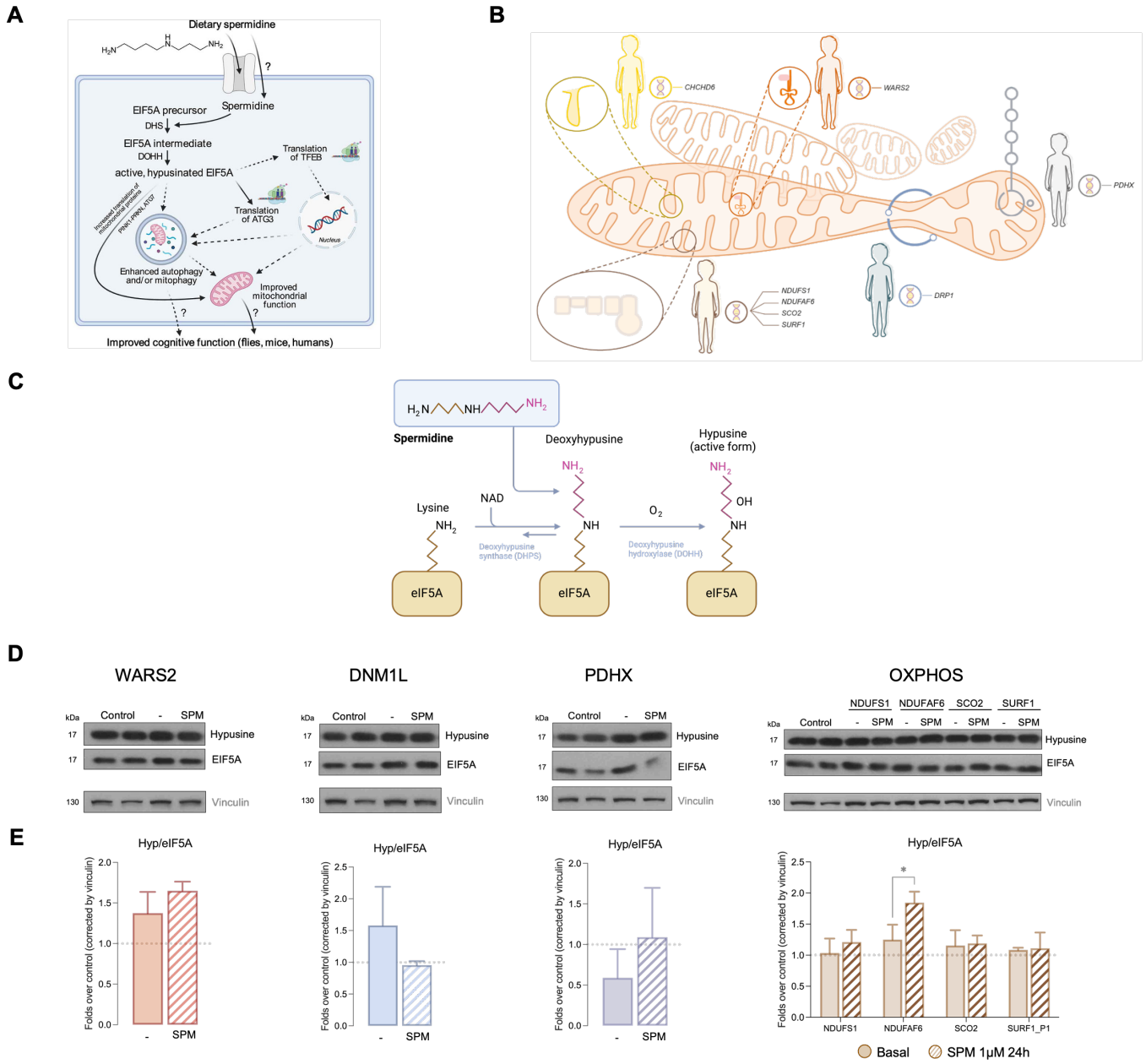

Figure 49. SPM mechanism of action and mitochondrial pediatric patients studied. (A) Schematic representation of SPM mechanism of action: SPM improves mitochondrial function exerting a direct effect on the organelle or through hypusination of the transcription factor eIF5A (adapted from (Hofer et al., 2021)). (B) Schematic representation of the eight patients studied that are classified in five functional categories: mitochondrial cristae structure (*CHCHD6*), gene translation (*WARS2*), fission dynamics (*DNM1L*), and OXPHOS-related genes (*NDUFS1*, *NDUFAF6*, *SCO2*, *SURF1*). (C) SPM gives the aminobutyl group to the eIF5A lysine residue to form hypusine, changing the transcription factor into its active form; created with BioRender. (D) Representative image of hypusine and total eIF5A expression in two controls (each lane represents a different cell line) and in patients' fibroblasts before and after 1 µM SPM treatment for 24 hours, detected by Western blot. (E) Densitometry quantification of the ratio hypusine over total eIF5A, corrected by vinculin. Data represented as mean + SD. (Brown-Forsythe) ANOVA test for comparisons between control vs. patient and basal vs. SPM 1 µM; two-way ANOVA for comparisons for OXPHOS patients. *P* value represents *<0.05.

Effect of spermidine on the bioenergetic profile of mitochondrial patients

As we have previously described, the bioenergetic profile is altered in the mitochondrial patients in terms of mitochondrial ATP synthesis and ROS production. All patients with mutations affecting genes involved in mitochondrial structure maintenance, gene translation, fission dynamics and intermediate metabolism showed different responses when treated with spermidine at 1 µM concentration for 24 hours (Fig. 50A).

For instance, fibroblasts from CHCHD6-patient did not show ameliorations in mitochondrial ATP, although a 17% decrease in $O_2^{\cdot-}$ production was detected in SPM-treated cells compared to non-treated. Opposite to this, WARS2-, DNM1L_P4- (which had decreased mitochondrial ATP) and PDHX-patients showed significative increases in mitochondrial ATP synthesis (1.87 folds, 1.39 folds and 1.43 folds respectively) without alterations in ROS, compared to non-treated condition. To investigate if this increase in mitochondrial ATP was paired to an increase in OXPHOS complexes expression after SPM treatment, we performed a Western blot to detect the expression of each complex (CI-CV) (Fig. 50B). Fibroblasts from CHCHD6-patient in basal conditions showed decreased expression in complexes I (0.54 folds), II (0.55 folds), III (0.61 folds) and IV (0.61 folds) compared to healthy controls, which were not corrected by spermidine treatment. *WARS2*-mutated cells showed trends of decreased expression of CI and CII (although not statistically significant), that were corrected with SPM treatment in 2.18 and 1.61 folds respectively, compared to basal condition. Dnm1L deficient cells from patient 4 had a decreased trend in CIV expression that was augmented in 1.51 times after SPM treatment compared to non-treated cells. PDHX-patient fibroblasts showed a 44% decrease in CIV expression compared to controls without significant ameliorations with SPM treatment. In brief, SPM was able to increase mitochondrial ATP synthesis in WARS2, DNM1L and PDHX patients without exacerbations in ROS production and not paired to general increases in OXPHOS complexes expression.

The last studied group encloses four patients with mutations in genes responsible for complex I subunits (NDUFS1) and assembly factors (NDUFAF6), and complex IV assembly factors (SCO2 and SURF1 patient P1). Fibroblasts of all these patients were, as well, previously detected with decreases in mitochondrial ATP synthesis and increased $O_2^{\cdot-}$ production. Treatment with spermidine of these fibroblasts resulted in an increase in mitochondrial ATP synthesis of 2.1 folds for NDUSFS1-, 1.47 folds for NDUFAF6-, 1.58 folds for SCO2- and 2.34 folds for SURF1- patient cells, compared to their basal conditions (Fig. 50C). In addition, ROS generation in terms of $O_2^{\cdot-}$ showed a 35% decrease in NDUFS1- patient fibroblasts but a 1.72-fold increase in NDUFAF6 ones, compared to basal, without significative changes for the complex IV assembly factors (SCO2 and SURF1 patients).

Regarding OXPHOS complexes expression (Fig. 50D), CI was decreased in 48% for NDUFS1-deficient fibroblasts, while CIV was significantly increased in 1.45 folds compared to controls. SPM treatment in this patient decreased the expression in complexes III (0.62 folds) and IV (0.33 folds) compared to non-treated condition. In the NDUAF6 patient cells, we detected an absence of CI expression (91%) as described previously, together with a significant 34% decrease in CIV compared to controls, without correction with SPM. For the complex IV assembly factors, in SCO2-deficient cells we detected decreases in complex I (0.75 folds), III (0.79 folds) and IV (0.56 folds), while in SURF1 patient fibroblasts we detected an 86% decrease in the expression of CIV compared to controls. No significant corrections were detected in the SPM-treated condition for both patients. Therefore, these results suggest that SPM mechanism to increase mitochondrial ATP production is not necessarily occurring through an increase in OXPHOS complexes expression.

(see next page)

Figure 50. Evaluation of spermidine (SPM) effect on the bioenergetic function in mitochondrial patients' fibroblasts. (A, C) Mitochondrial ATP detection by bioluminescence after incubation with 2-DG (n=2-9 experiments with minimum technical triplicates) and $O_2^{\cdot-}$ detection with MitoSOX™ probe measured by flow cytometry (n=2-4 experiments with minimum technical triplicates). (B, D) Representative image of OXPHOS complexes expression and densitometry quantification, detected by Western blot and corrected over vinculin (n=3-12 experiments).

Data expressed as folds over control and represented as mean for parametric data or median for non-parametric data, with individual values; a grey line at y=1 denotes mean value for controls. Comparative analysis basal *vs*. SPM done with Welch's test for parametric, and Mann-Whitney for non-parametric data; two-way ANOVA analysis with multiple comparisons between control, patient basal and patient SPM-treated for each OXPHOS complex. *P* value represents *0.05, **<0.01, ***<0.001, ****<0.0001.

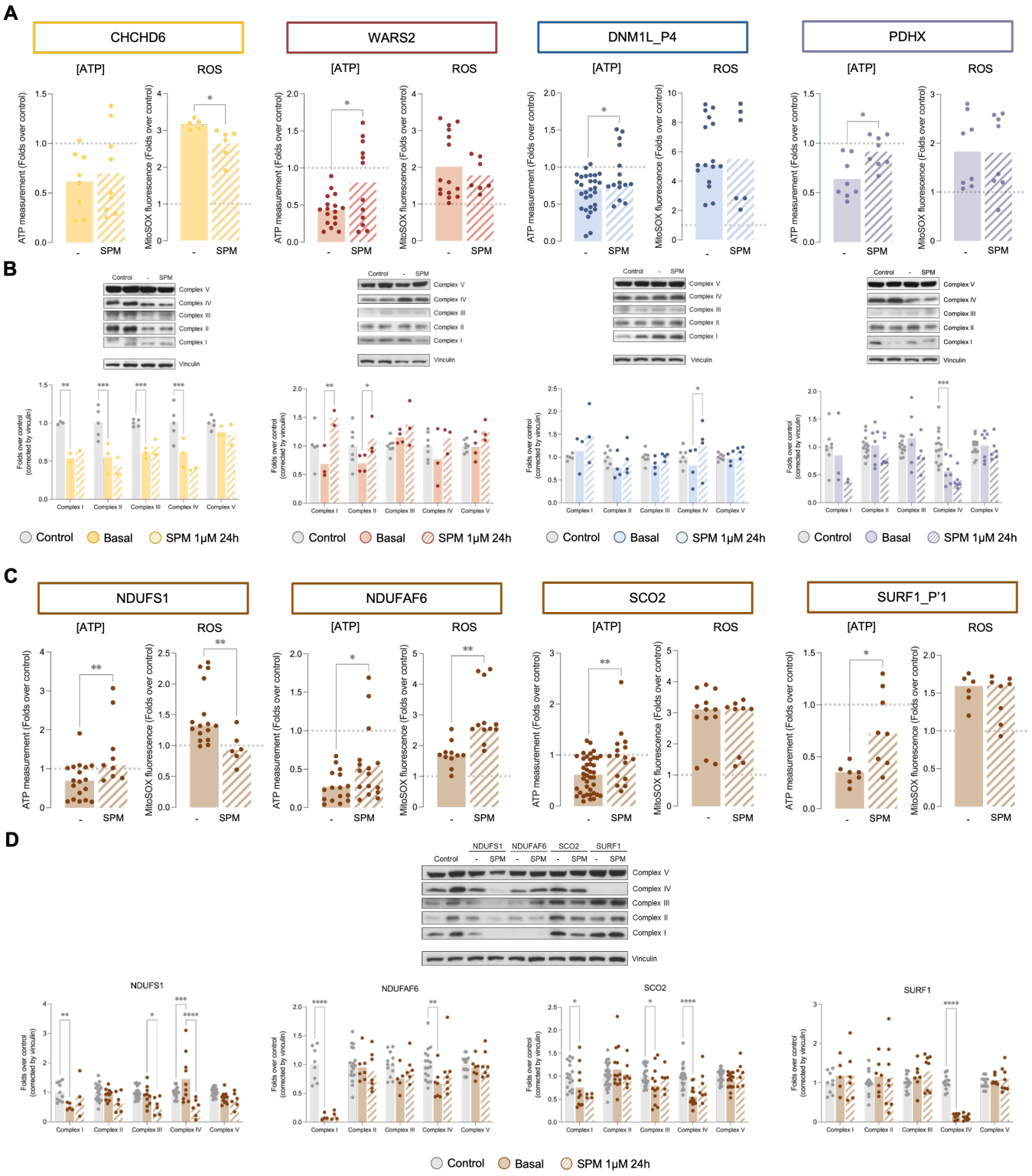

Figure 50. Evaluation of spermidine (SPM) effect on the bioenergetic function in mitochondrial patients' fibroblasts.
(see previous page)

Effect of spermidine treatment on the clinical phenotype of mitochondrial patients

Enlightened by the *in vitro* results, we studied the clinical efficacy of SPM in four of the eight mitochondrial patients studied. The patients that participated in the clinical trial were CHCHD6, NDUFAF6, SCO2 and SURF1_P1 and were supplemented with oral spermidine for three months at a dose of 6 mg/day, in three 2 mg doses per day. Neurodevelopment was assessed through the Vineland test, which measures adaptive behavior across multiple domains. Four neurodevelopmental aspects were evaluated before and after treatment: (1) communication in terms of receptive, expressive and written communication; (2) daily living skills – personal, domestic and community; (3) socialization, through interpersonal relationships, games (play and leisure) and coping strategies; and (4) psychomotor development regarding fine and gross motor skills. The evaluations were expressed as Growth Scale Values (GSV).

CHCHD6 patient showed improvements in fine motor skills, in socialization through coping strategies and play, in community and personal daily life aspects and communication, in terms of written and expressive communication (Fig. 51A). NDUFAF6 patient, however, did not show changes after the 3-month SPM treatment (Fig. 51B). SCO2 patient showed improvements in socialization through coping strategies and written and expressive communication (Fig. 51C). SURF1_P1 showed improvements in fine motor skills, socialization through games and interpersonal relationships, in personal daily life skills and expressive communication (Fig. 51D). When analyzed together, the mitochondrial patients showed significative improvements in socialization through play (Two-way ANOVA, p=0.0266) and expressive communication (Two-way ANOVA, p=0.0073). Therefore, SPM clinical effect after three months of treatment was noticeable in three of the four mitochondrial patients, and particularly relevant in expressive communication, socialization through play, fine motricity and personal everyday skills.

Additionally, DNM1L_P4 and NDUFS1 patients that were not part of the clinical trial started with SPM dietary supplementation at a dose between 4-6 mg/day taken twice a day. After two months treatment, DNM1L_P4 family reported a notable improvement in the respiratory pattern and a rise on the “global energy” and motor skills improvement, with both more stable walk and ability to walk longer periods of time without stopping, persisting, however, a serious truncal ataxia and spasticity in lower limbs. The patient also improved his school performance, due to greater ability to articulate words and some phonemes and sensation of more energy to carry out the school activities. Nowadays the patient is stable, but no further improvements have been reported. Regarding NDUFS1 patient, after 6 months treatment, she was able to support her head and turn it to both sides, had more interest for the environment and better response to extern stimulus. She started again to say monosyllables and was less irritable. Oral feeding was restarted, and sleep pattern was improved with apneas disappearance.

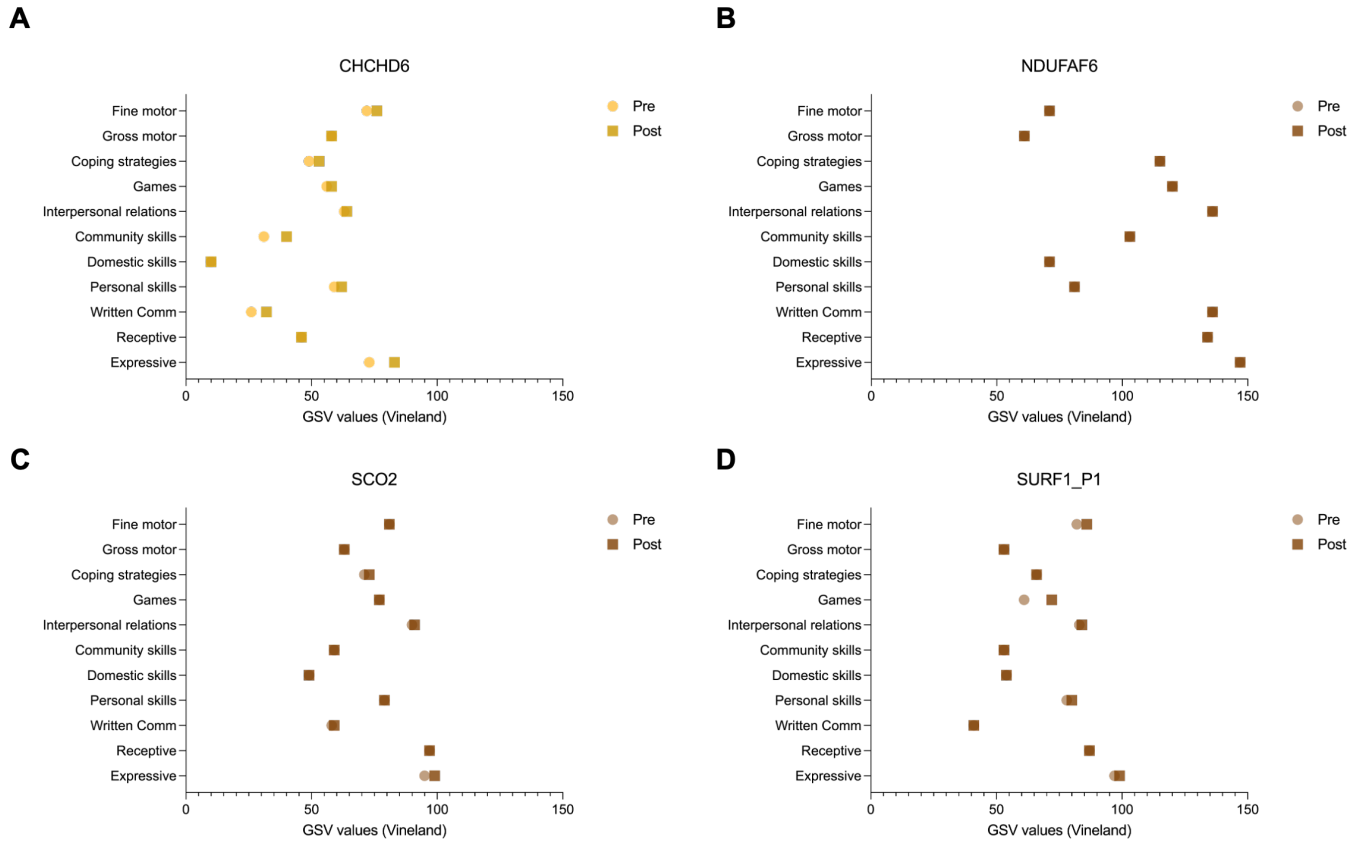

Figure 51. Evaluation of SPM clinical effect on mitochondrial pediatric patients through Vineland test. The test assesses neurodevelopment according to four domains: communication (expressive and receptive), daily living skills (personal, domestic and community), socialization (interpersonal relationships, games and coping strategies) and psychomotor development (fine and gross motricity). The test was performed on patients (A) CHCHD6, (B), NDUFAF6, (C) SCO2 and (D) SURF1 patient 1.
Data represented as individual value per variable, in round shape for pre (before treatment) and square for post (post SPM treatment at a 6 mg/day dose for three months).

Spermidine accumulation consequences on mitochondrial function

SPM can be detrimental in cases in which there is already an accumulation of the polyamine, as the case of spermine synthase (*SMS*) mutation. Here we characterized the mitochondrial dysfunction in fibroblasts of a patient with a suspected *SMS* variant and studied the bioenergetic response after SPM 1 µM treatment for 24 hours.

She was diagnosed with congenital but progressive cerebellar ataxia, strabismus and did not present epilepsy. Symptomatology was compatible with a mitochondrial disorder. The patient was detected with a variant in the X-linked *SMS* gene (OMIM *300105). This gene codes for spermine synthase, one of the four enzymes involved in the synthesis of polyamines from arginine and methionine. It catalyzes the production of spermine from spermidine and decarboxylated S-adenosylmethionine (dcSAM) (Fig. 52A). Mutations in this gene have been associated with developmental disorders in males. The patient was female and inherited the mutation c.733G>T (p.Pro258Leu) in heterozygosis from the mother, detected by Sanger sequencing (Fig. 52B). The suspected variant was not previously reported, was classified as VUS and could be causing an altered ordered interface in the protein (probability 0.36, $p = 4 \times 10^{-3}$), together with many pathogenic mechanisms with lower probability. However, more diagnostic tests are needed for confirming the mutation as causative of the symptomatology. *In vitro* analysis of SMS protein expression did not show any significant alterations, detected by Western blot (Fig. 52C). However, eIF5A hypusination was increased in the patient compared to controls, and furtherly augmented when treated with SPM (yet results not-statistically significant) (Fig. 52D).

Since symptoms were compatible with a mitochondrial disorder and the polyamine pathway was detected to be altered, we studied the mitochondrial homeostasis in the patient and validated SPM effect on the bioenergetic function. Mitochondrial network morphology evaluation through TOMM20 IF (Fig. 52E) showed an increase of 1.52 folds in total area in the patient compared to healthy controls, without statistically significant differences for the other parameters (Fig. 52F). Bioenergetic analysis showed unaltered total ATP synthesis while decreased mitochondrial ATP in 31% compared to controls (Fig. 52G). When cells were treated with SPM 1 µM for 24 hours, we detected an additional significant 52% decrease in mitochondrial ATP compared to basal. $O_2^{\cdot-}$ production detection revealed a 1.73-fold increase in the patient compared to controls, without significant differences for SPM-treated condition (Fig. 52H). Antioxidant enzymes detection showed 60% decreased expression for MnSOD without changes for GPx compared to controls (Fig. 52I).

These results suggest an increase in mitochondrial mass with defective bioenergetic function in the suspected *SMS*-mutated patient cells. The decrease in ATP after SPM treatment suggests that accumulation of SPM in patients with alterations in polyamine pathways could be toxic for mitochondria furtherly worsening its function.

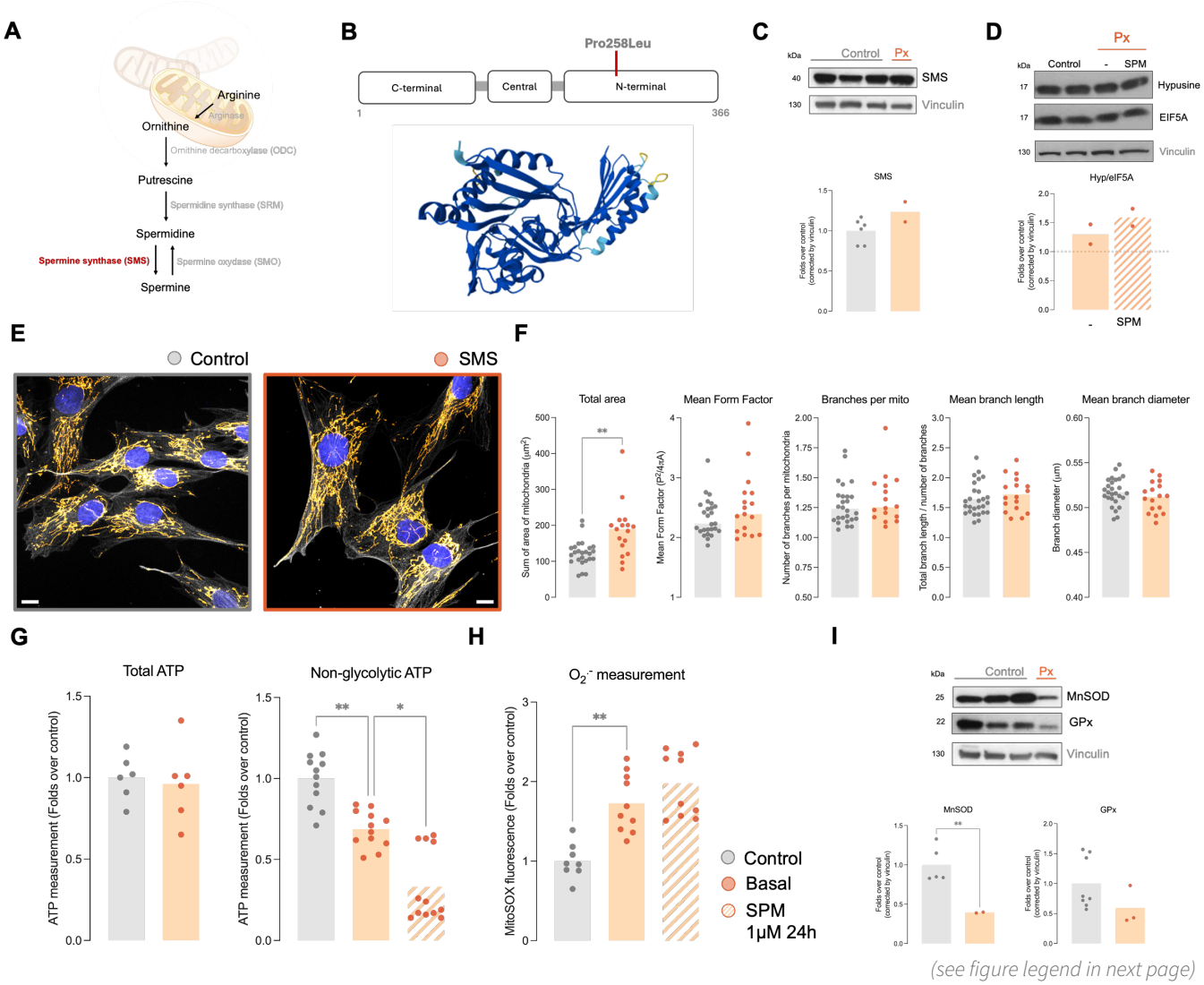

(see figure legend in next page)

(from previous page)

Figure 52. Evaluation of the mutation in SMS patient fibroblasts and its effect on mitochondrial homeostasis maintenance. (A) Schematic representation of SMS in polyamine synthesis. (B) Schematic representation of the mutation Pro258Leu in the N-terminal domain of the SMS protein, necessary for its activity (Wu et al., 2008), and 3D protein structure, observed through PyMOL. Detection of (C) SMS protein expression in patient and three controls and (D) ratio hypusination/eIF5A in patient (basal and SPM-treated) and two controls (each lane represents a different cell line) by Western blot, with vinculin used as loading control. (E-I) Mitochondrial network structure and bioenergetics studies on SMS fibroblasts. (E) Representative image of the mitochondrial network IF (TOMM20 in yellow, tubulin in grey, nuclei in blue; scale bar 10 µm). (F) Parametrization of the total area, mean form factor, number of branches per mitochondrial network, and mean branch length and diameter (n=25 control, n=17 patient mitochondria). (G) Total and mitochondrial (non-glycolytic) ATP concentration in the patient in basal and treated conditions compared to controls, measured by luciferin-luciferase bioluminescence after incubation with 2-DG (n=2 experiments with duplicates for total ATP and quadruplicates for mitochondrial ATP). (H) $O_2^{\cdot-}$ production in basal and treated patient compared to controls, measured by flow cytometry with MitoSOX™ probe (n=2 experiments with minimum quadruplicates). (I) Antioxidant enzymes MnSOD and GPx expression detected by Western blot, densitometry quantification corrected over vinculin, in three controls (each lane represents a different cell line) and patient (n=2-3 experiments).
Data represented as mean + SD for parametric data or median + interquartile range for non-parametric data, or with individual values. Comparative analysis control *vs*. SMS done with Welch's test for parametric, and Mann-Whitney for non-parametric data; Kruskal-Wallis for non-parametric data comparison between groups control *vs*. SMS and SMS *vs*. SPM. *P* value represents **<0.01, ***<0.001, ****<0.0001. Px = patient.

2.3 Metabolic treatment: ketogenic diet

Ketogenic diet (KD) consists of high-fat and low-protein and carbohydrate diet and has been widely used for the treatment of refractory epilepsies, that is, failure of at least two anti-epileptic drugs to achieve sustained relief of seizures (Meira et al., 2019). The diet mimics the fasting state, altering the metabolism to use fats as a primary fuel source. In the liver, catabolism of fatty acids produces ketone bodies (KB), process called ketosis. During ketosis, there is an increase in GABAergic output and ion channel activity (Bough and Rho, 2007), which could protect against epileptic seizures. In addition, KD has direct mitochondrial effects on bioenergetics, decreasing oxidative stress, modulating mitochondrial dynamics and increasing mitochondrial mass (Qu et al., 2021; Hasan-Olive et al., 2019). Given that AFG2A-deficiency produces a refractory epilepsy phenotype that was responsive to KD treatment, we hypothesized whether KD could be recovering the mitochondrial phenotype in AFG2A-related encephalopathy.

To investigate the effect of KD on mitochondrial function in these patients, we treated the fibroblasts with a KD-mimicking media that consisted of the ketone bodies β-hydroxybutyrate and acetoacetate at 5 mM for five consecutive days in DMEM with low glucose (1 g/L).

Regarding mitochondrial dynamics and morphology detected with time-lapse confocal microscopy in live cells (Fig. 53A), AFG2A patients were described with an aberrant mitochondrial network with less, round-shaped and slightly more branched mitochondria. They had an undirected and slower bursting-like movement together with a decreased fusion:fission ratio, causing a fragmented morphology. When patients' cells were treated with KD, all the motility parameters were restored (Fig. 53B). We detected an increase in 3 µm/s for median speed, 8% increase in median:max speed ratio (i.e., rapid movements of mitochondria), 18% increase in directionality, and more importantly, a 1.78-fold increase in fusion:fission ratio compared to non-treated cells. In addition, the morphology parameters were corrected as well (Fig. 53C). We detected a 1.45-fold increase in mitochondrial area, 1.29-fold increase in perimeter, 10% increase in aspect ratio and 3% decrease in solidity, considered as branching of mitochondrial networks, compared to basal condition. In this context, KD-mimicking media corrects the motility and morphology alterations in AFG2A patients' fibroblasts *in vitro*, particularly the recovery of the fusion:fission ratio and mitochondrial mass in the treated patients.

Total ATP production was decreased in fibroblasts from the patients AFG2A_P1 and P2, described previously. Treatment with KD recovered the alterations for both patients, in 3 folds and 2.19 folds respectively, without significative changes for AFG2A_P3 (Fig. 53D). OXPHOS complexes expression analysis detected by Western blot revealed also distinctive alterations and KD effect between the patients (Fig. 53E). Expression in CII was detected to be 1.6-fold increased in AFG2A_P3, and CIII was increased for patients AFG2A_P2 and P3, 1.47 and 1.9 folds respectively. In CIV expression we detected significant decreases for AFG2A_P1 (88%) and P2 (37%), which were corrected with KD treatment in 2.55 folds for P1 and 1.69 folds for P2. No changes were detected for CI nor CV expressions (Fig. 53F). These results suggest that KD is able to recover the ATP synthesis in the patients, while also increasing complex IV expression in the mitochondrial respiratory chain.

ROS production was increased for the three patients cells. KD was able to significantly reduce $O_2^{\cdot-}$ generation in all the patients (Fig. 53G): 38% for AFG2A_P1, 22% for P2, and 39% for P3. On the other hand, antioxidant enzymes expression differed between the patients, detected by Western blot (Fig 53H). MnSOD expression, which was 4.39-

fold increased in AFG2A_P3, was corrected with KD showing a decrease of 85% compared to non-treated patient cells. Whereas GPx expression, which was decreased in AFG2A_P1 and increased for P2, did not show recovery with KD treatment. Therefore, ROS production is similarly corrected in all the KD-treated patients, together with MnSOD expression in AFG2A_P3.

Two of the three patients studied *in vitro* were treated with KD (AFG2A_P1 and P3). P1 had a seizure onset at 27 months of age, which consisted of drug-resistant infantile spasms. Six months later he started with KD in combination with anti-epileptic drugs, and after one month of treatment he became seizure-free. At 7 years old, he continues seizure free on monotherapy with KD. AFG2A_P3 started with infantile spasms at 14 months old. At 6 years he presented atonic seizures that were treated with several anti-epileptic drugs. At this age he started KD, and after a year he presented a 30% seizure reduction together with attentional and motor improvements. Endorsed by the *in vitro* observations and the clinical improvement, KD could be a suitable treatment and safe option for patients with AFG2A-RE with refractory epilepsy.

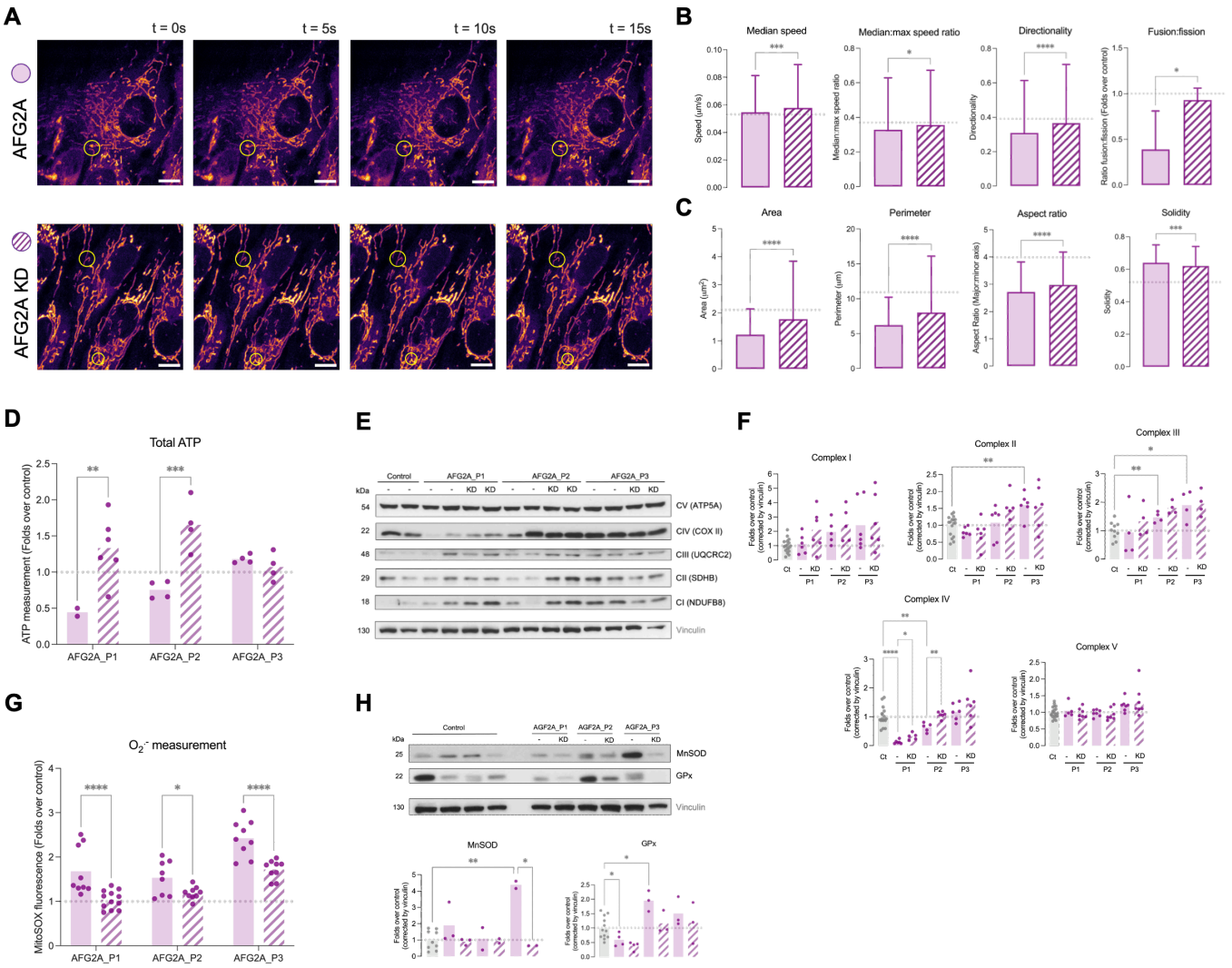

Figure 53. Evaluation of the KD-mimicking media effect on mitochondrial dynamics and bioenergetics in the three AFG2A patients' fibroblasts. (A-C) Mitochondrial dynamics and shape characterization of control and patients' fibroblasts using MATLAB add-in Mitometer. (A) Frames obtained from time-lapse images at different time points (0s, 5s, 10s, 15s) showing in yellow the fusion-fission dynamics in the mitochondrial network, detected with MitoTracker™ Green (ImageJ LUT inferno, scale bar 10 µm). (B) Quantification of the dynamics parameters: median speed (µm/s), median:max speed ratio (capacity of burst movement), directionality (defined as the total distance traveled divided by the maximum displacement of the track), and fusion:fission ratio. (C) Quantification of mitochondrial shape parameters: area occupied by signal, perimeter and aspect ratio (calculated as the ratio between the major and minor axes of mitochondria) (n=1616-1895 tracks for basal, n=4388-5159 tracks for KD mitochondria; n=7-9 patients' cells). (D) Total ATP production in fibroblasts from the three AFG2A patients, detected by bioluminescence assay and expressed as folds over control (n=3 experiments with minimum duplicates). (E) Representative image of the detection of OXPHOS complexes expression by Western blot, in the three patients in basal and KD conditions per duplicate, compared to two healthy controls. (F) Densitometry quantification of the five complexes, expressed as folds over control and corrected over vinculin (n=5 experiments). (G) $O_2^{\cdot-}$ production expressed as folds over controls, measured by flow cytometry with MitoSOX™ probe (n=3 experiments with triplicates). (H) Antioxidant enzymes MnSOD and GPx expression detected by Western blot, and densitometry analysis corrected to vinculin and expressed as folds over average of four controls (each lane represents a different cell line; n=2 experiments).

(cont. next page)

(from previous page)
Data represented as mean for parametric data or median for non-parametric data, (B, C) with interquartile range or standard deviation respectively, and (D, F, G, H) individual values. Comparative analysis basal *vs*. KD-treated done with Welch's test for parametric, and Mann-Whitney for non-parametric data. (Brown-Forsythe and Welch) ANOVA for parametric data and Kruskal-Wallis for non-parametric, with multiple comparisons between controls and the three patients, and each patient *vs*. treatment. Two-way ANOVA for comparison between basal *vs*. KD per patient. *P* value represents *<0.05, **<0.01, ***<0.001, ****<0.0001. P1 = AFG2A patient 1, P2 = AFG2A patient 2, P3 = AFG2A patient 3.

2.4 Non-responsive (non-treated) patients

GFM1 patient presented a dysfunction in mitochondrial homeostasis, characterized by an increased ATP production that was evident under stress conditions with galactose, and increased oxidative stress. Tetracyclines are a family of antibiotics that inhibit bacterial protein synthesis and have previously shown beneficial effects on mitochondrial function for *GFM1* mutations through mitochondrial unfolded protein response (UPR^{mt}) (Suárez-Rivero et al., 2022). Therefore, we assayed a treatment with the tetracycline doxycycline (DOX) at 40 µM for 48 hours in the GFM1 patient fibroblasts.

Regarding mitochondrial ATP synthesis, we did not detect a recovery in DOX-treated cells (Fig. 54A). In addition, OXPHOS complexes expression detected by Western blot (Fig. 54B) was decreased in the patient for complex I (51%) and IV (52%), compared to healthy controls, without correction with DOX treatment. Whereas complex V was decreased in 12% with DOX compared to basal. DOX treatment did not correct the increased ROS production in GFM1 fibroblasts, but it furtherly increased it by 1.86 folds compared to non-treated condition (Fig. 54C). Therefore, we did not detect a recovery in mitochondrial function in GFM1 patient fibroblasts at the assayed DOX concentration and time. The response to the treatment should be further analyzed in mitochondrial-forced respiration with galactose.

COASY patient mitochondrial dysfunction was detected with increased oxidative stress without alterations in mitochondrial ATP synthesis. We assayed two different treatment approaches: nutraceutical with SPM and pharmacologic with LGZ, to modulate the bioenergetic function. However, both treatments failed in achieving modulation in mitochondrial ATP and correction in oxidative stress in the patient (Fig. 54D), at the assayed conditions. SPM is considered to be inside the group of caloric restriction mimetics (CRMs), that is, compounds that would pharmacologically mimic the beneficial effects of caloric or dietary restriction (Madeo et al., 2018). CRM can induce autophagy though the inhibition of the synthesis of acetyl coenzyme A (CoA). Therefore, SPM would not be the best therapeutic option for patients with *COASY* mutations. Santambrogio and collaborators (Santambrogio et al., 2023) showed amelioration of the PKAN (Pantothenate kinase-2 associated Neurodegeneration) phenotype in astrocytes after LGZ treatment. This enzyme catalyzes the first reaction of the CoA biosynthetic pathway, which is the same pathway as COASY. Other conditions should be assayed, such as forcing a mitochondrial dependent environment with galactose (as we did not detect a decrease in mitochondrial ATP), or assaying on neurons derived from patient progenitor cells.

SLC25A22 patient fibroblasts were detected with lowered mitochondrial ATP synthesis and increased ROS production. SPM treatment was assayed for this patient's cells (Fig. 54E). Mitochondrial ATP synthesis showed no significant differences compared to basal conditions. $O_2^{\cdot-}$ detection showed 20% increase for SLC25A22 SPM-treated cells. Perhaps more targeted approaches, such as gene replacement therapies, could be considered to directly address the underlying deficiencies. However, the development and approval of such therapies require significant time, which is not feasible given the patient's critical condition.

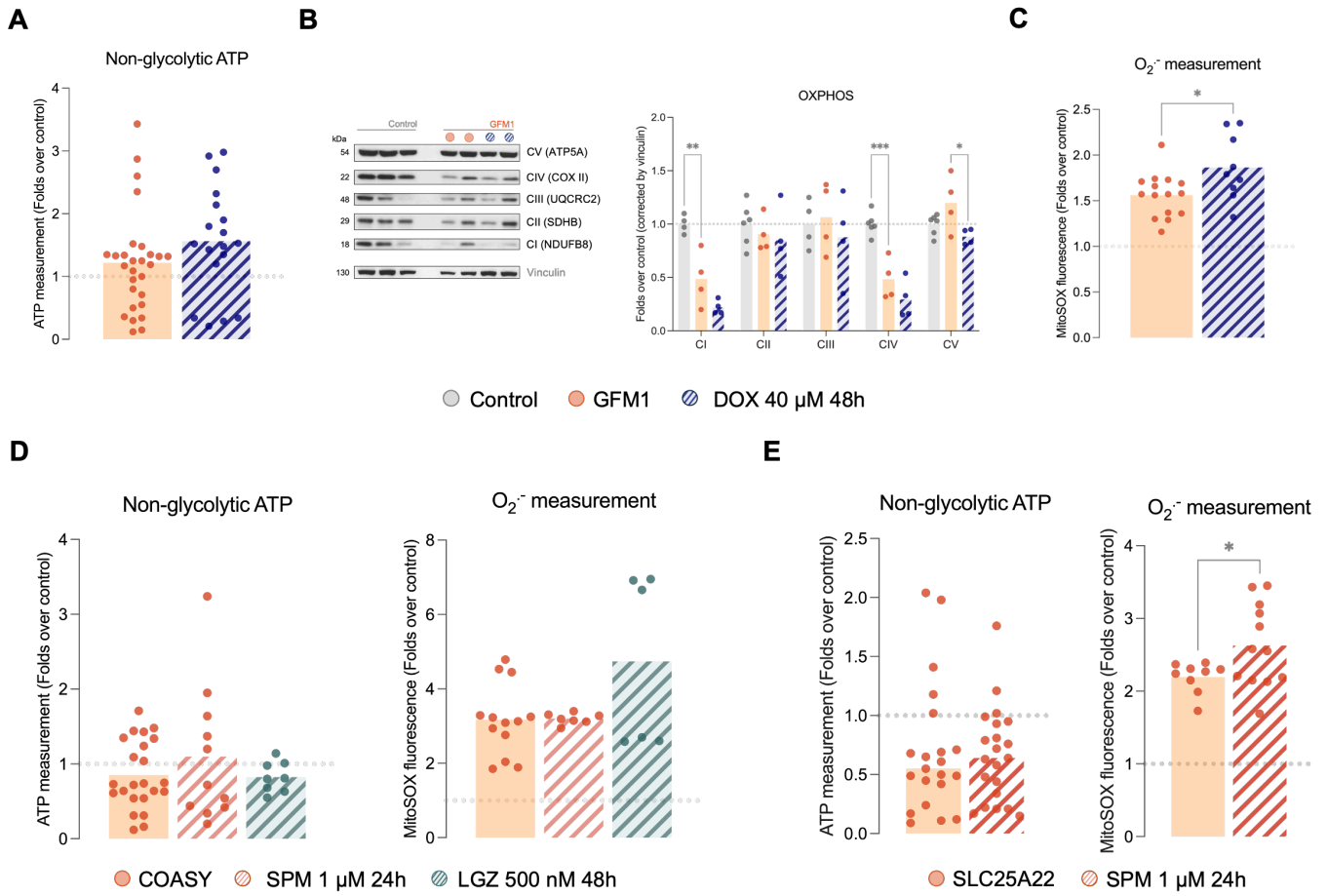

Figure 54. Assessment of mitochondrial function in GFM1, COASY and SLC25A22 patients' fibroblasts after different personalized treatments. (A-C) Bioenergetic response in GFM1 patient to 40 µM DOX treatment for 48 hours. (A) Mitochondrial ATP concentration in treated patient compared to basal, measured by luciferin-luciferase bioluminescence after incubation with 2-DG (n=4 experiments with minimum technical quadruplicates). (B) Representative image of the detection of OXPHOS complexes expression by Western blot, in the GFM1 patient in basal and DOX conditions per duplicate, compared to three healthy controls (each lane represents a different cell line), and densitometry quantification of the five complexes, expressed as folds over control and corrected over vinculin (n=2 experiments with technical duplicates). (C) $O_2^{\cdot-}$ production compared to controls, measured by flow cytometry with MitoSOX™ probe (n=2 experiments with triplicates). (D) Bioenergetic response in COASY patient to the treatments 1 µM SPM for 24 hours and 500 nM LGZ for 48 hours, in terms of mitochondrial ATP bioluminescence detection after 2-DG incubation (n=3 experiments with technical quadruplicates) and $O_2^{\cdot-}$ detection by flow cytometry with MitoSOX™ probe (n=2 experiments with technical triplicates). (E) Bioenergetic response in SLC25A22 patient to 1 µM SPM for 24 hours, measuring mitochondrial ATP detection by bioluminescence after 2-DG incubation (n=4 experiments experiment with 6 technical replicates) and $O_2^{\cdot-}$ detection with MitoSOX™ probe measured by flow cytometry in basal and SPM-treated conditions (n=3 experiments with minimum triplicates).
Data represented as mean for parametric data or median for non-parametric data, with individual values (a grey line at y=1 denotes mean value for controls). Comparative analysis basal *vs*. treatment done with Welch's test for parametric, and Mann-Whitney for non-parametric data if two groups; if more than two groups, ANOVA or Kruskal-Wallis analysis was performed. Two-way ANOVA analysis with OXPHOS complexes comparisons between the different groups (control, basal, DOX). *P* value represents *<0.05, **<0.01, ***<0.001.

2.5 Summary of mitochondrial dysfunctions and responses to personalized treatments

Table 14 summarizes the results obtained for the 20 neuropediatric patients studied. It includes predictions of the pathogenicity of the mutations, potential molecular alterations induced in the protein (for missense mutations only), mitochondrial homeostasis alterations, and their recovery, if detected, with the treatments tested. The response of each patient to the corresponding treatment is specified for *in vitro* conditions and, where possible, for clinical observations.

Table 14. Summary of the main findings for each patient studied: prediction of the pathogenicity of the mutation, molecular alteration prediction, report of the mutation and association to clinical phenotype, functional alterations, and response to treatment (*in vitro* and clinical).
P = pathogenic; LP = likely pathogenic; VUS = variant of unknown significance.

Patient	Mutation	Patho-genicity	Mol. prediction (missense)	Report	Functional alterations	Treatment (*in vitro*)	Treatment (clinical effect)
DNM1L_P1	-	-	-	-	↓ Drp1 expression ↑ OPA1 80:100 expression Hyperfused network ↑ Total and mitochondrial ATP ↑ ROS, ↓ GPx expression	**LGZ**: ↑ Branch diameter ↓ ROS	Not applicable.
DNM1L_P2	-	-	-	-	↓ Drp1, Fis1 expression Hyperfused network ↑ Total and mitochondrial ATP ↑ ROS, ↓ GPx expression	**LGZ**: ↓ ROS	Not applicable.
DNM1L_P3	-	-	-	-	↓ Drp1 expression ↑ OPA1 expression Hyperfused network ↑ Total and mitochondrial ATP ↑ ROS, ↓ MnSOD expression	**LGZ**: ↑ ROS	Not applicable.
DNM1L_P4	c.2167A>G (p.Arg723Gly)	P	Altered coiled coil	Novel phenotype	↑ Drp1 (oligomeric) expression ↑ OPA1 expression Hyperfused network ↓ Mitochondrial ATP ↑↑ ROS	**LGZ**: ↑ Branch diameter ↑ ROS **SPM**: ↑ Mitochondrial ATP ↑ Complex IV expression	**SPM (4-6 mg/day for two months)**: Respiratory pattern improvement and rise on "global energy". Motor skills improvement, however, a serious truncal ataxia and spasticity in lower limbs. Improved his school performance, (word and phonemes articulation) and sensation of more energy. Nowadays the patient is stable, but no further improvements have been reported.
DNM1L_P5	c.1084G>A (p.Gly362Ser)	P	Altered ordered interface	Reported (Sheffer et al., 2016)	↑ Drp1 (oligomeric) expression ↑ OPA1 expression Hyperfused network ↑ Total ATP ↓ ROS	No detected changes	Not applicable.
AFG2A_P1	c.251G>A (p.Arg84Gln)	LP	Loss of allosteric site at Arg84	Reported (Tanaka et al., 2015)	↓ Bursting, directionality, fusion:fission ↓ Area, perimeter, aspect ratio, ↑ solidity ↓ Total ATP ↓ Complex IV expression ↑ ROS, ↓ GPx expression	**KD**: ↑ Median speed, bursting, directionality, fusion: fission ↑ Area, perimeter, aspect ratio, ↓ solidity ↑ Total ATP ↑ Complex IV expression ↓ ROS	**KD (4 years)**: Seizure free.
AFG2A_P2	c.327_328del (p.Lys110fs)	VUS	No prediction	Not reported	↓ Bursting, directionality, fusion:fission ↓ Area, perimeter, aspect ratio, ↑ solidity ↓ Total ATP	**KD**: ↑ Median speed, bursting, directionality, fusion: fission ↑ Area, perimeter, aspect ratio, ↓ solidity	Not applicable.
	c.1631T>G (p.Leu544Arg)	VUS	No prediction	Not reported			

					↑ Complex III, ↓ complex IV expression ↑ ROS, ↑ GPx expression	↑ Total ATP ↑ Complex IV expression ↓ ROS	
AFG2A_P3	c.251G>A (p.Arg84Gln)	LP	Loss of allosteric site at R84	Reported (Tanaka et al., 2015)	↓ Bursting, directionality, fusion:fission ↓ Area, perimeter, aspect ratio, ↑ solidity ↑ Complex II and III expressions ↑ ROS, ↑ MnSOD expression	**KD**: ↓ ROS ↓ MnSOD expression	**KD (1 year)**: 30% seizure reduction. Attentional and motor improvements.
	c.1064T>C (p.Ile355Thr)	LP	Loss of allosteric site at Y352	Not reported			
CHCHD6	c.142C>T (p.Pro48Ser)	VUS	No prediction	Not previously associated with disease	↑↑ Total area, ↑ Indep. networks, ↓ branch diameter ↓ Mitochondrial ATP ↓ Complex I, II, III, IV expression ↑↑ ROS	**SPM**: ↓ ROS	**SPM (6 mg/day for 3 months)**: Improvements in fine motor skills, socialization (coping strategies and play), community and personal daily life aspects and communication (written and expressive).
	c.572G>A (p.Arg191His)	VUS	No prediction				
WARS2	c.515+5 G>A	VUS	No prediction	Not reported	↓ Total and mitochondrial ATP ↑ ROS, ↓ MnSOD expression	**SPM**: ↑ Mitochondrial ATP ↑ Complex I and II expression	Not applicable.
GFM1	c.2011C>T (p.Arg671Cys)	P	Altered metal binding	Reported (Galmiche et al., 2012)	↑ Branch length ↑ ATP in Galactose medium ↓ Complex I and IV expression ↑ ROS, ↓ MnSOD expression	**DOX**: ↓ Complex V expression ↑ ROS	Not applicable.
NDUFS1	c.2144G>A (p.Ser715Asn)	VUS	Gain of allosteric site at Arg716	Not reported	↑ Indep. networks, ↓ branch length ↑ Total ATP, ↓ mitochondrial ATP ↓ Complex I, ↑ complex IV expression ↑ ROS	**LGZ**: ↑ Mitochondrial ATP ↓ ROS **SPM**: ↑ Mitochondrial ATP ↓ ROS ↓ Complex III and IV expression	**SPM (4-6 mg/day for 6 months)**: Support and movement of her head, more interest for the environment and better response to stimulus. She started again to say monosyllables and was less irritable. Oral feeding was restarted, and sleep pattern was improved with apneas disappearance.
NDUFAF6	c.523G>C (p.Ala178Pro)	P	Altered coiled coil	Reported (Catania et al., 2018)	↑ Total area, ↓ aspect ratio, ↓ branch length ↓ Mitochondrial ATP ↓ Complex I (absence) and IV expression ↑ ROS	**SPM**: ↑ Mitochondrial ATP ↑ ROS	**SPM (6 mg/day for 3 months)**: No amelioration.
	c.420+784C>T	P	No prediction				
SCO2	c.244_246delAAG (p.Lys82del)	LP	No prediction	Reported for high myopia (Zheng et al., 2021)	↑ Total area, ↓ MFF, ↓ numbers of branches, ↓ branch length ↓ Mitochondrial ATP ↓ Complex I, III and IV expressions ↑ ROS	**SPM**: ↑ Mitochondrial ATP	**SPM (6 mg/day for 3 months)**: Improvements in socialization (coping strategies) and written and expressive communication.
	c.703G>A (p.Gly235Ser)	LP	Altered metal binding	Not reported			

SURF1_P1	c.817C>T (p.Gln273*)	P	No prediction	Reported (Dixon-Salazar et al., 2012)	↑ Total area, ↓ branch diameter ↓ Mitochondrial ATP ↓ Complex IV expression (absence) ↑ ROS	**SPM**: ↑ Mitochondrial ATP	**SPM (6 mg/day for 3 months)**: Improvements in fine motor skills, socialization (games and interpersonal relationships), in personal daily life skills and expressive communication.
	c.503T>G (p.Val177Gly)	P	Altered stability	Reported (Yuksel et al., 2006)			
SURF1_P2	c.809_826dup AGCATCTGCAGTACATCG (p.Glu270_Ile275dup)	P	No prediction	Not reported	↑ Total area, ↓ branch diameter ↓ Total and mitochondrial ATP ↓ Complex IV expression (absence) ↓ ROS	Not applicable	Not applicable.
	c.815_825dup TGCAGTACATC (p.Val276Cysfs*5)	LP	No prediction	Not reported			
SLC25A22	-	-	-	-	↓ Branch length ↓ Mitochondrial ATP ↑ ROS	**SPM**: ↑ ROS	Not applicable.
COASY	c.140dupT (p.Ala48fs)	LP	No prediction	Not reported	↑ Indep. networks, ↓ MFF, ↓ branches, ↓ branch length and diameter ↑ ROS, ↑ MnSOD expression	**SPM, LGZ**: No changes	Not applicable.
PDHX	c.906delT (p.Tyr302fs)	LP	No prediction	Not reported	↑ Total area, ↑ branch length ↓ Mitochondrial ATP ↓ Complex IV expression ↑ ROS, ↓ MnSOD expression	**SPM**: ↑ Mitochondrial ATP	Not applicable.
SMS	c.733G>T (p.Pro258Leu)	VUS	Altered ordered interface	Not confirmed diagnosis	↑ Total area ↓ Mitochondrial ATP ↑ ROS, ↓ MnSOD expression	**SPM**: ↓ Mitochondrial ATP	Not applicable.

3 SYNAPSE ON A CHIP (SoC): AN ADVANCED TOOL FOR STUDYING THE IMPLICATION OF MITOCHONDRIA IN SYNAPTIC COMMUNICATION IN NEURODEVELOPMENTAL DISORDERS

1 Microfluidic device “synapse on a chip” (SoC): design and characterization

1.1. Synapse on a chip device design and fabrication
1.2. Synapse on a chip device characterization

2 Cortical neurons growth and characterization in the microfluidic device

2.1. Human neural progenitor cell (hNPC)-derived cortical neurons growth and differentiation in the microfluidic device
2.2. Characterization of cortical neurons in the microfluidic device
2.3. Neurotransmitters’ measurement in the synaptic chamber

3 Dopaminergic neurons growth and characterization in the microfluidic device

3.1. Human ventral midbrain neural progenitor cell (vmNPC)-derived dopaminergic neurons growth and differentiation in the microfluidic device
3.2. Mitochondrial characterization of dopaminergic neurons in the microfluidic device
3.3. Dopamine measurement and mitochondrial disturbance in the synaptic chamber

Most of the patients discussed in Chapter 2, who carried mutations in proteins critical for maintaining mitochondrial homeostasis, were diagnosed as pediatric parkinsonism clinical courses and/or neurotransmitters defects, presenting decreased concentrations of homovanillic acid (HVA) in CSF, a metabolite of dopamine and surrogate for its detection. While the relationship between mitochondrial dysfunction and parkinsonism has been already established (Bose and Beal, 2016), more research is needed to elucidate how mitochondrial homeostasis is influencing dopaminergic neurotransmission in these and other patients. We find ourselves with the need of new systems to characterize these processes.

The synapse on a chip (SoC) microfluidic device is an advanced tool for studying *in vitro* the relationship between synaptic communication and any biological process relevant for neurotransmission. Here, we explored the relationship between mitochondrial function and synapse, particularly the dopaminergic neurotransmission. To do so, we designed and manufactured the SoC device starting from the idea shown in Figure 55A. First, we characterized the optimality of the device in terms of structure for neuronal growth and axonal guidance for establishing organized connections. Then we validated the device using two different cell types from healthy controls (Fig. 55B): (1) cortical neurons derived from human neural progenitor cells (hNPCs) to validate the SoC device as optimal for neuron growth and differentiation; and (2) dopaminergic neurons (DAn) obtained from human ventral midbrain progenitor cells (vmNPCs). In the cells cultured in the chip we studied the appropriate DA neuron differentiation and explored the mitochondrial function together with its influence on synaptic function.

This work has been carried out at Institut de Bioenginyeria de Catalunya (IBEC) for device fabrication, and in collaboration with Stem Cells and Neurodegenerative Diseases group led by Dr. Antonella Consiglio at Institut d'Investigació Biomèdica de Bellvitge (IDIBELL), who kindly assisted us in validating the device with hNPCs. The results presented in this last chapter are preliminary and aim to set the groundwork for better understanding how mitochondrial function could impact dopaminergic synaptic communication in the context of neurodevelopmental disorders.

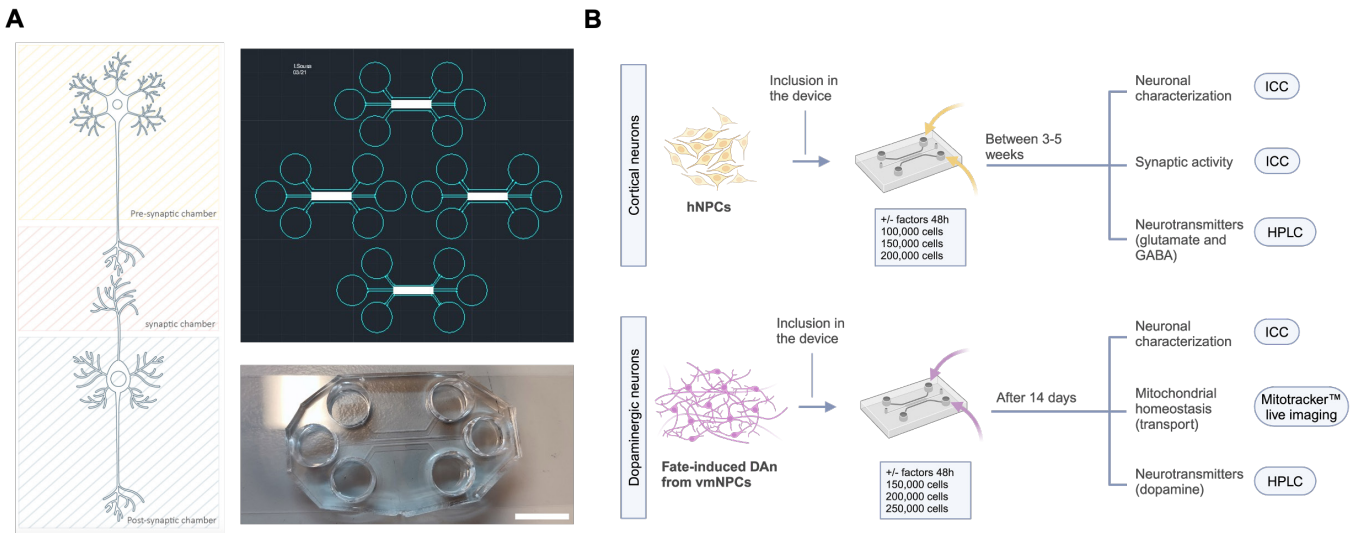

Figure 55. Workflow followed for synapse on a chip (SoC) device fabrication and validation. (A) The initial idea for the synaptic function precise study (left), mask design with AutoCAD for fabrication of the device (right, above) and SoC microfluidic device (right, below; scale bar 10,000 µm). (B) Neuron inclusion in the device from NPCs for cortical neurons and fate-induced DA neurons from vmNPCs as specified in Materials and Methods, and methods used for their characterization; created with BioRender.

1 Microfluidic device “synapse on a chip” (SoC): design and characterization

1.1 Synapse on a chip device design and fabrication

We developed a synapse on a chip (SoC) microfluidic device based on a design consisting of two lateral chambers, where cells of different type can be cultured, connected by conically shaped microchannels to a third central chamber named “synaptic chamber”. The cellular bodies would be situated in both lateral chambers (namely pre- and post-synaptic chambers) and the neuronal axons would grow unidirectionally from these chambers through the microchannels and should converge and connect synaptically in the central chamber (Fig. 56A). The cells in the three chambers are fed by two reservoirs of 8 mm diameter on the sides connected with the chambers (considered inlets and outlets). All chambers were 10 mm in length and the lateral chambers (pre- and post-synaptic) were 1 mm width, while the synaptic chamber was thinner with 500 µm width (Fig. 56B); all the chambers were 200 µm in height (Fig. 56C). The lateral chambers were connected to the synaptic chamber through 189 parallel microchannels of 500 µm length, 5 µm height and asymmetric shape for axon guidance: starting from 5 µm on the lateral chambers, to end at 2 µm on the central chamber. The 500 µm length of the microchannels assured that only axons would enter the synaptic chamber since dendrites cannot grow more than 450 µm long, as has been previously determined in (Taylor et al., 2005).

The chip was manufactured in poly-dimethyl-siloxane (PDMS) by standard photolithography (Fig. 56D). Photolithography is a microfabrication technique that uses light to transfer precise patterns from a mask onto a photosensitive material (e.g. SU-8), coated on a silicon wafer, creating a mold with microscale features. For this, we designed the necessary masks using AutoCAD. The fabrication of a chip with two heights is more complex than those in one height, as requires a mask on silicon wafer for each height and a two layers fabrication process microalligned with the first layer. These processes, which were previously performed at IBEC and are not part of this Thesis, are described in Materials and Methods (detailed in section 4.1. Design and SU-8 master fabrication). The silicon master, which now serves as a template for producing the microfluidic devices, allowed for the fabrication of four devices (or chips) at a time (Fig. 56E). Once the PDMS chips were cross-linked, the PDMS was removed with the transferred master shape and the chips were individually cut. The microfluidic channel was closed by bonding the PDMS to glass slides after plasma activation.

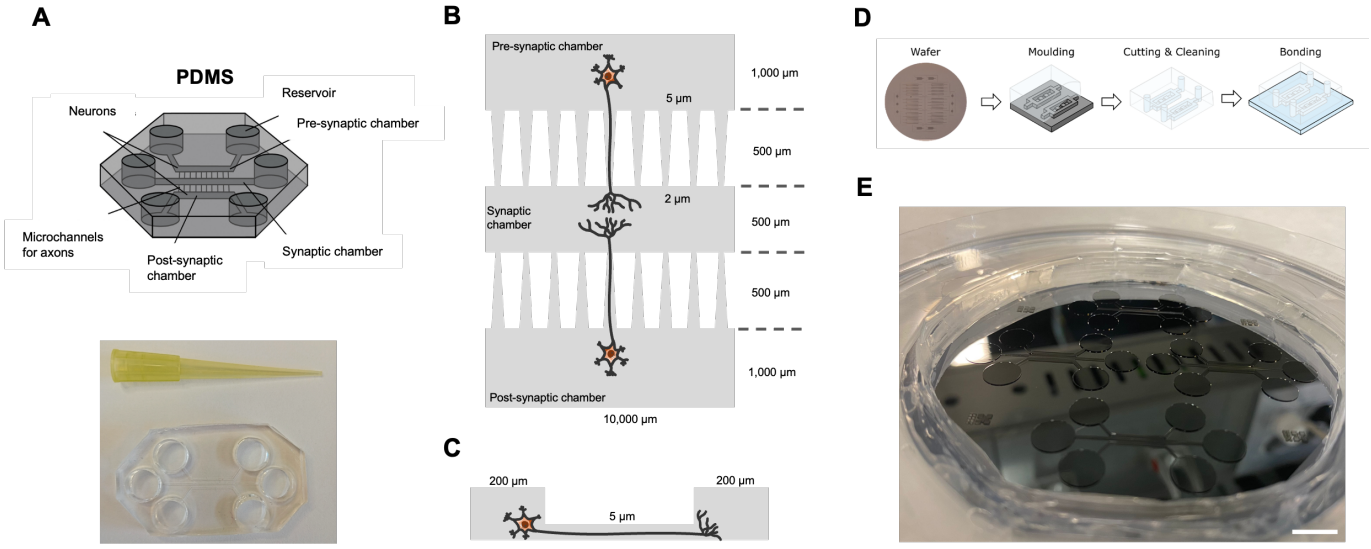

Figure 56. PDMS microfluidic device synapse on a chip (SoC) fabrication. (A) Representation of the PDMS chip with its different compartments (image adapted from (Coquinco et al., 2014)) and full-scale image of the chip compared to a 200 µL yellow pipette tip. (B) 2D schematic representation of the lateral (pre- and post-synaptic) chambers and synaptic chamber, with the funnel-shaped axonal microchannels, and their sizes and (C) heights. (D) Process followed for the creation of a microfluidic chip: starting from a master, the system is molded with PDMS polymer, trimmed and cleaned, and finally attached to a glass or slide for the growth of neurons and their study (image adapted from (Tauber et al., 2021)). (E) Full-scale image of the silicon master produced through photolithography (scale bar 10,000 µm).

1.2 Synapse on a chip device characterization

Once the mold was obtained, and before using it to generate the chips, we confirmed that it was optimal for its use. To do so, we verified by interferometry the height and width of the microchannels through which the axons will pass (Fig. 57A). This technique uses the interference of light waves to measure small displacements, surface irregularities, or changes in refractive index with high precision. Next, we reviewed the structure of the microchannels by optical microscopy (Fig. 57B). We measured that the wide end, which connects with the lateral chamber, ranges between 4.04 µm and 4.19 µm approximately, and the narrow end, which connects with the synaptic chamber, ranges between 1.77 µm and 1.84 µm. These values were considered to be inside the error design, thus determining that the microchannels were correctly formed during the photolithography process.

Ultimately, as with the master, we checked by optical microscopy the generation of the axonal microchannels in the chips (Fig. 57C). Manual counting of not finished or folded channels revealed that between 85-90% of the microchannels were functional, since they did not present errors, and the axons would be able to grow and enter the synaptic chamber.

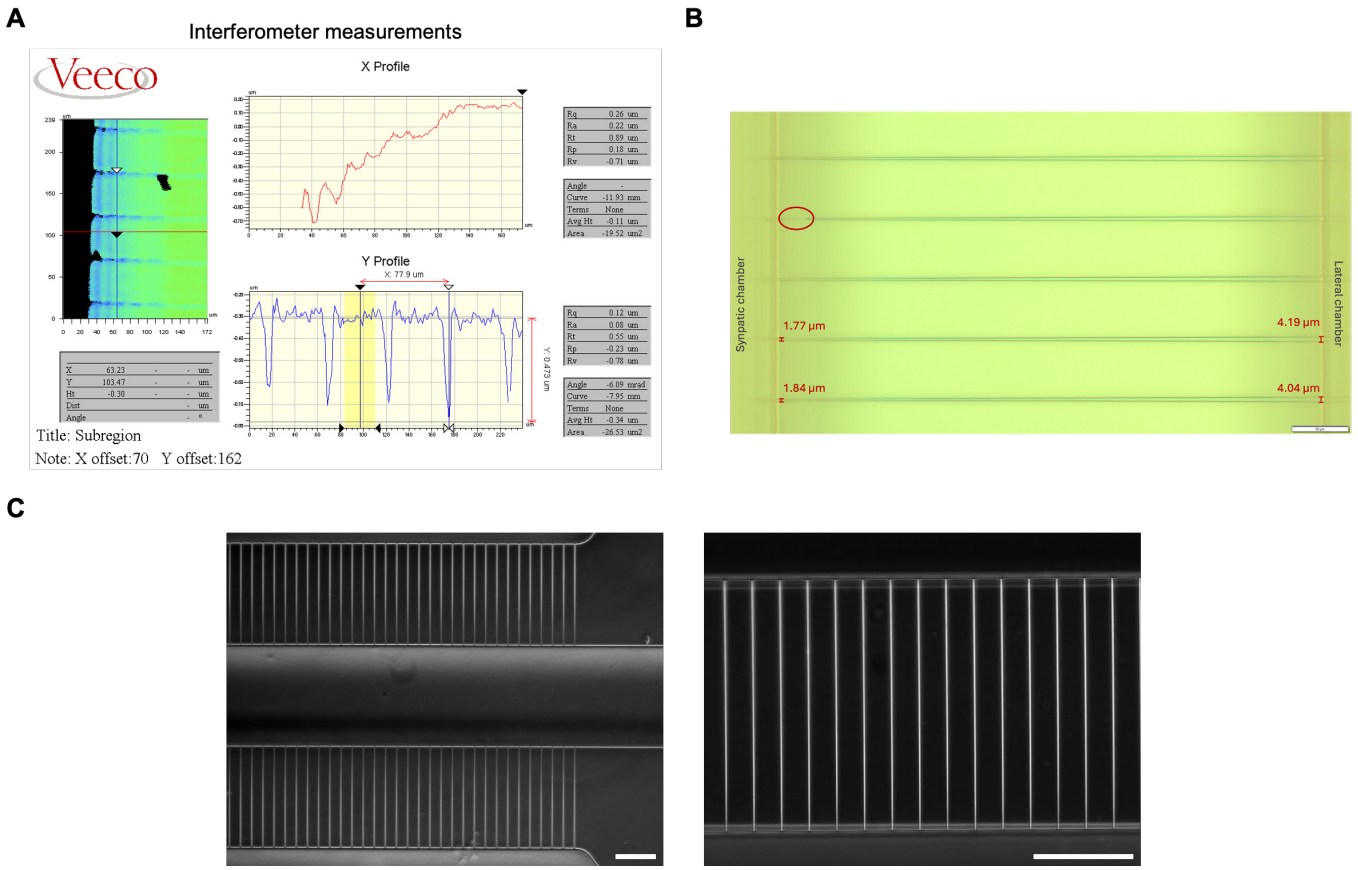

Figure 57. PDMS microfluidic device synapse on a chip (SoC) characterization. (A) Characterization of axonal microchannel height and width in the master using an interferometer (red line shows X profile and blue line shows Y profile, revealing the height of the microchannel; white arrow highlights the measurement of interest). (B) Observation by optical microscopy of the axonal microchannels in the master, from the wide end that starts from the lateral chamber to the narrow end that finishes in the synaptic chamber; two representative measurements and red circle shows broken microchannel during the manufacturing process (scale bar 50 µm). (C) Representative phase-contrast microscopy images of the SoC microchannels and synaptic chamber (scale bar 200 µm).

2 Cortical neurons growth and characterization in the microfluidic device

Once the SoC microfluidic device was characterized and confirmed that the fabrication process was successful, we assayed the growth and differentiation of hNPC-derived cortical neurons of a healthy control line, namely CTRL2#8, which was obtained at IDIBELL as specified in Materials and Methods (section 2.3. Human neural progenitor cells (hNPCs)). By this, we aimed to proof that the device was indeed suitable for the growth and study of neuronal cells. Shortly, we tested different conditions regarding cell number per chamber and differentiation times for optimal development inside the device. Then, when neurons were considered completely mature, we tested neuronal markers by immunofluorescence and measured neurotransmitters concentrations in the synaptic chamber media by high performance liquid chromatography (HPLC).

2.1 hNPC-derived cortical neurons growth in the microfluidic device

To establish the optimal conditions for cortical neurons growth in the lateral chambers of the microfluidic device we first assayed two seeding cell numbers (100,000 and 200,000 progenitor cells) and two differentiation conditions: maintaining the proliferation factors EGF and FGF2 at 10 ng/mL for 48 hours after seeding or starting the differentiation to cortical neurons at the moment of seeding (Fig. 58A). We observed that the 200,000 cells

condition filled the chamber completely with approximately 100% confluency whereas the 100,000 cells condition resulted to be too low cell density, which could affect differentiation. The maintenance of proliferation factors for 48 hours after seeding in the microfluidic device aided for an improved cell attachment and distribution inside the chamber. Already at day 9 after seeding, we observed that the cells direct their neurites to the microchannels and at day 13 we could observe that the neurites entered the central synaptic chamber, and therefore, they were considered axons. At day 22 after seeding, when hNPC-derived cortical neurons were considered to be fully mature, axons from opposite chambers connected between each other, establishing cortical axon-axon communications. At the same time, a control condition in 24 multi-well plates was maintained to compare neuronal differentiation in the chip with conventional conditions (Fig. 58B).

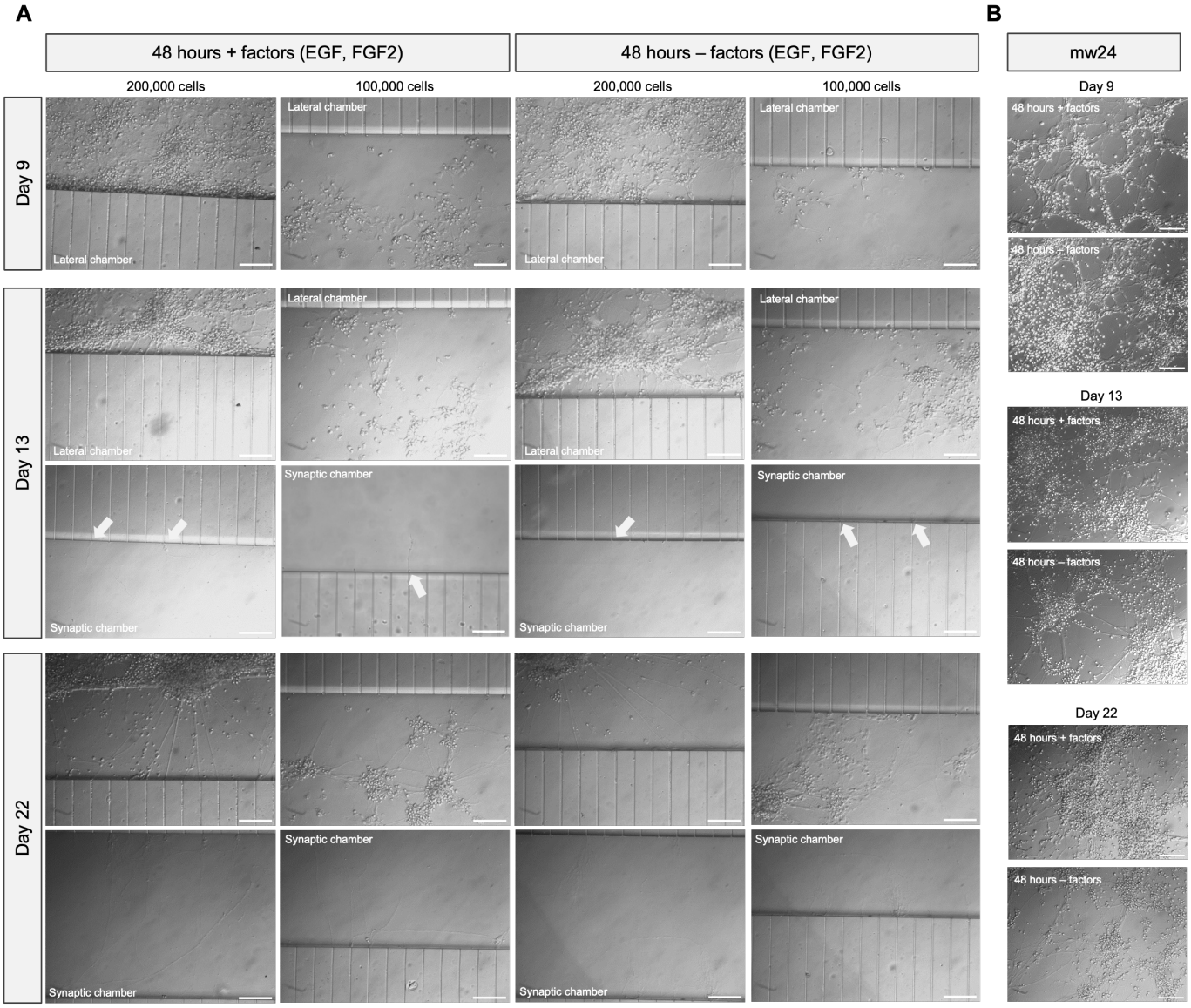

Figure 58. Optimization of cell seeding conditions in the SoC microfluidic device for cortical neuron differentiation from hNPCs. Bright-field microscopy images of hNPC-derived cortical neurons from healthy control CTRL2#8 at days 9, 13 and 22 after seeding in (A) the microfluidic device and (B) 24 multi-well plates, in conditions of cell number (100,000 and 200,000 progenitors; only 100,000 cells for mw24) and proliferation factors EGF and FGF2 at 10 ng/mL in proneural media (maintained for 48 hours after seeding in the device or started the neuron differentiation directly at seeding); images from lateral and synaptic chambers (white arrow highlights axons entering the synaptic chamber; scale bar 100 µm).

Since we considered 200,000 seeded cells to be too dense, while 100,00 cells would be not enough for a correct neuronal differentiation, we assayed a 150,000 cell-seeding condition and maintained the proliferation factors for 48 hours in the SoC microfluidic device to facilitate the cell proliferation and growth. This resulted to be the optimal condition, since progenitors were attached and distributed evenly throughout the lateral chambers (Fig. 59A) and grew their axons to enter the synaptic (central) chamber, after two-week differentiation in the device, to start synaptic connections in the central chamber (Fig. 59B). However, the established connections were not merely from neurons grown in the opposite chamber, but also axons connected to other axons that entered from the same chamber. This pointed towards a potential limitation of the device, as it seemed that the synaptic chamber is too large for establishing most synapses from the opposite chamber.

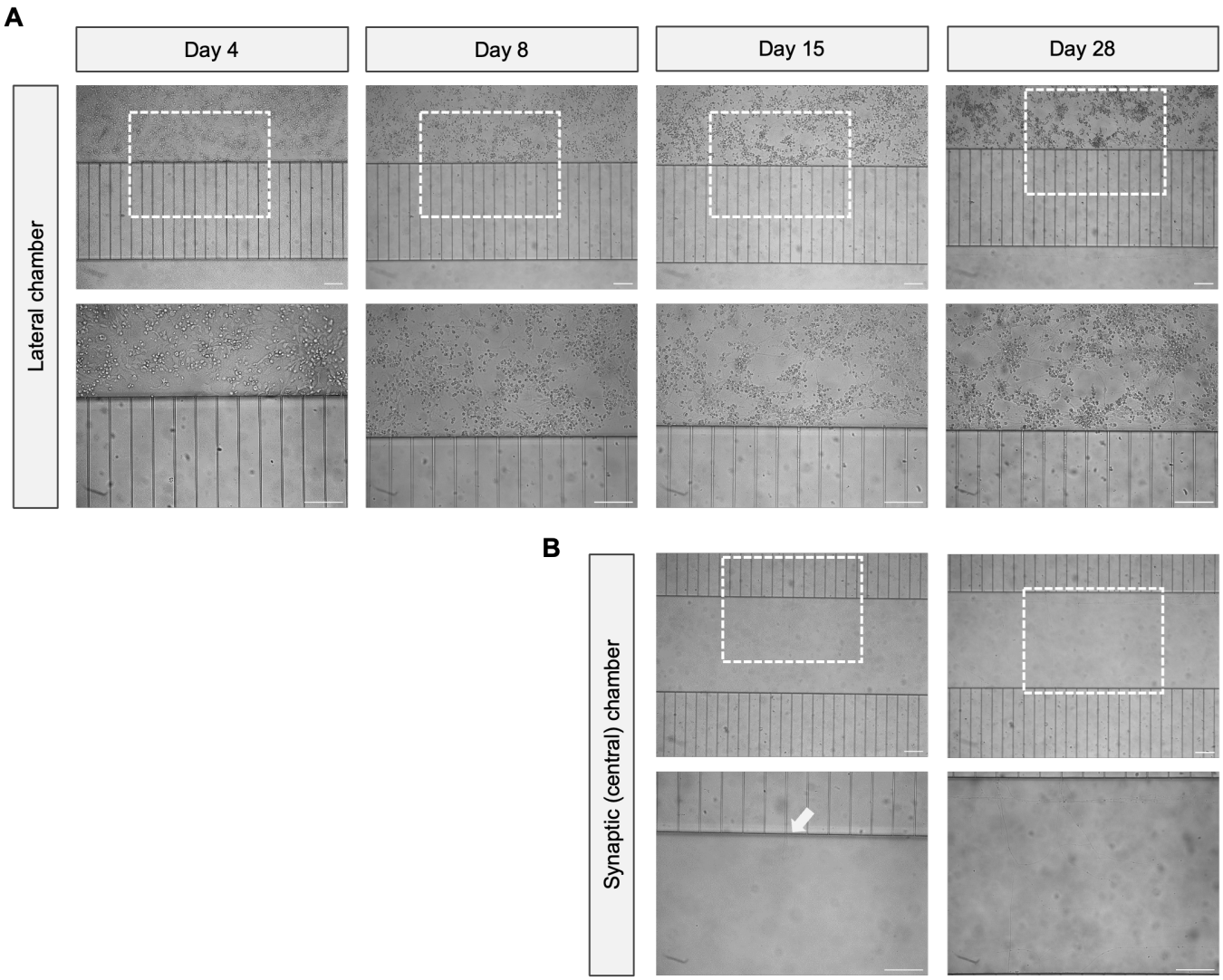

Figure 59. Cortical neuron differentiation in the SoC microfluidic device seeding 150,000 progenitors and maintaining proliferation factors EGF and FGF2 for 48 hours. Bright-field microscopy images of hNPC-derived cortical neurons from healthy control CTRL2#8 at days 4, 8, 15 and 28 after seeding in the (A) lateral chambers of the microfluidic device, and (B) images of the synaptic chamber, showing axonal passing through the microchannels into the central chamber (white dashed box represents the enlarged image beneath; white arrow highlights axons entering the synaptic chamber; scale bar 100 µm).

2.2 Characterization of cortical neurons in the microfluidic device

Based on previous experience, the cortical neurons were considered fully mature after 3-5 weeks of differentiation inside the SoC microfluidic device. This was confirmed by the expression of neuronal-specific markers, such as TUJ-1 and MAP2, that were detected by immunofluorescence (Fig. 60A). MAP2 (Microtubule-Associated Protein 2) stabilizes microtubules in the dendrites of postmitotic neurons and is considered a marker for mature neurons. TUJ-1 (class III β-tubulin) is a structural component of microtubules and is expressed in axons. The results show that TUJ-1 was better than MAP2 in staining neuronal prolongations and, consequently staining the axons that crossed the microchannels from the lateral chambers to enter the synaptic chamber (Fig. 60B). Some nuclei were also detected in the microchannels, suggesting that neuronal somas could pass into the synaptic chamber.

However, we did not achieve a complete staining of the axons along the microchannels. In this manner, we assayed staining with the probe phalloidin, which is a toxin used for staining actin filaments of the cytoskeleton, although not specific for neurons (Fig. 60C). We observed that phalloidin was able to effectively stain the axons crossing the microchannels, but did not have a homogeneous staining for all the neuronal structures, as while axons were properly stained, cell bodies staining was sub-optimal. In conclusion, we detected mature neuronal-specific structures with both MAP2 and TUJ-1 markers, the latter being more efficient in axonal staining, and validated the microchannel crossing of axons into the synaptic chamber; however, some nuclei crossed as well. Ultimately, we selected the marker TUJ-1 for neuronal staining in the SoC microfluidic device.

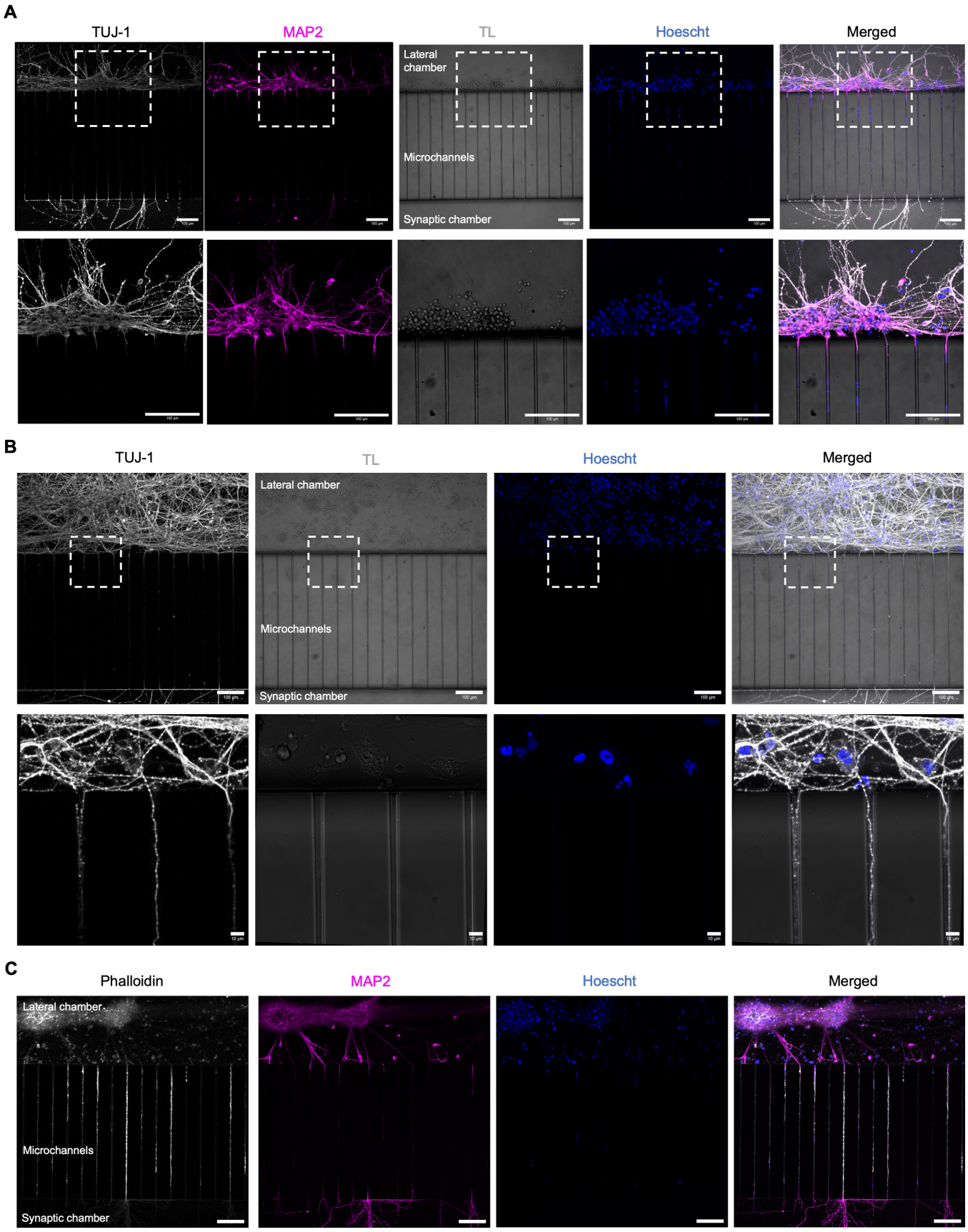

(see figure legend in next page)

(from previous page)

Figure 60. Characterization of CTRL2#8 hNPC-derived cortical neurons in the SoC microfluidic device. (A-C) Representative confocal microscopy IF images of the differentiated and mature cortical neurons in the lateral chamber which axons enter the synaptic chamber through the funnel-shaped microchannels. (A, B) TUJ-1 in grey, MAP2 in magenta, nuclei in blue stained with Hoescht; white dashed box denotes the enlarged image situated beneath; (A) scale bar 100 µm for both magnifications; (B) scale bars 100 µm for the upper image and 10 µm for the enlarged lower image. (C) Phalloidin in grey, MAP2 in magenta, nuclei in blue; scale bar 100 µm. TL = transmitted light.

Finally, we wondered if synaptic activity could be modulated by stimulating one of the chambers individually. This was of great interest, as potentially could be evolved into the differential study of pre and post-synaptic neurons in specific circuits. We evaluated if we could stimulate the neurons in one of the lateral chambers, which would become the pre-synaptic chamber, and exert an effect in the synaptic chamber or if the stimulation could be translated into changes in the non-stimulated lateral chamber, which would become the post-synaptic chamber. For this, we incubated the pre-synaptic neurons with 50 mM KCl for 10 minutes or with 50 µM FCCP for 30 minutes before adding KCl for stimulation and measured the active synapse marker Bassoon in the synaptic chamber (Fig. 61A). FCCP was added to cause mitochondrial function impairment through respiratory chain uncoupling and dissipation of mitochondrial membrane potential, to detect if alterations in mitochondrial homeostasis would affect synaptic activity.

In addition, we measured the ratio between phosphorylated-CAMKII and total CAMKII (pCAMKII/CAMKII) in the soma of post-synaptic neurons in basal conditions and after stimulation with 50 mM KCl for 10 minutes of the pre-synaptic chamber (Fig. 61B). CAMKII (Ca^{2+}/calmodulin-dependent protein kinase II) is a major signaling protein in neurons, essential for regulating synaptic strength and plasticity, which phosphorilation is an indicator of its active state.

After quantification of the synaptic activity markers in the synaptic chamber, we did not detect any significant differences for Bassoon count nor area occupied by signal, for the stimulated and the FCCP-induced mitochondrial damage conditions compared to basal (Fig. 61C). Regarding post-synaptic signaling, we did not detect significant differences in the fluorescence ratio pCAMKII/CAMKII in the soma of post-synaptic neurons after KCl stimulation in pre-synaptic chamber (Fig. 61D). These negative results suggest that the assayed conditions were insufficient for exerting an effect on synaptic activity and post-synaptic signaling.

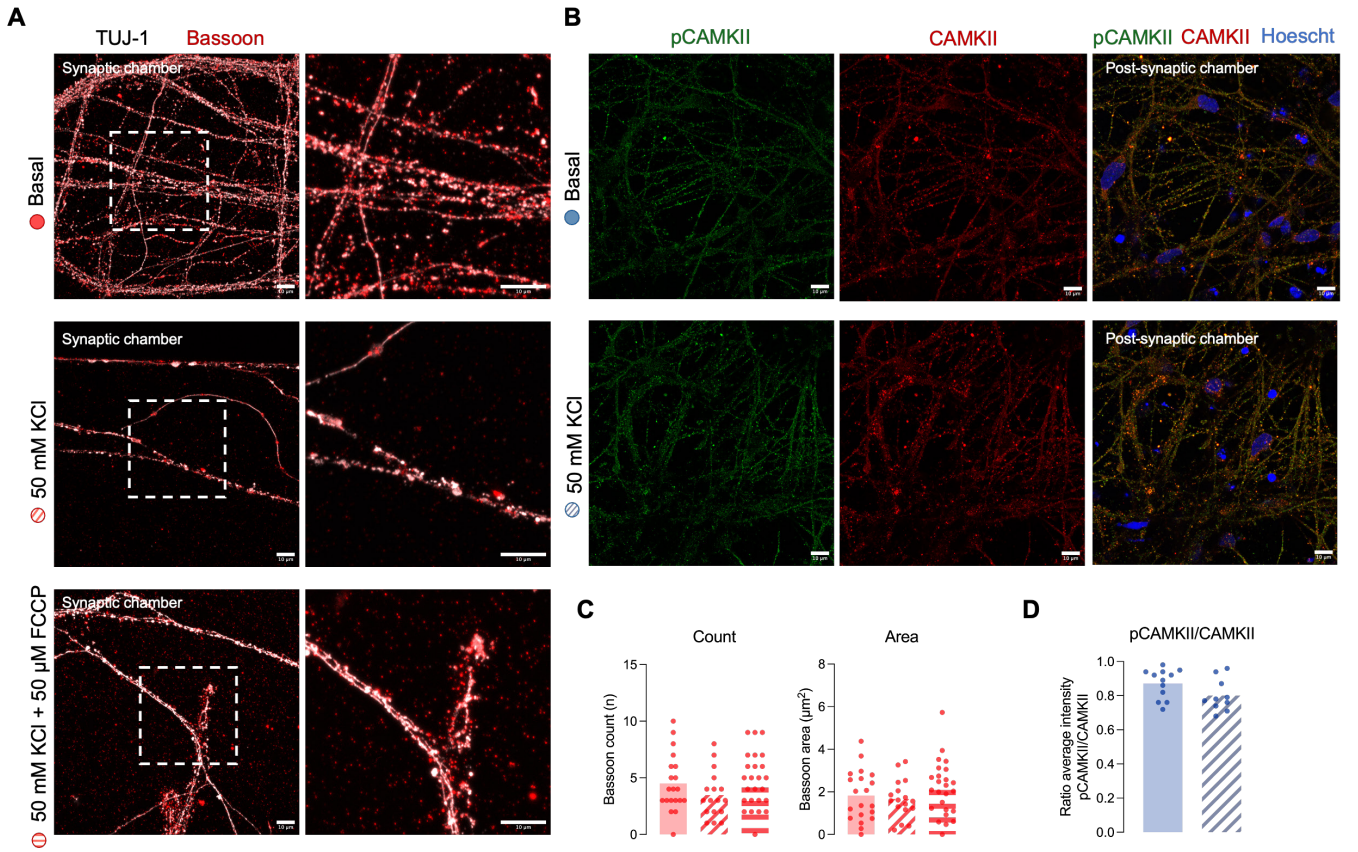

Figure 61. Synaptic activity evaluation of cortical neurons in SoC microfluidic device. (A) Representative confocal microspy images of active synapse marker Bassoon IF in the synaptic chamber, in basal condition and after stimulation of the pre-synaptic chamber with 50 mM KCl for 10 minutes, and 50 µM FCCP for 30 minutes together with 50 mM KCl for 10 minutes (TUJ-1 in grey, Bassoon in red; white dashed box represents the 2.5x enlarged image on the right side; scale bar 10 µm).

(cont. next page)

(from previous page)
(B) Representative confocal microspy images of phosphorilated CAMKII and total CAMKII IF in the post-synaptic chamber, in basal condition and after stimulation with 50 mM KCl for 10 minutes in the pre-synaptic chamber (pCAMKII in green, CAMKII in red, nuclei in blue stained with Hoescht; scale bar 10 µm). Quantifications of (C) Bassoon count and area occupied by signal in synaptic chamber (n=5 ROIs per image, from four images per condition), and (D) average intensity ratio pCAMKII/CAMKII in soma of post-synaptic neurons, quantified with ImageJ (n=17 nuclei for basal, n=13 nuclei for KCl condition).
Data represented as mean and individual values. Comparative analysis done with (Brown-Forsythe and Welch) ANOVA if more than two groups, and Welch's test if two groups.

2.3 Neurotransmitters' measurement in the synaptic chamber

One of the main applications of the SoC microfluidic device is to detect neurotransmitters' concentrations in the synaptic chamber. This would validate the device as an *in vitro* tool for synaptic characterization of neurodevelopmental disorders, and multiply its potential for the study of neurotransmitters modulators. To do so, we measured by HPLC the concentrations of the neurotransmitters glutamate and GABA (Gamma-Aminobutyric Acid) in the media of the synaptic chamber, obtained from the reservoir and without disturbing the synaptic connections (Fig. 62A). The media was collected from the reservoir of SoC devices with 150,000 cells plated on each lateral chamber. The conditions assayed in the device were basal, pre-synaptic stimulation with 50 mM KCl for 10 minutes, and pre-synaptic mitochondrial disturbance with 50 µM FCCP incubation for 30 minutes together with KCl stimulation for 10 minutes.

The results are preliminary and should be considered carefully since for the stimulated conditions we only have one or very few measurements. We detected a 2.17-fold increased trend in glutamate concentration after pre-synaptic stimulation with KCl (yet not significative because of the n) in the CTRL2#8 cortical neurons, which seemed to be maintained after mitochondrial homeostasis disturbance with FCCP (Fig. 62B). Regarding the main inhibitory neurotransmitter GABA, we detected very low concentrations with no-significative changes after KCl stimulation and was almost depleted when cells were incubated with FCCP+KCl (0.02 µmol/L) (Fig. 62C). Therefore, these results could demonstrate that glutamatergic neurotransmission would be more robust against mitochondrial alterations, whereas GABAergic neurotransmission would be affected by the disturbance, although no stimulation was initially detected. In this sense, GABA measurements were very low and disperse, since it is a very sensitive and difficult amino acid to measure (Rea et al., 2005) and more measurements are needed to confirm the obtained results.

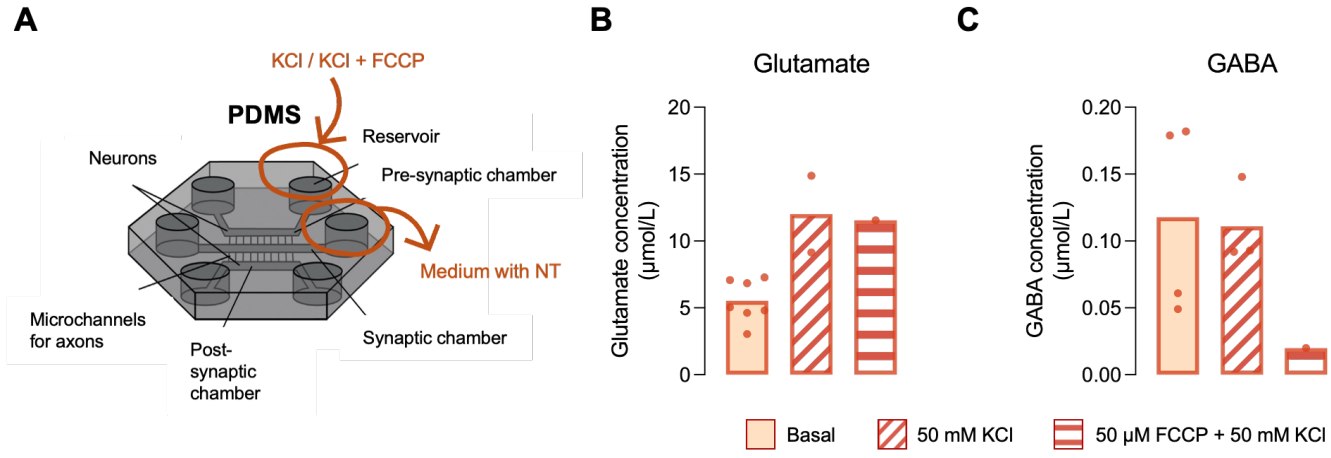

Figure 62. Neurotransmitters' measurement through HPLC in synaptic chamber of SoC microfluidic devices. (A) Schematic representation of the device and procedure to obtain the media for measurement: 50 mM KCl for 10 minutes or 50 µM FCCP for 30 minutes together with 50 mM KCl for 10 minutes were added to the reservoir of the pre-synaptic chamber and maintained at 37°C and 5% CO_2 for the corresponding times, and then media was collected from the synaptic chamber reservoir. HPLC measurements of the neurotransmitters (B) glutamate and (C) GABA in basal, KCl and FCCP+KCl conditions (n=3-4 devices, whereas only n=1 device for FCCP+KCl).
Data represented as mean and individual values. Comparative analysis between basal and KCl conditions was performed with Welch's t test. NT = neurotransmitters.

3 Dopaminergic neurons growth and characterization in the microfluidic device

After confirming that the SoC microfluidic device is suitable for hNPC-derived cortical neurons growth and differentiation, we moved forward and investigated if ventral midbrain NPC (vmNPC)-derived dopaminergic (DA) neurons would differentiate accordingly in the device. For this, we used a healthy human control line previously generated at IDIBELL, named SP11, which is tyrosine hydroxylase (TH)-TdTomato reporter, similar to the specified in (Calatayud et al., 2019). The cell line is engineered so that the gene encoding TH, a specific marker of DA neurons, is coupled to the TdTomato fluorescent protein. When the TH gene is expressed in differentiated DA neurons, TdTomato fluorescence is produced.

We tested different seeding conditions regarding cell number and terminal DA neuron differentiation times. When DA neurons were considered completely mature, we tested DA neuronal markers by immunofluorescence, evaluated mitochondrial dynamics (given the relationship between dopaminergic neurotransmission and mitochondrial function), and measured DA neurotransmitter concentration in the synaptic chamber media through HPLC.

3.1 vmNPC-derived dopaminergic neuron growth and differentiation in the microfluidic device

To establish the optimal conditions for DA neuron growth and differentiation in the lateral chambers of the microfluidic device we assayed three seeding cell numbers (150,000, 200,000 and 250,000 cells) and two differentiation times, one beginning the DA neuron terminal differentiation at the time of seeding (N2B27 medium supplemented with 20 ng/mL BDNF and 20 ng/mL GDNF, as detailed in Materials and Methods), and another 48 hours later. The latter was the optimized condition in the cortical neurons seeding in the SoC device, described in section 2.1. of the present chapter. Here, we increased the cell number plating since the seeding step is performed when cells are already DA-inducted neurons and not undifferentiated progenitors, which could imply less cell viability after seeding.

We seeded cells in both lateral chambers for the 48-hour non-terminal DA differentiation condition, whereas seeded only one chamber for the terminal differentiation condition. We observed that as the number of seeded cells increased in the lateral chambers, more aggregates formed in the non-terminal DA differentiation condition (Fig. 63A), whereas if the DA-induced cells started the terminal differentiation at the time of seeding (adding the factors BDNF and GDNF), the cells were more homogeneously distributed throughout the chamber. Axonal prolongations were observed in the synaptic chamber already at day 9 post-seeding in the device for the conditions of 200,000 and 250,000 cells undifferentiated for 48 hours, and at day 14 for all the conditions. In addition, we maintained a control well of a 12 multi-well plate (p12) with or without BNDF and GDNF factors for 48 hours after seeding (Fig. 63B). Here, the cells non-differentiated for 48 hours showed different aggregation patterns compared to the cells seeded in the microfluidic device for the same condition. These results suggest that the optimal conditions for DA-induced cell inclusion in the device are the intermediate number of 200,000 cells and starting the DA terminal differentiation at the time of seeding for a homogeneous cell distribution.

After day 14 post-seeding and DA terminal differentiation induction, the SP11 line is considered to be fully mature and DA neurons should be completely differentiated. To evaluate if the differentiation process was resulting in DA neurons, we observed the cultured cells in the lateral chambers of the SoC microfluidic device through an inverted epi-fluorescence microscope (Fig. 63C). We detected TH-TdT reporter cells in the lateral chambers of the device, meaning that we achieved DA neuron differentiation without differences between the assayed conditions.

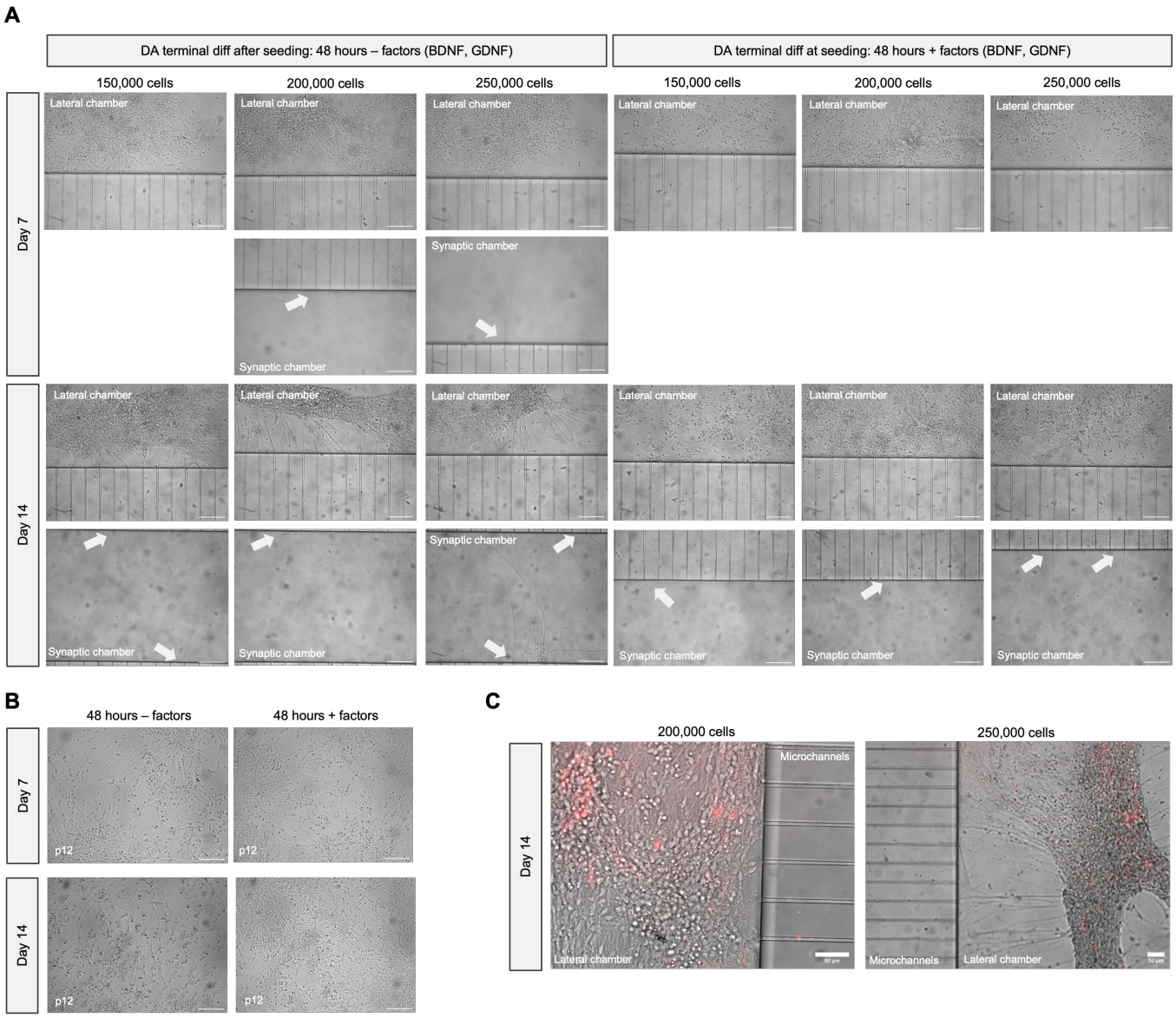

Figure 63. Optimization of cell seeding conditions in the SoC microfluidic device for DA neuron differentiation from vmNPCs. Bright-field microscopy images of vmNPC-derived DA neurons from healthy control SP11 at days 7 and 14 after seeding in (A) the microfluidic device and (B) 12 multi-well plates, in conditions of cell number (150,000, 200,000, and 250,000 cells) and proliferation factors BDNF and GDNF at 20 ng/mL in N2B27 media for terminal DA neuron differentiation (not added for 48 hours or added at seeding for starting terminal differentiation); images from lateral and synaptic chambers (white arrow highlights axons entering the synaptic chamber; scale bar 100 µm). (C) Bright-field representative images of TH-TdTomato reporter cells in live imaging through inverted epi-fluorescence microscope (TH-reporter DA neurons in red for 200,000 and 250,000 cell conditions without factors for 48 hours post-seeding; scale bar 50 µm).

To confirm the fidelity of the reporter, on day 18 post-seeding in the SoC microfluidic device, DA neurons were fixed and immunostaining was observed by confocal microscopy, as can be seen in Figure 64. The markers used were anti-TUJ-1 for mature neurons, anti-RFP (Red Fluorescent Protein) for amplification of the TdTomato signal and anti-TH for comprobation of the TH-positive neurons. We observed a correlation in the signals for RFP and TH, suggesting that the genetic reporter is correctly identifying TH-positive neuronal populations in the device. In addition, we observed that DA neurons passed from the lateral chamber through the microchannels into the synaptic chamber, as well as some nuclei (similar to what happenned in the devices with cortical neurons). In this manner, we validated the differentiation of vmNPCs to mature DA neurons in the SoC microfluidic device and the passage of the axons through the microchannels into the synaptic chamber.

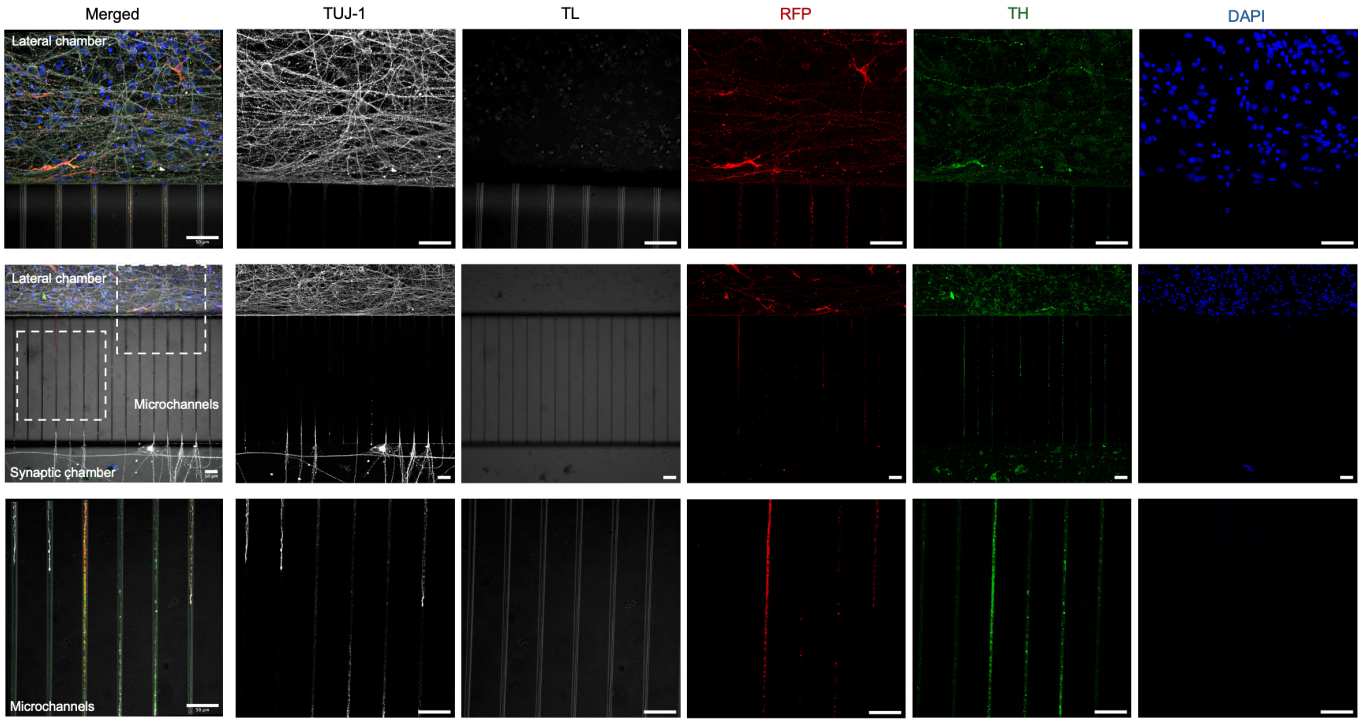

Figure 64. Characterization of DA neurons derived from the SP11 TH-reporter TdT line in the SoC microfluidic device. Representative confocal microscopy IF images of the differentiated and mature DA neurons in the lateral chamber which axons enter the synaptic chamber through the funnel-shaped microchannels. TUJ-1 in grey, RFP in red, TH in green, nuclei in blue stained with DAPI; white dashed boxes denote for the enlarged image situated above (lateral chamber) and beneath (microchannels); scale bar 50 µm. TL = transmitted light.

3.2 Mitochondrial characterization of dopaminergic neurons in the microfluidic device

Since most of the neurodevelopmental diseases with mitochondrial alterations studied in Chapter 2 involve dopaminergic alterations in their clinical pathophysiology, we wondered if we could study some aspects of mitochondrial homeostasis in the DA neuron-microfluidic devices as a preliminary work for the future development of personalized models. For this, MitoTracker™ Green probe was used for detection of mitochondrial structure and dynamics, observed through time-lapse image acquisition in live cells. We assayed a basal condition and 50 mM KCl stimulation of the pre-synaptic chamber for 10 minutes before image acquisition.

We were able to detect mitochondrial movement and its entry into the microchannels, suggesting axonal transport into the synaptic chamber (Fig. 65A). However, when adding 50 mM KCl to the reservoir of the pre-synaptic chamber, the signal was diffused and finally lost (Fig. 65B). The results suggest that the probe is not compatible with the KCl treatment and other systems should be explored, as viral tagging.

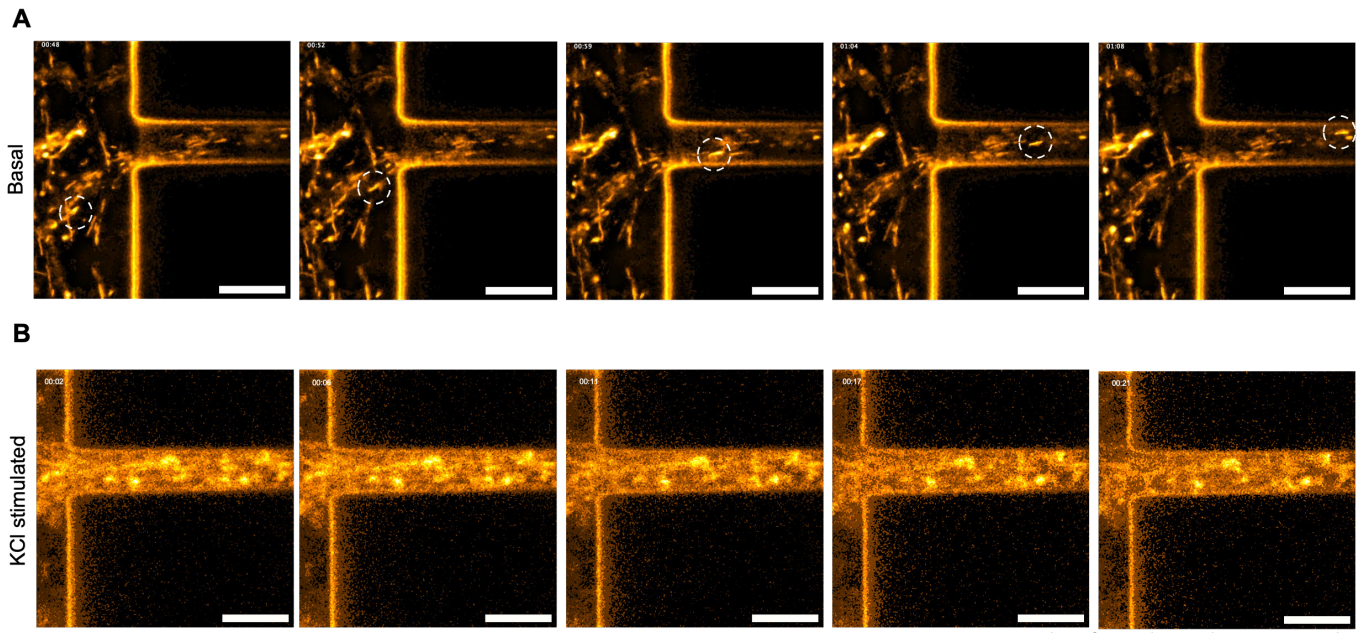

(see figure legend in next page)

(from previous page)

Figure 65. Mitochondrial dynamics characterization in the DA neuron-microfluidic device. Representative frames of the mitochondrial network of SP11 DA neurons derived from TH reporter vmNPCs, stained with MitoTracker™ Green in (A) basal conditions and (B) after stimulation of pre-synaptic chamber with 50 mM KCl for 10 minutes. White dashed circle highlights the transport of a mitochondrion from the pre-synaptic chamber into the microchannel at different time points (mitochondria in Orange Hot LUT; scale bar 10 µm).

3.3 Dopamine measurement and mitochondrial disturbance in the synaptic chamber

As previously shown in the SoC seeded with cortical neurons, the chip offers the possibility of analyzing neurotransmitters (glutamate and GABA concentrations) in the synaptic chamber of the *in vitro* model. Here the objective is the measurement of dopamine concentration by HPLC in the media of the synaptic chamber. This also, would allow to study the potential mitochondrial implications on the synapse in a DA neuron model. To do so, we obtained the media from the corresponding reservoir, without disturbing the synaptic connections during the liquid extraction (Fig. 66A). The conditions assayed in the device were basal, pre-synaptic stimulation with 50 mM KCl for 10 minutes, and pre-synaptic mitochondrial disturbance with 50 µM FCCP incubation for 30 minutes together with KCl stimulation for 10 minutes.

The results are preliminary and should be considered carefully. We detected an increased trend of 2.23 folds in DA concentration after pre-synaptic stimulation with KCl in the SP11 dopaminergic neurons (Fig. 66B). When pre-synaptic chamber was treated with FCCP and later stimulated with KCl, a decrease of 88% in DA concentration was detected. This could mean that dopaminergic neurons respond to stimulation, but when mitochondrial function is disturbed, dopaminergic neurotransmission is affected, since DA neurons are heavily reliant on correct mitochondrial homeostasis. However, more replicates are needed to confirm these results.

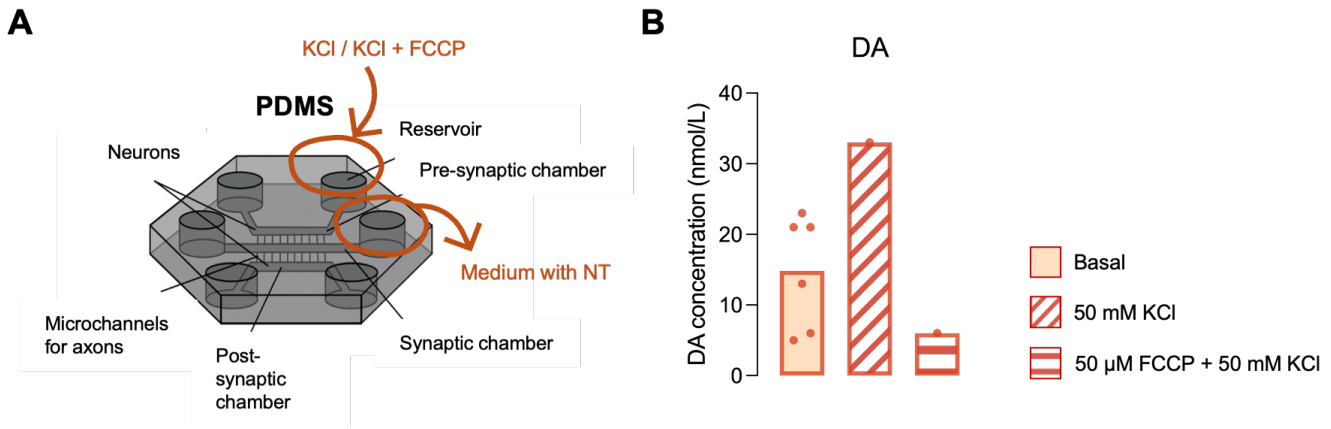

Figure 66. Neurotransmitters' measurement through HPLC in synaptic chamber of SoC microfluidic devices. (A) Schematic representation of the device and procedure to obtain the media for measurement: 50 mM KCl for 10 minutes or 50 µM FCCP for 30 minutes together with 50 mM KCl for 10 minutes were added to the reservoir of the pre-synaptic chamber and maintained at 37°C and 5% CO_2 for the corresponding times, and then media was collected from the synaptic chamber reservoir. (B) HPLC measurements of the dopamine (DA) neurotransmitter in basal, KCl and FCCP+KCl conditions (n=3 devices for basal, whereas only n=1 device for KCl and FCCP+KCl). Data represented as mean and individual values. NT = neurotransmitters.

DISCUSSION

In this Thesis, we have studied mitochondrial metabolism as a potential target for the treatment of neurodevelopmental disorders. We have described that mitochondrial alterations play a role in the pathophysiology of different neurodevelopmental diseases, which can either be the primary cause of the disease or underly as part of their pathophysiology. In both scenarios, we have demonstrated that their study and modulation can lead to new therapeutic strategies. To achieve that, we have divided this Thesis in three complementary sections. We first studied the paradigmatic neurodevelopmental disorder Rett syndrome, in which we described the mitochondrial dysfunction in two models of the disease, and assayed a treatment with a metabolic modulator, the PPARγ agonist leriglitazone, observing pre-clinical improvements. Then, we moved towards the study of the shared mitochondrial dysfunction of several neuropediatric patients with disorders caused by mitochondrial proteins alterations, assayed different treatment approaches (pharmacologic, nutraceutical and metabolic), and when possible, translated them into the clinic observing cognitive and symptomatic ameliorations. All the studied patients have in common, besides the mitochondrial dysfunction, clinical and/or biochemical presentations suggestive of "neurotransmitter-related diseases", along with a neurological phenotype, leading to the establishment of a relationship between the alterations in the bioenergetic metabolism and neurotransmission. Finally, since advanced models for a precise study of the mitochondrial involvement in the synaptic function are needed, we accomplished the first steps in the assessment and validation of the microfluidic system "synapse on a chip" for future personalized studies of neurodevelopmental disorders and discern how the assayed drugs could be influencing synaptic communication.

1 Mitochondrial homeostasis is altered in Rett syndrome and represents a new potential therapeutic target

Rett syndrome is a devastating neurodevelopmental disease without specific treatment. It is a complex disorder in which multiple physiological routes and different cell types are altered (Ribeiro et al., 2020a). Since the discovery of *MECP2* as the disease-causing gene (Amir et al., 1999), most of the research has been focused on its function in the brain, the main affected organ, and how its disfunction causes the observed phenotype. The main pillars of Rett pathophysiology are neuronal maturation delay, a disruption in excitatory/inhibitory neurotransmission and glial cell dysfunction (Banerjee et al., 2019; Gold et al., 2024). Besides them, other pathways have been described as part of Rett syndrome pathophysiology as well. These components include metabolic, and particularly, mitochondrial dysfunction (Justice et al., 2014), oxidative stress (Felice et al., 2012) and systemic inflammation (Pecorelli et al., 2020), which have been suggested to play a role in the disease development. In the last years, it is being proposed whether mitochondrial alterations can constitute a new therapeutic target for this disorder (Shulyakova et al., 2017).

In this Thesis, we have explored mitochondrial dysfunction in Rett syndrome based on two aspects of its homeostasis: mitochondrial network and ultrastructure shape, and bioenergetic function, regarding energy production and oxidative stress. Limiting our description to these features instead of profiling the full mitochondrial landscape (Monzel et al., 2023) has allowed us to analyze a larger number of samples and models, focusing on the aspects with the greatest therapeutic potential and translational scalability between fibroblasts and brain tissue. For this, we used two models of the disease: for the first analysis, we have used primary fibroblasts derived from Rett patients and controls. Fibroblasts are a useful and cost-effective resource to study mitochondrial abnormalities in neurodevelopmental disorders (Cordone et al., 2020; Olesen et al., 2022). They are easily accessible and maintain the patient's genetic background, allowing the study of genotype-phenotype aspects. Rett patients' fibroblasts are considered as a "disease-in-a-dish" model, particularly helpful for studying mitochondrial functions in terms of structure and bioenergetic function. On a second phase of the study, we moved towards the analysis in female "Rett" mice, a disease model that recapitulates most of the symptomatology and has allowed us to study specific brain alterations.

Mitochondrial homeostasis alterations are detected in the two studied Rett syndrome models

According to our results on **mitochondrial network analysis** in fibroblasts, Rett mitochondria form less interconnected and "simpler" networks with less, shorter and thinner branches compared to controls. Previous reports in this regard were unconclusive: in other models such as hippocampal astrocytes of *Mecp2*$^{-/y}$ mice, mitochondrial mass was reported to be increased (Bebensee et al., 2017), while other studies have reported

hyperfused mitochondria in fibroblasts (Crivellari et al., 2021) or normal mitochondrial mass in neurons from human embryonic stem cells (Li et al., 2013). The increase in mitochondrial networks in Rett fibroblasts has been proposed as a consequence of an impaired clearance of mitochondria through PINK1/Parkin mediated pathway (Cicaloni et al., 2020; Crivellari et al., 2021). Interestingly, while overall fibroblasts showed the described alterations, individually, the patients grouped in two different "mitochondrial network phenotypes". We found a more severely affected phenotype in patients RTT_P2, with mutation in c.916C>T (p.Arg306Cys), and RTT_P4, bearing a mutation in c.808C>T (p.Arg270*). Both mutations are located on the transcription repression domain and nuclear localization sequence, respectively. On the other hand, we saw a milder phenotype in patients RTT_P1 and PTT_P3, both with the mutation c.502C>T (p.Arg168*), located on the inter-domain region. These results suggest that there could be a mitochondrial network phenotype mutation-dependent, that should be further investigated and corroborated with a higher number of samples.

Related to mitochondrial network structure, **mitochondrial dynamics** show decreased fission-to-fusion ratio in Rett fibroblasts. This was detected both from live-cell confocal imaging and dynamics markers expression, and is in line with other studies that reported decreases in Drp1 and Fis1 protein expression (Crivellari et al., 2021; Hirofuji et al. 2018). Rett mitochondria also display alterations in movement with a slow but directed and bursting-like behavior, which could imply impaired mitochondrial transport along microtubules. Noteworthy, these results were more homogeneous among patients than the network analysis. Further studies should evaluate the potential mitochondrial transport disruption in Rett neuronal axons and how this can be affecting synaptic function.

Regarding **mitochondrial ultrastructure**, Rett mitochondria show, compared to controls, a more electro-dense matrix, usually associated to a higher protein content, and a reduced number of cristae, which are wider and 'disorganized', alterations that could suggest homeostasis alterations and have been described before in pro-apoptotic states (Cogliati et al., 2016). Some of these alterations have been already described in Rett peripheral blood mononuclear cells (Pecorelli et al., 2016), in dendrites and axons of motor cortex from Rett female mice (Belichenko et al., 2009), and skeletal muscle from *Mecp2* KO mice (Park et al., 2014); the latter, however, showing electron-lucent matrices. Changes in cristae number and shape have been widely associated with reduced respiratory efficiency and cell viability, and reported in many diseases, including Leigh syndrome and Parkinson's disease (Huang et al., 2023, Navaratnarajah et al., 2021).

Moving towards the **bioenergetic profile**, we have observed that Rett mitochondria show a decreased respiration rate in terms of basal respiration, maximal respiration and ATP-associated oxygen consumption, in accordance with previous studies on fibroblasts (Cervellati et al., 2015) and neurons (Li et al., 2013; Zlatic et al., 2022). However, others have reported increased oxygen consumption in Rett male mice (Can et al., 2019; Kriaucionis et al., 2006) suggesting a greater but less efficient respiratory capacity. Our results were coherent through experiments, as the decreased "oligomycin-sensitive respiration", this is, the oxygen consumption linked to ATP synthesis, was indeed paired to a reduced mitochondrial ATP synthesis, with Rett mitochondria producing half the ATP than controls do. This bioenergetic dysfunction adds to previous transcriptomics analyses that reported altered genes for mitochondrial dysfunction and oxidative phosphorylation in Rett patients' blood (Aldosary et al., 2020). Not only Rett mitochondria present a deficient ATP production, but they also generate more Reactive Oxygen Species (ROS) resulting in an increased oxidative damage. ROS are highly reactive forms of molecular oxygen, including the superoxide anion radical ($O_2^{\cdot-}$), hydrogen peroxide (H_2O_2), singlet oxygen ($^1O_2$), and hydroxyl radical (·OH) (Sies and Jones, 2020), and they are a byproduct of aerobic metabolism. While in physiological concentrations (maintained through the action of antioxidant enzymes) they play important roles in cellular function, their accumulation or excessive production lead to a toxic state named as oxidative stress, resulting in impairment of cellular functions. This "energy-wasting" state associated with oxidative stress in Rett syndrome was described in previous studies on microglia (Jin et al., 2015), female mouse brains (De Filippis et al., 2015b) and fibroblasts (Cervellati et al., 2015; Signorini et al., 2014). Importantly, Leoncini and colleagues correlated high levels of oxidative stress markers in blood with more severe phenotypes in patients (Leoncini et al., 2013).

Altogether, we have described that both mitochondrial shape and function are altered in Rett syndrome fibroblasts. While previous descriptions in such regard had been made, the preceding data was mostly partial and scattered, leading to even contradictory conclusions depending on the study. We have expanded on the description of mitochondrial network shape together with the bioenergetic function impairment, especially interesting since most studies focus mainly on the latter. Mitochondria undergo structural and functional adaptations in response to metabolic demands (Liesa and Shirihai, 2013), therefore the relationship between shape and bioenergetic function

is crucial. In Rett fibroblasts there is decreased fission and impaired mitochondrial turnover (Cicaloni et al., 2020), implying that quality control is altered, and dysfunctional or damaged mitochondria are not being eliminated. The question remains if this is a consequence or an adaptive behavior for maintaining more mitochondria to produce enough ATP for survival despite the resulting increase in oxidative stress.

Rett patients' fibroblasts reflect the mitochondrial dysfunction as a pathophysiological aspect of the disease. Besides the discussed characterization, these results confirm fibroblasts as a valid and understudied model for the research on mitochondrial alterations in this disease, enabling the study of patient-specific differences, that shall be further explored.

Despite the usefulness of fibroblasts to study mitochondrial alterations, they do not fully capture the complexity of the disease at the brain level. To understand the implications of mitochondrial dysfunction in the most affected organ in Rett syndrome, and more importantly, to study the differences in mitochondrial alterations both between brain areas and through development, we used a mouse model of the disease. Rett "Bird's model" (B6.129P2(C)-*Mecp2*$^{tm1.1Bird}$/J strain) was selected since they recapitulate many elements of the disorder. As in humans, female mice first show an apparent normal early development and later develop the symptomatology, being considered fully symptomatic around 6-7 months old. Opposite to humans, male Rett mice do survive pregnancy phase and are born normally compared to their littermates, but life-threatening symptoms already appear around 3 weeks of age, and life expectancy rarely surpasses 8 weeks. Given this fast progression, it is not uncommon to find research done on male mice. However, female mice, despite the difficulties they present, such as later development of symptoms and phenotype heterogeneity, recapitulate better the disease than males and have a higher translational value as a pre-clinical model (Ribeiro and MacDonald, 2020). For this, in this work we have focused on the study of mitochondrial dysfunction in female Rett mice exclusively.

To deepen our understanding on mitochondrial performance in this model, we have studied two stages of the disease – pre-symptomatic (established at 3 months old) and symptomatic (at 7 months old) – to elucidate if alterations are already present in prodromic stages of the disease and if are maintained through development. Also, we differentiated between three brain regions (cortex, hippocampus and cerebellum) to evaluate if the dysfunction could be area dependent. We limited the description to the study of bioenergetic function, through ATP detection and lipid peroxidation as a marker for oxidative stress, and neuroinflammation regarding cytokine production and inflammatory markers, of especial interest given the interplay between mitochondria and inflammation (Riley et al., 2020).

As in fibroblasts, **brain ATP concentration** was altered in symptomatic mice. Previous studies reported a decrease in brain ATP synthesis in "Bird" mice (Saywell et al., 2006; Valenti et al., 2017; Zuliani et al., 2020); however, knowledge was mostly limited to whole brain analysis and specific-area differences could be masked. We detected reduced ATP concentrations in hippocampus and cerebellum, whereas surprisingly cortex showed an increase in ATP synthesis. This could be explained as a compensatory mechanism for local energetic demand, in which cortex would be more robust against mitochondrial dysfunction, whereas hippocampus and cerebellum would be more vulnerable to mitochondrial alterations (Cabré et al., 2016; Lax et al., 2012). Toloe et al. reported increased resting ATP levels in hippocampal neurons from *Mecp2*$^{-/y}$ mice, which were reduced during epileptiform-like activity, suggesting higher susceptibility of hippocampal neurons to seizures (Toloe et al., 2014). Interestingly, while acute epilepsy is associated with increased ATP demand due to hypersynchronous neuronal discharges, chronic epilepsy often results in reduced ATP production capacity (Liotta et al., 2024). Therefore, these differences found in hippocampal ATP concentration could be attributed to a later disease stage in our symptomatic mice, whereas in the study by Toloe et al. they used hippocampal cells from postnatal day P3 mice that would not have developed chronic epileptic activity yet.

While descriptions on hippocampal alterations are more extensive, cerebellum implication in Rett syndrome remains understudied. Interestingly, we have not only described cerebellar bioenergetic alterations but found that they are already detectable in prodromic phases (3 m.o. mice), underlining its importance in disease progression. In *Mecp2* null mice models, cerebellum shows a downregulation of the majority of genes (Ben-Shachar et al., 2009) and is consistently impaired showing a noticeable reduced volume as soon as 3 weeks of age (Belichenko et al., 2009; Ward et al., 2008), although it was not detected in heterozygous females. Recent experiments show that deleting *Mecp2* from the cerebellum is responsible for the delay in motor learning in mice (Achilly et al., 2021). In Rett patients, alterations in cerebellum function have lately been suggested through MRI (Takeguchi et al., 2022). In fact, a parallelism could be established between cerebellar dysfunctions and early presenting features of the disease such as the movement disorders (Singh et al., 2021) or stereotypes (Dean et al., 2022).

The gap in the knowledge between cerebellum and other brain areas as cortex or hippocampus (Achilly et al., 2021) is bigger if we focus in cerebellar bioenergetic performance. Cerebellum contains approximately 75% of

all neurons in the brain while accounting for only 10% of total brain volume (Herculano-Houzel, 2009). Purkinje cells consume a large amount of ATP to maintain their spontaneous firing activity and strategically distribute mitochondria throughout their highly arborized dendrites (Chen et al., 2020; Fukumitsu et al., 2016). Therefore, bioenergetic alterations can be playing an even more important role in cerebellum than in other brain areas. Cerebellar dysfunction has been described in neurodevelopmental disorders, including autism spectrum disorders, as one of the earliest and most consistent reported alterations (Stoodley, 2015) with not only motor but cognitive consequences in the patients.

As done in fibroblasts, we have aimed to relate bioenergetic alterations with **oxidative damage**. Rather than focusing on the measurement of superoxide anion or other ROS, which characterize oxidative stress, we moved towards the quantification of lipid peroxidation, as an endpoint of the resulting oxidative damage. Previous results in brain context reported an increase in the rate of H_2O_2 generation due to dysfunctional complex II in Rett whole brain (De Filippis et al., 2015b), which would be expected to result in an increased brain damage (De Felice et al., 2014). Opposite to that, in symptomatic Rett mice, we have observed an increase in lipid peroxidation in cortex but a decrease in both hippocampus and cerebellum. While the results for the latests were apparently opposite to the initially expected, it is important to bear in mind that our analysis differs from previous reports as we have differentiated three brain regions, while the others analyzed whole brain homogenates. Cortex is the most voluminous area in the brain, and therefore the results in that area might overshadow the differences in other brain areas. On top of that, previous reports suggest an alteration in lipid metabolism, profiled both in Rett mice (Kyle et al., 2018; Lopez et al., 2017) and patient's plasma (Segatto et al., 2014) and cerebrospinal fluid (Zandl-Lang et al., 2022), probably affecting the overall lipid peroxidation detection. In an attempt to limit this potential bias in the results interpretation, we measured oxidative damage in hippocampus and cerebellum with the DNA-oxidative marker 8-OHdG. The detected increase in 8-OHdG fluorescence in cerebellum supported that oxidative damage is also involved in brain mitochondrial dysfunction, in agreement with previous reports.

Besides oxidative stress, another recently described element of Rett's pathophysiology is the **inflammatory component** (Pecorelli et al., 2020). Inflammation is closely related to mitochondrial homeostasis; other than ROS, dysfunctional mitochondria can release "damage-associated molecular patterns" (DAMPs), such as mitochondrial DNA, which activate molecular driving inflammatory signaling (Marchi et al., 2023). Alterations in inflammatory profiles have been described in patients' peripheral tissues, such as plasma (Leoncini et al., 2015), serum (Pecorelli et al., 2019), peripheral blood mononuclear cells (O'Driscoll et al., 2015), and saliva (Byiers et al., 2020), together with plasma of female Rett mice (Cortelazzo et al., 2017). As Zalosnik and collaborators show (Zalosnik et al., 2021), MeCP2 deficiency results in defective induction of anti-inflammatory responses in experimental setups. In fact, cultured and isolated glial cells of both female and male mouse models of the disease have shown alterations in immune markers (Nance 2017; Zhao 2017), some of them already present in prodromal stages of the disease (Cronk et al., 2015). While our studies did not show alterations for cortex or hippocampus at pre-symptomatic stages of the disease, interestingly, and similar to the bioenergetic alterations, cerebellum did show a pro-inflammatory profile in the prodromal stage. When we moved towards symptomatic mice, however, we detected a pro-inflammatory profile in cortex, whereas hippocampus and cerebellum were characterized by decreased expression of pro-inflammatory cytokine IL-1α (and TNF-α in hippocampus), suggesting a dynamic behavior of the cytokine profile through neurodevelopment. It is important to take into account that, besides inflammation, IL-1α and TNF-α can modulate synaptic function and plasticity as well (Khairova et al., 2009; Ross et al., 2003), potentially contributing to cognitive impairments when dysregulated.

In conclusion, our results on the bioenergetic and neuroinflammatory characterization of Rett female mice highlight the brain-area specific differences and the changes that occur in the pre-symptomatic stages of the disease. The studies on symptomatic 7 m.o. Rett mice evidence the diversity on mitochondrial performance through the brain, in which cortex may contribute with a metabolic hyperactivity profile characterized by increases in both energy synthesis and oxidative stress, together with neuroinflammation. Ultimately, our results point to the cerebellum as a major and early player in the pathophysiology of Rett syndrome regarding bioenergetic dysfunction. Taking cerebellum into consideration, together with its involvement in other neurodevelopmental disorders, is especially relevant on the design of new therapies and complete understanding of its pathophysiology. The systematic description and delineation of the involvement of mitochondria in Rett syndrome's pathophysiology sets the base for its study as a potential therapeutic target for the treatment of the disease.

Mitochondrial modulation through leriglitazone is a potential treatment for Rett syndrome

Despite the ongoing research on potential treatments for Rett syndrome, there is still no effective therapy for the disease, with the exception of the drug trofinetide (Neul et al., 2023). Trofinetide is an IGF-1 (Insulin Growth Factor 1) synthetic analog that has been very recently approved by the Food and Drug Administration (FDA) for

the treatment of Rett syndrome in the United States (U.S. Food and Drug Administration 2023). While it is the first treatment approved, clinical trials have shown many severe secondary effects and an over 50% abandonment rate, along with very limited amelioration in symptomatology (Camillo et al., 2024). Therefore, effective treatments for Rett syndrome are a clinical and social urgent need. In this context, several alternatives are currently being explored, ranging from pharmacological interventions and dietary supplements to genetic therapy, with two ongoing clinical trials (Percy et al., 2024).

Based on the aforementioned mitochondrial alterations, we explored whether mitochondria could be targeted with a therapeutic purpose in Rett syndrome. While this had already been attempted with other drugs, the effects observed were mild and have not been clinically translatable, leaving high room for improvement. Some examples of these approaches include the metabolic modulator metformin, which normalized electron transport chain (ETC) (Zuliani et al., 2020); pharmacological stimulation of serotonin receptor 7 (5-HT7R), which rescued mitochondrial ETC impairments and translated into phenotype recovery in Rett mice (De Filippis et al., 2015a; Valenti 2017); CNF1-toxin activation of Rho GTPases, which operated through remodeling of mitochondrial shape (Cittadini et al., 2023; De Filippis et al., 2012; De Filippis et al., 2015b; Urbinati et al., 2021); pharmacological inhibition of the CB1 cannabinoid receptor, which rescued bioenergetic and behavioral phenotypes (Cosentino et al., 2024); and several antioxidant therapies with the vitamin E analogue Trolox (Baroncelli et al., 2022; Bebensee et al., 2017; Janc et al., 2016) and flavonoids (Dave et al., 2019). In addition, there have been metabolic approaches with polyunsaturated fatty acids (Dave and Pillai, 2022; Marballi and MacDonald, 2021) and triglycerides such as triheptanoin (Park et al., 2014). Nevertheless, antioxidant therapies are considered controversial, and some of these approaches have failed in exerting a phenotypical amelioration on mice (Zuliani et al., 2020) or have failed in clinical trials (Percy et al., 2024), without achieving a clinical translation.

We have assayed the **metabolic modulator leriglitazone** for the correction of Rett syndrome dysfunctions. Leriglitazone (LGZ) is an oral bioavailable and a selective PPAR-ɣ agonist (Peroxisome Proliferator-Activated Receptor-gamma agonist) with an improved profile over other glitazones for treating neurodegenerative diseases. LGZ shows superior brain penetration and a favorable safety profile, allowing interaction with PPAR-ɣ in the central nervous system (CNS) above the level that can be safely achieved with pioglitazone and other glitazones (Pizcueta et al., 2023), and thereby, offering potential benefit to treat CNS diseases. PPAR-ɣ agonists have demonstrated the ability to induce a neuroprotective and restorative effect in various preclinical models of neurodegenerative diseases, such as amyotrophic lateral sclerosis (ALS) (Kiaei et al., 2005), Parkinson's disease (Dehmer et al., 2004; Swanson et al.,2011), Friedreich' ataxia (FA) (Coppola et al., 2009) and Alzheimer's disease (Chen et al., 2012). PPAR-ɣ agonists act through nuclear receptors that bind to DNA sequences in the promoter sites of key genes that counteract oxidative stress, stimulate mitochondrial biogenesis, and decrease inflammation through NF-κB activation (Rodríguez-Pascau et al., 2021a), thus preventing axonal degeneration and neuroinflammation. LGZ has been validated in preclinical models of various neurodegenerative diseases, showing clinical benefits for X-ALD (X-linked adrenoleukodystrophy) patients and clinical proof of concept in FA patients (Golse et al., 2024; Köhler et al., 2023; Pandolfo et al., 2022; Rodríguez-Pascau et al., 2021a; Rodríguez-Pascau et al., 2021b).

To unveil the potential of LGZ in mitochondrial modulation in Rett syndrome we have used both aforementioned pre-clinical models: patients' fibroblasts and female mice. In fibroblasts we studied the effect of a short 48-hour *in vitro* treatment on mitochondrial dynamics and bioenergetics, whereas the Rett mice were treated orally with LGZ from weaning until sacrifice at a dose of 75 mg/kg/day. In Rett mice we evaluated the drug effect on the bioenergetic performance and the neuroinflammatory component, together with the phenotype outcome and behavioral assessment.

As previously mentioned, LGZ is a selective PPAR-ɣ agonist that activates the PPARɣ-signaling pathway. PPAR-ɣ is a nuclear transcription factor that, upon activation, binds to PPAR response elements (PPREs) in target genes. Through transcription regulation, it modulates key pathways in lipid metabolism, glucose homeostasis, and inflammation, promoting adipogenesis, fatty acid storage, and insulin sensitivity, as well as anti-inflammatory pathways by inhibiting NF-κB and AP-1 signaling (Lehrke and Lazar, 2005; Savage, 2005). Additionally, PPAR-ɣ modulates mitochondrial biogenesis and oxidative stress responses (Corona and Duchen, 2016).

We first proved that in patients' fibroblasts, LGZ can effectively activate PPAR-ɣ, through assessment of a selection of its key targets. According to the transcription activation, LGZ exerts an effect in Rett fibroblasts in terms of mitochondrial biogenesis and antioxidant metabolism, but not regarding lipid metabolism, as increases in *PGC-1α* and *MnSOD* expression were detected, but not in *SREBP2*, the master regulator responsible for activation of genes involved in cholesterol synthesis.

For the study of LGZ effect we followed the same scheme as in the description of basal alterations, studying fibroblasts' response in first instance. LGZ recovered the alterations in **mitochondrial bioenergetics** in Rett primary fibroblasts. Both the decrease in mitochondrial ATP synthesis and the increase in $O_2^{\cdot-}$ generation in the assayed patients' fibroblasts were corrected by 48-hour incubation with LGZ, accompanied by an amelioration in

oxidative damage in the cells. This dual action highlights LGZ's potential to improve mitochondrial efficiency and reduce oxidative stress, both critical hallmarks in Rett syndrome pathophysiology.

On the contrary, the assayed *in vitro* conditions were insufficient to exert an effect on **mitochondrial network structure and dynamics** in the patients' fibroblasts. Given the promising effects on mitochondrial biogenesis and bioenergetics, the lack of impact on the general picture of Rett fibroblasts network morphology and dynamics could suggest that the bioenergetic enhancement is occurring in a shape-independent manner, while does not discard the possibility that these pathways may require longer treatment durations to observe significant changes. Importantly, as already mentioned, the studied patients' fibroblasts showed some differences and grouped in two network phenotypes, a more severe profile in patients' cells with mutations in c.916C>T (p.Arg306Cys) and c.808C>T (p.Arg270*) – patients RTT_P2 and P4 respectively – and a milder pheotype in patients RTT_P1 and P3 with the mutation c.502C>T (p.Arg168*). LGZ furtherly increased the alterations found in the milder phenotype and exerted a slight correction in one of the patient's cells with severe network phenotype. These results evidence the heterogeneous genetic background and point towards the relationship between mitochondrial phenotype, patient genotype and treatment response that should be considered for future studies.

While we expected an amelioration in the mitochondrial network morphology through LGZ treatment, unmatching changes between dynamics and bioenergetic profile have been previously described. Mitochondrial dynamics are complex and tighly regulated processes that determine the morphology and distribution of mitochondria in the cell, closely related to mitochondrial bioenergetics (Chen et al., 2023; Mishra et al., 2016). Dynamics alterations, including a disrupted fission-to-fusion ratio, are commonly associated with mitochondrial structural abnormalities and impaired functionality. Treatments targeting dynamics key players have shown a benefitial effect in different pathologies (as reviewed in Chen et al., 2023), whereas interventions not targeting directly dynamics could take longer to exert an effect on the morphology. Moreover, some strategies as mitochondrial transplantations have reported increased bioenergetic function without altering mitochondrial dynamics (Pour et al., 2020). In conclusion, besides the close relationship between dynamics and bioenergetics, therapeutic improvements might not necessarily have an effect on both parameters.

Building on the positive results registered in Rett fibroblasts, we moved on to the evaluation of the effect of LGZ in Rett mice. For that, we treated the mice with an oral dose of 75 mg/kg/day from weaning to sacrifice at 7 months old. LGZ had been previously used on mice models for other diseases as FA (Rodríguez-Pascau, 2021a) or X-ALD (Rodríguez-Pascau et al., 2021b) at doses of 50 mg/kg/day and 75 mg/kg/day respectively, situating us within the safety dose range, and as expected, no toxic effects were observed.

As occurred in fibroblasts, LGZ corrected the **bioenergetic function in the mouse model** of the disease. In Rett mice brains, LGZ prevented the decrease in ATP concentration and normalized lipid peroxidation profiles and oxidative damage markers both in hippocampus and cerebellum, without significative differences in any of both parameters in cortex. In general terms, our results are in concordance with the observations made in X-ALD (Rodríguez-Pascau et al., 2021b). Importantly, the recovery observed in Rett syndrome was higher compared to the basal situation. As mentioned, previous studies were performed in whole-brain homogenates. While we have taken a step forward, differentiating in three brain areas, it is important to bear in mind that cortex is the largest brain region and most heterogeneous between the studied areas (Herculano-Houzel, 2009). Studying cortex as a unity rather than focusing on different areas or cell types has been a limitation of the study, as neuronal-type specific responses to LGZ are potentially being masked. Consequently, further studies should evaluate LGZ treatment on neuronal and areas sub-populations. Future work should also explore to which extent the correction in lipid peroxidation is affected by the amelioration of oxidative stress and a potential alteration in lipid metabolism due to LGZ treatment.

On top of mitochondrial homeostasis correction, LGZ also reduced **neuroinflammation** in Rett mice. PPAR-ɣ activation has anti-inflammatory effects by downregulating pro-inflammatory cytokines, inhibiting NF-κB and Egr-1 pathways, and modulating immune cell functions in different tissues (Straus and Glass, 2007). Bioenergetic alterations were more prominent in cerebellum and already detectable at pre-symptomatic stages together with a pro-inflammatory profile. However, in the symptomatic phase, the neuroinflammatory component was only noticeable in cortex, which was corrected with LGZ. In hippocampus, LGZ treatment upregulated the expression of cytokines IL-17A and IL-1β . As previously mentioned, cytokines expression in hippocampus are not only related with inflammation but also with other features such as cognitive performance or long-term potentiation (Ross et al., 2003), so the interpretation of this rise in their expression might not be as straightforward as in cortex. Although mitochondrial dysfunction has recently been proposed as an inflammatory trigger in several scenarios (Casaril et al., 2021; Vringer and Tait, 2023), these results suggest that mitochondrial dysfunction and neuroinflammation are not necessarily interrelated in Rett syndrome or at least their correction with LGZ. The neuroinflammatory component of the disease sets a new therapeutic target for Rett syndrome. Further studies shall investigate its contribution to the disease progression.

Importantly, as happened in the other diseases as X-ALD, sustained treatment with leriglitazone results in an amelioration of the **phenotype** of female Rett mice, both in the general observed health and in the exploratory activity. Interestingly, an affectation regarding the general health index of Rett mice was detectable already at 3 months of age, a period that was generally considered as pre-symptomatic, and was improved in the LGZ-treated group. As a matter of fact, the paradigm of regular early development is also being challenged by recent evidence focusing on subtle cognitive and motor deficits in the patients before symptoms onset (Cosentino et al., 2019). Considering all the above, we highlight the importance of early diagnosis and treatment in Rett syndrome, which can also be applied to other neurodevelopmental disorders (Meredith et al., 2012).

Similar phenotypic modulation through mitochondrial targeting had been previously achieved through serotonin receptor stimulation (De Filippis et al., 2015a; Valenti et al., 2017) and Rho GTPases modulation (De Filippis 2015b; Urbinati et al., 2021) but not accomplished through other approaches as metformin (Zuliani et al., 2020). Recent studies have shown cognitive improvements in female mice treated with an inhibitor of an endocannabinoid receptor located on brain mitochondrial membranes (Cosentino et al., 2024), validating mitochondria as a remarkable therapeutic target for the treatment of neurological disorders with metabolic components. We believe the success of LGZ effect in Rett syndrome relies on both the treatment time (from weaning until sacrifice) and on its mechanism of action, increasing mitochondrial performance and biogenesis, exerting an anti-inflammatory effect and promoting neuronal growth and myelination (Rodríguez-Pascau et al., 2021b). In the counter side, this treatment scheme might be leading to an overestimation of the impact of LGZ; while we have proven its ability to modulate the natural history of Rett syndrome, future studies should focus on assessing its efficacy when administered after the onset of symptoms.

In conclusion, the results obtained in this work on the study of the mitochondrial dysfunction confirm that Rett syndrome is indeed a neurodevelopmental disorder with a key metabolic component, which can be purposed as a therapeutic target. The cerebellar bioenergetic dysfunction is already evident at the pre-symptomatic stage, together with an inflammatory profile that is present in other regions in later stages of the disease (Fig. 67). This underlines the importance of timing in the study and treatment of Rett syndrome, urging for a prompt mitochondria-targeted intervention upon disease diagnosis. Beyond highlighting cerebellum as one of the most afected areas -and however, still understudied-, we have demonstrated that the bioenergetic status and inflammatory alterations can be corrected in the studied models through treatment with the PPAR-γ agonist LGZ**.** These biochemical recoveries result in a phenotypic improvement of Rett female mice.

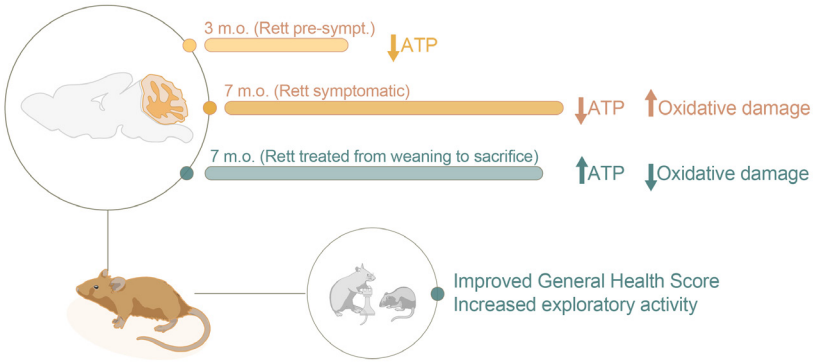

Figure 67. Schematic representation of the alterations in Rett mice brain cerebellum. Summary of the bioenergetic alterations affecting cerebellum and their correction with leriglitazone treatment.

Given these results and the knowledge on LGZ safety on both healthy subjects and pediatric patients (Pandolfo et al., 2022; Traver et al., 2024), this work constitutes the preclinical evidence for a clinical trial with LGZ in Rett syndrome and other diseases with mitochondrial involvement. In October 2024, it has been approved the TREE clinical trial, a phase 2a, double-blind, placebo-controlled clinical study designed to assess the safety and tolerability of LGZ in pediatric patients with Rett Syndrome (EU Clinical Trials Register 2025; Minoryx Therapeutics 2025).

2 Personalized treatment approach for mitochondrial disorders

Besides their involvement in the pathophysiology of neurodevelopmental and neurodegenerative diseases, as we reviewed in 2021 (Oyarzabal et al., 2021), mitochondrial alterations are also the direct cause of a group of diseases referred to as "primary mitochondrial disorders" or "mitochondriopathies". They are due to either *de novo* or inherited mutations in both nuclear and mitochondrial DNA (mtDNA) genes affecting any of the mitochondrial functions. Clinically, they represent a heterogeneous group of diseases, but usually show a chronic, slowly progressive course varying onset between birth and late adulthood. While these conditions are typically **multisystemic**, one of the most affected organs is usually the brain, given its high energy demand. The severity and pattern of involvement vary depending on the specific mutation and its distribution, but in many mitochondrial disorders, neurological symptoms are prominent due to the CNS's sensitivity to energy stress. Other frequently affected tissues are those highly dependent on mitochondrial function, such as skeletal muscle, heart, liver, and kidneys (Gorman et al., 2016).

Overall, mitochondrial disorders have an incidence in the general population of 11.5 per 100,000 (Chinnery, 2000), half of which develop a neurological syndrome (van der Ven et al., 2021), constituting the largest class of inborn errors of metabolism. Treatments of mitochondrial diseases currently focus on symptomatic management rather than ameliorating the biochemical defect caused by a particular mutation (Russell et al., 2020), so there is an urgent need to define therapeutic agents (drugs or other compounds, such as nutraceuticals), which correct aspects of mitochondrial dysfunction. Due to the high functional heterogeneity of mitochondrial alterations, personalized therapies are one promising avenue to solve this gap in their treatment.

In this context, to advance in the establishment of precision therapies for mitochondrial diseases we have studied a selection of 20 pediatric patients with neurological symptoms and due to different defects affecting mitochondrial homeostasis. Strategically, we excluded from this selection the most frequent and well-documented mitochondrial diseases such as mutations affecting *POLG* (OMIM *174763) – encoding DNA polymerase subunit ɣ1, which is the catalytic subunit of mtDNA polymerase, or the m.3243A>G mutation in *MT-TL1* (OMIM *590050), associated with mitochondrial encephalomyopathy with lactic acidosis and stroke-like episodes (MELAS) syndrome. Conversely, we focused on some underexplored mutations on a variety of nuclear genes encoding proteins essential for mitochondrial homeostasis to have a broader view of energy metabolism disturbances and how they affect brain development. The selected patients were grouped in five functional categories affecting different aspects of mitochondrial homeostasis: (1) mitochondrial dynamics, (2) mitochondrial cristae structure, (3) mitochondrial gene translation, (4) electron transport chain complexes subunits and assembly, and (5) intermediate metabolism related to mitochondria.

One of the objectives of this part of the study was to develop an algorithm for the design of personalized therapies in mitochondrial diseases. Setting the focus on placing the patient at the center of the research, the ultimate goal was that this algorithm could be implemented in the clinical practice, making it truly beneficial for patients. Therefore, all decisions were guided by this principle, ensuring that the approach was time-sensitive, cost-effective, and feasible without requiring highly specialized equipment beyond what is typically available in a molecular biology laboratory.

As previously proven, fibroblast are a bona-fide and cost-effective material for the study of some mitochondrial alterations. Although partialized, they are an accessible and relatively rapid window into the patient's precise pathophysiology. More importantly, they can be cultured in most reference centers. Therefore, we used primary fibroblasts derived from the patients in which we predicted *in silico* molecular mechanisms of disease and validated the mutation effect on the protein expression. To study the consequence of the mutation on mitochondrial homeostasis, we focused on two main aspects: network morphology and bioenergetics. We selected these parameters for their informative capacity, the accessibility to standardized methodology, their sensitivity to treatments, their impact in the pathophysiology of most mitochondrial diseases and their potential to be part of a medium-throughput analysis for drugs development. Ultimately, we proposed a series of personalized therapies based on pharmacological, nutraceutical and metabolic approaches, and when possible, we translated them into a clinical study.

Characterization of mitochondrial homeostasis in selected disorders

From the 20 studied patients, the information for the confirmed or suspected mutation was available for 15 of them. 53% (8 patients) carried mutations that either had not been previously associated with any known disease or the presenting variants are linked to emerging and novel phenotypes. The other 47% (7 patients) were due to known mutations or previously described genes. In this section we have focused in the discussion of the former,

as these findings expand our understanding of mitochondrial pathology and on the potential roles that new pathogenic variants can have in these rare conditions.

To deepen our understating of the pathophysiology of diseases due to alterations in **mitochondrial dynamics**, we have studied two sets of patients: samples from five patients harboring different mutations in *DNM1L*, which encodes for the key player in mitochondrial fission, the dynamin related protein 1 (Drp1, or Dnm1l), and samples from three patients with mutations in *AFG2A*, which encodes a protein equally named (previously referred to as SPATA5), which specific functions remain unclear but is suspected to be involved in mitochondrial transformations during spermatogenesis.

Mutations in ***DNM1L*** have been previously associated with lethal encephalopathy due to defective mitochondrial and peroxisomal fission-1 (EMPF1) (Waterham et al., 2007), refractory epilepsy (Vanstone et al., 2016) and optic atrophy 5 (Gerber et al., 2017), and ablations of Drp1 in neurons cause synaptic dysfunction, memory deficits and hippocampal atrophy (Oettinghaus et al., 2016). Within our analyzed patients, we present a novel phenotype in two of them, characterized by pediatric parkinsonism in a patient bearing a novel mutation in c.2167A>G (p.Arg723Gly), affecting the GED domain, and a patient with the mutation c.1084G>A (p.Gly362Ser), affecting the middle domain. We also characterized the mitochondrial dysfunction with other three DNM1L patients for whom the mutation has not been available.

In brief, Drp1 assembles at mitochondria-ER contact sites and forms homo-oligomeric complexes that subsequently hydrolyze GTP to drive conformational changes, resulting in scission of the mitochondrial inner and outer membrane (Friedman and Nunnari, 2014). Each monomer has an N-terminal GTPase domain, a middle domain (MD), a variable domain (VD, inset B), and a GTPase effector domain (GED). Attending the tertiary structure, the middle and GED domains form a “stalk”, bridging between the GTPase and Variable domains. Drp1 self-assembly is primarily driven via intramolecular stalk interactions (Francy et al., 2017; Kalia et al., 2018); several mutations in these regions have been shown to disrupt Drp1 oligomerization and are associated with developmental defects in humans.

To assess the functional impact of the mutations, we analyzed the expression of Drp1 in the five patients. We found that patients DNM1L_P1, P2 and P3 had decreased Drp1 monomeric expression; while the mutation for these patients was not available, the protein expression suggested a defective function. Interestingly, the mutations of both P4 and P5 were located in the stalk region of the protein, crucial for dimerization and the stability of Drp1 polymers, as mentioned in (Ramachandran, 2017). None of them had a decrease in the expression of the monomeric form, and we therefore analyzed the oligomeric form of Drp1 in these patients. We found that both showed an increase in the oligomeric-to-monomeric forms ratio compared to controls, pointing towards an alteration in the oligomerization (and de-oligomerization) process supporting the pathogenicity of the mutation. Other aspects related to Drp1 function such as GTPase activity, post-translational mechanisms as phosphorylation or interaction with lipids as cardiolipin have not been explored.

Despite the importance of mitochondrial fusion and fission cycles for the maintenance of the bioenergetic function, us and others report a normal ATP production in Dnm1L-patients (Gerber et al., 2017; Nolden et al., 2022; Robertson et al., 2023; Vanstone et al., 2016). Although these structural alterations affect processes such as mitophagy, mitochondrial distribution and cellular stress response, in some patients, mitochondria can maintain relatively normal bioenergetic activity in certain contexts. Further systematic studies shall explore to which extent bioenergetic alterations are contributing to Dnm1L deficiency, as this may shape future therapeutic strategies.

Given the clinical heterogeneity and the diversity of mutational spectrum, interpreting variants of unknown significance (VUS) for *DNM1L* can be challenging. This is aggravated by the often lack of correlation between the mutations and decreased protein expression or altered oligomerization, as reported by us and others (Gerber et al., 2017; Longo et al., 2020; Nolden et al., 2022). Therefore, there is a need to identify a molecular signature that supports pathogenicity evaluation. Mitochondrial network shape could be a specific biomarker in such regard. The hyperfused profile described in the five DNM1L patients is consistent with previously reported variants (Gerber et al., 2017; Hogarth et al., 2018; Longo et al., 2020; Nolden et al., 2022; Robertson et al., 2023; Scheffer et al., 2016; Vanstone et al., 2016; Waterham et al., 2007; Whitley et al., 2018). To explore its potential to discern between DNM1L patients and other mitochondrial diseases, we compared the characteristic polygonal-shaped network in DNM1L patients’ fibroblasts to a group of various mitochondrial disorders, revealing that this conformation is unique along the studied patients. Based on these findings, we propose mitochondrial network morphology parametrization as a marker to guide the diagnosis of patients with potential *DNM1L* mutations.

While *DNM1L* function and mechanisms of action are well documented, such is not the case of *AFG2A.* Mutations in ***AFG2A*** (*SPATA5*) are associated with an encephalopathy phenotype (AFG2A-RE), first described in 2015 (Tanaka et al., 2015). The major hallmark present in the disease is refractory epilepsy, present in up to 75% of the described patients and usually associated with intellectual disability and spasticity (Braun et al., 2021; Puusepp et al., 2018;

Tanaka et al., 2015; Zanus et al., 2020). The cardinal clinical features of AFG2A-RE mimic a mitochondrial disease, and as a matter of fact, in terms of pathophysiology, deficiency of AFG2A includes a mitochondrial dysfunction. As us and others have recently described (Puusepp et al., 2018), AFG2A deficiency is characterized by altered mitochondrial dynamics, in terms of decrease in the fusion-to-fission ratio along with mitochondrial movement speed and lowered mitochondrial mass. Although our results regarding the bioenergetic function are aligned with the defect described in the work of Raggio and collaborators (Raggio et al., 2023), some differences were shown between our studied patients' cells: all three patients had altered ROS production and metabolism, whereas respiratory activity, with a subsequently decreased cellular level of ATP, was only present in patients AFG2A_P1 and P2. In conclusion, mutations in *AFG2A* cause mitochondrial homeostasis disturbances, resulting in encephalopathy.

Shifting the focus from dynamics to **mitochondrial ultrastructure**, we have described the first patient ever with a neurological phenotype due to mutations in the gene ***CHCHD6***. The patient showcased a phenotype of pediatric parkinsonism with decreased concentration of homovanillic acid (HVA) in CSF. *CHDH6* encodes for the protein Mic25, part of the MICOS complex (Mitochondrial Contact site and Cristae Organizing System). It had not previously been causative of disease, particularly, of neuropediatric disease, although genome association studies had linked variants in *CHCHD6* to non-alcoholic fatty liver disease (NAFLD) (Krishnan et al., 2018), and to the progression of Alzheimer's disease (Shang et al., 2022).

The MICOS complex subunits are key players in the mitochondrial inner membrane structure and cristae formation. Mitochondria are two-membrane organelles in which the inner membrane invaginates, creating the mitochondria cristae. Cristae allocate the ETC supercomplexes, coupling TCA cycle with oxidative phosphorylation (OXPHOS) and energy production (Cogliati et al., 2016). While cristae formation and maintenance are intricate processes in which new components are still being described, MICOS proteins are the main participants. This complex is formed by at least seven subunits (Pfanner et al., 2014) and multiple interactors. However, there is no clear consensus on the complex core elements. While some report Mic19 (*CHCHD3*), Mic60/Mitofilin (*IMMT*) and Mic25 (*CHCHD6*) (Ding et al. 2015; Huynen et al., 2016) as the key components, others set the core in Mic19-Mic60 and Sam50 (Ott et al., 2015; Tang et al. 2020), that will interact with Mitofilin and Mic25 to sustain cristae morphology.

The results obtained for the fibroblasts of the CHCHD6 patient are consistent with an affectation of mitochondrial ultrastructure and are in agreement with previous descriptions in different models, such as decrease in cristae number (Ding et al., 2015), decrease in ATP production (An et al., 2012), and increase in ROS (Vue et al., 2024). Our results highlight the effect of *CHCHD6* mutations on the mitochondrial morphology and bioenergetic function, which despite the decrease in functional cristae number in this patient, their ATP synthesis capacity is "only" reduced in half compared to controls.

Aligned with the bioenergetic function of mitochondria, the last group of patients to be discussed are those related to **Electron Transport Chain (ETC) complexes subunits and assembly.** The ETC is a series of protein complexes (I-IV) located in the inner mitochondrial membrane that facilitates the transfer of electrons derived from metabolic substrates. This electron flow drives the pumping of protons across the membrane, creating an electrochemical gradient. Oxidative phosphorylation (OXPHOS) harnesses this gradient, as protons flow back through ATP synthase (complex V), generating ATP from ADP and inorganic phosphate. The ETC and OXPHOS are the basis of mitochondrial energy production, and mutations in the genes coding for these complexes (or assembling factors) cause a plethora of phenotypes, including Leigh syndrome (Distelmaiter et al., 2009; Kim et al., 2022), progressive leukoencephalopathies (Björkman et al., 2015; Ferreira et al., 2011; Zhang et al., 2019), movement disorders (Baide-Mairena et al., 2019), Acadian variant Fanconi syndrome (Hartmannová et al., 2016) or axonal polyneuropathy (Rebelo et al., 2018; Rucheton et al., 2021), and have been linked to neurodegenerative disorders as Parkinson's disease (Fato et al., 2008; González-Rodríguez et al., 2021; Epifane-de-Assunção et al., 2024).

Two main elements are to be considered in the pathophysiology of defects in the ETC: the bioenergetic function (and mitochondrial ATP production) and ROS generation and metabolism. As reviewed by Sharma and colleagues (Sharma et al., 2009), complexes I (NADH-coenzyme Q oxidoreductase) and III (coenzyme Q-cytochrome c oxidoreductase) are the main sites of ROS production in the mitochondria, particularly complex I, where electron leaks react with oxygen producing superoxide anion ($O_2^{\cdot-}$). As discussed, while reactive oxygen species are involved in many signaling pathways, ranging from apoptosis to cell proliferation (Sies and Jones, 2020), their uncontrolled production and/or defective metabolism leads to pathogenic conditions. In fibroblasts of patients with mutations in ***NDUFS1*** and ***NDUFAF6*** we found the expected decrease in mitochondrial ATP (more severe for NDUFAF6 patient with 70% decrease), together with increase in ROS production. Interestingly, analysis of total ATP production revealed an increase in NDUFS1 patient, and control-range concentrations for NDUFAF6 patient cells compared to controls, suggesting some glycolytic compensatory mechanisms for ATP production. These results have been reported in previous studies, in which these mutations caused a metabolic shift towards a glycolytic state (Ni et al., 2019) and the deficient cells maintain ATP production even in stress conditions (Morán et al., 2010).

The ETC ends in complex IV, the final acceptor of the transported electrons, which catalyze the transformation of O_2 into H_2O. In this work we have studied three patients with mutations in two genes affecting complex IV assembly: the patients with mutations in ***SCO2*** and ***SURF1***. Fibroblasts of all three patients showed similar alterations in mitochondrial network structure (together with complex I-related mutations), but different bioenergetic profiles. We found that *SURF1* mutations had a more severe effect on complex IV assembly than *SCO2*; however, others have reported the opposite (Sue et al., 2000), suggesting a potential mutation-specific effect.

In summary, four of the five studied patients with mutations in subunits and assembly factors of OXPHOS system (all except SURF1_P2), present similar bioenergetic alterations, with decreases in mitochondrial ATP paired to increases in ROS production. Interestingly, total cellular ATP production was not altered or even increased in some scenarios, suggesting a compensatory activity of other routs as glycolysis. It has to be taken into account that while these compensatory mechanisms are part of the adaptative changes some cells can undergo, some specific functions or cellular subdomains are highly dependent on mitochondrial bioenergetic function, such as synaptic communication.

In conclusion, mitochondrial homeostasis disturbances can be due to different molecular pathways, resulting in network structure and bioenergetic alterations. Even though only the most significant cases have been discussed (based on their complexity or description of new phenotypes), these alterations have been found in the several neurodevelopmental disorders studied in this Thesis, associating mitochondrial disfunction with a plethora of clinical features, such as movement disorders and neurodevelopmental delay. More importantly, this work has had a clinical impact as it has confirmed the potential genetic diagnosis in all cases in which it was dubious. Any amelioration on the burden (in terms of treatment, diagnosis biomarkers, or mere advance in the knowledge of the disease) supposes a huge leverage for these groups of patients. Diagnosing, characterizing and setting the base for future treatment of this ultra-rare diseases will be life changing for the patients and their families and caregivers, as they are fully dependent persons with a huge disability.

Therapeutic approaches for neurodevelopmental disorders with mitochondrial involvement

Mitochondrial diseases aggregate a wide range of symptoms, usually of great severity, resulting in high degrees of neurodevelopmental, physical and economic consequences for the patients and, consequently, families, social groups and society. The symptoms are life-lasting, so families are hindered (in any life aspect imaginable) for their lives. According to the 2019 report of the American Journal of Managed Care (AJMC 2021), the mean total per member per month (PMPM) costs were significantly higher in the mitochondrial disease group compared with the general population ($3,958 versus $427), and the 3 highest PMPM claims were inpatient hospitalizations ($769), surgery ($746), and prescription drugs ($582). These are comparable to the costs of patients with ALS and MS.

As per the national Rare Diseases Federation (FEDER) statistics, 47% of patients with a rare disease receive a treatment that is inadequate for their disease, so there is a great urge to fill this gap. This is especially significative in mitochondrial diseases, for which there is no specific treatment (Kerr, 2013; Pfeffer et al., 2012). Based on the pathophysiology of mitochondrial defects, the most frequent strategies in their management include the use of antioxidant cocktails such as vitamins and cofactors, as recently reviewed (Tragni et al., 2022). The most used are thiamine, riboflavin, niacin, and coenzyme Q_{10} (CoQ_{10}) either in the reduced form as ubiquinol or oxidized as ubiquinone. However, these therapies are not yet standardized or definitively proven to be effective. Advancing in therapeutic options for these diseases is not only a moral obligation but an urgent need for the National Health System.

As previously discussed, given the genetic and pathophysiological heterogeneity of mitochondrial diseases, one promising avenue for their treatment walks through a **Personalized Therapies** approach. After confirmation of the new diagnosis, we have evaluated the efficiency of three potential therapeutic strategies for the treatment of mitochondrial diseases: a pharmacological approach with leriglitazone, treatment with a nutraceutical (spermidine), and a metabolic approach with ketogenic diet. Rather than comparing the different approaches between them we aimed to evaluate their specific impact on mitochondrial performance and confirm the potential usefulness of this Personalized Treatment in the clinical management of mitochondrial diseases.

Based on the positive results on mitochondrial function enhancement obtained for the pre-clinical models of Rett syndrome, we wondered whether **leriglitazone (LGZ)** could have a beneficial effect on primary mitochondrial disorders. For this end, we assayed the drug in two groups of patients representing two key aspects of mitochondrial homeostasis: (1) one patient with impaired bioenergetic function (*NDUFS1* gene), and (2) the five-patients set with impaired mitochondrial dynamics (*DNM1L* gene).

As previously discussed, the PPAR-γ agonist LGZ counteracts oxidative stress, stimulates mitochondrial biogenesis, and decreases inflammation through NF-κB activation (Rodríguez-Pascau et al., 2021a), preventing axonal degeneration and neuroinflammation. Treatment with LGZ of the NDUFS1-deficient patient fibroblasts resulted in an increase of mitochondrial ATP concentration and decreased oxidative stress production, in a greater extent than those obtained with dibutyryl-cAMP, a synthetic derivative of cyclic adenosine monophosphate (cAMP) that promotes complex I activity through PKA phosphorylations (Iuso et al., 2006). These results, never reported before, highlight LGZ as a potential treatment for mitochondrial diseases, at least in those conditions in which a bioenergetic deficiency outstands in the pathophysiology. Given the two-faced improvement at a molecular level (both in ATP generation and ROS production), future work should explore the reproducibility in other mitochondrial conditions and, in those with positive results, its potential clinical application through a clinical trial.

Encouraged by the positive response in NDUFS1-deficiency, we next explored the effect of LGZ on patients' fibroblasts with mutations in the *DNM1L* gene. Conversely, results in this scenario were either negative or unconclusive. Treatment with LGZ corrected the oxidative stress in two patients, DNM1L_P1 and P2, whereas increased it for patients DNM1L_P3 and P4. In addition, no improvements in mitochondrial ATP nor in the hyperfused network morphology were detected for the five patients. Previously, other PPAR agonists such as bezafibrate, have been used to treat mitochondrial dysfunction due to *DNM1L* mutations, achieving an increase in ATP production, although at the expense of increased ROS (Douiev et al., 2020). It is important to remind that these results are aligned with those observed in Rett syndrome fibroblasts, in which network dynamics were not corrected with the assayed conditions. Further studies should consider more prolonged treatments for the correction of mitochondrial homeostasis in fibroblasts of patients with disturbances in the dynamics function before discarding LGZ as a potential treatment.

Besides pharmacological strategies, we find a growing use of nutraceuticals aimed at increasing mitochondrial performance in different diseases (Tarnopolsky et al., 2008), which can be as varied as macular degeneration (Luján et al., 2022), fetal brain inflammation in animal models (Sun and Zhang, 2022), ischemia (Marshall et al., 2022) or Alzheimer's disease (Jayatunga et al., 2021). Examples of nutraceuticals under investigation in neurodevelopmental pathology include vitamins (Stewart et al., 2015), sulforaphane (Singh et al., 2014) or *N*-acetylcysteine (Hardan et al., 2012). Lately, the **nutraceutical spermidine** has been proposed as a potential regulator of mitochondrial performance (Han et al., 2022). Although its functions as a regulator of autophagy have been better studied (Diaz-Osorio et al., 2025; McCarty et al., 2022), in recent years it has been shown to stimulate mitophagy and mitochondrial biogenesis in the aged mouse heart (Messerer et al., 2021) and improve mitochondrial function and respiration (Han et al., 2022; Wang et al., 2020).

Spermidine (SPM) is a naturally occurring polyamine that can be safely used as a dietary supplement, and indeed SPM-rich diets correlate with cognitive performance in humans (Schroeder et al., 2021). SPM is considered to be inside the group of caloric restriction mimetics (CRMs), that is, compounds that would pharmacologically mimic the beneficial effects of caloric or dietary restriction (Madeo et al., 2018). These CRM can induce autophagy though different molecular mechanisms, among others. The fact that it is a dietary supplement establishes a broad safety frame and facilitates patients access to the treatment. It has low toxicity, yet can exert a strong efficacy (Madeo et al., 2018). Notwithstanding, it has never been used in the treatment of primary mitochondrial disorders.

To unveil the potential role of SPM in the treatment of mitochondrial patients, we selected eight patients representative of the five functional groups studied: (1) mitochondrial cristae structure (CHCHD6), (2) gene translation (WARS2), (3) dynamics (DNM1L_P4), (4) intermediate metabolism (PDHX), and (5) OXPHOS-related functions (NDUFS1, NDUFAF6, SCO2, SURF1_P1).

In general terms, *in vitro* SPM treatment increased mitochondrial ATP synthesis in all the patients' fibroblasts without further increases in ROS production. This is a great feature of this treatment, as us and others have described how increased ROS is part of the pathophysiology of many diseases (Al Shahrani et al., 2017), and increases in ATP production in defective environments can be usually paired with an increase in ROS production, as is the case of ascorbate (vitamin C) (Douiev et al., 2016). Two exceptions were found: on one hand, while CHCHD6-deficient fibroblasts did not increase ATP synthesis after SPM-treatment, ROS production was decreased, therefore considering the treatment as positive overall. On the other hand, NDUFAF6-patient fibroblasts, in which treatment with SPM exerted an increase in [ATP] but it was paired with an increase in ROS. Interestingly, this patient's fibroblasts had the most significant increase (almost 2 folds) in hypusination of eIF5A after treatment, which could mean an exacerbated effect of SPM at the assayed concentration and consequently more oxidative stress compared to the other patients' fibroblasts. Future experiments to either confirm or discard SPM as a potential treatment in this patient should include tests at lower doses, reinforcing the importance of a personalized approach.

The improvement in the bioenergetic performance was not accompanied by increases in OXPHOS complexes expression, suggesting that SPM mechanism of action regarding mitochondrial diseases could include more effective coupling in the respiratory chain complexes, which should be validated. Considering its role as an autophagy modulator (Diaz-Osorio et al., 2025; McCarty et al., 2022), other mechanisms such as better tunning of mitophagy should be considered as well.

Since SPM is *a priori* a safe-to-use nutraceutical, as aforementioned, in those cases where it was possible, we translated this approach to the clinic through a series of n-of-1 trials, providing an important basis for the development of personalized medicine. The patients that participated in the clinical trial were CHCHD6 and the OXPHOS-related patients NDUFAF6, SCO2 and SURF1_P1. After only three months of 6 mg daily oral SPM supplementation, patients experimented a significant improvement in their neurodevelopment, that had been stagnated (or in deterioration) previous to the treatment, as measured by a Vineland test pre- and post-treatment. While advancements in the different evaluated domains were found, they were particularly significant in expressive communication and socialization through games. This improvement was especially significant in the CHCHD6 patient, who surprisingly had the most severe initial punctuation, although it was not detected in patient NDUFAF6. Due to the limited number of patients clinically assayed, it is not safe to establish a correlation between molecular and clinical response to the treatment.

Two other patients were treated with spermidine: DNM1L_P4 and NDUFS1. They were both treated for longer periods, but since their response to the intervention was not systematically evaluated, they have not been considered into our analysis. In summary, after treatment, DNM1L_P4 reported a notable improvement in the respiratory pattern, and the family (and the patient himself) reported a rise on the “global energy” and motor skills improvement, with both more stable walk and ability to walk longer periods of time without stopping; he even manages to run short distances. On the other hand, NDUFS1 patient parents and doctors could notice an improvement after two months treatment. After over 6 months treatment, she was able to support her head and turn it to both sides, had more interest for the environment and better response to extern stimulus. While, as mentioned, these results cannot be included into the complete analysis, they point towards an encouraging view of SPM as a potential treatment for mitochondrial disorders.

Importantly, these positive effects are being reported as the evaluation after a very short treatment, so we expect a continued improvement with longer-term treatments. More powerful upcoming clinical studies will determine the effect of SPM on a wider range of mitochondrial diseases. Results might as well be escalated to adult Parkinson’s disease, in which nutraceuticals are being assayed (Brakedal et al., 2022). Not only SPM itself can be a potential treatment but shall be assayed in combination with antioxidant therapies (such as Trolox, a vitamin E analogue) (Distelmaier et al., 2009).

No unexpected or negative side effects were detected upon treatment with SPM. Nonetheless, despite the used doses being within the approved ranges by the European Union for food supplementation with spermidine, its long-term effect in pediatric population should be carefully explored through standardized observational studies. These should discard metabolic dysregulation or pro-tumor effects, as polyamines may favor cell proliferation and be associated with tumor progression, especially if there is a genetic or environmental predisposition (Sari et al., 2021).

Aligned with the special attention to specific genetic backgrounds, spermidine supplementation should not be considered for patients with alterations in the polyamine pathway. In this work we included a patient with a variant in the *SMS* gene, that despite not confirmed as causative of the symptomatology, has an impairment in the metabolism of spermidine into spermine. As shown by the *in vitro* results, spermidine supplementation would overload the polyamine metabolic route and could have secondary effects, without any amelioration in mitochondrial function. These results ultimately validate the personalized treatment approach for neurodevelopmental disorders, since not all patients will respond similarly or beneficiate from the assayed treatments.

Finally, the third and last assessed approach was a metabolic treatment with **ketogenic diet (KD)**. This high-fat and low-carbohydrate diet has been widely described for its use on mitochondrial disorders as can be reviewed in (Gano et al., 2014; Lee et al., 2021; Qu et al., 2021; Zweers et al., 2021), as well for the management of refractory epilepsies (Meira et al., 2019; Rho, 2017), autism spectrum disorders (Ruskin et al., 2013), and diabetes (Feinman et al., 2015). However, the exact mechanism of action has not been elucidated yet. Previous studies have reported that KD inhibits the fission of mitochondria and enhances mitochondrial activity through the AMPK/mTOR signaling in diabetic mice’s myocardium (Guo et al., 2020), and increases neuronal metabolism through the PGC1α-SIRT3-UCP2 axis (Hasan-Olive et al., 2019). Therefore, we assayed a KD-mimicking *in vitro* treatment on AFG2A-RE patients’ fibroblasts, who present refractory epilepsy, to understand how KD is modulating the mitochondrial dysfunction present in these patients and if it could be considered as a potential therapeutic option.

In vitro analysis showed that, upon a 5-days exposure to the KD-mimicking medium, AFG2A-deficient fibroblasts restored their bioenergetic profile and the mitochondrial dynamics. The dynamics and network morphology parameters were corrected in a similar manner for the studied patients' cells, outstanding the correction in fusion-to-fission ratio and increase in mitochondrial area. The bioenergetic response to the treatment was analogue to the detected defects in basal condition: AFG2_P1 and P2 cells recovered ATP synthesis, which was paired to a significant increase in complex IV expression, whereas AFG2A_P3 did not show changes. ROS generation was corrected for the three patients' cells, particularly for AFG2A_P3 who showed an important correction in superoxide dismutase (MnSOD) expression. Altogether, these results endorsed KD as a potential treatment for AFG2A-RE.

As done in the spermidine evaluation, and based on these positive results, AFG2A_P1 and P3 patients were treated with KD, together with other two AFG2A-RE patients, not presented in this Thesis. All treated patients had observable clinical improvements. The patients treated earlier in development, that is, before 3 years of age, presented a very significant seizure frequency reduction from 95% to 100% (including AFG2A_P1, who was on KD for four years at the moment of the study), whereas in the two older patients seizure reduction was lower, 0% to 30% (AFG2A_P3, who was with KD for 1 year at the moment of the study). Despite not presenting such good results in terms of seizures control, improvements in social interaction, awareness, and motor symptoms were noted. These differences in treatment responsiveness come with no surprise, and reinforce the need of early diagnosis for early treatment implementation in neurodevelopmental diseases, in which timing is crucial. The abnormal connection networks generated by repeated seizures over the years would make it more difficult to achieve seizure control in older patients, while other neurological improvements could still be achievable (Jiruska et al., 2023). Moreover, early initiation of KD grants immediate action in the direction of neuroprotection and modulation of neuroinflammation (Falsaperla et al., 2023), topped by an improvement in neurobehavior (Zhu et al., 2022).

Endorsed by the *in vitro* and *in vivo* observations, we propose KD as a suitable treatment and safe option for patients with AFG2A-RE with refractory epilepsy. Among other mechanisms, KD appears to restore mitochondrial bioenergetic function and dynamics. This suggests that KD could be a plausible treatment option for those diseases or life processes in which such functions are compromised, such as mitochondrial dynamics disorders and, furthermore, cardiovascular disease, cancer or aging (Sharma et al., 2019; Tozzi et al., 2022). It has yet to be taken into account that ketogenic diet has some limitations. Adherence to the KD is one of the main challenges in its use as a therapeutic intervention, as its strict requirements can be socially and emotionally demanding. Additionally, the initial adaptation phase often causes "keto flu," characterized by symptoms such as fatigue, nausea, headaches, and dizziness, which may discourage patients (Batch et al., 2020). The diet's restrictive nature, eliminating foods like fruits, grains, and legumes, can lead to long-term micronutrient deficiencies, such as vitamin C, B vitamins, calcium, or fiber, that require continuous monitoring.

In conclusion, we have assayed three different therapeutic approaches for the amendment of mitochondrial defects: a pharmacological treatment (with leriglitazone), a nutraceutical (spermidine) and a metabolic modulation (ketogenic diet). In the context of a Personalized Therapies program, this has been assayed both in the patients fibroblasts and, when possible, translated into clinical trials. The treatments have achieved to variable degrees both recoveries in the mitochondrial homeostasis and improvements in the patients cognitive and motor function. While we have demonstrated their potential in the management of these pathologies, we are not advocating for their indiscriminate use in mitochondrial diseases but rather to be implemented in each scenario in a personalized fashion, depending on the molecular pathways involved in the pathology. Our results endorse the need for (1) expanding our knowledge on the pathophysiological bases of mitochondrial diseases, and (2) finding new therapeutic options that address these alterations. Since many of these diseases are rare or ultra-rare and the number of patients can be a limitation of study (e.g. CHCHD6, there were no previously described patients with mutations in this gene), finding shared molecular alterations can help in the research for new therapies for these and other disorders with mitochondrial involvement.

3 Advanced *in vitro* platforms for synaptic function analysis

The study of the mitochondrial involvement in brain development and synaptic function requires of novel tools. While, as we have discussed, fibroblasts are a versatile and accessible model for the characterization of neurodevelopmental disorders, and highly valuable since they maintain the genetic background of the patients (Cordone et al., 2020), they have some limitations to the study of specific processes as synaptic communication. To overcome this, for the study of synaptic alterations in neurodevelopmental patients, fibroblasts generally are reprogrammed into iPSCs and then differentiated into the neuronal type of interest (Vitrac and Cloët-Tayarani, 2018). However, conventional two-dimensional neuronal cultures have shown many limitations for the recreation of controlled neuronal circuits for the study of synaptic communication *in vitro*, and therefore, new approaches are being developed and implemented. Among these new tools are three-dimensional cell cultures based on biomaterials, and brain organoids, which are three-dimensional cell cultures that self-assemble to form specialized structures formed by different cell types (Coronel et al., 2024); although their heterogenity, reproducibility and scalability are still major limitations to overcome. Another advanced tool for the precise study of synaptic function are microfluidic devices or "organs on a chip". These chips are biologically inert structures (usually made of PDMS) consisting of small microchannels that allow for cell compartmentalization in specific shapes and manipulation of small amounts of fluids (Park et al., 2006). Many different cell types can be combined and allow 2D and 3D cell culturing, recreating biological complex structures such as the blood brain barrier (BBB) (Palma-Florez et al., 2023), leading to a better recapitulation of organ biology in health and disease (Palasantzas et al., 2023).

To overcome the limitations of conventional neuronal cultures, we developed a specialization of an organ-on-chip, the **synapse on a chip (SoC) microfluidic device**. This platform allows us to compartmentalize the pre- and post-synaptic neurons and the synaptic space to gain independent insight into the processes occurring in each part. In this manner, we can study more precisely the relationship of mitochondrial homeostasis with the synaptic communication, and how it may be affected in neurodevelopmental diseases. Similar PDMS microfluidic systems have previously been used to study neurodegenerative diseases such as Huntington's (Virlogeux et al., 2018), Alzheimer's (Deleglise et al., 2014), or Parkinson's (Freundt et al., 2012), to better understand the mechanism of these pathologies and accelerate the development of effective and personalized therapies.

In this preliminary work, we have validated the on-chip growth and differentiation of cortical and dopaminergic neuron models from healthy human neural progenitors. The models studied showed optimal differentiations in the device, which led to large axonal structures that connected in the synaptic chamber. Interestingly, these axons were considerably larger than the neurites formed in conventional culture, which were disoriented and disorganized, suggesting that the microfluidic environment facilitates the maturation of the neurons (Babaliari et al., 2023). Nonetheless, these are the first steps of a long path ahead of us, and many improvements need to be made to achieve better neuronal circuits. In our studies, some nuclei were detected in the microchannels, meaning that cell bodies were able to migrate into the channels, and ultimately enter the synaptic chamber. The number of nuclei found in the synaptic chambers were residual and were not considered affecting the synaptic measurements performed. Yet, to avoid these issues in the future, reducing microchannel heights should be considered. Goshi and collaborators (Goshi et al., 2023) reported that ideal microchannel height without affecting the ability of axons to enter the channels would be 1.5 µm, whereas our height was 5 µm. The synaptic chamber length should also be decreased (from 500 µm to perhaps 100 µm), since in some devices we found that axons would preferably form synaptic connections with axons originating from the same chamber instead from the opposite. This could affect pre- *vs*. post-synaptic studies, and it is crucial for neuronal circuits involving two different neuronal types, such as the cortico-striatal pathway (Virlogeux et al., 2018).

Another limitation was the staining of the axons in the microchannels and the measurement of synaptic markers after pre-synaptic stimulation with 50 mM KCl. Our microchannel width of 5 µm to 2 µm did not allow for complete staining of the axon along the structure, which was achieved in other studies with the same width but using primary neuron culture from mice as shown in (Virlogeux et al., 2018). Increasing microchannel width could be an option if experiments of single axon imaging are not performed, since this would improve robust synaptic activity in the central chamber (Goshi et al., 2023) and would facilitate the entry of the antibodies used into the microchannels, although it will permit the migration of more soma as a counterpart. Another option to consider is the systematic use of viral transfections for improved and stable signal, as achieved in the model developed by Iannielli and collaborators (Iannielli et al., 2019) between human iPSC-derived midbrain dopaminergic neurons and striatal medium spiny neurons. In their study, they were able to detect dopaminergic neuron signaling after stimulation with 56 mM KCl in a ACSF buffer (Artificial Cerebrospinal Fluid buffer). For mitochondrial transport measurements along the axon, viral transfections such as Mito-DsRed should be considered, which is stable after repeated stimulations with 90 mM KCl (Li et al., 2004), whereas MitoTracker™ signal could be affected, as detected in our studies. In conclusion, channel height and width and synaptic chamber length, together with the use of viral transfections and more robust stimulation techniques and conditions should be considered for further validations.

One of the advantages of the SoC system is the possibility to collect the medium of the synaptic environment, allowing the measurement of metabolites and neurotransmitters without the disturbances (and dilution) of the media of whole cultures. This allows for better characterization of the study models. In our case, the neurodevelopmental patients studied in this Thesis, in addition to a very severe clinical picture of infantile parkinsonism, presented alterations of monoamines in CSF, and therefore they were oriented as a neurotransmitter defect. It is remarkable how, in contrast to classical mitochondrial diseases, these cases were not oriented by a lactic acidemia, and part of their pathophysiology could be more related to the effect of mitochondria on neurotransmitters than to energetic dysfunction *per se*. We studied the potential mitochondrial influence on neurotransmitters concentration, such as dopamine for DA neurons and glutamate and GABA for cortical neurons. The preliminary results obtained suggested that DA neurons could be more dependent on correct mitochondrial function than cortical neurons, which would explain the parkinsonism symptomatology of many mitochondrial disorders, similarly as found in (Chen et al., 2017) for Leigh syndrome. These initial results open an interesting path to expand research in this direction and unveil a causal explanation for these alterations.

Besides the mitochondrial patients studied, neurodevelopmental disorders with underlying mitochondrial dysfunction, such as Rett syndrome, have alterations in the dopaminergic circuitry leading to motor, social and executive functions impairment (Hirofuji et al., 2018; Robinson and Gradinaru, 2018). This personalized approach through patient's iPSCs to study the mitochondrial function in the synaptic communication, particularly the dopaminergic circuitry, will allow for a better understanding of these rare neurological disorders in which mitochondrial impairment is part of their pathophysiology, and evaluate how treatments that modulate mitochondrial function can eventually have an impact on neurotransmission.

In conclusion, this preliminary work on the SoC microfluidic device has established the foundation for the study of the **relationship between mitochondrial homeostasis and synaptic function in neurodevelopmental disorders**. These results allow us to establish the optimal conditions for the differentiation and characterization of neural progenitors to the neuronal type of interest in the microfluidic system. In this context, we will be able to perform a personalized study of neurodevelopmental diseases, in addition to the potential effect of different treatments modulating mitochondrial function on the synapse. In the near future, this microfluidic device is expected to be used as a diagnostic and personalized therapy model for mitochondrial diseases, allowing for modelling specific neuronal types (e.g. glutamatergic/GABAergic neurons), neuron-glia co-cultures, and neuronal circuits such as cortico-striatal or cortico-cerebellar networks, which can be achieved by using patients' iPSC-derived neurons.

4 Integrative view of mitochondria as a therapeutic target

Mitochondria have an essential role in neurodevelopment and correct synaptic communication. Through their bioenergetics and signaling functions, they are involved in neurogenesis, stem cell fate decision and migration, programmed cell death, axogenesis and synaptogenesis, processes during which they undergo morphologic and metabolic shifts. At the synapse, they are responsible for generating the sufficient ATP and buffering of calcium, processes necessary for neuronal communication. Their role is also essential in generation of oxygen species for ROS signaling, post-synaptic density and plasticity, and synthesis of neurotransmitters and vesicle trafficking.

Mitochondrial alterations, in terms of morphological aspects and bioenergetic function, are present in neurodevelopmental disorders, as the paradigmatic neurological disorder Rett syndrome, traditionally characterized by neuronal maturation delay and imbalance of excitatory/inhibitory neurotransmission without integrating an energy metabolism perspective in these alterations. The systematic characterization of mitochondrial disturbances in Rett syndrome in preclinical models of the disease and the bioenergetic dysfunction correction with the PPARγ leriglitazone has resulted in the necessary evidence for a clinical trial in Rett syndrome patients. This highlights the importance of expanding the knowledge on the pathophysiology of the disease to find new therapeutic options and the potential of metabolism for the treatment of even “non-metabolic” neurodevelopmental diseases.

Additionally, primary defects in any of mitochondrial functions and aspects can lead to disorders, many of which present with a severe neurological component and motor dysfunction. From a patient-focused perspective, the precise knowledge of the mutation effect on mitochondrial functions can provide new horizons on personalized therapeutic approaches. For this, it is mandatory to implement a medium-throughput algorithm that allows for detection of mitochondrial homeostasis alterations in a real clinical-time response, aiding for diagnosis confirmation and resulting in a true benefit for the patient. Based on these alterations, new therapeutic approaches targeting mitochondrial homeostasis can be assayed. New treatments include pharmacological interventions with PPARγ agonists, which have shown clinical ameliorations in neurological disorders with underlying mitochondrial impairment, and supplementation with nutraceuticals, resulting in cognitive improvements changing the natural course of disease. Traditionally established metabolic approaches, such as ketogenic diet for the treatment of refractory epilepsies, has shown beneficial effects on a novel non-treated mitochondrial encephalopathy. Importantly, nutraceutical supplementation and dietary approach with ketogenic diet are readily available for implementation, and their application in a patient-specific approach reduces the requirement for pharmacological intervention. In addition, these different approaches are potentially not mutually exclusive and neither should be considered as the only option. For example, ketogenic diet exerts an effect on mitochondria by the PGC-1α pathway and simultaneous treatments with PPARγ agonists should be evaluated, discarding potential toxic effects and exploring a possible synergic outcome.

Deeper characterization on the relationship between mitochondrial function and synaptic communication will result in a better understanding of the pathophysiological features of each disease, yielding to better and more precise treatments. For that, new *in vitro* tools for the personalized study of the disease are needed, such as the “organ on a chip” advancement “synapse on a chip”. As our preliminary results have shown, these systems better recapitulate the *in vivo* environment than traditional models as cell cultures and allow selective modulation of the agents involved in synaptic communication.

Altogether, this Thesis explores the involvement of mitochondria in the pathophysiology of neurodevelopmental diseases, and endorses mitochondrial homeostasis as a therapeutic target for their treatment. Further studies will refine the algorithm for the description of mitochondrial alterations along with the development of advanced tools for their study. All approaches shall set the focus on enabling Personalized Treatments evaluation within clinical-relevant timeframes, shortening the usual research timelines to ensure prompt translation into clinical practice.

CONCLUSIONS

1. Mitochondrial homeostasis alterations are detected in Rett patients' fibroblasts, characterized by simpler and less interconnected networks, decreased fission dynamics, defective ATP production and increased oxidative stress.

2. Bioenergetic dysfunction is detectable in brains of female murine model of Rett syndrome, showing significant differences between cortex, hippocampus and cerebellum.

3. Bioenergetic alterations in cerebellum are already evident in pre-symptomatic stages of Rett female mice models, underscoring the importance of early mitochondria-targeted therapeutic interventions.

4. Neuroinflammation is a critical component of Rett syndrome pathophysiology.

5. Leriglitazone corrects the bioenergetic alterations in Rett patients' fibroblasts without exerting morphological and dynamics changes in mitochondrial network.

6. Sustained leriglitazone treatment in female Rett mice corrects the bioenergetic alterations in hippocampus and cerebellum and mitigates cortical neuroinflammation, leading to significant phenotypic and behavioral improvements in symptomatic Rett mice.

7. These findings position mitochondrial dysfunction as a promising therapeutic target for Rett syndrome treatment.

8. The characterization of mitochondrial function in terms of bioenergetics and network structure represents an optimal compromise between in-depth functional analysis, the technical capabilities available in hospital-based molecular biology laboratories, and the clinical response time requirements.

9. Leriglitazone is able to correct the bioenergetic alterations in fibroblasts of a patient with defects in the electron transport chain complex I, but not in patients with alterations in fission dynamics at the assayed *in vitro* conditions.

10. Spermidine treatment is able to increase mitochondrial ATP production without causing significant variations in oxidative stress in fibroblasts of most patients with primary mitochondrial disorders, and ameliorates cognitive and motor deficits in patients, establishing it as a possible therapeutic strategy.

11. Treatment with ketogenic diet improves *in vitro* ATP production and mitochondrial dynamics in fibroblasts from patients with AFG2A-related encephalopathy and achieves seizure control in patients, suggesting ketogenic diet as a safe and plausible treatment option.

12. The three tested compounds —leriglitazone, spermidine, and ketone bodies— highlight three complementary therapeutic strategies (pharmacological, nutraceutical, and metabolism-based), offering a base for personalized treatment of mitochondrial disorders.

13. The preliminary work on the "synapse on a chip" microfluidic device allows for the precise study of the mitochondrial implication on the synapse using human-derived cortical and dopaminergic neurons. This tool paves the way for personalized medicine studies focusing on synaptic and mitochondrial dysfunction.

14. Mitochondria represent a cross-sectional axis for the treatment of neurodevelopmental disorders, offering a shared therapeutic target for conditions in which mitochondrial dysfunction underlies disease pathophysiology, such as Rett syndrome, and for primary mitochondrial disorders.

BIBLIOGRAPHY

A, O., U, M., Lf, B. & A, G.-C. (2021). Energy metabolism in childhood neurodevelopmental disorders. EBioMedicine, 69, 103474. https://doi.org/10.1016/j.ebiom.2021.103474

Achilly, N. P., He, L., Kim, O. A., Ohmae, S., Wojaczynski, G. J., Lin, T., Sillitoe, R. V., Medina, J. F. & Zoghbi, H. Y. (2021). Deleting Mecp2 from the cerebellum rather than its neuronal subtypes causes a delay in motor learning in mice. eLife, 10, e64833. https://doi.org/10.7554/elife.64833

Agostini, M., Romeo, F., Inoue, S., Niklison-Chirou, M. V., Elia, A. J., Dinsdale, D., Morone, N., Knight, R. A., Mak, T. W. & Melino, G. (2016). Metabolic reprogramming during neuronal differentiation. 23(9), 1502–1514. https://doi.org/10.1038/cdd.2016.36

Alba, G., Dakhaoui, H., Santa-Maria, C., Palomares, F., Cejudo-Guillen, M., Geniz, I., Sobrino, F., Paz, S. M. la & Lopez-Enriquez, S. (2023). Nutraceuticals as Potential Therapeutic Modulators in Immunometabolism. Nutrients, 15(2), 411. https://doi.org/10.3390/nu15020411

Aldosary, M., Al-Bakheet, A., Al-Dhalaan, H., Almass, R., Alsagob, M., Al-Younes, B., AlQuait, L., Mustafa, O. M., Bulbul, M., Rahbeeni, Z., Alfadhel, M., Chedrawi, A., Al-Hassnan, Z., AlDosari, M., Al-Zaidan, H., Al-Muhaizea, M. A., AlSayed, M. D., Salih, M. A., AlShammari, M., … Colak, D. (2020). Rett Syndrome, a Neurodevelopmental Disorder, Whole-Transcriptome, and Mitochondrial Genome Multiomics Analyses Identify Novel Variations and Disease Pathways. OMICS: A Journal of Integrative Biology, 24(3), 160–171. https://doi.org/10.1089/omi.2019.0192

Amin, S., Ruban-Fell, B., Newell, I., Evans, J., Vyas, K., Nortvedt, C. & Chin, R. F. (2024). Treatment guidelines for rare, early-onset conditions associated with epileptic seizures: a literature review on Rett syndrome and tuberous sclerosis complex. 19(1), 89. https://doi.org/10.1186/s13023-023-02994-x

Amir, R. E., Veyver, I. B. V. den, Wan, M., Tran, C. Q., Francke, U. & Zoghbi, H. Y. (1999). Rett syndrome is caused by mutations in X-linked MECP2, encoding methyl-CpG-binding protein 2. Nature Genetics, 23(2), 185–188. https://doi.org/10.1038/13810

Amirifar, L., Shamloo, A., Nasiri, R., Barros, N. R. de, Wang, Z. Z., Unluturk, B. D., Libanori, A., Ievglevskyi, O., Diltemiz, S. E., Sances, S., Balasingham, I., Seidlits, S. K. & Ashammakhi, N. (2022). Brain-on-a-chip: Recent advances in design and techniques for microfluidic models of the brain in health and disease. Biomaterials, 285, 121531. https://doi.org/10.1016/j.biomaterials.2022.121531

Amsen, D., Visser, K. E. de & Town, T. (2009). Inflammation and Cancer, Methods and Protocols: Volume 1: Experimental Models and Practical Approaches. Methods in Molecular Biology (Clifton, N.J.), 511, 107–142. https://doi.org/10.1007/978-1-59745-447-6_5

An, J., Shi, J., He, Q., Lui, K., Liu, Y., Huang, Y. & Sheikh, M. S. (2012). CHCM1/CHCHD6, Novel Mitochondrial Protein Linked to Regulation of Mitofilin and Mitochondrial Cristae Morphology*. Journal of Biological Chemistry, 287(10), 7411–7426. https://doi.org/10.1074/jbc.m111.277103

Antoni, D., Burckel, H., Josset, E. & Noel, G. (2015). Three-Dimensional Cell Culture: A Breakthrough in Vivo. International Journal of Molecular Sciences, 16(3), 5517–5527. https://doi.org/10.3390/ijms16035517

Ariani, F., Hayek, G., Rondinella, D., Artuso, R., Mencarelli, M. A., Spanhol-Rosseto, A., Pollazzon, M., Buoni, S., Spiga, O., Ricciardi, S., Meloni, I., Longo, I., Mari, F., Broccoli, V., Zappella, M. & Renieri, A. (2008). FOXG1 Is Responsible for the Congenital Variant of Rett Syndrome. The American Journal of Human Genetics, 83(1), 89–93. https://doi.org/10.1016/j.ajhg.2008.05.015

Audouard, E., Khefif, N., Gillet-Legrand, B., Nobilleau, F., Bouazizi, O., Stanga, S., Despres, G., Alves, S., Lamazière, A., Cartier, N. & Piguet, F. (2024). Modulation of Brain Cholesterol Metabolism through CYP46A1 Overexpression for Rett Syndrome. Pharmaceutics, 16(6). https://doi.org/10.3390/pharmaceutics16060756

Babaliari, E., Ranella, A. & Stratakis, E. (2023). Microfluidic Systems for Neural Cell Studies. Bioengineering, 10(8), 902. https://doi.org/10.3390/bioengineering10080902

Bacman, S. R., Kauppila, J. H. K., Pereira, C. V., Nissanka, N., Miranda, M., Pinto, M., Williams, S. L., Larsson, N.-G., Stewart, J. B. & Moraes, C. T. (2018). MitoTALEN reduces mutant mtDNA load and restores tRNAAla levels in a mouse model of heteroplasmic mtDNA mutation. 24(11), 1696–1700. https://doi.org/10.1038/s41591-018-0166-8

Baide-Mairena, H., Gaudó, P., Marti-Sánchez, L., Emperador, S., Sánchez-Montanez, A., Alonso-Luengo, O., Correa, M., Grau, A. M., Ortigoza-Escobar, J. D., Artuch, R., Vázquez, E., Toro, M. D., Garrido-Pérez, N., Ruiz-Pesini, E., Montoya, J., Bayona-Bafaluy, M. P. & Pérez-Dueñas, B. (2019). Mutations in the mitochondrial complex I assembly factor NDUFAF6 cause isolated bilateral striatal necrosis and progressive dystonia in childhood. Molecular Genetics and Metabolism, 126(3), 250–258. https://doi.org/10.1016/j.ymgme.2019.01.001

Bak, L. K. & Walls, A. B. (2018). CrossTalk opposing view: lack of evidence supporting an astrocyte-to-neuron lactate shuttle coupling neuronal activity to glucose utilisation in the brain. The Journal of Physiology, 596(3), 351–353. https://doi.org/10.1113/jp274945

Balicza, P., Gezsi, A., Fedor, M., Sagi, J. C., Gal, A., Varga, N. A. & Molnar, M. J. (2024). Multilevel evidence of MECP2-associated mitochondrial dysfunction and its therapeutic implications. Frontiers in Psychiatry, 14, 1301272. https://doi.org/10.3389/fpsyt.2023.1301272

Banerjee, A., Miller, M. T., Li, K., Sur, M. & Kaufmann, W. E. (2019). Towards a better diagnosis and treatment of Rett syndrome: a model synaptic disorder. Brain, 142(2), 239–248. https://doi.org/10.1093/brain/awy323

Baroncelli, L., Auel, S., Rinne, L., Schuster, A.-K., Brand, V., Kempkes, B., Dietrich, K. & Müller, M. (2022). Oral Feeding of an Antioxidant Cocktail as a Therapeutic Strategy in a Mouse Model of Rett Syndrome: Merits and Limitations of Long-Term Treatment. Antioxidants, 11(7), 1406. https://doi.org/10.3390/antiox11071406

Barritt, S. A., DuBois-Coyne, S. E. & Dibble, C. C. (2024). Coenzyme A biosynthesis: mechanisms of regulation, function and disease. Nature Metabolism, 6(6), 1008–1023. https://doi.org/10.1038/s42255-024-01059-y

Bassuk, A. G. (2022). Gene therapy for Rett syndrome. Genes, Brain and Behavior, 21(1), e12754. https://doi.org/10.1111/gbb.12754

Batch, J. T., Lamsal, S. P., Adkins, M., Sultan, S. & Ramirez, M. N. (2020). Advantages and Disadvantages of the Ketogenic Diet: A Review Article. Cureus, 12(8), e9639. https://doi.org/10.7759/cureus.9639

Bebensee, D. F., Can, K. & Müller, M. (2017). Increased Mitochondrial Mass and Cytosolic Redox Imbalance in Hippocampal Astrocytes of a Mouse Model of Rett Syndrome: Subcellular Changes Revealed by Ratiometric Imaging of JC-1 and roGFP1 Fluorescence. Oxidative Medicine and Cellular Longevity, 2017, 1–15. https://doi.org/10.1155/2017/3064016

Beckervordersandforth, R., Ebert, B., Schäffner, I., Moss, J., Fiebig, C., Shin, J., Moore, D. L., Ghosh, L., Trinchero, M. F., Stockburger, C., Friedland, K., Steib, K., Wittgenstein, J. von, Keiner, S., Redecker, C., Hölter, S. M., Xiang, W., Wurst, W., Jagasia, R., … Lie, D. C. (2017). Role of Mitochondrial Metabolism in the Control of Early Lineage Progression and Aging Phenotypes in Adult Hippocampal Neurogenesis. Neuron, 93(3), 560-573.e6. https://doi.org/10.1016/j.neuron.2016.12.017

Bedogni, F., Rossi, R. L., Galli, F., Gigli, C. C., Gandaglia, A., Kilstrup-Nielsen, C. & Landsberger, N. (2014). Rett syndrome and the urge of novel approaches to study MeCP2 functions and mechanisms of action. Neuroscience & Biobehavioral Reviews, 46, 187–201. https://doi.org/10.1016/j.neubiorev.2014.01.011

Belichenko, P. V., Wright, E. E., Belichenko, N. P., Masliah, E., Li, H. H., Mobley, W. C. & Francke, U. (2009). Widespread changes in dendritic and axonal morphology in Mecp2-mutant mouse models of rett syndrome: Evidence for disruption of neuronal networks. Journal of Comparative Neurology, 514(3), 240–258. https://doi.org/10.1002/cne.22009

Benke, D. & Möhler, H. (2018). Impact on GABA systems in monogenetic developmental CNS disorders: Clues to symptomatic treatment. Neuropharmacology, 136, 46–55. https://doi.org/10.1016/j.neuropharm.2017.07.030

Ben-Shachar, S., Chahrour, M., Thaller, C., Shaw, C. A. & Zoghbi, H. Y. (2009). Mouse models of MeCP2 disorders share gene expression changes in the cerebellum and hypothalamus. Human Molecular Genetics, 18(13), 2431–2442. https://doi.org/10.1093/hmg/ddp181

Bienvenu, T. & Chelly, J. (2006). Molecular genetics of Rett syndrome: when DNA methylation goes unrecognized. Nature Reviews Genetics, 7(6), 415–426. https://doi.org/10.1038/nrg1878

Björkman, K., Sofou, K., Darin, N., Holme, E., Kollberg, G., Asin-Cayuela, J., Dahle, K. M. H., Oldfors, A., Moslemi, A.-R. & Tulinius, M. (2015). Broad phenotypic variability in patients with complex I deficiency due to mutations in NDUFS1 and NDUFV1. Mitochondrion, 21, 33–40. https://doi.org/10.1016/j.mito.2015.01.003

Bose, A. & Beal, M. F. (2016). Mitochondrial dysfunction in Parkinson's disease. Journal of Neurochemistry, 139(S1), 216–231. https://doi.org/10.1111/jnc.13731

Bough, K. J. & Rho, J. M. (2007). Anticonvulsant Mechanisms of the Ketogenic Diet. Epilepsia, 48(1), 43–58. https://doi.org/10.1111/j.1528-1167.2007.00915.x

Brakedal, B., Dölle, C., Riemer, F., Ma, Y., Nido, G. S., Skeie, G. O., Craven, A. R., Schwarzlmüller, T., Brekke, N., Diab, J., Sverkeli, L., Skjeie, V., Varhaug, K., Tysnes, O.-B., Peng, S., Haugarvoll, K., Ziegler, M., Grüner, R., Eidelberg, D. & Tzoulis, C. (2022). The NADPARK study: A randomized phase I trial of nicotinamide riboside supplementation in Parkinson's disease. Cell Metabolism, 34(3), 396-407.e6. https://doi.org/10.1016/j.cmet.2022.02.001

Braun, F., Hentschel, A., Sickmann, A., Marteau, T., Hertel, S., Förster, F., Prokisch, H., Wagner, M., Wortmann, S., Marina, A. D., Kölbel, H., Roos, A. & Schara-Schmidt, U. (2021). Muscular and Molecular Pathology Associated with SPATA5 Deficiency in a Child with EHLMRS. International Journal of Molecular Sciences, 22(15), 7835. https://doi.org/10.3390/ijms22157835

Brekke, E., Morken, T. S. & Sonnewald, U. (2015). Glucose metabolism and astrocyte–neuron interactions in the neonatal brain. 82, 33–41. https://doi.org/10.1016/j.neuint.2015.02.002

Buchanan, C. B., Stallworth, J. L., Joy, A. E., Dixon, R. E., Scott, A. E., Beisang, A. A., Benke, T. A., Glaze, D. G., Haas, R. H., Heydemann, P. T., Jones, M. D., Lane, J. B., Lieberman, D. N., Marsh, E. D., Neul, J. L., Peters, S. U., Ryther, R. C., Skinner, S. A., Standridge, S. M., … Percy, A. K. (2022). Anxiety-like behavior and anxiolytic treatment in the Rett syndrome natural history study. 14(1), 31. https://doi.org/10.1186/s11689-022-09432-2

Buchovecky, C. M., Turley, S. D., Brown, H. M., Kyle, S. M., McDonald, J. G., Liu, B., Pieper, A. A., Huang, W., Katz, D. M., Russell, D. W., Shendure, J. & Justice, M. J. (2013). A suppressor screen in Mecp2 mutant mice implicates cholesterol metabolism in Rett syndrome. 45(9), 1013–1020. https://doi.org/10.1038/ng.2714

Byiers, B. J., Merbler, A. M., Barney, C. C., Frenn, K. A., Panoskaltsis-Mortari, A., Ehrhardt, M. J., Feyma, T. J., Beisang, A. A. & Symons, F. (2019). Evidence of altered salivary cytokine concentrations in Rett syndrome and associations with clinical severity. Brain, Behavior, & Immunity - Health, 1, 100008. https://doi.org/10.1016/j.bbih.2019.100008

Cabré, R., Jové, M., Naudí, A., Ayala, V., Piñol-Ripoll, G., Gil-Villar, M. P., Dominguez-Gonzalez, M., Obis, È., Berdun, R., Mota-Martorell, N., Portero-Otin, M., Ferrer, I. & Pamplona, R. (2016). Specific Metabolomics Adaptations Define a Differential Regional Vulnerability in the Adult Human Cerebral Cortex. Frontiers in Molecular Neuroscience, 9, 138. https://doi.org/10.3389/fnmol.2016.00138

Calatayud, C., Carola, G., Fernández-Carasa, I., Valtorta, M., Jiménez-Delgado, S., Díaz, M., Soriano-Fradera, J., Cappelletti, G., García-Sancho, J., Raya, Á. & Consiglio, A. (2019). CRISPR/Cas9-mediated generation of a tyrosine hydroxylase reporter iPSC line for live imaging and isolation of dopaminergic neurons. Scientific Reports, 9(1), 6811. https://doi.org/10.1038/s41598-019-43080-2

Camillo, L., Pozzi, M., Bernardo, P., Pisano, S. & Nobile, M. (2024). Profile of Trofinetide in the Treatment of Rett Syndrome: Design, Development and Potential Place in Therapy. Drug Design, Development and Therapy, 18, 5023–5040. https://doi.org/10.2147/dddt.s383133

Can, K., Menzfeld, C., Rinne, L., Rehling, P., Kügler, S., Golubiani, G., Dudek, J. & Müller, M. (2019). Neuronal Redox-Imbalance in Rett Syndrome Affects Mitochondria as Well as Cytosol, and Is Accompanied by Intensified Mitochondrial O2 Consumption and ROS Release. Frontiers in Physiology, 10, 479. https://doi.org/10.3389/fphys.2019.00479

Cardaioli, E., Dotti, M., Hayek, G., Zappella, M. & Federico, A. (1999). Studies on mitochondrial pathogenesis of Rett syndrome: ultrastructural data from skin and muscle biopsies and mutational analysis at mtDNA nucleotides 10463 and 2835. Journal of Submicroscopic Cytology and Pathology, 31(2), 301—304. http://europepmc.org/abstract/MED/10457616

Carter, J. C., Lanham, D. C., Pham, D., Bibat, G., Naidu, S. & Kaufmann, W. E. (2008). Selective Cerebral Volume Reduction in Rett Syndrome: A Multiple-Approach MR Imaging Study. American Journal of Neuroradiology, 29(3), 436–441. https://doi.org/10.3174/ajnr.a0857

Casado, M., Sierra, C., Batllori, M., Artuch, R. & Ormazabal, A. (2018). A targeted metabolomic procedure for amino acid analysis in different biological specimens by ultra-high-performance liquid chromatography–tandem mass spectrometry. Metabolomics, 14(6), 76. https://doi.org/10.1007/s11306-018-1374-4

Casaril, A. M., Dantzer, R. & Bas-Orth, C. (2021). Neuronal Mitochondrial Dysfunction and Bioenergetic Failure in Inflammation-Associated Depression. Frontiers in Neuroscience, 15, 725547. https://doi.org/10.3389/fnins.2021.725547

Casarin, A., Giorgi, G., Pertegato, V., Siviero, R., Cerqua, C., Doimo, M., Basso, G., Sacconi, S., Cassina, M., Rizzuto, R., Brosel, S., Davidson, M. M., DiMauro, S., Schon, E. A., Clementi, M., Trevisson, E. & Salviati, L. (2012). Copper and bezafibrate cooperate to rescue cytochrome c oxidase deficiency in cells of patients with sco2 mutations. Orphanet Journal of Rare Diseases, 7(1), 21. https://doi.org/10.1186/1750-1172-7-21

Catania, A., Ardissone, A., Verrigni, D., Legati, A., Reyes, A., Lamantea, E., Diodato, D., Tonduti, D., Imperatore, V., Pinto, A. M., Moroni, I., Bertini, E., Robinson, A., Carrozzo, R., Zeviani, M. & Ghezzi, D. (2018). Compound heterozygous missense and deep intronic variants in NDUFAF6 unraveled by exome sequencing and mRNA analysis. Journal of Human Genetics, 63(5), 563–568. https://doi.org/10.1038/s10038-018-0423-1

Cervellati, C., Sticozzi, C., Romani, A., Belmonte, G., Rasmo, D. D., Signorile, A., Cervellati, F., Milanese, C., Mastroberardino, P. G., Pecorelli, A., Savelli, V., Forman, H. J., Hayek, J. & Valacchi, G. (2015). Impaired enzymatic defensive activity, mitochondrial dysfunction and proteasome activation are involved in RTT cell oxidative damage. Biochimica et Biophysica Acta (BBA) - Molecular Basis of Disease, 1852(10), 2066–2074. https://doi.org/10.1016/j.bbadis.2015.07.014

Chahrour, M., Jung, S. Y., Shaw, C., Zhou, X., Wong, S. T. C., Qin, J. & Zoghbi, H. Y. (2008). MeCP2, a Key Contributor to Neurological Disease, Activates and Represses Transcription. Science, 320(5880), 1224–1229. https://doi.org/10.1126/science.1153252

Chahrour, M. & Zoghbi, H. Y. (2007). The Story of Rett Syndrome: From Clinic to Neurobiology. Neuron, 56(3), 422–437. https://doi.org/10.1016/j.neuron.2007.10.001

Chao, H.-T., Chen, H., Samaco, R., Xue, M., Chahrour, M., Yoo, J., Neul, J., Gong, S., Lu, H.-C., Heintz, N., Ekker, M., Rubenstein, J., Noebels, J., Rosenmund, C. & Zoghbi, H. (2010). GABAergic dysfunction mediates autism-like stereotypies and Rett syndrome phenotypes. 468, 263–269. https://doi.org/10.1038/nature09582

Chaudhry, A., Shi, R. & Luciani, D. S. (2020). A pipeline for multidimensional confocal analysis of mitochondrial morphology, function, and dynamics in pancreatic β-cells. American Journal of Physiology-Endocrinology and Metabolism, 318(2), E87–E101. https://doi.org/10.1152/ajpendo.00457.2019

Chen, A., Kristiansen, C. K., Hong, Y., Kianian, A., Fang, E. F., Sullivan, G. J., Wang, J., Li, X., Bindoff, L. A. & Liang, K. X. (2021). Nicotinamide Riboside and Metformin Ameliorate Mitophagy Defect in Induced Pluripotent Stem Cell-Derived Astrocytes With POLG Mutations. Frontiers in Cell and Developmental Biology, 9, 737304. https://doi.org/10.3389/fcell.2021.737304

Chen, B., Hui, J., Montgomery, K. S., Gella, A., Bolea, I., Sanz, E., Palmiter, R. D. & Quintana, A. (2017). Loss of Mitochondrial Ndufs4 in Striatal Medium Spiny Neurons Mediates Progressive Motor Impairment in a Mouse Model of Leigh Syndrome. Frontiers in Molecular Neuroscience, 10, 265. https://doi.org/10.3389/fnmol.2017.00265

Chen, R. Z., Akbarian, S., Tudor, M. & Jaenisch, R. (2001). Deficiency of methyl-CpG binding protein-2 in CNS neurons results in a Rett-like phenotype in mice. Nature Genetics, 27(3), 327–331. https://doi.org/10.1038/85906

Chen, W., Zhao, H. & Li, Y. (2023). Mitochondrial dynamics in health and disease: mechanisms and potential targets. Signal Transduction and Targeted Therapy, 8(1), 333. https://doi.org/10.1038/s41392-023-01547-9

Chen, Y., Landin-Romero, R., Kumfor, F., Irish, M., Hodges, J. R. & Piguet, O. (2020). Cerebellar structural connectivity and contributions to cognition in frontotemporal dementias. Cortex, 129, 57–67. https://doi.org/10.1016/j.cortex.2020.04.013

Chen, Y.-C., Wu, J.-S., Tsai, H.-D., Huang, C.-Y., Chen, J.-J., Sun, G. Y. & Lin, T.-N. (2012). Peroxisome Proliferator-Activated Receptor Gamma (PPAR-γ) and Neurodegenerative Disorders. Molecular Neurobiology, 46(1), 114–124. https://doi.org/10.1007/s12035-012-8259-8

Cheng, A., Wan, R., Yang, J.-L., Kamimura, N., Son, T. G., Ouyang, X., Luo, Y., Okun, E. & Mattson, M. P. (2012). Involvement of PGC-1α in the formation and maintenance of neuronal dendritic spines. 3(1), 1250. https://doi.org/10.1038/ncomms2238

Cicaloni, V., Pecorelli, A., Tinti, L., Rossi, M., Benedusi, M., Cervellati, C., Spiga, O., Santucci, A., Hayek, J., Salvini, L., Tinti, C. & Valacchi, G. (2020). Proteomic profiling reveals mitochondrial alterations in Rett syndrome. Free Radical Biology and Medicine, 155, 37–48. https://doi.org/10.1016/j.freeradbiomed.2020.05.014

Ciccoli, L., Felice, C. D., Paccagnini, E., Leoncini, S., Pecorelli, A., Signorini, C., Belmonte, G., Valacchi, G., Rossi, M. & Hayek, J. (2012). Morphological changes and oxidative damage in Rett Syndrome erythrocytes. Biochimica et Biophysica Acta (BBA) - General Subjects, 1820(4), 511–520. https://doi.org/10.1016/j.bbagen.2011.12.002

Cittadini, C., Germinario, E. A. P., Maroccia, Z., Cosentino, L., Maselli, V., Gambardella, L., Giambenedetti, M., Guidotti, M., Travaglione, S., Fallerini, C., Renieri, A., Marcillo, D. I. E., Ricceri, L., Fortini, P., Filippis, B. D., Fiorentini, C. & Fabbri, A. (2023). Effects of the Rho GTPase-activating toxin CNF1 on fibroblasts derived from Rett syndrome patients: A pilot study. Journal of Cellular and Molecular Medicine, 27(10), 1315–1326. https://doi.org/10.1111/jcmm.17624

Cogliati, S., Enriquez, J. A. & Scorrano, L. (2016). Mitochondrial Cristae: Where Beauty Meets Functionality. Trends in Biochemical Sciences, 41(3), 261–273. https://doi.org/10.1016/j.tibs.2016.01.001

Cogliati, S., Frezza, C., Soriano, M. E., Varanita, T., Quintana-Cabrera, R., Corrado, M., Cipolat, S., Costa, V., Casarin, A., Gomes, L. C., Perales-Clemente, E., Salviati, L., Fernandez-Silva, P., Enriquez, J. A. & Scorrano, L. (2013). Mitochondrial Cristae Shape Determines Respiratory Chain Supercomplexes Assembly and Respiratory Efficiency. Cell, 155(1), 160–171. https://doi.org/10.1016/j.cell.2013.08.032

Coppola, G., Marmolino, D., Lu, D., Wang, Q., Cnop, M., Rai, M., Acquaviva, F., Cocozza, S., Pandolfo, M. & Geschwind, D. H. (2009). Functional genomic analysis of frataxin deficiency reveals tissue-specific alterations and identifies the PPARγ pathway as a therapeutic target in Friedreich's ataxia. Human Molecular Genetics, 18(13), 2452–2461. https://doi.org/10.1093/hmg/ddp183

Coquinco, A., Kojic, L., Wen, W., Wang, Y. T., Jeon, N. L., Milnerwood, A. J. & Cynader, M. (2014). A microfluidic based in vitro model of synaptic competition. Molecular and Cellular Neuroscience, 60, 43–52. https://doi.org/10.1016/j.mcn.2014.03.001

Cordone, V., Pecorelli, A., Amicarelli, F., Hayek, J. & Valacchi, G. (2020). The complexity of Rett syndrome models: Primary fibroblasts as a disease-in-a-dish reliable approach. Drug Discovery Today: Disease Models, 31, 11–19. https://doi.org/10.1016/j.ddmod.2019.11.001

Cornford, M. E., Philippart, M., Jacobs, B., Scheibel, A. B. & Vinters, H. V. (1994). Neuropathology of Rett Syndrome: Case Report With Neuronal and Mitochondrial Abnormalities in the Brain. Journal of Child Neurology, 9(4), 424–431. https://doi.org/10.1177/088307389400900419

Corona, J. C. & Duchen, M. R. (2016). PPARγ as a therapeutic target to rescue mitochondrial function in neurological disease. Free Radical Biology and Medicine, 100, 153–163. https://doi.org/10.1016/j.freeradbiomed.2016.06.023

Coronel, R., García-Moreno, E., Siendones, E., Barrero, M. J., Martínez-Delgado, B., Santos-Ocaña, C., Liste, I. & Cascajo-Almenara, M. V. (2024). Brain organoid as a model to study the role of mitochondria in neurodevelopmental disorders: achievements and weaknesses. Frontiers in Cellular Neuroscience, 18, 1403734. https://doi.org/10.3389/fncel.2024.1403734

Cortelazzo, A., Felice, C. D., Filippis, B. D., Ricceri, L., Laviola, G., Leoncini, S., Signorini, C., Pescaglini, M., Guerranti, R., Timperio, A. M., Zolla, L., Ciccoli, L. & Hayek, J. (2017). Persistent Unresolved Inflammation in the Mecp2-308 Female Mutated Mouse Model of Rett Syndrome. Mediators of Inflammation, 2017, 1–9. https://doi.org/10.1155/2017/9467819

Cosentino, L., Urbinati, C., Lanzillotta, C., Rasmo, D. D., Valenti, D., Pellas, M., Quattrini, M. C., Piscitelli, F., Kostrzewa, M., Domenico, F. D., Pietraforte, D., Bisogno, T., Signorile, A., Vacca, R. A. & Filippis, B. D. (2024). Pharmacological inhibition of the CB1 cannabinoid receptor restores abnormal brain mitochondrial CB1 receptor expression and rescues bioenergetic and cognitive defects in a female mouse model of Rett syndrome. Molecular Autism, 15(1), 39. https://doi.org/10.1186/s13229-024-00617-1

Cosentino, L., Vigli, D., Franchi, F., Laviola, G. & Filippis, B. D. (2019). Rett syndrome before regression: a time window of overlooked opportunities for diagnosis and intervention. Neuroscience & Biobehavioral Reviews, 107, 115–135. https://doi.org/10.1016/j.neubiorev.2019.05.013

Crivellari, I., Pecorelli, A., Cordone, V., Marchi, S., Pinton, P., Hayek, J., Cervellati, C. & Valacchi, G. (2021). Impaired mitochondrial quality control in Rett Syndrome. Archives of Biochemistry and Biophysics, 700, 108790. https://doi.org/10.1016/j.abb.2021.108790

Croci, S., Carriero, M. L., Capitani, K., Daga, S., Donati, F., Papa, F. T., Frullanti, E., Lopergolo, D., Lamacchia, V., Tita, R., Giliberti, A., Benetti, E., Niccheri, F., Furini, S., Rizzo, C. L., Conticello, S. G., Renieri, A. & Meloni, I. (2020). AAV-mediated FOXG1 gene editing in human Rett primary cells. 28(10), 1446–1458. https://doi.org/10.1038/s41431-020-0652-6

Cronk, J. C., Derecki, N. C., Ji, E., Xu, Y., Lampano, A. E., Smirnov, I., Baker, W., Norris, G. T., Marin, I., Coddington, N., Wolf, Y., Turner, S. D., Aderem, A., Klibanov, A. L., Harris, T. H., Jung, S., Litvak, V. & Kipnis, J. (2015). Methyl-CpG Binding Protein 2 Regulates Microglia and Macrophage Gene Expression in Response to Inflammatory Stimuli. Immunity, 42(4), 679–691. https://doi.org/10.1016/j.immuni.2015.03.013

Cuddapah, V. A., Pillai, R. B., Shekar, K. V., Lane, J. B., Motil, K. J., Skinner, S. A., Tarquinio, D. C., Glaze, D. G., McGwin, G., Kaufmann, W. E., Percy, A. K., Neul, J. L. & Olsen, M. L. (2014). Methyl-CpG-binding protein 2 (MECP2) mutation type is associated with disease severity in Rett syndrome. Journal of Medical Genetics, 51(3), 152. https://doi.org/10.1136/jmedgenet-2013-102113

Dave, A. & Pillai, P. P. (2022). Docosahexaenoic acid increased MeCP2 mediated mitochondrial respiratory complexes II and III enzyme activities in cortical astrocytes. Journal of Biochemical and Molecular Toxicology, 36(4), e23002. https://doi.org/10.1002/jbt.23002

Dave, A., Shukla, F., Wala, H. & Pillai, P. (2019). Mitochondrial Electron Transport Chain Complex Dysfunction in MeCP2 Knock-Down Astrocytes: Protective Effects of Quercetin Hydrate. Journal of Molecular Neuroscience, 67(1), 16–27. https://doi.org/10.1007/s12031-018-1197-9

Davies, K. M., Strauss, M., Daum, B., Kief, J. H., Osiewacz, H. D., Rycovska, A., Zickermann, V. & Kühlbrandt, W. (2011). Macromolecular organization of ATP synthase and complex I in whole mitochondria. Proceedings of the National Academy of Sciences, 108(34), 14121–14126. https://doi.org/10.1073/pnas.1103621108

Dean, S. L., Tochen, L., Augustine, F., Ali, S. F., Crocetti, D., Rajendran, S., Blue, M. E., Mahone, E. M., Mostofsky, S. H. & Singer, H. S. (2022). The Role of the Cerebellum in Repetitive Behavior Across Species: Childhood Stereotypies and Deer Mice. The Cerebellum, 21(3), 440–451. https://doi.org/10.1007/s12311-021-01301-3

Dehmer, T., Heneka, M. T., Sastre, M., Dichgans, J. & Schulz, J. B. (2004). Protection by pioglitazone in the MPTP model of Parkinson's disease correlates with IκBα induction and block of NFκB and iNOS activation. Journal of Neurochemistry, 88(2), 494–501. https://doi.org/10.1046/j.1471-4159.2003.02210.

Deleglise, B., Magnifico, S., Duplus, E., Vaur, P., Soubeyre, V., Belle, M., Vignes, M., Viovy, J.-L., Jacotot, E., Peyrin, J.-M. & Brugg, B. (2014). β-amyloid induces a dying-back process and remote trans-synaptic alterations in a microfluidic-based reconstructed neuronal network. Acta Neuropathologica Communications, 2(1), 145. https://doi.org/10.1186/s40478-014-0145-3

Derecki, N. C., Cronk, J. C., Lu, Z., Xu, E., Abbott, S. B. G., Guyenet, P. G. & Kipnis, J. (2012). Wild-type microglia arrest pathology in a mouse model of Rett syndrome. Nature, 484(7392), 105–109. https://doi.org/10.1038/nature10907

Desnous, B., Beretti, T., Muller, N., Neveu, J., Villeneuve, N., Lépine, A., Daquin, G. & Milh, M. (2024). Efficacy and tolerance of cannabidiol in the treatment of epilepsy in patients with Rett syndrome. Epilepsia Open, 9(1), 397–403. https://doi.org/10.1002/epi4.12796

Ding, C., Wu, Z., Huang, L., Wang, Y., Xue, J., Chen, S., Deng, Z., Wang, L., Song, Z. & Chen, S. (2015). Mitofilin and CHCHD6 physically interact with Sam50 to sustain cristae structure. Scientific Reports, 5(1), 16064. https://doi.org/10.1038/srep16064

Distelmaier, F., Koopman, W. J. H., Heuvel, L. P. van den, Rodenburg, R. J., Mayatepek, E., Willems, P. H. G. M. & Smeitink, J. A. M. (2009). Mitochondrial complex I deficiency: from organelle dysfunction to clinical disease. Brain, 132(4), 833–842. https://doi.org/10.1093/brain/awp058

Dixon-Salazar, T. J., Silhavy, J. L., Udpa, N., Schroth, J., Bielas, S., Schaffer, A. E., Olvera, J., Bafna, V., Zaki, M. S., Abdel-Salam, G. H., Mansour, L. A., Selim, L., Abdel-Hadi, S., Marzouki, N., Ben-Omran, T., Al-Saana, N. A., Sonmez, F. M., Celep, F., Azam, M., … Gleeson, J. G. (2012). Exome Sequencing Can Improve Diagnosis and Alter Patient Management. Science Translational Medicine, 4(138), 138ra78. https://doi.org/10.1126/scitranslmed.3003544

Dotti, M. T., Manneschi, L., Malandrini, A., Stefano, N. D., Caznerale, F. & Federico, A. (1993). Mitochondrial dysfunction in Rett syndrome An ultrastructural and biochemical study. Brain and Development, 15(2), 103–106. https://doi.org/10.1016/0387-7604(93)90045-a

Dotto, V. D., Fogazza, M., Carelli, V., Rugolo, M. & Zanna, C. (2018). Eight human OPA1 isoforms, long and short: What are they for? Biochimica et Biophysica Acta (BBA) - Bioenergetics, 1859(4), 263–269. https://doi.org/10.1016/j.bbabio.2018.01.005

Douiev, L., Sheffer, R., Horvath, G. & Saada, A. (2020). Bezafibrate Improves Mitochondrial Fission and Function in DNM1L-Deficient Patient Cells. Cells, 9(2), 301. https://doi.org/10.3390/cells9020301

Douiev, L., Soiferman, D., Alban, C. & Saada, A. (2016). The Effects of Ascorbate, N-Acetylcysteine, and Resveratrol on Fibroblasts from Patients with Mitochondrial Disorders. Journal of Clinical Medicine, 6(1), 1. https://doi.org/10.3390/jcm6010001

Du, F., Nguyen, M. V. C., Karten, A., Felice, C. A., Mandel, G. & Ballas, N. (2016). Acute and crucial requirement for MeCP2 function upon transition from early to late adult stages of brain maturation. 25(9), 1690–1702. https://doi.org/10.1093/hmg/ddw038

Duarte, S. T., Armstrong, J., Roche, A., Ortez, C., Pérez, A., O'Callaghan, M. del M., Pereira, A., Sanmartí, F., Ormazábal, A., Artuch, R., Pineda, M. & García-Cazorla, A. (2013). Abnormal Expression of Cerebrospinal Fluid Cation Chloride Cotransporters in Patients with Rett Syndrome. PLoS ONE, 8(7), e68851. https://doi.org/10.1371/journal.pone.0068851

Eeg-Olofsson, O., Al-Zuhair, A. G. H., Teebi, A. S., Daoud, A. S., Zaki, M., Besisso, M. S. & Al-Essa, M. M. N. (1990). Rett Syndrome: A Mitochondrial Disease? Journal of Child Neurology, 5(3), 210–214. https://doi.org/10.1177/088307389000500311

Eeg-Olofsson, O., Al-Zuhair, A. G., Teebi, A. S. & Al-Essa, M. M. (1988). Abnormal mitochondria in the Rett syndrome. Brain and Development, 10(4), 260–262. https://doi.org/10.1016/s0387-7604(88)80010-x

Ehrhart, F., Coort, S. L. M., Cirillo, E., Smeets, E., Evelo, C. T. & Curfs, L. M. G. (2016). Rett syndrome – biological pathways leading from MECP2 to disorder phenotypes. Orphanet Journal of Rare Diseases, 11(1), 158. https://doi.org/10.1186/s13023-016-0545-5

Epifane-de-Assunção, M. C., Bispo, A. G., Ribeiro-dos-Santos, Â. & Cavalcante, G. C. (2024). Molecular Alterations in Core Subunits of Mitochondrial Complex I and Their Relation to Parkinson's Disease. Molecular Neurobiology, 1–15. https://doi.org/10.1007/s12035-024-04526-5

Esch, E. W., Bahinski, A. & Huh, D. (2015). Organs-on-chips at the frontiers of drug discovery. Nature Reviews Drug Discovery, 14(4), 248–260. https://doi.org/10.1038/nrd4539

Esch, H. V., Bauters, M., Ignatius, J., Jansen, M., Raynaud, M., Hollanders, K., Lugtenberg, D., Bienvenu, T., Jensen, L. R., Gécz, J., Moraine, C., Marynen, P., Fryns, J.-P. & Froyen, G. (2005). Duplication of the MECP2 Region Is a Frequent Cause of Severe Mental Retardation and Progressive Neurological Symptoms in Males. The American Journal of Human Genetics, 77(3), 442–453. https://doi.org/10.1086/444549

Faitg, J., Lacefield, C., Davey, T., White, K., Laws, R., Kosmidis, S., Reeve, A. K., Kandel, E. R., Vincent, A. E. & Picard, M. (2021). 3D neuronal mitochondrial morphology in axons, dendrites, and somata of the aging mouse hippocampus. Cell Reports, 36(6), 109509. https://doi.org/10.1016/j.celrep.2021.109509

Falsaperla, R., Marino, S. D., Salomone, G., Madia, F., Marino, S., Tardino, L. G., Scalia, B. & Ruggieri, M. (2023). Impressive efficacy of the ketogenic diet in a KCNQ2 encephalopathy infant: a case report and exhaustive literature review. Translational Pediatrics, 0(0), 0–0. https://doi.org/10.21037/tp-22-258

Fang, D., Yan, S., Yu, Q., Chen, D. & Yan, S. S. (2016). Mfn2 is Required for Mitochondrial Development and Synapse Formation in Human Induced Pluripotent Stem Cells/hiPSC Derived Cortical Neurons. 6(1), 31462. https://doi.org/10.1038/srep31462

Fato, R., Bergamini, C., Leoni, S., Strocchi, P. & Lenaz, G. (2008). Generation of Reactive Oxygen Species by Mitochondrial Complex I: Implications in Neurodegeneration. Neurochemical Research, 33(12), 2487–2501. https://doi.org/10.1007/s11064-008-9747-0

Fecher, C., Trovò, L., Müller, S. A., Snaidero, N., Wettmarshausen, J., Heink, S., Ortiz, O., Wagner, I., Kühn, R., Hartmann, J., Karl, R. M., Konnerth, A., Korn, T., Wurst, W., Merkler, D., Lichtenthaler, S. F., Perocchi, F. & Misgeld, T. (2019). Cell-type-specific profiling of brain mitochondria

reveals functional and molecular diversity. Nature Neuroscience, 22(10), 1731–1742. https://doi.org/10.1038/s41593-019-0479-z

Fehr, S., Wilson, M., Downs, J., Williams, S., Murgia, A., Sartori, S., Vecchi, M., Ho, G., Polli, R., Psoni, S., Bao, X., Klerk, N. de, Leonard, H. & Christodoulou, J. (2013). The CDKL5 disorder is an independent clinical entity associated with early-onset encephalopathy. European Journal of Human Genetics, 21(3), 266–273. https://doi.org/10.1038/ejhg.2012.156

Feinman, R. D., Pogozelski, W. K., Astrup, A., Bernstein, R. K., Fine, E. J., Westman, E. C., Accurso, A., Frassetto, L., Gower, B. A., McFarlane, S. I., Nielsen, J. V., Krarup, T., Saslow, L., Roth, K. S., Vernon, M. C., Volek, J. S., Wilshire, G. B., Dahlqvist, A., Sundberg, R., … Worm, N. (2015). Dietary carbohydrate restriction as the first approach in diabetes management: Critical review and evidence base. Nutrition, 31(1), 1–13. https://doi.org/10.1016/j.nut.2014.06.011

Feldman, D., Banerjee, A. & Sur, M. (2016). Developmental Dynamics of Rett Syndrome. Neural Plasticity, 2016, 1–9. https://doi.org/10.1155/2016/6154080

Felice, C. D., Ragione, F. D., Signorini, C., Leoncini, S., Pecorelli, A., Ciccoli, L., Scalabrì, F., Marracino, F., Madonna, M., Belmonte, G., Ricceri, L., Filippis, B. D., Laviola, G., Valacchi, G., Durand, T., Galano, J.-M., Oger, C., Guy, A., Bultel-Poncé, V., … D'Esposito, M. (2014). Oxidative brain damage in Mecp2-mutant murine models of Rett syndrome. Neurobiology of Disease, 68(100), 66–77. https://doi.org/10.1016/j.nbd.2014.04.006

Felice, C. D., Signorini, C., Leoncini, S., Pecorelli, A., Durand, T., Valacchi, G., Ciccoli, L. & Hayek, J. (2012). The role of oxidative stress in Rett syndrome: an overview. Annals of the New York Academy of Sciences, 1259(1), 121–135. https://doi.org/10.1111/j.1749-6632.2012.06611.x

Ferreira, M., Torraco, A., Rizza, T., Fattori, F., Meschini, M. C., Castana, C., Go, N. E., Nargang, F. E., Duarte, M., Piemonte, F., Dionisi-Vici, C., Videira, A., Vilarinho, L., Santorelli, F. M., Carrozzo, R. & Bertini, E. (2011). Progressive cavitating leukoencephalopathy associated with respiratory chain complex I deficiency and a novel mutation in NDUFS1. Neurogenetics, 12(1), 9–17. https://doi.org/10.1007/s10048-010-0265-2

Filippis, B. D., Chiodi, V., Adriani, W., Lacivita, E., Mallozzi, C., Leopoldo, M., Domenici, M. R., Fuso, A. & Laviola, G. (2015). Long-lasting beneficial effects of central serotonin receptor 7 stimulation in female mice modeling Rett syndrome. Frontiers in Behavioral Neuroscience, 9, 86. https://doi.org/10.3389/fnbeh.2015.00086

Filippis, B. D., Fabbri, A., Simone, D., Canese, R., Ricceri, L., Malchiodi-Albedi, F., Laviola, G. & Fiorentini, C. (2012). Modulation of RhoGTPases Improves the Behavioral Phenotype and Reverses Astrocytic Deficits in a Mouse Model of Rett Syndrome. Neuropsychopharmacology, 37(5), 1152–1163. https://doi.org/10.1038/npp.2011.301

Filippis, B. D., Valenti, D., Bari, L. de, Rasmo, D. D., Musto, M., Fabbri, A., Ricceri, L., Fiorentini, C., Laviola, G. & Vacca, R. A. (2015). Mitochondrial free radical overproduction due to respiratory chain impairment in the brain of a mouse model of Rett syndrome: protective effect of CNF1. Free Radical Biology and Medicine, 83, 167–177. https://doi.org/10.1016/j.freeradbiomed.2015.02.014

Filosa, S., Pecorelli, A., D'Espositoc, M., Valacchi, G. & Hajek, J. (2015). Exploring the possible link between MeCP2 and oxidative stress in Rett syndrome. Free Radical Biology and Medicine, 88(Pt A), 81–90. https://doi.org/10.1016/j.freeradbiomed.2015.04.019

Forlani, G., Giarda, E., Ala, U., Cunto, F. D., Salani, M., Tupler, R., Kilstrup-Nielsen, C. & Landsberger, N. (2010). The MeCP2/YY1 interaction regulates ANT1 expression at 4q35: novel hints for Rett syndrome pathogenesis. Human Molecular Genetics, 19(16), 3114–3123. https://doi.org/10.1093/hmg/ddq214

Francy, C. A., Clinton, R. W., Fröhlich, C., Murphy, C. & Mears, J. A. (2017). Cryo-EM Studies of Drp1 Reveal Cardiolipin Interactions that Activate the Helical Oligomer. Scientific Reports, 7(1), 10744. https://doi.org/10.1038/s41598-017-11008-3

Frega, M., Mossink, B., Linda, K., Keller, J., Schubert, D. & Kasri, N. N. (2018). Brain-on-a Chip Technologies for Investigating Neuronal Diseases: Toward Precision Medicine Applications. 2018 IEEE International Symposium on Circuits and Systems (ISCAS), 1–3. https://doi.org/10.1109/iscas.2018.8351848

Freundt, E. C., Maynard, N., Clancy, E. K., Roy, S., Bousset, L., Sourigues, Y., Covert, M., Melki, R., Kirkegaard, K. & Brahic, M. (2012). Neuron-to-neuron transmission of α-synuclein fibrils through axonal transport. Annals of Neurology, 72(4), 517–524. https://doi.org/10.1002/ana.23747

Frezza, C., Cipolat, S., Brito, O. M. de, Micaroni, M., Beznoussenko, G. V., Rudka, T., Bartoli, D., Polishuck, R. S., Danial, N. N., Strooper, B. D. & Scorrano, L. (2006). OPA1 Controls Apoptotic Cristae Remodeling Independently from Mitochondrial Fusion. Cell, 126(1), 177–189. https://doi.org/10.1016/j.cell.2006.06.025

Friedman, J. R. & Nunnari, J. (2014). Mitochondrial form and function. Nature, 505(7483), 335–343. https://doi.org/10.1038/nature12985

Fukumitsu, K., Hatsukano, T., Yoshimura, A., Heuser, J., Fujishima, K. & Kengaku, M. (2016). Mitochondrial fission protein Drp1 regulates mitochondrial transport and dendritic arborization in cerebellar Purkinje cells. Molecular and Cellular Neuroscience, 71, 56–65. https://doi.org/10.1016/j.mcn.2015.12.006

Galmiche, L., Serre, V., Beinat, M., Zossou, R., Assouline, Z., Lebre, A.-S., Chretien, F., Shenhav, R., Zeharia, A., Saada, A., Vedrenne, V., Boddaert, N., Lonlay, P. de, Rio, M., Munnich, A. & Rötig, A. (2012). Toward genotype phenotype correlations in GFM1 mutations. Mitochondrion, 12(2), 242–247. https://doi.org/10.1016/j.mito.2011.09.007

Gano, L. B., Patel, M. & Rho, J. M. (2014). Ketogenic diets, mitochondria, and neurological diseases. Journal of Lipid Research, 55(11), 2211–2228. https://doi.org/10.1194/jlr.r048975

Gerber, S., Charif, M., Chevrollier, A., Chaumette, T., Angebault, C., Kane, M. S., Paris, A., Alban, J., Quiles, M., Delettre, C., Bonneau, D., Procaccio, V., Amati-Bonneau, P., Reynier, P., Leruez, S., Calmon, R., Boddaert, N., Funalot, B., Rio, M., … Lenaers, G. (2017). Mutations in DNM1L, as in OPA1, result indominant optic atrophy despite opposite effectson mitochondrial fusion and fission. Brain, 140(10), 2586–2596. https://doi.org/10.1093/brain/awx219

Gibson, J. H., Slobedman, B., KN, H., Williamson, S. L., Minchenko, D., El-Osta, A., Stern, J. L. & Christodoulou, J. (2010). Downstream targets of methyl CpG binding protein 2 and their abnormal expression in the frontal cortex of the human Rett syndrome brain. BMC Neuroscience, 11(1), 53. https://doi.org/10.1186/1471-2202-11-53

Gimeno-Agud, H., Díaz-Osorio, Y. & Oyarzábal, A. (2025). Biological Basis of Cell Trafficking: A General Overview. Journal of Inherited Metabolic Disease, 48(1), e12839. https://doi.org/10.1002/jimd.12839

Gold, W.A., Williamson, S. L., Kaur, S., Hargreaves, I. P., Land, J. M., Pelka, G. J., Tam, P. P. L. & Christodoulou, J. (2014). Mitochondrial dysfunction in the skeletal muscle of a mouse model of Rett syndrome (RTT): Implications for the disease phenotype. Mitochondrion, 15, 10–17. https://doi.org/10.1016/j.mito.2014.02.012

Gold, Wendy A., Percy, A. K., Neul, J. L., Cobb, S. R., Pozzo-Miller, L., Issar, J. K., Ben-Zeev, B., Vignoli, A. & Kaufmann, W. E. (2024). Rett syndrome. Nature Reviews Disease Primers, 10(1), 84. https://doi.org/10.1038/s41572-024-00568-0

Goldsmith, J., Ordureau, A., Harper, J. W. & Holzbaur, E. L. F. (2022). Brain-derived autophagosome profiling reveals the engulfment of nucleoid-enriched mitochondrial fragments by basal autophagy in neurons. Neuron, 110(6), 967-976.e8. https://doi.org/10.1016/j.neuron.2021.12.029

Golse, M., Weinhofer, I., Blanco, B., Barbier, M., Yazbeck, E., Huiban, C., Chaumette, B., Pichon, B., Fatemi, A., Pascual, S., Martinell, M., Berger, J., Perlbarg, V., Galanaud, D. & Mochel, F. (2024). Leriglitazone halts disease progression in adult patients with early cerebral adrenoleukodystrophy. Brain, 147(10), 3344–3351. https://doi.org/10.1093/brain/awae169

González-Rodríguez, P., Zampese, E., Stout, K. A., Guzman, J. N., Ilijic, E., Yang, B., Tkatch, T., Stavarache, M. A., Wokosin, D. L., Gao, L., Kaplitt, M. G., López-Barneo, J., Schumacker, P. T. & Surmeier, D. J. (2021). Disruption of mitochondrial complex I induces progressive parkinsonism. Nature, 599(7886), 650–656. https://doi.org/10.1038/s41586-021-04059-0

Gorman, G. S., Chinnery, P. F., DiMauro, S., Hirano, M., Koga, Y., McFarland, R., Suomalainen, A., Thorburn, D. R., Zeviani, M. & Turnbull, D. M. (2016). Mitochondrial diseases. Nature Reviews Disease Primers, 2(1), 16080. https://doi.org/10.1038/nrdp.2016.80

Goshi, N., Girardi, G., Souza, F. da C., Gardner, A., Lein, P. J. & Seker, E. (2022). Influence of microchannel geometry on device performance and electrophysiological recording fidelity during long-term studies of connected neural populations. Lab on a Chip, 22(20), 3961–3975. https://doi.org/10.1039/d2lc00683a

Grimm, N.-B. & Lee, J. T. (2022). Selective Xi reactivation and alternative methods to restore MECP2 function in Rett syndrome. Trends in Genetics, 38(9), 920–943. https://doi.org/10.1016/j.tig.2022.01.007

Großer, E., Hirt, U., Janc, O. A., Menzfeld, C., Fischer, M., Kempkes, B., Vogelgesang, S., Manzke, T. U., Opitz, L., Salinas-Riester, G. & Müller, M. (2012). Oxidative burden and mitochondrial dysfunction in a mouse model of Rett syndrome. Neurobiology of Disease, 48(1), 102–114. https://doi.org/10.1016/j.nbd.2012.06.007

Gruetter, R. (2003). Glycogen: The forgotten cerebral energy store. Journal of Neuroscience Research, 74(2), 179–183. https://doi.org/10.1002/jnr.10785

Guo, Y., Zhang, C., Shang, F.-F., Luo, M., You, Y., Zhai, Q., Xia, Y. & Suxin, L. (2020). Ketogenic Diet Ameliorates Cardiac Dysfunction via Balancing Mitochondrial Dynamics and Inhibiting Apoptosis in Type 2 Diabetic Mice. Aging and Disease, 11(2), 229–240. https://doi.org/10.14336/ad.2019.0510

Guy, J., Cheval, H., Selfridge, J. & Bird, A. (2011). The Role of MeCP2 in the Brain. Annual Review of Cell and Developmental Biology, 27(Volume 27, 2011), 631–652. https://doi.org/10.1146/annurev-cellbio-092910-154121

Guy, J., Gan, J., Selfridge, J., Cobb, S. & Bird, A. (2007). Reversal of Neurological Defects in a Mouse Model of Rett Syndrome. Science, 315(5815), 1143–1147. https://doi.org/10.1126/science.1138389

Guy, J., Hendrich, B., Holmes, M., Martin, J. E. & Bird, A. (2001). A mouse Mecp2-null mutation causes neurological symptoms that mimic Rett syndrome. Nature Genetics, 27(3), 322–326. https://doi.org/10.1038/85899

Hagberg, B. (1995). Rett syndrome: clinical peculiarities and biological mysteries. Acta Pædiatrica, 84(9), 971–976. https://doi.org/10.1111/j.1651-2227.1995.tb13809.x

Hagberg, Bengt, Aicardi, J., Dias, K. & Ramos, O. (1983). A progressive syndrome of autism, dementia, ataxia, and loss of purposeful hand use in girls: Rett's syndrome: Report of 35 cases. Annals of Neurology, 14(4), 471–479. https://doi.org/10.1002/ana.410140412

Halbach, N. S. J., Smeets, E. E. J., Braak, N. van den, Roozendaal, K. E. P. van, Blok, R. M. J., Schrander-Stumpel, C. T. R. M., Frijns, J.-P., Maaskant, M. A. & Curfs, L. M. G. (2012). Genotype–phenotype relationships as prognosticators in Rett syndrome should be handled with care in clinical practice. American Journal of Medical Genetics Part A, 158A(2), 340–350. https://doi.org/10.1002/ajmg.a.34418

Han, T., Lv, Y., Wang, S., Hu, T., Hong, H. & Fu, Z. (2019). PPARγ overexpression regulates cholesterol metabolism in human L02 hepatocytes. Journal of Pharmacological Sciences, 139(1), 1–8. https://doi.org/10.1016/j.jphs.2018.09.013

Han, X., Shangguan, J., Wang, Z., Li, Y., Fan, J., Ren, A. & Zhao, M. (2022). Spermidine Regulates Mitochondrial Function by Enhancing eIF5A Hypusination and Contributes to Reactive Oxygen Species Production and Ganoderic Acids Biosynthesis in Ganoderma lucidum. Applied andEnvironmental Microbiology, AEM0203721. https://doi.org/10.1128/aem.02037-21

Hardan, A. Y., Fung, L. K., Libove, R. A., Obukhanych, T. V., Nair, S., Herzenberg, L. A., Frazier, T. W. & Tirouvanziam, R. (2012). A Randomized Controlled Pilot Trial of Oral N-Acetylcysteine in Children with Autism. Biological Psychiatry, 71(11), 956–961. https://doi.org/10.1016/j.biopsych.2012.01.014

Harris, J. J., Jolivet, R. & Attwell, D. (2012). Synaptic Energy Use and Supply. Neuron, 75(5), 762–777. https://doi.org/10.1016/j.neuron.2012.08.019

Hartmannová, H., Piherová, L., Tauchmannová, K., Kidd, K., Acott, P. D., Crocker, J. F. S., Oussedik, Y., Mallet, M., Hodaňová, K., Stránecký, V., Přistoupilová, A., Barešová, V., Jedličková, I., Živná, M., Sovová, J., Hůlková, H., Robins, V., Vrbacký, M., Pecina, P., … Kmoch, S. (2016). Acadian variant of Fanconi syndrome is caused by mitochondrial respiratory chain complex I deficiency due to a non-coding mutation in complex I assembly factor NDUFAF6. Human Molecular Genetics, 25(18), 4062–4079. https://doi.org/10.1093/hmg/ddw245

Hasan-Olive, M. M., Lauritzen, K. H., Ali, M., Rasmussen, L. J., Storm-Mathisen, J. & Bergersen, L. H. (2019). A Ketogenic Diet Improves Mitochondrial Biogenesis and Bioenergetics via the PGC1α-SIRT3-UCP2 Axis. Neurochemical Research, 44(1), 22–37. https://doi.org/10.1007/s11064-018-2588-6

Herculano-Houzel, S. (2009). The Human Brain in Numbers: A Linearly Scaled-up Primate Brain. Frontiers in Human Neuroscience, 3, 31. https://doi.org/10.3389/neuro.09.031.2009

Hill, R. L., Kulbe, J. R., Singh, I. N., Wang, J. A. & Hall, E. D. (2018). Synaptic Mitochondria are More Susceptible to Traumatic Brain Injury-induced Oxidative Damage and Respiratory Dysfunction than Non-synaptic Mitochondria. 386, 265–283. https://doi.org/10.1016/j.neuroscience.2018.06.028

Hirano, M., Emmanuele, V. & Quinzii, C. M. (2018). Emerging therapies for mitochondrial diseases. Essays in Biochemistry, 62(3), 467–481. https://doi.org/10.1042/ebc20170114

Hirofuji, S., Hirofuji, Y., Kato, H., Masuda, K., Yamaza, H., Sato, H., Takayama, F., Torio, M., Sakai, Y., Ohga, S., Taguchi, T. & Nonaka, K. (2018). Mitochondrial dysfunction in dopaminergic neurons differentiated from exfoliated deciduous tooth-derived pulp stem cells of a child with Rett syndrome. Biochemical and Biophysical Research Communications, 498(4), 898–904. https://doi.org/10.1016/j.bbrc.2018.03.077

Hofer, S. J., Liang, Y., Zimmermann, A., Schroeder, S., Dengjel, J., Kroemer, G., Eisenberg, T., Sigrist, S. J. & Madeo, F. (2021). Spermidine-induced hypusination preserves mitochondrial and cognitive function during aging. Autophagy, 17(8), 2037–2039. https://doi.org/10.1080/15548627.2021.1933299

Hogarth, K. A., Costford, S. R., Yoon, G., Sondheimer, N. & Maynes, J. T. (2018). DNM1L Variant Alters Baseline Mitochondrial Function and Response to Stress in a Patient with Severe Neurological Dysfunction. Biochemical Genetics, 56(1–2), 56–77. https://doi.org/10.1007/s10528-017-9829-2

Hong, N. & Nam, Y. (2022). Neurons-on-a-Chip: In Vitro NeuroTools. Molecules and Cells, 45(2), 76–83. https://doi.org/10.14348/molcells.2022.2023

Horejs, C. (2021). Organ chips, organoids and the animal testing conundrum. Nature Reviews Materials, 6(5), 372–373. https://doi.org/10.1038/s41578-021-00313-z

Huang, C., Deng, K. & Wu, M. (2023). Mitochondrial cristae in health and disease. International Journal of Biological Macromolecules, 235, 123755. https://doi.org/10.1016/j.ijbiomac.2023.123755

Huynen, M. A., Mühlmeister, M., Gotthardt, K., Guerrero-Castillo, S. & Brandt, U. (2016). Evolution and structural organization of the mitochondrial contact site (MICOS) complex and the mitochondrial intermembrane space bridging (MIB) complex. Biochimica et Biophysica Acta (BBA) - Molecular Cell Research, 1863(1), 91–101. https://doi.org/10.1016/j.bbamcr.2015.10.009

Iannielli, A., Ugolini, G. S., Cordiglieri, C., Bido, S., Rubio, A., Colasante, G., Valtorta, M., Cabassi, T., Rasponi, M. & Broccoli, V. (2019). Reconstitution of the Human Nigro-striatal Pathway on-a-Chip Reveals OPA1-Dependent Mitochondrial Defects and Loss of Dopaminergic Synapses. Cell Reports, 29(13), 4646-4656.e4. https://doi.org/10.1016/j.celrep.2019.11.111

Illescas, S., Diaz-Osorio, Y., Serradell, A., Toro-Soria, L., Musokhranova, U., Juliá-Palacios, N., Ribeiro-Constante, J., Altafaj, X., Olivella, M., O'Callaghan, M., Darling, A., Armstrong, J., Artuch, R., García-Cazorla, À. & Oyarzábal, A. (2023). Metabolic characterization of neurogenetic disorders involving glutamatergic neurotransmission. Journal of Inherited Metabolic Disease. https://doi.org/10.1002/jimd.12689

Inak, G., Rybak-Wolf, A., Lisowski, P., Pentimalli, T. M., Jüttner, R., Glažar, P., Uppal, K., Bottani, E., Brunetti, D., Secker, C., Zink, A., Meierhofer, D., Henke, M.-T., Dey, M., Ciptasari, U., Mlody, B., Hahn, T., Berruezo-Llacuna, M., Karaiskos, N., … Prigione, A. (2021). Defective metabolic programming impairs early neuronal morphogenesis in neural cultures and an organoid model of Leigh syndrome. Nature Communications, 12(1), 1929. https://doi.org/10.1038/s41467-021-22117-z

Ingber, D. E. (2022). Human organs-on-chips for disease modelling, drug development and personalized medicine. Nature Reviews Genetics, 23(8), 467–491. https://doi.org/10.1038/s41576-022-00466-9

Ioannou, M. S., Jackson, J., Sheu, S.-H., Chang, C.-L., Weigel, A. V., Liu, H., Pasolli, H. A., Xu, C. S., Pang, S., Matthies, D., Hess, H. F., Lippincott-Schwartz, J. & Liu, Z. (2019). Neuron-Astrocyte Metabolic Coupling Protects against Activity-Induced Fatty Acid Toxicity. Cell, 177(6), 1522-1535.e14. https://doi.org/10.1016/j.cell.2019.04.001

Ip, J. P. K., Mellios, N. & Sur, M. (2018). Rett syndrome: insights into genetic, molecular and circuit mechanisms. Nature Reviews Neuroscience, 19(6), 368–382. https://doi.org/10.1038/s41583-018-0006-3

Ip, P., Ho, F. K. W., Rao, N., Sun, J., Young, M. E., Chow, C. B., Tso, W. & Hon, K. L. (2017). Impact of nutritional supplements on cognitive development of children in developing countries: A meta-analysis. Scientific Reports, 7(1), 10611. https://doi.org/10.1038/s41598-017-11023-4

Iuso, A., Scacco, S., Piccoli, C., Bellomo, F., Petruzzella, V., Trentadue, R., Minuto, M., Ripoli, M., Capitanio, N., Zeviani, M. & Papa, S. (2006). Dysfunctions of Cellular Oxidative Metabolism in Patients with Mutations in the NDUFS1 and NDUFS4 Genes of Complex I*. Journal of Biological Chemistry, 281(15), 10374–10380. https://doi.org/10.1074/jbc.m513387200

Janc, O. A., Hüser, M. A., Dietrich, K., Kempkes, B., Menzfeld, C., Hülsmann, S. & Müller, M. (2016). Systemic Radical Scavenger Treatment of a Mouse Model of Rett Syndrome: Merits and Limitations of the Vitamin E Derivative Trolox. Frontiers in Cellular Neuroscience, 10, 266. https://doi.org/10.3389/fncel.2016.00266

Janc, O. A. & Müller, M. (2014). The free radical scavenger Trolox dampens neuronal hyperexcitability, reinstates synaptic plasticity, and improves hypoxia tolerance in a mouse model of Rett syndrome. Frontiers in Cellular Neuroscience, 8, 56. https://doi.org/10.3389/fncel.2014.00056

Jang, S., Nelson, J. C., Bend, E. G., Rodríguez-Laureano, L., Tueros, F. G., Cartagenova, L., Underwood, K., Jorgensen, E. M. & Colón-Ramos, D. A. (2016). Glycolytic Enzymes Localize to Synapses under Energy Stress to Support Synaptic Function. Neuron, 90(2), 278–291. https://doi.org/10.1016/j.neuron.2016.03.011

Jayatunga, D. P. W., Hone, E., Khaira, H., Lunelli, T., Singh, H., Guillemin, G. J., Fernando, B., Garg, M. L., Verdile, G. & Martins, R. N. (2021). Therapeutic Potential of Mitophagy-Inducing Microflora Metabolite, Urolithin A for Alzheimer's Disease. Nutrients, 13(11), 3744. https://doi.org/10.3390/nu13113744

Jian, L., Nagarajan, L., Klerk, N. de, Ravine, D., Christodoulou, J. & Leonard, H. (2007). Seizures in Rett syndrome: An overview from a one-year calendar study. European Journal of Paediatric Neurology, 11(5), 310–317. https://doi.org/10.1016/j.ejpn.2007.02.008

Jin, L.-W., Horiuchi, M., Wulff, H., Liu, X.-B., Cortopassi, G. A., Erickson, J. D. & Maezawa, I. (2015). Dysregulation of Glutamine Transporter SNAT1 in Rett Syndrome Microglia: A Mechanism for Mitochondrial Dysfunction and Neurotoxicity. The Journal of Neuroscience, 35(6), 2516–2529. https://doi.org/10.1523/jneurosci.2778-14.2015

Jiruska, P., Freestone, D., Gnatkovsky, V. & Wang, Y. (2023). An update on the seizures beget seizures theory. Epilepsia, 64(S3), S13–S24. https://doi.org/10.1111/epi.17721

Johnson, S. C., Yanos, M., Sangesland, M., Bitto, A., Castanza, A., Gagnidze, A., Cordoba, J., Gonzalez, B., Gupta, K., Hui, J., Jarvie, C., Johnson, B., Letexier, N., McCanta, L., Tamis, O., Van-Den-Ende, A., Uhde, L., Rabinovitch, P., Suh, Y. & Kaeberlein, M. (2015). Dose-dependent effects of mTOR inhibition on weight and mitochondrial disease in mice. Frontiers in Genetics, 6. https://doi.org/10.3389/fgene.2015.00247

Joseph, X., Akhil, V., Arathi, A. & Mohanan, PV. (2022). Comprehensive Development in Organ-On-A-Chip Technology. Journal of Pharmaceutical Sciences, 111(1), 18–31. https://doi.org/10.1016/j.xphs.2021.07.014

Justice, M. J., Buchovecky, C. M., Kyle, S. M. & Djukic, A. (2014). A role for metabolism in Rett syndrome pathogenesis. Rare Diseases, 1(1), e27265. https://doi.org/10.4161/rdis.27265

Kaddoum, L., Panayotis, N., Mazarguil, H., Giglia-Mari, G., Roux, J. & Joly, E. (2013). Isoform-specific anti-MeCP2 antibodies confirm that expression of the e1 isoform strongly predominates in the brain. 2. https://doi.org/10.12688/f1000research.2-204.v1

Kahanovitch, U., Cuddapah, V. A., Pacheco, N. L., Holt, L. M., Mulkey, D. K., Percy, A. K. & Olsen, M. L. (n.d.). MeCP2 Deficiency Leads to Loss of Glial Kir4.1. Eneuro, 5(1), ENEURO.0194-17.2018. https://doi.org/10.1523/eneuro.0194-17.2018

Kahanovitch, U., Patterson, K. C., Hernandez, R. & Olsen, M. L. (2019). Glial Dysfunction in MeCP2 Deficiency Models: Implications for Rett Syndrome. International Journal of Molecular Sciences, 20(15). https://doi.org/10.3390/ijms20153813

Kalia, R., Wang, R. Y.-R., Yusuf, A., Thomas, P. V., Agard, D. A., Shaw, J. M. & Frost, A. (2018). Structural basis of mitochondrial receptor binding and constriction by DRP1. Nature, 558(7710), 401–405. https://doi.org/10.1038/s41586-018-0211-2

Kamudzandu, M., Köse-Dunn, M., Evans, M. G., Fricker, R. A. & Roach, P. (2019). A micro-fabricated in vitro complex neuronal circuit platform. Biomedical Physics & Engineering Express, 5(4), 045016. https://doi.org/10.1088/2057-1976/ab2307

Kapel, A., Kovacic, T., Kos, N. & Velnar, T. (2022). Impact of a 12-month multifaceted neurological physiotherapy intervention on gross motor function in women with Rett syndrome. JIN, 21(2), 59-null. https://doi.org/10.31083/j.jin2102059

Kasischke, K. (2011). Lactate Fuels the Neonatal Brain. Frontiers in Neuroenergetics, 3. https://doi.org/10.3389/fnene.2011.00004

Kaufmann, W. E., Luu, S. & Budimirovic, D. B. (2025). Drug Treatments for Neurodevelopmental Disorders: Targeting Signaling Pathways and Homeostasis. Current Neurology and Neuroscience Reports, 25(1), 7. https://doi.org/10.1007/s11910-024-01394-3

Kaufmann, W. E., Sprouse, J., Rebowe, N., Hanania, T., Klamer, D. & Missling, C. U. (2019). ANAVEX®2-73 (blarcamesine), a Sigma-1 receptor agonist, ameliorates neurologic impairments in a mouse model of Rett syndrome. 187, 172796. https://doi.org/10.1016/j.pbb.2019.172796

Kerr, D. S. (2013). Review of Clinical Trials for Mitochondrial Disorders: 1997–2012. Neurotherapeutics, 10(2), 307–319. https://doi.org/10.1007/s13311-013-0176-7

Khacho, M., Clark, A., Svoboda, D. S., Azzi, J., MacLaurin, J. G., Meghaizel, C., Sesaki, H., Lagace, D. C., Germain, M., Harper, M.-E., Park, D. S. & Slack, R. S. (2016). Mitochondrial Dynamics Impacts Stem Cell Identity and Fate Decisions by Regulating a Nuclear Transcriptional Program. Cell Stem Cell, 19(2), 232–247. https://doi.org/10.1016/j.stem.2016.04.015

Khacho, M., Clark, A., Svoboda, D. S., MacLaurin, J. G., Lagace, D. C., Park, D. S. & Slack, R. S. (2017). Mitochondrial dysfunction underlies cognitive defects as a result of neural stem cell depletion and impaired neurogenesis. 26(17), 3327–3341. https://doi.org/10.1093/hmg/ddx217

Khacho, M. & Slack, R. S. (2018). Mitochondrial dynamics in the regulation of neurogenesis: From development to the adult brain. Developmental Dynamics, 247(1), 47–53. https://doi.org/10.1002/dvdy.24538

Khairova, R. A., Machado-Vieira, R., Du, J. & Manji, H. K. (2009). A potential role for pro-inflammatory cytokines in regulating synaptic plasticity in major depressive disorder. International Journal of Neuropsychopharmacology, 12(4), 561–578. https://doi.org/10.1017/s1461145709009924

Khan, H. A. (2003). Bioluminometric assay of ATP in mouse brain: Determinant factors for enhanced test sensitivity. Journal of Biosciences, 28(4), 379–382. https://doi.org/10.1007/bf02705114

Khoury, E. S., Patel, R. V., O'Ferrall, C., Fowler, A., Sah, N., Sharma, A., Gupta, S., Scafidi, S., Kurtz, J. S., Olmstead, S. J., Kudchadkar, S. R., Kannan, R. M., Blue, M. E. & Kannan, S. (2024). Dendrimer nanotherapy targeting of glial dysfunction improves inflammation and neurobehavioral phenotype in adult female Mecp2-heterozygous mouse model of Rett syndrome. Journal of Neurochemistry, 168(5), 841–854. https://doi.org/10.1111/jnc.15960

Kiaei, M., Kipiani, K., Chen, J., Calingasan, N. Y. & Beal, M. F. (2005). Peroxisome proliferator-activated receptor-gamma agonist extends survival in transgenic mouse model of amyotrophic lateral sclerosis. Experimental Neurology, 191(2), 331–336. https://doi.org/10.1016/j.expneurol.2004.10.007

Kim, J., Lee, J. & Jang, D.-H. (2022). NDUFAF6-Related Leigh Syndrome Caused by Rare Pathogenic Variants: A Case Report and the Focused Review of Literature. Frontiers in Pediatrics, 10, 812408. https://doi.org/10.3389/fped.2022.812408

Kirby, D. M., Crawford, M., Cleary, M. A., Dahl, H.-H. M., Dennett, X. & Thorburn, D. R. (1999). Respiratory chain complex I deficiency: An underdiagnosed energy generation disorder. Neurology, 52(6), 1255–1255. https://doi.org/10.1212/wnl.52.6.1255

Kleele, T., Rey, T., Winter, J., Zaganelli, S., Mahecic, D., Lambert, H. P., Ruberto, F. P., Nemir, M., Wai, T., Pedrazzini, T. & Manley, S. (2021). Distinct fission signatures predict mitochondrial degradation or biogenesis. Nature, 593(7859), 435–439. https://doi.org/10.1038/s41586-021-03510-6

Korobova, F., Ramabhadran, V. & Higgs, H. N. (2013). An Actin-Dependent Step in Mitochondrial Fission Mediated by the ER-Associated Formin INF2. Science, 339(6118), 464–467. https://doi.org/10.1126/science.1228360

Kriaucionis, S. & Bird, A. (2004). The major form of MeCP2 has a novel N-terminus generated by alternative splicing. 32(5), 1818–1823. https://doi.org/10.1093/nar/gkh349

Kriaucionis, S., Paterson, A., Curtis, J., Guy, J., MacLeod, N. & Bird, A. (2006). Gene Expression Analysis Exposes Mitochondrial Abnormalities in a Mouse Model of Rett Syndrome. Molecular and Cellular Biology, 26(13), 5033–5042. https://doi.org/10.1128/mcb.01665-05

Krishnan, K. C., Kurt, Z., Barrere-Cain, R., Sabir, S., Das, A., Floyd, R., Vergnes, L., Zhao, Y., Che, N., Charugundla, S., Qi, H., Zhou, Z., Meng, Y., Pan, C., Seldin, M. M., Norheim, F., Hui, S., Reue, K., Lusis, A. J. & Yang, X. (2018). Integration of Multi-omics Data from Mouse Diversity Panel Highlights Mitochondrial Dysfunction in Non-alcoholic Fatty Liver Disease. Cell Systems, 6(1), 103-115.e7. https://doi.org/10.1016/j.cels.2017.12.006

Kuznetsov, A. V., Hermann, M., Saks, V., Hengster, P. & Margreiter, R. (2009). The cell-type specificity of mitochondrial dynamics. Mitochondrial Dynamics and Function in Biology and Medicine, 41(10), 1928–1939. https://doi.org/10.1016/j.biocel.2009.03.007

Kuzniewska, B., Cysewski, D., Wasilewski, M., Sakowska, P., Milek, J., Kulinski, T. M., Winiarski, M., Kozielewicz, P., Knapska, E., Dadlez, M., Chacinska, A., Dziembowski, A. & Dziembowska, M. (2020). Mitochondrial protein biogenesis in the synapse is supported by local translation. EMBO Reports, 21(8), e48882. https://doi.org/10.15252/embr.201948882

Kyle, S. M., Vashi, N. & Justice, M. J. (2018). Rett syndrome: a neurological disorder with metabolic components. Open Biology, 8(2), 170216. https://doi.org/10.1098/rsob.170216

Lagger, S., Connelly, J. C., Schweikert, G., Webb, S., Selfridge, J., Ramsahoye, B. H., Yu, M., He, C., Sanguinetti, G., Sowers, L. C., Walkinshaw, M. D. & Bird, A. (n.d.). MeCP2 recognizes cytosine methylated tri-nucleotide and di-nucleotide sequences to tune transcription in the mammalian brain. PLOS Genetics, 13(5), e1006793. https://doi.org/10.1371/journal.pgen.1006793

Landes, T., Emorine, L. J., Courilleau, D., Rojo, M., Belenguer, P. & Arnauné-Pelloquin, L. (2010). The BH3-only Bnip3 binds to the dynamin Opa1 to promote mitochondrial fragmentation and apoptosis by distinct mechanisms. EMBO Reports, 11(6), 459-465–465. https://doi.org/10.1038/embor.2010.50

Lassus, B., Naudé, J., Faure, P., Guedin, D., Boxberg, Y. V., Cour, C. M. la, Millan, M. J. & Peyrin, J.-M. (2018). Glutamatergic and dopaminergic modulation of cortico-striatal circuits probed by dynamic calcium imaging of networks reconstructed in microfluidic chips. Scientific Reports, 8(1), 17461. https://doi.org/10.1038/s41598-018-35802-9

Lax, N. Z., Hepplewhite, P. D., Reeve, A. K., Nesbitt, V., McFarland, R., Jaros, E., Taylor, R. W. & Turnbull, D. M. (2012). Cerebellar Ataxia in Patients With Mitochondrial DNA Disease: A Molecular Clinicopathological Study. Journal of Neuropathology & Experimental Neurology, 71(2), 148–161. https://doi.org/10.1097/nen.0b013e318244477d

Lee, I.-C. & Chiang, K.-L. (2021). Clinical Diagnosis and Treatment of Leigh Syndrome Based on SURF1: Genotype and Phenotype. Antioxidants, 10(12), 1950. https://doi.org/10.3390/antiox10121950

Lees, R. M., Johnson, J. D. & Ashby, M. C. (2020). Presynaptic Boutons That Contain Mitochondria Are More Stable. Frontiers in Synaptic Neuroscience, 11. https://doi.org/10.3389/fnsyn.2019.00037

Leesnitzer, L. M., Parks, D. J., Bledsoe, R. K., Cobb, J. E., Collins, J. L., Consler, T. G., Davis, R. G., Hull-Ryde, E. A., Lenhard, J. M., Patel, L., Plunket, K. D., Shenk, J. L., Stimmel, J. B., Therapontos, C., Willson, T. M. & Blanchard, S. G. (2002). Functional Consequences of Cysteine Modification in the Ligand Binding Sites of Peroxisome Proliferator Activated Receptors by GW9662. Biochemistry, 41(21), 6640–6650. https://doi.org/10.1021/bi0159581

Lefebvre, A. E. Y. T., Ma, D., Kessenbrock, K., Lawson, D. A. & Digman, M. A. (2021). Automated segmentation and tracking of mitochondria in live-cell time-lapse images. Nature Methods, 18(9), 1091–1102. https://doi.org/10.1038/s41592-021-01234-z

Lehrke, M. & Lazar, M. A. (2005). The Many Faces of PPARγ. Cell, 123(6), 993–999. https://doi.org/10.1016/j.cell.2005.11.026

Lenoir, S., Genoux, A., Agasse, F., Saudou, F. & Humbert, S. (2021). Recreating mouse cortico-hippocampal neuronal circuit in microfluidic devices to study BDNF axonal transport upon glucocorticoid treatment. STAR Protocols, 2(1), 100382. https://doi.org/10.1016/j.xpro.2021.100382

Leonard, H., Cobb, S. & Downs, J. (2017). Clinical and biological progress over 50 years in Rett syndrome. Nature Reviews Neurology, 13(1), 37–51. https://doi.org/10.1038/nrneurol.2016.186

Leoncini, S., Felice, C. D., Signorini, C., Pecorelli, A., Durand, T., Valacchi, G., Ciccoli, L. & Hayek, J. (2013). Oxidative stress in Rett syndrome: Natural history, genotype, and variants. Redox Report, 16(4), 145–153. https://doi.org/10.1179/1351000211y.0000000004

Leoncini, S., Felice, C. D., Signorini, C., Zollo, G., Cortelazzo, A., Durand, T., Galano, J.-M., Guerranti, R., Rossi, M., Ciccoli, L. & Hayek, J. (2015). Cytokine Dysregulation in MECP2- and CDKL5-Related Rett Syndrome: Relationships with Aberrant Redox Homeostasis, Inflammation, and ω-3 PUFAs. Oxidative Medicine and Cellular Longevity, 2015, 1–18. https://doi.org/10.1155/2015/421624

Li, G., Zhou, J., Budhraja, A., Hu, X., Chen, Y., Cheng, Q., Liu, L., Zhou, T., Li, P., Liu, E. & Gao, N. (2014). Mitochondrial translocation and interaction of cofilin and Drp1 are required for erucin-induced mitochondrial fission and apoptosis. Oncotarget, 6(3), 1834–1849. https://doi.org/10.18632/oncotarget.2795

Li, W. (2022). Excitation and Inhibition Imbalance in Rett Syndrome. Frontiers in Neuroscience, 16. https://doi.org/10.3389/fnins.2022.825063

Li, W. & Pozzo-Miller, L. (2012). Beyond Widespread Mecp2 Deletions to Model Rett Syndrome: Conditional Spatio-Temporal Knockout, Single-Point Mutations and Transgenic Rescue Mice. Autism- Open Access, 01(S1), 5. https://doi.org/10.4172/2165-7890.s1-005

Li, W. & Pozzo-Miller, L. (2014). BDNF deregulation in Rett syndrome. Neuropharmacology, 76, 737–746. https://doi.org/10.1016/j.neuropharm.2013.03.024

Li, Y., Wang, H., Muffat, J., Cheng, A. W., Orlando, D. A., Lovén, J., Kwok, S., Feldman, D. A., Bateup, H. S., Gao, Q., Hockemeyer, D., Mitalipova, M., Lewis, C. A., Vander Heiden, M. G., Sur, M., Young, R. A. & Jaenisch, R. (2013). Global Transcriptional and Translational Repression in Human-Embryonic-Stem-Cell-Derived Rett Syndrome Neurons. Cell Stem Cell, 13(4), 446–458. https://doi.org/10.1016/j.stem.2013.09.001

Li, Z., Okamoto, K.-I., Hayashi, Y. & Sheng, M. (2004). The Importance of Dendritic Mitochondria in the Morphogenesis and Plasticity of Spines and Synapses. Cell, 119(6), 873–887. https://doi.org/10.1016/j.cell.2004.11.003

Liang, Y., Piao, C., Beuschel, C. B., Toppe, D., Kollipara, L., Bogdanow, B., Maglione, M., Lützkendorf, J., See, J. C. K., Huang, S., Conrad, T. O. F., Kintscher, U., Madeo, F., Liu, F., Sickmann, A. & Sigrist, S. J. (2021). eIF5A hypusination, boosted by dietary spermidine, protects from premature brain aging and mitochondrial dysfunction. Cell Reports, 35(2), 108941. https://doi.org/10.1016/j.celrep.2021.108941

Liebhaber, G. M., Riemann, E. & Baumeister, F. A. M. (2003). Ketogenic Diet in Rett Syndrome. Journal of Child Neurology, 18(1), 74–75. https://doi.org/10.1177/08830738030180011801

Liesa, M. & Shirihai, O. S. (2013). Mitochondrial Dynamics in the Regulation of Nutrient Utilization and Energy Expenditure. Cell Metabolism, 17(4), 491–506. https://doi.org/10.1016/j.cmet.2013.03.002

Liotta, A., Loroch, S., Wallach, I., Klewe, K., Marcus, K. & Berndt, N. (2024). Metabolic Adaptation in Epilepsy: From Acute Response to Chronic Impairment. International Journal of Molecular Sciences, 25(17), 9640. https://doi.org/10.3390/ijms25179640

Lioy, D. T., Garg, S. K., Monaghan, C. E., Raber, J., Foust, K. D., Kaspar, B. K., Hirrlinger, P. G., Kirchhoff, F., Bissonnette, J. M., Ballas, N. & Mandel, G. (2011). A role for glia in the progression of Rett's syndrome. 475(7357), 497–500. https://doi.org/10.1038/nature10214

Livide, G., Patriarchi, T., Amenduni, M., Amabile, S., Yasui, D., Calcagno, E., Rizzo, C. L., Falco, G. D., Ulivieri, C., Ariani, F., Mari, F., Mencarelli, M. A., Hell, J. W., Renieri, A. & Meloni, I. (2015). GluD1 is a common altered player in neuronal differentiation from both MECP2-mutated and CDKL5-mutated iPS cells. 23(2), 195–201. https://doi.org/10.1038/ejhg.2014.81

Liyanage, V. R. B. & Rastegar, M. (2014). Rett Syndrome and MeCP2. NeuroMolecular Medicine, 16(2), 231–264. https://doi.org/10.1007/s12017-014-8295-9

Longo, F., Benedetti, S., Zambon, A. A., Sora, M. G. N., Resta, C. D., Ritis, D. D., Quattrini, A., Maltecca, F., Ferrari, M. & Previtali, S. C. (2020). Impaired turnover of hyperfused mitochondria in severe axonal neuropathy due to a novel DRP1 mutation. Human Molecular Genetics, 29(2), 177–188. https://doi.org/10.1093/hmg/ddz211

Lopes, A. G., Loganathan, S. K. & Caliaperumal, J. (2024). Rett Syndrome and the Role of MECP2: Signaling to Clinical Trials. Brain Sciences, 14(2), 120. https://doi.org/10.3390/brainsci14020120

Lopez, A. M., Chuang, J.-C., Posey, K. S. & Turley, S. D. (2017). Suppression of brain cholesterol synthesis in male Mecp2-deficient mice is age dependent and not accompanied by a concurrent change in the rate of fatty acid synthesis. Brain Research, 1654(Pt A), 77–84. https://doi.org/10.1016/j.brainres.2016.10.021

Low, L. A., Mummery, C., Berridge, B. R., Austin, C. P. & Tagle, D. A. (2021). Organs-on-chips: into the next decade. Nature Reviews Drug Discovery, 20(5), 345–361. https://doi.org/10.1038/s41573-020-0079-3

Lozovaya, N., Nardou, R., Tyzio, R., Chiesa, M., Pons-Bennaceur, A., Eftekhari, S., Bui, T.-T., Billon-Grand, M., Rasero, J., Bonifazi, P., Guimond, D., Gaiarsa, J.-L., Ferrari, D. C. & Ben-Ari, Y. (2019). Early alterations in a mouse model of Rett syndrome: the GABA developmental shift is abolished at birth. Scientific Reports, 9(1), 9276. https://doi.org/10.1038/s41598-019-45635-9

Luikenhuis, S., Giacometti, E., Beard, C. F. & Jaenisch, R. (2004). Expression of MeCP2 in postmitotic neurons rescues Rett syndrome in mice. Proceedings of the National Academy of Sciences, 101(16), 6033–6038. https://doi.org/10.1073/pnas.0401626101

Luján, L. M. L., McCarty, M. F., Nicolantonio, J. J. D., Ruiz, J. C. G., Rosas-Burgos, E. C., Plascencia-Jatomea, M. & Assanga, S. B. I. (2022). Nutraceuticals/Drugs Promoting Mitophagy and Mitochondrial Biogenesis May Combat the Mitochondrial Dysfunction Driving Progression of Dry Age-Related Macular Degeneration. Nutrients, 14(9), 1985. https://doi.org/10.3390/nu14091985

Lund, T. M., Risa, Ø., Sonnewald, U., Schousboe, A. & Waagepetersen, H. S. (2009). Availability of neurotransmitter glutamate is diminished when β-hydroxybutyrate replaces glucose in cultured neurons. Journal of Neurochemistry, 110(1), 80–91. https://doi.org/10.1111/j.1471-4159.2009.06115.x

Lust, W. D., Pundik, S., Zechel, J., Zhou, Y., Buczek, M. & Selman, W. R. (2003). Changing Metabolic and Energy Profiles in Fetal, Neonatal, and Adult Rat Brain. 18(3), 195–206. https://doi.org/10.1023/a:1025503115837

Ly, C. V. & Verstreken, P. (2006). Mitochondria at the Synapse. The Neuroscientist, 12(4), 291–299. https://doi.org/10.1177/1073858406287661

Lykken, E. A., Shyng, C., Edwards, R. J., Rozenberg, A. & Gray, S. J. (2018). Recent progress and considerations for AAV gene therapies targeting the central nervous system. 10(1), 16. https://doi.org/10.1186/s11689-018-9234-0

Lyst, M. J., Ekiert, R., Ebert, D. H., Merusi, C., Nowak, J., Selfridge, J., Guy, J., Kastan, N. R., Robinson, N. D., Alves, F. de L., Rappsilber, J., Greenberg, M. E. & Bird, A. (2013). Rett syndrome mutations abolish the interaction of MeCP2 with the NCoR/SMRT co-repressor. Nature Neuroscience, 16(7), 898–902. https://doi.org/10.1038/nn.3434

Ma, C., Peng, Y., Li, H. & Chen, W. (2021). Organ-on-a-Chip: A New Paradigm for Drug Development. Trends in Pharmacological Sciences, 42(2), 119–133. https://doi.org/10.1016/j.tips.2020.11.009

Madeo, F., Eisenberg, T., Pietrocola, F. & Kroemer, G. (2018). Spermidine in health and disease. Science, 359(6374). https://doi.org/10.1126/science.aan2788

Maezawa, I. & Jin, L.-W. (2010). Rett Syndrome Microglia Damage Dendrites and Synapses by the Elevated Release of Glutamate. The Journal of Neuroscience, 30(15), 5346–5356. https://doi.org/10.1523/jneurosci.5966-09.2010

Maezawa, I., Swanberg, S., Harvey, D., LaSalle, J. M. & Jin, L.-W. (n.d.). Rett Syndrome Astrocytes Are Abnormal and Spread MeCP2 Deficiency through Gap Junctions. The Journal of Neuroscience, 29(16), 5051. https://doi.org/10.1523/jneurosci.0324-09.2009

Mancini, J., Dubus, J.-C., Jouve, E., Roux, J.-C., Franco, P., Lagrue, E., Castelnau, P., Cances, C., Chaix, Y., Rougeot-Jung, C., Cornu, C., Desportes, V., Vallée, L., Bahi-Buisson, N., Truillet, R., Attolini, L., Villard, L., Blin, O. & Micallef, J. (2018). Effect of desipramine on patients with breathing disorders in RETT syndrome. Annals of Clinical and Translational Neurology, 5(2), 118–127. https://doi.org/10.1002/acn3.468

Mandal, S., Lindgren, A. G., Srivastava, A. S., Clark, A. T. & Banerjee, U. (2011). Mitochondrial Function Controls Proliferation and Early Differentiation Potential of Embryonic Stem Cells. 29(3), 486–495. https://doi.org/10.1002/stem.590

Manrique, J. F. M., Voit, P. R., Windsor, K. E., Karla, A. R., Rodriguez, S. R. & Beaudoin, G. M. J. (2021). SynapseJ: An Automated, Synapse Identification Macro for ImageJ. Frontiers in Neural Circuits, 15, 731333. https://doi.org/10.3389/fncir.2021.731333

Mao, Y., Evans, E. E., Mishra, V., Balch, L., Eberhardt, A., Zauderer, M. & Gold, W. A. (2021). Anti-Semaphorin 4D Rescues Motor, Cognitive, and Respiratory Phenotypes in a Rett Syndrome Mouse Model. International Journal of Molecular Sciences, 22(17), 9465. https://doi.org/10.3390/ijms22179465

Marballi, K. & MacDonald, J. L. (2021). Proteomic and transcriptional changes associated with MeCP2 dysfunction reveal nodes for therapeutic intervention in Rett syndrome. Neurochemistry International, 148, 105076. https://doi.org/10.1016/j.neuint.2021.105076

Marchi, S., Guilbaud, E., Tait, S. W. G., Yamazaki, T. & Galluzzi, L. (2022). Mitochondrial control of inflammation. Nature Reviews Immunology, 1–15. https://doi.org/10.1038/s41577-022-00760-x

Marshall, R. A., Luchkanych, A. M. S., Morton, J. S., Boyes, N. G., Zhai, A., Marciniuk, D. D., Mei, Y., Allison, E. Y., Shoemaker, J. K., Al-Khazraji, B. K., Allen, M. D., Tomczak, C. R. & Olver, T. D. (2022). Cerebral haemodynamics during arrhythmia in health, ischaemic heart disease and heart failure with reduced ejection fraction, and in a preclinical swine model. The Journal of Physiology, 600(10), 2311–2325. https://doi.org/10.1113/jp283112

Mattson, M. P., Gleichmann, M. & Cheng, A. (2008). Mitochondria in Neuroplasticity and Neurological Disorders. Neuron, 60(5), 748–766. https://doi.org/10.1016/j.neuron.2008.10.010

Mattson, M. P. & Partin, J. (1999). Evidence for mitochondrial control of neuronal polarity. Journal of Neuroscience Research, 56(1), 8–20. https://doi.org/10.1002/(sici)1097-4547(19990401)56:1<8::aid-jnr2>3.0.co;2-g

Maunakea, A. K., Chepelev, I., Cui, K. & Zhao, K. (2013). Intragenic DNA methylation modulates alternative splicing by recruiting MeCP2 to promote exon recognition. Cell Research, 23(11), 1256–1269. https://doi.org/10.1038/cr.2013.110

McCarty, M. F. (2022). Nutraceutical and Dietary Strategies for Up-Regulating Macroautophagy. International Journal of Molecular Sciences, 23(4), 2054. https://doi.org/10.3390/ijms23042054

McFarland, R., Taylor, R. W. & Turnbull, D. M. (2010). A neurological perspective on mitochondrial disease. The Lancet Neurology, 9(8), 829–840. https://doi.org/10.1016/s1474-4422(10)70116-2

McGraw, C., Samaco, R. & Zoghbi, H. (2011). Adult Neural Function Requires MeCP2. 333, 186–186. https://doi.org/10.1126/science.1206593

McKenzie, M., Tucker, E. J., Compton, A. G., Lazarou, M., George, C., Thorburn, D. R. & Ryan, M. T. (2011). Mutations in the Gene Encoding C8orf38 Block Complex I Assembly by Inhibiting Production of the Mitochondria-Encoded Subunit ND1. Journal of Molecular Biology, 414(3), 413–426. https://doi.org/10.1016/j.jmb.2011.10.012

Meira, I. D., Romão, T. T., Prado, H. J. P. do, Krüger, L. T., Pires, M. E. P. & Conceição, P. O. da. (2019). Ketogenic Diet and Epilepsy: What We Know So Far. Frontiers in Neuroscience, 13, 5. https://doi.org/10.3389/fnins.2019.00005

Meredith, R. M., Dawitz, J. & Kramvis, I. (2012). Sensitive time-windows for susceptibility in neurodevelopmental disorders. Trends in Neurosciences, 35(6), 335–344. https://doi.org/10.1016/j.tins.2012.03.005

Messerer, J., Wrede, C., Schipke, J., Brandenberger, C., Abdellatif, M., Eisenberg, T., Madeo, F., Sedej, S. & Mühlfeld, C. (2021). Spermidine supplementation influences mitochondrial number and morphology in the heart of aged mice. Journal of Anatomy. https://doi.org/10.1111/joa.13618

Michele, F. di, Luchetti, S., Bernardi, G., Romeo, E. & Longone, P. (2013). Neurosteroid and neurotransmitter alterations in Parkinson's disease. Frontiers in Neuroendocrinology, 34(2), 132–142. https://doi.org/10.1016/j.yfrne.2013.03.001

Miliotou, A. N., Foltopoulou, P. F., Ingendoh-Tsakmakidis, A., Tsiftsoglou, A. S., Vizirianakis, I. S., Pappas, I. S. & Papadopoulou, L. C. (2023). Protein Transduction Domain-Mediated Delivery of Recombinant Proteins and In Vitro Transcribed mRNAs for Protein Replacement Therapy of Human Severe Genetic Mitochondrial Disorders: The Case of Sco2 Deficiency. Pharmaceutics, 15(1), 286. https://doi.org/10.3390/pharmaceutics15010286

Mishra, P. & Chan, D. C. (2016). Metabolic regulation of mitochondrial dynamics. Journal of Cell Biology, 212(4), 379–387. https://doi.org/10.1083/jcb.201511036

Monrós, E., Armstrong, J., Aibar, E., Poo, P., Canós, I. & Pineda, M. (2001). Rett syndrome in Spain: mutation analysis and clinical correlations. Brain and Development, 23, S251–S253. https://doi.org/10.1016/s0387-7604(01)00374-6

Monteggia, L. M. & Kavalali, E. T. (2009). Rett Syndrome and the Impact of MeCP2 Associated Transcriptional Mechanisms on Neurotransmission. Biological Psychiatry, 65(3), 204–210. https://doi.org/10.1016/j.biopsych.2008.10.036

Monzel, A. S., Enríquez, J. A. & Picard, M. (2023). Multifaceted mitochondria: moving mitochondrial science beyond function and dysfunction. Nature Metabolism, 5(4), 546–562. https://doi.org/10.1038/s42255-023-00783-1

Morán, M., Rivera, H., Sánchez-Aragó, M., Blázquez, A., Merinero, B., Ugalde, C., Arenas, J., Cuezva, J. M. & Martín, M. A. (2010). Mitochondrial bioenergetics and dynamics interplay in complex I-deficient fibroblasts. Biochimica et Biophysica Acta (BBA) - Molecular Basis of Disease, 1802(5), 443–453. https://doi.org/10.1016/j.bbadis.2010.02.001

Morris, R. L. & Hollenbeck, P. J. (1995). Axonal transport of mitochondria along microtubules and F-actin in living vertebrate neurons. 131(5), 1315–1326. https://doi.org/10.1083/jcb.131.5.1315

Moutaux, E., Christaller, W., Scaramuzzino, C., Genoux, A., Charlot, B., Cazorla, M. & Saudou, F. (2018). Neuronal network maturation differently affects secretory vesicles and mitochondria transport in axons. Scientific Reports, 8(1), 13429. https://doi.org/10.1038/s41598-018-31759-x

Müller, M. (2019). Disturbed redox homeostasis and oxidative stress: Potential players in the developmental regression in Rett syndrome. Neuroscience & Biobehavioral Reviews, 98, 154–163. https://doi.org/10.1016/j.neubiorev.2018.12.009

Musokhranova, U., Grau, C., Vergara, C., Rodríguez-Pascau, L., Xiol, C., Castells, A. A., Alcántara, S., Rodríguez-Pombo, P., Pizcueta, P., Martinell, M., García-Cazorla, A. & Oyarzábal, A. (2023). Mitochondrial modulation with leriglitazone as a potential treatment for Rett syndrome. Journal of Translational Medicine, 21(1), 756. https://doi.org/10.1186/s12967-023-04622-5

Naegelin, Y., Kuhle, J., Schädelin, S., Datta, A. N., Magon, S., Amann, M., Barro, C., Ramelli, G. P., Heesom, K., Barde, Y.-A., Weber, P. & Kappos, L. (2021). Fingolimod in children with Rett syndrome: the FINGORETT study. 16(1), 19. https://doi.org/10.1186/s13023-020-01655-7

Navaratnarajah, T., Anand, R., Reichert, A. S. & Distelmaier, F. (2021). The relevance of mitochondrial morphology for human disease. The International Journal of Biochemistry & Cell Biology, 134, 105951. https://doi.org/10.1016/j.biocel.2021.105951

Neul, J. L., Kaufmann, W. E., Glaze, D. G., Christodoulou, J., Clarke, A. J., Bahi-Buisson, N., Leonard, H., Bailey, M. E. S., Schanen, N. C., Zappella, M., Renieri, A., Huppke, P., Percy, A. K. & Appendix), for the R. C. (Members listed in the. (2010). Rett syndrome: Revised diagnostic criteria and nomenclature. Annals of Neurology, 68(6), 944–950. https://doi.org/10.1002/ana.22124

Neul, J. L., Percy, A. K., Benke, T. A., Berry-Kravis, E. M., Glaze, D. G., Marsh, E. D., Lin, T., Stankovic, S., Bishop, K. M. & Youakim, J. M. (2023). Trofinetide for the treatment of Rett syndrome: a randomized phase 3 study. Nature Medicine, 29(6), 1468–1475. https://doi.org/10.1038/s41591-023-02398-1

Nguyen, M., Du, F., Felice, C., Shan, X., Nigam, A., Mandel, G., Robinson, J. & Ballas, N. (2012). MeCP2 Is Critical for Maintaining Mature Neuronal Networks and Global Brain Anatomy during Late Stages of Postnatal Brain Development and in the Mature Adult Brain. 32, 10021–10034. https://doi.org/10.1523/jneurosci.1316-12.2012

Nguyen, M. V. C., Felice, C. A., Du, F., Covey, M. V., Robinson, J. K., Mandel, G. & Ballas, N. (n.d.). Oligodendrocyte Lineage Cells Contribute Unique Features to Rett Syndrome Neuropathology. The Journal of Neuroscience, 33(48), 18764. https://doi.org/10.1523/jneurosci.2657-13.2013

Ni, Y., Hagras, M. A., Konstantopoulou, V., Mayr, J. A., Stuchebrukhov, A. A. & Meierhofer, D. (2019). Mutations in NDUFS1 Cause Metabolic Reprogramming and Disruption of the Electron Transfer. Cells, 8(10), 1149. https://doi.org/10.3390/cells8101149

Nolden, K. A., Egner, J. M., Collier, J. J., Russell, O. M., Alston, C. L., Harwig, M. C., Widlansky, M. E., Sasorith, S., Barbosa, I. A., Douglas, A. G., Baptista, J., Walker, M., Donnelly, D. E., Morris, A. A., Tan, H. J., Kurian, M. A., Gorman, K., Mordekar, S., Deshpande, C., … Oláhová, M. (2022). Novel DNM1L variants impair mitochondrial dynamics through divergent mechanisms. Life Science Alliance, 5(12), e202101284. https://doi.org/10.26508/lsa.202101284

O'Driscoll, C. M., Kaufmann, W. E. & Bressler, J. P. (2013). MeCP2 deficiency enhances glutamate release through NF-κB signaling in myeloid derived cells. 265(1), 61–67. https://doi.org/10.1016/j.jneuroim.2013.09.002

O'Driscoll, C. M., Lima, M. P., Kaufmann, W. E. & Bressler, J. P. (2015). Methyl CpG binding protein 2 deficiency enhances expression of inflammatory cytokines by sustaining NF-κB signaling in myeloid derived cells. Journal of Neuroimmunology, 283, 23–29. https://doi.org/10.1016/j.jneuroim.2015.04.005

Oettinghaus, B., Schulz, J. M., Restelli, L. M., Licci, M., Savoia, C., Schmidt, A., Schmitt, K., Grimm, A., Morè, L., Hench, J., Tolnay, M., Eckert, A., D'Adamo, P., Franken, P., Ishihara, N., Mihara, K., Bischofberger, J., Scorrano, L. & Frank, S. (2016). Synaptic dysfunction, memory deficits and hippocampal atrophy due to ablation of mitochondrial fission in adult forebrain neurons. Cell Death & Differentiation, 23(1), 18–28. https://doi.org/10.1038/cdd.2015.39

Olesen, M. A., Villavicencio-Tejo, F. & Quintanilla, R. A. (2022). The use of fibroblasts as a valuable strategy for studying mitochondrial impairment in neurological disorders. Translational Neurodegeneration, 11(1), 36. https://doi.org/10.1186/s40035-022-00308-y

Olichon, A., Emorine, L. J., Descoins, E., Pelloquin, L., Brichese, L., Gas, N., Guillou, E., Delettre, C., Valette, A., Hamel, C. P., Ducommun, B., Lenaers, G. & Belenguer, P. (2002). The human dynamin-related protein OPA1 is anchored to the mitochondrial inner membrane facing the inter-membrane space. FEBS Letters, 523(1–3), 171–176. https://doi.org/10.1016/s0014-5793(02)02985-x

Otera, H., Ishihara, N. & Mihara, K. (2013). New insights into the function and regulation of mitochondrial fission. 1833(5), 1256–1268. https://doi.org/10.1016/j.bbamcr.2013.02.002

Ott, C., Dorsch, E., Fraunholz, M., Straub, S. & Kozjak-Pavlovic, V. (2015). Detailed Analysis of the Human Mitochondrial Contact Site Complex Indicate a Hierarchy of Subunits. PLoS ONE, 10(3), e0120213. https://doi.org/10.1371/journal.pone.0120213

Oyarzabal, A., Xiol, C., Castells, A. A., Grau, C., O'Callaghan, M., Fernández, G., Alcántara, S., Pineda, M., Armstrong, J., Altafaj, X. & García-Cazorla, A. (2020). Comprehensive Analysis of GABAA-A1R Developmental Alterations in Rett Syndrome: Setting the Focus for Therapeutic Targets in the Time Frame of the Disease. International Journal of Molecular Sciences, 21(2), 518. https://doi.org/10.3390/ijms21020518

Palasantzas, V. E. J. M., Tamargo-Rubio, I., Le, K., Slager, J., Wijmenga, C., Jonkers, I. H., Kumar, V., Fu, J. & Withoff, S. (2023). iPSC-derived organ-on-a-chip models for personalized human genetics and pharmacogenomics studies. Trends in Genetics. https://doi.org/10.1016/j.tig.2023.01.002

Palma, F. R., Gantner, B. N., Sakiyama, M. J., Kayzuka, C., Shukla, S., Lacchini, R., Cunniff, B. & Bonini, M. G. (2024). ROS production by mitochondria: function or dysfunction? Oncogene, 43(5), 295–303. https://doi.org/10.1038/s41388-023-02907-z

Palma-Florez, S., López-Canosa, A., Moralez-Zavala, F., Castaño, O., Kogan, M. J., Samitier, J., Lagunas, A. & Mir, M. (2023). BBB-on-a-chip with integrated micro-TEER for permeability evaluation of multi-functionalized gold nanorods against Alzheimer's disease. Journal of Nanobiotechnology, 21(1), 115. https://doi.org/10.1186/s12951-023-01798-2

Palmieri, M., Pozzer, D. & Landsberger, N. (2023). Advanced genetic therapies for the treatment of Rett syndrome: state of the art and future perspectives. Frontiers in Neuroscience, 17, 1172805. https://doi.org/10.3389/fnins.2023.1172805

Panayotis, N., Ehinger, Y., Felix, M. S. & Roux, J. (2023). State-of-the-art therapies for Rett syndrome. Developmental Medicine & Child Neurology, 65(2), 162–170. https://doi.org/10.1111/dmcn.15383

Pandey, K. B. & Rizvi, S. I. (2010). Markers of Oxidative Stress in Erythrocytes and Plasma During Aging in Humans. Oxidative Medicine and Cellular Longevity, 3(1), 2–12. https://doi.org/10.4161/oxim.3.1.10476

Pandolfo, M., Reetz, K., Darling, A., Rivera, F. J. R. de, Henry, P.-G., Joers, J., Lenglet, C., Adanyeguh, I., Deelchand, D., Mochel, F., Pousset, F., Pascual, S., Eede, D. V. den, Martin-Ugarte, I., Vilà-Brau, A., Mantilla, A., Pascual, M., Martinell, M., Meya, U. & Durr, A. (2022). Efficacy and Safety of Leriglitazone in Patients With Friedreich Ataxia: A Phase 2 Double-Blind, Randomized Controlled Trial (FRAMES). Neurology Genetics, 8(6), e200034. https://doi.org/10.1212/nxg.0000000000200034

Park, J. W., Vahidi, B., Taylor, A. M., Rhee, S. W. & Jeon, N. L. (2006). Microfluidic culture platform for neuroscience research. Nature Protocols, 1(4), 2128–2136. https://doi.org/10.1038/nprot.2006.316

Park, M. J., Aja, S., Li, Q., Degano, A. L., Penati, J., Zhuo, J., Roe, C. R. & Ronnett, G. V. (2014). Anaplerotic Triheptanoin Diet Enhances Mitochondrial Substrate Use to Remodel the Metabolome and Improve Lifespan, Motor Function, and Sociability in MeCP2-Null Mice. PLoS ONE, 9(10), e109527. https://doi.org/10.1371/journal.pone.0109527

Pathak, D., Shields, L. Y., Mendelsohn, B. A., Haddad, D., Lin, W., Gerencser, A. A., Kim, H., Brand, M. D., Edwards, R. H. & Nakamura, K. (2015). The Role of Mitochondrially Derived ATP in Synaptic Vesicle Recycling *♦ Journal of Biological Chemistry, 290(37), 22325–22336. https://doi.org/10.1074/jbc.m115.656405

Payne, B. A. I., Wilson, I. J., Yu-Wai-Man, P., Coxhead, J., Deehan, D., Horvath, R., Taylor, R. W., Samuels, D. C., Santibanez-Koref, M. & Chinnery, P. F. (2013). Universal heteroplasmy of human mitochondrial DNA. 22(2), 384–390. https://doi.org/10.1093/hmg/dds435

Pecorelli, A., Cervellati, C., Cordone, V., Amicarelli, F., Hayek, J. & Valacchi, G. (2019). 13-HODE, 9-HODE and ALOX15 as potential players in Rett syndrome OxInflammation. Free Radical Biology and Medicine, 134, 598–603. https://doi.org/10.1016/j.freeradbiomed.2019.02.007

Pecorelli, A., Cervellati, C., Cordone, V., Hayek, J. & Valacchi, G. (2020). Compromised immune/inflammatory responses in Rett syndrome. Free Radical Biology and Medicine, 152(1), 100–106. https://doi.org/10.1016/j.freeradbiomed.2020.02.023

Pecorelli, A., Cervellati, F., Belmonte, G., Montagner, G., Waldon, P., Hayek, J., Gambari, R. & Valacchi, G. (2016). Cytokines profile and peripheral blood mononuclear cells morphology in Rett and autistic patients. Cytokine, 77, 180–188. https://doi.org/10.1016/j.cyto.2015.10.002

Pecorelli, A., Leoni, G., Cervellati, F., Canali, R., Signorini, C., Leoncini, S., Cortelazzo, A., Felice, C. D., Ciccoli, L., Hayek, J. & Valacchi, G. (2013). Genes Related to Mitochondrial Functions, Protein Degradation, and Chromatin Folding Are Differentially Expressed in Lymphomonocytes of Rett Syndrome Patients. Mediators of Inflammation, 2013, 1–18. https://doi.org/10.1155/2013/137629

Pejaver, V., Urresti, J., Lugo-Martinez, J., Pagel, K. A., Lin, G. N., Nam, H.-J., Mort, M., Cooper, D. N., Sebat, J., Iakoucheva, L. M., Mooney, S. D. & Radivojac, P. (2020). Inferring the molecular and phenotypic impact of amino acid variants with MutPred2. Nature Communications, 11(1), 5918. https://doi.org/10.1038/s41467-020-19669-x

Pekkurnaz, G. & Wang, X. (2022). Mitochondrial heterogeneity and homeostasis through the lens of a neuron. Nature Metabolism, 1–11. https://doi.org/10.1038/s42255-022-00594-w

Pellerin, L. & Magistretti, P. J. (1994). Glutamate uptake into astrocytes stimulates aerobic glycolysis: a mechanism coupling neuronal activity to glucose utilization. Proceedings of the National Academy of Sciences, 91(22), 10625–10629. https://doi.org/10.1073/pnas.91.22.10625

Percy, A. K., Ananth, A. & Neul, J. L. (2024). Rett Syndrome: The Emerging Landscape of Treatment Strategies. CNS Drugs, 38(11), 851–867. https://doi.org/10.1007/s40263-024-01106-y

Percy, A. K., Lane, J. B., Childers, J., Skinner, S., Annese, F., Barrish, J., Caeg, E., Glaze, D. G. & MacLeod, P. (2007). Rett Syndrome: North American Database. Journal of Child Neurology, 22(12), 1338–1341. https://doi.org/10.1177/0883073807308715

Petriti, U., Dudman, D. C., Scosyrev, E. & Lopez-Leon, S. (2023). Global prevalence of Rett syndrome: systematic review and meta-analysis. Systematic Reviews, 12(1), 5. https://doi.org/10.1186/s13643-023-02169-6

Pfanner, N., Laan, M. van der, Amati, P., Capaldi, R. A., Caudy, A. A., Chacinska, A., Darshi, M., Deckers, M., Hoppins, S., Icho, T., Jakobs, S., Ji, J., Kozjak-Pavlovic, V., Meisinger, C., Odgren, P. R., Park, S. K., Rehling, P., Reichert, A. S., Sheikh, M. S., … Nunnari, J. (2014). Uniform nomenclature for the mitochondrial contact site and cristae organizing system. Journal of Cell Biology, 204(7), 1083–1086. https://doi.org/10.1083/jcb.201401006

Pfeffer, G., Majamaa, K., Turnbull, D. M., Thorburn, D. & Chinnery, P. F. (2012). Treatment for mitochondrial disorders. Cochrane Database of Systematic Reviews, 4, CD004426. https://doi.org/10.1002/14651858.cd004426.pub3

Picard, M. & Shirihai, O. S. (2022). Mitochondrial signal transduction. Cell Metabolism, 34(11), 1620–1653. https://doi.org/10.1016/j.cmet.2022.10.008

Pierro, D. D., Ciaccio, C., Sbardella, D., Tundo, G. R., Bernardini, R., Curatolo, P., Galasso, C., Pironi, V., Coletta, M. & Marini, S. (2020). Effects of oral administration of common antioxidant supplements on the energy metabolism of red blood cells. Attenuation of oxidative stress-induced changes in Rett syndrome erythrocytes by CoQ10. Molecular and Cellular Biochemistry, 463(1–2), 101–113. https://doi.org/10.1007/s11010-019-03633-5

Pizcueta, P., Vergara, C., Emanuele, M., Vilalta, A., Rodríguez-Pascau, L. & Martinell, M. (2023). Development of PPARγ Agonists for the Treatment of Neuroinflammatory and Neurodegenerative Diseases: Leriglitazone as a Promising Candidate. International Journal of Molecular Sciences, 24(4), 3201. https://doi.org/10.3390/ijms24043201

Pour, P. A., Kenney, M. C. & Kheradvar, A. (2020). Bioenergetics Consequences of Mitochondrial Transplantation in Cardiomyocytes. Journal of the American Heart Association, 9(7), e014501. https://doi.org/10.1161/jaha.119.014501

Przanowski, P., Wasko, U., Zheng, Z., Yu, J., Sherman, R., Zhu, L. J., McConnell, M. J., Tushir-Singh, J., Green, M. R. & Bhatnagar, S. (2018). Pharmacological reactivation of inactive X-linked Mecp2 in cerebral cortical neurons of living mice. Proceedings of the National Academy of Sciences, 115(31), 7991–7996. https://doi.org/10.1073/pnas.1803792115

Puigserver, P., Adelmant, G., Wu, Z., Fan, M., Xu, J., O'Malley, B. & Spiegelman, B. M. (1999). Activation of PPARγ Coactivator-1 Through Transcription Factor Docking. Science, 286(5443), 1368–1371. https://doi.org/10.1126/science.286.5443.1368

Pulido, C. & Ryan, T. A. (n.d.). Synaptic vesicle pools are a major hidden resting metabolic burden of nerve terminals. Science Advances, 7(49), eabi9027. https://doi.org/10.1126/sciadv.abi9027

Puusepp, S., Kovacs-Nagy, R., Alhaddad, B., Braunisch, M., Hoffmann, G. F., Kotzaeridou, U., Lichvarova, L., Liiv, M., Makowski, C., Mandel, M., Meitinger, T., Pajusalu, S., Rodenburg, R. J., Safiulina, D., Strom, T. M., Talvik, I., Vaarmann, A., Wilson, C., Kaasik, A., … Õunap, K. (2018). Compound heterozygous SPATA5 variants in four families and functional studies of SPATA5 deficiency. European Journal of Human Genetics, 26(3), 407–419. https://doi.org/10.1038/s41431-017-0001-6

Qu, C., Keijer, J., Adjobo-Hermans, M. J. W., Wal, M. van de, Schirris, T., Karnebeek, C. van, Pan, Y. & Koopman, W. J. H. (2021). The ketogenic diet as a therapeutic intervention strategy in mitochondrial disease. The International Journal of Biochemistry & Cell Biology, 138, 106050. https://doi.org/10.1016/j.biocel.2021.106050

Rafiki, A., Boulland, J. L., Halestrap, A. P., Ottersen, O. P. & Bergersen, L. (2003). Highly differential expression of the monocarboxylate transporters MCT2 and MCT4 in the developing rat brain. 122(3), 677–688. https://doi.org/10.1016/j.neuroscience.2003.08.040

Raggio, V., Graña, M., Winiarski, E., Mansilla, S., Simoes, C., Rodríguez, S., Brandes, M., Tapié, A., Rodríguez, L., Cibils, L., Alonso, M., Martínez, J., Fernández-Calero, T., Domínguez, F., Mezquida, M. R., Castro, L., Cerisola, A., Naya, H., Cassina, A., … Spangenberg, L. (2023). Computational and mitochondrial functional studies of novel compound heterozygous variants in SPATA5 gene support a causal link with epileptogenic encephalopathy. Huan Genomics, 17(1), 14. https://doi.org/10.1186/s40246-023-00463-x

Ragione, F. D., Vacca, M., Fioriniello, S., Pepe, G. & D'Esposito, M. (2016). MECP2, a multi-talented modulator of chromatin architecture. Briefings in Functional Genomics, 15(6), 420–431. https://doi.org/10.1093/bfgp/elw023

Rahman, J. & Rahman, S. (2018). Mitochondrial medicine in the omics era. The Lancet, 391(10139), 2560–2574. https://doi.org/10.1016/s0140-6736(18)30727-x

Rahn, J. J., Stackley, K. D. & Chan, S. S. L. (n.d.). Opa1 Is Required for Proper Mitochondrial Metabolism in Early Development. PLOS ONE, 8(3), e59218. https://doi.org/10.1371/journal.pone.0059218

Rai, P. K., Craven, L., Hoogewijs, K., Russell, O. M. & Lightowlers, R. N. (2018). Advances in methods for reducing mitochondrial DNA disease by

replacing or manipulating the mitochondrial genome. 62(3), 455–465. https://doi.org/10.1042/ebc20170113

Ramachandran, R. (2018). Mitochondrial dynamics: The dynamin superfamily and execution by collusion. Seminars in Cell & Developmental Biology, 76, 201–212. https://doi.org/10.1016/j.semcdb.2017.07.039

Ramadan, Q. & Zourob, M. (2020). Organ-on-a-chip engineering: Toward bridging the gap between lab and industry. Biomicrofluidics, 14(4), 041501. https://doi.org/10.1063/5.0011583

Rangaraju, V., Calloway, N. & Ryan, T. A. (2014). Activity-Driven Local ATP Synthesis Is Required for Synaptic Function. Cell, 156(4), 825–835. https://doi.org/10.1016/j.cell.2013.12.042

Rangaraju, V., Lauterbach, M. & Schuman, E. M. (2019). Spatially Stable Mitochondrial Compartments Fuel Local Translation during Plasticity. Cell, 176(1–2), 73-84.e15. https://doi.org/10.1016/j.cell.2018.12.013

Rangaraju, V., Lewis, T. L., Hirabayashi, Y., Bergami, M., Motori, E., Cartoni, R., Kwon, S.-K. & Courchet, J. (2019). Pleiotropic Mitochondria: The Influence of Mitochondria on Neuronal Development and Disease. Journal of Neuroscience, 39(42), 8200–8208. https://doi.org/10.1523/jneurosci.1157-19.2019

Rawson, R. L., Yam, L., Weimer, R. M., Bend, E. G., Hartwieg, E., Horvitz, H. R., Clark, S. G. & Jorgensen, E. M. (2014). Axons Degenerate in the Absence of Mitochondria in C. elegans. Current Biology, 24(7), 760–765. https://doi.org/10.1016/j.cub.2014.02.025

Rea, K., Cremers, T. I. F. H. & Westerink, B. H. C. (2005). HPLC conditions are critical for the detection of GABA by microdialysis. Journal of Neurochemistry, 94(3), 672–679. https://doi.org/10.1111/j.1471-4159.2005.03218.x

Rebelo, A. P., Saade, D., Pereira, C. V., Farooq, A., Huff, T. C., Abreu, L., Moraes, C. T., Mnatsakanova, D., Mathews, K., Yang, H., Schon, E. A., Zuchner, S. & Shy, M. E. (2018). SCO2 mutations cause early-onset axonal Charcot-Marie-Tooth disease associated with cellular copper deficiency. Brain, 141(3), 662–672. https://doi.org/10.1093/brain/awx369

Rho, J. M. (2017). How does the ketogenic diet induce anti-seizure effects? Neuroscience Letters, 637, 4–10. https://doi.org/10.1016/j.neulet.2015.07.034

Ribeiro, M. C. & MacDonald, J. L. (2020). Sex differences in Mecp2-mutant Rett syndrome model mice and the impact of cellular mosaicism in phenotype development. Brain Research, 1729, 146644. https://doi.org/10.1016/j.brainres.2019.146644

Ribeiro, M. C., Moore, S. M., Kishi, N., Macklis, J. D. & MacDonald, J. L. (2020). Vitamin D supplementation rescues aberrant NF-κB pathway activation and partially ameliorates Rett syndrome phenotypes in Mecp2 mutant mice. eNeuro, 7(3), ENEURO.0167-20.2020. https://doi.org/10.1523/eneuro.0167-20.2020

Ricciardi, S., Boggio, E. M., Grosso, S., Lonetti, G., Forlani, G., Stefanelli, G., Calcagno, E., Morello, N., Landsberger, N., Biffo, S., Pizzorusso, T., Giustetto, M. & Broccoli, V. (2011). Reduced AKT/mTOR signaling and protein synthesis dysregulation in a Rett syndrome animal model. 20(6), 1182–1196. https://doi.org/10.1093/hmg/ddq56

Riley, J. S. & Tait, S. W. (2020). Mitochondrial DNA in inflammation and immunity. EMBO Reports, 21(4), EMBR201949799. https://doi.org/10.15252/embr.201949799

Rinholm, J. E., Hamilton, N. B., Kessaris, N., Richardson, W. D., Bergersen, L. H. & Attwell, D. (n.d.). Regulation of Oligodendrocyte Development and Myelination by Glucose and Lactate. The Journal of Neuroscience, 31(2), 538. https://doi.org/10.1523/jneurosci.3516-10.2011

Robertson, G. L., Riffle, S., Patel, M., Bodnya, C., Marshall, A., Beasley, H. K., Garza-Lopez, E., Shao, J., Vue, Z., Hinton, A., Stoll, M. S., Wet, S. de, Theart, R. P., Chakrabarty, R. P., Loos, B., Chandel, N. S., Mears, J. A. & Gama, V. (2023). DRP1 mutations associated with EMPF1 encephalopathy alter mitochondrial membrane potential and metabolic programs. Journal of Cell Science, 136(3), jcs260370. https://doi.org/10.1242/jcs.260370

Robinson, J. E. & Gradinaru, V. (2018). Dopaminergic dysfunction in neurodevelopmental disorders: recent advances and synergistic technologies to aid basic research. Current Opinion in Neurobiology, 48, 17–29. https://doi.org/10.1016/j.conb.2017.08.003

Rodrigues, R. O., Sousa, P. C., Gaspar, J., Bañobre-López, M., Lima, R. & Minas, G. (2020). Organ-on-a-Chip: A Preclinical Microfluidic Platform for the Progress of Nanomedicine. Small, 16(51), e2003517. https://doi.org/10.1002/smll.202003517

Rodríguez-Pascau, L., Britti, E., Calap-Quintana, P., Dong, Y. N., Vergara, C., Delaspre, F., Medina-Carbonero, M., Tamarit, J., Pallardó, F. V., Gonzalez-Cabo, P., Ros, J., Lynch, D. R., Martinell, M. & Pizcueta, P. (2021). PPAR gamma agonist leriglitazone improves frataxin-loss impairments in cellular and animal models of Friedreich Ataxia. Neurobiology of Disease, 148, 105162. https://doi.org/10.1016/j.nbd.2020.105162

Rodríguez-Pascau, L., Vilalta, A., Cerrada, M., Traver, E., Forss-Petter, S., Weinhofer, I., Bauer, J., Kemp, S., Pina, G., Pascual, S., Meya, U., Musolino, P. L., Berger, J., Martinell, M. & Pizcueta, P. (2021). The brain penetrant PPARγ agonist leriglitazone restores multiple altered pathways in models of X-linked adrenoleukodystrophy. Science Translational Medicine, 13(596), eabc0555. https://doi.org/10.1126/scitranslmed.abc0555

Rogue, A., Spire, C., Brun, M., Claude, N. & Guillouzo, A. (2010). Gene Expression Changes Induced by PPAR Gamma Agonists in Animal and Human Liver. PPAR Research, 2010(1), 325183. https://doi.org/10.1155/2010/325183

Romano, A., Rosa, G. D., Tisano, A., Fabio, R. A. & Lotan, M. (2022). Effects of a remotely supervised motor rehabilitation program for individuals with Rett syndrome at home. Disability and Rehabilitation, 44(20), 5898–5908. https://doi.org/10.1080/09638288.2021.1949398

Ross, F. M., Allan, S. M., Rothwell, N. J. & Verkhratsky, A. (2003). A dual role for interleukin-1 in LTP in mouse hippocampal slices. Journal of Neuroimmunology, 144(1–2), 61–67. https://doi.org/10.1016/j.jneuroim.2003.08.030

Rossignol, R., Gilkerson, R., Aggeler, R., Yamagata, K., Remington, S. J. & Capaldi, R. A. (2004). Energy Substrate Modulates Mitochondrial Structure and Oxidative Capacity in Cancer Cells. Cancer Research, 64(3), 985–993. https://doi.org/10.1158/0008-5472.can-03-1101

Rubenstein, J. L. R. & Merzenich, M. M. (2003). Model of autism: increased ratio of excitation/inhibition in key neural systems. Genes, Brain and Behavior, 2(5), 255–267. https://doi.org/10.1034/j.1601-183x.2003.00037.x

Rucheton, B., Ewenczyk, C., Gaignard, P., Agathe, J.-M. de S., Fauret, A.-L., Saillour, V., Leonard-Louis, S., Touitou, V. & Mochel, F. (2021). Adult Cerebellar Ataxia, Axonal Neuropathy, and Sensory Impairments Caused by Biallelic SCO2 Variants. Neurology: Genetics, 7(6), e630. https://doi.org/10.1212/nxg.0000000000000630

Ruskin, D. N., Svedova, J., Cote, J. L., Sandau, U., Rho, J. M., Kawamura, M., Boison, D. & Masino, S. A. (2013). Ketogenic Diet Improves Core Symptoms of Autism in BTBR Mice. PLoS ONE, 8(6), e65021. https://doi.org/10.1371/journal.pone.0065021

Russell, O. M., Gorman, G. S., Lightowlers, R. N. & Turnbull, D. M. (2020). Mitochondrial Diseases: Hope for the Future. Cell, 181(1), 168–188. https://doi.org/10.1016/j.cell.2020.02.051

Sala, G. D. & Pizzorusso, T. (2014). Synaptic plasticity and signaling in rett syndrome. Developmental Neurobiology, 74(2), 178–196. https://doi.org/10.1002/dneu.22114

Sari, I. N., Setiawan, T., Kim, K. S., Wijaya, Y. T., Cho, K. W. & Kwon, H. Y. (2021). Metabolism and function of polyamines in cancer progression. Cancer Letters, 519, 91–104. https://doi.org/10.1016/j.canlet.2021.06.020

Savage, D. B. (2005). PPARγ as a metabolic regulator: insights from genomics and pharmacology. Expert Reviews in Molecular Medicine, 7(1), 1–16. https://doi.org/10.1017/s1462399405008793

Saxton, W. M. & Hollenbeck, P. J. (2012). The axonal transport of mitochondria. 125(9), 2095–2104. https://doi.org/10.1242/jcs.053850

Saywell, V., Viola, A., Confort-Gouny, S., Fur, Y. L., Villard, L. & Cozzone, P. J. (2006). Brain magnetic resonance study of Mecp2 deletion effects on anatomy and metabolism. Biochemical and Biophysical Research Communications, 340(3), 776–783. https://doi.org/10.1016/j.bbrc.2005.12.080

Schroeder, S., Hofer, S. J., Zimmermann, A., Pechlaner, R., Dammbrueck, C., Pendl, T., Marcello, G. M., Pogatschnigg, V., Bergmann, M., Müller, M., Gschiel, V., Ristic, S., Tadic, J., Iwata, K., Richter, G., Farzi, A., Üçal, M., Schäfer, U., Poglitsch, M., … Madeo, F. (2021). Dietary spermidine improves cognitive function. Cell Reports, 35(2), 108985. https://doi.org/10.1016/j.celrep.2021.108985

Schulman, I. G. (2017). Liver X receptors link lipid metabolism and inflammation. FEBS Letters, 591(19), 2978–2991. https://doi.org/10.1002/1873-3468.12702

Scott, S. M. & Ali, Z. (2021). Fabrication Methods for Microfluidic Devices: An Overview. Micromachines, 12(3), 319. https://doi.org/10.3390/mi12030319

Segatto, M., Trapani, L., Tunno, I. D., Sticozzi, C., Valacchi, G., Hayek, J. & Pallottini, V. (2014). Cholesterol Metabolism Is Altered in Rett Syndrome: A Study on Plasma and Primary Cultured Fibroblasts Derived from Patients. PLoS ONE, 9(8), e104834. https://doi.org/10.1371/journal.pone.0104834

Shahrani, M. A., Heales, S., Hargreaves, I. & Orford, M. (2017). Oxidative Stress: Mechanistic Insights into Inherited Mitochondrial Disorders and Parkinson's Disease. Journal of Clinical Medicine, 6(11), 100. https://doi.org/10.3390/jcm6110100

Shang, Y., Sun, X., Chen, X., Wang, Q., Wang, E. J., Miller, E., Xu, R., Pieper, A. A. & Qi, X. (2022). A CHCHD6–APP axis connects amyloid and mitochondrial pathology in Alzheimer's disease. Acta Neuropathologica, 144(5), 911–938. https://doi.org/10.1007/s00401-022-02499-0

Sharma, K., Singh, J., Frost, E. & Pillai, P. (2018). MeCP2 in central nervous system glial cells: current updates. 78 1, 30–40. https://doi.org/10.21307/ane-2018-007

Sharma, L., Lu, J. & Bai, Y. (2009). Mitochondrial Respiratory Complex I: Structure, Function and Implication in Human Diseases. Current Medicinal Chemistry, 16(10), 1266–1277. https://doi.org/10.2174/092986709787846578

Sheffer, R., Douiev, L., Edvardson, S., Shaag, A., Tamimi, K., Soiferman, D., Meiner, V. & Saada, A. (2016). Postnatal microcephaly and pain insensitivity due to a de novo heterozygous DNM1L mutation causing impaired mitochondrial fission and function. American Journal of Medical Genetics Part A, 170(6), 1603–1607. https://doi.org/10.1002/ajmg.a.37624

Sheng, Z.-H. & Cai, Q. (2012). Mitochondrial transport in neurons: impact on synaptic homeostasis and neurodegeneration. 13(2), 77–93. https://doi.org/10.1038/nrn3156

Shulyakova, N., Andreazza, A. C., Mills, L. R. & Eubanks, J. H. (2017). Mitochondrial Dysfunction in the Pathogenesis of Rett Syndrome: Implications for Mitochondria-Targeted Therapies. Frontiers in Cellular Neuroscience, 11, 58. https://doi.org/10.3389/fncel.2017.00058

Shyh-Chang, N., Daley, G. Q. & Cantley, L. C. (2013). Stem cell metabolism in tissue development and aging. 140(12), 2535–2547. https://doi.org/10.1242/dev.091777

Siegmund, S. E., Yang, H., Sharma, R., Javors, M., Skinner, O., Mootha, V., Hirano, M. & Schon, E. A. (2017). Low-dose rapamycin extends lifespan in a mouse model of mtDNA depletion syndrome. 26(23), 4588–4605. https://doi.org/10.1093/hmg/ddx341

Sies, H. & Jones, D. P. (2020). Reactive oxygen species (ROS) as pleiotropic physiological signalling agents. Nature Reviews Molecular Cell Biology, 21(7), 363–383. https://doi.org/10.1038/s41580-020-0230-3

Signorini, C., Leoncini, S., Felice, C. D., Pecorelli, A., Meloni, I., Ariani, F., Mari, F., Amabile, S., Paccagnini, E., Gentile, M., Belmonte, G., Zollo, G., Valacchi, G., Durand, T., Galano, J.-M., Ciccoli, L., Renieri, A. & Hayek, J. (2014). Redox Imbalance and Morphological Changes in Skin Fibroblasts in Typical Rett Syndrome. Oxidative Medicine and Cellular Longevity, 2014, 1–10. https://doi.org/10.1155/2014/195935

Silva, B., Mantha, O. L., Schor, J., Pascual, A., Plaçais, P.-Y., Pavlowsky, A. & Preat, T. (2022). Glia fuel neurons with locally synthesized ketone bodies to sustain memory under starvation. 4(2), 213–224. https://doi.org/10.1038/s42255-022-00528-6

Singh, J., Lanzarini, E., Nardocci, N. & Santosh, P. (2021). Movement disorders in patients with Rett syndrome: A systematic review of evidence and associated clinical considerations. Psychiatry and Clinical Neurosciences, 75(12), 369–393. https://doi.org/10.1111/pcn.13299

Singh, K., Connors, S. L., Macklin, E. A., Smith, K. D., Fahey, J. W., Talalay, P. & Zimmerman, A. W. (2014). Sulforaphane treatment of autism spectrum disorder (ASD). Proceedings of the National Academy of Sciences, 111(43), 15550–15555. https://doi.org/10.1073/pnas.1416940111

Sinnamon, J. R., Jacobson, M. E., Yung, J. F., Fisk, J. R., Jeng, S., McWeeney, S. K., Parmelee, L. K., Chan, C. N., Yee, S.-P. & Mandel, G. (2022). Targeted RNA editing in brainstem alleviates respiratory dysfunction in a mouse model of Rett syndrome. Proceedings of the National Academy of Sciences, 119(33), e2206053119. https://doi.org/10.1073/pnas.2206053119

Sissler, M., González-Serrano, L. E. & Westhof, E. (2017). Recent Advances in Mitochondrial Aminoacyl-tRNA Synthetases and Disease. Trends in Molecular Medicine, 23(8), 693–708. https://doi.org/10.1016/j.molmed.2017.06.002

Smith, H. L., Bourne, J. N., Cao, G., Chirillo, M. A., Ostroff, L. E., Watson, D. J. & Harris, K. M. (2016). Mitochondrial support of persistent presynaptic vesicle mobilization with age-dependent synaptic growth after LTP. eLife, 5, e15275. https://doi.org/10.7554/elife.15275

Son, G. & Han, J. (n.d.). Roles of mitochondria in neuronal development. BMB Reports, 51(11), 549–556. https://doi.org/10.5483/bmbrep.2018.51.11.226

Spoto, G., Saia, M. C., Amore, G., Gitto, E., Loddo, G., Mainieri, G., Nicotera, A. G. & Rosa, G. D. (2021). Neonatal Seizures: An Overview of Genetic Causes and Treatment Options. Brain Sciences, 11(10), 1295. https://doi.org/10.3390/brainsci11101295

Stewart, P. A., Hyman, S. L., Schmidt, B. L., Macklin, E. A., Reynolds, A., Johnson, C. R., James, S. J. & Manning-Courtney, P. (2015). Dietary Supplementation in Children with Autism Spectrum Disorders: Common, Insufficient, and Excessive. Journal of the Academy of Nutrition and Dietetics, 115(8), 1237–1248. https://doi.org/10.1016/j.jand.2015.03.026

Stoll, E. A., Cheung, W., Mikheev, A. M., Sweet, I. R., Bielas, J. H., Zhang, J., Rostomily, R. C. & Horner, P. J. (2011). Aging Neural Progenitor Cells Have Decreased Mitochondrial Content and Lower Oxidative Metabolism * . Journal of Biological Chemistry, 286(44), 38592–38601. https://doi.org/10.1074/jbc.m111.252171

Stoodley, C. J. (2016). The Cerebellum and Neurodevelopmental Disorders. The Cerebellum, 15(1), 34–37. https://doi.org/10.1007/s12311-015-0715-3

Straus, D. S. & Glass, C. K. (2007). Anti-inflammatory actions of PPAR ligands: new insights on cellular and molecular mechanisms. Trends in Immunology, 28(12), 551–558. https://doi.org/10.1016/j.it.2007.09.003

Suárez-Rivero, J. M., Pastor-Maldonado, C. J., Povea-Cabello, S., Álvarez-Córdoba, M., Villalón-García, I., Talaverón-Rey, M., Suárez-Carrillo, A., Munuera-Cabeza, M., Reche-López, D., Cilleros-Holgado, P., Piñero-Perez, R. & Sánchez-Alcázar, J. A. (2022). UPRmt activation improves pathological alterations in cellular models of mitochondrial diseases. Orphanet Journal of Rare Diseases, 17(1), 204. https://doi.org/10.1186/s13023-022-02331-8

Sue, C. M., Karadimas, C., Checcarelli, N., Tanji, K., Papadopoulou, L. C., Pallotti, F., Guo, F. L., Shanske, S., Hirano, M., Vivo, D. C. D., Coster, R. V., Kaplan, P., Bonilla, E. & DiMauro, S. (2000). Differential features of patients with mutations in two COX assembly genes, SURF-1 and SCO2. Annals of Neurology, 47(5), 589–595.

Suen, D.-F., Norris, K. L. & Youle, R. J. (2008). Mitochondrial dynamics and apoptosis. Genes & Development, 22(12), 1577–1590. https://doi.org/10.1101/gad.1658508

Sugino, K., Hempel, C. M., Okaty, B. W., Arnson, H. A., Kato, S., Dani, V. S. & Nelson, S. B. (n.d.). Cell-Type-Specific Repression by Methyl-CpG-Binding Protein 2 Is Biased toward Long Genes. The Journal of Neuroscience, 34(38), 12877. https://doi.org/10.1523/jneurosci.2674-14.2014

Sun, J. & Zhang, W. (2022). Supplementation with dietary omega-3 PUFA mitigates fetal brain inflammation and mitochondrial damage caused by high doses of sodium nitrite in maternal rats. PLoS ONE, 17(3), e0266084. https://doi.org/10.1371/journal.pone.0266084

Swanson, C. R., Joers, V., Bondarenko, V., Brunner, K., Simmons, H. A., Ziegler, T. E., Kemnitz, J. W., Johnson, J. A. & Emborg, M. E. (2011). The PPAR-γ agonist pioglitazone modulates inflammation and induces neuroprotection in parkinsonian monkeys. Journal of Neuroinflammation, 8(1), 91. https://doi.org/10.1186/1742-2094-8-91

Takubo, K., Nagamatsu, G., Kobayashi, C. I., Nakamura-Ishizu, A., Kobayashi, H., Ikeda, E., Goda, N., Rahimi, Y., Johnson, R. S., Soga, T., Hirao, A., Suematsu, M. & Suda, T. (2013). Regulation of Glycolysis by Pdk Functions as a Metabolic Checkpoint for Cell Cycle Quiescence in Hematopoietic Stem Cells. Cell Stem Cell, 12(1), 49–61. https://doi.org/10.1016/j.stem.2012.10.011

Tanaka, A. J., Cho, M. T., Millan, F., Juusola, J., Retterer, K., Joshi, C., Niyazov, D., Garnica, A., Gratz, E., Deardorff, M., Wilkins, A., Ortiz-Gonzalez, X., Mathews, K., Panzer, K., Brilstra, E., van Gassen, K. L. I., Volker-Touw, C. M. L., van Binsbergen, E., Sobreira, N., … Chung, W. K. (2015). Mutations in SPATA5 Are Associated with Microcephaly, Intellectual Disability, Seizures, and Hearing Loss. The American Journal of Human Genetics, 97(3), 457–464. https://doi.org/10.1016/j.ajhg.2015.07.014

Tang, J., Zhang, K., Dong, J., Yan, C., Hu, C., Ji, H., Chen, L., Chen, S., Zhao, H. & Song, Z. (2020). Sam50–Mic19–Mic60 axis determines mitochondrial cristae architecture by mediating mitochondrial outer and inner membrane contact. Cell Death & Differentiation, 27(1), 146–160. https://doi.org/10.1038/s41418-019-0345-2

TARNOPOLSKY, M. A. (2008). Sex Differences in Exercise Metabolism and the Role of 17-Beta Estradiol. Medicine & Science in Sports & Exercise, 40(4), 648–654. https://doi.org/10.1249/mss.0b013e31816212ff

Täuber, S., Schmitz, J., Blöbaum, L., Fante, N., Steinhoff, H. & Grünberger, A. (2021). How to Perform a Microfluidic Cultivation Experiment—A Guideline to Success. Biosensors, 11(12), 485. https://doi.org/10.3390/bios11120485

Taylor, A. M., Blurton-Jones, M., Rhee, S. W., Cribbs, D. H., Cotman, C. W. & Jeon, N. L. (2005). A microfluidic culture platform for CNS axonal injury, regeneration and transport. Nature Methods, 2(8), 599–605. https://doi.org/10.1038/nmeth777

Taylor, A. M., Dieterich, D. C., Ito, H. T., Kim, S. A. & Schuman, E. M. (2010). Microfluidic Local Perfusion Chambers for the Visualization and Manipulation of Synapses. Neuron, 66(1), 57–68. https://doi.org/10.1016/j.neuron.2010.03.022

Thornton, B., Cohen, B., Copeland, W. & Maria, B. L. (2014). Mitochondrial Disease: Clinical Aspects, Molecular Mechanisms, Translational Science, and Clinical Frontiers. Journal of Child Neurology, 29(9), 1179–1207. https://doi.org/10.1177/0883073814537379

Tian, J., Jia, K., Wang, T., Guo, L., Xuan, Z., Michaelis, E. K., Swerdlow, R. H., Initiative, A. D. N. & Du, H. (2024). Hippocampal transcriptome-wide association study and pathway analysis of mitochondrial solute carriers in Alzheimer's disease. Translational Psychiatry, 14(1), 250. https://doi.org/10.1038/s41398-024-02958-0

Toloe, J., Mollajew, R., Kügler, S. & Mironov, S. L. (2014). Metabolic differences in hippocampal 'Rett' neurons revealed by ATP imaging. Molecular and Cellular Neuroscience, 59, 47–56. https://doi.org/10.1016/j.mcn.2013.12.008

Tomasello, D. L., Barrasa, M. I., Mankus, D., Alarcon, K. I., Lytton-Jean, A. K. R., Liu, X. S. & Jaenisch, R. (2024). Mitochondrial dysfunction and increased reactive oxygen species production in MECP2 mutant astrocytes and their impact on neurons. Scientific Reports, 14(1), 20565. https://doi.org/10.1038/s41598-024-71040-y

Tozzi, R., Campolo, F., Baldini, E., Venneri, M. A., Lubrano, C., Ulisse, S., Gnessi, L. & Mariani, S. (2022). Ketogenic Diet Increases Serum and White Adipose Tissue SIRT1 Expression in Mice. International Journal of Molecular Sciences, 23(24), 15860. https://doi.org/10.3390/ijms232415860

Tragni, V., Primiano, G., Tummolo, A., Beltrame, L. C., Piana, G. L., Sgobba, M. N., Cavalluzzi, M. M., Paterno, G., Gorgoglione, R., Volpicella, M., Guerra, L., Marzulli, D., Servidei, S., Grassi, A. D., Petrosillo, G., Lentini, G. & Pierri, C. L. (2022). Personalized Medicine in Mitochondrial Health and Disease: Molecular Basis of Therapeutic Approaches Based on Nutritional Supplements and Their Analogs. Molecules, 27(11), 3494. https://doi.org/10.3390/molecules27113494

Traver, E., Rodríguez-Pascau, L., Meya, U., Pina, G., Pascual, S., Poli, S., Eckland, D., Wetering, J. van de, Ke, A., Lindauer, A., Martinell, M. & Pizcueta, P. (2024). Clinical pharmacokinetics of leriglitazone and a translational approach using PBPK modeling to guide the selection of the starting dose in children. CPT: Pharmacometrics & Systems Pharmacology, 13(6), 982–993. https://doi.org/10.1002/psp4.13132

Tropea, D., Giacometti, E., Wilson, N. R., Beard, C., McCurry, C., Fu, D. D., Flannery, R., Jaenisch, R. & Sur, M. (2009). Partial reversal of Rett Syndrome-like symptoms in MeCP2 mutant mice. Proceedings of the National Academy of Sciences, 106(6), 2029–2034. https://doi.org/10.1073/pnas.0812394106

Turovsky, E., Karagiannis, A., Abdala, A. P. & Gourine, A. V. (2015). Impaired CO2 sensitivity of astrocytes in a mouse model of Rett syndrome. The Journal of Physiology, 593(14), 3159–3168. https://doi.org/10.1113/jp270369

Urbinati, C., Cosentino, L., Germinario, E. A. P., Valenti, D., Vigli, D., Ricceri, L., Laviola, G., Fiorentini, C., Vacca, R. A., Fabbri, A. & Filippis, B. D. (2021). Treatment with the Bacterial Toxin CNF1 Selectively Rescues Cognitive and Brain Mitochondrial Deficits in a Female Mouse Model of Rett Syndrome Carrying a MeCP2-Null Mutation. International Journal of Molecular Sciences, 22(13), 6739. https://doi.org/10.3390/ijms22136739

Urdinguio, R. G., Fernández, A. F., Lopez-Nieva, P., Rossi, S., Huertas, D., Kulis, M., Liu, C.-G., Croce, C. M., Calin, G. A. & Esteller, M. (2010). Disrupted microRNA expression caused by Mecp2 loss in a mouse model of Rett syndrome. Epigenetics, 5(7), 656–663. https://doi.org/10.4161/epi.5.7.13055

Ure, K., Lu, H., Wang, W., Ito-Ishida, A., Wu, Z., He, L., Sztainberg, Y., Chen, W., Tang, J. & Zoghbi, H. Y. (2016). Restoration of Mecp2 expression in GABAergic neurons is sufficient to rescue multiple disease features in a mouse model of Rett syndrome. eLife, 5, e14198. https://doi.org/10.7554/elife.14198

Valenti, D., Bari, L. de, Vigli, D., Lacivita, E., Leopoldo, M., Laviola, G., Vacca, R. A. & Filippis, B. D. (2017). Stimulation of the brain serotonin receptor 7 rescues mitochondrial dysfunction in female mice from two models of Rett syndrome. Neuropharmacology, 121, 79–88. https://doi.org/10.1016/j.neuropharm.2017.04.024

Vanstone, J. R., Smith, A. M., McBride, S., Naas, T., Holcik, M., Antoun, G., Harper, M.-E., Michaud, J., Sell, E., Chakraborty, P., Tetreault, M., Majewski, J., Baird, S., Boycott, K. M., Dyment, D. A., MacKenzie, A. & Lines, M. A. (2016). DNM1L-related mitochondrial fission defect presenting as refractory epilepsy. European Journal of Human Genetics, 24(7), 1084–1088. https://doi.org/10.1038/ejhg.2015.243

Ven, A. T. van der, Johannsen, J., Kortüm, F., Wagner, M., Tsiakas, K., Bierhals, T., Lessel, D., Herget, T., Kloth, K., Lisfeld, J., Scholz, T., Obi, N., Wortmann, S., Prokisch, H., Kubisch, C., Denecke, J., Santer, R. & Hempel, M. (2021). Prevalence and clinical prediction of mitochondrial disorders in a large neuropediatric cohort. Clinical Genetics, 100(6), 766–770. https://doi.org/10.1111/cge.14061

Venkatachalam, G., Kumar, A. P., Yue, L. S., Pervaiz, S., Clement, M. V. & Sakharkar, M. K. (2009). Computational identification and experimental validation of PPRE motifs in NHE1 and MnSOD genes of Human. BMC Genomics, 10(Suppl 3), S5. https://doi.org/10.1186/1471-2164-10-s3-s5

Vidal, S., Xiol, C., Pascual-Alonso, A., O'Callaghan, M., Pineda, M. & Armstrong, J. (2019). Genetic Landscape of Rett Syndrome Spectrum: Improvements and Challenges. International Journal of Molecular Sciences, 20(16), 3925. https://doi.org/10.3390/ijms20163925

Villani, C., Sacchetti, G., Bagnati, R., Passoni, A., Fusco, F., Carli, M. & Invernizzi, R. W. (2016). Lovastatin fails to improve motor performance and survival in methyl-CpG-binding protein2-null mice. eLife, 5, e22409. https://doi.org/10.7554/elife.22409

Viola, A., Saywell, V., Villard, L., Cozzone, P. J. & Lutz, N. W. (n.d.). Metabolic Fingerprints of Altered Brain Growth, Osmoregulation and Neurotransmission in a Rett Syndrome Model. PLOS ONE, 2(1), e157. https://doi.org/10.1371/journal.pone.0000157

Virlogeux, A., Moutaux, E., Christaller, W., Genoux, A., Bruyère, J., Fino, E., Charlot, B., Cazorla, M. & Saudou, F. (2018). Reconstituting Corticostriatal Network on-a-Chip Reveals the Contribution of the Presynaptic Compartment to Huntington's Disease. Cell Reports, 22(1), 110–122. https://doi.org/10.1016/j.celrep.2017.12.013

Viscomi, C., Bottani, E., Civiletto, G., Cerutti, R., Moggio, M., Fagiolari, G., Schon, E. A., Lamperti, C. & Zeviani, M. (2011). In Vivo Correction of COX Deficiency by Activation of the AMPK/PGC-1α Axis. Cell Metabolism, 14(1), 80–90. https://doi.org/10.1016/j.cmet.2011.04.011

Vitrac, A. & Cloëz-Tayarani, I. (2018). Induced pluripotent stem cells as a tool to study brain circuits in autism-related disorders. Stem Cell Research & Therapy, 9(1), 226. https://doi.org/10.1186/s13287-018-0966-2

Vringer, E. & Tait, S. W. G. (2023). Mitochondria and cell death-associated inflammation. Cell Death & Differentiation, 30(2), 304–312. https://doi.org/10.1038/s41418-022-01094-w

Vue, Z., Murphy, A., Le, H., Neikirk, K., Garza-Lopez, E., Marshall, A. G., Mungai, M., Jenkins, B., Vang, L., Beasley, H. K., Ezedimma, M., Manus, S., Whiteside, A., Forni, M. F., Harris, C., Crabtree, A., Albritton, C. F., Jamison, S., Demirci, M., … Hinton, A. (2024). MICOS Complex Loss Governs Age-Associated Murine Mitochondrial Architecture and Metabolism in the Liver, While Sam50 Dictates Diet Changes. bioRxiv, 2024.06.20.599846. https://doi.org/10.1101/2024.06.20.599846

Wakabayashi, J., Zhang, Z., Wakabayashi, N., Tamura, Y., Fukaya, M., Kensler, T. W., Iijima, M. & Sesaki, H. (2009). The dynamin-related GTPase Drp1 is required for embryonic and brain development in mice. 186(6), 805–816. https://doi.org/10.1083/jcb.200903065

Wakai, S., Kameda, K., Ishikawa, Y., Miyamoto, S., Nagaoka, M., Okabe, M., Minami, R. & Tachi, N. (1990). Rett syndrome: findings suggesting axonopathy and mitochondrial abnormalities. Pediatric Neurology, 6(5), 339–343. https://doi.org/10.1016/0887-8994(90)90028-y

Wang, Jieqi, Wegener, J. E., Huang, T.-W., Sripathy, S., Jesus-Cortes, H. D., Xu, P., Tran, S., Knobbe, W., Leko, V., Britt, J., Starwalt, R., McDaniel, L., Ward, C. S., Parra, D., Newcomb, B., Lao, U., Nourigat, C., Flowers, D. A., Cullen, S., … Pieper, A. A. (2015). Wild-type microglia do not reverse pathology in mouse models of Rett syndrome. 521(7552), E1–E4. https://doi.org/10.1038/nature14444

Wang, Junying, Li, S., Wang, J., Wu, F., Chen, Y., Zhang, H., Guo, Y., Lin, Y., Li, L., Yu, X., Liu, T. & Zhao, Y. (2020). Spermidine alleviates cardiac aging by improving mitochondrial biogenesis and function. Aging (Albany NY), 12(1), 650–671. https://doi.org/10.18632/aging.102647

Wang, W., Esbensen, Y., Kunke, D., Suganthan, R., Rachek, L., Bjørås, M. & Eide, L. (n.d.). Mitochondrial DNA Damage Level Determines Neural Stem Cell Differentiation Fate. The Journal of Neuroscience, 31(26), 9746. https://doi.org/10.1523/jneurosci.0852-11.2011

Wang, W., Osenbroch, P., Skinnes, R., Esbensen, Y., Bjørås, M. & Eide, L. (2010). Mitochondrial DNA Integrity Is Essential For Mitochondrial Maturation During Differentiation of Neural Stem Cells. 28(12), 2195–2204. https://doi.org/10.1002/stem.542

Ward, B. C., Agarwal, S., Wang, K., Berger-Sweeney, J. & Kolodny, N. H. (2008). Longitudinal brain MRI study in a mouse model of Rett Syndrome and the effects of choline. Neurobiology of Disease, 31(1), 110–119. https://doi.org/10.1016/j.nbd.2008.03.009

Waterham, H. R., Koster, J., Roermund, C. W. T. van, Mooyer, P. A. W., Wanders, R. J. A. & Leonard, J. V. (2007). A Lethal Defect of Mitochondrial and Peroxisomal Fission. The New England Journal of Medicine, 356(17), 1736–1741. https://doi.org/10.1056/nejmoa064436

Weaving, L. S., Ellaway, C. J., Gécz, J. & Christodoulou, J. (2005). Rett syndrome: clinical review and genetic update. Journal of Medical Genetics, 42(1), 1–7. https://doi.org/10.1136/jmg.2004.027730

Wevers, N. R., Vught, R. van, Wilschut, K. J., Nicolas, A., Chiang, C., Lanz, H. L., Trietsch, S. J., Joore, J. & Vulto, P. (2016). High-throughput compound evaluation on 3D networks of neurons and glia in a microfluidic platform. Scientific Reports, 6(1), 38856. https://doi.org/10.1038/srep38856

Whitley, B. N., Lam, C., Cui, H., Haude, K., Bai, R., Escobar, L., Hamilton, A., Brady, L., Tarnopolsky, M. A., Dengle, L., Picker, J., Lincoln, S., Lackner, L. L., Glass, I. A. & Hoppins, S. (2018). Aberrant Drp1-mediated mitochondrial division presents in humans with variable outcomes. Human Molecular Genetics, 27(21), 3710–3719. https://doi.org/10.1093/hmg/ddy287

Wu, H., Min, J., Zeng, H., McCloskey, D. E., Ikeguchi, Y., Loppnau, P., Michael, A. J., Pegg, A. E. & Plotnikov, A. N. (2008). Crystal Structure of Human Spermine Synthase IMPLICATIONS OF SUBSTRATE BINDING AND CATALYTIC MECHANISM. Journal of Biological Chemistry, 283(23), 16135–16146. https://doi.org/10.1074/jbc.m710323200

Xiol, C., Vidal, S., Pascual-Alonso, A., Blasco, L., Brandi, N., Pacheco, P., Gerotina, E., O'Callaghan, M., Pineda, M., Armstrong, J., Aguirre, F. J., Aleu, M., Alonso, X., Alsius, M., Amorós, M. I., Antiñolo, G., Aquino, L., Arellano, C., Arriola, G., … Villar, C. (2019). X chromosome inactivation does not necessarily determine the severity of the phenotype in Rett syndrome patients. Scientific Reports, 9(1), 11983. https://doi.org/10.1038/s41598-019-48385-w

Yasui, D. H., Peddada, S., Bieda, M. C., Vallero, R. O., Hogart, A., Nagarajan, R. P., Thatcher, K. N., Farnham, P. J. & LaSalle, J. M. (2007). Integrated epigenomic analyses of neuronal MeCP2 reveal a role for long-range interaction with active genes. Proceedings of the National Academy of Sciences, 104(49), 19416–19421. https://doi.org/10.1073/pnas.0707442104

Youle, R. J. & Bliek, A. M. van der. (2012). Mitochondrial Fission, Fusion, and Stress. Science, 337(6098), 1062–1065. https://doi.org/10.1126/science.1219855

Young, J. I., Hong, E. P., Castle, J. C., Crespo-Barreto, J., Bowman, A. B., Rose, M. F., Kang, D., Richman, R., Johnson, J. M., Berget, S. & Zoghbi, H. Y. (2005). Regulation of RNA splicing by the methylation-dependent transcriptional repressor methyl-CpG binding protein 2. Proceedings of the National Academy of Sciences, 102(49), 17551–17558. https://doi.org/10.1073/pnas.0507856102

Yüksel, A., Seven, M., Cetincelik, Ü., Yeşil, G. & Köksal, V. (2006). Facial Dysmorphism in Leigh Syndrome With SURF-1 Mutation and COX Deficiency. Pediatric Neurology, 34(6), 486–489. https://doi.org/10.1016/j.pediatrneurol.2005.10.020

Zalosnik, M. I., Fabio, M. C., Bertoldi, M. L., Castañares, C. N. & Degano, A. L. (2021). MeCP2 deficiency exacerbates the neuroinflammatory setting and autoreactive response during an autoimmune challenge. Scientific Reports, 11(1), 10997. https://doi.org/10.1038/s41598-021-90517-8

Zandl-Lang, M., Züllig, T., Trötzmüller, M., Naegelin, Y., Abela, L., Wilken, B., Scholl-Buergi, S., Karall, D., Kappos, L., Köfeler, H. & Plecko, B. (2022). Changes in the Cerebrospinal Fluid and Plasma Lipidome in Patients with Rett Syndrome. Metabolites, 12(4), 291. https://doi.org/10.3390/metabo12040291

Zanus, C., Costa, P., Faletra, F., Musante, L., Russo, A., Grazian, L. & Carrozzi, M. (2020). Description of a peculiar alternating ictal electroclinical pattern in a young boy with a novel SPATA5 mutation*. Epileptic Disorders, 22(5), 659–663. https://doi.org/10.1684/epd.2020.1204

Zhang, B., Korolj, A., Lai, B. F. L. & Radisic, M. (2018). Advances in organ-on-a-chip engineering. Nature Reviews Materials, 3(8), 257–278. https://doi.org/10.1038/s41578-018-0034-7

Zhang, J., Liu, M., Zhang, Z., Zhou, L., Kong, W., Jiang, Y., Wang, J., Xiao, J. & Wu, Y. (2019). Genotypic Spectrum and Natural History of Cavitating Leukoencephalopathies in Childhood. Pediatric Neurology, 94, 38–47. https://doi.org/10.1016/j.pediatrneurol.2019.01.002

Zhao, D., Mokhtari, R., Pedrosa, E., Birnbaum, R., Zheng, D. & Lachman, H. M. (2017). Transcriptome analysis of microglia in a mouse model of Rett syndrome: differential expression of genes associated with microglia/macrophage activation and cellular stress. Molecular Autism, 8(1), 17. https://doi.org/10.1186/s13229-017-0134-z

Zhao, H. H. & Haddad, G. (2024). Brain organoid protocols and limitations. Frontiers in Cellular Neuroscience, 18, 1351734. https://doi.org/10.3389/fncel.2024.1351734

Zhao, X., Yu, M., Zhang, W., Hou, Y., Yuan, Y. & Wang, Z. (2024). Demographic characteristics, diagnostic challenges, treatment patterns, and caregiver burden of mitochondrial diseases: a retrospective cross-sectional study. 19(1), 287. https://doi.org/10.1186/s13023-024-03289-5

Zheng, Y.-H., Cai, X.-B., Xia, L.-Q., Zhou, F.-Y., Wen, X.-R., Chen, D.-F., Han, F., Zhou, K.-J., Jin, Z.-B., Zhuang, W.-J. & Lin, B. (2021). Mutational screening of AGRN, SLC39A5, SCO2, P4HA2, BSG, ZNF644, and CPSF1 in a Chinese cohort of 103 patients with nonsyndromic high myopia. Molecular Vision, 27, 706–717.

Zhu, H., Bi, D., Zhang, Y., Kong, C., Du, J., Wu, X., Wei, Q. & Qin, H. (2022). Ketogenic diet for human diseases: the underlying mechanisms and potential for clinical implementations. Signal Transduction and Targeted Therapy, 7(1), 11. https://doi.org/10.1038/s41392-021-00831-w

Zlatic, S. A., Duong, D., Gadalla, K. K. E., Murage, B., Ping, L., Shah, R., Fink, J. J., Khwaja, O., Swanson, L. C., Sahin, M., Rayaprolu, S., Kumar, P., Rangaraju, S., Bird, A., Tarquinio, D., Carpenter, R., Cobb, S. & Faundez, V. (2022). Convergent cerebrospinal fluid proteomes and metabolic ontologies in humans and animal models of Rett syndrome. iScience, 25(9), 104966. https://doi.org/10.1016/j.isci.2022.104966

Zuliani, I., Urbinati, C., Valenti, D., Quattrini, M. C., Medici, V., Cosentino, L., Pietraforte, D., Domenico, F. D., Perluigi, M., Vacca, R. A. & Filippis, B. D. (2020). The Anti-Diabetic Drug Metformin Rescues Aberrant Mitochondrial Activity and Restrains Oxidative Stress in a Female Mouse Model of Rett Syndrome. Journal of Clinical Medicine, 9(6), 1669. https://doi.org/10.3390/jcm9061669

Zweers, H., Wegberg, A. M. J. van, Janssen, M. C. H. & Wortmann, S. B. (2021). Ketogenic diet for mitochondrial disease: a systematic review on efficacy and safety. Orphanet Journal of Rare Diseases, 16(1), 295. https://doi.org/10.1186/s13023-021-01927-w

PAPER PUBLICATIONS

1 PUBLICATIONS DIRECTLY RELATED TO THE CONTENT OF THIS THESIS

Oyarzábal, A., Musokhranova, U., Barros, Lf., & García-Cazorla, A. (2021). Energy metabolism in childhood neurodevelopmental disorders. EBioMedicine, 69, 103474. https://doi.org/10.1016/j.ebiom.2021.103474

Musokhranova, U., Grau, C., Vergara, C., Rodríguez-Pascau, L., Xiol, C., Castells, A. A., Alcántara, S., Rodríguez-Pombo, P., Pizcueta, P., Martinell, M., García-Cazorla, A. & Oyarzábal, A. (2023). Mitochondrial modulation with leriglitazone as a potential treatment for Rett syndrome. Journal of Translational Medicine, 21(1), 756. https://doi.org/10.1186/s12967-023-04622-5

EBioMedicine 69 (2021) 103474

Contents lists available at ScienceDirect

EBioMedicine

journal homepage: www.elsevier.com/locate/ebiom

Review

Energy metabolism in childhood neurodevelopmental disorders

Oyarzábal A[a], Musokhranova U[a], Barros LF[b], García-Cazorla A[a,*]

[a] Neurometabolic Unit and Laboratory of Synaptic Metabolism. IPR, CIBERER (ISCIII) and MetabERN, Hospital Sant Joan de Déu, Barcelona, Spain
[b] Center for Scientific Studies – CECs, Valdivia 5110466, Chile

ARTICLE INFO

Article History:
Received 4 December 2020
Revised 30 January 2021
Accepted 18 June 2021
Available online 10 July 2021

Keywords:
Brain energy metabolism
Neurodevelopment
Inborn errors of energy metabolism
Rett syndrome
Autism

ABSTRACT

Whereas energy function in the aging brain and their related neurodegenerative diseases has been explored in some detail, there is limited knowledge about molecular mechanisms and brain networks of energy metabolism during infancy and childhood. In this review we describe current insights on physiological brain energetics at prenatal and neonatal stages, and in childhood. We then describe the main groups of inborn errors of energy metabolism affecting the brain. Of note, scarce basic neuroscience research in this field limits the opportunity for these disorders to provide paradigms of energy utilization during neurodevelopment. Finally, we report energy metabolism disturbances in well-known non-metabolic neurodevelopmental disorders. As energy metabolism is a fundamental biological function, brain energy utilization is likely altered in most neuropediatric diseases. Precise knowledge on mechanisms of brain energy disturbance will open the possibility of metabolic modulation therapies regardless of disease etiology.
© 2021 The Author(s). Published by Elsevier B.V. This is an open access article under the CC BY-NC-ND license (http://creativecommons.org/licenses/by-nc-nd/4.0/)

1. The importance of energy metabolism in the brain

Information processing is expensive. The mammalian brain, gram per gram, consumes energy 10 times faster than the rest of the body, chiefly for the recovery of ion gradients, challenged by excitatory synaptic activity and action potentials [1,2]. In addition to high energy expenditure, the brain stands out for its unusual reliance on glucose, metabolic isolation by the blood-brain barrier, local recycling of metabolites, and marked division of metabolic labor between cell types. Neuronal signaling may account for most of the brain's energy budget, but astrocytes bear the brunt of the metabolic load, controlling the composition of the interstitial fluid, storing energy in the form of glycogen, supplying neurons with fuels and precursors for biosynthesis, and recycling neurotransmitters, oxidized scavengers, and other waste products [3]. In children, the brain demands even more energy, for growth and plasticity, and is relatively bigger, reaching up to 44% of the body's metabolic rate [4]. The adult brain is fueled almost exclusively by the oxidation of glucose, but other substrates become relevant when abundant in the circulation. During exercise, blood-borne lactate provides up to 25% of energy, with a corresponding reduction in fractional brain glucose consumption [5], whereas for every 1 mM increase in ketone bodies blood concentration, brain glucose consumption goes down by 10% [6,7], an effect of relevance during prolonged fasting and for the dietary treatment of seizures. In healthy neonates, ketone bodies supply about 10% of the energy consumed by the brain, a biochemical readiness that protects them against hypoglycemia [8].

Most glucose entering the brain is fully oxidized to CO_2, but the process is not homogeneous. In some regions a small but constant fraction of glucose metabolism stops at lactate, despite the presence of oxygen, a phenomenon termed aerobic glycolysis or Warburg Effect. Tonic aerobic glycolysis, which is actively studied in cancer [9], correlates with the expression of genes associated with synaptic formation and growth [10]. Noteworthy, these regions are also conspicuous for Alzheimer's beta-amyloid deposition [11]. A second instance of aerobic glycolysis is transient, lasting seconds to minutes, and is directly caused by local neural activity [12]. It is not obvious why lactate formation is preferred over full glucose oxidation, which yields 15 times more ATP. One hypothesis is that aerobic glycolysis serves to redistribute oxygen and fuel from astrocytes to neurons [13–16].

A related, but conceptually different question, is whether neurons are energized solely by glucose or co-energized by astrocytic lactate, as first proposed by Pellerin and Magistretti [17]. Thanks to technical advances in the last decade, including the measurement of glucose, lactate, NADH and other metabolites with high temporal resolution in individual cells *in vitro* and *in vivo*, it is now generally accepted that lactate produced by astrocytes serves to fuel neurons to some extent. The interested reader may like to peruse over the evidence in a CrossTalk debate and its associated correspondence [18,19]. More comprehensive reviews are also available although mostly focused on the adult brain [20,21]. In addition, it has emerged that lactate plays important signaling roles in brain tissue [22]. Much remains to

* Corresponding author.
E-mail address: agarcia@sjdhospitalbarcelona.org (G.-C. A).

https://doi.org/10.1016/j.ebiom.2021.103474
2352-3964/© 2021 The Author(s). Published by Elsevier B.V. This is an open access article under the CC BY-NC-ND license (http://creativecommons.org/licenses/by-nc-nd/4.0/)

be elucidated. Neurons differ greatly in terms of synaptic input and firing regime, eg, excitatory versus inhibitory. Do they follow different fuelling strategies? Does a given neuron transit from one fuel to another at different stimulation levels? Are neurons located in brain regions characterized by tonic aerobic glycolysis and higher lactate levels fueled in a different manner? Future technical developments shall address the issues of neuronal subcompartments, ie, somatodendritic versus axonal, astrocytic subtypes, and the metabolic roles of oligodendrocytes and microglia.

In this article we aim to expose the current knowledge about both the physiological basis of brain energy metabolism and the disorders that disturb bioenergetics during neurodevelopment. To elaborate this review, we focus not only on inborn errors of energy metabolism but also on neurodevelopmental disorders in which brain energy dysfunction has been reported.

2. Energy metabolism and neurodevelopment: where are we now?

Whereas energy function in the aging brain and their related diseases has been explored in more detail, there is only limited knowledge about the molecular mechanisms and brain networks of energy metabolism at infancy and childhood. Despite its great interest, we only have scarce understanding on substrate utilization during neonatal and following periods, with most knowledge coming from studies in animal models such as rodents. Evidence demonstrates that neural development extends from the embryonic period through adolescence, in a sequence of events comparable among species [23]. While the differences between humans and rodent models have to be taken into account, analogous structures can be identified, and inferences regarding the maturation of specific brain structures or neural circuits in rodents and humans, can be made. Through this review, data from animal models (mouse and rat) or humans will be explained, clearly stating which is being analyzed. These models provide metabolic insight during the neonatal period, however, they need to be proven useful at reproducing human-specific development.

2.1. Brain energy during neonatal development

From an energy metabolism point of view, the main players to be taken into account in neurodevelopment are glucose, lactate and ketone bodies. On one side, glucose is metabolized through the glycolytic pathway to pyruvate, and further metabolized either to lactate or to Acetyl-CoA, entering the mitochondrial TCA (tricarboxylic acid) cycle. On the other side, lactate may be metabolized back to pyruvate, further processed in mitochondria, and ketone bodies are transported into the mitochondria for metabolism into Acetyl-CoA (Fig. 1).

Compared to the adult brain, the ratio of lactate and ketone bodies versus glucose utilization is higher in neonates. Taking data from animal models, in a 7 days postnatal rat glucose supports 63% of brain energy demands and ketone bodies provide 30% [24], while in fed non-ketotic adult rats glucose is the principal fuel of the brain. Lactate and other monocarboxylate (MCT) utilization by the fetal brain can be up to three-fold higher than the neonatal brain [25], highlighting the use of lactate during neurodevelopment.

The glucose/lactate utilization discrepancy is reflected in the expression of their blood-brain barrier (BBB) specific transporters. Neonate rat and mouse studies show a predominant expression of the monocarboxylate transporters [26], responsible for ketone body and lactate crossing, and a lowered expression of glucose transporters GLUT1 and GLUT3, responsible for the transport of glucose in the BBB and into neurons and glial cells [27,28]. The dynamic regulation of glucose transporters goes along with the expression of glycolytic enzymes, that change several fold between the neonate period and adult age in the studied models, such as PFK1 (Phosphofrucktokinase 1) or Hexokinase [24].

Ketone bodies (KBs) (acetoacetate, acetone and b-hydroxybutyrate) are an indispensable energy source in neurodevelopment at the fetal stage [29]. They provide acetoacetyl-CoA and acetyl-CoA for the synthesis of lipids, fatty acids and cholesterol, preferred over glucose for such biomolecules [30]. They are metabolized from medium and short fatty acids and imported into the brain through specific transporters such as MCT1. Regarding their energetic role, upon importation they are oxidized into acetyl-CoA, and enter into the TCA cycle. In suckling rodents, KB absorption and MCT1 expression is homogeneous throughout the brain, while in adult brains we find differences in their distribution. Interestingly, glucose and KB metabolism keep playing an important role through adult life. While glucose metabolic rate decreases in older adults, acetoacetate metabolism remains similar between the young and old, once again showing spatial differences across the brain. It should be noted that KBs are not only highly energetic but also precursors of cholesterol biosynthesis, which is over-represented in fetal metabolism compared to adults.

To what extent these pathways meet the energy needs of the neonatal brain was addressed by Ivanov et al. [31], who proved in neonatal hippocampal brain tissue preparations that synaptic function depended on oxidative metabolism; glycolysis alone not being able to meet its energetic needs. Simultaneously measuring field potentials, oxygen levels and NAD(*P*)*H* fluorescence, they proved that lactate not only sustained synaptic activity but enhanced it, together with oxygen utilization. Culturing hippocampal slices with 5 mM glucose and 5 mM lactate resulted in an increase of oxygen consumption and local field potentials (31% and 41% increase respectively), compared to activation with glucose alone. These results were further enhanced when lactate was the only substrate in the medium, confirming lactate as a neonatal brain fuel and implying that in neonates, lactate might be preferentially used over glucose when both substrates are present at equal concentrations [32].

Both lactate and KB metabolism converge in the mitochondria. Also, the complete oxidation of glucose requires the sequential action of glycolysis in the cytosol, followed by the mitochondrial decarboxylation of pyruvate mediated by PDH (pyruvate dehydrogenase), the incorporation of acetyl-CoA in the TCA cycle and the oxidation of reducing equivalents in the respiratory chain (Fig. 1). This review does not intend to cover mitochondrial function through development; however, its role has to be taken into consideration. Together with its bioenergetics function, mitochondria are a metabolic and signaling hub in the neuron. As a consequence of oxidative respiration, mitochondria produce reactive oxygen species (ROS). Under physiological circumstances, they act as signaling molecules that are required for synaptic plasticity [33] but they get severely deregulated upon mitochondrial insult. ROS overproduction can be found in many diseases [33] and, compared to other organs, the immature brain is especially vulnerable to ROS.

2.2. Beyond the neonatal period

After the neonatal period, brain lactate metabolism decreases through early infancy to childhood, while glucose uptake and metabolism rises. *In vivo* studies using hyperpolarized ^{13}C imaging reveal that the conversion rate of pyruvate to lactate on developing mouse brain models [34] decreases through development (Fig. 1b). In humans, following the early neonatal period, glucose consumption rapidly increases. Glucose PET scanning shows that, after the second year of life, when adult values are reached, glucose metabolic rates continue increasing. Then, in the third year of postnatal development, they exceed the adult values and sustain this rate until adolescence, when it gradually decays to adult values [35–37].

In the human neonatal brain, PET scans reveal early activation of subcortical areas such as the thalamus, brain stem, cerebellar vermis, amygdala, hippocampus, or cingulate cortex. These are evolutionarily preserved structures and related to neonate behavior as reflexes or

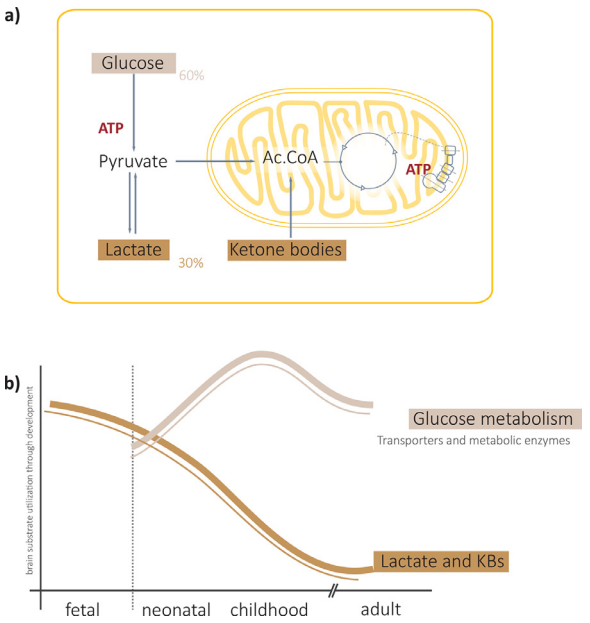

Fig. 1. *Energy metabolism during neurodevelopment: key molecules and their dynamics.* Glucose, lactate and ketone bodies (KBs) are key players in energy metabolism during neurodevelopment. (a) Basic pathways for energy production. In a 7-days postnatal rat, glucose supports around 60% of brain energy demands, and KBs support 30% (24). (b) Substrate utilization dynamics in the brain throughout development.

emotional processing and bonding. Later on, as functional complexity increases, maturation and glucose uptake augment in frontal eye fields, parietal cortex, basal ganglia and cerebellar cortex, ending in frontal cortex maturation [36].

Data on brain substrate utilization does not reveal the pathways the substrates undergo. Interestingly, an increase in oxygen consumption through development is delayed from glucose increase, suggesting the non-oxidative metabolism of glucose through this period. The oxygen-glucose index (OGI) has a theoretical maximum value of 6, meaning 1 molecule of glucose is fully oxidized with 6 molecules of O_2 to 6 CO_2 and water. This index drops below 6 when glucose is consumed by the brain but not oxidized, ie, non-oxidative metabolism of glucose despite oxygen availability (also referred to as aerobic glycolysis (AG) or Warbug effect). As a reference frame, in adult brains, AG accounts for 10–12% of total glucose metabolism, and is related to the most neotenous regions [10]. This ratio is increased in the developing brain by several fold [38], when synaptic growth is at its highest. While AG has been well documented in different contexts, such as cancer metabolism, as previously explained, its role on brain development remains to be elucidated. It has been proposed that this AG imbalance represents a way to sustain synaptogenesis as brain mass increases, but this has been ruled out as the only explanation since the theoretical increase in mass due to the AG ratio differs from the actual increase. Lactate production as the sole final fate of glucose was also discarded by performing a meta-analysis of lactate brain concentrations during childhood and noting that it did not peak as glucose did [39]. A combination of multiple routes appears to be the most plausible explanation. Other possible destinations for glucose carbon have to be taken into account, such as the pentose phosphate pathway (PPP) or biosynthetic precursors.

Although we have discussed the role of lactate in the neonatal brain, it is important not to obviate the role of glucose metabolism in brain development. Energetic metabolism of substrates such as lactate and KBs permit the utilization of glucose in alternative metabolic routes of crucial importance during neurodevelopment (Fig. 2). Basal PPP activity for instance accounts for 5–15% of glucose metabolism in the 7 day postnatal rat brain [40,41], showing a larger use of glucose in this pathway in the neonate compared to the adult [24]. Additionally, glucose is essential for a diverse number of key processes such as neurotransmitter homeostasis [19,42] or myelination [43] - a

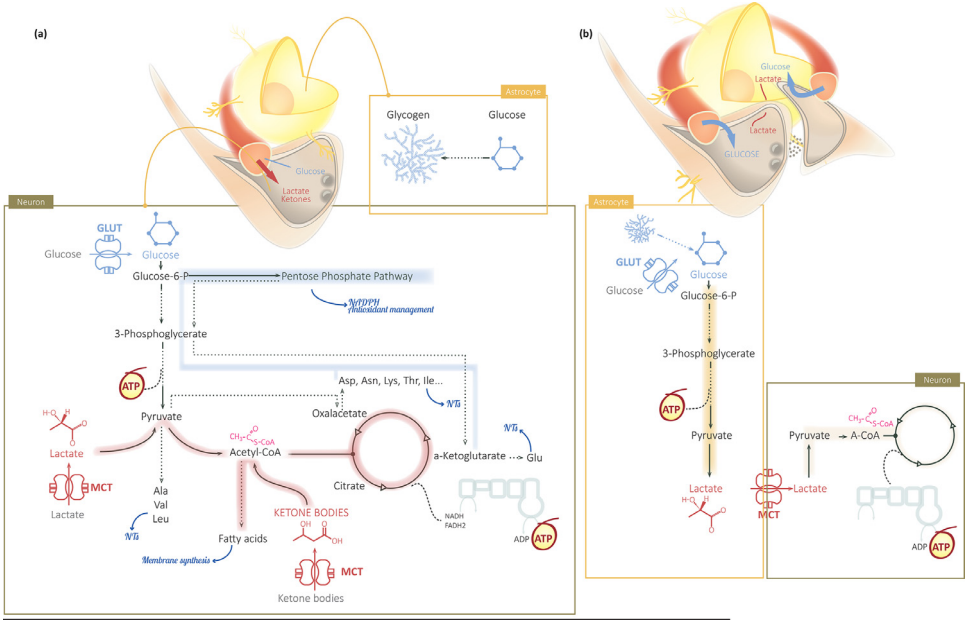

Fig. 2. *Perinatal to early infancy versus childhood to adolescence brain metabolism.* Only main variations between both development times are shown. (a) In the neonatal brain, lactate and ketone bodies (KBs) uptake versus glucose ratio is higher than in the adult brain. Upon importation of glucose into the neuron, it will be preferentially metabolized through the pentose phosphate pathway, generating both NADPH and precursors for the synthesis of nucleotides, as well as key element in the antioxidant defense of the cell. Glucose might also be further metabolized for the generation of oxalacetate, a-Ketoglutarate and pyruvate, all precursors of amino acids which also have specific roles as neurotransmitters (NTs), as is the synthesis of glutamate. Lactate and KBs are taken up by the cell at much higher rates than found in adults. They undergo metabolism for the production of Acetyl CoA, which can either enter the TCA cycle, producing NADH used by the mitochondrial electron transport chain for ATP synthesis, or for sterol synthesis, such as cholesterol, a key element for neurodevelopment signaling and essential component of membranes. KBs are preferentially used over lactate for fatty acid synthesis. (b) The astrocyte neuron lactate shuttle metabolism model is roughly represented for the adult brain metabolism scheme. Multichannel Transporters (MCRs) transport metabolites through membranes into the specified compartment.

high energy-demanding process used by oligodendrocytes that occurs throughout development as glucose consumption peaks. Glucose is also essential for oligodendrocyte precursor cell differentiation and migration [44], and mature oligodendrocytes rely on glycolysis for ATP production even in the presence of oxygen [45,46]. The switch from mitochondrial to glycolytic metabolism for ATP production might also respond to the necessity to reduce the production of ROS, a necessary by-product of respiratory chain activity [47]. Surprisingly, oligodendrocytes rely on lactate for myelin production and, as astrocytes, they supply lactate to the axon through MCT1 transporters [43]. We therefore find that both glucose and lactate are critical for brain function and development.

2.3. Common therapeutic strategies based on energy metabolism modulation

We have reviewed how energy metabolism is a crucial element of neurodevelopment. Given this, it can constitute not only a common pathway through different diseases (as will be further explained), but also a common therapeutic target. Besides their energetic functions, both lactate and KBs show neuroprotective roles [48,49], being candidates for common therapeutic development. Lactate produces a therapeutic effect in neonatal hypoxia-ischemia models [50,51]. It not only acts as an energetic substrate, but can also act directly on cell signaling through the activation of the HCAR1 receptor, potentiating angiogenesis [52] and neurogenesis in experimental intra-cerebral hemorrhage [53]. These results have been translated into clinical practice in adult traumatic brain-injured patients [54]. A similar effect has been demonstrated in neonatal hypoxia-ischemia rat models, where multiple sequential lactate injections after ischemic damage resulted in reduced brain damage and improved cognitive and sensorimotor deficits [50].

The therapeutic application of KBs is found in ketogenic diets (KD), used in the management of intractable epilepsy in children. Reported as a therapeutic option in 1921 [55], its antiepileptic mechanisms remain poorly understood. This therapeutic approximation is especially effective in the management of GLUT1-deficiency syndrome. This disease results from dominant mutations in *SLC2A1*, which encodes the facilitative transporter GLUT1, located in endothelial cells of the BBB and astrocytes and mediates the entrance of glucose into the brain. Deleterious mutations in *SLC2A1* reduce glucose availability to astrocytes and neurons, most commonly resulting in infancy-onset epilepsy, associated with movement disorders, cerebellar ataxia, and deceleration of head growth. Around 60% of the patients on KD become seizure-free, suggesting that 4-carbon KBs can compensate a glucose deficit. The results of KD in GLUT1 management [56] and other forms of intractable epilepsy and other conditions [57–59] exemplify the potential of energy metabolism as a therapeutic approach in neurodevelopmental diseases.

Defining alterations in energy metabolism and pathology in specific diseases, will be further reviewed. Understanding brain energy metabolism through development and its intricate relationship with neurodevelopment diseases sets the targets and time frames for therapeutic intervention [60,61] and proper development [62].

3. Monogenic disorders of energy metabolism

The importance of brain energy metabolism is completely reflected in the diseases that arise from primary defects of brain energy homeostasis [58,63]. These are genetic diseases of brain metabolism (inborn errors of metabolism: IEM) with symptoms due, at least in part, to a deficiency in energy production or utilization within the nervous system. In these IEM, other high-energy consumption organs (eg, muscle, heart, liver, eyes), are frequently involved. Most of them are pediatric-onset diseases. Therefore, they represent excellent models to study how energy is used in the neurodevelopmental brain. Functional tests measuring glucose, lactate, ketones and other energetic molecules (amino acids, organic acids, acylcarnitines) are useful diagnostic tools. According to a recently published simplified classification of IEM [64], these disorders could be divided into defects of membrane carriers of energetic molecules, cytoplasmic energy defects, and mitochondrial defects. Table 1 gives a global overview of these disorders. They encompass numerous diseases with diverse clinical manifestations from early-onset global encephalopathies to late-onset presentations, which may appear as movement disorders, stroke-like episodes, and neuromuscular signs amongst others.

Despite well-characterized clinical and biochemical descriptions, the cellular and molecular basis of brain energy impairment is still poorly understood in most of these IEM. As an example, in Glut1-deficiency syndrome, which is one of the most paradigmatic diseases, there is still insufficient knowledge regarding how energy is utilized on different nervous cells and compartments. However, ketogenic diet, an energy replacement therapy, shows important benefits for the patients [56].

Combined proton MRS (^{1}H MRS) and glucose metabolism PET could provide useful biomarkers of brain energetics in these rare disorders. However, there are only a few studies using this approach, and most reports in mitochondrial disorders have been performed in adults. In two children with congenital lactic acidosis, researchers found a massive increase of glycolysis to accommodate energy requirements in brain tissue [65]. Other than glucose, PET studies could also be used to trace pyruvate, lactate, and other energy molecules in the brain, leading to interesting data about the utilization of diverse fuels in the nervous system. However, these brain imaging techniques are not universally available and age-dependent control studies are scarce.

4. Energy metabolism in neurodevelopmental diseases

As reviewed so far, energy metabolism is essential for normal brain function and development, and can be both a common pathway of disease and - more importantly - a shared therapeutic strategy. Defects on brain metabolism result in neurodevelopmental diseases, as reviewed in the previous sections. Yet, remaining questions to be answered include: how is energy metabolism affected in monogenic neurodevelopmental diseases when it is not the primary cause of the disease? Can its modulation constitute a viable therapeutic strategy? As summarized in Table 1, in this section we review those neurodevelopmental diseases in which brain energy dysfunction has been reported in the scientific literature. First, we report on the studies of brain energy in neurological syndromes such as: (i)-autism spectrum and psychiatric disorders;-epileptic encephalopathies. Then we focused on specific genetic diseases: (ii) -Rett syndrome; -fragile-*X* syndrome; -Down syndrome, considered as the most common causes of intellectual disability.

4.1. Autism spectrum and psychiatric disorders

Autism Spectrum Disorder (ASD) is a complex neurodevelopmental disorder that involves deficits in sociability and communication and increased restrictive and/or repetitive behavioral patterns.

Molecular pathways involved in ASD are as diverse as their etiology [66], including mitochondrial function, suspected to be involved in ASD development since 1985, when lactic acidosis was described in 5% of autistic patients [67]. Several studies support the linkage between mitochondria and ASD, which can be distributed into four categories [68]: (a) many genes coding for mitochondrial proteins have been described as ASD-risk genes, (b) studies in ASD patients' brain show impaired mitochondrial function, (c) blood studies point towards mitochondrial malfunctioning in ASD patients, and (d) abnormal mitochondrial function has been described in peripheral

Table 1

DISEASE	NEUROLOGICAL SYMPTOMS/TREATMENT	BIOCHEMICAL AND CELL BIOLOGY CHARACTERIZATION	BRAIN MAPPING
Inborn errors of metabolism primarily involving brain energy utilization			
Cell membrane carriers of energetic molecules			
GLUT1 *(SLC2A1)*	GLUT1 deficiency syndrome (GLUT1DS) is characterized by epilepsy, a complex movement disorder, and developmental delay. Variants of the classical form present with only one or two of the three items. Non-epileptic paroxysmal events: episodes of ataxia, dystonia, exercise induced.[1] Treatment: ketogenic diet	GLUT1 is a membrane glycosylated protein that transport glucose across the BBB and is also expressed in astrocytes (not in neurons). GLUT1DS causes a chronic neuroglycopenia which in turn produces the whole repertoire of clinical symptoms It should be suspected in any patient with a CSF glucose concentration < 2.5 mmol/l (normal >3.3 mmol/l). Values are age-specific and may vary considerably (range 0.9 - 2.9 mmol/l).[2]	PET studies: cortical hypometabolism in the mesial temporal regions and thalami; signal increase in the basal ganglia. Hypometabolism in bilateral thalami and increased uptake in bilateral lenticular nuclei.[3]
PAST-A (*SLC45A1*)	Intellectual disability, epilepsy and neuropsychiatric features. Facial dysmorphism. Stereotyped hand movements and behavioral problems including anxiety and autism.[4] There is no effective treatment	PAST-A is a proton-associated sugar transporter expressed in neurons. It links glucose transport to the gradient of protons allowing regulatory effects. Impaired uptake of glucose into neurons by this dysfunctional transporter results in the reported symptoms. Both plasma and CSF glucose are within normal limits	Brain MRI is normal. PET studies are not conclusive as diagnostic marker
MCT1 *(SLC16A1)*	Profound ketoacidosis after poor feeding and vomiting (van Hazzel, 2014). Homozygous mutations may cause severe developmental delay and abnormal brain MRI. Treatment: iv glucose or dextrose + bicarbonate	MCT1 is a protein that transport Lactate, Pyruvate and Ketones. MCT1 deficiency causes ketoacidosis due to ketone-body transport deficiency, necessary to maintain acid-base balance.	Homozygous mutations: White matter and sucortical U fibers involvement,. CC, Thalami and BBGG also Heterotopias.[5]
MCT12 (*SLC16A12*) Creatine transport	X-linked Intellectual disability, autistic features, behavioral disturbances, seizures and movement disorders (van Kamp, 2013). Treatment: high dose creatine, arginine, glycine and S-adenosylmethionine may offer some improvement	Creatine is involved in energy production and acts as an ATP shuttle from the inner mitochondria to the cytosol High urine creatine to creatinine ratio is a biomarker of the disease	Brain spectroscopy shows low creatine peak but a detailed study about anatomic areas and creatine quantification has not been published
Cytoplasmic energy defects			
Glycolysis and PPP defects	Most disorders present with myopathy. Those with prominent central nervous system have poor therapeutic options and are the following: **TPI deficiency:** movement disorders, spinal motor neuron involvement seizures and psychomotor delay. Haemolytic anemia There is no effective treatment. **PGK deficiency:** Haemolytic anemia, myopathy. ID and early-onset parkinsonism. **RPI deficiency:** leukoencephalopathy, seizures, spasticity, ataxia, neuroregression. **TKT deficiency**: developmental delay and short stature		
Glycogen defects Synthesis and catabolism	The neurological aspects of these disorders are due to complications of profound and/or recurrent hypoglycaemias. In the neonatal period and early infancy occipital and parieto-temporal areas are predominantly affected and may cause visual dysfunctions, seizures, acquired microcephaly and developmental delay.[6]		
Creatine defects	**AGAT deficiency:** non-syndromic ID with speech and language delay, microcephaly, hand stereotypies. **GAMT deficiency:** ID with speech and language delay, behavioral problems and epilepsy. Treatment: creatine supplementation in both defects. Ornithine in GAMT	Systemic and cerebral creatine deficiency AGAT: Low guanidinoacetate in urine GAMT: Elevated guanidinoacetate in urine Profound cerebral creatine deficiency *in vivo* brain MRS in all creatine defects.[7]	GAMT deficiency: globus pallidus involvement with T2 prolongation.
Mitochondrial defects			
General oxidative metabolism: energy components of the TCA cycle and Pyruvte metabolism that feed into OXPHOS			
Fatty acid oxidation	Most are treatable disorders. The neurological aspects of these disorders are due to complications of profound and/or recurrent hypoglycaemias but there are also some other symptoms depending on specific diseases: **LCHAD deficiency:** peripheral neuropathy; **Crotonase deficiency, *NADK2***: neurodegeneration; *ETFA, ETFB, ETFDH, CPTII:* brain malformations. **Riboflavin transport and metabolism defects** may impair beta-oxidation and produce ponto-bulbar palsy, deafness and peripheral neuropathy.		
Ketones metabolism	Most are treatable disorders. Other than the consequences of recurrent and/or profound hypoglycaemias, specific signs dependeing on every disease are the following: **Ketogenesis defects: - HMG-CoA lyase deficiency**: myelination abnormalities, cerebral atrophy and basal ganglia abnormalities. **Defects of KBs utilization or transport: succinyl-CoA:3-oxoacid CoA transferase (SCOT), mitochondrial acetoacetyl-CoA thiolase (T2) and monocarboxylate transporter 1 (MCT1):** severe ketoacidosis starting in early childhood, abnormalities in the basal ganglia in a number of patients with T2 deficiency. Some of these patients have presented with hypotonia, dystonia or chorea without any preceding episodes of acidosis. Abnormalities in the basal ganglia in a number of patients with T2 deficiency. Some of these patients have presented with hypotonia, dystonia or chorea without any preceding episodes of acidosis		
Pyruvate/lactate oxidation	**PC deficiency:** lactacidosis, ketosis, severe neonatal encephalopathy, episodic lactacidosis and ataxia, periventricular lesions. **PDH deficiency:** delayed development, hypotonia, seizures and ataxia, hyperpyruvicaemia, lactic acidaemia. Basal ganglia abnormalities. May respond to high thiamine doses and/or ketogenic diet. **Mitochondrial Pyruvate Carrier deficiency:** neonatal and mild progressive encephalopathy, hyperlactacidaemia with normal lacte/pyruvate ratio.		
Krebs cycle	**These defects include KDHC, SUCL, SDH, FH, ACO, MAS, and NAD(P)HX system repair defects.** Most of them cause encephalopathies with basal ganglia involvement (Leigh-like) and lactacidosis with specific organic acid profile. High doses of vitamin D3 (nicotinamide) has been suggested to be a treatment in NAD(P)HX system repair defects. Pyridoxine and serine in MAS deficiency.		

(*continued*)

Table ? 1 (*Continued*)

DISEASE	NEUROLOGICAL SYMPTOMS/TREATMENT	BIOCHEMICAL AND CELL BIOLOGY CHARACTERIZATION	BRAIN MAPPING
Respiratory chain and other mitochondrial functions			
OXPHOS subunits, assembly factors and electron carriers, mtDNA maintenance, mtDNA expression, mt aminoacyl tRNA synthetases, enzyme cofactors, mitochondrial homeostasis and quality control This is a large category of diseases that encompass about 300 genes[8]. About 200 genes have a primary role in OXPHOS biogenesis. Pathogenic mutations have been reported in all 37 mtDNA genes and all tRNA synthetases (19 genes). Only few are treatable so far: Vitamins, CoQ, Xenobiotic. Neurological manifestations are heterogeneous. Basal ganglia and cerebellar involvement are frequent. Most of them have a progressive character[9].			
DISEASE	**NEUROLOGICAL SYMPTOMS/TREATMENT**	**BIOCHEMICAL AND CELL BIOLOGY CHARACTERIZATION**	**BRAIN MAPPING**
Neurogenetic disorders in which brain energy dysfunction is a major mechanism of disease			
Rett syndrome (*MECP2*)	Regression in neurodevelopment between 6 and 18 months of age. Communicative ability and purposeful use of hands are lost, and stereotypies, autism signs, and seizure appear over time	Decrease in the OXPHOS complexes which results in ATP levels decrease, ROS production increase and an exaggerated redox responses both in cytosol and mitochondria has been shown. Abnormal mitochondrial morphology	Frontal lobe hypoperfusion, increased choline, and reduced NAA. However, glucose metabolism PET showed *hypermetabolism* of the frontal lobe (related to increased glutamate cycling in synapses).[10]
X-Fragile syndrome (*FMR1*)	Intellectual disability, diverse behavioral abnormalities, autistic signs, epilepsy	Respiratory chain complexes are up-regulated, elevated ROS production, decrease in ATP production, increased synthesis of TCA cycle and glycolytic enzymes	No energy brain mapping studies reported
Down syndrome	Intellectual disability, epilepsy and behavioral abnormalities may appear	Decrease of ATP production and increase in oxidative stress and altered mitochondrial dynamics.	Enhanced resting neuronal activity in cortical areas involved in reasoning, cognition, and speech This difference is confined to the dominant (left) hemisphere.[11]
Autism	Neurodevelopmental disorder that involves deficits in sociability and communication and increased restrictive and/or repetitive behavioral patterns	Impaired mitochondrial function: diverse respiratory chain abnormalities 1/3 of patients show elevated respiratory rates, approximately 200% of controls, for respiratory parameters associated with adenosine triphosphate production.[12]	PET studies: hypometabolism in parietal lobe, frontal premotor and eye-fields areas and amygdala. Rates increased in the posterior cingulate, occipital cortex, hippocampus and basal ganglia.[13]
Schizophrenia	Symptoms can include delusions, hallucinations, disorganized speech, trouble with thinking and lack of motivation	Decreased ATP production and increased oxidative stress. Increased lactate and decreased pH in schizophrenia brain.	PET studies: hypometabolism in the frontal lobe, anterior cingulate, superior temporal gyrus, amygdala and medial thalamic nuclei.[13]
Epileptic Encephalopathies	Other than epilepsy, neurodevelopmental delay motor symptoms and behavioral dysfunction are common	ATP depletion but transient ATP increase at the synaptic level, ROS increase. Oxidative damage, neurotransmitter uptake and release dysfunction.[14]	PET studies show different patterns of hypometabolism

Names of genes are in italics. ACO: Mitochondrial Aconitase deficiency; AGAT: Glycine Amidinotransferase Deficiency; BBB: blood brain barrier; GAMT: Guanidinoacetate Methyltransferase Deficiency; FH: Fumarase Deficiency; HMG-CoA: Mitochondrial 3-Hydroxy-3-Methylglutaryl-CoA; ID: intellectual disability; IV: intravenous; KBs: ketone bodies; KDHC: 2-Ketoglutarate Dehydrogenase Complex Deficiency; LCHAD: long-chain 3-hydroxyacil-CoA dehydrogenase deficiency. MAS: Malate-aspartate shuttle defects; MCT: monocarboxylate transporter; NAA: N-Acetylaspartate; NAD(P)HX system repair defects; NADK2: Dienoyl-CoA reductase; PC: pyruvate carboxylase deficiency; PDH: pyruvate deshydrogenase deficiency. PGK: Phosphoglycerate Kinase. PPP: pentose phosphate pathway; RPI: Ribose-5-Phosphate Isomerase; SDH: Succinate Dehydrogenase Deficiency; SUCL: Succinyl-CoA Ligase Deficiency Succinyl-CoA ligase deficiency; TKT: Transketolase deficiency; TPI: Triosephosphate Isomerase.

REFERENCES.

[1] Leen WG, Klepper J, Verbeek MM, Leferink M, Hofste T, van Engelen BG, et al. Glucose transporter-1 deficiency syndrome: the expanding clinical and genetic spectrum of a treatable disorder. Brain. 2010 Mar;133(Pt 3):655–70.

[2] Leen WG, Wevers RA, Kamsteeg E-J, Scheffer H, Verbeek MM, Willemsen MA. Cerebrospinal fluid analysis in the workup of GLUT1 deficiency syndrome: a systematic review. JAMA Neurol. 2013 Nov;70(11):1440–4.

[3] Natsume J, Ishihara N, Azuma Y, Nakata T, Takeuchi T, Tanaka M, et al. Lenticular nuclei to thalamic ratio on PET is useful for diagnosis of GLUT1 deficiency syndrome. Brain Dev. 2021 Jan;43(1):69–77.

[4] Srour M, Shimokawa N, Hamdan FF, Nassif C, Poulin C, Al Gazali L, et al. Dysfunction of the Cerebral Glucose Transporter SLC45A1 in Individuals with Intellectual Disability and Epilepsy. Am J Hum Genet. 2017 May;100(5):824–30.

[5] Nicolas-Jilwan M, Medlej R, Sulaiman RA, AlSayed M. The neuroimaging findings of monocarboxylate transporter 1 deficiency. Neuroradiology. 2020 Jul;62(7):891–4.

[6] Ferreira GC, McKenna MC. L-Carnitine and Acetyl-L-carnitine Roles and Neuroprotection in Developing Brain. Neurochem Res. 2017;42(6):1661–75.

[7] Fons C, Campistol J. Creatine Defects and Central Nervous System. Semin Pediatr Neurol. 2016 Nov;23(4):285–9.

[8] Frazier AE, Thorburn DR., Compton AG. Mitochondrial energy generation disorders: genes, mechanisms, and clues to pathology. J Biol Chem. 2019 Apr;294(14):5386–95.

[9] Saudubray J-M, Mochel F, Lamari F, Garcia-Cazorla A. Proposal for a simplified classification of IMD based on a pathophysiological approach: A practical guide for clinicians. J Inherit Metab Dis. 2019 Jul;42(4):706–27.

[10] Chugani HT. Positron Emission Tomography in Pediatric Neurodegenerative Disorders. Pediatr Neurol. 2019 Nov;100:12–25.

[11] Lengyel Z, Balogh E, Emri M, Szikszai E, Kollár J, Sikula J, et al. Pattern of increased cerebral FDG uptake in Down syndrome patients. Pediatr Neurol. 2006 Apr;34(4):270–5.

[12] Frye RE. Mitochondrial Dysfunction in Autism Spectrum Disorder: Unique Abnormalities and Targeted Treatments. Semin Pediatr Neurol. 2020 Oct;35:100,829.

[13] Mitelman SA, Bralet M-C, Mehmet Haznedar M, Hollander E, Shihabuddin L, Hazlett EA, et al. Positron emission tomography assessment of cerebral glucose metabolic rates in autism spectrum disorder and schizophrenia. Brain Imaging Behav. 2018 Apr;12(2):532–46.

[14] **Zhou Z**, Austin GL, Young LEA, Johnson LA, Sun R. **Mitochondrial** Metabolism in Major **Neurological Diseases**.Cells. 2018 Nov 23;7(12):229.

tissues and cells of autistic patients. These reports are complemented by studies in animal models, leading to the same conclusions. It has been proposed that systemic mitochondrial mutations can cause tissue-specific brain defects accompanied by regional neurophysiological alterations that result in autistic endophenotypes, as was demonstrated in a mouse strain bearing an mtDNA gene missense mutation [69].

Metabolic dysfunction can be either the primary cause (ie, IEM with features of ASD), or secondary contributions to precise ASD pathophysiology [70]. Different types of biomarkers (respiratory chain activities, lactate, pyruvate, alanine, lysine, carnitine, acyl carnitines) suggest the prevalence of abnormal mitochondrial function is much higher than the prevalence of classic mitochondrial disease, perhaps around 30−50% [71]. Additionally, studies in lymphoblastoid cell lines [72,73] derived from children show that one-third of patients present mitochondrial hyperactivity with elevated respiratory rates, approximately 200% that of controls, for respiratory parameters associated with adenosine triphosphate production [71].

One therapeutic strategy based on metabolic manipulation in ASDs is KD, but other strategies are being explored, such as supplementation with vitamins [74], N-acetylcysteine [75] or sulforaphane [76].

Regarding psychiatric disorders, we will focus on the three major psychiatric diseases: schizophrenia, bipolar disorder (BPD), and major depressive disorder (MDD). All three show differential expression in a substantial number of proteins related to energy metabolism (92 in SCZ, 95 in BPD, and 41 in MDD), five of which are common in the three diseases, such as citrate synthase [77], pointing towards impaired oxidative phosphorylation [78], increased glycolysis [79] and altered ROS-detoxification systems [80].

Schizophrenia is a developmental disorder that encompasses synaptic dysfunction. As in ASD, metabolic disturbances might be either the primary cause or secondary elements to the disease [81]. Moreover, metabolic studies in schizophrenia are hampered as most antipsychotics produce metabolic changes in patients [82]. Alterations in the electron transport chain activity, resulting in decreased ATP production and increased oxidative stress, have been reported [83−85] and these dysfunctions might be region- or cell-specific [81]. Additionally, multiple studies point to increased lactate and decreased pH in the schizophrenic brain. There is evidence to suggest that increased brain lactate may be directly related to diminished cognitive function [79] while decreased brain pH has been associated with increased emotional withdrawal [86]. Increased brain lactate seems to be driven by a high glycolysis rate and low TCA cycle and oxidative phosphorylation activity [87].

Psychiatric disorders continue to grow with a great impact on health, social and human rights [88]. Narrowing down the metabolic aspects of these diseases and investigating if they can constitute a therapeutic target is key for their proper management, as is the use of eicosapentaenoic acid (EPA) and docosahexaenoic acid (DHA) in mood disorders, in particular for the treatment of depressive symptoms in unipolar and bipolar depression [89−91].

4.1.1. *Epilepsy and epileptic encephalopathies*

It is beyond the scope of this review to provide a detailed summary of early epileptic encephalopathies and energy metabolism disruption. Major evidence of the involvement of bioenergetics in the epileptic phenomenon comes from clinical practice: the use of KD as an alternative fuel supply and a membrane potential stabilizer. However, the connection between mitochondrial dysfunction, energy metabolism, and epilepsy in childhood has not been described in detail. Regardless of the etiology, seizure activity significantly decreases ATP levels in neurons, suggestive of energy depletion. Because neurons lack glycolytic capacities, the metabolic strain of post-seizure activity increases the demand for oxidative phosphorylation and may trigger an excess ROS and Ca^{2+} fluctuations (Table 1).

4.1.2. *RETT syndrome*

Rett syndrome (OMIM # 312,750) affects 1 in 10,000 people, usually due to *de novo* mutations in *MECP2*, located on the X chromosome. It is the second most common cause of intellectual disability in women and is characterized by a regression in neurodevelopment between 6 and 18 months of age. Communicative ability and purposeful use of hands are lost, and stereotypies, autism signs, and seizures appear over time [92,93]. Despite the great complexity of the disease, it seems clear that Rett syndrome is a disorder that arises from an imbalance between excitatory and inhibitory activity, and failure in the maturation of neural circuits, which remain in an immature state throughout development [94].

Prior to the description of *MECP*2 as the causative gene for Rett syndrome, it was questioned by the earliest studies to be a mitochondrial disease, as it shares many features with classic mitochondrial disorders (eg, early symptomatic debut, neurodevelopment delay, motor and intellectual regression, movement disorders), suggesting energy metabolism impairment [95]. An imbalance in the redox state has been described in fibroblasts from patients, which translates into oxidative damage in lipids and proteins, lowering of antioxidant defences (GSH) and morphological changes in the cell [96,97]. Furthermore, in murine models, a decrease in the OXPHOS complexes has been shown [98], resulting in a decrease in ATP levels, an increase in ROS production [99], and an exaggerated redox-response both in cytosol and mitochondria. Although a common pathway or element that explains mitochondrial dysfunction in Rett syndrome has not yet been found, there are many cases in which associated mitochondrial dysfunction is described as being responsible [100].

In spite of promising clinical trials [101], Rett syndrome lacks a specific treatment. Interestingly, correcting mitochondrial dysfunction is a potential therapeutic strategy [102]. Pharmacological stimulation of the mitochondrial serotonin receptor 5-HT7R effectively restores mitochondrial impairments in mouse models. Indeed, restoration of respiratory chain complexes together with the correction of mitochondrial ROS overproduction in different models of Rett syndrome, has resulted in a sustained phenotypic amelioration of the disease [99,103].

Setting the focus on mitochondria as a target for Rett syndrome could result in repurposing known drugs. Such is the case with metformin, used for decades in the treatment of type 2 diabetes [104−106], but whose mechanism of action has only been partially solved. Treatment of symptomatic Rett syndrome mouse models with 100 mg/kg metformin for 10 days resulted in an improvement of ATP brain levels and ROS production [107]. As concluded by the authors, “by improving brain mitochondrial dysfunction, metformin may rescue the neurological phenotype, thus representing an innovative and repurposable therapeutic strategy for Rett”.

4.1.3. *Fragile* X *syndrome*

Fragile *X* syndrome (FXS) (OMIM # 312,750) is the most frequent form of hereditary intellectual disability and genetic cause of autism. It associates epilepsy and behavioral abnormalities and is normally caused by a CGG triplet expansion within the X-located gene *FMR1*, resulting in the loss of expression of FMRP. FMRP is an mRNA-binding protein that controls different processes such as mRNA transport, splicing and translation or DNA damage response. This phenotype is accompanied by immature synapses and synaptic plasticity and excitotoxicity.

Besides the RNA-modulating function of FMRP, metabolic alterations have been described in FXS, suggesting a defect in mitochondrial physiology and oxidative phosphorylation [108]. These defects, including altered mitochondrial dynamics and increased oxidative stress, result in deficits in dendritic maturation, and have been described both in FXS mouse and *Drosophila* models [109,110]. Respiratory chain complexes are up-regulated in FXS mouse models [111], accounting for the elevated ROS production, but surprisingly, paired

to a decrease in ATP production. During early stages of development, ATP synthase subunit c accounts for a mitochondrial inner membrane leak, which favors glycolytic metabolism over oxidative phosphorylation. This leak is closed between embryonic days 11 and 13 in wild-type mouse cardiomyocites [112], when oxidative phosphorylation starts. As recently reported, such closure does not occur in FXS cells, resulting in the increased synthesis of TCA cycle and glycolytic flux-supporting enzymes. Pharmacological inhibition of the leakage results in recovery of the metabolic phenotype, favoring synapse maturation, and correction of autistic behaviors in FXS models [113].

Metabolic alterations have been described in plasma of both FXS models and patients. Plasmatic metabolites suggest a deregulation in glucose and lipid homeostasis, with a shifted metabolism towards the use of lipids and increased response to insulin stimulation [114]. Several studies report an increase in creatine and in BCAAs, asparagine and phosphocholine metabolism as well [114,115].

The role of glial metabolism in the pathophysiology of FXS is gaining relevance. Recent studies in *Drosophila* suggest FMRP has a role in insulin receptors activation in glia [116]. Although FXS-astrocytes mitochondria do not appear to have respiratory impairments, they show an increased ROS production [117], and extracellular vesicles in *Fmr1 KO* mouse models have been proved to be depleted mitochondrial components, specially those secreted from cortical astrocytes, endorsing the mitochondrial dysfunction in FXS pathophysiology [118].

Analogous with Rett syndrome, mitochondrial metabolism represents a potential target for the treatment of a generalized neurodevelopment disease. A study of nine FXS patients between the ages of 2 to 7 years old, treated with metformin, reported beneficial effects in language and behavior [119]. These results support the need for a controlled trial of metformin in young children with FXS to determine the effect of the treatment in a wider population.

4.1.4. Down syndrome

Down syndrome (DS) is the most common cause of intellectual disability, resulting from the presence of an either total or partial extra chromosome 21. Among other factors, the trisomy on this chromosome encompasses metabolic and mitochondrial alterations, that could be summarized by impaired glucose and lipid metabolism and defective mitochondrial activity, resulting in a decrease of ATP production and increase in oxidative stress [120]. Part of these alterations can be explained since key regulatory metabolic enzymes are encoded in chromosome 21, such as phosphofructokinase or cystathionine beta synthase. Studies in animal models suggest that abnormal glucose metabolism is already occurring during neurodevelopment, probably contributing to Down's brain function impairment.

Although not strictly falling into energy metabolism, brain lipid metabolism is also altered [121]. Reduced levels of glycerophosphoethanolamine and glycerophospholipid metabolism were observed in the DS prefrontal cortex. These results are complemented with the description of altered levels of sphingosine derivatives in DS fibroblasts [122].

4.2. Outstanding questions

There is still little knowledge about brain energy metabolism during neurodevelopment in both physiological and pathological conditions. Compared to advances in adult neurodegenerative disorders, energy dysfunction in neuropediatric diseases still represents a universe to be explored. However, energy homeostasis in neurodevelopmental diseases is probably a major pathophysiological feature. In fact, energy utilization is a fundamental biological mechanism carefully preserved across species and human evolution. Advanced in metabolomics, brain MRI spectroscopy and PET techniques will expand the knowledge of brain energy in neuropediatrics. Would intelligent integrative platforms using clinical, genetic, metabolic and pathophysiological data be robust enough to improve this knowledge? Whatever the methodology used, it is very likely that precise information on energy metabolism through neurodevelopment could provide new horizons in energy-based treatments regardless of the etiology of the neurological disease.

4.3. Search strategy and selection criteria

Data for this Review were identified by searches of PubMed mainly focused in the last 10 years (2011−2021). References from relevant articles were obtained using the search terms "neurodevelopment", "brain energy metabolism", "glycolysis", "oxidative phosphorylation", "lactate" "pyruvate", "monocarboxylate transporters", "ketone bodies", "inborn errors of metabolism", "mitochondrial disorders", "Rett syndrome", "X-fragile syndrome", "Autism", "Psychiatric diseases", "brain MRS", "Glucose PET".

5. Contributors

AO covered the issues of brain metabolism through neurodevelopment and neurodevelopmental diseases.

UM collaborated on the writing of neurodevelopmental diseases and energy metabolism.

LFB wrote the introductory aspects of this review, framing the importance of energy metabolism in brain function and setting the ground aspects for its development.

AGC conceived the whole manuscript structure and idea, supervised its contents and directly covered the monogenic disorders of energy metabolism.

All authors have read and approved the final version of this manuscript.

Declaration of Competing Interest

Dr Oyarzábal, MsC Musokhranova, Dr Barros and Dr García-Cazorla, have nothing to disclose

Acknowledgments

AGC is funded by Fondo de Investigación Sanitaria (FIS) P118/00111 (Instituto de Salud Carlos III: ISCIII and "Fondo Europeo de desarrollo regional" FEDER). We acknowledge the Spanish Patient Associations, "Mi Princesa Rett" and "Rettando al síndrome de Rett", for their continuous support to the "Synaptic Metabolism Laboratory" research at Sant Joan de Déu Hospital, Barcelona. The Centro de Estudios Científicos (CECs) is funded by the Chilean Government through the Centers of Excellence Basal Financing Program of ANID.

Refrences

[1] Erecińska M, Silver IA. Ions and energy in mammalian brain. Prog Neurobiol 1994;43(1):37–71 May.
[2] Attwell D, Laughlin SB. An energy budget for signaling in the grey matter of the brain. J Cereb blood flow Metab 2001;21(10):1133–45 Off J Int Soc Cereb Blood Flow MetabOct.
[3] Weber B, Barros LF. The astrocyte: powerhouse and recycling center. Cold Spring Harb Perspect Biol 2015;7(12) Feb.
[4] Drunin. Basal metabolic rate in man. Joint FAO/WHO/UNU expert consultation on energy and protein requirements. Rome: WHO; 1981 http://www.fao.org/3/M2845E/m2845e00.htm.
[5] Rasmussen P, Wyss MT, Lundby C. Cerebral glucose and lactate consumption during cerebral activation by physical activity in humans. FASEB J 2011;25(9):2865–73 Off Publ Fed Am Soc Exp BiolSep.
[6] LaManna JC, Salem N, Puchowicz M, Erokwu B, Koppaka S, Flask C, et al. Ketones suppress brain glucose consumption. Adv Exp Med Biol 2009;645:301–6.
[7] Zhang Y, Kuang Y, Xu K, Harris D, Lee Z, LaManna J, et al. Ketosis proportionately spares glucose utilization in brain. J Cereb blood flow Metab 2013;33(8):1307–11 Off J Int Soc Cereb Blood Flow MetabAug.

[8] Vannucci RC, Vannucci SJ. Glucose metabolism in the developing brain. Semin Perinatol 2000;24(2):107–15 Apr.
[9] Vander Heiden MG, Cantley LC, Thompson CB. Understanding the Warburg effect: the metabolic requirements of cell proliferation. Science 2009;324(5930):1029–33 May.
[10] Goyal MS, Hawrylycz M, Miller JA, Snyder AZ, Raichle ME. Aerobic glycolysis in the human brain is associated with development and neotenous gene expression. Cell Metab 2014;19(1):49–57.
[11] Bero AW, Yan P, Roh JH, Cirrito JR, Stewart FR, Raichle ME, et al. Neuronal activity regulates the regional vulnerability to amyloid-β deposition. Nat Neurosci 2011;14(6):750–6 Jun.
[12] Fox PT, Raichle ME, Mintun MA, Dence C. Nonoxidative glucose consumption during focal physiologic neural activity. Science 1988;241(4864):462–4 Jul.
[13] Lerchundi R, Fernández-Moncada I, Contreras-Baeza Y, Sotelo-Hitschfeld T, Mächler P, Wyss MT, et al. NH4(+) triggers the release of astrocytic lactate via mitochondrial pyruvate shunting. Proc Natl Acad Sci U S A 2015;112(35):11090–5 Sep.
[14] San Martín A, Arce-Molina R, Galaz A, Pérez-Guerra G, Barros LF. Nanomolar nitric oxide concentrations quickly and reversibly modulate astrocytic energy metabolism. J Biol Chem 2017;292(22):9432–8 Jun.
[15] Fernández-Moncada I, Ruminot I, Robles-Maldonado D, Alegría K, Deitmer JW, Barros LF. Neuronal control of astrocytic respiration through a variant of the Crabtree effect. Proc Natl Acad Sci U S A 2018;115(7):1623–8 Feb.
[16] Barros LF, Ruminot I, San Martín A, Lerchundi R, Fernández-Moncada I, Baeza-Lehnert F. Aerobic glycolysis in the brain: warburg and crabtree contra pasteur. Neurochem Res 2020 Jan.
[17] Pellerin L, Magistretti PJ. Glutamate uptake into astrocytes stimulates aerobic glycolysis: a mechanism coupling neuronal activity to glucose utilization. Proc Natl Acad Sci U S A 1994;91(22):10625–9 Oct.
[18] Barros LF, Weber B. CrossTalk proposal: an important astrocyte-to-neuron lactate shuttle couples neuronal activity to glucose utilisation in the brain. J Physiol 2018;596(3):347–50.
[19] Bak LK, Walls AB. CrossTalk opposing view: lack of evidence supporting an astrocyte-to-neuron lactate shuttle coupling neuronal activity to glucose utilisation in the brain. J Physiol 2018;596(3):351–3.
[20] Magistretti PJ, Allaman I. Lactate in the brain: from metabolic end-product to signalling molecule. Nat Rev Neurosci 2018;19(4):235–49 Apr.
[21] Dienel GA. Brain glucose metabolism: integration of energetics with function. Physiol Rev 2019;99(1):949–1045 Jan.
[22] Barros LF. Metabolic signaling by lactate in the brain. Trends Neurosci 2013;36(7):396–404 Jul.
[23] Rice D, Barone SJ. Critical periods of vulnerability for the developing nervous system: evidence from humans and animal models. Environ Health Perspect 2000;108(3):511–33 JunSuppl(Suppl.
[24] Brekke E, Morken TS, Sonnewald U. Glucose metabolism and astrocyte–neuron interactions in the neonatal brain. Neurochem Int 2015;82:33–41.
[25] Lust WD, Pundik S, Zechel J, Zhou Y, Buczek M, Selman WR. Changing metabolic and energy profiles in fetal, neonatal, and adult rat brain. Metab Brain Dis 2003;18(3):195–206.
[26] Rafiki A, Boulland JL, Halestrap AP, Ottersen OP, Bergersen L. Highly differential expression of the monocarboxylate transporters MCT2 and MCT4 in the developing rat brain. Neuroscience 2003;122(3):677–88.
[27] Pellerin L, Pellegri G, Bittar PG, Charnay Y, Bouras C, Martin JL, et al. Evidence supporting the existence of an activity-dependent astrocyte-neuron lactate shuttle. Dev Neurosci 1998;20(4–5):291–9.
[28] Kishimoto A, Takahashi-Iwanaga H, MW M, Iwanaga T. Differential expression of endothelial nutrient transporters (MCT1 and GLUT1) in the developing eyes of mice. Exp Eye Res 2016;153:170–7.
[29] Adam PA, Räihä N, Rahiala EL, Kekomäki M. Oxidation of glucose and D-B-OH-butyrate by the early human fetal brain. Acta Paediatr Scand 1975;64(1):17–24 Jan.
[30] Yeh YY, Sheehan PM. Preferential utilization of ketone bodies in the brain and lung of newborn rats. Fed Proc 1985;44(7):2352–8 Apr.
[31] Ivanov A, Mukhtarov M, Bregestovski P, Zilberter Y. Lactate Effectively Covers Energy Demands during Neuronal Network Activity in Neonatal Hippocampal Slices. Front Neuroenergetics 2011;3:2.
[32] Kasischke K. Lactate Fuels the Neonatal Brain. Front Neuroenergetics 2011;3:4.
[33] Beckhauser TF, Francis-Oliveira J, De Pasquale R. Reactive oxygen species: physiological and physiopathological effects on synaptic plasticity. J Exp Neurosci 2016;10(1):23–48 Suppl.
[34] Chen Y, Kim H, Bok R, Sukumar S, Mu X, Sheldon RA, et al. Pyruvate to lactate metabolic changes during neurodevelopment measured dynamically using hyperpolarized 13C imaging in juvenile murine brain. Dev Neurosci 2016;38(1):34–40.
[35] Chugani HT. A critical period of brain development: studies of cerebral glucose utilization with PET. Prev Med 1998;27(2):184–8 (Baltim).
[36] Chugani HT. Imaging brain metabolism in the newborn. J Child Neurol 2018;33(13):851–60.
[37] Chugani HT, Phelps ME, Mazziotta JC. Positron emission tomography study of human brain functional development. Ann Neurol 1987;22(4):487–97 Oct.
[38] Hyder F, Herman P, Bailey CJ, Møller A, Globinsky R, Fulbright RK, et al. Uniform distributions of glucose oxidation and oxygen extraction in gray matter of normal human brain: no evidence of regional differences of aerobic glycolysis. J Cereb blood flow Metab 2016;36(5):903–16 Off J Int Soc Cereb Blood Flow MetabMay.
[39] Benveniste H, Dienel G, Jacob Z, Lee H, Makaryus R, Gjedde A, et al. Trajectories of brain lactate and re-visited oxygen-glucose index calculations do not support elevated non-oxidative metabolism of glucose across childhood. Front Neurosci 2018;12:631.
[40] Brekke EMF, Morken TS, Widerøe M, Håberg AK, Brubakk AM, Sonnewald U. The pentose phosphate pathway and pyruvate carboxylation after neonatal hypoxic-ischemic brain injury. J Cereb blood flow Metab 2014;34(4):724–34 Off J Int Soc Cereb Blood Flow MetabApr.
[41] Morken TS, Brekke E, Håberg A, Widerøe M, Brubakk AM, Sonnewald U. Neuron-astrocyte interactions, pyruvate carboxylation and the pentose phosphate pathway in the neonatal rat brain. Neurochem Res 2014;39(3):556–69.
[42] Lund TM, Risa O, Sonnewald U, Schousboe A, Waagepetersen HS. Availability of neurotransmitter glutamate is diminished when beta-hydroxybutyrate replaces glucose in cultured neurons. J Neurochem 2009;110(1):80–91 Jul.
[43] Rinholm JE, Hamilton NB, Kessaris N, Richardson WD, Bergersen LH, Attwell D. Regulation of oligodendrocyte development and myelination by glucose and lactate. J Neurosci 2011;31(2):538–48.
[44] Yan H, Rivkees SA. Hypoglycemia influences oligodendrocyte development and myelin formation. Neuroreport 2006;17(1):55–9 Jan.
[45] Fünfschilling U, Jockusch WJ, Sivakumar N, Möbius W, Corthals K, Li S, et al. Critical time window of neuronal cholesterol synthesis during neurite outgrowth. J Neurosci 2012;32(22):7632–45 May.
[46] Rao VTS, Khan D, Cui QL, Fuh SC, Hossain S, Almazan G, et al. Distinct age and differentiation-state dependent metabolic profiles of oligodendrocytes under optimal and stress conditions. PLoS ONE 2017;12(8):e0182372.
[47] Rosko L, Smith VN, Yamazaki R, Huang JK. Oligodendrocyte bioenergetics in health and disease. Neurosci. 2019;25(4):334–43.
[48] Berthet C, Lei H, Thevenet J, Gruetter R, Magistretti PJ, Hirt L. Neuroprotective role of lactate after cerebral ischemia. J Cereb blood flow Metab 2009;29(11):1780–9 Off J Int Soc Cereb Blood Flow MetabNov.
[49] Lee BS, Woo DC, Woo CW, Kim KS. Exogenous β-hydroxybutyrate treatment and neuroprotection in a suckling rat model of hypoxic-ischemic encephalopathy. Dev Neurosci 2018;40(1):73–83.
[50] Roumes H, Dumont U, Sanchez S, Mazuel L, Blanc J, Raffard G, et al. Neuroprotective role of lactate in rat neonatal hypoxia-ischemia. J Cereb Blood Flow Metab 2020 0271678 × 2090835.
[51] Tassinari ID, Andrade MKG, Rosa LAda, Hoff MLM, Nunes RR, Vogt EL, et al. Lactate administration reduces brain injury and ameliorates behavioral outcomes following neonatal hypoxia-ischemia. Neuroscience 2020. doi: 10.1016/j.neuroscience.2020.09.006.
[52] Morland C, Andersson KA, Haugen ØP, Hadzic A, Kleppa L, Gille A, et al. Exercise induces cerebral VEGF and angiogenesis via the lactate receptor HCAR1. Nat Commun 2017;8:15557. May.
[53] Zhou J, Liu T, Guo H, Cui H, Li P, Feng D, et al. Lactate potentiates angiogenesis and neurogenesis in experimental intracerebral hemorrhage. Exp Mol Med 2018;50(7):1–12.
[54] Ichai C, Armando G, Orban JC, Berthier F, Rami L, Samat-Long C, et al. Sodium lactate versus mannitol in the treatment of intracranial hypertensive episodes in severe traumatic brain-injured patients. Intensiv Care Med 2009;35(3):471–9 Mar.
[55] Wheless JW. History of the ketogenic diet. Epilepsia 2008;49(8):3–5 NovSuppl.
[56] Klepper J, Akman C, Armeno M, Auvin S, Cervenka M, Cross HJ, et al. Glut1 deficiency syndrome (Glut1DS): state of the art in 2020 and recommendations of the international Glut1DS study group. Epilepsia Open 2020;5(3):354–65 Sep.
[57] Barry D, Ellul S, Watters L, Lee D, Haluska R, White R. The ketogenic diet in disease and development. Int J Dev Neurosci 2018;68:53–8 [Internet]Available from http://www.sciencedirect.com/science/article/pii/S0736574818300960.
[58] Oyarzabal A, Marin-Valencia I. Synaptic energy metabolism and neuronal excitability, in sickness and health. J Inherit Metab Dis 2019;42(2):220–36.
[59] Kass HR, Winesett SP, Bessone SK, Turner Z, Kossoff EH. Use of dietary therapies amongst patients with GLUT1 deficiency syndrome. Seizure 2016;35:83–7 Feb.
[60] Wachs TD, Georgieff M, Cusick S, McEwen BS. Issues in the timing of integrated early interventions: contributions from nutrition, neuroscience, and psychological research. Ann N Y Acad Sci 2014;1308(1):89–106.
[61] Georgieff MK, Brunette KE, Tran PV. Early life nutrition and neural plasticity. Dev Psychopathol 2015;27(2):411–23.
[62] Schwarzenberg SJ, Georgieff MK, COMMITTEE ON NUTRITION. Advocacy for improving nutrition in the first 1000 days to support childhood development and adult health. Pediatrics 2018;141(2):e20173716.
[63] Frazier AE, Thorburn DR, Compton AG. Mitochondrial energy generation disorders: genes, mechanisms, and clues to pathology. J Biol Chem 2019;294(14):5386–95 Apr.
[64] Saudubray JM, Mochel F, Lamari F, Garcia-Cazorla A. Proposal for a simplified classification of IMD based on a pathophysiological approach: a practical guide for clinicians. J Inherit Metab Dis 2019;42(4):706–27 Jul.
[65] Duncan DB, Herholz K, Kugel H, Roth B, Ruitenbeek W, Heindel W, et al. Positron emission tomography and magnetic resonance spectroscopy of cerebral glycolysis in children with congenital lactic acidosis. Ann Neurol 1995;37(3):351–8 Mar.
[66] Kumar S, Reynolds K, Ji Y, Gu R, Rai S, Zhou CJ. Impaired neurodevelopmental pathways in autism spectrum disorder: a review of signaling mechanisms and crosstalk. J Neurodev Disord 2019;11(1):10.
[67] Coleman M, Blass JP. Autism and lactic acidosis. J Autism Dev Disord 1985;15(1):1–8 Mar.
[68] Cheng N, Rho JM, Masino SA. Metabolic dysfunction underlying autism spectrum disorder and potential treatment approaches. Front Mol Neurosci 2017;10:34.
[69] Yardeni T, Cristancho AG, McCoy AJ, Schaefer PM, McManus MJ, Marsh ED, et al. An mtDNA mutant mouse demonstrates that mitochondrial deficiency can result in autism endophenotypes. Proc Natl Acad Sci U S A 2021;118(6) Feb.

[70] Mierau SB, Neumeyer AM. Metabolic interventions in autism spectrum disorder. Neurobiol Dis 2019;132:104544.
[71] Frye RE. Mitochondrial dysfunction in autism spectrum disorder: unique abnormalities and targeted treatments. Semin Pediatr Neurol 2020;35:100829 Oct.
[72] Rose S, Bennuri SC, Wynne R, Melnyk S, James SJ, Frye RE. Mitochondrial and redox abnormalities in autism lymphoblastoid cells: a sibling control study. FASEB J 2017;31(3):904–9 Off Publ Fed Am Soc Exp BiolMar.
[73] Rose S, Frye RE, Slattery J, Wynne R, Tippett M, Melnyk S, et al. Oxidative stress induces mitochondrial dysfunction in a subset of autistic lymphoblastoid cell lines. Transl Psychiatry 2014;4(4):e377. Apr.
[74] Stewart PA, Hyman SL, Schmidt BL, Macklin EA, Reynolds A, Johnson CR, et al. Dietary supplementation in children with autism spectrum disorders: common, insufficient, and excessive. J Acad Nutr Diet 2015;115(8):1237–48 Aug.
[75] Hardan AY, Fung LK, Libove RA, Obukhanych TV, Nair S, Herzenberg LA, et al. A randomized controlled pilot trial of oral N-acetylcysteine in children with autism. Biol Psychiatry 2012;71(11):956–61 Jun.
[76] Singh K, Connors SL, Macklin EA, Smith KD, Fahey JW, Talalay P, et al. Sulforaphane treatment of autism spectrum disorder (ASD). Proc Natl Acad Sci U S A 2014;111(43):15550–5 Oct.
[77] Zuccoli GS, Saia-Cereda VM, Nascimento JM, Martins-de-Souza D. The energy metabolism dysfunction in psychiatric disorders postmortem brains: focus on proteomic evidence. Front Neurosci 2017;11:493.
[78] Maurer I, Zierz S, Möller H. Evidence for a mitochondrial oxidative phosphorylation defect in brains from patients with schizophrenia. Schizophr Res 2001;48(1):125–36 Mar.
[79] Rowland LM, Pradhan S, Korenic S, Wijtenburg SA, Hong LE, Edden RA, et al. Elevated brain lactate in schizophrenia: a 7 T magnetic resonance spectroscopy study. Transl Psychiatry 2016;6(11):e967. Nov.
[80] Martins-de-Souza D, Harris LW, Guest PC, Bahn S. The role of energy metabolism dysfunction and oxidative stress in schizophrenia revealed by proteomics. Antioxid Redox Signal 2011;15(7):2067–79 Oct.
[81] Sullivan CR, O'Donovan SM, McCullumsmith RE, Ramsey A. Defects in bioenergetic coupling in schizophrenia. Biol Psychiatry 2018;83(9):739–50.
[82] Pillinger T, McCutcheon RA, Vano L, Mizuno Y, Arumuham A, Hindley G, et al. Comparative effects of 18 antipsychotics on metabolic function in patients with schizophrenia, predictors of metabolic dysregulation, and association with psychopathology: a systematic review and network meta-analysis. Lancet Psychiatry 2020;7(1):64–77 Jan.
[83] Dror N, Klein E, Karry R, Sheinkman A, Kirsh Z, Mazor M, et al. State-dependent alterations in mitochondrial complex I activity in platelets: a potential peripheral marker for schizophrenia. Mol Psychiatry 2002;7(9):995–1001.
[84] Mahadik SP, Evans D, Lal H. Oxidative stress and role of antioxidant and omega-3 essential fatty acid supplementation in schizophrenia. Prog Neuropsychopharmacol Biol Psychiatry 2001;25(3):463–93 Apr.
[85] Kuloglu M, Atmaca M, Tezcan E, Gecici O, Tunckol H, Ustundag B. Antioxidant enzyme activities and malondialdehyde levels in patients with obsessive-compulsive disorder. Neuropsychobiology 2002;46(1):27–32.
[86] Shioiri T, Someya T, Murashita J, Kato T, Hamakawa H, Fujii K, et al. Multiple regression analysis of relationship between frontal lobe phosphorus metabolism and clinical symptoms in patients with schizophrenia. Psychiatry Res 1997;76(2–3):113–22 Dec.
[87] Pruett BS, Meador-Woodruff JH. Evidence for altered energy metabolism, increased lactate, and decreased pH in schizophrenia brain: a focused review and meta-analysis of human postmortem and magnetic resonance spectroscopy studies. Schizophr Res 2020;223:29–42 Sep.
[88] Trautmann S, Rehm J, Wittchen H. The economic costs of mental disorders. EMBO Rep 2016;17(9):1245–9.
[89] Sublette ME, Ellis SP, Geant AL, Mann JJ. Meta-analysis of the effects of eicosapentaenoic acid (EPA) in clinical trials in depression. J Clin Psychiatry 2011 Dec;72(12):1577–84.
[90] Nemets B, Stahl Z, Belmaker RH. Addition of omega-3 fatty acid to maintenance medication treatment for recurrent unipolar depressive disorder. Am J Psychiatry 2002;159(3):477–9 Mar.
[91] Bozzatello P, Brignolo E, De Grandi E, Bellino S. Supplementation with omega-3 fatty acids in psychiatric disorders: a review of literature data. J Clin Med 2016 Jul;5(8).
[92] Feldman D, Banerjee A, Sur M. Developmental dynamics of rett syndrome. Neural Plast 2016;2016:6154080.
[93] Leonard H, Cobb S, Downs J. Clinical and biological progress over 50 years in Rett syndrome. Nat Rev Neurol 2017;13(1):37–51 Jan.
[94] Banerjee A, Rikhye RV, Breton-Provencher V, Tang X, Li C, Li K, et al. Jointly reduced inhibition and excitation underlies circuit-wide changes in cortical processing in Rett syndrome. Proc Natl Acad Sci U S A 2016;113(46):E7287–96 Nov.
[95] Dotti MT, Manneschi L, Malandrini A, De Stefano N, Caznerale F, Federico A. Mitochondrial dysfunction in Rett syndrome. An ultrastructural and biochemical study. Brain Dev 1993;15(2):103–6.
[96] De Felice C, Ciccoli L, Leoncini S, Signorini C, Rossi M, Vannuccini L, et al. Systemic oxidative stress in classic Rett syndrome. Free Radic Biol Med 2009;47(4):440–8 Aug.
[97] Signorini C, Leoncini S, De Felice C, Pecorelli A, Meloni I, Ariani F, et al. Redox imbalance and morphological changes in skin fibroblasts in typical Rett syndrome. Oxid Med Cell Longev 2014;2014:195935.
[98] Can K, Menzfeld C, Rinne L, Rehling P, Kügler S, Golubiani G, et al. Neuronal redox-imbalance in rett syndrome affects mitochondria as well as cytosol, and is accompanied by intensified mitochondrial O_2 consumption and ROS release. Front Physiol 2019;10:479.
[99] Valenti D, de Bari L, Vigli D, Lacivita E, Leopoldo M, Laviola G, et al. Stimulation of the brain serotonin receptor 7 rescues mitochondrial dysfunction in female mice from two models of Rett syndrome. Neuropharmacology 2017;121:79–88.
[100] Panneman DM, Smeitink JA, Rodenburg RJ. Mining for mitochondrial mechanisms: linking known syndromes to mitochondrial function. Clin Genet 2018;93(5):943–51 May.
[101] Sandweiss AJ, Brandt VL, Zoghbi HY. Advances in understanding of Rett syndrome and MECP2 duplication syndrome: prospects for future therapies. Lancet Neurol 2020;19(8):689–98 Aug.
[102] Shulyakova N, Andreazza AC, Mills LR, Eubanks JH. Mitochondrial dysfunction in the pathogenesis of rett syndrome: implications for mitochondria-targeted therapies. Front Cell Neurosci 2017;11:58.
[103] De Filippis B, Nativio P, Fabbri A, Ricceri L, Adriani W, Lacivita E, et al. Pharmacological stimulation of the brain serotonin receptor 7 as a novel therapeutic approach for Rett syndrome. Neuropsychopharmacol 2014;39(11):2506–18 Off Publ Am Coll NeuropsychopharmacolOct.
[104] United Kingdom Prospective Diabetes Study (UKPDS). 13: relative efficacy of randomly allocated diet, sulphonylurea, insulin, or metformin in patients with newly diagnosed non-insulin dependent diabetes followed for three years. BMJ 1995;310(6972):83–8 Jan.
[105] Effect of intensive blood-glucose control with metformin on complications in overweight patients with type 2 diabetes (UKPDS 34). UK Prospective Diabetes Study (UKPDS) Group. Lancet 1998;352(9131):854–65 Sep.
[106] Knowler WC, Barrett-Connor E, Fowler SE, Hamman RF, Lachin JM, Walker EA, et al. Reduction in the incidence of type 2 diabetes with lifestyle intervention or metformin. N Engl J Med 2002;346(6):393–403 Feb.
[107] Zuliani I, Urbinati C, Valenti D, Quattrini MC, Medici V, Cosentino L, et al. The anti-diabetic drug metformin rescues aberrant mitochondrial activity and restrains oxidative stress in a female mouse model of rett syndrome. J Clin Med 2020;9(6):1669.
[108] Lumaban JG, Nelson DL. The Fragile X proteins Fmrp and Fxr2p cooperate to regulate glucose metabolism in mice. Hum Mol Genet 2015;24(8):2175–84.
[109] Shen M, Wang F, Li M, Sah N, Stockton ME, Tidei JJ, et al. Reduced mitochondrial fusion and Huntingtin levels contribute to impaired dendritic maturation and behavioral deficits in Fmr1-mutant mice. Nat Neurosci 2019;22(3):386–400 Mar.
[110] Weisz ED, Towheed A, Monyak RE, Toth MS, Wallace DC, Jongens TA. Loss of Drosophila FMRP leads to alterations in energy metabolism and mitochondrial function. Hum Mol Genet 2018;27(1):95–106 Jan.
[111] D'Antoni S, de Bari L, Valenti D, Borro M, Bonaccorso CM, Simmaco M, et al. Aberrant mitochondrial bioenergetics in the cerebral cortex of the Fmr1 knockout mouse model of fragile X syndrome. Biol Chem 2020;401(4):497–503.
[112] Hom JR, Quintanilla RA, Hoffman DL, de Mesy, Bentley KL, Molkentin JD, Sheu SS, et al. The permeability transition pore controls cardiac mitochondrial maturation and myocyte differentiation. Dev Cell 2011;21(3):469–78 Sep.
[113] Licznerski P, Park HA, Rolyan H, Chen R, Mnatsakanyan N, Miranda P, et al. ATP synthase c-subunit leak causes aberrant cellular metabolism in fragile X syndrome. Cell 2020;182(5):1170–85 e9.
[114] Leboucher A, Pisani DF, Martinez-Gili L, Chilloux J, Bermudez-Martin P, Van Dijck A, et al. The translational regulator FMRP controls lipid and glucose metabolism in mice and humans. Mol Metab 2019;21:22–35 Mar.
[115] Menzies C, Naz S, Patten D, Alquier T, Bennett BM, Lacoste B. Distinct basal metabolism in three mouse models of neurodevelopmental disorders. eNeuro 2021;8(2).
[116] Vita DJ, Meier CJ, Broadie K. Neuronal fragile X mental retardation protein activates glial insulin receptor mediated PDF-Tri neuron developmental clearance. Nat Commun 2021;12(1) Feb.
[117] Vandenberg GG, Dawson NJ, Head A, Scott GR, Scott AL. Astrocyte-mediated disruption of ROS homeostasis in Fragile X mouse model. Neurochem Int 2021;146:105036 Jun.
[118] Ha BG, Heo JY, Jang YJ, Park TS, Choi JY, Jang WY, et al. Depletion of mitochondrial components from extracellular vesicles secreted from astrocytes in a mouse model of fragile X syndrome. Int J Mol Sci 2021;22(1) Jan.
[119] Biag HMB, Potter LA, Wilkins V, Afzal S, Rosvall A, Salcedo-Arellano MJ, et al. Metformin treatment in young children with fragile X syndrome. Mol Genet genomic Med 2019;7(11):e956. Nov.
[120] Dierssen M, Fructuoso M, Martínez de, Lagrán M, Perluigi M, Barone E. Down syndrome is a metabolic disease: altered insulin signaling mediates peripheral and brain dysfunctions. Front Neurosci 2020;14:670.
[121] Yu Q, He Z, Zubkov D, Huang S, Kurochkin I, Yang X, et al. Lipidome alterations in human prefrontal cortex during development, aging, and cognitive disorders. Mol Psychiatry 2020;25(11):2952–69 Nov.
[122] Hwang S, Williams JF, Kneissig M, Lioudyno M, Rivera I, Helguera P, et al. Suppressing aneuploidy-associated phenotypes improves the fitness of trisomy 21 cells. Cell Rep 2019;29(8):2473–88 Nove5.

Journal of Translational Medicine

RESEARCH

Open Access

Mitochondrial modulation with leriglitazone as a potential treatment for Rett syndrome

Uliana Musokhranova[1], Cristina Grau[1], Cristina Vergara[2], Laura Rodríguez-Pascau[3], Clara Xiol[4], Alba A. Castells[5], Soledad Alcántara[5], Pilar Rodríguez-Pombo[6,7], Pilar Pizcueta[3], Marc Martinell[2,3], Angels García-Cazorla[1,7*] and Alfonso Oyarzábal[1,7*]

Abstract

Background Rett syndrome is a neuropediatric disease occurring due to mutations in *MECP2* and characterized by a regression in the neuronal development following a normal postnatal growth, which results in the loss of acquired capabilities such as speech or purposeful usage of hands. While altered neurotransmission and brain development are the center of its pathophysiology, alterations in mitochondrial performance have been previously outlined, shaping it as an attractive target for the disease treatment.

Methods We have thoroughly described mitochondrial performance in two Rett models, patients' primary fibroblasts and female Mecp2$^{tm1.1Bird-/+}$ mice brain, discriminating between different brain areas. The characterization was made according to their bioenergetics function, oxidative stress, network dynamics or ultrastructure. Building on that, we have studied the effect of leriglitazone, a PPARγ agonist, in the modulation of mitochondrial performance. For that, we treated Rett female mice with 75 mg/kg/day leriglitazone from weaning until sacrifice at 7 months, studying both the mitochondrial performance changes and their consequences on the mice phenotype. Finally, we studied its effect on neuroinflammation based on the presence of reactive glia by immunohistochemistry and through a cytokine panel.

Results We have described mitochondrial alterations in Rett fibroblasts regarding both shape and bioenergetic functions, as they displayed less interconnected and shorter mitochondria and reduced ATP production along with increased oxidative stress. The bioenergetic alterations were recalled in Rett mice models, being especially significant in cerebellum, already detectable in pre-symptomatic stages. Treatment with leriglitazone recovered the bioenergetic alterations both in Rett fibroblasts and female mice and exerted an anti-inflammatory effect in the latest, resulting in the amelioration of the mice phenotype both in general condition and exploratory activity.

Conclusions Our studies confirm the mitochondrial dysfunction in Rett syndrome, setting the differences through brain areas and disease stages. Its modulation through leriglitazone is a potential treatment for this disorder, along with other diseases with mitochondrial involvement. This work constitutes the preclinical necessary evidence to lead to a clinical trial.

Keywords Rett syndrome, Metabolic modulation, Bioenergetics, Neuroinflammation, Leriglitazone, Mitochondria

*Correspondence:
Angels García-Cazorla
Alfonso Oyarzábal
alfonsoluis.oyarzabal@sjd.es
Full list of author information is available at the end of the article

© The Author(s) 2023. **Open Access** This article is licensed under a Creative Commons Attribution 4.0 International License, which permits use, sharing, adaptation, distribution and reproduction in any medium or format, as long as you give appropriate credit to the original author(s) and the source, provide a link to the Creative Commons licence, and indicate if changes were made. The images or other third party material in this article are included in the article's Creative Commons licence, unless indicated otherwise in a credit line to the material. If material is not included in the article's Creative Commons licence and your intended use is not permitted by statutory regulation or exceeds the permitted use, you will need to obtain permission directly from the copyright holder. To view a copy of this licence, visit http://creativecommons.org/licenses/by/4.0/. The Creative Commons Public Domain Dedication waiver (http://creativecommons.org/publicdomain/zero/1.0/) applies to the data made available in this article, unless otherwise stated in a credit line to the data.

Background

Rett syndrome (OMIM # 312750) is a neurodevelopmental disorder that affects 1 in 10,000 people, mostly girls. Usually caused by de novo mutations in the X-linked *MECP2* gene, it is a clinically and molecularly complex disorder [1]. It is characterized by a regression in neurodevelopment between 6 and 18 months of age, after normal early development. Patients experience a loss of acquired abilities, such as communication skills, and symptoms that include features of severe autism, loss of purposeful use of the hands, stereotypies, apnoea / hyperpnoea and seizures [2].

Despite several attempts, Rett syndrome still lacks a specific therapeutic option. Importantly, it was proved several years ago that the reversal of many of the features that characterize Rett syndrome is possible [3, 4], encouraging for the research of potential therapeutic options. Diverse approaches targeting specific features such as epileptic activity or breathing abnormalities have been made, and while clinical trials focused on genetic therapy are in the horizon, their efficacy and reach is dubious [5]. Considering this, the study of the Rett syndrome's pathophysiology and the validation of new therapeutic targets and alternatives is a matter of urgency.

Among key features of the disease, such as an imbalance in excitatory/inhibitory neurotransmission and a delay in GABAergic neurotransmission maturation, mitochondrial dysfunction has been reported to play a role in Rett's pathophysiology as well [6, 7]. Several alterations in mitochondrial homeostasis have been partially described as ultrastructure differences, decrease in electron transport chain complexes expression, with consequent reduction in ATP concentration [8]. A dysregulation in the redox state has also been described, translating into oxidative damage and lowered antioxidant defenses [9]. Metabolic and mitochondrial dysfunctions have been proposed as a potential therapeutic target. Few attempts to amend its homeostasis have been made, as through the stimulation of the brain serotonin receptor 7 (5-HT7R) with LP-211 [10] or the repurpose of known drugs such as metformin [11], used for decades in the treatment of type 2 diabetes, or triheptanoin [12], which anaplerotic function enhanced mitochondrial function in Rett models. Notwithstanding the great results in different models, none of these approaches has met successful clinical trials.

In our work we have studied mitochondrial homeostasis focusing on mitochondrial shape and bioenergetic function in both several Rett patients' fibroblasts and female mice models. Importantly, we have determined how mitochondrial performance varies through different brain areas across neurodevelopment. Advancing from this concise description, we have evaluated the effect of a novel PPARγ-agonist, leriglitazone. It is a drug from the glitazone family that shows a superior brain penetration and a favorable safety profile, as proven in healthy controls and other neuropediatric diseases [13, 14]. Its efficacy on mitochondrial function enhancement and phenotypic amendment in Rett models endorses leriglitazone as a potential new treatment for Rett syndrome and other neurodevelopmental diseases with mitochondrial involvement.

Methods

Cell culturing

We used primary cultures of skin fibroblasts from patients (defined through the results section) and age-matching controls. Dermal fibroblasts were grown following standard culture conditions in minimal essential medium (MEM) supplemented with 1% glutamine, 10% fetal bovine serum (FBS) and 1% penicillin–streptomycin. Unless stated otherwise, experiments were accomplished when fibroblasts were at 80% confluence and between the 7th and 14th passages.

Leriglitazone (MW: 408.9 g/mol) was resuspended in 100% DMSO to obtain a stock solution at 10 mM concentration. We prepared a stock solution at 0.1 mM diluted in DMEM and 10% DMSO, stored at − 20 °C for less than one month. For the working solutions, we prepare an intermediate 1 µM working solution 1% DMSO from the 0.1 mM stock solution. For leriglitazone treatment, cells were incubated for 48 h with 100 nM or 500 nM leriglitazone in the same medium, complemented with 1% DMSO.

GW9662 (M6191, Sigma-Aldrich) was used as a PPARγ antagonist. 5 mg of GW9662 were resuspended in 1.8 mL of DMSO to obtain a stock solution at 10 mM, stored at − 20 °C. From this, we prepared an intermediate stock solution at 1 mM diluted in DMEM and 10% DMSO. Cells were treated with a working solution at 1 µM in DMEM and 1% DMSO for 72 h.

Mice colony maintenance and sample collection

Both B6.129P2(C)-*Mecp2*$^{tm1.1Bird}$/J and control littermates mice were used. To increase the translational value of the work, only female mice have been used, as they have been reported to better recapitulate the disease phenotype. Mice were housed in standard cages with ad libitum access to food and water and in controlled environmental conditions of light (12 h dark/light cycle starting at 7:30 am), temperature (22 °C) and humidity (60%). Mice were genotyped following the provider recommendations.

When stated, leriglitazone was delivered orally with the food at a dose equivalent to 75 mg/kg/day. Mice were fed pellets with or without leriglitazone from weaning until

7 months (symptomatic mice). Leriglitazone plasmatic levels were confirmed by LC–MS/MS post animal sacrifice to confirm the proper intake.

Behavioral tests

Novel object recognition (NOR) test

The NOR test is widely used to evaluate object recognition memory in mice. To test recognition, on the first day of the test (familiarization phase) mice were placed in a box (35×35×35 cm) with two identical objects (such as chess figures) and let freely explore the objects (meaning physically interact with them) for a total of 20 s of physical contact, or a maximum of 10 min in the cage even if the exploration time did not sum 20 s. 24 h later, on the second day of the test (test phase), mice were placed again in the box with the initial object explored during the familiarization phase and a novel object, during 10 min. The time spent exploring each object was calculated manually (exploration of an object was defined as the mouse placing its nose within 2 cm of the zone where the object located). Maximum exploration time was recorded at 20 s.

General health score

The health scale was carried out every two weeks, from 3 months to the day of sacrifice. Mice were placed onto a laboratory bench for observation and received a score for each category (0 = absent or normal appearance; 1 = present or moderate phenotype; 2 = severe phenotype). The resulted phenotype was calculated by the sum of the scores of each mouse and then averaging all animals within each group. The categories taken into account were gait, mobility, breathing, hind limb clasping, tremors, general condition, kyphosis (i.e., increased curvature of the frontal part of the spine), fur and seizures.

Immunofluorescence and confocal microscopy

Cells were seeded onto coverslips at 80% confluence and fixed with paraformaldehyde 4% for 20 min. Primary antibodies were used against TOMM20 (1:250, Rb; ab186735, Abcam) and α-tubulin (1:250, Ms; ab7291, Abcam) for mitochondrial network imaging, and 8-OHdG (1:250, Ms; sc-66036, Santa Cruz Biotechnology, TX, USA) for RNA oxidative damage imaging. After 1 h blocking at room temperature in a solution of 10% FBS in PBS, primary antibody was incubated for 1 h at room temperature in a solution of PBS 1% FBS. Secondary antibodies anti-Rabbit (Alexa Fluor 488, Goat; Thermo Fisher) and anti-Mouse (Alexa Fluor 546, Goat; Thermo Fisher) were incubated for 1 h at room temperature at concentrations 1:1000 in the same solution. Fluorescence was visualized using Leica TCS SP8 microscope (Leica, Wetzlar, Germany) with 63×, 1.4 N.A. immersion oil objective. Images were analyzed using Fiji software and the Mitochondria Analyzer plug-in [15].

In vivo time-lapse imaging

Cells were incubated with 300 nM MitoTracker Green (Invitrogen) for 30 min at 37 °C and 5% CO_2. Immunofluorescence was visualized using Leica TCS SP8 microscope (Leica, Wetzlar, Germany) with a 63x, 1.4 N.A. oil-immersion objective, 2.75 electronic zoom, and at a frame size of 512×512 pixels. We used a 495 nm white laser, and recorded for 2 min with 0.73 s between each frame, maintaining cell culture conditions. Mitochondrial dynamics analysis was performed with the MATLAB add-in Mitometer [16], which gives the fusion and fission number of events per track.

Electron transmission microscopy

Mitochondrial ultrastructure was analyzed by electron microscopy. Fibroblasts were fixed in the culture plate at room temperature for 1 h with a mixture of 4% paraformaldehyde and 2% glutaraldehyde in phosphate buffer (pH 7.4) and post-fixed with 1% osmium tetroxide plus 1% potassium ferricyanide in distilled water for 1 h at 4 °C. Fibroblasts were dehydrated in ethanol and embedded in epoxy resin EML-812 (TAAB Laboratories), still attached to the culture plate. Small pieces of the thin layer of resin containing the cells were separated from the culture plate and glued to blocks of resin to cut ultrathin sections (70 nm) oriented parallel to the cell base. Sections were collected on 100-meshgrids, stained with uranyl acetate and lead citrate, and examined at 80 kV in a Jeol JEM-1010 (Tokyo, Japan) electron microscope. Images were recorded with 4 k CMOS F416 camera from TVIPS (Gauting, Germany). Electron transmission images were taken at the Electron Microscopy Service at Centro de Biología Molecular Severo Ochoa in Madrid.

Images were analysed using Fiji software measuring the following ultrastructure parameters: (1) mitochondrial major: minor axis ratio; (2) cristae length and (3) cristae width.

Immunohistochemistry

Mice were anaesthetized with Ketamine/Xylazine at a concentration of 100 mg/kg and 10 mg/kg respectively and perfused intracardially with 4% paraformaldehyde (PFA). Brains were extracted and post-fixed in a solution of 4% PFA overnight, cryoprotected in 30% sucrose and kept frozen at − 80 °C. Sagittal sections of 40-µm thick were obtained using a cryostat, collected in a cryoprotective solution (30% glycerol, 30% ethylene glycol in 0.1 M phosphate buffer) and kept at − 20 °C until processing. For immunohistochemistry analysis, the slices were washed three times with washing

solution (0.01% Triton X-100 in PBS), permeabilized with 0.25% Triton X-100 in PBS for 15 min and incubated with blocking solution (0.25% Triton X-100, 10% Horse Serum, 2% BSA) for 2 h at room temperature. Subsequently, slices were incubated with mouse anti-8-OHdG (1:1000; Santa Cruz Biotechnology), rabbit anti-calbindin (1:100; Proteintech), rabbit anti-GFAP (1:500; Dako) or rabbit anti-Iba1 (1:200; Wako) in blocking solution at 4 °C overnight. The slices were then washed with washing solution before the incubation with Alexa Fluor 488-conjugated goat anti-rabbit IgG or Alexa Fluor 546-conjugated goat anti-mouse IgG antibody (1:400; Thermo Fisher), and Hoechst (1:10,000, Thermo Fisher), in blocking solution for 2 h at room temperature. Finally, slices were washed three times with PBS and then mounted with Fluoromount Aqueous Mounting Medium (Sigma-Aldrich, MO, USA) in glass slides coated with 0.2% gelatin. Fluorescence images at 10x, 0.45 N.A. were captured using a Zeiss LSM 880 confocal microscope (Zeiss, Germany). Scales bar have been added in each representative figure.

Western blotting

Proteins were extracted from cultured fibroblasts or mouse brain tissue through a 30' cold incubation with RIPA and protease and phosphatase inhibitors. Following extraction, proteins were quantified by Bradford method and prepared at a homogenous concentration in Laemmli Buffer in reductive denaturing conditions and subjected to SDS-PAGE 8 or 10% and transferred to a nitrocellulose membrane at 100 V 1 h. Membranes were blocked with TBS-Tween (0.05%): milk 5% for 1 h at room temperature. Primary antibodies were incubated O/N at 4 °C in blocking buffer, at the following concentrations: Drp1 (1:1000, Rb; ab184247, Abcam), Fis1 (1:500, Ms; sc-376469, Santa Cruz Biotechnology), OPA1 (1:2000, Ms; BD-612607, BD Biosciences), Mfn2 (1:500, ab124773, Rb; Abcam), MnSOD (1:80,000, Rb; ADI-SOD-111-F, Enzo Life Sciences) and GPx1 (1:1000, Rb; ab108427, Abcam). Vinculin (1:20,000, Ms; sc-59803, Santa Cruz Biotechnology) was used as a loading control. For the OXPHOS complexes detection, proteins were denatured in a non-reductive buffer, and incubated after SDS-PAGE and Western blot with OXPHOS Human WB Antibody Cocktail (1:1000, Ms; 45-8199, Thermo Fisher). The secondary antibodies used were HRP-conjugated goat anti-Rabbit and goat anti-Mouse IgG antibodies (Thermo Fisher) and were detected using the Pierce™ ECL Western Blotting substrate (Thermo Fisher). Quantification of protein expression was performed using Fiji software by calculating protein densitometry relative to controls and normalized to vinculin.

RT-qPCR

RNA for RT-qPCR was extracted using RNeasy Fibrous Tissue Mini Kit (Qiagen), following the manufacturer's instructions. The total RNA was eluted in 40 µL of RNAse-free water and stored at − 80 °C. The RNA concentration was measured using the NanoDrop 2000 Spectrophotometer (Thermo Fisher). qPCRs were carried out following a two-step protocol. First, cDNA was synthesized from a total of 500 ng of RNA per reaction, following the recommendations provided with SuperScript III First-Strand Synthesis SuperMix for RT-qPCR (Invitrogen). After the RT-PCR reaction, the cDNA from control and Rett fibroblasts was pooled. Second, qPCR was performed in a QuantStudio 6 Flex Real Time PCR System (Thermo Fisher) with PowerUp SYBR Green Master Mix (Thermo Fisher). The data were analyzed using a comparative method, correlating the initial template concentration with the cycle threshold (Ct) to obtain the relative quantity (RQ) of the RNA. The RQ is defined as $2^{-\Delta\Delta Ct}$, where ΔΔCt is the ΔCt of the patient cell line minus the ΔCt of the control cell line, and ΔCt is the Ct of the target gene minus Ct of the endogenous gene (*RPLP0*).

Primers used for determination of mitochondrial mass were: *mtND1, CO1, CO2, CO3* and *HK2*. Primers used for detection of PPARγ pathway and known to be altered in Rett were: *PGC1a, PKM, MnSOD, SREBF2.*

ATP content measurement

ATP concentration was evaluated both in fibroblasts and mice brains.

In the former, cells were harvested and resuspended in boiling ATP extraction buffer (100 mM Tris–HCl, 4 mM EDTA pH 7.7). Finally, ATP concentration was assayed by bioluminescence using a luciferin-luciferase system (ATP Bioluminescence Assay Kit CLS II, Roche) according to manufacturer's instructions. ATP concentration was corrected per mg of protein. To discriminate between glycolytic and non-glycolytic ATP, cells were grown either in complete MEM 10% FBS or supplemented with the hexokinase inhibitor 2′-deoxy-D-glucose (D8375, Sigma-Aldrich) at a concentration of 100 mM for 2 h prior to extraction.

For analysis of ATP concentration in different brain areas, brains were dissected, and samples were kept in cryopreservation buffer at − 80 °C until experiment. Samples were weighted, homogenized in pre-cooled 10% $HClO_4$, neutralized with KOH 2.5 M and the supernatant diluted in 100 mM Tris–4 mM EDTA [17]. Total ATP was detected by luciferin–luciferase bioluminescence assay (ATP Bioluminescence Assay Kit CLS II, Roche). ATP concentration was corrected by mg of tissue.

Oxygen consumption rate

Oxygen consumption rate (OCR) was measured using the XF24 Extracellular Flux Analyzer (Seahorse Bioscience, Izasa Scientific). 80,000 fibroblasts per well were seeded in XF 24-well cell culture microplates (Seahorse Bioscience) in 250 µL of MEM 10% FBS and incubated in normal conditions for 24 h in MEM containing 1 g/L of glucose. Two hours previous to the assay, the growth medium was replaced with 700 µL of fresh medium, allowing the media temperature and pH to reach equilibrium before the first measurement. After an OCR baseline measurement, 50 µL of oligomycin, carbonyl cyanide-4-(trifluoromethoxy) phenylhydrazone (FCCP), rotenone and antimycin solutions were sequentially added to each well to reach working concentrations of 6 µM, 50 µM, 1 µM and 1 µM respectively. Results were normalized per cell counting after the experiment and normalized to 30,000 cells. To determine Oligomycin Sensitive Respiration (OSR) we calculated the difference between oxygen consumption before and after adding oligomycin to the medium, considered as ATP-linked respiration.

Analysis of intracellular $O2^{\cdot-}$ by flow cytometry

Superoxide anion concentration was measured using MitoSOX™ Red probe (M36008, Invitrogen). Alive fibroblasts were incubated with the dye at a concentration of 5 µM for 10 min at 37 °C according to manufacturer's instructions. Cells were subsequently resuspended in complete Hanks Balanced-Buffered Saline (HBSS) and analyzed by flow cytometry in a NovoCyte Flow Cytometer (ACEA Biosciences).

TBARS assay

Lipid peroxidation in brain samples was detected using a colorimetric assay (ab118970, Abcam) in which the malonaldehyde (MDA) present in the samples reacted with thiobarbituric acid (TBA) to form the MDA-TBA adduct. In brief, samples were homogenized in 303 µL lysis solution (MDA lysis buffer + BHT) for hippocampus and cerebellum, and 606 µL for cortex, and centrifuged at 13,000*g* for 10 min. 200 µL of supernatant were collected and added 600 µL of TBA reagent. Samples were incubated at 95 °C for 30 min and cooled to room temperature previous to absorbance measurement at 532 nm. Measurements were corrected by mg of protein.

Cytokines multiplex

A panel of thirteen cytokines (IL-1α, IL-1β, IL-6, IL-10, IL-12p70, IL-23, IL-27, IFN-β, IL-17A, MCP-1, TNF-α, IFN-γ, GM-CSF) was detected by flow cytometry using an immunoassay based on bead-fluorescence detection on a V-bottom plate (#740446, BioLegend) according to the manufacturer's guidelines. For sample preparation, samples were weighted, homogenized with lysis buffer (PBS 1×, NP-40 1% and 1× protease inhibitor) as specified in [18], incubated with rotation for 1 h at 4 °C, sonicated and centrifuged at 14,000 rpm (19,500*g*) for 15 min at 4 °C. Supernatant was collected and centrifuged at 14,000 rpm (19,500*g*) for 15 min at 4 °C. In brief, 25 µL of sample were added to 25 µL of assay buffer and 25 µL mixed beads and incubated for 2 h shaking at room temperature. Beads were spun down, washed and 25 µL of detection antibodies were added and incubated for 1 h shaking at room temperature. Then 25 µL of SA-PE were added and incubated for 30 min shaking at room temperature. Finally, beads were spun down, samples were added 150 µL of wash buffer and were read on a flow cytometer. Measurements were corrected by mg of protein.

Statistical analysis

GraphPad Prism 9.0 (La Jolla, CA, USA) software was used for statistical analysis. First, outliers are identified by ROUT test and discarded, and then data normality was determined. ANOVA for parametric data or Kruskal–Wallis for non-parametric data were performed, with posterior multiple comparisons analysis correction when appropriate. Equal standard deviations were not assumed. Two-way ANOVA was used for comparing groups with two or more variables. Results are represented as mean + individual values, mean ± SD, lower to upper quartile box + individual values, or min to max box plot with line at mean. RStudio was used for histogram representation.

Differences were considered as statistically significant at $p < 0.05$, and coded through the figures as follows: $^{*}p < 0.05$, $^{**}p < 0.01$, $^{***}p < 0.001$, and $^{****}p < 0.0001$.

Results

Mitochondrial shape and bioenergetic functions are altered in Rett syndrome fibroblasts

Within the multiple physiological routes affected in Rett syndrome, mitochondrial dysfunctions had been previously suggested. We have studied both mitochondrial shape (ultrastructure and network dynamics) and bioenergetic homeostasis (energy metabolism and oxidative stress) in fibroblasts from eight Rett patients with different *MECP2* mutations and different severity presentations of the disease (Additional file 1: Table S1), compared to four different healthy controls.

We first analyzed mitochondrial network by immunofluorescence of the mitochondrial marker TOMM20, and parametrization of its structure with Mitochondria Analyzer algorithms. It revealed alterations in mitochondrial grid number and morphology, as Rett mitochondrial

networks were less interconnected (higher number of independent networks) and less ramified (Fig. 1A, B) than controls. While they summarize the general picture, these results were, however, not homogeneous within all patients, and some individualities have been found along the different cell lines, as shown in Additional file 1: Fig. S1A.

As mitochondrial network maintenance is closely regulated through mitochondrial dynamics, we upraised the expression of fission and fusion-mediating proteins through Western blot. We registered a significant decrease in the expression of both proteins involved in mitochondrial fission, Drp1 and Fis1 (Fig. 1C, D). On the contrary, we did not detect changes in the proteins responsible for the fusion processes OPA1 or Mfn2, (Fig. 1C, E), suggesting a reduction in the fission: fusion rate. This was corroborated by in vivo time-lapse image acquisition of mitochondria, stained with the probe MitoTracker^{TM} and visualized by confocal microscopy, recording during 2 min with 0.7 s between each frame. Subsequent analysis of the fusion and fission events with the MATLAB add-in Mitometer confirmed a decrease in the fission rate of Rett mitochondria (Fig. 1F and Additional file 2, 3: Videos S1, S2). These results are compatible within each other and support that Rett fibroblasts bear elongated and non-fragmented mitochondria.

Next, we analyzed mitochondrial structure differences between Rett fibroblasts and controls through imaging by Transmission Electron Microscopy (TEM). Agreeing with the previous results [19], we found a hyper fused mitochondria phenotype, as the major: minor axis ratio was higher in Rett mitochondria. On top of that, Rett fibroblasts' mitochondria showed some structural abnormalities regarding cristae, such as a reduction in their number, which were also shorter and wider than control ones (Fig. 1G, H).

Since mitochondrial form and function follow each other, we next analyzed the mitochondrial bioenergetic performance, focusing on ATP production, respiratory capacity, and Reactive Oxygen Species (ROS) generation and metabolism. To discriminate between total ATP and non-glycolytic (and hence mitochondrial) ATP, we measured ATP concentration in the presence of the glycolysis inhibitor 2-deoxy-D-glucose, revealing that Rett mitochondria produced half the ATP controls did (Fig. 1I). For its corroboration, we measured real-time oxygen consumption rate (OCR) of Rett and control fibroblasts, revealing an overall reduction in the OCR in the MeCP2 deficient cells. Rett fibroblasts showed a lowered respiratory capacity in both basal and maximal respiration, calculated after the addition of the uncoupler FCCP. Moreover, they also showed a significant reduction in the Oligomycin-Sensitive Respiration (OSR), this is, the fraction of oxygen consumed for ATP production (Fig. 1J). These results were consistent with an impairment in mitochondrial bioenergetic function.

Mitochondrial respiration defects often result in ROS generation, that can end in oxidative damage. Therefore, we quantified the ROS superoxide anion ($O_2^{\cdot -}$) by detection through flow cytometry and using the probe MitoSOX. We recorded that Rett fibroblasts were exposed to two-fold higher concentrations of superoxide anion compared to controls (Fig. 1K). Surprisingly, we did not detect any differences in the expression of the antioxidant enzymes MnSOD or GPX between Rett and control fibroblasts (Fig. 1L, M). Moreover, this increase in

(See figure on next page.)

Fig. 1 Rett syndrome primary fibroblasts recapitulate alterations in mitochondrial homeostasis. We have focused the analysis on mitochondrial shape (**A**–**H**) and energy production (**I**–**N**). Mitochondrial network shape was studied by immunofluorescence of mitochondrial marker TOMM20 and parametrization with "Mitochondria Analyzer" plugin; **A** representative image of mitochondrial network IF (TOMM20 in yellow, nuclei in blue, and tubulin in grey; scale bar 10 µm; 6× zoomed section included in the white box) and **(B)** parametrization of number of independent networks corrected by area and mean form factor (a shape measure given by: P^2/(4piA): 1 indicates round object and increases with elongation, expressed as mean FF of objects in image), number of branches per mitochondrial network, and mean branch length and diameter. **C**–**E** Analysis and densitometry quantification of mitochondrial dynamics associated proteins Mfn2, OPA1, Drp1 and Fis1 by Western blot and corrected by vinculin. **F** Quantification of the fission and fusion events from in vivo imaging of mitochondrial network. Analysis of mitochondrial ultrastructure was performed by transmission electron microscopy; **G** representative images (scale bar 300 nm) and **H** parametrization of number of cristae per mitochondria, cristae length and width, and mitochondrial major:minor axis ratio. **I** Non-glycolytic ATP production –assumed as mitochondrial ATP– measured by luciferin-luciferase luminescence upon incubation with 2-deoxyglucose. **J** Mitochondrial respiration profile was measured by Seahorse in the presence of oligomycin, FCCP and Antimycin A. Oligomycin Sensitive Respiration (OSR) was calculated as the difference of oxygen consumption before and after adding oligomycin (considered as ATP-linked respiration). **K** $O_2^{\cdot -}$ production measured by flow cytometry with the MitoSOX probe **L** Expression of antioxidant enzymes MnSOD and GPX by Western blot, and **M** quantification of densitometry corrected by vinculin. **N** Oxidative damage was detected based on the fluorescence of RNA oxidative damage marker 8-OHdG, showed with the intensity-revealing LUT "royal" (calibration bar shown at the lower right corner of the panel), at 63× magnification; scale bar represents 10 µm, and represented as relative frequency of intensity values, calculated with Fiji software. All experiments were done in at least two different Rett and control cell lines, with three technical replicates and each experiment was done in triplicates. Statistical analyses were performed as described in Materials and Methods. *$p < 0.05$, **$p < 0.01$, ***$p < 0.001$, ****$p < 0.0001$. Absence of asterisk means no statistically significant difference. Control fibroblasts in grey; Rett patients' fibroblasts in yellow

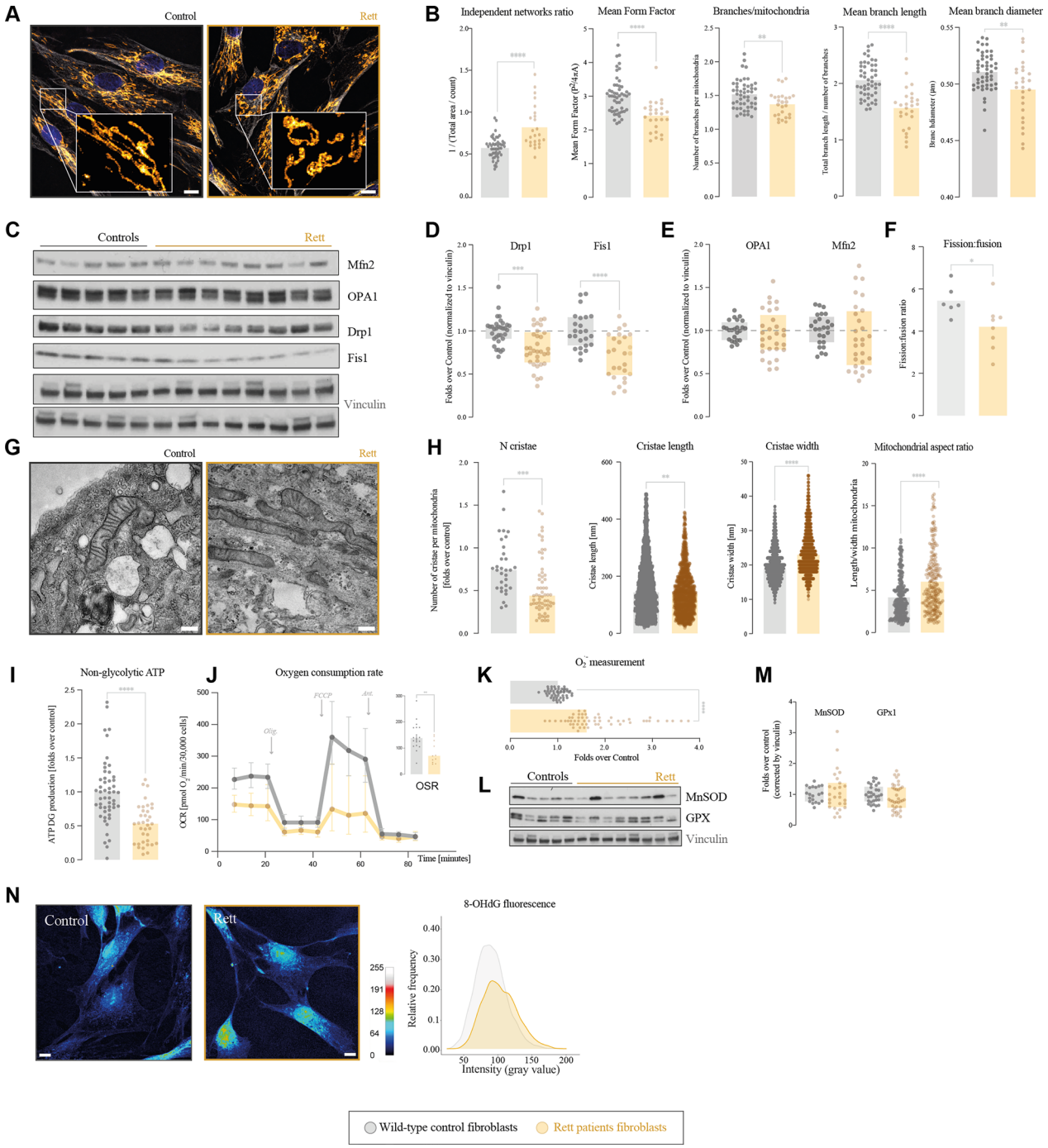

Fig. 1 (See legend on previous page.)

oxidative stress resulted in an enhanced oxidative damage in Rett cells, measured by the detection of 8-OHdG, (Fig. 1N), a widely accepted marker of oxidative damage easily quantifiable by immunofluorescence.

We have worked with 8 Rett lines and observed different degrees of harshness among patients specially regarding mitochondrial network shape and antioxidant defense, both the decrease in mitochondrial ATP production and the increase in ROS and oxidative damage were consistent along the studied cell lines (Additional file 1: Fig. S1B, C). These differences were not mutation-dependent, as patients bearing the same mutations showed differences in mitochondrial performance. Skin fibroblasts are a useful and cost-effective resource to

investigate mitochondrial abnormalities in neurodevelopmental disorders [20, 21].

Altogether, our data supported an alteration in mitochondrial form and function.

Bioenergetic dysfunction is also detectable in Rett syndrome female mice models, displaying differences among brain areas and already evident at pre-symptomatic stages

Encouraged by the alterations found in fibroblasts, we moved towards the analysis of mitochondrial dysfunction in the Rett animal model, wondering whether the dysfunction was homogeneous through the different brain areas and steady through neurodevelopment. For that, we studied female mice from the B6.129P2(C)-*Mecp2*$^{tm1.1Bird}$/J strain, as they recapitulate many elements of the disease. Building on previous reports on mitochondrial dysfunction in whole brain samples, we have analyzed three different brain areas separately- cortex, hippocampus and cerebellum, regarding ATP concentration and oxidative stress (assessed through lipid peroxidation). Interestingly, as patients do, female mice also go through an early normal or non-phenotypic phase, and only after a few months develop the full Rett phenotype. Therefore, we have brought neurodevelopment into the equation, studying differences at two developmental stages: pre-symptomatic (3 months old) and fully symptomatic (7 months old) mice.

Pre-symptomatic mice showed already alterations in both ATP concentration and lipid peroxidation, which were brain area-specific (Fig. 2A): cerebellums from Rett mice had a decreased concentration of ATP, which was within control values in hippocampus and cortex samples. Lipid peroxidation displayed differences as well, as we observed a significant decrease in pre-symptomatic Rett cortex samples along with non-significant differences in hippocampus and cerebellum.

As expected, the variations in these two parameters were more evident when we moved into symptomatic 7 months old mice brains (Fig. 2B). The observed reduction in cerebellum ATP concentration of pre-symptomatic mice was continued in the symptomatic ones, and also evident in Rett hippocampus at this stage. Opposite to that, an increase in [ATP] was detected in Rett cortex, suggesting that alterations are dynamic both between brain areas and through neurodevelopment. ATP concentration is also dynamic through time, and while Rett and control samples varied analogously throughout development, the differences between Rett and WT increased over time (Additional file 1: Fig. S2). On the other hand, a decrease in lipid peroxidation was detected in both hippocampus and cerebellum of symptomatic mice, opposite to a significant increase observed in Rett mice cortex.

Leriglitazone corrects bioenergetic but not dynamics alterations in Rett fibroblasts

Given the mitochondrial alterations in the studied models, we next investigated if these dysfunctions could be corrected with leriglitazone (LGZ). Leriglitazone is a selective peroxisome proliferator-activated receptor gamma (PPARγ) agonist that can efficiently cross the blood–brain barrier (BBB) [13]. Activation of the PPARγ/PGC1α pathway stimulates mitochondrial biogenesis, reduces oxidative stress and improves mitochondrial function (Fig. 3A). Leriglitazone has demonstrated preclinical efficacy in the correction of the phenotype in in vitro and in vivo models of other neurodevelopmental diseases such as X-linked adrenoleukodystrophy (X-ALD)[13] and Friedreich's ataxia (FA) [22] and clinical benefit for X-ALD and FA patients in clinical trials [14, 23].

We initially investigated the effect of leriglitazone in Rett fibroblasts incubating the cells at two different concentrations, 100 and 500 nM, for 48 h (Fig. 3B). The target engagement of LGZ treatment was assessed by measuring the expression of four genes under PPARγ regulation (*PGC1α, PKM, MnSOD* and *SREBF2*), that represent four key pathways under its modulation. Analysis by qPCR revealed an increase in the transcripts' detection upon LGZ incubation, verifying that leriglitazone effectively modulated PPARγ-signaling pathway in the patients' fibroblasts (Additional file 1: Fig. S3A). Leriglitazone treatment resulted also in an increase in the expression ratio of *mtND1*, *CO1*, *CO2* and *CO3* corrected over *HK2*, pointing towards an

(See figure on next page.)

Fig. 2 Bioenergetic characterization of pre-symptomatic (3 m.o.) and symptomatic (7 m.o.) Rett mice. Given the time-dependent character of Rett syndrome, we studied both wild-type and Rett mice at two development time points: **A** pre-symptomatic (3 months) and **B** post-symptomatic (7 months) brains. At the time points, mice brains were dissected and subjected to analysis. ATP concentration by luciferin-luciferase luminescence and lipid peroxidation by TBARS were analysed in three brain areas: cortex, hippocampus and cerebellum. All experiments were done in at least three different mice, with three technical replicates. The ATP production experiment was done in triplicates, while lipid peroxidation was a unique experiment. Statistical analyses were performed as described in Materials and Methods. *$p < 0.05$, **$p < 0.01$, ***$p < 0.001$, ****$p < 0.0001$. Absence of asterisk means no statistically significant difference. Wild-type female mice in grey; Rett female mice in yellow

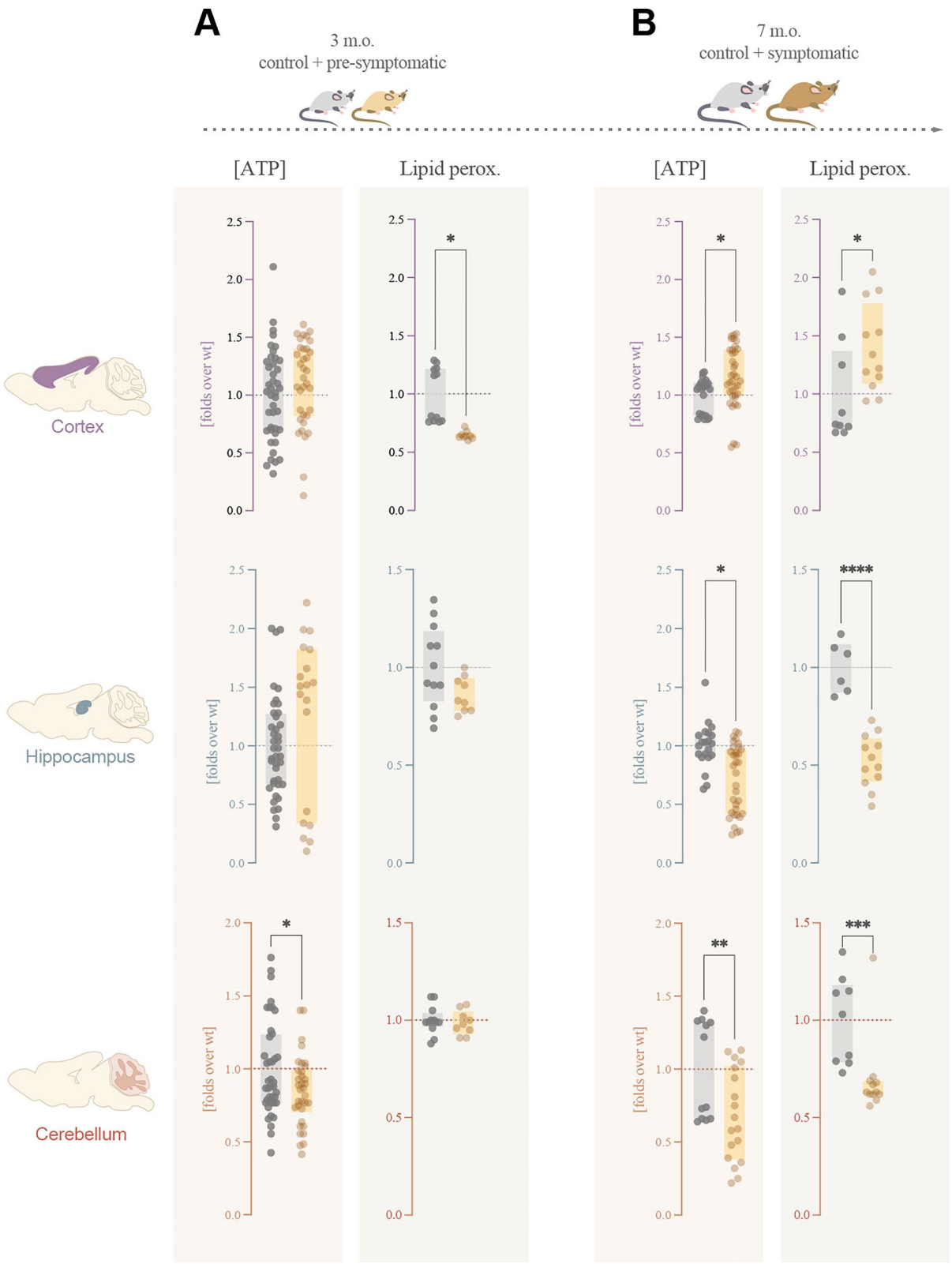

Fig. 2 (See legend on previous page.)

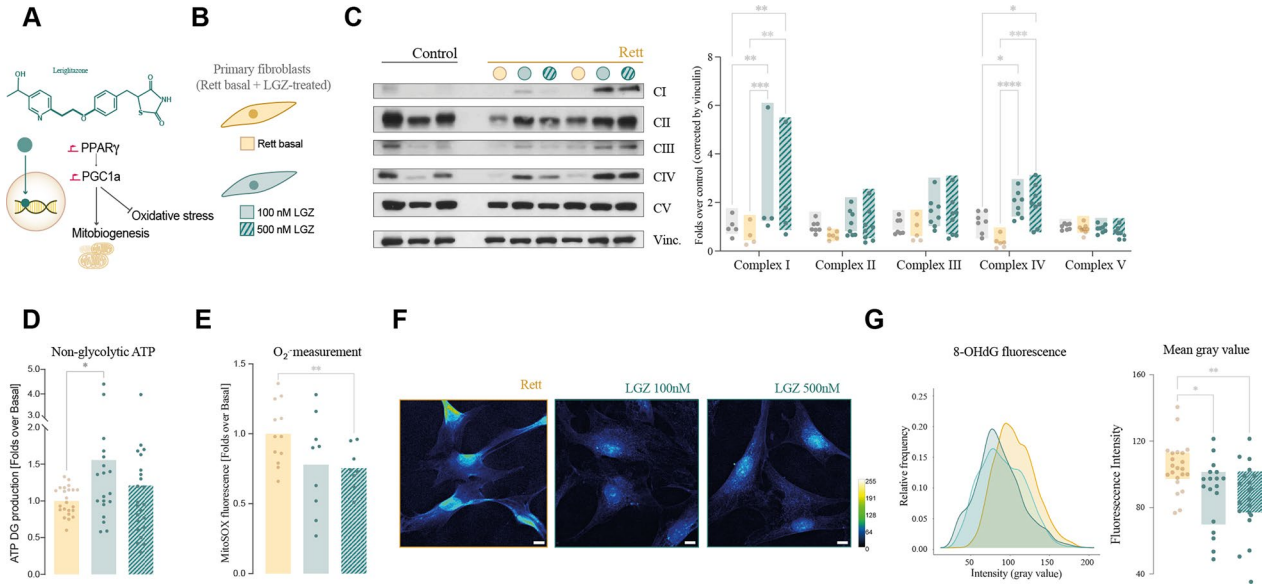

Fig. 3 Correction by leriglitazone of both bioenergetics and oxidative stress in Rett fibroblasts. **A** Schematic representation of leriglizatone (LGZ) and its activity as a PPARγ agonist in a cell. LGZ binds to PPARγ, activating the expression of the genes under its regulation through interaction with PGC1α. **B** LGZ effect was evaluated first on Rett fibroblasts at two concentrations, 100 nM and 500 nM for 48 h. **C** PPARγ pathway activation has an effect on the detection of all electron-transport chain complexes, detected by Western blot and densitometry quantification corrected by vinculin. The ultimate goal of LGZ treatment was to correct the previously described alterations, observing significant corrections in ATP (**D**), ROS production (**E**) and (**F**) oxidative damage measured in terms of 8-OHdG detection. Images are shown with the intensity-revealing LUT "royal", at a 63× magnification; scale bar represents 10 µm. Images were quantified and statistical significance of corrections was evaluated (**G**). All experiments were done in at least two different control and Rett cell lines, with three technical replicates and each experiment was done in triplicates. Statistical analysis was performed as described in Materials and Methods. *$p < 0.05$, **$p < 0.01$, ***$p < 0.001$, ****$p < 0.0001$. Absence of asterisk means no statistically significant difference. Control fibroblasts in grey; Rett patients' fibroblasts in yellow; LGZ-treated Rett patients' fibroblasts in green

increase in the expression of respiratory complexes (Additional file 1: Fig. S3B). These results were confirmed by anti-OXPHOS complexes Western blot, as all four complexes expression was increased upon treatment with Leriglitazone (Fig. 3C), being statistically significant the increases in complex I and IV. This was paired to an increase in the expression of several mitochondrial mass markers (Additional file 1: Fig. S2C).

Upon confirmation of the effective PPARγ-signaling pathway, we evaluated leriglitazone's efficacy in the correction of the described mitochondrial alterations in Rett fibroblasts. Treatment with leriglitazone resulted in a 50% increase in the production of mitochondrial ATP, suggesting an enhancement on mitochondrial energy production in Rett fibroblasts (Fig. 3D). Importantly, these changes were accompanied by a significant 20% decrease in superoxide anion concentration in LGZ-treated cells (Fig. 3E), and a reduction of oxidative damage in Rett fibroblasts, evidenced by a lower detection of 8-OHdG fluorescence intensity (Fig. 3F, G). These changes were not associated to a significant change in antioxidant enzymes expression (Additional file 1: Fig. S3D).

Opposite to the positive effects regarding the bioenergetic performance, we did not observe a recovery in mitochondrial network shape or dynamics, as neither network structure (measured by anti-TOMM20 immunofluorescence), expression of dynamic markers (measured by Western blot) or fusion and fission events (analyzed by in vivo imaging) showed significant differences after treatment with leriglitazone (Additional file 1: Fig. S4; Additional files 3, 4: videos S2, S3).

To confirm that these changes were a direct consequence of PPARγ pathway activation, we treated the cells with the PPARγ-signaling inhibitor GW9662 at a concentration 1 µM for 72 h. Pathway inhibition blocked the effect of leriglitazone regarding all the observed measures. As shown in Additional file 1: Fig. S5A, ATP production was even decreased when Rett fibroblasts were treated with either GW9662 or a combination of leriglitazone + GW9662. Analogously, superoxide anion production was not reduced after treatment with leriglitazone + GW9662 Additional file 1: Fig. S5B). These results confirmed the beneficial effect of PPARγ pathway activation in the recovery of the bioenergetic deficits in Rett syndrome fibroblasts.

Leriglitazone corrects the bioenergetic alterations in symptomatic Rett female mice, together with the amelioration of their phenotypic outcome

Encouraged by the positive results in fibroblasts and the description in animal models, we then studied the effect of leriglitazone in the Rett animal model (Fig. 4A). The drug was orally administered mixed with the diet at a dose equivalent to 75 mg/kg/day from weaning and until analysis at 7 months, and its intake was controlled at sacrifice through quantification of leriglitazone concentration in plasma by LC–MS/MS (Additional file 1: Fig. S6).

Both ATP concentration deficit and lipid peroxidation profile were corrected in hippocampus and cerebellum, with no significant changes observed in cortex (Fig. 4B–D). These corrections were especially noticeably in cerebellum, as the increase in ATP concentration reached levels over the control values, and lipid peroxidation was normalized with respect to control mice.

The results regarding lipid peroxidation were opposite to the expected, as we initially predicted an increase in lipid peroxidation and subsequent correction through treatment with leriglitazone. However, lipid metabolism has been described to be altered in several Rett syndrome samples [24, 25], thus alterations in lipids profiles could be contributing to the counterintuitive interpretation of the results. On top of that, PPARγ activation regulates lipids biosynthesis and we have demonstrated that leriglitazone is effectively regulating the expression of the cholesterol master-regulator *SREBF2.* To by-pass the effect of lipid metabolism in the assessment of oxidative stress, we measured oxidative damage through the quantification of 8-OHdG. Rett mice cerebellum showed increased levels of 8-OHdG, that were within control values in leriglitazone-treated mice (Fig. 4E; Additional file 1: Fig. S7).

To deepen the analysis of the effect of leriglitazone in the management of oxidative stress, we analyzed the expression of the ROS-metabolizing enzymes MnSOD and GPX in LGZ-treated Rett mice by Western blot (Fig. 4F). As happened in the ATP concentration and lipid peroxidation corrections, the most significant effect of leriglitazone was a 20 to 30% decrease in both MnSOD and GPX expression in cerebellum (Fig. 4G). These results outstand cerebellum not only as one of the most affected areas regarding bioenergetic functions but also as one of the most leriglitazone-respondent areas in Rett animal models.

Finally, to assess the ultimate effect of leriglitazone as a potential drug for the treatment of Rett syndrome, we studied its effect on Rett mice phenotype correction. Leriglitazone effectively ameliorated the overall mice status, assessed through the General Health Score, a scale that evaluates the most relevant features as mobility, breathing abnormalities, tremor or physical deterioration. The treated mice developed a milder form of the disease, which difference was evident from the beginning of the assessment (12 weeks) (Fig. 4H), and especially significant in fully symptomatic mice (7 months old) (Fig. 4I). On top of that, treated mice increased the exploring time, measured as time spent analyzing objects in Novel Object Recognition Test (NORT), suggesting an enhanced explorative behavior (Fig. 4J).

Neuroinflammatory component underlies in Rett syndrome, which is prevented with leriglitazone

Previous reports had suggested an increased inflammatory signaling in Rett syndrome, detected in peripheral tissues in both Rett models and patient samples [26, 27]. Yet, the neuroinflammatory component of the disease had not been previously explored. To unveil its potential role in the pathogenesis of the disease, we performed a cytokine detection panel in symptomatic 7 months old Rett mice compared to age-paired controls. We observed a significant increase in the expression of several cytokines in Rett samples cortex compared to the wild-type (Fig. 5A, Additional file 1: Fig. S8A), although no differences were observed in cerebellum (Additional file 1: Fig. S8B). Since leriglitazone exerts an anti-inflammatory effect through NF-κB modulation, we studied its effect on the neuroinflammatory landscape in Rett syndrome, noting a correction in leriglitazone-treated animals (Fig. 5A). These results were ratified by the presence of microglia (through the expression of the marker Iba1) and mature astrocytes (through the marker GFAP) in Rett mice brains compared to wild-type, as we observed an increase in both GFAP and Iba1 in Rett mice cortex, which was significantly corrected through treatment with leriglitazone (Fig. 5B–E). Regarding the role of inflammation through neurodevelopment, we did not detect an inflammatory profile in pre-symptomatic mice (Additional file 1: Fig. S8C).

PPARγ activation can result in the amelioration of the energetic deficits in other mitochondrial diseases

After showing that leriglitazone can modulate mitochondrial dysfunction in Rett syndrome, we next asked whether it could be useful in the correction of mitochondrial deficits in the context of primary mitochondrial diseases. Mitochondrial diseases affect 1 in every 4300 people, and result from mutations in genes directly responsible for any of their functions, encoded either in mitochondrial or nuclear DNA. To test the effect of leriglitazone in primary mitochondrial disorders we have selected fibroblasts from a patient bearing a mutation in *NDUFS1*, which has been confirmed as the cause of the disease. We limited our study to the effect of leriglitazone in mitochondrial ATP production and ROS exposure,

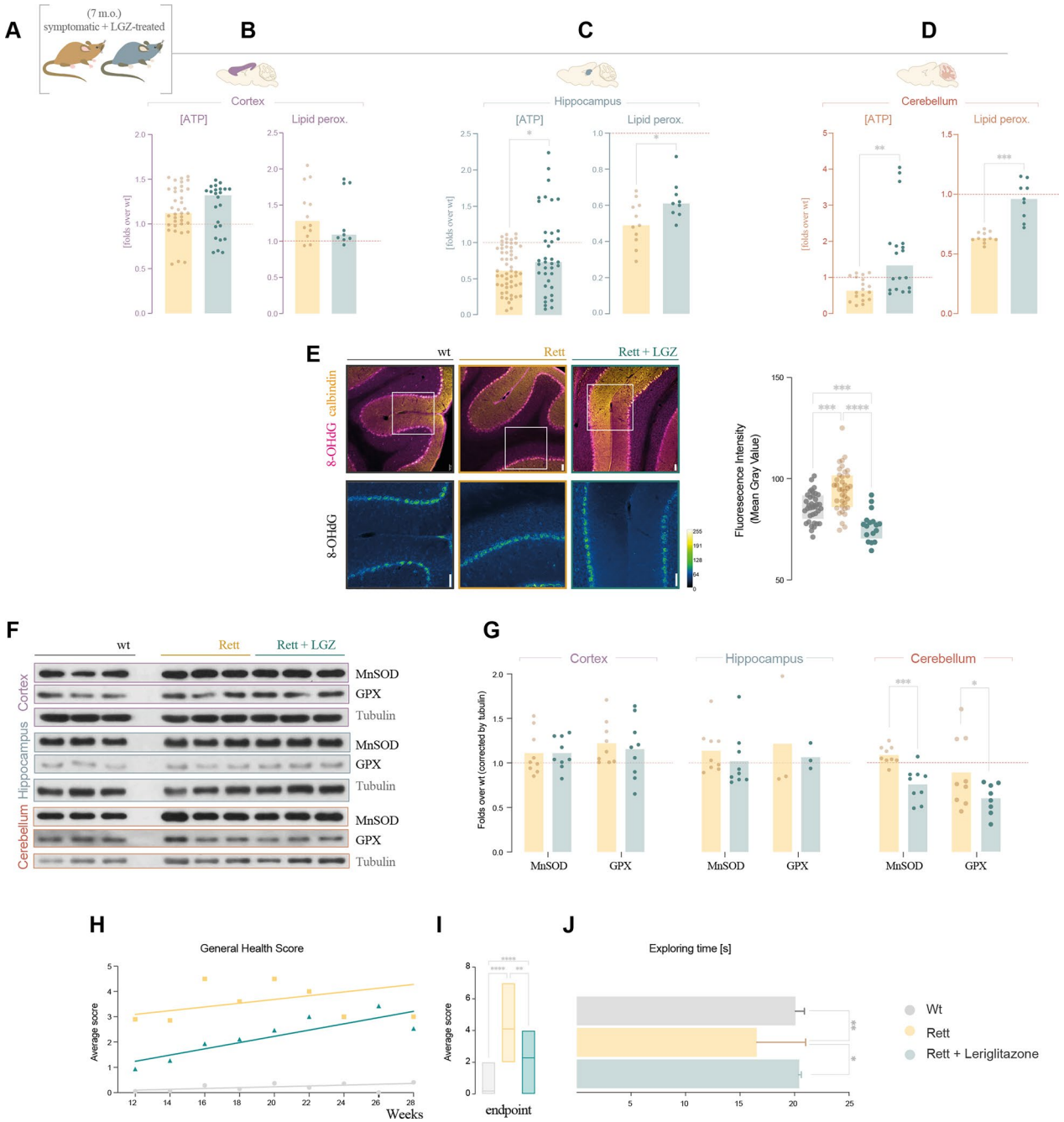

Fig. 4 Correction by LGZ of the bioenergetic component in hippocampus and cerebellum, together with a phenotypic amelioration in symptomatic Rett mice. **A** Treatment with LGZ was assayed in Rett mice, treating them from weaning until sacrifice at the symptomatic stage (7 m.o.). Both ATP concentration (detected by bioluminescence) and lipid peroxidation (detected by TBARS) were assayed in untreated and LGZ-treated Rett mice in **B** cortex, **C** hippocampus and **D** cerebellum. **E** to **G** show results regarding oxidative stress and antioxidant markers in the brain areas of interest. **E** Detection of the RNA oxidative damage marker 8-OHdG in cerebellum by immunofluorescence. 8-OHdG staining is shown in magenta and calbindin in yellow for Purkinje cells in the upper images at 10× magnification; in the lower images 8-OHdG is shown with the intensity-revealing LUT "Green Fire Blue", with a 2× electronic zoom; scale bar represents 50 µm in both images. **F** Antioxidant markers MnSOD and GPX in cortex, hippocampus and cerebellum detected by western blot, and their respective densitometry quantification, normalized by tubulin (**G**). Phenotypical characterization of the treated mice, registering an improvement in the General Health Score (**H**), which was maintained until the endpoint (**I**) and a recovery of the explorative behaviour of Rett mice upon treatment in the NOR-test (**J**). All experiments were done in at least three different mice, with three technical replicates and each experiment was done in triplicated (except for lipid peroxidation). Statistical analysis was performed as described in Materials and Methods. *$p < 0.05$, **$p < 0.01$, ***$p < 0.001$, ****$p < 0.0001$. Absence of asterisk means no statistically significant difference. Wild-type female mice in grey; Rett female mice in yellow; LGZ-treated Rett female mice in green

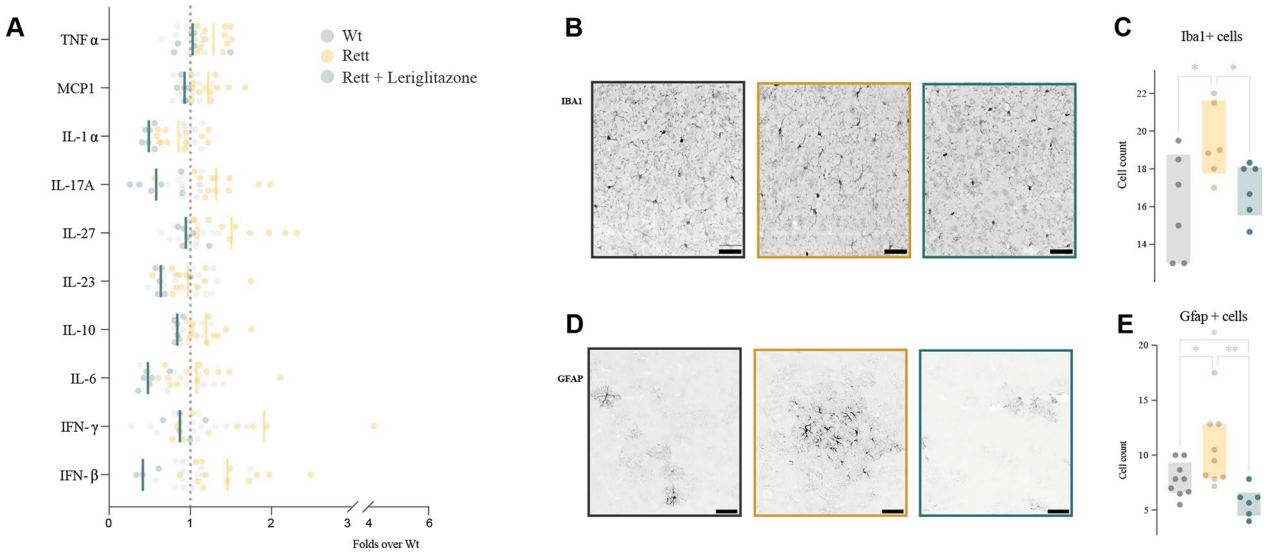

Fig. 5 Neuroinflammatory component in cerebral cortex of symptomatic Rett mice is corrected after leriglitazone treatment. **A** Rett cerebral cortex at 7 m.o. showed a pattern of increased cytokines expression detected by flow cytometry, that was corrected in leriglitazone-treated mice (Nested one-way ANOVA analysis; *p*-value Rett *vs* wt = ** 0.0016; Rett *vs* Rett + leriglitazone = **** < 0.0001) **B** Iba1 and **D** GFAP cell-positive number were appraised, as microglia and astrocytic specific markers, respectively. **C**, **E** Quantifications of Iba1- and GFAP-positive cells revealed an increase in microglia and active astrocytes in symptomatic Rett mice cortex compatible with neuroinflammation, that was corrected with LGZ for both markers. Images were taken at a 10 × magnification (and 2.5 × electronic zoom for Iba1 images). Scale bar represents 50 µm. Statistical analyses were performed as described in Materials and Methods. *$p < 0.05$, **$p < 0.01$. Absence of asterisk means no statistically significant difference. Wild-type female mice in grey; Rett female mice in yellow; LGZ-treated Rett female mice in green

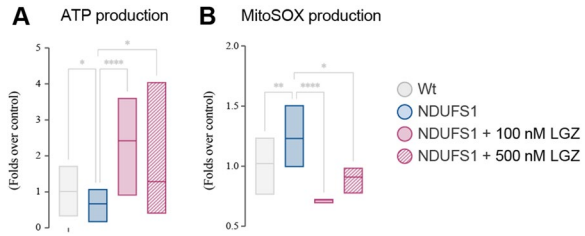

Fig. 6 Effect of leriglitazone in fibroblasts from primary mitochondrial diseases. Given LGZ mechanism of action we investigated its potential effect on the treatment of mitochondrial diseases. For that, we selected fibroblasts from a patient bearing mutations in *NDUFS1*, which affect the bioenergetic function. **A** Non-glycolytic ATP concentration detected by luciferin-luciferase luminescence upon incubation with 2-deoxyglucose, and **B** O_2^- generation—detected with MitoSOX probe by flow cytometry—were evaluated, confirming the effect of leriglitazone in mitochondrial patients. All experiments were done in at least two technical replicates and each experiment was done in triplicates. Statistical analyses were performed as described in Materials and Methods. *$p < 0.05$, **$p < 0.01$, ****$p < 0.0001$. Absence of asterisk means no statistically significant difference. Control fibroblasts in grey; NDUFS1-patient's fibroblasts in blue; LGZ-treated NDUFS1-patient's fibroblasts in rouge

altered in the patient (Fig. 6A, B). Treatment with leriglitazone for 48 h effectively corrected the mitochondrial phenotype, increasing the mitochondria-derived ATP concentration in the patient fibroblasts, and significantly reducing the oxidative stress. These results suggest that leriglitazone could be efficient in the treatment of primary mitochondrial diseases in which bioenergetic functions are altered.

Discussion

Rett syndrome is a devastating neurodevelopmental disease without specific treatment. While a disruption of excitatory/inhibitory neurotransmission stands out in its pathophysiology, mitochondrial dysfunction has been suggested to play a role in the disease development as well [6], and in the last years it is being proposed whether mitochondrial alterations can constitute a new therapeutic target for this disorder [7]. In our work, we have explored mitochondrial dysfunction focusing on mitochondrial shape and bioenergetic function. We have defined the specific alterations in patients' fibroblasts and in Rett female mice brains, highlighting the brain-area specific differences and the changes that occur in the pre-symptomatic stages. Building on that, we have studied the effect of the novel drug leriglitazone on mitochondrial function enhancement, showing that it increases ATP production and reduces oxidative damage, ultimately improving the phenotype of symptomatic female mice. Our data endorse leriglitazone as a potential therapy not only for Rett syndrome, but also for other mitochondrial diseases.

Rett mitochondria form less interconnected and "simpler" less ramified networks with reduced fission: fusion ratio, along with several structural differences. These changes in cristae number and shape have been previously associated with reduced respiratory efficiency and cell viability, and reported in many diseases, including Leigh syndrome and Parkinson's disease [28, 29]. We have observed that Rett mitochondria produce half the ATP than controls do, also reflected in the respiration rates measured by Seahorse flux analytics, as the ATP-associated oxygen consumption is reduced with respect to controls. Not only Rett mitochondria produce less ATP, but they also generate more ROS ($O_2^{\cdot -}$), resulting in an increased oxidative damage. These results build on previous studies reporting mitochondrial alterations in the context of Rett syndrome such as decreased respiration and ATP production [30, 31], enhanced oxidative stress [32] or mitochondrial elongation [19]. They also confirm fibroblasts as a valid, and understudied, model for the research on mitochondrial alterations in this disease, enabling the study patient-specific differences. Further works shall explore the potential correlation between patients and fibroblasts response to a drug, advancing towards personalized medicine in Rett syndrome.

The bioenergetic alterations are maintained in Rett mice brains. This agrees with studies that reported a decrease in brain ATP synthesis [33–35], but while knowledge was mostly limited to whole brain analysis, we have studied bioenergetic function both between different brain areas and at two different time-points through the phenotype progression. Our results in symptomatic 7 m.o. Rett mice evidence the diversity on mitochondrial performance through the brain, and point to the cerebellum as a major player in the pathophysiology of Rett syndrome with respect to bioenergetic dysfunction. Previous results reported an increase in the rate of H_2O_2 generation due to dysfunctional complex II in Rett whole brain [36], which would be expected to result in an increase in lipid peroxidation. Opposite to that, we have observed a decrease in lipid peroxidation in both hippocampus and cerebellum of Rett mice and an increase in cortex. This discrepancy might be sustained on two aspects: on one hand, cortex is the most voluminous area in the brain, and therefore the results in that area might overshadow the differences in other brain areas. On the other hand, previous reports suggest an alteration in lipids metabolism, profiled both in Rett mice [24, 37, 38] and patient's cerebrospinal fluid [25], probably affecting the overall lipid peroxidation detection. Clarifying this, the increase in 8-OHdG in cerebellum supports oxidative damage is also involved in brain mitochondrial dysfunction, in agreement with previous reports. Cerebellar bioenergetic alterations are already detectable in pre-symptomatic phases (3 m.o. mice), underlining its importance in disease progression. Alterations in cerebellum function had been suggested in Rett patients through MRI [39], and recent experiments show that deleting Mecp2 from the cerebellum is responsible for the delay in motor learning in mice [40]. In fact, a parallelism could be established between cerebellar dysfunctions and early-presenting features of the disease such as the movement disorders [41] or stereotypes [42]. Despite all this, cerebellum remains understudied in Rett syndrome compared to other brain areas as cortex or hippocampus [40]. This gap in the knowledge is bigger if we focus in bioenergetic performance, that can be playing an even more important role in cerebellum than in other brain areas. Taking cerebellum into consideration as an important player in the pathophysiology of Rett syndrome is especially relevant on the design of new therapies, such as transcranial electrical stimulation (tES) [43, 44] or genetic therapy, where reach of the transgene can be a limitation [45].

This systematic description and delineation of the involvement of mitochondria in Rett syndrome's pathophysiology sets the base for its study as a potential therapeutic target for the treatment of the disease. While this had already been attempted with other drugs, the effects observed were mild and have not been clinically translatable [10, 11, 46]. Building on that, we have studied the effect of the novel drug leriglitazone on the correction of Rett dysfunctions. Leriglitazone (LGZ) is an oral bioavailable selective PPARγ agonist that has an improved profile compared with other drugs acting on the same target for treating neurodegenerative diseases. It shows superior brain penetration and a favorable safety profile, allowing interaction with PPARγ in the CNS above the level that can be safely achieved with pioglitazone and other glitazones [13]. It promotes the transcription of key genes that counteract oxidative stress, stimulate mitochondrial biogenesis and repress Nf-kB activation [22]. It has been validated in preclinical models of other neurodegenerative diseases, showing clinical benefits for X-ALD patients and clinical proof of concept in FA patients [13, 14, 22, 23, 47].

Treatment with leriglitazone restores mitochondrial homeostasis in Rett models. Our studies show that LGZ increases mitochondrial ATP production and reduces oxidative stress, which can be defined as an improved bioenergetic status. These effects were recorded both in fibroblasts and in animal models, in which leriglitazone recovered the decrease in ATP concentration and normalized lipid peroxidation profiles and oxidative damage markers both in hippocampus and cerebellum.

On top of mitochondrial homeostasis correction, leriglitazone also reduced inflammation in Rett mice. Inflammatory involvement in the disease had been previously

pointed out in patients' plasma and fibroblasts [26, 48], and this is the first report on a neuroinflammatory activity in Rett brain, evidenced by the cytokine panel and the increase in microglia in cortex. Surprisingly, while bioenergetic alterations were more prominent in cerebellum and already detectable at a pre-symptomatic stage, inflammatory alterations were only noticeable in symptomatic brain cortex. Although mitochondrial dysfunction has recently been proposed as an inflammatory trigger in several scenarios [49, 50], our results suggest that mitochondrial dysfunction and neuroinflammation are not necessarily interrelated in Rett syndrome and nor is their correction with leriglitazone. Neuroinflammatory component of the disease sets a new therapeutic target for Rett syndrome. Further studies shall investigate its contribution to the disease progression.

Importantly, sustained treatment with leriglitazone results in an amelioration of the phenotype of female Rett mice, both in the general observed health and in the exploratory activity. Similar phenotypic modulation through mitochondrial targeting had been previously achieved through serotonin receptor stimulation [10, 46], but not accomplished through other approaches as metformin [11]. We believe the success in leriglitazone effect in Rett syndrome relies on both the treatment time (from weaning until sacrifice) and on the mechanism of action of leriglitazone, increasing mitochondrial performance and biogenesis, exerting an anti-inflammatory effect and promoting neuronal growth and myelination [13]. Working with female mice greatly increases the translational value of these results.

Given the effect of leriglitazone on mitochondrial function enhancement, and its prompt availability in other neuropediatric diseases, we wondered whether it will be effective on primary mitochondrial diseases. To such end, we treated with leriglitazone fibroblasts from mitochondrial patients bearing a mutation in *NDUFS1*, which showed alterations affecting directly the electron transport chain. Treatment with leriglitazone resulted in an increase in ATP concentration and decreased oxidative stress, outstanding as a potential treatment for mitochondrial diseases.

Taken together, our work provides evidence of mitochondrial dysfunction in Rett syndrome, sustained from patient fibroblasts to Rett female mice, complementing previous reports on total brain metabolic defect and highlighting the importance of the cerebellum. Noteworthy, cerebellar mitochondrial dysfunction is already evident at the pre-symptomatic stage, which underlines the importance of timing in the study and treatment of Rett syndrome. Our results confirm that Rett syndrome is indeed a neurodevelopmental disorder with a key metabolic component, which can be purposed as a therapeutic target, urging for a prompt mitochondria-targeted intervention upon disease diagnosis.

The bioenergetic and inflammatory alterations are corrected in the studied models through treatment with the PPARγ agonist leriglitazone, resulting in a phenotypic improvement of Rett female mice. Given these results and the knowledge on leriglitazone safety on both healthy subjects and pediatric patients [13], this work constitutes the preclinical evidence for a clinical trial with leriglitazone in Rett syndrome and other diseases with mitochondrial involvement.

Conclusions

- Both mitochondrial shape and bioenergetic functions are altered in Rett syndrome fibroblasts, which display simpler and less interconnected networks, with defective ATP production and increased oxidative stress.
- The bioenergetic dysfunction is also detectable in Rett syndrome female mice models, displaying differences among brain areas and already evident at pre-symptomatic stages.
- Cerebellum, an understudied area in the pathophysiology of Rett syndrome, outstands regarding the bioenergetic dysfunction.
- Leriglitazone corrects bioenergetic alterations in all the studied Rett models, together with the amelioration of the phenotypic outcome in symptomatic Rett female mice.
- Rett syndrome pathophysiology includes a neuroinflammatory component, which is prevented with leriglitazone.
- This work provides preclinical evidence foundational for a clinical trial with leriglitazone for the treatment of Rett syndrome.

Abbreviations

8-OHdG	8-Hydroxy-2′-deoxyguanosine
Drp1	Dynamin-related protein 1
FA	Friedreich's ataxia
Fis1	Mitochondrial fission 1 protein
GPX	Glutathione peroxidase 1
MECP2	Methyl-CpG binding protein 2
Mfn2	Mitofusin 2
MnSOD	Manganese superoxide dismutase
OPA1	OPA1 mitochondrial dynamin like GTPase
PGC1α	Peroxisome proliferator activated receptor gamma coactivator 1
PPARγ	Peroxisome proliferator-activated receptor-gamma
TOMM20	Translocase of the outer mitochondrial membrane complex subunit 20.
XALD	X-linked adrenoleukodystrophy

Supplementary Information

The online version contains supplementary material available at https://doi.org/10.1186/s12967-023-04622-5.

Additional file 1: Table S1. MeCP2 mutations correspondent to each studied patients' fibroblasts. **Figure S1**. Individualities between Rett patients' fibroblasts regarding mitochondrial network and bioenergetics. **Figure S2**. ATP production in brain areas through development. **Figure S3**. Leriglitazone (LGZ) upregulates genes under the PPARγ pathway and exerts an effect on mitochondrial biogenesis, without changes in antioxidant markers expression. **Figure S4**. Leriglitazone (LGZ) does not exert an effect on mitochondrial dynamics in Rett fibroblasts. **Figure S5**. Blocking PPARγ pathway with GW9662 results in a decrease in ATP production, without changes in superoxide anion generation. **Figure S6.** LGZ plasma detection in symptomatic Rett female mice. **Figure S7**. Oxidative stress in cerebellum of symptomatic Rett female mice. **Figure S8**. Neuroinflammatory component is not detected in cerebellum of symptomatic mice nor presymptomatic cerebral cortex.

Additional file 2: Video S1. Time-lapse video of mitochondrial network dynamics of control fibroblasts (2 minutes, scale bar 10 µm).

Additional file 3: Video S2. Time-lapse video of mitochondrial network dynamics of Rett fibroblasts (2 minutes, scale bar 10 µm).

Additional file 4: Video S3. Time-lapse video of mitochondrial network dynamics of LGZ-treated Rett fibroblasts (2 minutes, scale bar 10 µm).

Acknowledgements
The authors wish to acknowledge Centres Científics i Tecnològics, especially Benjamín Torrejon (Universitat de Barcelona, Bellvitge Campus, Barcelona, Spain), electronic microscopy service of Centro de Biologia Molecular Severo Ochoa, especially Maite Rejas (CBMSO, Madrid, Spain) and Hospital Sant Joan de Déu Confocal Microscopy Service and Biobanc for their support and technical assistance.

Author contributions
AO, AGC, PP, MM conceptualized the study. AO, AC designed the methodology. UM, CG, CV, LRP, AO performed the investigation. UM, CX, AO visualized the data. AO, AGC, PP, MM, SA, UM acquired funding for the experiments. AO, AGC were responsible for project administration. AO, AGC, PRP, SA, PP, MM provided supervision. AO, UM wrote the original draft. AO, UM, CX, AC, CG, SA, PRP, CV, LRP, PP, MM, AGC reviewed, edited and approved the final manuscript.

Funding
Spanish Ministry of Science and Innovation "Retos Colaboración" Grant RTC-2017-5867-1 (AO, AGC, UM, PP, MM). Spanish Ministry of Science and Innovation grant PID2020-115748RB-I00 (SA). Generalitat de Catalunya "PIF-Salut" Grant PFP00201-PERIS (UM, AGC, AO). Princesa Rett and Rettando al Síndrome de Rett donations (AGC, AO, UM, CG, CX).

Availability of data and materials
The datasets used and/or analysed during the current study are available from the corresponding author on reasonable request.

Declarations

Ethics approval and consent to participate
Fibroblast samples were collected with legal tutors informed consent, and ethical approval for its collection, use and storage was granted by the Institutional Ethics Committee of the Hospital Sant Joan de Déu. Controls were unrelated surgery surpluses from healthy donors. The mouse colony was maintained in the Animal Facilities of the University of Barcelona. All animal procedures were carried out according to European Union guidelines (Directive 2010/63/EU) and were approved by the University of Barcelona Committee on Animal Use and Care.

Consent for publication
Not applicable.

Competing interests
Pilar Pizcueta, Cristina Vergara, Laura Rodríguez-Pascau and Marc Martinell are staff from the pharmaceutic company Minoryx Therapeutics. Marc Martinell and Pilar Pizcueta report a patent application (10198126) issued on January 15th 2019 for the use of leriglitazone described in this paper. The patent will be owned by those authors. Marc Martinell is the cofounder of Minoryx Threapeutics, focused on the development of therapies for rare neurodegenerative diseases. The rest of the authors declare no competing interests.

Author details
[1]Synaptic Metabolism and Personalized Therapies Lab, Department of Neurology and MetabERN, Institut de Recerca Sant Joan de Déu, 39-57 Santa Rosa Street, Esplugues de Llobregat , 08950 Barcelona, Spain. [2]Minoryx Therapeutics BE S.A., Gosselies, Charleroi, Belgium. [3]Minoryx Therapeutics S.L., Barcelona, Spain. [4]Department of Medical Genetics, Institut de Recerca Pediàtrica, Hospital Sant Joan de Déu, Barcelona, Spain. [5]Neural Development Lab, Departament de Patologia i Terapèutica Experimental, Institut de Neurociències, IDIBELL, Universitat de Barcelona, L'Hospitalet de Llobregat, Barcelona, Spain. [6]Centro de Diagnóstico de Enfermedades Moleculares, Centro de Biología Molecular Severo Ochoa, CBM-CSIC, Departamento de Biología Molecular, Institute for Molecular Biology-IUBM, Universidad Autónoma Madrid, IDIPAZ, Madrid, Spain. [7]CIBERER-Spanish Biomedical Research Centre in Rare Diseases, Madrid, Spain.

Received: 13 July 2023 Accepted: 12 October 2023
Published online: 26 October 2023

References

1. Feldman D, Banerjee A, Sur M. Developmental dynamics of Rett syndrome. Neural Plast. 2016;2016:6154080.
2. Leonard H, Cobb S, Downs J. Clinical and biological progress over 50 years in Rett syndrome. Nat Rev Neurol. 2017;13(1):37–51.
3. Ure K, Lu H, Wang W, Ito-Ishida A, Wu Z, He L-J, et al. Restoration of Mecp2 expression in GABAergic neurons is sufficient to rescue multiple disease features in a mouse model of Rett syndrome. Elife. 2016;5:e14198.
4. Guy J, Gan J, Selfridge J, Cobb S, Bird A. Reversal of neurological defects in a mouse model of Rett syndrome. Science. 2007;315(5815):1143–7.
5. Panayotis N, Ehinger Y, Felix MS, Roux J-C. State-of-the-art therapies for Rett syndrome. Dev Med Child Neurol. 2023;65(2):162–70.
6. Justice MJ, Buchovecky CM, Kyle SM, Djukic A. A role for metabolism in Rett syndrome pathogenesis. Rare Dis. 2014;1(1):e27265.
7. Shulyakova N, Andreazza AC, Mills LR, Eubanks JH. Mitochondrial dysfunction in the pathogenesis of Rett syndrome: implications for mitochondria-targeted therapies. Front Cell Neurosci. 2017;11:58.
8. Valenti D, de Bari L, Vigli D, Lacivita E, Leopoldo M, Laviola G, et al. Stimulation of the brain serotonin receptor 7 rescues mitochondrial dysfunction in female mice from two models of Rett syndrome. Neuropharmacology. 2017;121:79–88.
9. Signorini C, Leoncini S, De Felice C, Pecorelli A, Meloni I, Ariani F, et al. Redox imbalance and morphological changes in skin fibroblasts in typical Rett syndrome. Oxid Med Cell Longev. 2014;2014:195935.
10. Valenti D, de Bari L, Vigli D, Lacivita E, Leopoldo M, Laviola G, et al. Stimulation of the brain serotonin receptor 7 rescues mitochondrial dysfunction in female mice from two models of Rett syndrome. Neuropharmacology. 2017;121:79–88.
11. Zuliani I, Urbinati C, Valenti D, Quattrini MC, Medici V, Cosentino L, et al. The anti-diabetic drug metformin rescues aberrant mitochondrial activity and restrains oxidative stress in a female mouse model of Rett syndrome. J Clin Med. 2020;9(6):1669.
12. Park MJ, Aja S, Li Q, Degano AL, Penati J, Zhuo J, et al. Anaplerotic triheptanoin diet enhances mitochondrial substrate use to remodel the metabolome and improve lifespan, motor function, and sociability in MeCP2-null mice. PLoS ONE. 2014;9(10):e109527.
13. Rodríguez-Pascau L, Vilalta A, Cerrada M, Traver E, Forss-Petter S, Weinhofer I, et al. The brain penetrant PPARγ agonist leriglitazone restores multiple altered pathways in models of X-linked adrenoleukodystrophy. Sci Transl Med. 2021. https://doi.org/10.1126/scitranslmed.abc0555.

14. Pandolfo M, Reetz K, Darling A, Rodriguez de Rivera FJ, Henry P-G, Joers J, et al. Efficacy and safety of leriglitazone in patients with Friedreich ataxia: a phase 2 double-blind, randomized controlled trial (FRAMES). Neurol Genet. 2022;8(6):e200034.
15. Chaudhry A, Shi R, Luciani DS. A pipeline for multidimensional confocal analysis of mitochondrial morphology, function, and dynamics in pancreatic β-cells. Am J Physiol Endocrinol Metab. 2020;318(2):E87-101.
16. Lefebvre AEYT, Ma D, Kessenbrock K, Lawson DA, Digman MA. Automated segmentation and tracking of mitochondria in live-cell time-lapse images. Nat Methods. 2021;18(9):1091–102.
17. Khan HA. Bioluminometric assay of ATP in mouse brain: determinant factors for enhanced test sensitivity. J Biosci. 2003;28(4):379–82.
18. Amsen D, de Visser KE, Town T. Approaches to determine expression of inflammatory cytokines. Methods Mol Biol. 2009;511:107–42.
19. Belichenko PV, Wright EE, Belichenko NP, Masliah E, Li HH, Mobley WC, et al. Widespread changes in dendritic and axonal morphology in Mecp2-mutant mouse models of Rett syndrome: evidence for disruption of neuronal networks. J Comp Neurol. 2009;514(3):240–58.
20. Olesen MA, Villavicencio-Tejo F, Quintanilla RA. The use of fibroblasts as a valuable strategy for studying mitochondrial impairment in neurological disorders. Transl Neurodegener. 2022;11(1):36.
21. Cordone V, Pecorelli A, Amicarelli F, Hayek J, Valacchi G. The complexity of Rett syndrome models: primary fibroblasts as a disease-in-a-dish reliable approach. Drug Discov Today Dis Model. 2020;31:11–9.
22. Rodríguez-Pascau L, Britti E, Calap-Quintana P, Dong YN, Vergara C, Delaspre F, et al. PPAR gamma agonist leriglitazone improves frataxin-loss impairments in cellular and animal models of Friedreich Ataxia. Neurobiol Dis. 2021;148:105162.
23. Köhler W, Engelen M, Eichler F, Lachmann R, Fatemi A, Sampson J, et al. Safety and efficacy of leriglitazone for preventing disease progression in men with adrenomyeloneuropathy (ADVANCE): a randomised, double-blind, multi-centre, placebo-controlled phase 2–3 trial. Lancet Neurol. 2023;22(2):127–36.
24. Segatto M, Trapani L, Di Tunno I, Sticozzi C, Valacchi G, Hayek J, et al. Cholesterol metabolism is altered in Rett syndrome: a study on plasma and primary cultured fibroblasts derived from patients. PLoS ONE. 2014;9(8):e104834.
25. Zandl-Lang M, Züllig T, Trötzmüller M, Naegelin Y, Abela L, Wilken B, et al. Changes in the cerebrospinal fluid and plasma lipidome in patients with Rett syndrome. Metabolites. 2022;12(4):291.
26. Cortelazzo A, De FC, Guerranti R, Signorini C, Leoncini S, Pecorelli A, et al. Subclinical inflammatory status in Rett syndrome. Mediators Inflamm. 2014;2014:1–13.
27. Cortelazzo A, De FC, De FB, Ricceri L, Laviola G, Leoncini S, et al. Persistent unresolved inflammation in the Mecp2-308 female mutated mouse model of Rett syndrome. Mediators Inflamm. 2017;2017:1–9.
28. Huang C, Deng K, Wu M. Mitochondrial cristae in health and disease. Int J Biol Macromol. 2023;235:123755.
29. Navaratnarajah T, Anand R, Reichert AS, Distelmaier F. The relevance of mitochondrial morphology for human disease. Int J Biochem Cell Biol. 2021;134:105951.
30. Cicaloni V, Pecorelli A, Tinti L, Rossi M, Benedusi M, Cervellati C, et al. Proteomic profiling reveals mitochondrial alterations in Rett syndrome. Free Radic Biol Med. 2020;155:37–48.
31. Cervellati C, Sticozzi C, Romani A, Belmonte G, De Rasmo D, Signorile A, et al. Impaired enzymatic defensive activity, mitochondrial dysfunction and proteasome activation are involved in RTT cell oxidative damage. Biochim Biophys Acta. 2015;1852(10 Pt A):2066–74.
32. De Filippis B, Chiodi V, Adriani W, Lacivita E, Mallozzi C, Leopoldo M, et al. Long-lasting beneficial effects of central serotonin receptor 7 stimulation in female mice modeling Rett syndrome. Front Behav Neurosci. 2015;9:86.
33. Toloe J, Mollajew R, Kügler S, Mironov SL. Metabolic differences in hippocampal "Rett" neurons revealed by ATP imaging. Mol Cell Neurosci. 2014;59:47–56.
34. Saywell V, Viola A, Confort-Gouny S, Le Fur Y, Villard L, Cozzone PJ. Brain magnetic resonance study of Mecp2 deletion effects on anatomy and metabolism. Biochem Biophys Res Commun. 2006;340(3):776–83.
35. Jin L-W, Horiuchi M, Wulff H, Liu X-B, Cortopassi GA, Erickson JD, et al. Dysregulation of glutamine transporter SNAT1 in Rett syndrome microglia: a mechanism for mitochondrial dysfunction and neurotoxicity. J Neurosci Off J Soc Neurosci. 2015;35(6):2516–29.
36. De Filippis B, Valenti D, de Bari L, De Rasmo D, Musto M, Fabbri A, et al. Mitochondrial free radical overproduction due to respiratory chain impairment in the brain of a mouse model of Rett syndrome: protective effect of CNF1. Free Radic Biol Med. 2015;83:167–77.
37. Kyle SM, Vashi N, Justice MJ. Rett syndrome: a neurological disorder with metabolic components. Open Biol. 2018. https://doi.org/10.1098/rsob.170216.
38. Lopez AM, Chuang J-C, Posey KS, Turley SD. Suppression of brain cholesterol synthesis in male Mecp2-deficient mice is age dependent and not accompanied by a concurrent change in the rate of fatty acid synthesis. Brain Res. 2017;1654(Pt A):77–84.
39. Takeguchi R, Kuroda M, Tanaka R, Suzuki N, Akaba Y, Tsujimura K, et al. Structural and functional changes in the brains of patients with Rett syndrome: a multimodal MRI study. J Neurol Sci. 2022;441:120381.
40. Achilly NP, He L-J, Kim OA, Ohmae S, Wojaczynski GJ, Lin T, et al. Deleting Mecp2 from the cerebellum rather than its neuronal subtypes causes a delay in motor learning in mice. Elife. 2021. https://doi.org/10.7554/eLife.64833.
41. Singh J, Lanzarini E, Nardocci N, Santosh P. Movement disorders in patients with Rett syndrome: a systematic review of evidence and associated clinical considerations. Psychiatry Clin Neurosci. 2021;75(12):369–93.
42. Dean SL, Tochen L, Augustine F, Ali SF, Crocetti D, Rajendran S, et al. The role of the cerebellum in repetitive behavior across species: childhood stereotypies and deer mice. Cerebellum. 2022;21(3):440–51.
43. Fabio RA, Gangemi A, Capri T, Budden S, Falzone A. Neurophysiological and cognitive effects of transcranial direct current stimulation in three girls with Rett syndrome with chronic language impairments. Res Dev Disabil. 2018;76:76–87.
44. Fabio RA, Gangemi A, Semino M, Vignoli A, Canevini MP, Priori A, et al. Effects of combined transcranial direct current stimulation with cognitive training in girls with Rett syndrome. Brain Sci. 2020;10(5):276.
45. Fischell JM, Fishman PS. A multifaceted approach to optimizing AAV delivery to the brain for the treatment of neurodegenerative diseases. Front Neurosci. 2021;15:747726.
46. De Filippis B, Nativio P, Fabbri A, Ricceri L, Adriani W, Lacivita E, et al. Pharmacological stimulation of the brain serotonin receptor 7 as a novel therapeutic approach for Rett syndrome. Neuropsychopharmacol Off Publ Am Coll Neuropsychopharmacol. 2014;39(11):2506–18.
47. Pizcueta P, Vergara C, Emanuele M, Vilalta A, Rodríguez-Pascau L, Martinell M. Development of PPARγ agonists for the treatment of neuroinflammatory and neurodegenerative diseases: leriglitazone as a promising candidate. Int J Mol Sci. 2023;24(4):3201.
48. Cicaloni V, Pecorelli A, Cordone V, Tinti L, Rossi M, Hayek J, et al. A proteomics approach to further highlight the altered inflammatory condition in Rett syndrome. Arch Biochem Biophys. 2020;696:108660.
49. Vringer E, Tait SWG. Mitochondria and cell death-associated inflammation. Cell Death Differ. 2023;30(2):304–12.
50. Casaril AM, Dantzer R, Bas-Orth C. Neuronal mitochondrial dysfunction and bioenergetic failure in inflammation-associated depression. Front Neurosci. 2021;15:725547.

Publisher's Note

Springer Nature remains neutral with regard to jurisdictional claims in published maps and institutional affiliations.

2| OTHER PAPERS PUBLISHED DURING THE PRE-DOCTORAL PERIOD BUT NOT INCLUDED IN THIS THESIS

Illescas, S., Diaz-Osorio, Y., Serradell, A., Toro-Soria, L., Musokhranova, U., Juliá-Palacios, N., Ribeiro-Constante, J., Altafaj, X., Olivella, M., O'Callaghan, M., Darling, A., Armstrong, J., Artuch, R., García-Cazorla, À. & Oyarzábal, A. (2023). Metabolic characterization of neurogenetic disorders involving glutamatergic neurotransmission. Journal of Inherited Metabolic Disease. https://doi.org/10.1002/jimd.12689

Justel, M., Jou, C., Sariego-Jamardo, A., Juliá-Palacios, N. A., Ortez, C., Poch, M. L., Hedrera-Fernandez, A., Gomez-Martin, H., Codina, A., Dominguez-Carral, J., Muxart, J., Hernández-Laín, A., Vila-Bedmar, S., Zulaica, M., Cancho-Candela, R., Castro, M. del C., Osa-Langreo, A. de la, Peña-Valenceja, A., Marcos-Vadillo, E., …, Musokhranova, U, … Benito, D. N. (n.d.). Expanding the phenotypic spectrum of TRAPPC11-related muscular dystrophy: 25 Roma individuals carrying a founder variant. Journal of Medical Genetics, 60(10), 965. https://doi.org/10.1136/jmg-2022-109132

Check for updates

Received: 1 August 2023 | Revised: 28 September 2023 | Accepted: 2 November 2023

DOI: 10.1002/jimd.12689

ORIGINAL ARTICLE

JIMD SSIEM WILEY

Metabolic characterization of neurogenetic disorders involving glutamatergic neurotransmission

Sofía Illescas[1] | **Yaiza Diaz-Osorio**[1] | **Anna Serradell**[1] | **Lucía Toro-Soria**[1] | **Uliana Musokhranova**[1] | **Natalia Juliá-Palacios**[1,2] | **Juliana Ribeiro-Constante**[1,2] | **Xavier Altafaj**[3] | **Mireia Olivella**[4,5] | **Mar O'Callaghan**[1,2,6] | **Alejandra Darling**[1,2] | **Judith Armstrong**[6,7] | **Rafael Artuch**[6,8] | **Àngels García-Cazorla**[1,2,6] | **Alfonso Oyarzábal**[1,2,6]

[1]Synaptic Metabolism and Personalized Therapies Lab, Institut de Recerca Sant Joan de Déu, Department of Neurology and MetabERN, Esplugues de Llobregat, Barcelona, Spain

[2]Neurometabolic Unit, Hospital Sant Joan de Déu, Department of Neurology, Esplugues de Llobregat, Barcelona, Spain

[3]Neurophysiology Laboratory, Department of Biomedicine, Institute of Neurosciences, Faculty of Medicine and Health Sciences, University of Barcelona, August Pi i Sunyer Biomedical Research Institute (IDIBAPS), Barcelona, Spain

[4]School of International Studies, ESCI-UPF, Barcelona, Spain

[5]Bioinformatics and Bioimaging Group, Faculty of Science, Technology and Engineering, University of Vic—Central University of Catalonia, Vic, Spain

[6]CIBERER-Spanish Biomedical Research Centre in Rare Diseases, Barcelona, Spain

[7]Department of Medical Genetics, Institut de Recerca Pediàtrica, Hospital Sant Joan de Déu, Barcelona, Spain

[8]Clinical Biochemistry Department, Institut de Recerca Sant Joan de Déu, Hospital Sant Joan de Déu, Barcelona, Spain

Correspondence
Àngels García-Cazorla and Alfonso Oyarzábal, Synaptic Metabolism and Personalized Therapies Lab, Institut de Recerca Sant Joan de Déu, Department of Neurology and MetabERN, Esplugues de Llobregat, Barcelona, Spain.
Email: agarcia@sjdhospitalbarcelona.org and alfonsoluis.oyarzabal@sjd.es

Funding information
Instituto de Salud Carlos III, Grant/Award Number: FI21/0073; Fondo Europeo de desarrollo regional (FEDER); European Regional Development Fund (ERDF), Grant/Award Numbers: PI22/00525, PI19/00348

Communicating Editor: Nenad Blau

Abstract

The study of inborn errors of neurotransmission has been mostly focused on monoamine disorders, GABAergic and glycinergic defects. The study of the glutamatergic synapse using the same approach than classic neurotransmitter disorders is challenging due to the lack of biomarkers in the CSF. A metabolomic approach can provide both insight into their molecular basis and outline novel therapeutic alternatives. We have performed a semi-targeted metabolomic analysis on CSF samples from 25 patients with neurogenetic disorders with an important expression in the glutamatergic synapse and 5 controls. Samples from patients diagnosed with MCP2, CDKL5-, GRINpathies and STXBP1-related encephalopathies were included. We have performed univariate (UVA) and multivariate statistical analysis (MVA), using Wilcoxon rank-sum test, principal component analysis (PCA), and OPLS-DA. By using the results of both analyses, we have identified the metabolites that were significantly altered and that were important in clustering the respective groups. On these, we performed pathway- and network-based analyses to define which metabolic pathways were possibly altered in each pathology. We have observed alterations in the tryptophan and branched-chain amino acid metabolism pathways, which interestingly converge on LAT1 transporter-dependency to cross

 © 2023 SSIEM.

the blood–brain barrier (BBB). Analysis of the expression of LAT1 transporter in brain samples from a mouse model of Rett syndrome (MECP2) revealed a decrease in the transporter expression, that was already noticeable at pre-symptomatic stages. The study of the glutamatergic synapse from this perspective advances the understanding of their pathophysiology, shining light on an understudied feature as is their metabolic signature.

KEYWORDS

metabolomics, neurodevelopmental diseases, Rett syndrome, SLC7A5, tryptophan

1 | INTRODUCTION

Biochemical pathways of neurotransmission and their related diseases have been well-described during the last decades and mainly involve disorders of monoaminergic, GABAergic and glycinergic neurotransmission. These diseases are identified by the detection of abnormal concentration of metabolites related with these pathways. Glutamatergic neurotransmission has been poorly considered in this category of disorders probably because no validated markers have been described so far as possible biochemical signatures. However, glutamatergic signaling is the most abundant form of synaptic communication leading to the development of crucial functions in the brain such as excitability and neuronal plasticity. Therefore, it is not surprising that glutamatergic neurotransmission has been described to be impaired in a plethora of diseases with different clinical presentations, ranging from loss-of-function mutations in *GRIN2B* that result in the inability of NMDA receptors to respond to glutamate neurotransmission[1] to the increased glutamatergic signaling in Rett syndrome,[2] that, along with a reduction in the activity of the GABAergic system,[2] results in an shifted excitatory/inhibitory balance.

A systematic review of disorders of the glutamatergic synapse has found around 80 different genetic disorders primarily affecting key proteins of the glutamatergic synapse (i.e., receptors, presynaptic and postsynaptic pathways) leading to impaired glutamatergic transmission.[3] Neurophysiological studies in cellular and animal models have been the bases so far to determine how glutamatergic transmission is disturbed in these neuro genetic conditions.

High-throughput "omic" technologies are emerging as useful approaches to study complex diseases, advancing in their description and the identification of biomarkers.[4–8] Metabolomics can capture patient-specific variation such as response to treatment, exposure to environmental conditions, or disease progression, which makes it a promising avenue for personalized medicine.[9,10] One of the main advantages of metabolomics is that it allows researchers to study complete metabolic pathways in a single assay, providing a broader view of the effect that genomic and proteomic regulation have on the disease pathophysiology.

In this work we have studied the metabolic profile of patients affected with different genetic neurodevelopmental disorders (NDDs) in which glutamatergic neurotransmission has been proposed as a major event in the disease progression, comparing patient CSF samples with healthy controls. The joint study of different pathologies that display common molecular features has helped on the identification of shared pathophysiological mechanisms, common to neurodevelopmental diseases.

2 | MATERIALS AND METHODS

2.1 | Patients and samples

Cerebrospinal fluid (CSF) was collected from a total of 25 patients and 5 healthy controls as previously reported.[11–13] The metabolomic study was done on the last fraction collected (the first fraction consists of the first 5 drops extracted and the remaining of the following 10 drops each; the fractions were used for biochemistry studies, neurotransmitters detection, pterins, amino acids and omics studies respectively as described in references 11,12). Patients presented mutations in genes that have been widely reported to involve glutamatergic transmission: *CDKL5* ($n = 2$), *GRIN* genes ($n = 7$), *MECP2* ($n = 12$), and *STXBP1* ($n = 4$). The median age at the time of collection was 6 years, ranging from 1 to 18 years old, as seen in Table 1. The majority of patients were female ($n = 19$) due to the large proportion of Rett syndrome patients that were included in this study.

All samples were from pediatric population and were obtained and stored under the ethical approval of the Ethics Committee of Hospital Sant Joan de Déu with the assistance of Hospital Sant Joan de Déu Biobanc.

15732665, 2024, 3, Downloaded from https://onlinelibrary.wiley.com/doi/10.1002/jimd.12689 by Universitat De Barcelona Biblioteca, Wiley Online Library on [09/01/2025]. See the Terms and Conditions (https://onlinelibrary.wiley.com/terms-and-conditions) on Wiley Online Library for rules of use; OA articles are governed by the applicable Creative Commons License

TABLE 1 Patients major findings and description summary.

ID	Disease group	Age at LP	Sex	5HIAA (nmol/L)	HVA (nmol/L)	HVA/ 5-HIAA	Gene	Mutation	Clinical presentation	Medications at time of lumbar puncture
GRIN.1	GRIN	9	F	**62 (87–366)**	330 (202–596)	**5,32 (1,5-3,5)**	*GRIN2B* NM_015378	p.(Pro553Thr)	Neurodevelopmental encephalopathy, global developmental delay, profound intellectual disability, hypotonia, no ambulation, behavior disorder. Partial epilepsy (clonic and myoclonic seizures).	Levopromazine, carbamazepine, melatonin, L-Serine
GRIN.2	GRIN	3	M	**106 (106–316)**	**529 (304–658)**	4,99 (1,5-3,5)	*GRIN2B* NM_015378	p.(Arg696His)	Neurodevelopmental encephalopathy, severe intellectual disability, autism, hyperkinetic behavior, aggressiveness with autistic traits, multifocal epileptiform discharges without clinical seizures, hypotonia, walking with limitations.	None
GRIN.3	GRIN	0	F	**220 (217–1142)**	**439 (354–1328)**	2 (1,5-3,5)	*GRIN1* NM_007327	p.(Gly641Arg)	Global developmental delay, Severe intellectual disability, hyperkinesia, dyskinetic movements, hands-washing stereotypies, hypotonia, no ambulation. Partial epilepsy (oculocephalic crisis, onset at 5 months) that remitted with valproic acid.	None
GRIN.5	GRIN	14	M	**47 (63–185)**	**126 (156–410)**	2,68 (1,5-3,5)	*GRIN2B* NM_015378	t (1;12) (1;12)(p13;q13)	Global developmental delay, moderate intellectual disability, attention deficit hyperactivity disorder.	Guanfacine, Melatonin

(Continues)

15732665, 2024, 3, Downloaded from https://onlinelibrary.wiley.com/doi/10.1002/jimd.12689 by Universitat De Barcelona Biblioteca, Wiley Online Library on [09/01/2025]. See the Terms and Conditions (https://onlinelibrary.wiley.com/terms-and-conditions) on Wiley Online Library for rules of use; OA articles are governed by the applicable Creative Commons License

TABLE 1 (Continued)

ID	Disease group	Age at LP	Sex	5HIAA (nmol/L)	HVA (nmol/L)	HVA/ 5-HIAA	Gene	Mutation	Clinical presentation	Medications at time of lumbar puncture
GRIN.6	GRIN	14	F	**56 (63–185)**	**156 (156–410)**	2,79 (1,5-3,5)	*GRIN2B* NM_015378	p.(Arg926*)	Global developmental delay, mild intellectual disability, multifocal epileptiform discharges without clinical seizures, attention deficit hyperactivity disorder.	None
GRIN.7	GRIN	8	M	104 (87–366)	377 (202–596)	**3,63 (1,5-3,5)**	*GRIN2B* NM_015378	p.(Pro553Thr)	Neurodevelopmental encephalopathy, global developmental delay, profound intellectual disability, hypotonia, caregiver assistance walking, hyperkinetic movements, behavior disorder. Epileptic spasms.	Levetiracetam
STXBP1.1	STXBP1	5	F	124 (106–316)	310 (304–658)	2,5 (1,5-3,5)	*STXBP1* NM_001032221	p.(Arg406Cys)	Global developmental delay, congenital microcephaly. Epilepsy, generalized-onset and myoclonic seizure. Stereotypy. Limb dystonia and tremor. Severe intellectual disability.	Unknown
STXBP1.2	STXBP1	3	M	**164 (170–490)**	578 (344–906)	**3,52 (1,5-3,5)**	*STXBP1* NM_001032221	p.(Met602Val)	Global developmental delay. Epilepsy, infantile spasms and generalized-onset seizures. Severe intellectual disability.	Levetiracetam, valproic acid, carbamazepine
STXBP1.3	STXBP1	18	F	85 (63–185)	289 (156–410)	3,4 (1,5-3,5)	*STXBP1* NM_001032221	p.(Ile55Lys)	Infantile onset. Global developmental delay with prominent speech and language development. Autistic behavior. Intellectual disability, severe. Stereotypical body rocking. Behavioral abnormalities.	None

15732665, 2024, 3, Downloaded from https://onlinelibrary.wiley.com/doi/10.1002/jimd.12689 by Universitat De Barcelona Biblioteca, Wiley Online Library on [09/01/2025]. See the Terms and Conditions (https://onlinelibrary.wiley.com/terms-and-conditions) on Wiley Online Library for rules of use; OA articles are governed by the applicable Creative Commons License

TABLE 1 (Continued)

ID	Disease group	Age at LP	Sex	5HIAA (nmol/L)	HVA (nmol/L)	HVA/ 5-HIAA	Gene	Mutation	Clinical presentation	Medications at time of lumbar puncture
STXBP1.4	STXBP1	9	M	**70 (87–366)**	344 (202–596	**4,91 (1,5-3,5)**	*STXBP1* NM_001032221	p.(Gly417AlafsX7)	Neurodevelopmental delay. Generalized hypotonia. Postnatal microcephaly. Epileptic encephalopathy. Postnatal microcephaly. Action tremor. Nystagmus. Spastic tetraplegia Behavioral abnormality.	Valproic acid, clonazepam, pregabaline, rufinamide
CDKL5.1	CDKL5	7	F	144 (106–316)	434 (304–658)	3,01 (1,5-3,5)	*CDKL5* NM_001323289	p.(Ser196Trp)	Early onset epileptic encephalopathy.	Levetiracetam, vigabatrine
CDKL5.2	CDKL5	8	F	**65 (87–366)**	267 (158–596)	**4,25 (1,5-3,5)**	*CDKL5* NM_001323289	p.(Gln902Stop)	Early onset epileptic encephalopathy (1st month). Neurodevelopmental delay detected at 5 months. Behavioral abnormalities with autolysis.	Carbamazepine
MECP2.1	MECP2	9	F	176 (87–366)	590 (158–596)	3,35 (1,5-3,5)	*MECP2* NM_004992.4	p.(Glu137Gly)	Rett syndrome. Severe scoliosis and epilepsy	Valproic, levetiracetam
MECP2.2	MECP2	3	F	**117 (170–490)**	493 (344–906)	**4,21 (1,5-3,5)**	*MECP2* NM_004992.4	p.(Cys502Thr)	Rett syndrome. No epileptic activity. Apnea and hyperpnea that are well controlled with topamax.	None
MECP2.3	MECP2	9	F	123 (87–366)	391 (158–596)	3,18 (1,5-3,5)	*MECP2* NM_004992.4	p.(Arg255X)	Rett syndrome. Refractory epilepsy, dysphagia and severe apnea/hyperpnea. Recurrent pneumonia. Died at 11 y.o.	Valproic acid, phenobarbital, clobazam
MECP2.4	MECP2	6	F	242 (87–156)	510 (184–464)	2,11 (1,5-3,5)	*MECP2* NM_004992.4	p.(Lys321GlyfsX6)	Rett syndrome. Drug-responsive epilepsy. No scoliosis. Speech is preserved.	Zonisamide, Ethosuximide, risperidone

(Continues)

15732665, 2024, 3, Downloaded from https://onlinelibrary.wiley.com/doi/10.1002/jimd.12689 by Universitat De Barcelona Biblioteca, Wiley Online Library on [09/01/2025]. See the Terms and Conditions (https://onlinelibrary.wiley.com/terms-and-conditions) on Wiley Online Library for rules of use; OA articles are governed by the applicable Creative Commons License

TABLE 1 (Continued)

ID	Disease group	Age at LP	Sex	5HIAA (nmol/L)	HVA (nmol/L)	HVA/ 5-HIAA	Gene	Mutation	Clinical presentation	Medications at time of lumbar puncture
MECP2.5	MECP2	4	M	162 (106–316)	502 (304–658)	3,10 (1,5-3,5)	*MECP2* NM_004992.4	p.(Arg309Trp)	Male with Rett syndrome (his mother was a carrier for the mutation). Epilepsy with debut at 3 years old. Ocular revulsion with generalized hypertonia and clonus of 4 limbs.	Valproic acid, risperidone, Levomepromazine
MECP2.6	MECP2	6	F	**90 (106–316)**	292 (304–658)	3,24 (1,5-3,5)	*MECP2* NM_004992.4	p.(Arg270X)	Rett syndrome. Spastic tetraparesia with possible mandibular dystonia. Pathologic EEG without clinical crisis. Left scoliosis. Repetitive pneumonias. Died at 17 y.o.	
MECP2.7	MECP2	5	F	210 (87–366)	658 (237–596)	3,13 (1,5-3,5)	*MECP2* NM_004992.4	p.(Arg306Cys)		
MECP2.8	MECP2	16	F	140 (82–140)	336 (156–336)	2,40 (1,5-3,5)	*MECP2* NM_004992.4	p.(Arg294X)		Carbamazepine
MECP2.9	MECP2	11	F	**65 (63–185)**	298 (156–410)	**4,58 (1,5-3,5)**	*MECP2* NM_004992.4	p.(Ser229Leu)	Rett syndrome. Daily crises of facial clonus of the right hemiface lasting up to 10 min. Scoliosis.	Valproic acid, carbamazepine
MECP2.10	MECP2	2	F	**114 (170–490)**	586 (344–906)	**5,14 (1,5-3,5)**	*MECP2* NM_004992.4	p.(Arg255Stop)	Rett syndrome. Epilepsy. Scoliosis.	Valproic acid, clobazam
MECP2.11	MECP2	3	F	**87 (170–490)**	**256 (344–906)**	3,05 (1,5-3,5)	*MECP2* NM_004992.4	p.(Thr158Met)	Rett syndrome. Pharmacorefractory epilepsy with polymorphic seizures, debut at the age of 4 years 11 months, uncontrolled. Mild global developmental delay. Hypovitaminosis D.	None

15732665, 2024, 3, Downloaded from https://onlinelibrary.wiley.com/doi/10.1002/jimd.12689 by Universitat De Barcelona Biblioteca, Wiley Online Library on [09/01/2025]. See the Terms and Conditions (https://onlinelibrary.wiley.com/terms-and-conditions) on Wiley Online Library for rules of use; OA articles are governed by the applicable Creative Commons License

TABLE 1 (Continued)

ID	Disease group	Age at LP	Sex	5HIAA (nmol/L)	HVA (nmol/L)	HVA/ 5-HIAA	Gene	Mutation	Clinical presentation	Medications at time of lumbar puncture
MECP2.12	MECP2	4	F	**103 (106–316)**	428 (304–658)	**4,16 (1,5-3,5)**	*MECP2* NM_004992.4	p.(SerArg_fsTer12)	Rett syndrome. Progressive microcephaly. Developmental regression. Sudden episodic apnea. Stereotypy. Autistic behavior. Global developmental delay. Strabismus. EEG abnormality.	Topiramate

Note: Description of the main clinical and biochemical findings in the patients. Age at LP: age at the time lumbar puncture was taken; Sex: M = male, F = female; 5HIAA = 5-hydroxyindoleacetic acid, HVA = homovanillic acid, HVA/5-HIAA = ration between homovalinic and 5-hydroxyindoleacetic acids measured by HPLC at diagnosis. Control reference values are indicated between brackets. Values in bold represent those outside the control values. Gene = common name and RefSeq accession number of mutated gene.

2.2 | Metabolomics analysis

Samples were sent to the Centre for Omic Sciences (COS) Joint Unit of the Universitat Rovira i Virgili-Eurecat, where a targeted metabolomics analysis was conducted by liquid chromatography with tandem mass spectrometry (LC–MS–MS) for tryptophan related metabolites and acylcarnitines. Gas chromatography–mass spectrometry (GC–MS) was performed for organic acids and sugar metabolites related to energy metabolism and the TCA cycle. A total of 82 metabolites were detected, and the results were presented as micromolar (μM) concentrations.

2.2.1 | LC–MS/MS

CSF (50 μL) samples were diluted in methanol (200 μL, 100%) along with the set of labeled internal and concentration response curve standards (DL-kynurenine, DL-tryptophan, 5-hydroxyindole-3-acetic acid, L-citrulline, 2-picolinic acid, nicotinic acid, kynurenic acid, indole-3-acetic acid (Sigma Aldrich); serotonin hydrochloride, kynurenine-d4 trifluoroacetic acid salt, D-tryptophan-d5, 5-hydroxyindole-3-acetic acid-d2 (5-HIAA-d2), serotonin-d4 hydrochloride, 2-picolinic-d4 acid, nicotinic acid-d4, 3-hydroxyanthranilic acid, 3-hydroxyanthranilic acid-d3, kynurenic acid-d5, indole-2,4,5,6,7-d5-3-acetic-α,α-d2 acid, 3-indolepropionic-d2 acid, n-acetyl-5-hydroxytryptamine (Toronto Research Chemicals); trigonelline hydrochloride (TCI); anthranilic acid (Glentham life sciences); hydrocortisone, androstenedione, testosterone, progesterone (Sigma Aldrich and Toronto Research Chemicals). Following centrifugation (10 min, 15 000 rpm, 4°C), the supernatant was dried in a SpeedVac concentrator and reconstituted in methanol (50 μL, 100%).

The equipment consisted on an UHPLC 1290 Infinity II Series coupled to a QqQ/MS 6490 Series (Agilent Technologies) and a Kinetex 2.6 μm Polar C18, 100 Å, 150 × 2.1 mm (Phenomenex) analytical column. Chromatographic separation was performed in mode negative electrospray ionization (ESI) at 20°C with an injection volume of 1 μL. Mobile phase A was formic acid (0.1%) and mobile phase B was methanol: formic acid (10:1, v/v).

2.2.2 | GC–MS

CSF (50 μL) samples were diluted in water: methanol (200 μL, 8:2, v/v) and the set of labeled internal standards (Succinic-d4 acid, myristic-d27 acid, d-glucose 13C6 and L-Methionine-(carboxy-13C,methyl-d3) [Sigma Aldrich]). Following centrifugation (5 min, 15 000 rpm, 4°C), the supernatants were dried in a SpeedVac concentrator at

15732665, 2024, 3, Downloaded from https://onlinelibrary.wiley.com/doi/10.1002/jimd.12689 by Universitat De Barcelona Biblioteca, Wiley Online Library on [09/01/2025]. See the Terms and Conditions (https://onlinelibrary.wiley.com/terms-and-conditions) on Wiley Online Library for rules of use; OA articles are governed by the applicable Creative Commons License

45°C and reconstituted in methoxyamine (30 μL, 100%). Samples were incubated at 37°C for 90 min and then silylated with 45 μL of MSTFA +1% TMCS at room temperature for 60 min.

The separation was performed on a GC-QTOF 7200 and a HP5-MS UI capillary column (30 m × 250 μm I.D., 0.25 μm film thickness), both from Agilent Technologies. Helium (>99.999%) was used as the carrier gas with a constant flow 1.1 mL/min. Initial oven temperature was set at 60°C, then increased by 10°C/min to 320°C and held constant for 10 min. Samples were injected in split mode 1:20 at injection temperature 250°C. Compounds were detected through MS in electron ionization (70 eV) and full-scan monitoring mode (m/z 50–600) mode with an acquisition rate of 5 spectra/s. Ion source temperature was 250°C and quadrupole temperature was 200°C.

Organic acids were identified and semi-quantified using the spectra library Fiehn-pct-2013 and their pure analytical standards (pyruvic acid, lactic acid, glycolic acid, 3-hydroxybutyric acid, glycerol, succinic acid, glyceric acid, fumaric acid, malic acid, d-threitol, threonic acid, α-ketoglutaric acid, arabitol, glycerol-1-phosphate, 3-phosphoglyceric acid, citric acid, d-mannitol, myo-inositol, glucose-6-phosphate, d-sucrose and α-tocopherol [Sigma Aldrich]).

2.3 | Statistical analysis

The goal of the analysis was to compare the metabolic profiles of patients to those of healthy controls. All statistical tests were conducted in R version 4.3.0. Metabolic profiles of patients were compared to those of health controls, either all together or categorized on the glutamatergic behavior of the disease (hypoglutamatergic diseases vs. hyperglutamatergic + GABAergic).

The metabolite concentrations were log2-transformed in order to account for the expected high variability and noise found in metabolomics data. The statistical methods chosen for this study have been recently applied in several studies dealing with metabolomics and lipidomics data.[14–17]

Multivariate statistical methods were applied on the transformed data in order to account for the small sample size and the inherent multicollinearity of the data. Unsupervised principal component analysis (PCA) was performed in order to obtain an overall view of the variation between samples and their separation into clusters. Ward hierarchical clustering with Euclidian distance combined with a heatmap (pheatmap version 1.0.12) was used to compare the log-transformed concentrations of all the analyzed metabolites in patients and controls. The supervised classification model orthogonal partial least-squares discriminant analysis (OPLS-DA) from the ropls package (version 1.32.0) was used to identify metabolites responsible for group separation. This method has the advantage that it removes sources of variation unrelated to group labels, so it is particularly useful when dealing with heterogeneous data like metabolite concentrations.[18] The models were evaluated by goodness of fit (R2Y), goodness of prediction (Q2Y), and the root mean square error of estimation (RMSEE). 7-fold cross-validation was performed to mitigate the risk of overfitting caused by the high dimensionality of the data. Metabolites were selected based on their variable importance in projection (VIP) scores (VIP >1). Permutation testing ($n = 1000$) was used to determine the statistical significance of the results ($p < 0.05$).

Univariate statistical analysis was carried out by performing Wilcoxon Mann–Whitney U tests to find differences in individual metabolite concentrations between patients and controls. The non-parametric test was chosen because the small sample size not contain enough information to determine whether its underlying distribution was Gaussian. Correction for the false discovery rate (FDR) was applied in order to account for the issue of multiple testing ($p < 0.05$).

Pathway analysis was performed for metabolites with $p < 0.05$ or VIP score >1 using the Kyoto Encyclopedia of Genes and Genomes (KEGG) database and the KEGGREST package (version 1.40.0). Pathways were identified as important when two or more of their metabolite components were found to be altered between the disease groups and the healthy controls. The results were plotted after excluding pathways that are ubiquitous or unrelated to synaptic metabolism. Special attention was given to the tryptophan metabolism pathway, as well as to the amino acid substrates of Large Neutral Amino Acid Transporter (LAT1).

2.4 | Western blot

Proteins were extracted from brain tissue through a 30′ cold incubation with RIPA buffer and protease inhibitors. After extraction and protein quantification, equivalent solubilized amounts (10 μg) were mixed with Laemmli Buffer in reductive denaturing conditions, subjected to SDS-PAGE and transferred to a nitrocellulose membrane. Membranes were blocked with TBS-Tween (0.05%): milk 5% for 1 h at room temperature. Primary antibodies were incubated overnight at 4°C in blocking buffer, at the following concentrations: SLC7A5 (1:2000, 28 670, Proteintech). Tubulin (1:50 000, ab7291, Abcam) was used as a loading control. The secondary antibodies used were HRP-conjugated goat anti-Rabbit and goat anti-Mouse IgG antibodies (Thermo Fisher) and were detected using

15732665, 2024, 3, Downloaded from https://onlinelibrary.wiley.com/doi/10.1002/jimd.12689 by Universitat De Barcelona Biblioteca, Wiley Online Library on [09/01/2025]. See the Terms and Conditions (https://onlinelibrary.wiley.com/terms-and-conditions) on Wiley Online Library for rules of use; OA articles are governed by the applicable Creative Commons License

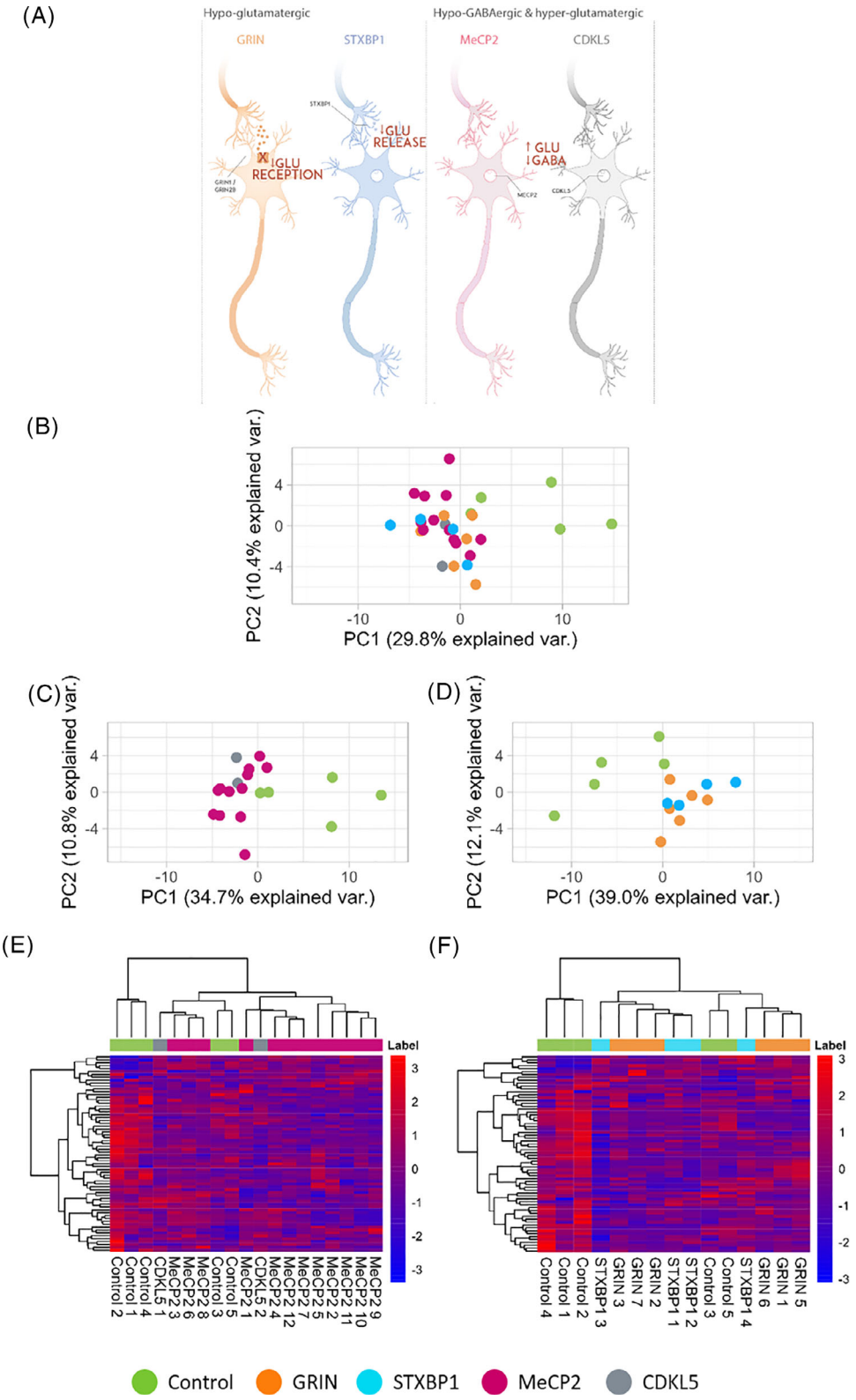

FIGURE 1 Unsupervised multivariate analysis of patient and control CSF metabolite concentrations. (A) Glutamatergic neurotransmission alterations in disease cohorts. Rett syndrome (MeCP2) and CDKL5-epileptic encephalopathy (CDKL5) were classified as hyperglutamatergic disorders, while GRIN-related pediatric encephalopathy (GRIN) and syntaxin encephalopathy (STXBP1) were classified as hypoglutamatergic disorders (B–F). Unsupervised multivariate analysis of patient and control CSF metabolite concentrations. PCA score plots showing the separation of patients from controls on the first two principal components. (B) Patients do not form distinct groups based on pathology or hyper/hypoglutamatergic alterations. Control samples are highly varied, although the majority separate from the patients. (C) Hyperglutamatergic patients. (D) Hypoglutamatergic patients. Ward hierarchical clustering showing log-transformed metabolite concentrations. Both (E) hyperglutamatergic and (F) hypoglutamatergic patients form homogeneous groups regardless of genotype. There is some overlap with controls, but mostly patients cluster together and have a markedly decreased concentration of most metabolites.

the PierceTM ECL Western Blotting substrate (Thermo Fisher). Quantification of protein expression was performed using Fiji software.

Both B6.129P2(C)-*Mecp2*$^{tm1.1Bird}$/J and control littermates mice (Jackson laboratory) were used. To increase the translational value of the work, only

15732665, 2024, 3, Downloaded from https://onlinelibrary.wiley.com/doi/10.1002/jimd.12689 by Universitat De Barcelona Biblioteca, Wiley Online Library on [09/01/2025]. See the Terms and Conditions (https://onlinelibrary.wiley.com/terms-and-conditions) on Wiley Online Library for rules of use; OA articles are governed by the applicable Creative Commons License

female mice have been used, as they have been reported to better recapitulate the disease phenotype. Mice were housed in standard cages with ad libitum access to food and water and in controlled environmental conditions of light (12 h dark/light cycle starting at 7:30 a.m.), temperature (22°C) and

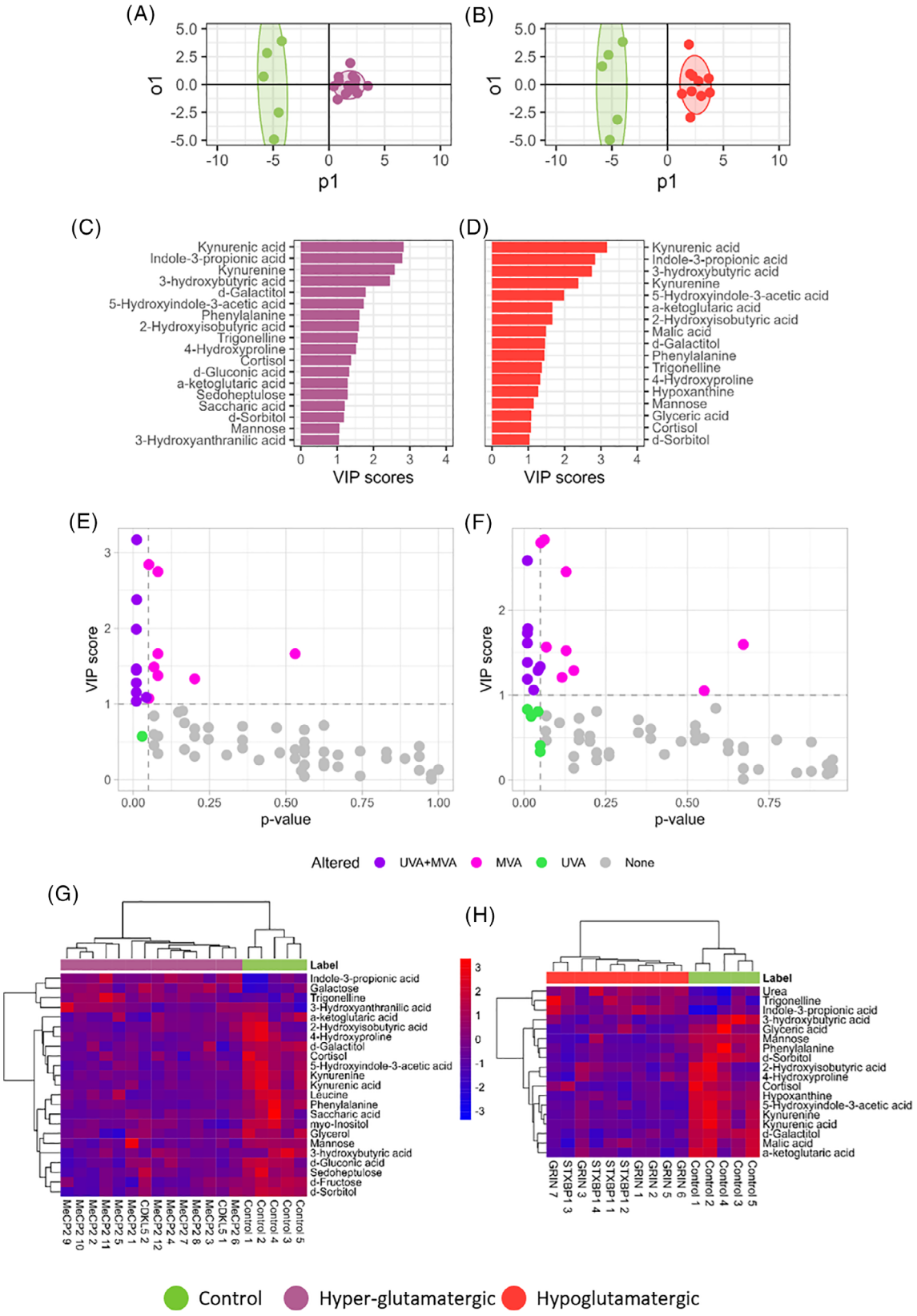

FIGURE 2 Legend on next page.

15732665, 2024, 3, Downloaded from https://onlinelibrary.wiley.com/doi/10.1002/jimd.12689 by Universitat De Barcelona Biblioteca, Wiley Online Library on [09/01/2025]. See the Terms and Conditions (https://onlinelibrary.wiley.com/terms-and-conditions) on Wiley Online Library for rules of use; OA articles are governed by the applicable Creative Commons License

humidity (60%). Mice were genotyped following the provider recommendations.

3 | RESULTS

Cerebrospinal fluid (CSF) samples were collected from 29 individuals with four different diseases related to glutamatergic neurotransmission (Figure 1A):

- Monogenic diseases which pathophysiology includes an increased glutamatergic neurotransmission: 12 patients with Rett syndrome (bearing mutations in *MECP2*) and 2 with mutations in *CDKL5*.[19]
- Monogenic disorders characterized by hypoglutamatergic function: A total of 10 patients, 6 GRIN patients with mutations functionally annotated as loss-of-function[1] and 4 STXP1 patients. GRIN patients bore mutations in either *GRIN1* or *GRIN2B*, that encode GluN1 and GluN2B subunit of NMDA receptors respectively, and LoF mutations in result in reduced transmission in response to glutamate activation,[20] leading to a neurodevelopmental disorder characterized by developmental delay, intellectual disability and epilepsy.[1,21] On the other hand, STXBP1 participates in the regulation of synaptic vesicle docking and fusion in the presynaptic terminal, and mutations affecting their expression have been associated with a globally reduced glutamatergic neurotransmission.[22,23]
- We have included 5 age-matched controls obtained from children who were visited in the emergency department of our hospital and underwent a lumbar puncture for a clinical suspicion of meningitis/encephalitis being finally this hypothesis not confirmed due to a CSF study negative for microbiology tests and with a normal cytology and biochemistry.

All patients and controls were within pediatric age, ranging from 0 to 15 years old. Patients and controls from both genders were included, though the majority were female because of the higher prevalence of Rett on girls. Summary of mutations and clinical characteristics has been summarized in Table 1.

All CSF samples were subjected to a semi-targeted metabolomic analysis, through which we measured the concentrations of metabolites related with energy and amino acid metabolism, with a special coverage of tryptophan and tyrosine metabolism, to deepen into the relationship between glutamatergic alterations and other neurotransmitters (monoamines) metabolism. The total concentration of metabolites detected was similar among all samples, giving confidence in the results and in the differences observed in each population. The analysis identified a total of 68 metabolites (Supplementary Table 1). Dimensionality reduction through PCA revealed that, despite some crossovers, patients from both groups were more similar to each other than to the controls, as they assembled in two different clusters (Figure 1B). This profile was maintained after separating Rett and *CDKL5* patients from hypoglutamatergic patients (Figure 1C,D), where again, both CDKL5 and MeCP2 patients, as well as STXBP1 and GRIN patients were more similar to each other than to controls. Hierarchical clustering with Ward's method criterion, a clustering algorithm that finds groups with the least internal variance, was performed using all the analyzed metabolites. This revealed that both groups had a similar underlying structure, with two main clusters containing metabolic alterations, that are consistent across these different pathologies.

In order to overcome the overlapping of controls and patients and to prioritize clinically relevant metabolic differences we performed feature selection through the supervised method OPLS-DA. This technique efficiently differentiated patients from controls in both scenarios (hyperglutamatergic and hypoglutamatergic samples)

FIGURE 2 Identification of significantly altered metabolites and their impact on group classification (A and B) OPLS-DA score plots showing separations of controls compared to (A) hyperglutamatergic and (B) hypoglutamatergic patients. Both OPLS-DA models showed good separation between the groups (R2Y (cum) > 0.9, Q2Y (cum) > 0.8, RMSEE <0.2), and both were statistically significant after permutation testing. C-D) VIP scores. Both diseases show similar metabolic alterations. (C) hyperglutamatergic patients had 18 metabolites with a Variable Importance in Projection (VIP) score >1 (D) hypoglutamatergic patients had 17. The highest VIP scores in both cases belonged to tryptophan metabolites. (E and F) Integrated results of UVA and MVA analysis. (E) hyperglutamatergic patients (F) hypoglutamatergic patients. For both groups there was a small number of metabolites identified as altered by both univariate and multivariate analyses. Both diseases showed similar metabolic alterations, though hyperglutamatergic (C) had a higher number of significantly altered metabolites. Interestingly, the hyperglutamatergic cohort showed significant alterations in metabolites that did not contribute to the performance of the OPLS-DA model. (G and H) Hierarchical clustering using only the selected metabolites showed perfect separation between patients and controls for both groups. (G) Hyperglutamatergic patients had increased concentrations of indole-3-propionic acid, galactose, and trigonelline, while (H) hypoglutamatergic patients had increased concentrations of urea, trigonelline, and indole-3-propionic acid. but the rest of the altered metabolites all had decreased concentrations in patient cohorts.

15732665, 2024, 3, Downloaded from https://onlinelibrary.wiley.com/doi/10.1002/jimd.12689 by Universitat De Barcelona Biblioteca, Wiley Online Library on [09/01/2025]. See the Terms and Conditions (https://onlinelibrary.wiley.com/terms-and-conditions) on Wiley Online Library for rules of use; OA articles are governed by the applicable Creative Commons License

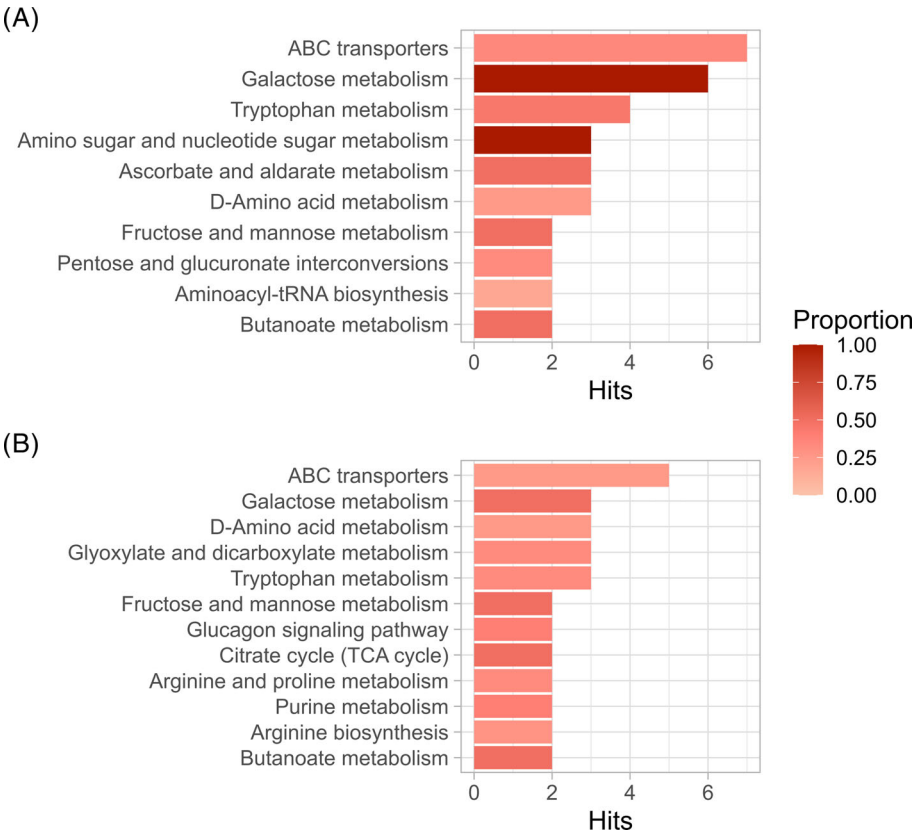

FIGURE 3 Pathways affected by selected metabolites. Selected metabolites were converted to their KEGG compound IDs and mapped to their corresponding pathways. Only human pathways were taken into account, and pathways unrelated to the nervous system were filtered out. ABC transporters, galactose metabolism, tryptophan metabolism, and amino sugar and nucleotide sugar metabolism had the highest numbers of altered metabolites for both (A) hyperglutamatergic, and (B) hypoglutamatergic patients.

(Figure 2A,B). The models showed a strong ability to discriminate between classes (R2Y = 0.939 and 0.960 for hyper and hypoglutamatergic respectively), and a prediction accuracy ≥0.8 (Q2Y = 0.816 and 0.866) after permutation ($n = 1000$).

The models identified possible shared metabolic pathways that contribute to their pathophysiology. Multivariate feature selection identified 18 influential metabolites for Rett patients and 17 for hypoglutamatergic disorders (Figure 2C,D; Supplementary Table 2). Univariate hypothesis testing found 17 significantly altered metabolites in hyperglutamatergic and 7 in hypoglutamatergic disorders. There were 10 metabolites in the first and 7 in hypoglutamatergic disorders that were selected by both methods (Figure 2E,F). Integrating the results of multivariate and univariate analysis, and performing hierarchical clustering including metabolites that had a $p < 0.5$ level or VIP score >1 resulted in separation of patients and controls (Figure 2G,H).

To determine which pathways were most impacted by the alterations in metabolite concentrations, we assessed KEGG pathway over-representation for metabolites that had a $p < 0.05$ level or VIP score >1. The most affected pathways were related to amino acid metabolism and transport, including tryptophan and its metabolites. (Figure 3).

In humans, tryptophan (Trp) metabolism occurs through two different pathways: the kynurenine pathway, through which Trp is degraded into kynurenic acid and 2-picolinic acid, and the serotonin pathway, converting Trp into 5-HT for final production of serotonin, metabolized into 5-hydroxyindoleacetic acid (5-HIAA) (Figure 4A). Several of these metabolites were found to be decreased in patients, although tryptophan itself was not. As shown in Figure 4B, even though there were no statistically significant differences in the concentration of tryptophan, we detected a tendency to decrease in the concentration of metabolites of both pathways. Samples from both disease groups showed a decrease in both kynurenine (hyperglutamatergic: 0.036 μM, hypoglutamatergic: 0.036 μM, controls: 0.172 μM; median values) and kynurenic acid (hyperglutamatergic: 0.004 μM, hypoglutamatergic: 0.003 μM, controls: 0.021 μM; median values), though only the hyperglutamatergic decrease in kynurenine was statistically significant. Moreover, both groups had significantly decreased concentrations of 5-hydroxy-3-indoleacetic acid (hyperglutamatergic: 0.215 μM, hypoglutamatergic: 0.183 μM controls: 0.562 μM; median values). Fifteen out of the 24 patients (62.5%) had reduced concentration of 5-HIAA in CSF (Table 1), measured by high-performance liquid chromatography with electrochemical detection and compared with age-matched reference values established by our laboratory (342 samples collected over the past 15 years). On top of

15732665, 2024, 3, Downloaded from https://onlinelibrary.wiley.com/doi/10.1002/jimd.12689 by Universitat De Barcelona Biblioteca, Wiley Online Library on [09/01/2025]. See the Terms and Conditions (https://onlinelibrary.wiley.com/terms-and-conditions) on Wiley Online Library for rules of use; OA articles are governed by the applicable Creative Commons License

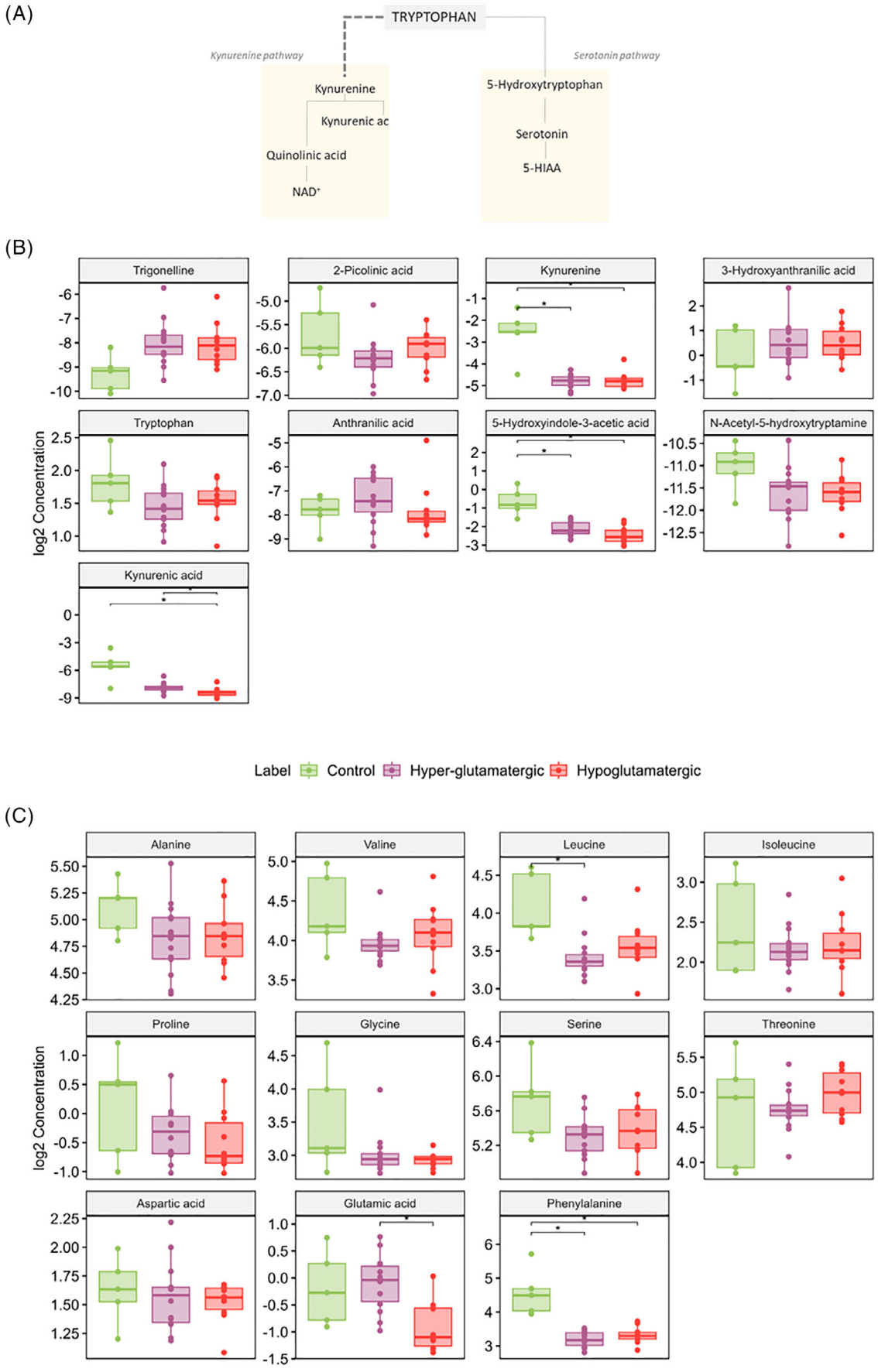

FIGURE 4 Legend on next page.

15732665, 2024, 3, Downloaded from https://onlinelibrary.wiley.com/doi/10.1002/jimd.12689 by Universitat De Barcelona Biblioteca, Wiley Online Library on [09/01/2025]. See the Terms and Conditions (https://onlinelibrary.wiley.com/terms-and-conditions) on Wiley Online Library for rules of use; OA articles are governed by the applicable Creative Commons License

that, other amino acids alterations such as significant decreases in the concentration of phenylalanine or leucine were detected as well (Figure 4C). There was no correlation between the decrease in metabolites concentration in CSF and any drugs the patients were taking at the moment, nor their age or sex (Supplementary Figures 1 and 2).

Tryptophan is preferentially transported across the blood–brain barrier through a facilitative Na^+-independent transporter named LAT1 (system L Amino Acid transporter), coded by the *SLC7A5* gene. This transporter also imports other amino acids as valine, leucine, isoleucine, or threonine into the brain. Interestingly, both valine and leucine were also reduced in the patients CSF (Val: hyperglutamatergic: 14.6 μM, hypoglutamatergic: 15.1 μM, controls: 20.3 μM; Leu: hyperglutamatergic: 10.2 μM, hypoglutamatergic: 10.6 μM, controls: 16.9 μM; median values). In contrast, all patients showed isoleucine and threonine concentration values within a control-range (Ile: hyperglutamatergic: 4.4 μM, hypoglutamatergic: 4.4 μM, controls: 4.7 μM; Thr: hyperglutamatergic: 26.7 μM, hypoglutamatergic: 32.2 μM, controls: 30.4 μM; median values) (Figure 5A).

Considering these amino acids shared the transport system, we investigated its expression in a model of Rett syndrome, the B6.129P2(C)-*Mecp2*$^{tm1.1Bird}$/J female mice. Remarkably, brain samples from Rett female mice showed a significant decrease in the expression of LAT1, compared to littermate controls (Figure 5B,C). This was observed already at a pre-symptomatic stage (3 months old mice), pointing toward a potential involvement of amino acid brain transport and metabolism in the evolution and pathophysiology of Rett syndrome.

4 | DISCUSSION

Defective glutamatergic neurotransmission is one of the main features outstanding in the pathophysiology of many genetic neurodevelopmental diseases. Yet, other elements contribute to the landscape such as inflammation,[24–27] neuronal and glia[28–30] maturation or metabolism and neuroimmunometabolism.[31–33] Specifically, metabolic alterations are known to play key roles in the pathophysiology of neurodevelopmental diseases, and they have been explored in several non-metabolic diseases, such as Rett syndrome,[31,34] autism spectrum disorders or epileptic encephalopathies.[31] The study of metabolism in neurodevelopmental pathologies will favor not only the advance in the knowledge of these diseases, but also the identification of biomarkers and new therapeutic targets.

In our work we have studied the neurometabolic component of four neurodevelopmental diseases in which the main described element of their pathophysiology is an altered glutamatergic neurotransmission. For that, we have analyzed cerebrospinal fluid 29 samples from patients and controls distributed in three different groups: (a) patients with conditions associated to *increased* glutamatergic activity (mutations in *MECP2*[35] and *CDKL5*[36]), (b) patients with encephalopathies associated to hypoglutamatergic activity (with mutations in *STXBP1*[22] and the *GRIN*[20] genes) and (c) controls. Rett syndrome and related disorders have shown vast evidence of altered glutamatergic neurotransmission, including higher levels of glutamate and a reduced expression of metabotropic glutamate receptors 5 and 7 (mGlu5, mGlu7),[37,38] alterations in NMDA receptors expression or elevated glutamate release.[39] These alterations occur along with a clear involvement of the GABAergic system, that contributes to a shift in the excitatory/inhibitory balance.[2] On the other hand, mutations in *STXBP1* and *GRIN* genes result in a reduced release and reception of glutamate respectively.

While analyzing these alterations in CSF can suppose a limitation to the study, especially due to the difficulty of obtaining samples from controls, it allows us to understand more accurately what is occurring in the patients brains during the course of the disease.[6,8,40] Regarding their metabolomic profile, and despite some overlapping between patients and controls when all metabolites were taken into account, patients clustered together regardless

FIGURE 4 Alterations in amino acid metabolism. Boxplots show medians and interquantile ranges, with significance expressed as $^*p < 0.05$ after FDR correction. (A) Summary of tryptophan metabolism pathways. (B) Alterations in tryptophan metabolism. Of the metabolites involved in tryptophan metabolism that were analyzed, only 5-hydroxyindole-3-acetic acid and kynurenine were significantly decreased in both disease groups, while kynurenic acid was significantly decreased in hypoglutamatergic patients and non-significantly decreased in hyperglutamatergic patients. Tryptophan and N-acetyl-5-hydroxytryptamine showed a slight decrease that was not statistically significant in both hyperglutamatergic and hypoglutamatergic patients, while trigonelline was non-significantly increased in both groups. Interestingly, kynurenic acid was also significantly decreased in hypoglutamatergic patients compared to hyperglutamatergic patients. (C) Alterations in other amino acids. Phenylalanine was significantly decreased in both patient cohorts, while leucine was significantly decreased in hyperglutamatergic patients. Additionally, several amino acids (glycine, serine, isoleucine, and valine) were non-significantly decreased in both patient groups. It is noteworthy that glutamate was found to be significantly decreased only in hypoglutamatergic patients compared to hyperglutamatergic patients, but not between either patient group and controls.

15732665, 2024, 3, Downloaded from https://onlinelibrary.wiley.com/doi/10.1002/jimd.12689 by Universitat De Barcelona Biblioteca, Wiley Online Library on [09/01/2025]. See the Terms and Conditions (https://onlinelibrary.wiley.com/terms-and-conditions) on Wiley Online Library for rules of use; OA articles are governed by the applicable Creative Commons License

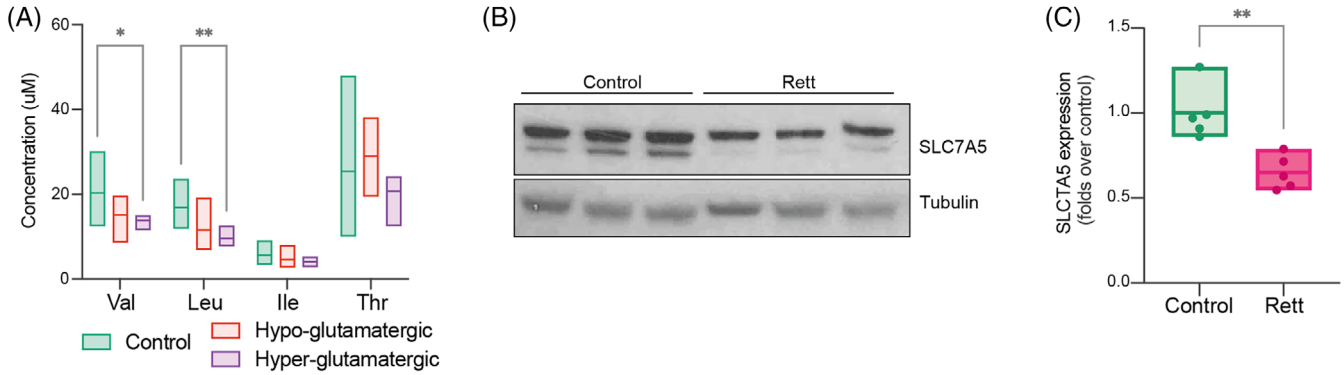

FIGURE 5 Tryptophan and BCAAs transport across the blood–brain barrier. (A) Alterations in LNAAs in CSF samples: Valine and leucine were decreased in patients compared to controls (statistically significant for hyperglutamatergic samples), while both groups had non-significantly altered levels of isoleucine and threonine. (B and C) Analysis of the expression of *SLC7A5* (LAT1) in brain samples from Rett mouse models. Three different brain samples were analyzed for each group (Rett and controls) in two independent experiments. (B) Representative blot of the expression of SLC7A5 is shown, where tubulin has been used as a loading control. (C) Quantification with ImageJ of all the experiments; ***p*-value <0.001.

of their mutation, pointing toward shared metabolic alterations underlying in the pathophysiology of glutamate-involved neurodevelopmental diseases.

Integration of multivariate and univariate analysis identified 25 metabolites in Rett + *CDKL5* and 17 in hypoglutamatergic disorders that were contributing to their pathophysiology. Pathway analysis of our data showed that the metabolic routes differing between patients and controls were mostly involved in amino acid and energy metabolism. As mentioned, one of the metabolic routes in which we have found alterations common to all diseases studied is tryptophan metabolism. Tryptophan is an essential amino acid and the precursor of several neuroactive compounds. The majority of tryptophan is catabolized through the kynurenine pathway, and on a lower rate, through the serotonin pathway, by which the neurotransmitter serotonin is synthesized.[41] We have found a decrease in the concentration of different metabolites in both metabolic branches, as samples from all disease groups showed a reduction in both kynurenine and kynurenic acid concentrations, together with lowered concentrations of 5-hydroxy-3-indoleacetic acid. The decrease in 5-HIAA was confirmed by HPLC in 62.5% of the samples. Noteworthy, we have not observed a decrease in tryptophan itself. The dependency of Trp concentration and other factors such as diet shall be explored in the future.

Similar decreases in peripheral tryptophan metabolism had been previously described in plasma of Rett syndrome patients[34] and animal models.[42] Likewise, alterations in tryptophan metabolism had been previously reported in developmental and epileptic encephalopathy patients, in which abnormal concentration of neurotransmitter was identified in 33% of the samples, being 5-HIAA deficit was the most prevalent alteration (91%).[43] It has also being studied in other diseases with unclear genetic etiology as diverse as migraine, schizophrenia, suicidality or autism spectrum disorders.[44–47]

On the other side, although not neurotransmitter-producing, the kynurenine pathway plays essential roles in cell function: it has a key function in energy metabolism by regulation of the coenzyme nicotinamide adenine dinucleotide (NAD+)[48] and has been implicated in the process of inflammation,[49,50] along with the neuroprotective role of kynurenic acid, an intermediate metabolite of the kynurenine pathway that acts as an antagonist to the N-methyl-D-aspartate receptors (NMDARs). Further studies in patients and animal models shall expand the knowledge of this downregulation and its direct relationship with glutamatergic neurotransmission, elucidating whether it is a cause of consequence of the pathology.[51] Aligned with that, it shall be explored whether the generalized tryptophan metabolism reduction is related with a reduced tryptophan brain availability due to increased peripheral kynurenine metabolism, associated with pro-inflammatory conditions.[52]

Alterations in tryptophan metabolism are often associated with alterations in other amino acids.[34] These are essential players in brain function and development: besides protein synthesis, they act as neuromodulators and are the biosynthetic precursors of various neurotransmitters. Primary dysregulation of amino acid metabolism results in neurodevelopmental pathologies that exemplify their importance in the function of the developing brain. Such is the case of aromatic L-amino acid decarboxylase (AADC) deficiency, in which both tyrosine and tryptophan metabolism is impaired,[53,54] or BCAAs metabolism that can lead to maple syrup urine disease

15732665, 2024, 3, Downloaded from https://onlinelibrary.wiley.com/doi/10.1002/jimd.12689 by Universitat De Barcelona Biblioteca, Wiley Online Library on [09/01/2025]. See the Terms and Conditions (https://onlinelibrary.wiley.com/terms-and-conditions) on Wiley Online Library for rules of use; OA articles are governed by the applicable Creative Commons License

(MSUD)[55] or to a treatable form of autism.[56] On top of that, previous work on the study of metabolic alterations in neurodevelopmental diseases has focused on pathways as energy metabolism, redox homeostasis or lipid metabolism, leaving the role of amino acids metabolism in non-metabolic diseases understudied. Given the importance of amino acids in the regulation of development and neurotransmission it is of great interest to study these pathways in pathologies whose main pathophysiological elements are not amino acid metabolism itself.

Specific analysis of the concentration of large neutral amino acids in our samples has revealed a generalized decrease in both disease groups, highlighting the decrease in leucine and phenylalanine. These are transported into the brain through the large neutral amino acids transporter (LAT1, coded by the *SLC7A5* gene), responsible for the transport tryptophan and other amino acids such as BCAAs or threonine. Besides amino acids transport, LAT1 has been reported to regulate Kv1.2 potassium channels,[57] modifying the functional outcomes of epilepsy-linked channelopathies.[58] On top of that, mutations *SLC7A5* (together with other variants in genes encoding for large amino acid transporters) increase the risk of autism spectrum disorder[59,60] and is essential for perinatal neuronal excitability[61] and survival and granule cell development through mTOR regulation.[62] We have analyzed the transporter expression in brain tissue from a mouse model of Rett syndrome, noticing a decrease that was already detectable at pre-symptomatic stages. This is the first report to our knowledge of a reduced expression of this transporter in Rett syndrome. Further studies shall investigate the relationship between this finding and the decreased expression of other transporters and the blood–brain barrier integrity,[63] with the potential implications in brain metabolism.

Studying neurodevelopmental and neurotransmitter-related diseases under the metabolic prism advances on their knowledge from a transversal view, favoring the identification of biomarkers and shared pathophysiological features that can be addressed as new therapeutic targets. Our work highlights the importance of metabolism in the pathophysiology of diseases related to glutamatergic neurotransmission, focusing on tryptophan metabolism, giving clues to better understand the vulnerability of serotonin in neuropediatric pathologies. It also reinforces the role of branched chain amino acids, which are crucial in energy metabolism, signaling and glutamate homeostasis among others. The study in CSF allows us to understand more faithfully the metabolism of the developing brain, and will benefit from future work in extended series of patients. These results propose new questions that will mark future lines of work, such as their implication in other neurodevelopmental pathologies and the study of how these alterations can be used for therapeutic purposes.

AUTHOR CONTRIBUTIONS

Sofía Illescas: Performed the data analysis and interpretation; manuscript drafting. **Yaiza Diaz-Osorio**: Data analysis; samples preparation and interpretation; manuscript drafting. **Anna Serradell**: Western blot experiments; manuscript drafting. **Lucía Toro-Soria**: Western blot experiments; manuscript drafting. **Uliana Musokhranova**: Samples preparation and interpretation; manuscript drafting. **Natalia Julià-Palacios**: Clinical care and assessment of the patients; manuscript drafting. **Juliana Ribeiro-Constante**: Clinical care and assessment of the patients; manuscript drafting. **Xavier Altafaj**: Evaluation of the impact of GRIN mutations; manuscript drafting. **Mireia Olivella**: Evaluation of the impact of GRIN mutations; manuscript drafting. **Mar O'Callaghan**: Clinical care and assessment of the patients; manuscript drafting. **Alejandra Darling**: Clinical care and assessment of the patients; manuscript drafting. **Judith Armstrong**: Genetic diagnosis of the patients; manuscript drafting. **Rafael Artuch**: Biochemical analysis in CSF; manuscript drafting. **Àngels García-Cazorla**: Study conceptualization, patients clinical care and assessment; manuscript writing. **Alfonso Oyarzábal**: Study conceptualization, data interpretation, manuscript writing.

ACKNOWLEDGEMENTS

The authors want to express their gratitude to patients and their families for their participation and support for this study. We also thank the patient associations Mi Princesa Rett, Rettando al Síndrome de Rett and Asociación Española Grinpatías. We thank FEDER (Federación Española de Enfermedades Raras) for their Support and funding. The authors wish to acknowledge Hospital Sant Joan de Déu Biobanc for their support and technical assistance.

FUNDING INFORMATION

This work has been funded with a FI21/0073 and "Instituto de Salud Carlos III (ISCIII)" and "Fondo Europeo de desarrollo regional (FEDER)" grant, both awarded to Àngels García-Cazorla. Xavier Altafaj and Mireia Olivella were supported by ISCIII, co-funded by European Regional Development Fund (ERDF), a way to build Europe (grants PI19/00348 and PI22/00525).

CONFLICT OF INTEREST STATEMENT

Àngels García-Cazorla has received honoraria for research support and lectures from PTC Therapeutics, Immedica and Nutricia, honoraria for lectures from

15732665, 2024, 3, Downloaded from https://onlinelibrary.wiley.com/doi/10.1002/jimd.12689 by Universitat De Barcelona Biblioteca, Wiley Online Library on [09/01/2025]. See the Terms and Conditions (https://onlinelibrary.wiley.com/terms-and-conditions) on Wiley Online Library for rules of use; OA articles are governed by the applicable Creative Commons License

Biomarin and Recordati Rare Diseases Foundation, and is a co-founder of the Hospital Sant Joan de Déu start-up "Neuroprotect Life Sciences." Alfonso Oyarzábal is a co-founder of the Hospital Sant Joan de Déu start-up "Neuroprotect Life Sciences." The content of the article has not been influenced by the sponsors.

DATA AVAILABILITY STATEMENT

Metabolomic raw data will be shared after publication.

AUTHORS WHO SERVE AS GUARANTOR FOR THE ARTICLE

Alfonso Oyarzabal and Àngels García-Cazorla.

ETHICS STATEMENT

All parents or legal representatives of the patients gave written informed consent. This study was approved by the local institutional ethics committee (Sant Juan de Déu Hospital ID number: PIC-131-18). All research work has been carried away following the principles under the Helsinki declaration. No vertebrate animals have been sacrificed ad hoc for this study. However, mouse brain protein samples, surpluses from other projects, have been used. Such extraction was made under approval from Committee for Animal Experimentation of Universitat de Barcelona.

REFERENCES

1. García-Recio A, Santos-Gómez A, Soto D, et al. GRIN database: a unified and manually curated repertoire of GRIN variants. *Hum Mutat*. 2021;42(1):8-18. doi:10.1002/humu.24141
2. Ure K, Lu H, Wang W, et al. Restoration of Mecp2 expression in GABAergic neurons is sufficient to rescue multiple disease features in a mouse model of Rett syndrome. *Elife*. 2016;5:e14198. doi:10.7554/elife.14198
3. Koopmans F, van Nierop P, Andres-Alonso M, et al. SynGO: an evidence-based, expert-curated knowledge base for the synapse. *Neuron*. 2019;103(2):217-234.e4. doi:10.1016/j.neuron.2019.05.002
4. Tebani A, Afonso C, Marret S, Bekri S. Omics-based strategies in precision medicine: toward a paradigm shift in inborn errors of metabolism investigations. *Int J Mol Sci*. 2016;17(9):1555. doi:10.3390/ijms17091555
5. Heywood WE, Galimberti D, Bliss E, et al. Identification of novel CSF biomarkers for neurodegeneration and their validation by a high-throughput multiplexed targeted proteomic assay. *Mol Neurodegener*. 2015;10:64. doi:10.1186/s13024-015-0059-y
6. Wang T, Li C, Ma Y, et al. Metabolomics of cerebrospinal fluid reveals prognostic biomarkers in pediatric status epilepticus. *CNS Neurosci Ther*. 2023;1-10. doi:10.1111/cns.14312
7. Peters TMA, Merx J, Kooijman PC, et al. Novel cerebrospinal fluid biomarkers of glucose transporter type 1 deficiency syndrome: implications beyond the brain's energy deficit. *J Inherit Metab Dis*. 2023;46(1):66-75. doi:10.1002/jimd.12554
8. Peters TMA, Engelke UFH, de Boer S, et al. Confirmation of neurometabolic diagnoses using age-dependent cerebrospinal fluid metabolomic profiles. *J Inherit Metab Dis*. 2020;43(5):1112-1120. doi:10.1002/jimd.12253
9. Jacob M, Lopata AL, Dasouki M, Abdel Rahman AM. Metabolomics toward personalized medicine. *Mass Spectrom Rev*. 2019;38(3):221-238. doi:10.1002/mas.21548
10. Karczewski KJ, Snyder MP. Integrative omics for health and disease. *Nat Rev Genet*. 2018;19(5):299-310. doi:10.1038/nrg.2018.4
11. Batllori M, Molero-Luis M, Ormazabal A, et al. Cerebrospinal fluid monoamines, pterins, and folate in patients with mitochondrial diseases: systematic review and hospital experience. *J Inherit Metab Dis*. 2018;41(6):1147-1158. doi:10.1007/s10545-018-0224-x
12. Cortès-Saladelafont E, Molero-Luis M, Cuadras D, et al. Gamma-aminobutyric acid levels in cerebrospinal fluid in neuropaediatric disorders. *Dev Med Child Neurol*. 2018;60(8):780-792. doi:10.1111/dmcn.13746
13. Ormazabal A, García-Cazorla A, Fernández Y, Fernández-Alvarez E, Campistol J, Artuch R. HPLC with electrochemical and fluorescence detection procedures for the diagnosis of inborn errors of biogenic amines and pterins. *J Neurosci Methods*. 2005;142(1):153-158. doi:10.1016/j.jneumeth.2004.08.007
14. Chen C, Luo F, Wu P, et al. Metabolomics reveals metabolite changes of patients with pulmonary arterial hypertension in China. *J Cell Mol Med*. 2020;24(4):2484-2496. doi:10.1111/jcmm.14937
15. Wang H, Li S, Wang C, Wang Y, Fang J, Liu K. Plasma and vitreous metabolomics profiling of proliferative diabetic retinopathy. *Invest Ophthalmol Vis Sci*. 2022;63(2):17. doi:10.1167/iovs.63.2.17
16. Zandl-Lang M, Züllig T, Trötzmüller M, et al. Changes in the cerebrospinal fluid and plasma lipidome in patients with Rett syndrome. *Metabolites*. 2022;12(4):291. doi:10.3390/metabo12040291
17. Zhang X, Li N, Cui Y, et al. Plasma metabolomics analyses highlight the multifaceted effects of noise exposure and the diagnostic power of dysregulated metabolites for noise-induced hearing loss in steel workers. *Front Mol Biosci*. 2022;9:907832. doi:10.3389/fmolb.2022.907832
18. Trygg J, Wold S. Orthogonal projections to latent structures (O-PLS). *J Chemometr*. 2002;16(3):119-128. doi:10.1002/cem.695
19. Li W. Excitation and inhibition imbalance in Rett syndrome. *Front Neurosci*. 2022;16:825063. doi:10.3389/fnins.2022.825063
20. Sabo SL, Lahr JM, Offer M, Weekes ALA, Sceniak MP. GRIN2B-related neurodevelopmental disorder: current understanding of pathophysiological mechanisms. *Front Synaptic Neurosci*. 2022;14:1090865. doi:10.3389/fnsyn.2022.1090865
21. Platzer K, Lemke JR. GRIN2B-Related neurodevelopmental disorder. In: Adam MP, Feldman J, Mirzaa GM, Pagon RA, Wallace SE, Bean LJH, Gripp KW, Amemiya A, eds. *GeneReviews® [Internet]*. University of Washington, Seattle; 1993-2023. PMID: 29851452.
22. Miyamoto H, Tatsukawa T, Shimohata A, et al. Impaired cortico-striatal excitatory transmission triggers epilepsy. *Nat Commun*. 2019;10(1):1917. doi:10.1038/s41467-019-09954-9

15732665, 2024, 3, Downloaded from https://onlinelibrary.wiley.com/doi/10.1002/jimd.12689 by Universitat De Barcelona Biblioteca, Wiley Online Library on [09/01/2025]. See the Terms and Conditions (https://onlinelibrary.wiley.com/terms-and-conditions) on Wiley Online Library for rules of use; OA articles are governed by the applicable Creative Commons License

23. Miyamoto H, Shimohata A, Abe M, et al. Potentiation of excitatory synaptic transmission ameliorates aggression in mice with Stxbp1 haploinsufficiency. *Hum Mol Genet*. 2017;26(24):4961-4974. doi:10.1093/hmg/ddx379
24. Pecorelli A, Cervellati C, Cordone V, Hayek J, Valacchi G. Compromised immune/inflammatory responses in Rett syndrome. *Free Radic Biol Med*. 2020;152:100-106. doi:10.1016/j.freeradbiomed.2020.02.023
25. Freitas BC, Beltrão-Braga PCB, Marchetto MC. Modeling inflammation on neurodevelopmental disorders using pluripotent stem cells. *Adv Neurobiol*. 2020;25:207-218. doi:10.1007/978-3-030-45493-7_7
26. Wang L, Wang B, Wu C, Wang J, Sun M. Autism spectrum disorder: neurodevelopmental risk factors, biological mechanism, and precision therapy. *Int J Mol Sci*. 2023;24(3):1819. doi:10.3390/ijms24031819
27. Matta SM, Hill-Yardin EL, Crack PJ. The influence of neuroinflammation in autism spectrum disorder. *Brain Behav Immun*. 2019;79:75-90. doi:10.1016/j.bbi.2019.04.037
28. Batool S, Raza H, Zaidi J, Riaz S, Hasan S, Syed NI. Synapse formation: from cellular and molecular mechanisms to neurodevelopmental and neurodegenerative disorders. *J Neurophysiol*. 2019;121(4):1381-1397. doi:10.1152/jn.00833.2018
29. Lim L, Mi D, Llorca A, Marín O. Development and functional diversification of cortical interneurons. *Neuron*. 2018;100(2):294-313. doi:10.1016/j.neuron.2018.10.009
30. Kim YS, Choi J, Yoon B-E. Neuron–glia interactions in neurodevelopmental disorders. *Cells*. 2020;9:10. doi:10.3390/cells9102176
31. Oyarzábal A, Musokhranova U, Barros LF, García-Cazorla A. Energy metabolism in childhood neurodevelopmental disorders. *EBioMedicine*. 2021;69:103474. doi:10.1016/j.ebiom.2021.103474
32. Mitra S, Banik A, Saurabh S, Maulik M, Khatri SN. Neuroimmunometabolism: a new pathological nexus underlying neurodegenerative disorders. *J Neurosci Off J Soc Neurosci*. 2022;42(10):1888-1907. doi:10.1523/JNEUROSCI.0998-21.2022
33. Douglas A, Stevens B, Lynch L. Interleukin-17 as a key player in neuroimmunometabolism. *Nat Metab*. 2023;5(7):1088-1100. doi:10.1038/s42255-023-00846-3
34. Neul JL, Skinner SA, Annese F, et al. Metabolic signatures differentiate Rett syndrome from unaffected siblings. *Front Integr Neurosci*. 2020;14:7. doi:10.3389/fnint.2020.00007
35. El-Khoury R, Panayotis N, Matagne V, Ghata A, Villard L, Roux J-C. GABA and glutamate pathways are spatially and developmentally affected in the brain of Mecp2-deficient mice. *PloS One*. 2014;9(3):e92169. doi:10.1371/journal.pone.0092169
36. De Rosa R, Valastro S, Cambria C, et al. Loss of CDKL5 causes synaptic GABAergic defects that can be restored with the neuroactive steroid pregnenolone-methyl-ether. *Int J Mol Sci*. 2023;24(1):68. doi:10.3390/ijms24010068
37. Gogliotti RG, Senter RK, Rook JM, et al. mGlu5 positive allosteric modulation normalizes synaptic plasticity defects and motor phenotypes in a mouse model of Rett syndrome. *Hum Mol Genet*. 2016;25(10):1990-2004. doi:10.1093/hmg/ddw074
38. Gogliotti RG, Senter RK, Fisher NM, et al. mGlu(7) potentiation rescues cognitive, social, and respiratory phenotypes in a mouse model of Rett syndrome. *Sci Transl Med*. 2017;9(403):eaai7459. doi:10.1126/scitranslmed.aai7459
39. Rakela B, Brehm P, Mandel G. Astrocytic modulation of excitatory synaptic signaling in a mouse model of Rett syndrome. *Elife*. 2018;7:e31629. doi:10.7554/eLife.31629
40. Mussap M, Antonucci R, Noto A, Fanos V. The role of metabolomics in neonatal and pediatric laboratory medicine. *Clin Chim Acta*. 2013;426:127-138. doi:10.1016/j.cca.2013.08.020
41. Ruddick JP, Evans AK, Nutt DJ, Lightman SL, Rook GAW, Lowry CA. Tryptophan metabolism in the central nervous system: medical implications. *Expert Rev Mol Med*. 2006;8(20):1-27. doi:10.1017/S1462399406000068
42. Samaco RC, Mandel-Brehm C, Chao H-T, et al. Loss of MeCP2 in aminergic neurons causes cell-autonomous defects in neurotransmitter synthesis and specific behavioral abnormalities. *Proc Natl Acad Sci U S A*. 2009;106(51):21966-21971. doi:10.1073/pnas.0912257106
43. Juliá-Palacios N, Molina-Anguita C, Sigatulina Bondarenko M, et al. Monoamine neurotransmitters in early epileptic encephalopathies: new insights into pathophysiology and therapy. *Dev Med Child Neurol*. 2022;64(7):915-923. doi:10.1111/dmcn.15140
44. Strasser B, Becker K, Fuchs D, Gostner JM. Kynurenine pathway metabolism and immune activation: peripheral measurements in psychiatric and co-morbid conditions. *Neuropharmacology*. 2017;112(Pt B):286-296. doi:10.1016/j.neuropharm.2016.02.030
45. Bryleva EY, Brundin L. Suicidality and activation of the kynurenine pathway of tryptophan metabolism. *Curr Top Behav Neurosci*. 2017;31:269-284. doi:10.1007/7854_2016_5
46. Lovelace MD, Varney B, Sundaram G, et al. Recent evidence for an expanded role of the kynurenine pathway of tryptophan metabolism in neurological diseases. *Neuropharmacology*. 2017;112(Pt B):373-388. doi:10.1016/j.neuropharm.2016.03.024
47. Fujigaki H, Yamamoto Y, Saito K. L-tryptophan-kynurenine pathway enzymes are therapeutic target for neuropsychiatric diseases: focus on cell type differences. *Neuropharmacology*. 2017;112(Pt B):264-274. doi:10.1016/j.neuropharm.2016.01.011
48. Castro-Portuguez R, Sutphin GL. Kynurenine pathway, NAD (+) synthesis, and mitochondrial function: targeting tryptophan metabolism to promote longevity and healthspan. *Exp Gerontol*. 2020;132:110841. doi:10.1016/j.exger.2020.110841
49. Savitz J. The kynurenine pathway: a finger in every pie. *Mol Psychiatry*. 2020;25(1):131-147. doi:10.1038/s41380-019-0414-4
50. Cervenka I, Agudelo LZ, Ruas JL. Kynurenines: tryptophan's metabolites in exercise, inflammation, and mental health. *Science*. 2017;357(6349):eaaf9794. doi:10.1126/science.aaf9794
51. Joisten N, Ruas JL, Braidy N, Guillemin GJ, Zimmer P. The kynurenine pathway in chronic diseases: a compensatory mechanism or a driving force? *Trends Mol Med*. 2021;27(10):946-954. doi:10.1016/j.molmed.2021.07.006
52. Wang Q, Liu D, Song P, Zou M-H. Tryptophan-kynurenine pathway is dysregulated in inflammation, and immune activation. *Front Biosci*. 2015;20(7):1116-1143. doi:10.2741/4363
53. Wassenberg T, Molero-Luis M, Jeltsch K, et al. Consensus guideline for the diagnosis and treatment of aromatic L-amino acid decarboxylase (AADC) deficiency. *Orphanet J Rare Dis*. 2017;12(1):12. doi:10.1186/s13023-016-0522-z
54. Rizzi S, Spagnoli C, Frattini D, Pisani F, Fusco C. Clinical features in aromatic L-amino acid decarboxylase (AADC) deficiency: a systematic review. *Behav Neurol*. 2022;2022:2210555. doi:10.1155/2022/2210555
55. Strauss KA, Carson VJ, Soltys K, et al. Branched-chain α-ketoacid dehydrogenase deficiency (maple syrup urine

15732665, 2024, 3, Downloaded from https://onlinelibrary.wiley.com/doi/10.1002/jimd.12689 by Universitat De Barcelona Biblioteca, Wiley Online Library on [09/01/2025]. See the Terms and Conditions (https://onlinelibrary.wiley.com/terms-and-conditions) on Wiley Online Library for rules of use; OA articles are governed by the applicable Creative Commons License

disease): treatment, biomarkers, and outcomes. *Mol Genet Metab*. 2020;129(3):193-206. doi:10.1016/j.ymgme.2020.01.006

56. Tangeraas T, Constante JR, Backe PH, et al. BCKDK deficiency: a treatable neurodevelopmental disease amenable to newborn screening. *Brain A J Neurol*. 2023;146(7):3003-3013. doi:10.1093/brain/awad010
57. Lamothe SM, Sharmin N, Silver G, et al. Control of Slc7a5 sensitivity by the voltage-sensing domain of Kv1 channels. *Elife*. 2020;9:e54916. doi:10.7554/eLife.54916
58. Baronas VA, Yang RY, Morales LC, Sipione S, Kurata HT. Slc7a5 regulates Kv1.2 channels and modifies functional outcomes of epilepsy-linked channel mutations. *Nat Commun*. 2018;9(1):4417. doi:10.1038/s41467-018-06859-x
59. Tărlungeanu DC, Deliu E, Dotter CP, et al. Impaired amino acid transport at the blood brain barrier is a cause of autism spectrum disorder. *Cell*. 2016;167(6):1481-1494.e18. doi:10.1016/j.cell.2016.11.013
60. Cascio L, Chen C-F, Pauly R, et al. Abnormalities in the genes that encode large amino acid transporters increase the risk of autism spectrum disorder. *Mol Genet Genomic Med*. 2020;8(1):e1036. doi:10.1002/mgg3.1036
61. Knaus LS, Basilico B, Malzl D, et al. Large neutral amino acid levels tune perinatal neuronal excitability and survival. *Cell*. 2023;186(9):1950-1967.e25. doi:10.1016/j.cell.2023.02.037
62. Sokolov AM, Holmberg JC, Feliciano DM. The amino acid transporter Slc7a5 regulates the mTOR pathway and is required for granule cell development. *Hum Mol Genet*. 2020;29(18):3003-3013. doi:10.1093/hmg/ddaa186
63. Pepe G, Fioriniello S, Marracino F, et al. Blood-brain barrier integrity is perturbed in a Mecp2-null mouse model of Rett syndrome. *Biomolecules*. 2023;13(4):606. doi:10.3390/biom13040606

SUPPORTING INFORMATION

Additional supporting information can be found online in the Supporting Information section at the end of this article.

How to cite this article: Illescas S, Diaz-Osorio Y, Serradell A, et al. Metabolic characterization of neurogenetic disorders involving glutamatergic neurotransmission. *J Inherit Metab Dis*. 2024;47(3):551-569. doi:10.1002/jimd.12689

15732665, 2024, 3, Downloaded from https://onlinelibrary.wiley.com/doi/10.1002/jimd.12689 by Universitat De Barcelona Biblioteca, Wiley Online Library on [09/01/2025]. See the Terms and Conditions (https://onlinelibrary.wiley.com/terms-and-conditions) on Wiley Online Library for rules of use; OA articles are governed by the applicable Creative Commons License

OPEN ACCESS

Original research

Expanding the phenotypic spectrum of *TRAPPC11*-related muscular dystrophy: 25 Roma individuals carrying a founder variant

Maria Justel,[1,2] Cristina Jou,[3,4,5] Andrea Sariego-Jamardo,[6] Natalia Alexandra Juliá-Palacios,[7] Carlos Ortez,[1,3] Maria Luisa Poch,[8] Antonio Hedrera-Fernandez,[9] Hilario Gomez-Martin,[10] Anna Codina,[3] Jana Dominguez-Carral,[11] Jordi Muxart,[12] Aurelio Hernández-Laín,[13] Sara Vila-Bedmar,[14] Miren Zulaica,[15] Ramon Cancho-Candela,[16] Margarita del Carmen Castro,[17] Alberto de la Osa-Langreo,[18] Alfonso Peña-Valenceja,[19] Elena Marcos-Vadillo,[20] Pablo Prieto-Matos,[2] Samuel Ignacio Pascual-Pascual,[21] Adolfo López de Munain,[15] Ana Camacho,[22] Berta Estevez-Arias,[1,23] Uliana Musokhranova,[7] Mireia Olivella,[24] Alfonso Oyarzábal,[7] Cecilia Jimenez-Mallebrera,[3,4,25] Cristina Domínguez-González ,[4,14] Andrés Nascimento,[1,3,4] Àngels García-Cazorla,[7] Daniel Natera-de Benito [1,3]

ABSTRACT

Background Limb-girdle muscular dystrophies (LGMD) are a heterogeneous group of genetically determined muscle disorders. TRAPPC11-related LGMD is an autosomal-recessive condition characterised by muscle weakness and intellectual disability.

Methods A clinical and histopathological characterisation of 25 Roma individuals with LGMD R18 caused by the homozygous *TRAPPC11* c.1287+5G>A variant is reported. Functional effects of the variant on mitochondrial function were investigated.

Results The c.1287+5G>A variant leads to a phenotype characterised by early onset muscle weakness, movement disorder, intellectual disability and elevated serum creatine kinase, which is similar to other series. As novel clinical findings, we found that microcephaly is almost universal and that infections in the first years of life seem to act as triggers for a psychomotor regression and onset of seizures in several individuals with *TRAPPC11* variants, who showed pseudometabolic crises triggered by infections. Our functional studies expanded the role of TRAPPC11 deficiency in mitochondrial function, as a decreased mitochondrial ATP production capacity and alterations in the mitochondrial network architecture were detected.

Conclusion We provide a comprehensive phenotypic characterisation of the pathogenic variant *TRAPPC11* c.1287+5G>A, which is founder in the Roma population. Our observations indicate that some typical features of golgipathies, such as microcephaly and clinical decompensation associated with infections, are prevalent in individuals with LGMD R18.

WHAT IS ALREADY KNOWN ON THIS TOPIC

⇒ *TRAPPC11*-related limb-girdle muscular dystrophies (LGMD), which has been reported so far in no more than 20 individuals, is clinically characterised by muscle weakness, intellectual disability and hyperkinetic movements.

WHAT THIS STUDY ADDS

⇒ Our phenotypic characterisation of the pathogenic variant *TRAPPC11* c.1287+5G>A, which is founder in the Roma population, indicates that some typical features of golgipathies, such as microcephaly and clinical decompensation associated with infections, are prevalent in individuals with *TRAPPC11*-related LGMD.

⇒ Our functional studies expanded the role of TRAPPC11 deficiency in mitochondrial function.

HOW THIS STUDY MIGHT AFFECT RESEARCH, PRACTICE OR POLICY

⇒ Our findings allow us to refine and expand the emerging concept of golgipathies through a better understanding of the phenotype associated with *TRAPPC11*-related LGMD.

INTRODUCTION

Limb-girdle muscular dystrophies (LGMD) are a heterogeneous group of genetically determined muscle disorders with predominant proximal weakness.[1] The age of onset, severity and clinical course may vary among LGMD subtypes, ranging from early onset myopathy with rapid progression to adult-onset with long-time preserved ambulation and normal life span.[2 3]

TRAPPC11-related LGMD R18, previously known as LGMD2S,[4] is an autosomal-recessive congenital disorder of glycosylation that is clinically

► Additional supplemental material is published online only. To view, please visit the journal online (http://dx.doi.org/10.1136/jmg-2022-109132).

For numbered affiliations see end of article.

Correspondence to
Dr Daniel Natera-de Benito, Neuromuscular Unit, Department of Neurology, Hospital Sant Joan de Déu, Barcelona, Spain; daniel.natera@sjd.es

ÀG-C and DN-dB contributed equally.

Received 30 December 2022
Accepted 28 March 2023
Published Online First 16 May 2023

Check for updates

© Author(s) (or their employer(s)) 2023. Re-use permitted under CC BY-NC. No commercial re-use. See rights and permissions. Published by BMJ.

To cite: Justel M, Jou C, Sariego-Jamardo A, *et al*. *J Med Genet* 2023;**60**:965–973.

J Med Genet: first published as 10.1136/jmg-2022-109132 on 16 May 2023. Downloaded from http://jmg.bmj.com/ on January 9, 2025 by guest. Protected by copyright.

characterised by muscle weakness, intellectual disability and hyperkinetic movements.[5–7] *TRAPPC11* encodes subunit 11 of the multiprotein TRAPP complex, a regulator of membrane trafficking and autophagy whose best characterised biochemical function is to act as a guanine nucleotide exchange factor to activate Ypt/Rab GTPases.[8–10] Pathogenic variants or deletions of TRAPP subunits are involved in several neurodevelopmental disorders, known as TRAPPopathies.[11 12] TRAPPopathies belong to the rapidly growing category of disorders of cell trafficking and in particular to membrane trafficking defects. The recent report of the cryo-EM structure of the *Drosophila* TRAPPIII complex has revealed how the TRAPP subunits assemble and the TRAPPC11 structure, shedding light on how disease-causing variants affect the structure and function of TRAPPC11.[13]

No more than 20 individuals and 12 variants in *TRAPPC11* have been reported so far.[5–7 14–19] Here, we report a founder pathogenic variant (*TRAPPC11* c.1287+5G>A; p.Ala372_Ser429del) in the Roma population and provide a comprehensive phenotypic characterisation based on the description of 25 previously unreported Spanish Roma individuals who harbour the variant in homozygosis. There are no previous reports of a direct link between *TRAPPC11* and mitochondrial function, but it is not uncommon to find associated mitochondrial defects in membrane trafficking disorders.[20 21] We have therefore studied mitochondrial energy metabolism in individuals with the variant *TRAPPC11* c.1287+5G>A to better understand the possible involvement of mitochondria in the pathophysiology of *TRAPPC11*-related muscular dystrophy.

METHODS

Recruitment of patients, clinical examinations and molecular genetic analyses

Data of individuals with a genetically confirmed LGMD R18 were collected at 12 Spanish hospitals after sending a request for collaboration to all the members of the Spanish Paediatric Neurology Society. Demographic, clinical, genetic, electroencephalographic, neuroradiological and muscle biopsy data were collected in accordance with the ethics guidelines of each of the institutions involved. The degree of intellectual disability was classified according to the impression of the neurologist who followed each individual, but a neuropsychological assessment was not carried out systematically in all individuals.

Genomic DNA samples were extracted from peripheral blood of affected individuals. Different next-generation sequencing methodologies were used to prepare and capture genomic DNA libraries, from customised panels for selected genes to exome sequencing. The same single nucleotide variant c.1287+5G>A in *TRAPPC11*, classified as pathogenic according to the American College of Medical Genetics and Genomics guidelines for germline variant classification,[22] was found in homozygosis in all the individuals. Segregation was performed on the asymptomatic parents of 13 individuals.

In silico analysis of variant *TRAPPC11* c.1287+5G>A

A homology molecular model for *human* TRAPPC11 (positions 1–574) and TRAPPC2L (positions 1–138) was constructed based on *Drosophila* TRAPPIII complex structures (7B6H and 7B6R),[13] using Modeller.[23] Positions 61–75 and 378–405, with no determined structure in the template structure, were also modelled. Sequence identity was 42.1% and 52.9% for TRAPPC11 and TRAPPC2L, respectively. *Human* TRAPPC11 structural model was visualised using Pymol[24] (http://www.pymol.org/pymol).

Muscle and skin biopsies, histological, immunohistochemical, immunofluorescence, ultrastructural studies and western blot analysis

Muscle biopsy samples were obtained for diagnostic purposes and processed following standard histological, histochemical and immunohistochemical protocols as previously described.[25] Skin biopsy samples were obtained and fibroblasts were cultered according to Hospital Sant Joan de Déu standard clinical procedures. Specific antibodies used for immunohistochemical or immunofluorescence studies are listed in online supplemental table 1. Electron microscopy studies were performed on muscle samples from individual 5. Semi-quantitative western blot analysis on fibroblasts and muscle lysates using antibodies against TRAPPC11 and alpha-dystroglycan (IIH6 and VIA4) was performed as previously described.[26] All the muscle biopsies and western blot analysis studies were expressly reviewed for this study by a pathologist (CJ), a clinical scientist (ACo) and a paediatric neurologist (DN-dB), all three specialists in neuromuscular disorders. Control muscle samples were taken from two children aged 5 and 10 years who did not have neuromuscular disease, from quadriceps and from an unknown muscle. Control fibroblasts were obtained from a skin biopsy of a child aged 10 years with no neuromuscular disease.

Characterisation of epilepsy

Classification of seizures, epilepsy course and available EEGs were reviewed by an epileptologist specialised in children (JD-C). Seizures and epilepsy were described and classified according to the International League Against Epilepsy classification.[27 28] Bilateral tonic-clonic seizures in which the onset of the seizure was not observed and which could be either 'generalised seizures' or 'focal seizures that evolve into bilateral tonic-clonic seizures' were referred to as 'bilateral tonic-clonic seizures'. Epilepsy course was classified as (a) 'early seizure freedom' (seizure-free within 6 months of starting treatment), (b) 'delayed seizure freedom' (seizures not immediately controlled by medication, but became seizure-free at some point after 6 months), (c) 'fluctuating course' (periods of seizure freedom of >12 months, interspersed with relapses) or (d) 'refractory' (never seizure-free for a continuous 12-month period) following the method defined by Brodie *et al*.[29]

Functional analysis of the variant on mitochondrial function

Functional studies have included the analysis of non-glycolytic ATP production and mitochondrial network visualisation. Mitochondrial (as in non-glycolytic) ATP concentration was measured as explained in the study by Oyarzabal *et al*.[30] Briefly, cells from individuals with TRAPPC11-related muscular dystrophy and cells from controls were incubated with 2-deoxy-D-glucose for 2 hours to discriminate between total and non-glycolytic ATP. Finally, ATP concentration was assayed by bioluminescence using a luciferin-luciferase system (ATP Bioluminescence Assay Kit CLS II, Roche) according to the manufacturer's instructions, corrected by protein concentration and expressed as folds over controls.

The mitochondrial network was visualised through immunofluorescence against TOMM20 (1:250, ab186735) following standard protocols. Fluorescence was imaged using Zeiss LSM 880 microscope (Zeiss, Germany) with a 63× magnification. Images were analysed using Fiji software and parametrised by Mitochondrial Analyzer plugin.[31] All experiments are done at least three times with triplicates.

J Med Genet: first published as 10.1136/jmg-2022-109132 on 16 May 2023. Downloaded from http://jmg.bmj.com/ on January 9, 2025 by guest. Protected by copyright.

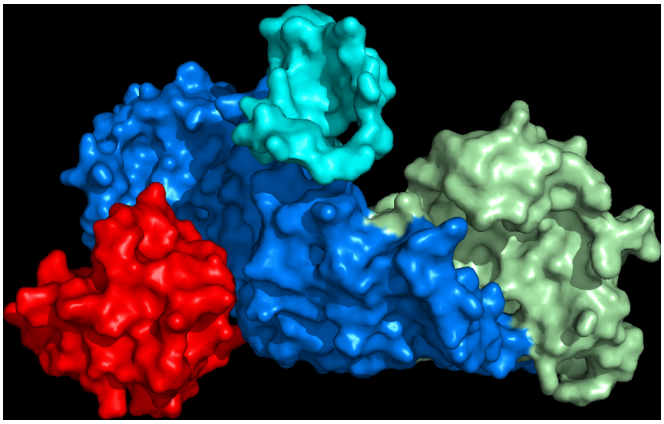

Figure 1 Molecular model of *human* TRAPPC11 (residues 1–574, in blue and green) interacting with *human* TRAPPC2L (residues 1–136, in red), in the TRAPPIII complex. TRAPPC11 foie gras domain (residues 181–566, in cyan blue) is essential for TRAPPC2L interaction. This domain contains residues 372–429 (in dark blue), which are lacking in *TRAPPC11* c.1287+5G>A splice-site variant. The N-terminal domain of TRAPPC11 is shown in green.

At the time the fibroblasts were biopsied, one of the individuals with TRAPPC11-related muscular dystrophy was 4 years old and the other was 12 years old. All controls, which included both males and females, were within this age range. All cells used were between passages 7 and 12.

RESULTS

Demographics and molecular genetics

A total of 25 individuals with TRAPPC11-related muscular dystrophy (13 males, 12 females) from 18 families were collected. All of them were Spanish with a Roma origin and 22 of 23 cases (96%) were born from consanguineous parents. The mean age at the last examination was 11.8 years old (range 2–23). The previously reported homozygous splice-site variant *TRAPPC11* (NM_021942.6) c.1287+5G>A was found in all the individuals. Segregation studies were performed on the parents of 13 individuals, confirming that the pathogenic variants were inherited each from one of the unaffected parents.

Structure consequence of *TRAPPC11* c.1287+5G>A variant

The splice-site variant *TRAPPC11* c.1287+5G>A results in an in-frame deletion of 58 amino acids (p.Ala372_Ser429del).[5] Figure 1 shows *human* TRAPPC11 and TRAPPC2L structural model interaction. The deletion of residues 372–429 in TRAPPC11 is located within the conserved foie gras domain (residues 181–566), which is responsible for the surface interaction with TRAPPC2L.[13] The lacking of this region has been recently described as resulting in defects in membrane trafficking,[5] autophagy and N-linked glycosylation.[17]

Clinical features

A history of late premature birth was reported in 3/24 individuals (12.5%) and low birth weight in 3/23 (13%). Progressive and highly significant microcephaly was almost universally found (21/23; 91%), being detected at birth in 38% of individuals and acquired during the first years of life in 52%. The mean head circumference SD score was −3.45, ranging from −1.55 to −7.2. Individuals tended to be short, with a mean height percentile of p12 compared with the Spanish population (range p<1–p35).[19] A height percentile below p2 was observed in 27% (4/15). Three individuals had neonatal hypotonia and none of them had congenital cataracts.

The most common initial presentation was a global psychomotor delay (21/25; 84%), while the presenting symptom was seizures in the four individuals who had seizures before the age of 7 months. A global psychomotor delay was observed at some point in 96% of individuals (24/25), and a subsequent intellectual disability was described in all individuals who were older than 4 years at the last follow-up (23/23). The intellectual disability was severe in eight individuals, moderate-to-severe in five, moderate in seven, mild in one and of an unknown degree in two. It is noteworthy that four individuals (16%) experienced a psychomotor regression, with loss of developmental milestones previously attained, triggered by infections. These triggering infections were even initially classified as encephalitis in these individuals, as there was drowsiness, febrile seizures and a slowed EEG. No causative microorganism was identified in the cerebrospinal fluid. These infections occurred at a median age of 13 months old (range: 4–36).

A severe language impairment was detected in 21/25 individuals (84%). Movement disorders, including hyperkinesia and choreiform movements, were reported in 79% of cases (19/24). None of the individuals with TRAPPC11-related muscular dystrophy showed signs of spasticity. The main clinical features are summarised in online supplemental table 2.

All individuals had elevated creatine kinase (CK) in serum, ranging from 300 to 5000 IU/L (mean: 1440 IU/L, SD: 1009 IU/L). Independent ambulation was acquired by 23 from 24 individuals (96%) at a mean age of 22 months, with a delay in the acquisition of autonomous ambulation—understood as above 18 months of age—observed in 40% (8/20). An early onset proximal weakness was detected in 71% of individuals (17/24), associated with myalgia and cramps in six of them (6/23; 26%). Rhabdomyolysis was not identified in any of the individuals.

Epilepsy, defined as recurrent seizures, was diagnosed in 12/25 individuals (48%), and the mean age at first seizure was 21 months (range: 4 months–8 years; median 12 months). All 12 individuals with epilepsy were treated with antiepileptic drugs. The most common type of seizure was bilateral tonic-clonic seizures, either with focal onset or with unknown onset, being experienced by 92% of individuals with epilepsy (11/12). Focal-onset seizures with impaired awareness were observed in 33% of individuals with epilepsy (4/12). Remarkably, half of individuals with epilepsy (6/12; 50%) had a history of status epilepticus, four of them in the context of fever. Seizures triggered by infections were observed in 83% of individuals (10/12). Seizure characteristics, as well as main electroclinical and neuroradiological features, are summarised in online supplemental table 2.

EEG reports were available in all 11 individuals with epilepsy. Selected illustrative EEG studies are shown in figure 2. Eight individuals (67%) showed interictal focal or multifocal epileptiform abnormalities. A high degree of variability was observed in the origin of the epileptiform abnormalities (online supplemental table 2). Although the temporal origin was slightly more frequent than in other locations, the difference was not significant and is not different from that observed in other individuals with epilepsy, given that temporal lobe epilepsy is the most common form of focal epilepsy.[32 33] Background activity was slow in 42% of individuals with epilepsy (5/12). Photosensitivity was not present in any of the individuals.

Long-term seizure control was assessed in the 12 individuals with epilepsy based on the Brodie classification system.[29] Six individuals (50%) were seizure-free within 6 months of starting treatment (a), two individuals (17%) were seizure-free after

J Med Genet: first published as 10.1136/jmg-2022-109132 on 16 May 2023. Downloaded from http://jmg.bmj.com/ on January 9, 2025 by guest. Protected by copyright.

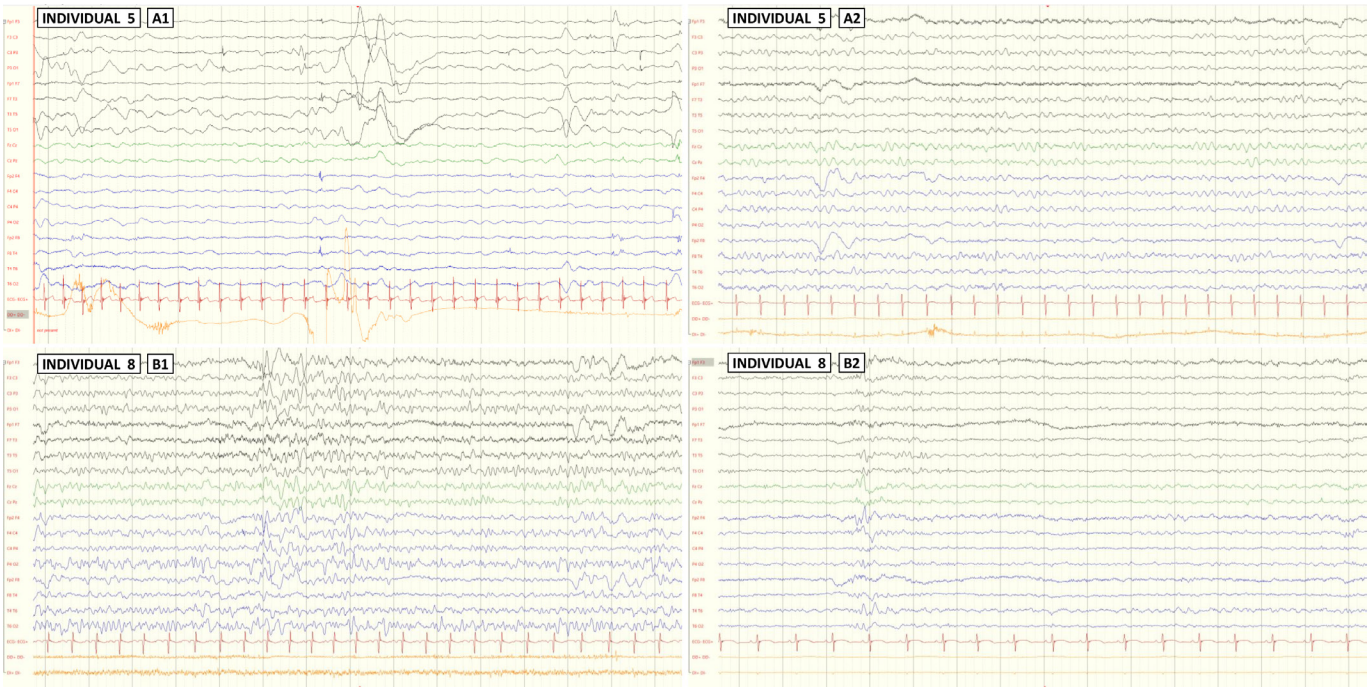

Figure 2 Awake EEG studies of individuals 5 and 8. Longitudinal bipolar montage at sensitivity 70 µV/cm is shown in all the cases. Individual 5: while EEG at 14 months old during his first seizures showed a slow and low voltage background activity without epileptic abnormalities (A1), the EEG at the age of 2 years, during wakefulness with eyes closed, showed a slow background activity without epileptiform abnormalities (A2). Individual 8: EEGs at the age of 13 years, during wakefulness with eyes closed (B1) and eyes open (B2) showed normal background activity, with epileptic abnormalities (sharp waves and spikes) in bilateral frontocentrotemporal region.

6 months of starting treatment (b) and 4 (33%) had a fluctuating course (c; periods of at least 12 months seizure-free, interspersed with relapses). A favourable response to monotherapy treatment was observed in 7/12 individuals (58%). A summary of medications used in each individual at the last follow-up is provided in online supplemental table 2. At the last visit, four individuals were seizure-free with levetiracetam monotherapy and three remained seizure-free after antiepileptic drug withdrawal. Non-pharmacological treatments, including the ketogenic diet, vagus nerve stimulation and epilepsy surgery, were not tried on any individual.

Brain MRI was performed in 84% of individuals (21/25). A generalised decrease in cortico-subcortical volume, including white matter, was found in 29% of them (6/21), with no other associated structural abnormalities. No hypomyelination was observed in the brain MRI of any individual. A prominence of the cerebellar folia was observed in individual 10 but obvious cerebellar atrophy or hypoplasia was not observed in any individual (figure 3 and online supplemental table 2).

Scoliosis was identified in 50% of individuals (5/10) over 13 years of age. No cardiac involvement was observed in the 15 individuals in whom cardiac evaluation with ECG and echocardiography was performed, except in one individual with mild dilatation of the aortic root and ascending aorta.

Morphological findings in muscle biopsies

Muscle biopsies were performed on seven individuals, taken from either the quadriceps (five individuals), the deltoids (one individual) or an unknown location (one individual), at a mean age of 5.5 years (SD: 4.5; median: 3). The main features of muscle biopsies are shown in figure 4 and in online supplemental table 3. Muscle histology showed myopathic changes with variability in fibre size and some fibres with internalised nuclei. Intermyofibrillar pattern disruptions, with areas devoid of staining for oxidative enzymes (Nicotinadmide adenine dinucleotide and Succinate dehydrogenase), were observed in all the individuals. Occasional myonecrosis and regeneration (displayed as neonatal myosin-positive fibres) were observed, while increased endomysial or perimysial connective tissue with fibrosis or fatty infiltration were not observed in any of the cases. Fibre-type distribution was normal, with a mosaic pattern, in five cases while atrophy of type II fibres was observed in two individuals.

Immunofluorescence labelling at the sarcolemma with two antibodies to alpha-dystroglycan (IIH6 and VIA4) showed a patchy or mosaic reduction of alpha-dystroglycan in 5/6 individuals, similar to four individuals with TRAPPC11-related muscular dystrophy recently described by Munot *et al*.[18] Immunohistochemical studies for spectrin, dystrophin, sarcoglycans,

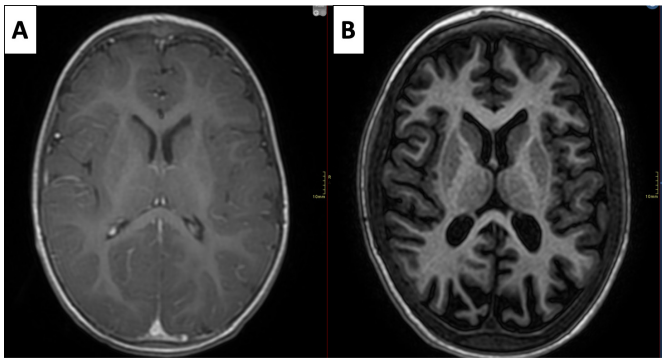

Figure 3 A progressive cortical and subcortical atrophy is observed in individual 5. MRIs at the age of 14 months (A) and 5 years (B) are shown, axial T1.

J Med Genet: first published as 10.1136/jmg-2022-109132 on 16 May 2023. Downloaded from http://jmg.bmj.com/ on January 9, 2025 by guest. Protected by copyright.

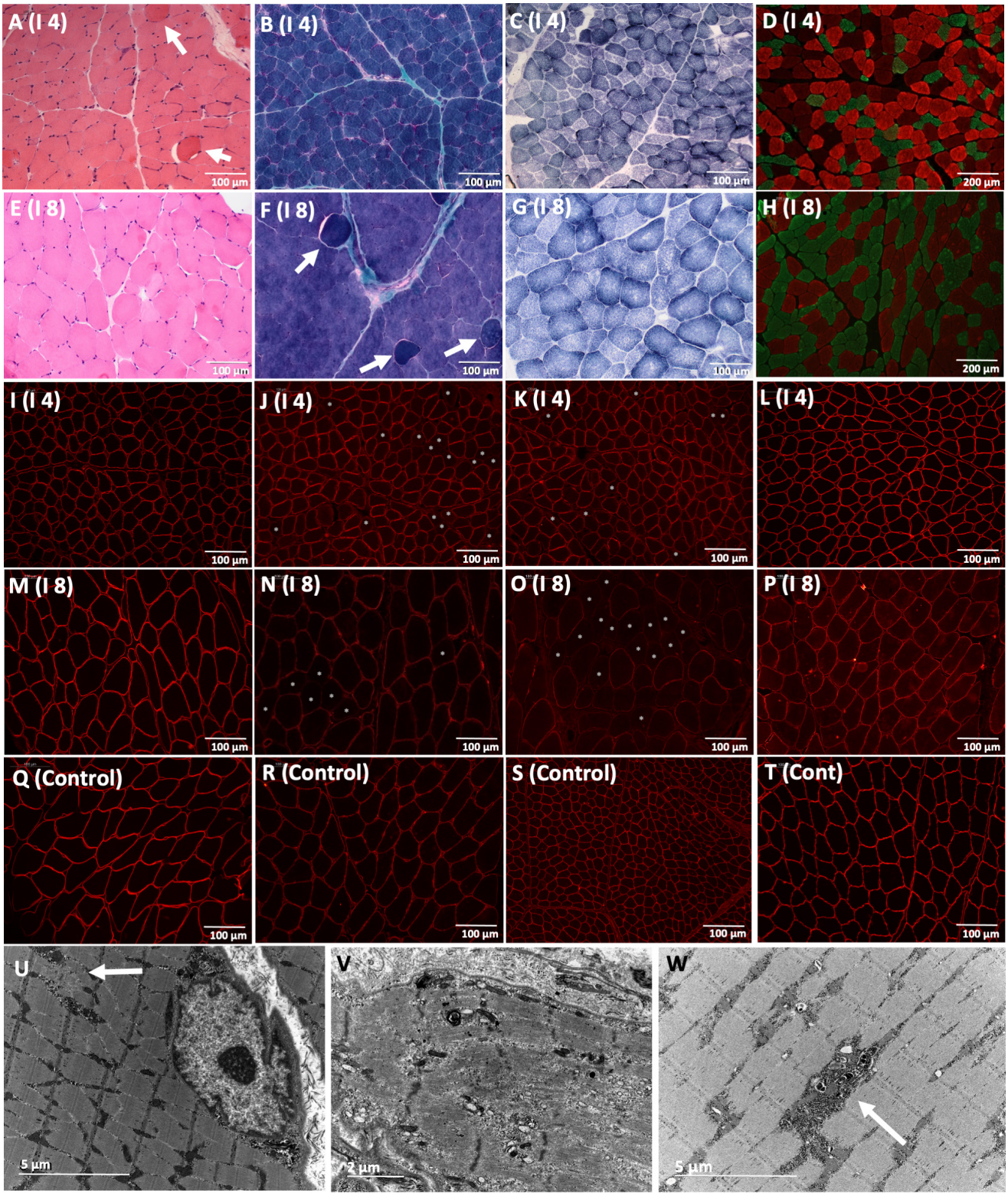

Figure 4 Myopathic muscle pathology from quadriceps and deltoid biopsies. Biopsy from Individual 4 (A–D, I–L and U–W) was taken from quadriceps at 3 years and biopsy from individual 8 (E–H and M–P) was taken from deltoid at 12 years. Variability in fibre size and fibres with internalised nuclei were observed with H&E stain in individuals 4 and 8 (A, E), as well as hypercontracted fibres (arrow A, F). Increased connective tissue with fibrosis or fatty infiltration were not observed (B, F). Blurred unstained areas in some fibres were noted with SDH (C, G). Selective atrophy of fast fibres is noted with double immunostaining of myosins. Slow-type fibres stained red and fast-type fibres stained green (D, H). Sarcolemmal beta-dystroglycan was normal (I, M) compared with control (Q), which implies that the integrity of the sarcolemma is not altered. A reduction of sarcolemmal alpha-dystroglycan with a mosaic pattern (asterisks in fibres with reduced alpha-dystroglycan) was noted in individuals 4 and 8 with IIH6 (J and N) and VIA 4 (K and O) antibodies, compared with control (R and S). Merosin immunolabelling was normal in individuals 4 (L) and 8 (P) compared with control (T). Electron microscopy (U, V and W) performed in individual 4 showed focal Z-band streamings (arrow in U), a necrotic fibre with a structural disruption of the sarcomere (V) and electron-dense degraded material (arrow in W). Scale bar=100 µm in A–T. Scale bar=5 µm in U and W. Scale bar=2 µm in V.

J Med Genet: first published as 10.1136/jmg-2022-109132 on 16 May 2023. Downloaded from http://jmg.bmj.com/ on January 9, 2025 by guest. Protected by copyright.

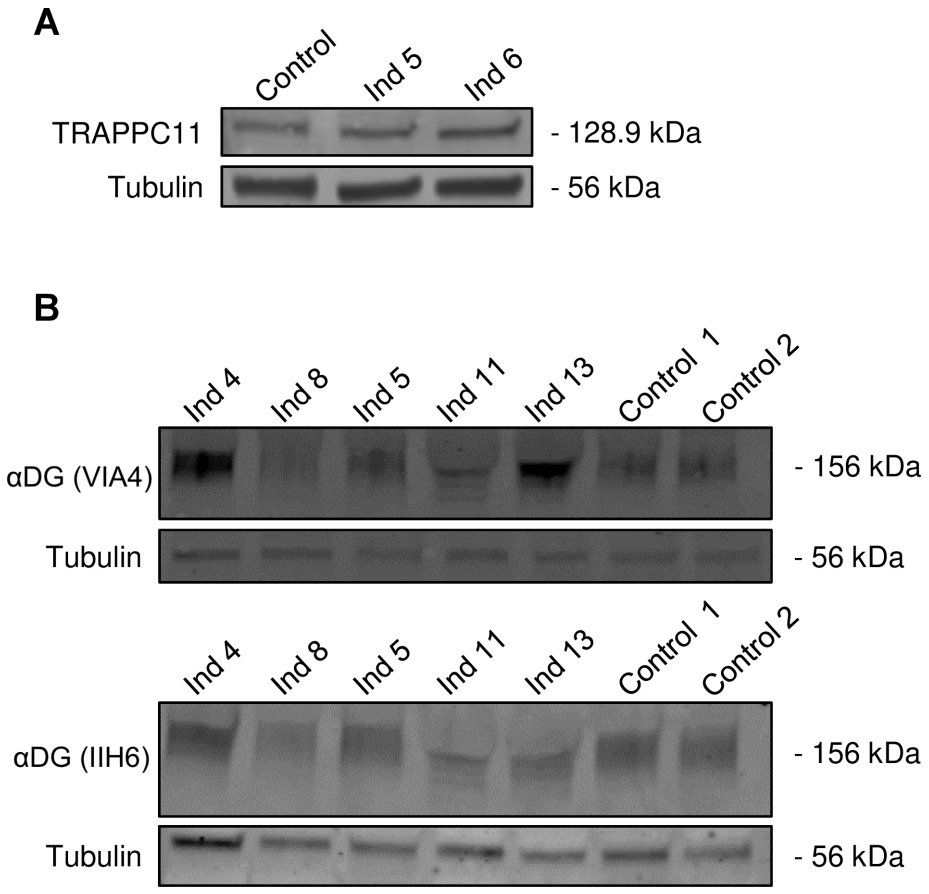

Figure 5 Western blot analyses of TRAPPC11 (in fibroblasts) and alpha-dystroglycan (αDG) glycosylation (in muscle) in some patients. TRAPPC11 expression (A) was not different in fibroblasts from individuals (Ind) 5 and 6 compared with control while αDG glycosylation in muscle was reduced in some individuals. A subtle-to-moderate reduction was noted in Ind 8 and 11 compared with controls with antibodies VIA4 and IIH6. No reductions were noted in Ind 4, 5 and 13.

beta-dystroglycan and laminin were normal. Overexpression of utrophin was not noted, except in regenerative fibres, which is physiological (figure 4).

Electron microscopy performed in individual 4 showed focal Z-band streamings, a necrotic fibre with an almost completely absent myofibrillar structure that was replaced by granular amorphous material as well as a fibre electron-dense degraded material (figure 4).

Variability in fibre size and the presence of atrophic fibres were the most prominent ultrastructural findings.

Western blot analysis studies

To study TRAPPC11 expression levels, a western blot analysis against TRAPPC11 was performed on fibroblast lysates from two individuals (individuals 5 and 6). No differences were observed compared with the control (figure 5A). An alpha-dystroglycan western blot analysis (VIA4 and IIH6 antibodies) was performed on five individuals and compared with controls to study whether glycosylation in muscle was altered. A reduction of alpha-dystroglycan expression was observed in two of the five individuals compared with the healthy control. The reduction in band intensity in individuals 8 and 11 was subtle-to-moderate. The intensity of the band in individuals 4, 5 and 13 was not reduced (figure 5B). No clear alteration in their mean molecular weight was observed compared with the control, except for individual 11, where the molecular weight appears slightly lower, which could be related to protein instability.

Pathophysiology of TRAPPC11 deficiency

We investigated the effect of TRAPPC11 deficiency on mitochondrial function in the fibroblasts of two individuals with TRAPPC11-related muscular dystrophy. Analysis of non-glycolytic ATP production (assumed as mitochondrial ATP) revealed a significant decrease of ~30% in the fibroblasts of individuals with TRAPPC11-related muscular dystrophy. Together with this finding, we observed some mild alterations in the mitochondrial network architecture, as individuals with TRAPPC11-related muscular dystrophy showed more mitochondria but with fewer and shorter branches, resulting in a 'less structured mesh' (figure 6).

DISCUSSION

We report a comprehensive description of the phenotype of 25 individuals with LGMD due to a homozygous c.1287+5G>A splice-site variant in *TRAPPC11*. Variant c.1287+5G>A has been previously reported in homozygosity in five individuals from two Hutterite families who had myopathy, infantile hyperkinetic movements, ataxia and intellectual disability.[5] Subsequently, it was also described in compound heterozygosity along with a frameshift variant (c.3379_3380insT) in a Spanish individual who was not Roma and showed hypotonia, spasticity, choreiform movements and remarkable cerebral atrophy.[17] To our knowledge, this is the first time such a large number of TRAPPC11-related LGMD R18 individuals with the same

J Med Genet: first published as 10.1136/jmg-2022-109132 on 16 May 2023. Downloaded from http://jmg.bmj.com/ on January 9, 2025 by guest. Protected by copyright.

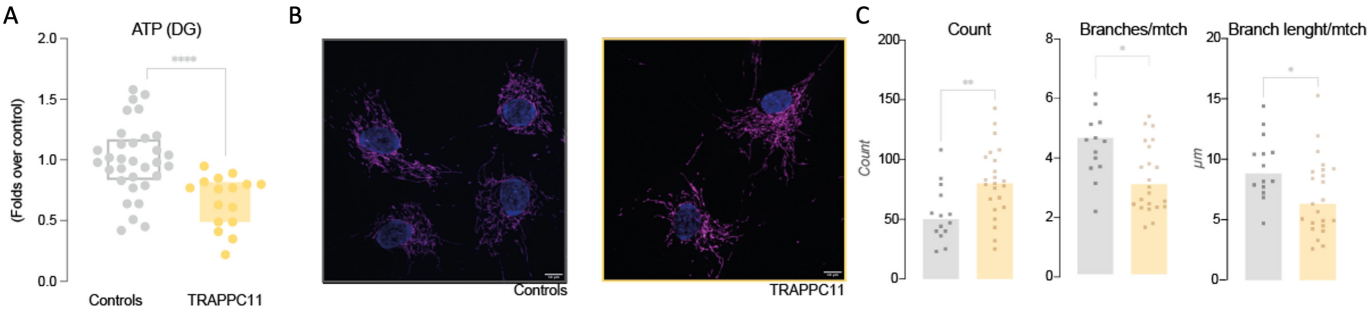

Figure 6 Analysis of the mitochondrial impact of TRAPPC11 deficiency. We explored mitochondrial function in terms of non-glycolytic ATP production (A) through a 2-hour incubation of fibroblasts from individuals with *TRAPPC11*-related muscular dystrophy and controls with 2-deoxy-D-glucose (DG) and a subsequent luciferin/luciferase assay. Results are presented as folds over control. Mitochondrial network was assayed by immunofluorescence against the mitochondrial marker TOMM20: representative images are shown in B and quantification results in C, showing an increase in mitochondrial counts, whose networks are less branched and with shorter mitochondria. Although only one representative image is shown for both control and patients, several fields of independent preparations in triplicate were analysed. The mitochondrial networks were analysed with the ImageJ plugin 'Mitochondrial Analyzer'. Nuclei are marked in blue and mitochondria in magenta. Scale bar marks 10 µm. Images have been parametrised through Mitochondrial Analyzer. Unpaired Welch's t-test was performed. *P<0.05; **p<0.01; ****p<0.0001.

homozygous variant are compiled in a single study. Furthermore, all individuals in our sample were Roma, suggesting *TRAPPC11* c.1287+5G>A is a founder pathogenic variant in Roma ethnicity.

Founder pathogenic variants are often responsible for the high prevalence of rare genetic disorders in specific populations. It is known that the Hutterite population, a communal ethnoreligious group currently settled in the USA and Canada, was first established in the 16th century in Austria and subsequently travelled through various regions of Europe.[34] In the 17th century, both Roma and Hutterite populations were present in Romania, which could be a hypothesis for the presence of the same variant in two ethnicities that are so remote from each other.

The main phenotypic characteristics of the individuals in our cohort do not differ substantially from those already described in previously reported individuals with pathogenic variants in *TRAPPC11*. Early onset muscle weakness, movement disorders, intellectual disability, epilepsy and elevation of CK in serum were almost constant findings in the individuals presented here. However, in our cohort, we have identified two additional phenotypic characteristics that are relevant and have not been previously reported. The first is a progressive and highly significant microcephaly that was almost universally found, often associated with a generalised decrease in cortico-subcortical volume. Although microcephaly has not been recognised as a feature associated with *TRAPPC11* until now, having been reported in only one individual so far,[18] postnatal microcephaly is a typical finding in most of the called 'golgipathies', a term used to describe those diseases caused by defects in Golgi-related genes.[35–40] The second novel finding is that, according to the information gathered in our cohort, infections in the first years of life seemed to act as triggers for a psychomotor regression and onset of seizures in some of the *TRAPPC11* individuals: psychomotor regression triggered by infections was observed in 16% of the individuals (4/25), and seizures triggered by infections were observed in 10/25 individuals (40%), including four who had a history of febrile status epilepticus. Even in four individuals with seizures and psychomotor regression the first diagnostic orientation was encephalitis. Indeed, other TRAPPopathies have been related to these episodes such as two novel homozygous variants in *TRAPPC2L* that associate postinfectious encephalopathy, developmental arrest, tetraplegia and rhabdomyolysis.[41 42]

These febrile illness-triggered seizures, usually presenting in the first 2 years of life, and occasionally associated with psychomotor regression, are a recognisable finding in many TRAPPC11 individuals and are similar to the phenotype showed by the few TRAPPC2L individuals reported so far.[42] In addition, individuals with pathogenic variants in *TRAPPC11* and *TRAPPC2L* share other clinical signs such as neurodevelopmental delay with speech difficulties, microcephaly and extrapyramidal symptoms. This marked phenotypic similarity leads us to hypothesise that variant *TRAPPC11* c.1287+5G>A, located in the foie gras domain, which is essential for interaction with TRAPPC2L, may alter the interaction between TRAPPC2L and TRAPPC11 (figure 1). In an analogous manner, it is possible that the variants described in *TRAPPC2L* weaken the interaction between the two proteins, thus explaining this unique phenotypic similarity. The reason why pathogenic variants of several subunits of the TRAPP complex result in microcephaly (TRAPPC2L, TRAPPC6, TRAPPC9, TRAPPC11) while others do not is unclear but may be related to the function of these proteins within the TRAPP complex and their role in membrane traffic.

On the other hand, the acute episodes observed in TRAPPC11 individuals partially resemble the acute pseudometabolic crises triggered by infections that are well-described in individuals with pathogenic variants in *TANGO2*[43] and other cell trafficking disorders. Cell trafficking disorders, which encompass 346 genes so far, are mostly progressive diseases due to the homeostatic loss of crucial molecular functions involved in neurodegeneration such as lipid transfer and membrane remodelling.[44] Although rhabdomyolysis and sustained CK elevation are hallmarks of some TRAPPopathies, they can also be observed in other anterograde trafficking disorders such as TANGO2, in which rhabdomyolysis during acute crises is associated with hypoglycaemia, hyperlactataemia and hyperammonaemia, or LPIN1, in which recurrent hyperCKaemia occurs.[40] All these features point towards a major metabolic involvement and make it advisable that cell trafficking disorders are included in the differential diagnoses of inborn errors of metabolism of small molecules (in particular intoxication disorders) and energy defects. These findings suggest that stressful situations such as infections impact the normal functioning of the trafficking machinery between the endoplasmic reticulum (ER) and the Golgi apparatus in individuals with *TRAPPC11* pathogenic variants and other disorders.

J Med Genet: first published as 10.1136/jmg-2022-109132 on 16 May 2023. Downloaded from http://jmg.bmj.com/ on January 9, 2025 by guest. Protected by copyright.

The precise mechanisms leading to these manifestations need to be further described.

Although epilepsy represents a significant symptom of LGMD R18 with a serious impact on quality of life, to date neither the types of seizures nor the electroencephalographic abnormalities had been studied systematically in a well-described cohort of individuals. In our cohort, epilepsy occurred in more than half of individuals with TRAPPC11-related muscular dystrophy and was typically presented with early childhood-onset long-lasting bilateral tonic-clonic seizures. EEG studies showed focal or multifocal interictal epileptiform abnormalities in most of the cases. The response to antiepileptic drugs was good in a significant proportion of individuals but not in all.

Our pathological studies on muscle biopsy from seven individuals revealed a myopathic pattern with degenerative-regenerative fibres, isolated hypercontracted fibres and alterations in the intermyofibrillar pattern. Although the fibre-type distribution pattern was normal in most individuals, selective atrophy of fast fibres was identified in two cases. We detected a patchy reduction of alpha-dystroglycan of variable intensity, both with immunofluorescence and western blot analysis, which validates similar findings recently reported by Munot *et al*.[18]

TRAPPC11 is a protein involved in membrane trafficking[10 44] and had been previously related to autophagy defects, with a role in membrane recruitment for the autophagosome formation.[45] Our results expand the role of TRAPPC11 in mitochondrial function, as we observe a decreased mitochondrial ATP production capacity and network architecture in TRAPPC11-deficient fibroblasts. This sets the base for further research on the potential role of TRAPPC11 within mitochondria-Golgi-ER triad and its specific role on mitochondrial functions, which should be delimited with further experiments that are beyond the scope of this work, analysing the involvement of other mitochondrial functions in *TRAPPC11*-related muscular dystrophies such as the activity and expression of electron transport chain complexes, mitochondrial ultrastructure, reactive oxygen species production and metabolism, mitophagy and mitochondrial signalling. These findings may also help to develop targeted therapies.

In summary, we provide a comprehensive phenotypic characterisation of the pathogenic variant *TRAPPC11* c.1287+5G>A, which is founder in the Roma population. Our observations indicate that glycosylation of alpha-dystroglycan is reduced in the skeletal muscle of individuals with LGMD R18 and we emphasise some features that are typical of golgipathies, such as microcephaly and clinical decompensation associated with infections, are probably more prevalent than previously thought.

Author affiliations
[1]Neuromuscular Unit, Department of Neurology, Hospital Sant Joan de Déu, Barcelona, Spain
[2]Department of Paediatrics, Complejo asistencial de Salamanca, Salamanca, Spain
[3]Applied Research in Neuromuscular Diseases, Sant Joan de Deu Research Institute, Barcelona, Spain
[4]Centre for Biomedical Network Research on Rare Diseases (CIBERER), Instituto de Salud Carlos III, Madrid, Spain
[5]Department of Pathology, Hospital Sant Joan de Déu, Barcelona, Spain
[6]Paediatric Neurology Unit, Hospital Universitario Marques de Valdecilla, Santander, Spain
[7]Neurometabolic Unit and Synaptic Metabolism Lab, Departments of Neurology, IPR (Institut Pediàtric de Recerca), CIBERER and MetabERN, Hospital Sant Joan de Déu, Barcelona, Spain
[8]Department of Paediatrics, Hospital San Pedro, Logrono, Spain
[9]Paediatric Neurology Unit, Hospital Universitario Central de Asturias, Oviedo, Spain
[10]Department of Paediatrics, Complejo Asistencial Universitario de Salamanca, Salamanca, Spain
[11]Unit of Epilepsy, Sleep and Neurophysiology, Department of Neurology, Hospital Sant Joan de Déu, Barcelona, Spain
[12]Department of Radiology, Hospital Sant Joan de Déu, Barcelona, Spain
[13]Neuropathology Unit, Hospital Universitario 12 de Octubre, Madrid, Spain
[14]Neuromuscular Unit, Department of Neurology, Hospital Universitario 12 de Octubre, Madrid, Spain
[15]Biodonostia, Neurosciences Area, Neuromuscular Diseases Laboratory, Hospital Universitario de Donostia, San Sebastian, Spain
[16]Paediatric Neurology Unit, Hospital Universitario Rio Hortega de Valladolid, Valladolid, Spain
[17]Department of Paediatrics, Hospital Clinico Universitario de Valladolid, Valladolid, Spain
[18]Department of Paediatrics, Hospital Universitario Doctor Peset, Valencia, Spain
[19]Department of Paediatrics, Hospital Rio Carrion, Palencia, Spain
[20]Department of Clinical Biochemistry, Complejo Asistencial Universitario de Salamanca, Salamanca, Spain
[21]La Paz University Hospital, Madrid, Spain
[22]Paediatric Neurology Unit, Hospital Universitario 12 de Octubre, Madrid, Spain
[23]Laboratory of Neurogenetics and Molecular Medicine—IPER, Sant Joan de Deu Research Institute, Barcelona, Spain
[24]Biosciences Department, Faculty of Sciences, Technology and Engineering, Universitat de Vic—Universitat Central de Catalunya, Vic, Spain
[25]Department of Genetics, Microbiology and Statistics, University of Barcelona, Barcelona, Spain

Twitter Maria Luisa Poch @PochMarisa

Acknowledgements We are indebted to the 'Biobanc de l'HospitalInfantil Sant Joan de Déu per a la Investigació', part of the Spanish Biobank Network of ISCIII for the sample and data procurement.

Contributors MJ had a major role in the acquisition of the data, analysed the data, interpreted the data and drafted the manuscript for intellectual content. ÀG-C and DN-dB designed and conceptualised the study, had major role in the acquisition of the data, analysed the data, interpreted the data and drafted the manuscript for intellectual content. DN-dB is responsible for the overall content as the guarantor. The rest of the authors collected the data, performed the analysis and revised the manuscript for intellectual content.

Funding DN-dB was supported by the Miguel Servet programme from Instituto de Salud Carlos III, Spain (CP22/00141). ÀG-C and NAJ-P are supportedby FIS P118/00111 and FI21/0073 'Instituto de Salud Carlos III' and 'Fondo Europeo de desarrollo regional (FEDER)'. CJ-M is partially supported by Instituto de Salud Carlos III and co-funded with European Regional Development Fund (ERDF) 'A way to achieve Europe' grant PI19/00122.

Competing interests Authors report no disclosures. ÀG-C has received honoraria for lectures from PTC Therapeutics International GT, Immedica, Biomarin and Recordati Rare Diseases Foundation; she has also received a research grant from PTC Therapeutics and is a co-founder of the Sant Joan de Déu start up 'Neuroprotect Life Sciences'.

Patient consent for publication Consent obtained from parent(s)/guardian(s).

Ethics approval This study was approved by Hospital Sant Joan de Déu Clinical Research Ethics Committee (reference PIC-131-18). Participants gave informed consent to participate in the study before taking part.

Provenance and peer review Not commissioned; externally peer reviewed.

Data availability statement Data are available on reasonable request.

Biobank The HSJD Biobank is officially registered in the Spanish Institute of Health (Instituto de Salud Carlos III) under the number B.0000599. It is also authorised by the autonomic health system of Catalonia. All the samples of HSJD Biobank used in research are collected, managed and stored under strict quality measures (the Biobank is accredited by ISO 9001:2015 standard) and all donors or their relatives have signed an informed consent form. The HSJD Biobank website is: https://www.irsjd.org/es/servicios-cientificotecnicos/biobanco-pediatrico-para-la-investigacion/.

Supplemental material This content has been supplied by the author(s). It has not been vetted by BMJ Publishing Group Limited (BMJ) and may not have been peer-reviewed. Any opinions or recommendations discussed are solely those of the author(s) and are not endorsed by BMJ. BMJ disclaims all liability and responsibility arising from any reliance placed on the content. Where the content includes any translated material, BMJ does not warrant the accuracy and reliability of the translations (including but not limited to local regulations, clinical guidelines, terminology, drug names and drug dosages), and is not responsible for any error and/or omissions arising from translation and adaptation or otherwise.

Open access This is an open access article distributed in accordance with the Creative Commons Attribution Non Commercial (CC BY-NC 4.0) license, which permits others to distribute, remix, adapt, build upon this work non-commercially, and license their derivative works on different terms, provided the original work is

J Med Genet: first published as 10.1136/jmg-2022-109132 on 16 May 2023. Downloaded from http://jmg.bmj.com/ on January 9, 2025 by guest. Protected by copyright.

properly cited, appropriate credit is given, any changes made indicated, and the use is non-commercial. See: http://creativecommons.org/licenses/by-nc/4.0/.

ORCID iDs
Cristina Domínguez-González http://orcid.org/0000-0001-5151-988X
Daniel Natera-de Benito http://orcid.org/0000-0001-7764-2085

REFERENCES

1 Wicklund MP. The limb-girdle muscular dystrophies. *CONTINUUM (Minneap Minn)* 2019;25:1599–618.
2 Nallamilli BRR, Chakravorty S, Kesari A, *et al*. Genetic landscape and novel disease mechanisms from a large LGMD cohort of 4656 patients. *Ann Clin Transl Neurol* 2018;5:1574–87.
3 Rosales XQ, al-Dahhak R, Tsao C-Y. Childhood onset of limb-girdle muscular dystrophy. *Pediatr Neurol* 2012;46:13–23.
4 Straub V, Murphy A, Udd B, *et al*. 229th ENMC International workshop: limb girdle muscular dystrophies – Nomenclature and reformed classification naarden, the Netherlands, 17–19 March 2017. *Neuromuscular Disorders* 2018;28:702–10.
5 Bögershausen N, Shahrzad N, Chong JX, *et al*. Recessive TRAPPC11 mutations cause a disease spectrum of limb girdle muscular dystrophy and myopathy with movement disorder and intellectual disability. *Am J Hum Genet* 2013;93:181–90.
6 Liang W-C, Zhu W, Mitsuhashi S, *et al*. Congenital muscular dystrophy with fatty liver and infantile-onset cataract caused by TRAPPC11 mutations: broadening of the phenotype. *Skelet Muscle* 2015;5:29.
7 Matalonga L, Bravo M, Serra-Peinado C, *et al*. Mutations in TRAPPC11 are associated with a congenital disorder of glycosylation. *Hum Mutat* 2017;38:148–51.
8 Lipatova Z, Segev N. Ypt/Rab GTPases and their TRAPP GEFs at the Golgi. *FEBS Lett* 2019;593:2488–500.
9 Jones S, Newman C, Liu F, *et al*. The TRAPP complex is a nucleotide exchanger for Ypt1 and ypt31/32. *Mol Biol Cell* 2000;11:4403–11.
10 Scrivens PJ, Noueihed B, Shahrzad N, *et al*. C4orf41 and TTC-15 are mammalian TRAPP components with a role at an early stage in ER-to-Golgi trafficking. *Mol Biol Cell* 2011;22:2083–93.
11 Brunet S, Sacher M. In sickness and in health: the role of TRAPP and associated proteins in disease. *Traffic* 2014;15:803–18.
12 Sacher M, Shahrzad N, Kamel H, *et al*. TRAPPopathies: an emerging set of disorders linked to variations in the genes encoding transport protein particle (TRAPP)-associated proteins. *Traffic* 2019;20:5–26.
13 Galindo A, Planelles-Herrero VJ, Degliesposti G, *et al*. Cryo-EM structure of metazoan TRAPPIII, the multi-subunit complex that activates the gtpase rab1. *EMBO J* 2021;40:e107608.
14 Koehler K, Milev MP, Prematilake K, *et al*. A novel *trappc11* mutation in two turkish families associated with cerebral atrophy, global retardation, scoliosis, achalasia and alacrima. *J Med Genet* 2017;54:176–85.
15 Fee DB, Harmelink M, Monrad P, *et al*. Siblings with mutations in TRAPPC11 presenting with limb-girdle muscular dystrophy 2S. *J Clin Neuromuscul Dis* 2017;19:27–30.
16 Larson AA, Baker PR, Milev MP, *et al*. TRAPPC11 and gosr2 mutations associate with hypoglycosylation of α-dystroglycan and muscular dystrophy. *Skelet Muscle* 2018;8:17.
17 Milev MP, Stanga D, Schänzer A, *et al*. Characterization of three trappc11 variants suggests a critical role for the extreme carboxy terminus of the protein. *Sci Rep* 2019;9:14036.
18 Munot P, McCrea N, Torelli S, *et al*. TRAPPC11-related muscular dystrophy with hypoglycosylation of alpha-dystroglycan in skeletal muscle and brain. *Neuropathol Appl Neurobiol* 2022;48:e12771.
19 Wang X, Wu Y, Cui Y, *et al*. Novel *trappc11* mutations in a chinese pedigree of limb girdle muscular dystrophy. *Case Rep Genet* 2018;2018:8090797.
20 Szymański J, Janikiewicz J, Michalska B, *et al*. Interaction of mitochondria with the endoplasmic reticulum and plasma membrane in calcium homeostasis, lipid trafficking and mitochondrial structure. *Int J Mol Sci* 2017;18:1576.
21 Cohen S, Valm AM, Lippincott-Schwartz J. Interacting organelles. *Curr Opin Cell Biol* 2018;53:84–91.
22 Richards S, Aziz N, Bale S, *et al*. Standards and guidelines for the interpretation of sequence variants: a joint consensus recommendation of the American College of medical genetics and genomics and the association for molecular pathology. *Genetics in Medicine* 2015;17:405–24.
23 Sali A, Blundell TL. Comparative protein modelling by satisfaction of spatial restraints. *J Mol Biol* 1993;234:779–815.
24 Schrödinger. DeLano WL. PyMOL. 2020. Available: http://www.pymol.org/pymol
25 Healy EG. Muscle biopsy a practical approach 5th edition. *Neuromuscular Disorders* 2022;32:98.
26 Brockington M, Torelli S, Sharp PS, *et al*. Transgenic overexpression of large induces α-dystroglycan hyperglycosylation in skeletal and cardiac muscle. *PLoS ONE* 2010;5:e14434.
27 Fisher RS, van Emde Boas W, Blume W, *et al*. Epileptic seizures and epilepsy: definitions proposed by the international league against epilepsy (ILAE) and the international bureau for epilepsy (IBE). *Epilepsia* 2005;46:470–2.
28 Berg AT, Berkovic SF, Brodie MJ, *et al*. Revised terminology and concepts for organization of seizures and epilepsies: report of the ILAE commission on classification and terminology, 2005-2009. *Epilepsia* 2010;51:676–85.
29 Brodie MJ, Barry SJE, Bamagous GA, *et al*. Patterns of treatment response in newly diagnosed epilepsy. *Neurology* 2012;78:1548–54.
30 Oyarzabal A, Bravo-Alonso I, Sánchez-Aragó M, *et al*. Mitochondrial response to the BCKDK-deficiency: some clues to understand the positive dietary response in this form of autism. *Biochimica et Biophysica Acta (BBA) - Molecular Basis of Disease* 2016;1862:592–600.
31 Chaudhry A, Shi R, Luciani DS. A pipeline for multidimensional confocal analysis of mitochondrial morphology, function, and dynamics in pancreatic β-cells. *Am J Physiol Endocrinol Metab* 2020;318:E87–101.
32 Gastaut H, Gastaut JL, Gonçalves e Silva GE, *et al*. Relative frequency of different types of epilepsy: a study employing the classification of the International League against epilepsy. *Epilepsia* 1975;16:457–61.
33 Ünver O, Keskin SP, Uysal S, *et al*. The epidemiology of epilepsy in children: a report from a Turkish pediatric neurology clinic. *J Child Neurol* 2015;30:698–702.
34 Hostetler JA. History and relevance of the Hutterite population for genetic studies. *Am J Med Genet* 1985;22:453–62.
35 Rasika S, Passemard S, Verloes A, *et al*. Golgipathies in neurodevelopment: a new view of old defects. *Dev Neurosci* 2019;40:396–416.
36 Passemard S, Perez F, Gressens P, *et al*. Endoplasmic reticulum and Golgi stress in microcephaly. *Cell Stress* 2019;3:369–84.
37 Passemard S, Perez F, Colin-Lemesre E, *et al*. Golgi trafficking defects in postnatal microcephaly: the evidence for "golgipathies." *Prog Neurobiol* 2017;153:46–63.
38 Rawlins LE, Almousa H, Khan S, *et al*. Biallelic variants in TRAPPC10 cause a microcephalic trappopathy disorder in humans and mice. *PLOS Genet* 2022;18:e1010114.
39 Kaur P, Kadavigere R, Girisha KM, *et al*. Recurrent bi-allelic splicing variant c.454+3a > G in TRAPPC4 is associated with progressive encephalopathy and muscle involvement. *Brain* 2020;143:e29.
40 Majethia P, Do Rosario MC, Kaur P, *et al*. Further evidence of muscle involvement in neurodevelopmental disorder with epilepsy, spasticity, and brain atrophy. *Ann Hum Genet* 2022;86:94–101.
41 Al-Deri N, Okur V, Ahimaz P, *et al*. A novel homozygous variant in TRAPPC2L results in a neurodevelopmental disorder and disrupts TRAPP complex function. *J Med Genet* 2021;58:592–601.
42 Milev MP, Graziano C, Karall D, *et al*. Bi-Allelic mutations in TRAPPC2L result in a neurodevelopmental disorder and have an impact on Rab11 in fibroblasts. *J Med Genet* 2018;55:753–64.
43 Bérat C-M, Montealegre S, Wiedemann A, *et al*. Clinical and biological characterization of 20 patients with TANGO2 deficiency indicates novel triggers of metabolic crises and NO primary energetic defect. *J Inherit Metab Dis* 2021;44:415–25.
44 García-Cazorla A, Oyarzábal A, Saudubray J-M, *et al*. Genetic disorders of cellular trafficking. *Trends Genet* 2022;38:724–51.
45 Stanga D, Zhao Q, Milev MP, *et al*. TRAPPC11 functions in autophagy by recruiting ATG2B-WIPI4/WDR45 to preautophagosomal membranes. *Traffic* 2019;20:325–45.

J Med Genet: first published as 10.1136/jmg-2022-109132 on 16 May 2023. Downloaded from http://jmg.bmj.com/ on January 9, 2025 by guest. Protected by copyright.

3| PUBLICATIONS IN PROCESS DIRECTLY RELATED TO THE CONTENT OF THIS THESIS (under review/manuscript in preparation)

AFG2A-RELATED ENCEPHALOPATHY: CLINICAL AND EPILEPTIC PHENOTYPE, KETOGENIC DIET EFFECT (IN VIVO AND IN VITRO)

Under review

Authors: Laia Nou-Fontanet, Uliana Musokhranova, Gaetano Cantalupo, Frederik Braun, Alia Ramírez Camacho, Verónica González Álvarez, Verónica Delgadillo Chilavert, Víctor Soto Insuga, Luisa Arrabal Fernández, Itziar Alonso-Colmenero, Alexis Arzimanoglou, Ángeles García Cazorla, Alfonso Oyarzabal*, Carmen Fons*.

In this paper, we present the in vitro functional studies on AFG2A-related encephalopathy patients' fibroblasts (including the three patients described in this Thesis) and the treatment with media mimicking ketogenic diet. In addition, we present the clinical and epileptic characterization of the patients with ketogenic diet treatment.

SPERMIDINE AS A POTENTIAL NOVEL THERAPEUTIC APPROACH IN MITOCHONDRIAL DISORDERS

Under review

Authors: Musokhranova U, Rivera N, Urreitzi R, Grau C, Grau L, Sigatullina M, Afonsi C, Juliá-Palacios N, O'Callaghan M, Darling A, Fernández-Alvarez E, Artuch R, Bayona P, Montoya J, García-Cazorla A* and Oyarzábal A*.

In this paper, we present the in vitro functional characterization of fibroblasts from eight mitochondrial patients presented in this Thesis: CHCHD6 (mitochondrial cristae), WARS2 (mitochondrial gene translation), DNM1L (mitochondrial fission), PDHX (intermediate metabolism), NDUFS1 (OXPHOS complex I structural subunit), NDUFAF6 (OXPHOS complex I assembly factor), SCO2 (OXPHOS complex IV assembly factor), SURF1 (OXPHOS complex IV assembly factor). In these patients, we assayed spermidine treatment in vitro evaluating the bioenergetic function correction. In addition, we present the clinical phenotype evolution before and after the treatment with spermidine in the patients.

MITOCHONDRIAL NETWORK CHARACTERIZATION AS A BIOMARKER TO AID THE CLINICAL DIAGNOSIS OF DNM1L PATIENTS WITH NEW VARIANTS

In preparation

In this paper, we present the mitochondrial network characterization in fibroblasts from patients with novel mutations on DNM1L, including the five patients presented in this Thesis. Also, we characterize the bioenergetic function and assay different treatment options that module the bioenergetic function depending on the alterations described.